AZERBAIJAN NATIONAL ACADEMY OF SCIENCES

ANAS TRANSACTIONS

EARTH SCIENCES

www.journalesgia.com

2024
№ 2

We are Crossref
Member

Crossref
This journal is included and indexed in the *GeoRef* database

ELSEVIER
Scopus

PETROGENETIC ROLE OF PYROXENES IN THE FORMATION OF PICRITES OF THE LESSER CAUCASUS AND TALYSH ZONE

Mammadov M.N., Babayeva G.J., Sariyev F.H.

Ministry of Science and Education of the Republic of Azerbaijan,

Institute of Geology and Geophysics, Azerbaijan

119, H.Javid ave., Baku, AZ1143: gultekin_babayeva@rambler.ru

Keywords: *The Lesser Caucasus, Talysh zone, picrite, zoned pyroxene, crystallization differentiation*

Summary. On the basis of microprobe, chemical and X-ray diffractometric analyses, the petrogenetic features of the formation of picrites depending on epycompositional variability of clinopyroxenes in the Lesser Caucasus and Talysh zone were studied. The Upper Jurassic picrites of the Murovdag anticlinorium were formed under similar geological and geodynamic conditions, while being controlled by the rift-type crack structure. Therefore, the petrographic type of rocks involved in the anticlinorium is homogeneous. Clinopyroxene megacrysts in subalkaline picrites in the Khojavend bend correspond to chromium diopside partially depleted in titanium oxide. Clinopyroxenes are included as phenocrysts, normal prismatic and megacrysts in the Santonian trachybasalt-trachydolerite, tephrite-teschenite complexes of the Khojavend synclinorium. The contact zone is noticeable in its parent rock. In the Talysh zone, the picrites belong to the subalkaline series and have a characteristic clay structure, and their main masses are dolerite and subdolerite. Along with olivine, clinopyroxene phenocrysts are present in the contents. Those phenocrysts in most cases form large elongated, sometimes plate-like crystals. In most cases, they are colorless. However, olivine and chromspinel inclusions of different sizes are observed in them. Rather large prismatic phenocrysts of clinopyroxenes are included in phlogopite and olivine picrites. These phenocrysts are xenomorphic to olivine. The composition of clinopyroxenes in the picrites of Talysh zone corresponds to diopside-salite. Thus, the change in the composition of pieroxenes in picrites of the Lesser Caucasus and Talysh zone is regulated by crystallization differentiation.

Introduction. The formation of picrites is related to the melting of the mantle substrate at high degree. Therefore, their geochemical composition corresponds mainly to the composition of the core mantle. Besides these, in most cases, picrites are homogeneous both in oceans and continents of the world. In some cases, they are formed by the direct control of crystallization differentiation. In this sense, the study of the genesis of picrites is of great importance.

According to the existing geological and petrological sources, the study of monoclinic and rhombic pyroxenes, which are part of picrites, is the most realistic source of genetic information in determining the evolutionary processes of their primary fusion, thermobaric conditions of their crystallization, as well as their potential mineralization.

Unlike other rock-forming minerals, pyroxenes are more resistant to derivative processes and can preserve their originality. In this sense, the study of their complex physico-chemical and petrological characteristics can be quite important in the research of the petrological and geological conditions of picrites occurrences of the Lesser Caucasus and Talysh zone.

Research methods. Microprobe, chemical and X-ray diffraction methods were used to determine the reliability of the presented pyroxene analyses. Microprobe analyses of pyroxene phenocrysts were carried out using an internal standard in electron probe microanalysis (JEOL, JSM-6610 LV, Oxford Instruments, X-MAX). All microprobe, X-ray diffraction and chemical analyses of pyroxenes were carried out at the analytical center of the Institute of Geology and Geophysics of the Ministry of Science and Education of the Republic of Azerbaijan. The crystallochemical formulas of the minerals were determined by the Kushiro method (Kushiro, 1965), and the crystallization temperature was determined by the Lindsley paleothermometer (Lindsley, 1983).

Geological and petrological conditions of the formation of picrites in the Lesser Caucasus and Talysh zone. Picrites of various petrochemical series have been discovered in the geological structure of the Murovdag uplift, Khojavand flexure of the Lesser Caucasus and Talysh zone in the territory of the Republic of Azerbaijan.

Normal alkaline impregnation-like picrites are located in the Bajocian-Bathonian volcanites on the northeastern slope of the Murovdag uplift, at its junction with the Dashkasan flexure (Fig. 1).

Picrites are dark black and macroscopically homogeneous. But greenish-gray colored olivine phenocrysts are visible to the naked eye. A weak thermal rim is observed with volcanites of the contact zone. Picrites have characteristic porphyritic structure under the microscope. Olivine completely dominates among the phenocrysts (25-30%). They form large dipyramidal grains. Serpentine loops divided the olivine into separate parts. Olivine remained completely unaltered among the loops. The composition of the olivine phenocryst corresponds to for-

sterite-chrysolite ($Fa_{8-14\%}$), and in most cases it forms mutual combinations with chrome spinel. They are partially xenomorphic compared to rhombic and monoclinic olivine, and have spread very partially. Picrites are intensively chloritized in contact zones. They are low-graded in silica from a petrochemical point of view, and are accumulated in the area of typical picrites in the classification chart (Table 1, Fig. 2). It is clearly observed in the abovementioned classification chart that their points are accumulated together revealing the limitation of the weak evolutionary process. However, the weak increase of sericitization and calcitization in pyroxene picrites caused a partial increase of diopside in their normative mineralogical composition.
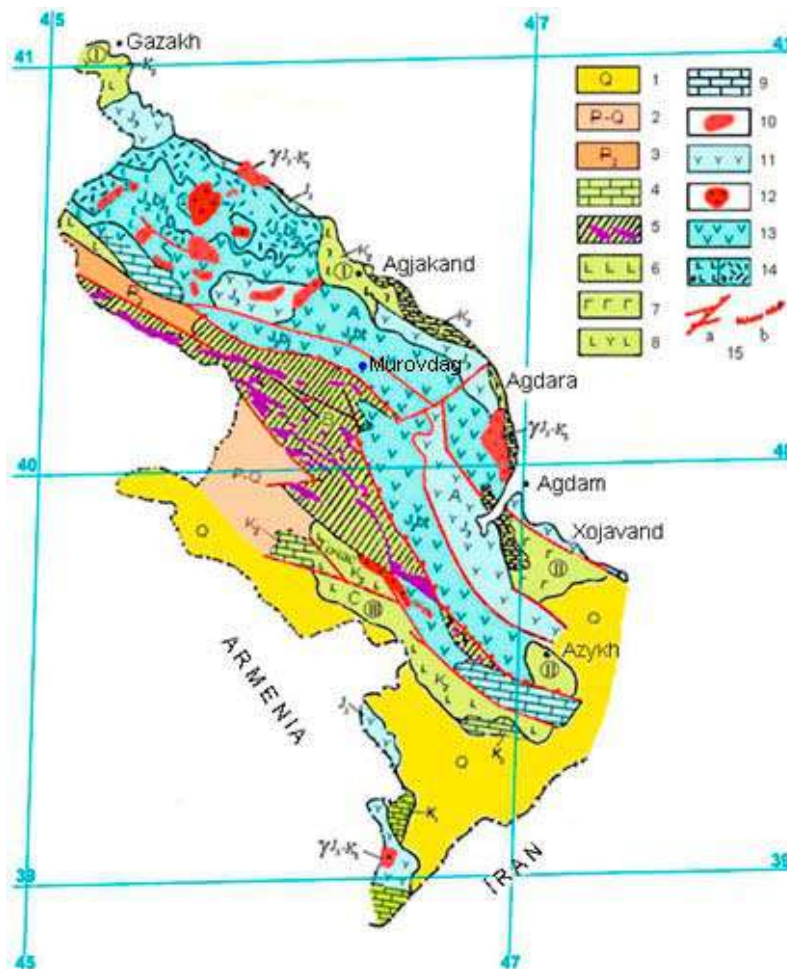
Fig. 1. Schematic geological map of the Lesser Caucasus (Шихалибейли, 1994)

I – Lok-Garabakh structural-formation zone (the Gazakh, the Agjakand, the Agdara depressions); II – Goycha-Akeri structural-formation zone (the Azykh and the Khojavand depressions), III – Miskhan-Kafan structural-formation zone (the Gochas depression)
1 – the contemporary sediments; 2 – the Paleogene-Neogene volcanogenic sedimentary deposits; 3 – the Paleogene volcanogenic sedimentary deposits; 4 – the Upper Cretaceous limestones; 5 –the ophiolite complexes; 6 – the Late Senonian basalt-andesibasalt and trachybasalt-trachyandesibasalt complexes (the Gochas depression); 7 – the Santonian basalt-andesibasalt and trachybasalt-trachyandesibasalt complexes (the Azykh depression), trachybasalt-trachydolerite and tephrite-teschenite (the Khojavand depression) complexes; 8 – the Late Coniacian-Early Santonian basalt-andesibasalt and the Late Santonian-Early Campanian rhyolite-rhyodacite complexes (the Gazakh depression), Coniacian-Santonian basalt-andesibasalt and rhyolite-rhyodacite complexes (the Agjakand and the Agdara depressions); 9 – the Upper Jurassic limestones; 10 – the Late Jura- Early Cretaceous gabbro-diorite-granite complex; 11 – the Late Jurassic- Early Cretaceous dacite complex; 12 – the Bathonian plagiogranite complex; 13 – the Bathonian basalt-andesite-dacite-rhyoilte complex; 14 – a) the Early Bajocian basalt complex, б) the Late Bajocian rhyolite complex; 15 – deep faults (a), flexures (b).

Chemical and CIPW compositions of picrites of the Murovdag anticlinorium

№№ Komp.	3	5	10	72	73	74	76	79
SiO$_2$	41.45	42.50	41.60	41.21	42.28	42.15	43.36	43.60
TiO$_2$	0.16	0.26	0.24	0.11	0.11	0.15	0.18	0.16
Al$_2$O$_3$	7.12	6.70	6.23	9.56	7.46	9.12	9.11	8.78
Cr$_2$O$_3$	0.38	0.34	0.24	0.46	0.38	0.42	0.58	0.46
Fe$_2$O$_3$	3.42	4.56	3.64	3.92	3.75	3.89	3.42	3.95
FeO	5.53	6.14	6.04	6.49	6.79	6.40	5.60	6.51
MnO	0.18	0.19	0.22	0.17	0.18	0.16	0.20	0.16
MgO	31.78	28.80	28.81	28.85	29.36	27.42	25.20	25.70
CaO	5.53	5.66	8.26	4.23	5.28	6.20	7.30	6.40
Na$_2$O	0.18	0.11	0.10	0.06	0.07	0.09	0.10	0.12
K$_2$O	0.05	0.14	0.15	0.09	0.08	0.08	0.08	0.04
P$_2$O$_5$	0.04	0.05	0.04	0.06	0.04	0.05	0.03	0.04
LOI	4.15	4.46	4.39	4.43	4.12	3.64	4.25	3.75
∑	99.97	99.91	99.96	99.64	99.90	99.77	99.41	99.67
Ap	0.1	0.1	0.1	0.1	0.1	0.1	0.1	0.1
Il	0.3	0.5	0.5	0.2	0.2	0.3	0.3	0.3
Mt	5.5	7.1	5.6	6.4	6.0	6.3	5.8	6.4
Or	0.3	0.8	0.9	0.5	0.5	0.5	0.5	0.2
Ab	1.5	0.9	0.8	0.5	0.6	0.8	0.8	1.0
An	18.5	17.4	16.1	20.6	19.8	24.2	24.2	23.3
Di	3.6	4.3	10.3	-	2.6	2.6	5.0	3.4
En	2.9	3.5	8.2	-	2.0	2.1	3.9	2.7
Fs	0.3	0.3	0.9	-	0.3	0.2	0.4	0.4
Fo	44.4	31.8	39.7	32.8	34.8	32.4	24.4	23.9
Fa	4.4	3.5	4.8	4.2	4.8	4.3	3.0	3.4
En	12.9	22.8	6.9	25.1	21.5	20.0	24.0	27.3
Fs	1.1	2.3	0.8	2.9	2.7	2.4	2.7	3.5
∑	95.8	95.3	95.6	93.3	95.9	96.2	95.1	95.9

3, 73 – olivine picrite, 5, 10, 72 ,74, 76, 79 – olivine-pyroxene picrite.

The results of the conducted petrochemical, petrographic and mineralogical studies show that indeed the picrite magma was poorly evolved in the Earth's crust.

The subalkaline analogs of picrites occur in association with tephrites, trachybasalts, and teshenites of the Khojavend Synclinorium of the Lesser Caucasian Megaanticlinorium. The described subalkaline picrites form a gradual transition with teschenite on the one hand, and tephrite on the other hand.

At the same time, a limited amount of chrome diopside and phlogopite inclusions of 0.5x5 cm size were found in the breccias of tephrite. A thin thermal contact is observed between those inclusions and tephrite. Teschenite is freckled-gray, dark-gray and gray-black colored and varies from top to bottom by gravity of rock types. Volcanites are located in the center of the Khojavand synclinorium surrounded by Santonian limestones.

Macroscopically, the picrites of the Khojavand synclinorium is dark black, and relatively greenish-black pyroxene grains, sometimes colorless and pale brown phlogopite grains are easily visible to the naked eye against their background.

Picrites of the Khojavand synclinorium is located in the contact zones of picrites and basalts in the classification chart (Table 2, Fig. 2) from the petrochemical point of view. The abundance of alkaline (Na$_2$O+K$_2$O), chrome and titanium oxides in contrast to the previous petrographic types of rocks shows some peculiarities of the primary fusion of these picrites. Besides these, the amount of magnesium oxide gradually decreases from 22.4% to 11.78%, starting from the subalkaline melanocrate type towards the leucocrate type due to other petrochemical characteristics of the subalkaline picrites. Such an alteration is also occurred in the normative mineralogical composition of picrites. So, the normative forsterite molecule decreases from olivine subalkaline picrites to leucocratic picrites (Table 2). The subalkaline picrites of the Khojavand synclinorium are nepheline normative.
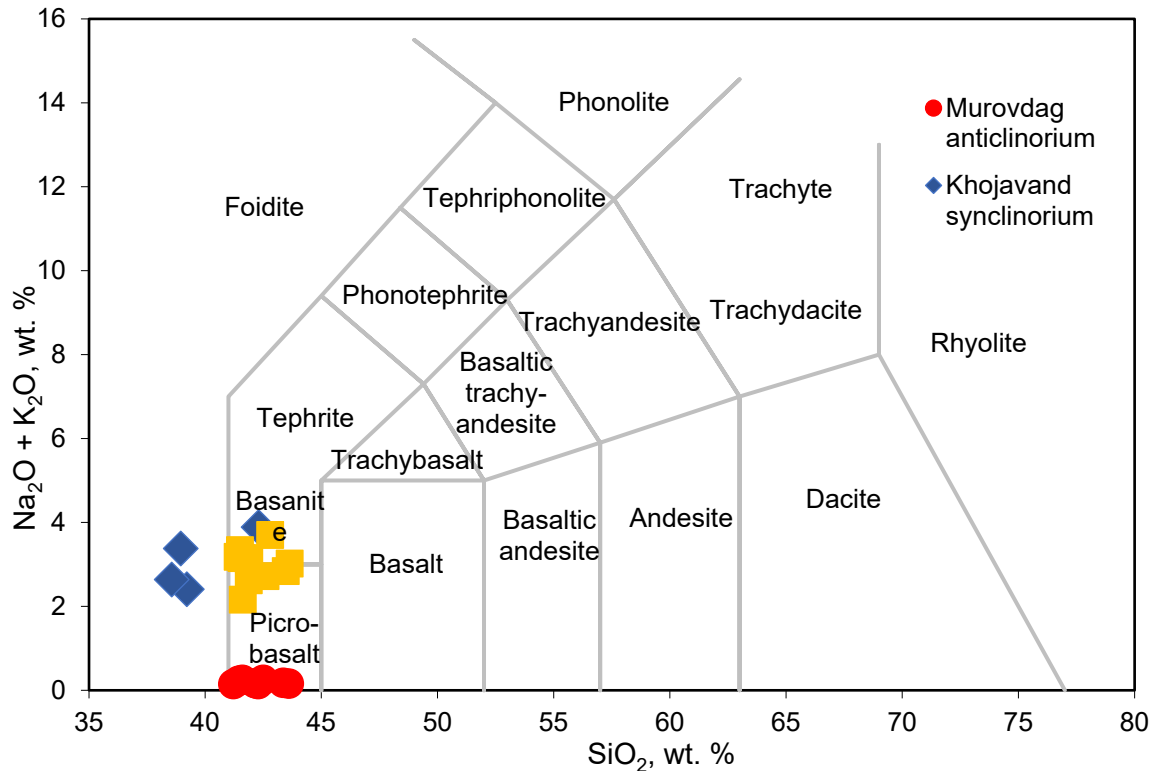
Fig. 2. Position of the chemical compositions of picrites of the Lesser Caucasus and Talysh zone on the TAS classification chart (Le Bas et al., 1986).

The Talysh zone is the northwestern continuation of the Alborz folding zone, it is traced from the valley of the Seyfirud (Agchay) River in the direction of the general Caucasus to the Germi settlement of the Islamic Republic of Iran (Fig. 3) (Азизбеков и др., 1979). The structures of the zone change the stretching direction from here and are observed along the latitudinal circle to the Garadag ophiolite outcrop (Мамедов, 1983; Рустамов, 2019). The picrites are of the subalkaline composition here and their age is mainly the Upper Eocene-Lower Oligocene. The subalkaline picrites form thin (2-4 m) layered outcrops alternating with the Paleocene and Eocene flysch sandstones in this zone. Besides these, picrite's limited outcrops of low thickness (2.5-3 m) are observed in places where picrites spread. But the subalkaline picrites are impregnated and fully crystalline. The large impregnations consist of monoclinic pyroxene of 0.3x1.2 cm size, olivine with relatively minor chrysotile, as well as phlogopite and small chrome spinel grains. The main mass of the rock is fully crystalline and consists of clinopyroxene grains. The subalkaline picrites are involved in serpentinization and amphibolization processes to one degree or another. The chemical and normative mineralogical composition of picrites is given in Table 3.

The amount of olivine, chrome diopside and chrome spinel in the composition of the subalkaline picrites gradually changes along the vertical section here too. Therefore, their plagioclase types are directly observed in the apical parts of picrites.

As abovementioned, the picrites found in the Lesser Caucasus and Talysh zones differ greatly in terms of their composition and occurrence conditions. Besides the geological and petrological properties of their formation, this diversity occurs in the compositional alteration of the rock-forming minerals involved in the composition of picrites, in the crystallization sequences and determination of thermal conditions. In this sense, the study of pyroxenes in the compositions of picrites of different ages and petrochemical series, which are distributed in the Lesser Caucasus and the Talysh zone, is of exceptional petrogenetic importance. So, the petrological and geological diversity of picrites developed in the abovementioned zones can be shown in the examples of pyroxenes that are part of their composition.

From this point of view, as abovementioned, the picrites found on the north-eastern slope of the Murovdag anticlinorium are less evolved and the monoclinic and rhombic pyroxenes in their compositions are almost homogeneous. According to the conducted microscopic research, rhombic and monoclinic pyroxenes are xenomorphic with a very small amount of impregnations compared to the olivine impregnations in the composition of picrites. Its impregnations are found in a short prismatic form (Fig. 4).

Table 2

Chemical and CIPW compositions of the subalkaline picrites
of the Khojavend synclinorium

Komp.＼an.	1	2	3	4
SiO_2	39.21	38.56	38.95	42.3
TiO_2	2.18	2.19	2.25	1.38
Al_2O_3	8.46	8.86	11.12	14.29
Cr_2O_3	1.48	1.49	0.84	0.64
Fe_2O_3	3.76	3.64	3.46	3.57
FeO	6.45	6.75	6.73	7.28
MnO	0.18	0.2	0.23	0.18
MgO	22.4	21.5	17.4	11.78
CaO	8.16	7.64	9.6	9.82
Na_2O	1.16	1.46	1.82	2.79
K_2O	1.25	1.18	1.56	1.1
P_2O_5	0.21	0.18	0.16	0.25
LOI	4.56	5.75	5.32	4.43
Σ	99.46	99.4	99.44	99.81
Ap	0.1	0.1	0.1	0.7
Il	4.1	4.1	4.2	2.6
Mgt	7.4*	7.5*	6.5*	5.6
Or	7.2	7.2	0	6.7
Ab	0.5	0.3	0	9.3
Ne	5.41	6.7	8.2	7.7
Le	0	0	7.0	0
An	14.2	13.9	17.8	23.0
Wo	10.7	9.6	12.1	10.0
En	8.7	7.6	9.4	7.1
Fs	0.7	0.9	1.3	2.0
Fo	33.1	32.2	24.2	15.6
Fa	2.8	4.1	3.9	4.9
Σ	94.91	94.2	94.7	95.2

But they form small prismatic grains in the dark black main mass (Fig 4). In some cases, besides the microscopic research, according to the results of microprobe analysis (Table 4), the composition of those rhombic and monoclinic pyroxenes is less variable compared to each other. So, the quantitative behaviors of the mineral-forming components in rhombic pyroxenes are really close to each other (Table 4, an. 3, 5, 10, 73). At the same time, the values of the magnesium coefficient are slightly different from each other (Mg#=0.80-0.85). Monoclinic pyroxenes are also homogeneous, their composition differs a little from each other (Table 4). One of their most characteristic features is that titanium, sodium and aluminum oxides from the mineral-forming components are low-grade. But they are rich in silicon and magnesium oxides. Trivalent iron fills aluminum deficiencies in the IV coordination of monoclinic pyroxenes while calculating crystallochemical formulas. As a direct consequence of this, aluminum does not participate in the VI coordination. Calcium chermak minal is almost absent in the minal composition calculated by the Kushiro method (Kushiro, 1965). According to the existing classifications (Добрецов и др., 1971; Morimoto, 1988) the rhombic pyroxenes of the Upper Jurassic picrites of the Murovdag anticlinorium are bronzite-bearing, and the monoclinic pyroxenes are mainly chromium-bearing diopside.

Crystallization temperature of rhombic and monoclinic pyroxenes are 820ºC and 900-1000ºC (Table 4, Fig. 5) according to Lindsley (Lindsley, 1983) paleothermometer.

The Upper Jurassic picrites of the Murovdag anticlinorium were formed under similar geological and geodynamic conditions, while being controlled by the rift-type fault structure. Therefore, the rocks of petrographic type in the composition of picrites are homogeneous. The pyroxenes of these evolved picrites are closely related in terms of mineralogy, crystallization temperature and end-members compositions.
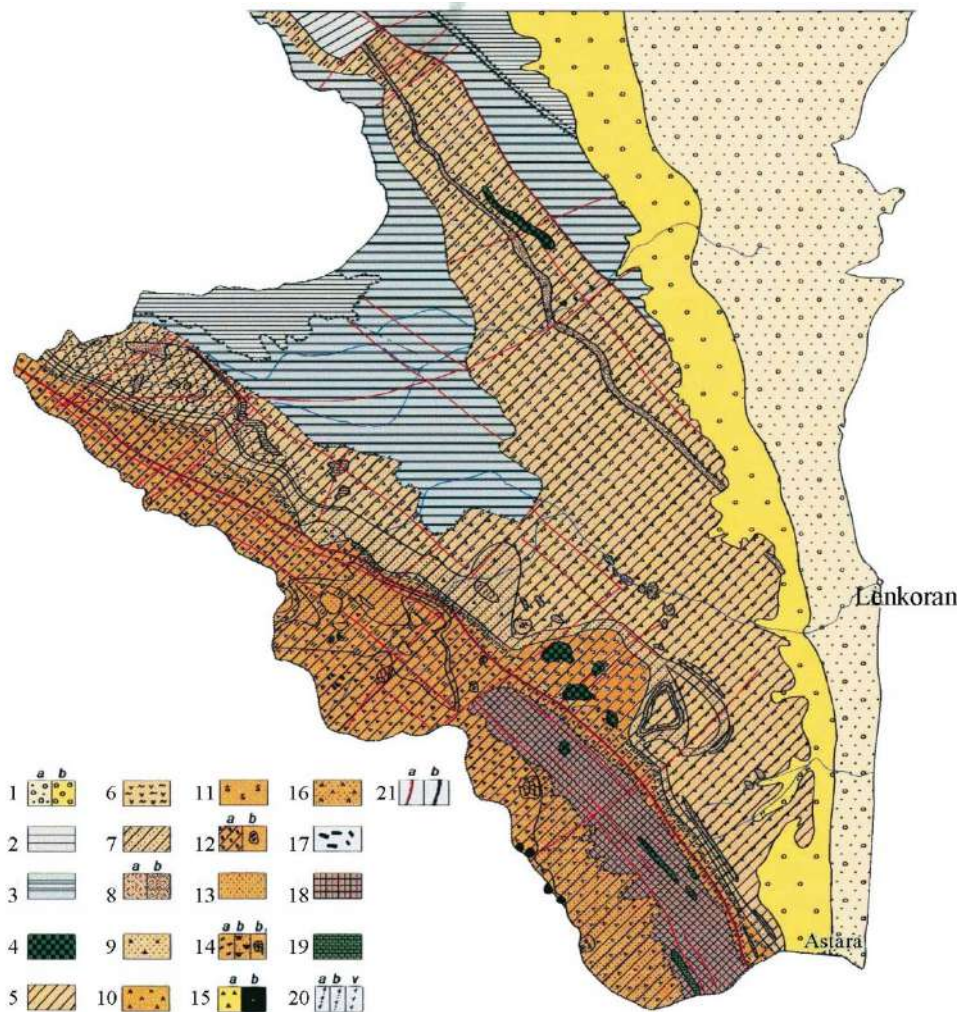
Fig. 3. Structural-formation map of the Talysh zone

1 – the Quaternary sediments: a) the Holocene sediments, b) the Pleistocene sediments; 2 – the Upper mollasse sediments (the Middle and the Upper Pliocene); 3 – the Lower mollasse sediments (the Oligocene and Upper Miocene); 4 – the subalkaline ultrabasic formation (the Upper Eocene-Lower Oligocene); the Eocene trachybasalt-trachyandezibasalt-phonolite formation; 5 – the trachybasalt-trachyandezibasalt (latite)-phonolite complex (the Upper Eocene); 6 – the layer of tuffaceous sandstones; 7 – the leucitic phonolite layer; 8 – the subalkaline trachybasalts, layer of trachydolerites: a) lava, pyroclastic facies, b) subvolcanic facies; 9 – the plagioporphyric trachyandezibasalt (latite) layer; 10 – the absarocite-shoshonite-alkaline basalt complex (the Lower-Middle Eocene); 11 – the łayer of sedimentary sandstones with flysch tuff; 12 – the alkaline basalts layer: a) lava, pyroclastic facies; b) subvolcanic facies; 13 – the layer of tuffaceous sedimentary sandstones; 14 – the layer of absarocites and leucite tephrites: a) lava, pyroclastic facies, b) subvolcanic facies, b₁) subvolcanic gabbro-techenites; 15 – the layer of trachybasalts; 16 – the layer of trachyandezibasalt tuffs; 17 – the dikes of trachybasalt, leucite tephrites and absarocites; 18 – the layer of flysch-tuffaceous sandstones (Paleocene); 19 – the limestone layer (the Upper Cretaceous); 20 – the fractures bordering structural floors: a) the Eocene age; b) the Oligocene age; v) the Miocene age; 21 – the magma-carrying and emplacement faults; a) connecting; b) separating.

Clinopyroxenes occur as phenocrysts, normal prismatic and megacrysts in the Santonian trachybasalt-trachydolerite, tephrite-teschenite complexes of the Khojavand synclinorium (0.5x2.5 cm) (Мамедов и др., 2012). Clinopyroxene megacrysts are dark black and are observed irregularly in gray tephrite-bearing breccias. A contact zone is noticeable in its source rock. Elongated prismatic crystals truncated by transverse crack are observed under the microscope. In most cases, fine and partially idiomorphic fine chrome spinel grains occur as inclusions. The subalkaline picrites have low-grade thermal contact with basic rocks.

As a result of the microprobe analysis, it was determined that it contains chrome diopside (Table 5). So, diopside molecule is 47.1%, and enstatite is about 45% in its end members. It is located in the area of modal diopside in the classification chart (Fig. 5).Unlike diopsides of normative alkaline picrites of the Murovdag anticlinorium, the concentration of aluminum and chromium is here significantly increased. If we compare the subalkaline picrites of the described megacrysts with the central part (Fig. 6a) of the zoned pyroxenes in the picrotephrites, it is observed that they have a similar composition (Table 5, an. 1).

Table 3

Chemical and normative mineralogical compositions of picrites of the Talysh zone

an. Komp.	1	2	3	4	5	6	7	8	9	10	11
SiO$_2$	41.4	41.50	41.82	41.57	41.62	41.88	41.9	42.8	42.6	43.47	43.64
TiO$_2$	0.53	0.59	0.5	0.4	0.37	0.44	0.69	0.4	0.55	0.61	0.78
Al$_2$O$_3$	6.32	6.31	5.65	5.53	5.63	5.91	7.92	9.39	12.16	12.40	12.26
Fe$_2$O$_3$	4.35	3.18	3.96	3.37	3.09	2.46	3.23	3.16	3.21	3.78	2.36
FeO	7.45	7.64	6.7	6.23	6.4	7.72	6.56	6.32	4.12	6.20	6.16
MnO	0.14	0.18	0.2	0.18	0.18	0.19	0.19	0.18	0.16	0.24	0.24
MgO	24.76	25.6	26.5	25.75	26.01	24.75	20.34	16.55	16.25	14.20	14.10
CaO	5.45	5.94	5.21	7.8	8.79	7.98	10.32	11.34	11.9	10.23	11.16
Na$_2$O	1.46	1.56	1.46	1.52	1.24	1.52	1.86	1.91	1.46	1.38	1.38
K$_2$O	1.72	1.78	1.69	1.63	0.92	1.1	1.2	1.79	1.26	1.46	1.64
P$_2$O$_5$	0.21	0.15	0.2	0.21	0.18	0.14	0.15	0.18	0.12	-	-
LOI	5.7	5.46	5.94	5.6	5.42	5.35	5.55	5.88	5.64	5.68	6.20
∑	99.49	99.89	99.83	99.79	99.85	99.44	99.91	99.9	99.43	99.65	99.92
Ap	0.3	0.3	0.3	0.3	0.3	0.3	0.3	0.3	0.1	-	-
Il	0.9	1.1	0.9	0.8	0.6	0.9	1.4	0.8	0.9	1.1	1.5
Mt	6.3	4.6	5.9	4.9	4.4	3.5	4.6	4.6	4.6	5.1	3.5
Or	10	10.6	10.0	4.2	4.2	6.7	3.3	4.5	7.2	8.3	9.5
Ab	5.0	0.9	4.7	-	-	0.7	-	-	1.4	10.0	4.6
An	4.3	5.0	3.3	3.6	7.0	5.8	9.7	11.7	22.8	23.6	22.5
Ne	4.1	6.7	4.3	2.7	5.7	6.7	8.5	8.8	6.0	0.8	3.8
Le	-	-	-	4.1	1.1	-	3.1	5.3	-	-	-
Wo	8.6	9.8	8.2	14.3	14.9	13.7	17.0	18.2	14.7	11.4	13.7
En	6.6	7.4	7.1	11.2	11.6	10.3	12.9	13.6	11.8	8.4	10.0
Fs	1.1	1.3	0.9	1.5	1.6	2.0	2.2	2.9	1.2	1.8	2.4
Fo	38.6	39.5	41.2	37.0	37.2	35.9	26.4	19.4	20.0	18.9	17.6
Fa	6.6	7.2	6.5	5.3	5.6	7.6	4.9	4.5	2.3	3.3	4.5

1, 2, 3, 4 – subalkaline olivine picrites, porphyritic; 5, 6, 7 – subalkaline olivine-clinopyroxene picrites, porphyritic; 8, 9 – subalkaline olivine-clinopyroxene-plagioclase picrites, porphyritic; 10, 11 – subalkaline clinopyroxene-plagioclase picrites
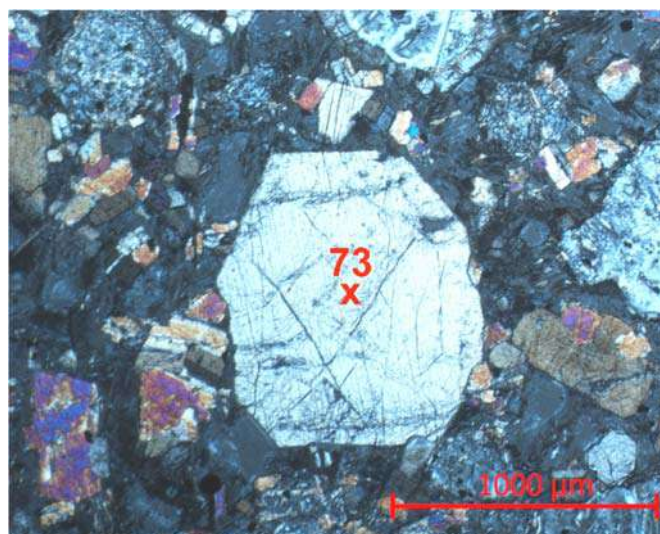

Fig. 4. Clinopyroxene phenocrystal in olivine picrite

Table 4

Chemical compositions, crystallochemical and end-members of pyroxenes of the Murovdag anticlinorium

minerals	clinopyroxene								orthopyroxene			
an. komp.	3	5	10	73	72	74	76	79	3	5	10	73
SiO$_2$	52.56	52.60	51.60	52.46	51.08	51.90	52.48	50.16	54.62	54.65	55.38	54.26
TiO$_2$	0.42	0.34	0.38	0.28	0.48	0.16	0.29	0.46	0.30	0.23	0.16	0.16
Al$_2$O$_3$	1.41	1.52	1.41	0.85	2.63	1.76	1.46	3.40	0.85	0.82	0.54	1.20
Cr$_2$O$_3$	0.54	0.63	0.74	0.68	0.32	0.72	0.64	0.16	0.52	0.58	0.39	0.39
Fe$_2$O$_3$	1.08	0.86	2.56	1.28	3.87	2.36	2.36	5.55	2.46	1.80	0.90	3.13
FeO	4.99	6.01	4.90	5.75	3.93	4.08	4.03	2.31	8.62	10.23	9.65	7.32
MnO	0.34	0.16	0.22	0.16	0.06	0.12	0.16	0.12	0.23	0.16	0.25	0.14
MgO	16.82	16.38	16.12	16.80	16.10	16.45	16.74	16.08	31.12	29.89	30.70	31.25
NiO	0.21	0.24	0.18	0.18	0.10	0.24	0.24	0.12	0.10	0.28	0.46	0.30
CoO	0.16	0.19	0.16	0.21	0.08	0.12	0.18	0.07	0.12	0.16	0.34	0.28
CaO	21.16	20.70	21.10	20.06	21.20	21.10	20.82	21.30	0.86	1.30	0.69	1.35
Na$_2$O	0.12	0.22	0.21	0.20	0.34	0.28	0.42	0.40	-	-	-	-
Σ	99.81	99.85	99.58	98.91	100.19	99.29	99.82	100.13	99.8	100.1	99.46	99.78
t°C	900	900	900	1000	880	880	900	820				
Mg#	0.83	0.81	0.80	0.80	0.79	0.82	0.83	0.80	0.84	0.82	0.84	0.85
T												
Si	1.939	1.944	1.918	1.950	1.882	1.926	1.933	1.849				
Al	0.061	0.056	0.061	0.037	0.114	0.074	0.063	0.147				
Fe^{+3}	-	-	0.021	0.013	0.004	-	0.004	0.004				
M1												
Al	-	0.010	-	-	-	0.001	-	-				
Fe^{+3}	0.030	0.024	0.050	0.024	0.104	0.066	0.062	0.15				
Ti	0.012	0.009	0.011	0.008	0.013	0.004	0.008	0.013				
Cr	0.015	0.018	0.022	0.020	0.009	0.021	0.019	0.004				
Mg	0.800	0.769	0.775	0.779	0.764	0.787	0.792	0.765				
Fe^{+2}	0.133	0.158	0.132	0.160	0.105	0.110	0.107	0.062				
Ni	0.006	0.007	0.005	0.005	0.003	0.007	0.007	0.004				
Co	0.004	0.006	0.005	0.006	0.002	0.004	0.005	0.002				
M2												
Fe^{+2}	0.021	0.027	0.020	0.031	0.016	0.017	0.017	0.009				
Mg	0.124	0.133	0.118	0.151	0.120	0.121	0.127	0.118				
Mn	0.011	0.005	0.007	0.005	0.002	0.004	0.005	0.004				
Ca	0.836	0.819	0.840	0.799	0.837	0.838	0.823	0.844				
Na	0.008	0.016	0.015	0.014	0.025	0.020	0.029	0.029				
Si	1.939	1.944	1.918	1.950	1.882	1.926	1.933	1.847	1.933	1.944	1.973	1.920
Ti	0.012	0.009	0.011	0.008	0.013	0.004	0.008	0.013	0.008	0.006	0.004	0.004
Al	0.061	0.066	0.061	0.037	0.114	0.075	0.063	0.148	0.035	0.034	0.023	0.050
Cr	0.015	0.018	0.022	0.020	0.009	0.021	0.019	0.004	0.015	0.016	0.011	0.011
Fe^{+3}	0.030	0.024	0.071	0.035	0.108	0.066	0.066	0.154	0.066	0.048	0.024	0.083
Fe^{+2}	0.154	0.186	0.152	0.191	0.121	0.127	0.124	0.071	0.255	0.304	0.288	0.217
Mn	0.011	0.005	0.007	0.005	0.002	0.004	0.005	0.004	0.007	0.005	0.008	0.004
Mg	0.924	0.901	0.893	0.930	0.884	0.908	0.919	0.883	1.642	1.585	1.631	1.649
Ni	0.006	0.007	0.005	0.005	0.003	0.007	0.007	0.003	0.003	0.003	0.003	0.003
Co	0.004	0.006	0.005	0.006	0.002	0.004	0.005	0.002	0.003	0.005	0.010	0.008
Ca	0.836	0.819	0.840	0.799	0.837	0.838	0.823	0.841	0.033	0.050	0.026	0.051
Na	0.008	0.016	0.015	0.014	0.025	0.020	0.029	0.030	-	-	-	-
Σ	4.000	4.000	4.000	4.000	4.000	4.000	4.000	4.000	4.000	4.000	4.000	4.000

End-members												
NaFe^{+3}Si$_2$O$_6$	0.9	1.6	1.5	1.4	2.5	2.0	2.9	3.0				
CaTiAl$_2$O$_6$	1.2	1.0	1.1	0.8	1.3	0.4	0.8	1.3				
CaAl$_2$SiO$_6$	0.4	1.5	2.1	1.3	0.4	0.3	0.4	0.5				
CaFeAlSi	3.7	2.7	3.6	1.8	8.6	6.7	4.7	12.0				
Ca$_2$Si$_2$O$_6$	39.3	38.5	38.6	37.9	36.6	38.3	38.2	35.1				
Mg$_2$Si$_2$O$_6$	46.3	45.2	45.2	47.0	44.4	45.8	46.5	44.4				
Fe$_2$Si$_2$O$_6$	8.2	9.6	7.9	9.8	6.2	6.5	6.5	3.7				
MgSiO$_3$	42.8	42.3	42.8	40.7	42.9	43.1	42.5	43.1	1.7	2.6	1.4	2.7
CaSiO$_3$	47.2	46.6	45.5	47.4	45.3	46.7	47.4	45.2	85.1	81.7	83.8	86.0
FeSiO$_3$	10.0	11.1	11.7	11.9	11.8	10.2	10.1	11.7	13.2	15.7	14.8	11.3
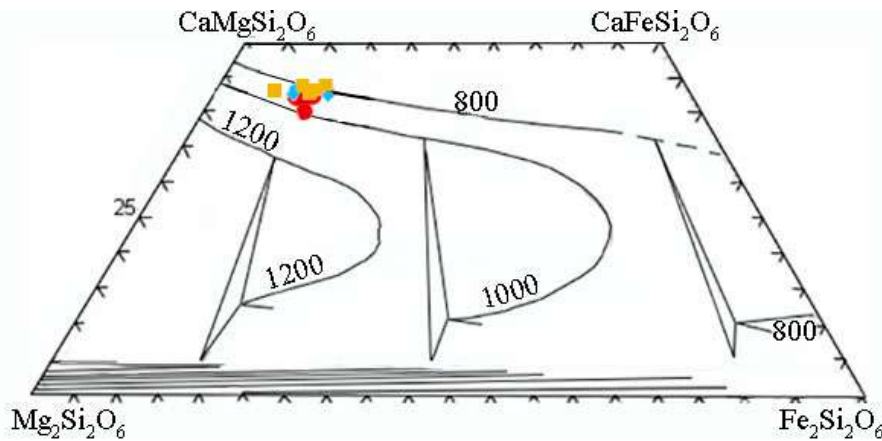
Fig. 5. Pyroxene compositions on the Di-Hd-En-Fs diagram (Lindsley, 1983; Rohrbach et al., 2005)

The concentrations of enstatite and diopside molecules are close to each other in the central part of zoned diopsides (Table 5, an. 2) (Fig. 6b). At the same time, the concentrations of chromium and aluminum oxides are relatively high here as in megacrysts.

The amount of aluminum oxide remains constant, while the amount of chromium and titanium gradually decreases from the center of the zoned crystals to the outside, i.e. under conditions of calcium dominance (CaO=23.20%) in the next zone (Table 5, an. 3) (Fig. 6b).

The clinopyroxenes in the composition of picrothechenites are prismatic, and the amount of silicon, chromium, and magnesium oxides in their composition decreases sharply. The amount of titanium and aluminum oxides increases significantly. The amount of calcium and iron oxides remains relatively constant. Essenite (CaFe^{+3}AlSiO$_6$) molecule increases in the composition of the end members.

An increase in aluminum and titanium oxides in the composition of clinopyroxenes is also observed in picrotephrites. The concentration of calcium oxide in mineral-forming clinopyroxenes is less variable.
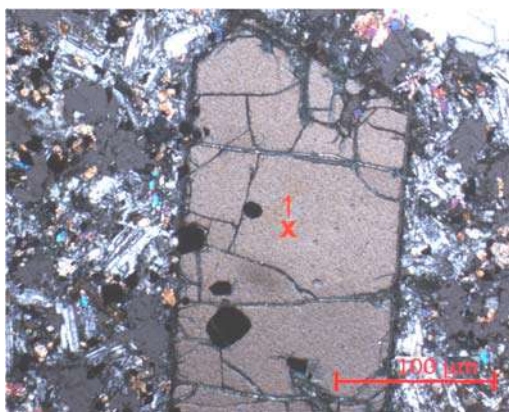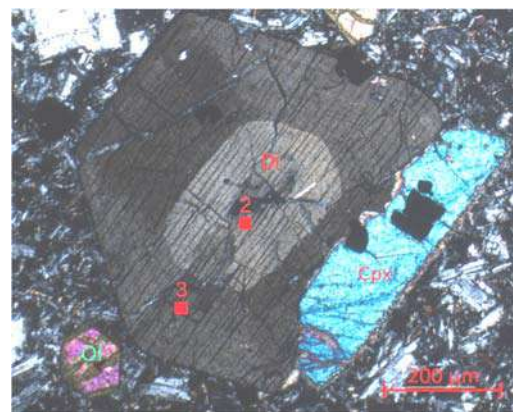
Fig. 6. a – zoned pyroxene phenocryst in picrotefrite; b – pyroxene megacrystal in picrotefrite

Table 5

Chemical, crystallochemical compositions and end-members of pyroxenes
of the Khojavand synclinorium

komp. \ an.		1	2	3	4
SiO_2		51.60	51.30	51.20	51.87
TiO_2		0.37	0.45	1.17	0.22
Al_2O_3		2.67	2.67	3.36	2.31
Cr_2O_3		1.20	1.16	0.76	0.21
Fe_2O_3		0.95	2.15	1.09	2.15
FeO		4.18	3.71	4.23	4.83
MnO		0.11	0.16	0.24	0.12
MgO		15.44	16.07	15.46	14.53
CaO		22.60	22.2	22.20	23.2
Na_2O		0.32	0.16	0.38	0.36
$\sum$		99.44	100.03	100.09	99.8
Mg#		0.83	0.83	0.77	0.76
t°C		820	840	780	820
Cations in T, M1, M2 positions					
T	Si	1.907	1.888	1.862	0.923
	Al	0.093	0.112	0.138	0.077
M_1	Al	0.027	0.006	0.009	0.024
	Fe^{+3}	0.026	0.059	0.030	0.060
	Ti	0.010	0.012	0.033	0.006
	Cr	0.035	0.034	0.022	0.006
	Mg	0.783	0.787	0.786	0.762
	Fe^{+2}	0.119	0.102	0.120	0.142
M_2	Fe^{+2}	0.010	0.012	0.011	0.008
	Mg	0.068	0.096	0.072	0.041
	Mn	0.003	0.005	0.007	0.004
	Ca	0.896	0.875	0.882	0.921
	Na	0.023	0.012	0.028	0.026
End members					
$NaFe^{+3}Si_2O_6$		2.3	1.2	2.7	2.6
$CaTiAl_2O_6$		1.0	1.2	3.3	0.6
$CaAl_2SiO_6$		2.4	0.4	0.9	2.2
$CaFeAlSiO_6$		3.9	8.2	2.5	4.1
$Ca_2Si_2O_6$		40.3	39.6	39.6	41.4
$Mg_2Si_2O_6$		38.3	39.8	38.3	36.1
$Fe_2Si_2O_6$		6.4	7.9	7.6	9.6
$CaSiO_3$		42.9	43.9	43.8	43.0
$MgSiO_3$		47.7	46.8	43.1	43.6
$FeSiO_3$		9.4	9.4	13.1	13.5

The clinopyroxenes in the Santonian picrites and picrothechenites of the Khojavand synclinorium correspond to chrome, partially aluminum diopsides. According to Lindsley paleothermometer, their crystallization temperature ranges between 780-840ºC (Table 5, Fig. 5). The chromium diopside megacryst has been formed as an accumulative inclusion. Therefore, it corresponds to the central part of the zoned crystals. At the same time, the absence of a thermal break between the zones of the zoned clinopyroxenes and the gradual alteration of clinopyroxene composition in the zones show that this process is regulated by crystallization differentiation. In this direction, crystallization temperature is also characterized by a gradual alteration.

The increase of titanium and aluminum oxides, the decrease of magnesium and chromium oxides are confirmed by the alteration of the modal mineralogical composition of the subalkaline picrites due to the partial intense fractionation in the last rim of the zoned crystals. So, chromium diopside is gradually replaced by salite, calcium augite and chrome spinel by chrome-magnetite.

Picrites belong to the subalkaline series and have a characteristic impregnation structure and their main masses are dolerite and subdolerite structured in the Talysh zone (Мамедов и др., 2017). Besides olivine, clinopyroxene phenocrysts are present in the impregnations. In most cases, those phenocrysts form large elongated, sometimes plate-like crystals. In most cases, they are colorless. However, olivine and chrome spinel inclusions of different sizes are observed in them. Relatively large prismatic phenocrysts (1.5-2.3 cm) of clinopyroxenes occur in phlogopite and olivine picrites. These phenocrysts are xenomorphic compared to olivine. According to their chemical composition (Table 6), these megacrysts are partial high-grade in magnesium, silicon and chrome oxides, and low-grade in aluminum and titanium oxides. This composition diversity is also reflected in the calculation of compositions of the end members. So, the concentration of enstatite in the composition of the abovementioned phenocrysts ranges between 42.0-46.8%. Correspondingly, titanium and calcium chermak molecules decrease significantly (Table 6, an. 1). According to Lindsley thermometer (Lindsley, 1983), the crystallization temperature of these phenocrysts ranges from 700 to 900°C (Table 6, Fig. 5).

The second group of clinopyroxene phenocrysts has a characteristic prismatic shape, and in most cases has a zoned structure.

Table 6

Chemical, crystallochemical compositions of clinopyroxenes in picrites of the Talysh zone

		1	2	3	4	5	6	7	8	9	10	11	12
	SiO_2	51.90	50.41	50.25	50.60	51.50	50.63	51.76	51.24	51.26	48.92	49.40	49.36
	TiO_2	0.16	0.53	0.73	0.41	0.41	0.58	0.43	0.66	0.75	0.64	0.61	0.53
	Al_2O_3	3.33	3.63	3.47	4.16	3.24	3.15	2.23	2.89	3.12	5.26	4.80	4.78
	Cr_2O_3	0.89	0.65	0.50	0.75	0.62	0.62	0.63	0.42	0.15	0	0	0
	Fe_2O_3	2.26	3.87	3.42	2.14	1.73	3.86	2.37	1.93	1.94	3.81	4.24	3.80
	FeO	2.17	4.03	2.69	4.73	3.12	4.47	3.59	3.05	4.46	5.69	4.52	5.38
	MnO	0.16	0.16	0.14	0.15	0.06	0.19	0.15	0.12	0.18	0.16	0.14	0.20
	MgO	16.93	15.50	15.15	15.40	16.32	15.20	15.98	15.48	15.66	13.41	13.46	13.42
	CaO	21.97	21.10	23.00	21.20	22.45	21.64	22.36	23.4	21.75	21.42	22.30	21.66
	Na_2O	0.36	0.39	0.34	0.26	0.21	0.35	0.29	0.26	0.40	0.46	0.54	0.46
	Mg#	0.87	0.79	0.82	0.80	0.86	0.77	0.83	0.85	0.82	0.72	0.74	0.73
	t°C	880	800	800	900	780	800	800	860	800	820	750	700
	∑	100.13	100.27	99.69	99.5	99.66	100.69	99.79	99.45	99.67	99.77	100.01	99.59
Cations in T, M1, M2 positions													
T	Si	1.893	1.859	1.860	1.869	1.893	1.865	1.909	1.895	1.893	1.920	1.921	1.893
	Al	0.107	0.141	0.140	0.131	0.107	0.135	0.091	0.105	0.107	0.080	0.079	0.107
M_1	Al	0.036	0.017	0.011	0.050	0.033	0.002	0.006	0.021	0.029	0.049	0.040	0.013
	Fe^{+3}	0.062	0.107	0.095	0.060	0.048	0.106	0.066	0.054	0.055	0.019	0.036	0.095
	Ti	0.004	0.015	0.020	0.011	0.011	0.016	0.012	0.018	0.021	0.012	0.016	0.012
	Cr	0.026	0.019	0.015	0.022	0.018	0.018	0.018	0.012	0.004	-	-	-
	Mg	0.809	0.730	0.778	0.731	0.804	0.736	0.797	0.806	0.770	0.699	0.688	0.717
	Fe^{+2}	0.063	0.112	0.081	0.126	0.086	0.122	0.101	0.089	0.122	0.211	0.220	0.163
M_2	Fe^{+2}	0.003	0.013	0.002	0.020	0.010	0.016	0.010	0.005	0.015	0.021	0.019	0.012
	Mg	0.111	0.121	0.057	0.116	0.089	0.099	0.081	0.045	0.091	0.072	0.059	0.052
	Mn	0.005	0.005	0.004	0.005	0.002	0.006	0.005	0.004	0.006	0.006	0.006	0.009
	Ca	0.856	0.833	0.912	0.839	0.884	0.855	0.883	0.927	0.860	0.879	0.886	0.901
	Na	0.025	0.028	0.025	0.019	0.015	0.024	0.021	0.019	0.028	0.022	0.030	0.026

End members	1	2	3	4	5	6	7	8	9	10	11	12
$NaFe^{+3}Si_2O_6$	2.5	2.8	2.4	1.9	1.5	2.5	2.1	1.9	2.9	2.2	3.0	2.6
$CaTiAl_2O_6$	0.4	1.5	2.0	1.1	1.1	1.6	1.2	1.8	2.1	1.2	1.6	1.2
$CaAl_2SiO_6$	3.4	1.6	1.0	5.0	3.3	0.2	0.6	2.0	2.7	4.7	4.0	1.3
$CaFeAlSi$	6.2	9.8	8.5	6.3	5.1	10.0	6.3	4.4	3.0	0.8	0.6	7.0
$Ca_2Si_2O_6$	39.1	37.6	41.0	37.8	40.0	38.6	39.9	41.7	38.8	38.2	39.8	38.6
$Mg_2Si_2O_6$	42.0	38.4	37.6	38.2	40.5	37.7	39.6	38.4	38.8	33.3	33.4	33.3
$Fe_2Si_2O_6$	6.1	10.7	8.2	9.5	6.5	11.3	8.0	6.7	7.7	10.5	9.1	10.2
$CaSiO_3$	43.7	43.4	44.0	42.2	46.0	44.0	45.5	43.5	44.8	42.0	46.8	45.8
$MgSiO_3$	49.9	44.3	45.8	44.7	46.4	43.0	45.2	47.8	45.0	39.0	39.3	39.4
$FeSiO_3$	7.4	12.3	10.2	11.1	7.6	13.0	9.3	8.7	10.2	19.0	13.9	14.8
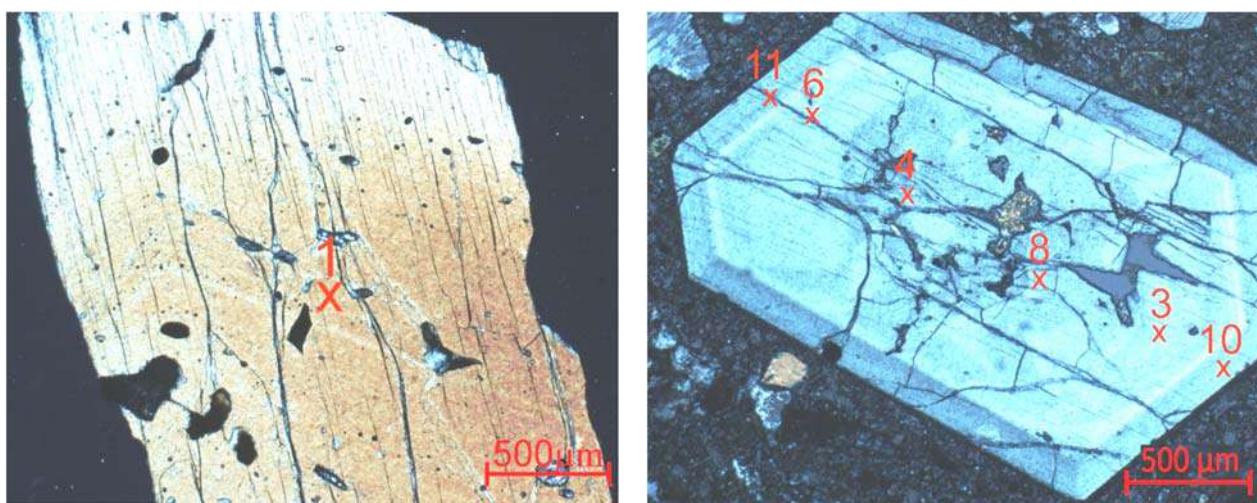
Fig. 7. a – pyroxene phenocryst in pycrite; b – zoned pyroxene phenocryst in pycrite

At the same time, the non-zoned phenocrysts are also found (Table 6, an. 1) (Fig. 7a). The compositions of the central part of the zoned prismatic clinopyroxene grains are almost completely similar to those phenocrysts. So, while the relative dominance of silicon and magnesium oxides in phenocrysts remains constant, the amount of aluminum oxide decreases. As a result of such decrease, the amount of calcium chermak molecule also decreases. The calcium chermak molecule partially increases, and the wollastonite molecule decreases in the composition of the end members (Table 6, an. 4, 8) in analysis of the central part of the zoned clinopyroxenes (Fig. 7b).

The transition of the zoned clinopyroxene grain to the next zone is gradual (Table 6, an. 6, 3) (Fig. 7b). The analysis of the composition of this zone shows that the concentrations of aluminum and iron oxides increase significantly, while the amount of silicon oxide decreases. Due to their minal composition, they correspond to diopside-salite. They are located in the area of diopside in the classification chart. Crystallization temperature ranges between 700-900°C (Table 6, Fig. 5).

The result of the analysis of the next rim of the zoned prismatic clinopyroxene shows that the concentration of iron oxide is slightly increased here. As a result, the ferrosilite molecule in the composition of this rim increases weakly, and the calcium chermak minal decreases sharply due to the decrease in the amount of silicon and calcium oxides ($CaAl_2SiO_6$=0.2%).

Finally, the amount of silicon and magnesium oxides in the last rim (Table 6, an. 10, 11 , Fig. 7b) of the zoned clinopyroxene phenocryst decreases significantly, while the amount of aluminum and iron oxides increases due to the gradual transition of the subalkaline olivine and clinopyroxene picrites to the subalkaline plagioclase picrites (Fig. 7b). Therefore, calcium chermak and ferrosilite molecules increase slightly. Calcium chermak and ferrosilite molecules gradually increase in the non-zoned clinopyroxene phenocrysts in the subalkaline picrobasalts (Table 6, an. 1) (Fig. 7a).

As it can be seen from the presented material, the alteration of the composition of clinopyroxene phenocrysts is related to the evolutionary process of the subalkaline picrite magma. So, the alteration of the composition of the subalkaline picrites is controlled by the effect of crystallization differentiation.

Results

So, summarizing the conducted research, the following results can be emphasized:

1. The layered picrites located among the Bajocian-Bathonian volcanites on the northeastern slope of the Murovdag anticlinorium are petrographically and petrochemically homogeneous. These signs of homogeneity are explained by the fact that the compositions of monoclinic and rhombic pyroxenes are similar. At the same time, the similarity of their crystallization temperature allows confirming this point of view. Besides, the partial lack of aluminum oxide in their composition caused the absence of the calcium chermak ($CaAl_2SiO_6$) molecule in the composition of clinopyroxene impregnation.

2. Clinopyroxene megacrysts in the Khojavend flexure contain chrome diopside with partial low-grade titanium oxide as phenocrysts in the subalkaline picrites. In this sense, the central part of the zoned phenocrysts is almost similar with megacrysts in terms of composition. The absence of discreteness and gradual transitions between the zones, as well as the decrease of chromium, magnesium oxides and the increase of aluminum and titanium oxides from the center to the outside can be considered a sign of the regulation of the evolution process of the subalkaline picrite magma by crystallization differentiation.

3. Alteration of primary subalkaline picrite fusion of the subalkaline picrites of the Talysh zone in intermediate magmatic focus was probably regulated by crystallization differentiation. So, forsterite-bearing olivine, magnesium-chrome chrome spinel, phlogopite and chrome diopside crystallized and accumulated in the lower part of the intermediate magmatic focus at the early stage of the crystallization process. The partial alteration in the effects of volatile components in the course of this process led to the formation of zoned phenocrysts and the variations in the components in their composition. The gradual variation shows that the leading factor controlling the process is crystallization differentiation. The decisiveness of this factor is explained by the alteration of the composition of clinopyroxene phenocrysts according to the general evolution of the subalkaline picrite magma.

REFERENCES

Azizbekov Sh.A., Bagirov A.E., Veliyev M.M., Ismail-Zade A.D., Nizheradzhe N.S., Emelyanova E.N., Mamedov M.N. et al. Geology and volcanism of Talysh. Nauka. Moscow, 1979, 241 p. (in Russian).

Dobretsov N.L., Kochkin Yu.N., Krivenko A.P., Kutolin V.A. Rock-forming pyroxenes. Nauka. Moscow, 1971, 455 p. (in Russian).

Mamedov M.N. Evolution of alkaline basic magmatism in the structures of the Talysh block (southeastern Azerbaijan). In: Evolution of magmatism of the main structures of the Earth, Moscow, 1983, p. 41 (in Russian).

Mamedov M.N., Babayeva G.J., Sadygov N.M. Clinopyroxenes of trachybasalt-trahydoleryte and tephrite-teschenite complexes of the Khojavend trough. Otechestvennaya geologiya, No. 6, 2012, pp. 48-55 (in Russian).

Mammedov M.N., Babayeva G.J., Kerimov V.M. Clinopyroxenes in formation process of sub-alkalic olivine-basalt magma of the Talysh zone of Caucasus. Uralian Geological Journal, No. 5, 2017, pp. 39-53 (in Russian).

Rustamov M.I. Geodinamics and magmatism of the Caspian-Caucasus segment of the Mediterranean belt of the Phanerozoic. Nafta-Press. Baku, 2019, 543 p. (in Russian).

Shikhalibeyli E.Sh. Geology and minerals of Nagorno-Karabakh of Azerbaijan. Baku, 1994, 284 p. (in Russian).

Kushiro I. Clinopyroxene solid solutions. Part I. The $CaAl_2SiO_2$ component. Jap. J. Geol. Geogr., No. 33, 1962, pp. 213-220.

Le Bas M.J., Le Mitre R.W., Streckeisen A., Zanettin B. A chemical classification of volcanic rocks based on the total alkali-silica (TAS) diagram. J. Petrol., Vol. 27, 1986, pp. 745-750, http://doi.org/10.1093/petrology/27.3.745/.

Lindsley D.H. Pyroxene thermometry. American Mineralogist, Vol. 68(5-6), 1983, pp. 477-493.

Morimoto N. Nomenclature of pyroxenes. Mineralogy and Petrology, Vol. 39, 1988, pp. 55-76, http://dx.doi.org/10.1007/BF01226262.

Rohrbach A., Schuth S., Ballhaus C., Miinker C., Matveev S., Qopoto C. Petrological constraints on the origin of arc picrites, New Georgia Group, Solomon Islands. Contrib Mineral Petrol, No. 149, No. 6, 2005, pp. 685-698, http://doi.org/10.1007/S00410-0675-6.

ЛИТЕРАТУРА

Азибеков Ш.А., Багиров А.Э., Велиев М.М., Исмаил-Заде А.Д., Нижерадже Н.Ш., Емельянова Е.Н., Мамедов М.Н. Геология и вулканизм Талыша. Элм. Баку, 1979, 241 с.

Добрецов Н.Л., Кочкин Ю.Н., Кривенко А.П., Кутолин В.А. Породообразующие пироксены. Наука. Москва, 1971, 455 с.

Мамедов М.Н. Эволюция щелочного основного магматизма в структурах Талышского блока (юго-восточный Азербайджан). В сб.: Эволюция магматизма в главнейших структурах Земли, Наука. Москва, 1983, с.41-44.

Мамедов М.Н., Бабаева Г.Д., Садыгов Н.М. Клинопироксены трахибазальт-трахидолеритового и тефрит-тешенитового комплексов Ходжавендского прогиба. Отечественная геология, No. 6, 2012, с. 48-55.

Мамедов М.Н., Бабаева Г.Д., Керимов В.М. Клинопироксены в процессе формирования субщелочной оливин-базальтовой магмы Талышской зоны Кавказа. Уральский геологический журнал, No. 5, 2017, с. 39-53.

Рустамов М.И. Геодинамика и магматизм Каспийско-Кавказского сегмента Средиземноморского пояса в фанерозое. Nafta-Press. Баку, 2019, 543 с.

Шихалибейли Э.Ш. Геология и полезные ископаемые Нагорного Карабаха Азербайджана. Элм. Баку, 1994, 284 с.

Kushiro I. Clinopyroxene solid solutions. Part I. The $CaAl_2SiO_2$ component. Jap. J. Geol. Geogr., Vol. 33, 1962, pp. 213-220.

Le Bas M.J., Le Mitre R.W., Streckeisen A., Zanettin B. A chemical classification of volcanic rocks based on the total alkali-silica (TAS) diagram. J. Petrol., Vol. 27, 1986, pp. 745-750, http://doi.org/10.1093/petrology/27.3.745/.

Lindsley D.H. Pyroxene thermometry. American Mineralogist, Vol. 68(5-6), 1983, pp. 477-493.

Morimoto N. Nomenclature of pyroxenes. Mineralogy and Petrology, Vol. 39, 1988, pp. 55-76, http://dx.doi.org/10.1007/BF01226262.

Rohrbach A., Schuth S., Ballhaus C., Miinker C., Matveev S., Qopoto C. Petrological constraints on the origin of arc picrites, New Georgia Group, Solomon Islands. Contrib Mineral Petrol, Vol. 149, No. 6, 2005, pp. 685-698, http://doi.org/10.1007/S00410-0675-6.

ПЕТРОГЕНЕТИЧЕСКАЯ РОЛЬ ПИРОКСЕНОВ В ФОРМИРОВАНИИ ПИКРИТОВ МАЛОГО КАВКАЗА И ТАЛЫША

Мамедов М.Н., Бабаева Г.Дж., Сариев Ф.Х.

Министерство науки и образования Азербайджанской Республики, Институт геологии и геофизики, Азербайджан
AZ1143, Баку, просп. Г.Джавида, 119: gultekin_babayeva@rambler.ru

Резюме. На основе микрозондового, химического и рентгенодифрактометрического анализов изучены петрогенетические особенности формирования пикритов в зависимости от изменчивости составов клинопироксенов Малого Кавказа и Талышской зоны. Верхнеюрские пикриты Муровдагского антиклинория формировались в сходных геолого-геодинамических условиях, но подчинялись рифтогенному строению трещин. Пироксены этих эволюционировавшихся пикритов близки по минералогическому составу, температурам кристаллизации и «минальному» составу. Мегакристаллы клинопироксена в субщелочных пикритах Ходжавендского прогиба соответствуют хромистому диопсиду, частично обедненному оксидом титана. Клинопироксены участвуют в виде вкрапленников, нормально-призматических и мегакристов (0.5x2.5 см) в составе сантонских трахибазальт-трахидолеритового, тефрит-тешенитового комплексов Ходжавендского прогиба. Мегакристаллы клинопироксена темно-черного цвета наблюдаются неравномерно в серых тефритсодержащих брекчиях. Зона контакта заметна в материнской породе. В Талышской зоне пикриты относятся к субщелочной серии и имеют характерное глинистое строение, а их основная масса представлена долеритом и субдолеритом. Наряду с оливином в составе пикритов присутствуют вкрапленники клинопироксена. Эти фенокристаллы в большинстве случаев образуют крупные удлиненные, иногда пластинчатые кристаллы. В большинстве случаев они бесцветны. Однако в них наблюдаются включения оливина и хромшпинелида разного размера. Довольно крупные призматические вкрапленники клинопироксенов (1.5-2.3 см) присутствуют во флогопитовых и оливиновых пикритах. Эти фенокристаллы ксеноморфны оливину. Состав клинопироксенов в пикритах Талышской зоны соответствует диопсид-салиту. Таким образом, изменение состава пикроксенов в пикритах Малого Кавказа и Талышской зоны регулируется кристаллизационной дифференциацией.

Ключевые слова: Малый Кавказ, Талышская зона, пикрит, зональный пироксен, кристаллизационная дифференциация

KİÇİK QAFQAZIN VƏ TALIŞ ZONASININ PİKRİTLƏRİNİN FORMALAŞMASINDA PİROKSENLƏRİN PETROGENETİK ROLU

Məmmədov M.N., Babayeva G.C., Sarıyev F.H.

Azərbaycan Respublikası Elm və Təhsil Nazirliyi, Geologiya və Geofizika İnstitutu, Azərbaycan
AZ1143, Bakı, H. Cavid pr., 119: gultekin56@rambler.ru

Xülasə. Mikrozond, kimyəvi və rentgen-difraktometrik analizlərlə Kiçik Qafqazın və Talış zonasında klinopiroksenlərin tərkib dəyişkənliyi əsasında pikritlərinin əmələgəlməsinin petrogenetik xüsusiyyətləri öyrənilmişdir. Murovdağ antiklinorisinin üst yura yaşlı pikritləri rift təbiətli qırılma strukturu ilə nəzarətlənməklə bərabər, oxşar geoloji-geodinamik şəraitdə formalaşmışdır. Buna görə də, antiklinorinin tərkiblərində iştirak edən petroqrafik tip süxurlar bircinslidirlər. Bu təkamülə uğramış pikritlərin piroksenləri mineraloji cəhətdən, kristallaşma temperaturlarına və "minal" tərkiblərinə görə çox yaxındır. Xocavənd əyilməsində subqələvi pikritlərdə klinopiroksen meqakristalları titan oksidi ilə qismən kasıblaşmış xrom diopsidə uyğundur. Klinopiroksenlər Xocavənd sinklinorisinin santon yaşlı traxibazalt-traxidolerit, tefrit-teşenit komplekslərinin tərkibində fenokristal, normal prizmatik və meqakristal qismində iştirak edirlər (0,5x2,5 sm). Klinopiroksen meqakristalları tünd qara rəngli olub, boz rəngli tefrit tərkibli brekçiyaların içərisində qeyri-düzgün formada müşahidə olunur. Onun ana süxurunda təmas zonası nəzərə çarpır. Talış zonasında da pikritlər subqələvi seriyaya aid, xarakterik möhtəvi strukturlu olub, onların əsas kütləri isə dolerit və subdolerit quruluşludur. Möhtəvilərin içərisində olivinlə yanaşı klinopiroksen fenokristalları iştirak edir. Həmin fenokristallar əksər hallarda iri uzunsov, bəzən lövhəvari kristallar əmələ gətirirlər. Əksər hallarda rəngsiz olurlar. Lakin onların içərisində müxtəlif ölçülü olivin və xromşpinel daxilolmaları müşahidə olunur. Klinopiroksenlərin kifayət qədər iri ölçülü prizmatik fenokristalları (1,5-2,3 sm) floqopitli, olivinli pikritlərin tərkiblərində iştirak edirlər. Bu fenokristallar olivinə nisbətən ksenomorfdur. Talış zonasınının pikritlərində isə klinopiroksenlərin tərkibi diopsid-salitə uyğun gəlir. Beləliklə, Kiçik Qafqaz və Talış zonasının pikritlərində pikroksenlərin tərkibinin dəyişməsi kristallaşma diferensiasiyası ilə tənzimlənir.

Açar sözlər: Kiçik Qafqaz, Talış zonası, pikrit, zonal piroksen, kristallaşma diferensiasiyası

GOLD-BEARING VOLCANOGENIC FIELDS OF NON-FERROUS METALS OF THE LESSER CAUCASUS AND THE EASTERN PONTIDES AND THEIR GENESIS

Babazadeh V.M.[1], Abdullayeva Sh.F.[1], Novruzova S.R.[1], Ibrahimov J.R.[2]

[1]Baku State University, Azerbaijan

33, acad. Zahid Khalilov Str., Baku, AZ1148: vasifbabazadeh1938@bsu.edu.az;
shakhla.a@gmail.com; samiranovruzova001@gmail.com;

[2]Azerbaijan International Mining Company Limited

2, Izmir Str., Baku, AZ1065: Javid.Ibrahimov@aimc.az

Keywords: *field, ore region, paleo-arc, inclusion, fluid, isotope*

Summary. In the countries of the South Caucasus and Türkiye, the most representative gold-bearing volcanogenic fields are known in the strata composing fragments of the Pontic-South Caucasian paleoarc, which was active during the Mesozoic Era. At that time, the oceanic crust was subducted under the arc, which was the marginal part of the Eurasian continent. Separate segments of the arc differed in their geodynamic development, due to which different types of volcanogenic fields occurred in them. Besides epigenetic deposits, hydrothermal-sedimentary deposits are also known within the Pontides (Türkiye) in the west.

The paper deals with the geological environments of deposits' occurrence in Türkiye, Azerbaijan, Armenia and Georgia. Most of them can be attributed to the Kuroko type and differ in the nature of ore accumulation: copper-zinc deposits, which were apparently formed in the conditions of a deep-sea basin, are known in Türkiye, and we have examples of only epigenetic fields to the east. The Gadabay and Alaverdi ore regions are interesting in that copper, copper-zinc and barite-sulfide ores are concentrated in the Jurassic volcanic depressions, and porphyry copper fields – Garadag and Tutkhun are known in the raised wedge-shaped blocks that limit the volcanic depressions. A mental logical geological and genetic model of volcanogenic fields was created based on the literary material, which has been collected for years, as well as our own data.

Fields of volcanogenic nature, despite the fact that they are formed in similar PTX conditions, have their own "appearance", taking into account which is extremely important when predicting fields in specific areas.

Introduction

The Caucasian folded mountain structure is perceived as the result of interaction of microcontinents – "fragments" of the Afro-Arabian and Eurasian lithosphere plates. As a rule, the marginal parts of microcontinents are composed of sediments of either marginal marine or oceanic origin that obducted on them (Fig. 1). According to the composition of the lithogeodynamic complexes, the southern margin of the European continent was occupied by an oceanic basin (Paleotethys) at the beginning of the Hercynian cycle, covering the time from the Silurian to the Early Triassic inclusive, as evidenced by the North Caucasian ophiolitic allochthons, Silurian-Devonian deepwater carbonaceous siliceous-argillaceous strata, as well as volcanites of the Front Range zone of the Greater Caucasus, which most likely belong to the formations of the ensimatic arc (fragments of which are exposed in the modern zone of the Main Range of the Greater Caucasus) based on the predominance of basites in them. There was obviously an ensialic arc to the south of the latter, on the slopes of which flyschoids accumulated during the Devonian-Carboniferous, and its root underwent metamorphism and granitization. It is assumed that part of Gondwana (in Fig. 1 – Taurides and Daralagoz block) was "soldered" to Eurasia at the end of the Triassic, and later – at the beginning of the Jurassic – torn away due to the laying of the Lesser Caucasus branch of the Neotethys. The diagram (see Fig. 1) shows that the central part of the Alpine-Himalayan mountain-fold belt consists of microplates: 1) Scythian and South Caucasian-Pontic (active paleo-margin of the Eurasian continent); 2) Kirshehir, Taurus and Daralagoz blocks (previously part of Gondwana). The continental blocks are separated by su-

ture zones (sutures), most of which are marked by ultramafic "mélange". Passive continental blocks of Gondwana appear to researchers (Vrielinck, 1994) drifted on oceanic lithospheric plates.

It follows from numerous publications (Адамия и др., 1977; Шихалибейли, 1996; Okay, Sahinturk, 1997; Sosson et al., 2010; Vrielinck, 1994; Yilmaz et.al., 1997) that the most important tectonic events that predetermined the geological appearance of the Alpides include: 1) the abruption of the Iranian plate in the Permian-Triassic from the edge of Gondwana and its joining to the active Eurasian margin; 2) opening of the Neotethys at the Late Triassic-Early Jurassic, possibly its two branches (Biju-Duval et.al., 1997) in connection with the laying of rift systems; obduction of oceanic complexes in the Senonian, as A. Knipper (Монин, Зоненшайн, 1987) put it figuratively, denoting the "death" of the ocean. Due to the abovementioned events, the main milestones of the historical and geological development in the Alpine cycle were also emphasized: the divergence of microplates (Triassic-Early Bajocian), accompanied by the formation of the Neotethys branches and the activa-

tion of mantle diapirism at the beginning; then their convergence (Late Bajocian-Early Cretaceous) with characteristic island-arc andesitoid volcanism on the edge and rift-related volcanism in the central part of the South Caucasus-Pontic microplate. Moreover, the maximum activation of island-arc volcanism in Transcaucasia falls on the Bajocian-Late Jurassic, and in the Pontides – on the Turonian-Santonian. Based on comparative structural-facies analysis, A. Yilmaz et al. (Yilmaz et.al, 2000) showed the difference in the geodynamic development of individual segments of the South Caucasus-Pontic system. The beginning of the collision (or the beginning of the collision of continental protrusions of microplates) in the western and eastern parts of the region was diachronous: if the "contact" of the South Caucasian and Daralagoz blocks occurred in the Coniacian (Монин, Зоненшайн, 1987), then the Pontides with the Taurida occurred in the Campanian (Dixon, Periere, 1974). Volcanic activity was occurred in the residual back-arc sea basins at the collision stage (Late Cretaceous-Eocene), and later in the depressions (Eocene volcanites) formed on the previously formed tectonic structures.
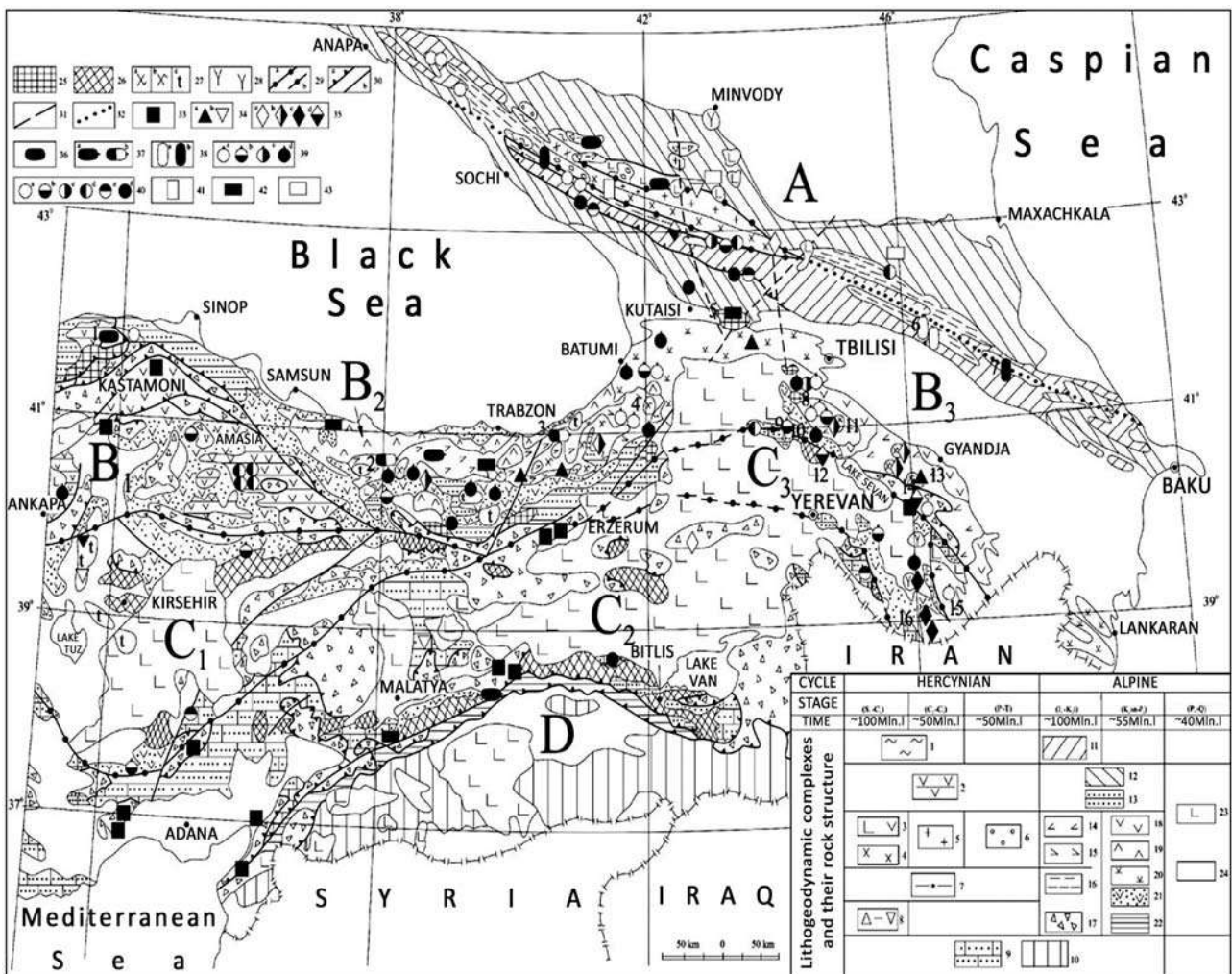
Fig. 1. The allocation pattern of lithogeodynamic complexes and the main types of metal fields of the central part (Pontides, Taurides, Greater and Lesser Caucasus) of the Alpine-Himalayan mountain-folded belt

Hercynian lithogeodynamic complexes: *active margin of the East European paleocontinent*: 1 - continental shelf zones and slopes (andesite-basalts, carbonaceous shales, limestones, Devon-Carbon, greenstone alterations, Greater Caucasus); 2 - continental shelf zones (sandstones, conglomerates, carbonaceous shales, andesite-basalts, Carboniferous-Triassic, greenstone alterations, Pontides); 3 - ensimatic island arc (basalts, rhyolites, siliceous shales, carbonate-rich sandstones, Devonian-Early Carboniferous, Greater Caucasus); 4 - ensialic island arc (gabbros, sodium granitoids, parametamorphites and crystalline schists, Pre-cambrian (?) – Early Paleozoic, Greater Caucasus); 5 - activated blocks of the ensialic arc (collisional potassium-sodium granitoids, staurolite and biotite-muscovite schists, late Paleozoic, Greater Caucasus); 6 - continental depressions (clay shales, sandstones, andesite-basalts, rhyolites, Permian-Triassic, Greater Caucasus); 7 - paleomarginal sea - slope and plain of the continent (carbonaceous shales, sandstones, andesite-basalts, olistostromes, limestones, Devonian-Triassic, greenstone alteration, southern slope of the Greater Caucasus); 8 - ocean floor (carbonate and siliceous shales, basalts, peridotites, dunites, rhyolites – in allochthonous occurrence, Greater Caucasus); *passive margin of Gondwana, and in the Mesozoic Afro-Arabian, paleocontinent*: 9 - shelf zones (clays, carbonate clays and sandstones, limestones, locally andesite-basalts, tuffites, Paleozoic-Cretaceous, Kirshehir, Taurus and Daralagoz blocks); 10 - shelf and continental zones of the Arabian uplift (sandstones, clays, limestones, conglomerates, Paleozoic-Eocene).

Alpine lithogeodynamic: active margin of the Eurasian paleocontinent: 11 - slopes and plain of the South Caucasian microcontinent (andesite-basalts, trachyandesites, terrigenous-carbonate flysch, carbonaceous clay shales, granodiorites, Jurassic-Early Cretaceous, southern slope of the Greater Caucasus); 12 - shelf zones of the Scythian and South Caucasian microcontinents (andesites, andesite-basalts, clay shales, sandstones, mottled clays with sulfates, limestones and dolomites, marls, tuffites, Jurassic-Paleogene, Greater Caucasus); 13 - shelf zones and slope of the Pontian microcontinent (andesite-basalts, sandstones, limestones, shales, Early Jurassic; conglomerates, limestones, basalts, coral rag, marls, Late Jurassic-Cretaceous; terrigenous-carbonate flysch, Late Cretaceous, Pontides); 14 - Lesser Caucasus ensimatic island arc (andesite-basalts, rhyodacites, tuffites, sandstones, clay shales, tonalites, diorites, Bajocian-Early Cretaceous, southern edge of the Transcaucasian microcontinent); 15 - Pontian ensimatic island arc (andesite-basalts, rhyodacites, marls, sandstones, clay shales, Late Creta-

ceous (Turonian-Santonian), Eastern Pontides); 16 - basins of the marginal paleosea (clay shales, basalts, rhyolites, gabbro-diabases, Early Jurassic, Greater Caucasus); 17 - oceanic zones in allochthonous bedding (in the composition of sutures and obducted thrust plate – ultramafic "mélange", harzburgites, serpentinites, gabbros, tholeitic and alkaline basalts, terrigenous-carbonate flysch with horizons of ophioclastic olistostromes, radiolarites; Pontides, Taurides and Lesser Caucasus); 18 - Lesser Caucasus residual back-arc volcanic depressions (andesites, rhyodacitic ignimbrites, rhyolites, trachyrhyolites, limestones, basalts, granodiorites, Senonian-Danian); 19 - Pontic residual back-arc volcanic depressions (basalts, rhyodacites, trachyrhyolites, coral rags, Campanian-Danian); 20 - intraplate rift-related volcanic depressions (trachyandesites, trachybasalts, volcanogenic-terrigenous flysch with olistostrome horizons, gabbro-diorites, monzonites, syenites, alkaline gabbroids and syenites, Eocene, Lesser Caucasus and Pontides); 21 - superimposed, mainly on pre-collision structures, marine volcanic depressions (andesites, trachyandesites, terrigenous-carbonate flysch, sandstones, clays, Eocene; Pontides, Taurida and Lesser Caucasus); 22 - flysch troughs (southern side of Taurus), formed at the beginning of the collision of the Taurus microcontinent with the Eurasian continent (sandstones, marls, clays, fragments of ultramafic, Senonian-Paleogene); 23 - activated blocks of folded mountain structures (andesites, andesite basalts, their pyroclastolites, Neogene-Quaternary); 24 - intermountain and foredeeps of folded mountain structures (marine and continental molasses, Oligocene-Quaternary); 25 - Crystalline basement of the Eurasian continent (Precambrian-Early Paleozoic); 26 - Crystalline basement of the Afro-Arabian continent (Precambrian); 27 - Granitoids (pre-collision: a- Early Cretaceous, b- Late Cretaceous; c- collision Eocene-Oligocene); 28 - Post-collision monzonites, syenites, granodiorites; 29 - Sutures (a- known, b- inferred under recent deposits); 30 - Ruptured zone (a-thrust and reverse-thrust faults, b-near-vertical faults); 31 - Caucasian lineaments based on the results of interpretation of space images; 32 - supposed boundary between the Scythian and Transcaucasian microplates.

Genetic types of fields: 33 - magmatic (chrome raw materials); 34 - skarn (a- iron ore, b- tungsten-molybdenum); 35 - hydrothermal plutonogenic (a- polymetallic, b- copper-porphyry, c- copper-molybdenum-porphyry, d- gold ore); 36 - hydrothermal-sedimentary in volcanic strata (copper with zinc); 37 - combined hydrothermal-sedimentary and epigenetic (stockwork) in volcanic strata (a-copper, b-copper-zinc); 38 - hydrothermal-sedimentary in clayey-shale strata (a- polymetallic, b- copper); 39 -

hydrothermal epigenetic in volcanic strata (a- copper; b- polymetallic with baryte; c- polyformational: copper, baryte, baryte-polymetallic, gold ore in secondary quartzites; d- properly gold ore); 40 - amagmatogenic ("telethermal") (a- mercury, b- arsenic (realgar-orpiment), c- arsenic (arsenopyrite with gold), d- gold with antimony, e- lead-zinc in carbonate strata, f-baryte); 41 - hydrothermal-metamorphogenic (tungsten); 42 - sedimentary and volcanogenic-sedimentary (manganese); 43 - sedimentary (celestine).

Significant fields of the Eurasian active paleoomargin: 1 - Ashikei (Cu), 2 - Lahanos (Cu, Zn, Pb), 3- Chayeli-Madenkoy (Cu, Zn), 4 - Murgul (Cu, Zn), 5 - Chiatura (Mn), 6 - Filizchai (Zn, Pb, Cu), 7 - Gizil-Dere (Cu), 8 - Madneuli (Cu, Zn, Pb, Au, BaSO₄), 9 - Alaverdi (Cu), 10 - Shamlug (Cu), 11 - Tekhut (Cu), 12 - Meghradzor (Au), 13 - Dashkesan (Fe,Co), 14 - Chovdar BaSO₄, 15 - Chovdar (Au), 16 - Zod (Au), 17 - Kafan (Cu), 18 - Kajaran (Mo, Cu).

Microplates: Eurasian paleocontinent: A - Scythian, B - Pontic-South Caucasian (B₁- Western Pontides, B₂ - Eastern Pontides, B₃ - South Caucasus); Afro-Arabian paleocontinent: C₁ - Kirshehir, C₂ - Taurus, C₃ - Daralagoz (North Iranian). Microplates are separated by sutures. D - Arabian ledge (its boundary with the Taurus is emphasized by a system of reverse-thrust faults).

The Caucasus is a relatively well-studied region and therefore it can be stated that its ore potential is determined by: plutonogenic hydrothermal (copper, molybdenum, gold), volcanogenic hydrothermal-sedimentary (copper, zinc, lead), volcanogenic epigenetic (copper, zinc, gold, barium), skarn (tungsten, molybdenum, iron) and sedimentary (manganese, strontium) fields. Besides that, "amagmatic" mercury, arsenic, antimony and lead-zinc (in carbonate strata), magmatogenic (chromium, titanium), pegmatoid (tin), greisen (niobium, tantalum) fields and ore occurrences are known here. Epigenetic gold-bearing volcanogenic fields of copper and baryte-polymetallic (Gadabay, Bitti-Bulag, Novo-Gorelovka, Gulyatag, Janyataq, Kapaz, Alaverdi, Shamlug, Kafan, Akhtala) first (Jurassic) occurred during the convergence of microplates in the folded mountain structure of the Lesser Caucasus, and copper-porphyry fields of the Garadag, Damirli, Tekhut types in the Early Cretaceous (Абдуллаева, 2013, 2018; Баба-заде др., 2003, 2012). All of them were observed in Azerbaijan and Armenia. Epigenetic copper, gold, baryte-polymetallic fields such as Bolnisi (Georgia), Dagkesaman (Azerbaijan), etc. were formed in the back-arc volcano-depressions at the early stage of the activated collision. In the west,

in the Eastern Pontides in the Late Cretaceous, volcanogenic-sedimentary copper-zinc ores (Chayeli and others, Türkiye) accumulated in intra-arc sea basins, and large-scale Murgul and other epigenetic ores fields were formed.

The fields show clear connections with certain volcanites and lithogeodynamic complexes of paleo-island-arc structures.

It is well known that ore fields are located in the upper, 10-kilometer "edge" of the Earth's crust. The topmost position is occupied by volcanogenic fields of non-ferrous and precious metals (0 - 1 km). They will be discussed in this article. The geological positions of the fields of the Eastern Pontides (Türkiye), Bolnisi (Georgia), Gadabay (Azerbaijan) and Alaverdi ore regions, as well as the copper-porphyry fields of Garadag and Tekhut, located in raised blocks near the Gadabay and Alaverdi (Armenia) gold-copper pyrite volcanogenic fields will be given as examples.

Eastern Pontides (Türkiye) and their ore-bearing

It has been found that volcano-plutonic activity led to the formation of significant accumulations of gold-bearing volcanogenic and plutonogenic ores of non-ferrous metals in the Eastern Pontides (Türkiye), which developed in the Alpine period as an island paleoarc. Moreover, volcanogenic fields were formed in volcano-depressions, which were parts of intra-arc sea basins in the Cenomanian-Campanian, and plutonogenic copper- and molybdenum-porphyry fields were formed due to the formation of granitoids in blocks raised relative to the depressions. Commercial fields are Ashikoy, Lahanos, Kutlular, Chayeli, Murgul, Cherratepe and Guzeyyayla (Cu, Mo). It should be emphasized that the Eastern Pontides are the only region of the Pontic-South Caucasian island paleoarc where hydrothermal-sedimentary accumulations of non-ferrous metal ores have been observed. Examples of these are the Chayeli (Madenkoy) and Ashikoy fields. The Chayeli field, which geologists call the pearl of the Pontides, contains significant reserves of non-ferrous metals. The massive sulphide ores (VMS) form a deposit with 920 m long (along the strike) here; it is traced to a depth of 650 m; its maximum thickness is 100 m. The deposit is covered by thin (up to 2 m) jasperlike quartzites as in the field of Kuroko type in Japan. This layer is covered by a series of interbedded tuffites and basalt covers, above which lie green tuffs with dolomite interlayers containing foraminifera fragments. According to Turkish geologists, the deposit is divided into two parts by a syn-ore fault. In connection with it, the body consists of two mutually overlapping "lenses". Sulfides are represented

by pyrite, chalcopyrite, sphalerite and in small quantities galena, bornite, tetrahedrite. Yellow (rich in chalcopyrite) and black (rich in sphalerite) ores are distinguished inside the body, as in the fields of Kuroko type. The sphalerite content exceeds 10% in the matrix of brecciated black ores. Veinlet-impregnated mineralization occurs in dacites under the massive ore deposit. The hydrothermal-sedimentary structure, which was preserved in the Late Cretaceous volcanites as an ore deposit, was subjected to repeated brecciation under the influence of explosive phenomena during the functioning the hydrosystem. Clastic ores are predominantly located in the upper parts of the deposit. Massive yellow ores and their powdery varieties form the lower parts of the body and are characteristic of the most powerful parts of the deposit. Massive ores superpose on hyaloclastites, which consist mainly of oriented felsite "fragments". The abovementioned rocks are overlain by a quartz-pyrite-chalcopyrite stockwork.

Another type of hydrothermal-sedimentary mineralization was found in the allochthon, apparently displaced to the paleoisland structure from the marginal sea basin of the Paleotethys. The rocks that form the allochthon are known in the literature as the "Cure complex": their age is Triassic, they consist of ultramafic tectonic plates, alternating clay shales and basalt covers, represented by island-arc and oceanic tholeiites, as well as rocks of the depleted mantle. According to Ustaomer (Ustaomer, Roberston, 1993), a geological picture similar to the Cyprus one is observed in places where ore mineralization occurs: serpentized peridotites are known in the lower part of the section, above which gabbro, a shale dolerite complex and greenstone-altered pillow lavas of basalts are occurred. The lavas that enclose the dolerite dykes are covered by clay shales. Copper-bearing massive sulphide deposits are located under the latter, on pillow lavas. One should agree with M. Guner, who attributed sulphur pyrite deposits refined with copper to the Cyprus VMS type.

Epigenetic sphalerite-chalcopyrite mineralization is observed at other exploited fields of the Pontides.

The Turkish and Western European geologists' works deal with the composition and structure of volcanic strata hosting non-ferrous metal fields in the Eastern Pontides (Altun, 1977; Akchay, Arar, 1999; etc.). The base for the Late Cretaceous rocks-carriers of the fields are andesitic volcanites and Lower-Middle Jurassic terrigenous rocks (Popović, 2004), as well as the Upper Jurassic-Cretaceous complex with minor copper and gold occurrences.

According to Akchay (Akchay, Arar, 1999), bimodal volcanites, in which VMS are located, are associated with large calderas and siliceous domes.

VMS were also known at the Murgul, Jerattepe, Kutluler, Kotarakdere, Hrzit and Lahanos fields. It follows from the archive and published materials that the massive non-ferrous metal ores of the Pontides were formed on the seabed of deep-sea basins, and before the diagenetic transformation of the sediments, the ore deposits were "ore hills". The sea basins were probably intra-arc, and their bottoms underwent rifting in the Late Cretaceous, as evidenced by the composition of the volcanites, as well as basalt dikes that intersect both the ore deposit and the upper basalts and purple tuffs. The rocks overlying the Chayeli ore deposit alter little, except for diagenetic alterations. Senonian fauna was found in the pink limestones of the upper series.

Massive ores are gold-bearing: gold is found in sphalerite in the form of inclusions with size of 200 μ. Researchers see vertical, poorly expressed zoning (from top to bottom) in the ore deposit: sphalerite-galena-baryte-chalcopyrite; pyrite-chalcopyrite-clay; pyrite-chalcopyrite-quartz.

It was found that the basalts of the ophiolite complex belong to the formations of spreading zones according to their chemical characteristics in the Kure region, at the Ashikoy-Taikopdu field (Chakir, 1995). It is assumed that the spreading zone was located in a back-arc basin in the Early Jurassic.

Examples of stockwork-vein fields, very similar to the Madneuli copper ores (Georgia), are in the Pontides – Lahanos and Murgul, associated with late Cretaceous volcanites. Hydrothermal-sedimentary deposits with "black" and "yellow" ores are known near Murgul, in the Gizilgaya area (Lethch, 1981), which were characterized by colloform banded and framboidal textures. The ore-bearing rocks with angular unconformity are overlain by andesite-dacite lavas here.

In conclusion, we state that gold occurrences are also known in the Eastern Pontides, for example, Behkesik (Yigit et al., 2000) and Maradit (Popović, 2004) in Late Cretaceous volcanites, as well as in Eocene quartz diorites. The commercial value of gold occurrences has yet to be determined.

Bolnisi ore region (Georgia) and its ore-bearing

The Cretaceous volcano-tectonic depression of the Bolnisi ore region was laid in the back-arc residual sea basin at the end of convergence, and was finally formed at the beginning of the collision of the South Caucasian and Iranian lithospheric microplates. The depression is filled with Albian-Campanian volcanogenic-terrigenous deposits, within which three complexes are distinguished (Назаров, 1966; Кекелия и др., 1993; Гугушвили и др., 2002, 2018; Баба-заде и др., 2015).

In the opinion of the authors (Назаров, 1966), copper, baryte-polymetallic and gold (in secondary quartzites) mineralizations of different ages are combined at the largest Madneuli field, where initially only baryte and later copper and gold ores were mined: at the small Tsitelisopelskoye - copper and gold, at Sakdriskoye – gold and baryte-polymetallic; at David - Garejinskoye – baryte, baryte-polymetallic and gold-silver. The example of Madneuli (Кекелия и др., 1991, 1993) shows that ore accumulation was preceded by the stage of formation of a metasomatic column, the upper parts of which are occupied by monoquartzites – solfataric formations, the lower ones – by quartz-sericite metasomatites, and the flanks and deep horizons – by propylites. Two ore levels are clearly distinguished under the screen of lava domes at Madneuli (Кекелия и др., 1993): the upper one is baryte and baryte-polymetallic, and the lower one is copper-pyrite. Gold-bearing quartzite bodies are occurred on the upper and partially lower layers.

Georgian geologists have carried out a large volume of thermobarogeochemical studies at the fields of Bolnisi region. According to previous researchers (Аревадзе, 1989; Kekeliya et al., 1993), two-phase gas-liquid inclusions in quartz of copper pyrite ores were homogenized at 320-370°C (maximums – 350-420°C), copper-zinc ores at 280-300°C, in baryte of polymetallic barytes at 260-270°C, and in barytes of baryte ores proper at 120°C. According to cryometric studies of fluid inclusions, the salinity of the solutions that deposited copper and polymetallic ores was low and equal to ~ 40 gram-equivalent of NaCl per liter of solution. The solutions were chloride-sulfate potassium-sodium, contained nitrogen and CO_2. Heavy hydrocarbons and methane were also observed (Кекелия и др., 1993), the total concentration of which did not exceed 4 mol%. The data on the isotopic composition of sulfur are following: the $\delta^{34}S$ values deviate slightly from the meteoritic standard in sulfides: the $\delta^{34}S$ values fluctuate within the range of +10 to +20% in most sulfates. Data on carbon, hydrogen and oxygen isotopes are ambiguous and can be interpreted in favor of the participation of both meteoric and magmatic waters during the ore-forming process. So, the values of $\delta^{13}C$ in calcite and fluid inclusions are grouped around the values of -7.1 ±2.1% and +0.3 ±1.6%; the isotopic composition of hydrogen (δD water) in fluids varies within the range of -70 -90%, and modern waters of the region from -50 to -70%; $\delta^{18}O$ in quartz of copper ores varies from +10.35 to +9.25%, and in baryte of baryte-polymetallic ores within the range of -1.07 to -1.53%.

It should also be stated that industrially significant volcanogenic fields are located in the upper parts of the blocks of Turonian-Santonian effusive-sedimentary rocks in the Bolnisi region, in places where the latter are complicated by extrusive and lava domes. The blocks are bounded by faults of NW and NE strike, which are magma and ore excurrent.

The authors of this paper have data (Гугушвили и др., 2002) on the isotopic composition of strontium and the concentrations of rubidium and strontium in rocks located near volcanogenic fields. It turned out that the basalts of the Bolnisi region ($^{87}Sr/^{86}Sr = 0.704910$) could be the products of differentiation of the undepleted mantle, and the rhyodacites at the Murgul field (Türkiye) could have originated in the lower crust ($^{87}Sr/^{86}Sr = 0.707739$); the rhyolites of the Madneuli field - in the lower upper crust ($^{87}Sr/^{86}Sr=0.710269$). The crustal source of the rhyolite and ignimbrite magmas is also indicated by the europium ratios (for rhyolites – Eu/Eu*=0.65-0.68, ignimbrites – 0.52-0.58) established in them, as well as the enrichment of the rocks in light REE and large-ion lithophylic elements.

It seems appropriate to present geochemical data (Гугушвили и др., 2002) on the rocks hosting the Rapu-Rapu field (Philippines), published in the scientific literature (Sherlock et al., 2003). The massive sulphide deposits of the Rapu-Rapu fields are spatially associated with dacites that have undergone greenstone transformation. This field is of the Kuroko type. Researchers (Sherlock et al., 2003) believe that the REE-rich volcanic rocks of the Rapu-Rapu field were formed during the active rifting of an oceanic arc or a Jurassic back-arc basin. It is interesting that there is a known Canatuan field also in the Philippines, which was formed in the environment of an immature arc that is confirmed by a sharp decrease in the content of light REE in acidic and basic rocks. The data presented for the Bolnisi ore region (Гугушвили и др., 2002) shows that the Zr/Y ratios are higher (for dacites 9.5-11.2; for rhyolites 2.7; for basalts 3.7-4.1) and we are probably dealing with a more mature paleo-arc.

Gadabay ore region (Azerbaijan) and its ore-bearing

It is located in the axial zone of the Shamkir horst-uplift, complicated by the Upper Jurassic-Lower Cretaceous Hajikend-Dashkesan superimposed trough. Its disjunctive framework consists of two faulting systems: the early, northwestern and the later, northeastern. The first of them also includes the Main Gadabay Fault zone, which can be traced in the southwest of the region (Абдуллаева, 2013, 2018; Баба-заде, 2003; Баба-заде, Абдуллаева, 2012).

A special place in the structure of the ore region is given to its central part, where the famous Gadabay gold-copper pyrite ore field is located, controlled by a volcano-dome structure and complicated by radial faults. Bitti-Bulag, Novo-Gorelovka, Maskhit and other gold-copper pyrite, gold-copper-arsenic, gold-copper-polymetallic ores fields are also located here, which represent together the Gadabay ore-magmatic system.

The ore bodies of the Gadabay field, described as stocks in the literature, are morphologically more likely to be flat lenticular bodies, which are confined to the upper horizons of the rhyolite and rhyodacites strata. Part of the ore bodies is concentrated in the early Bajocian main volcanites. These strata are broken by dikes associated with the formation of andesite-basalt-plagiorhyolite and basalt-andesite-dacite-rhyolite formations, as well as comagmatic Mesozoic plagiogranites (Atabey-Slavyan intrusion) and gabbro-diorites, quartz-diorites, etc. (Gadabay intrusion), which according to the entire complex of features, can be combined into a volcano-plutonic association.

The main ore bodies of the Gadabay field (Karl-shtok, Fedorov-stok) are confined to the most raised parts of the blocks at the intersection of a semicircular fault with a submeridional disturbance extending along the central part of the field. The formed blocks of the field were re-displaced relative to each other in the post-ore stage during renewed tectonic movements, along which part of the Fedorov-stock was faulted. The ore bodies in the footwalls have a predominantly pyrite composition with an admixture of chalcopyrite. Solid, massive structure of pyrite ores are replaced downwards, through veinlet, veinlet-impregnated ores, by practically barren hydrothermally altered rocks. The pyrite core of the ore bodies is laterally enveloped by copper-zinc ores, especially in the apical part. So two commercial types of ores are distinguished at the field: early pyrite ores and superimposed copper-zinc ores, which are broken in time, but spatially combined by the stage of ore mineralization. The latter was preceded by a stage of intensive metasomatic alteration of the ore-bearing rocks.

Of natural interest is the assumption of multi-level of Gadabay field. The abovementioned is reinforced by the fact that pyrite mineralization is found in the lower volcanogenic strata outside the Gadabay ore field in the samename and other ore regions of the Somkhito-Karabakh island arc (Bitti-Bulag, etc.).

The general morphology and structural peculiarities of the Garadag-Kharkhar group of porphyry copper fields are determined by the Maarif-Garadag ore-controlling fault of the northwestern direction, as well as diagonal ore-conduit faults, to which crushing and shear zones, small zones of eruptive breccias, subvolcanic and hydrothermal formations are confined. The zones of increased fracture adjacent to these faults turned out to be a reservoir of Late Jurassic (Early Cretaceous) stockworks of gold-bearing Cu-Mo-porphyry mineralization.

Alaverdi ore district (Armenia) and its ore-bearing

Copper-bearing stock-like ore bodies are concentrated in the late Bajocian horizons of siltstones and sandstones in the Alaverdi region, and vertical vein-like ones are in rhyodacitic hyaloclastites and effusives of andesite-basalts of the early Bajocian age. Vein bodies are marked by narrow zones of quartz-sericite-chlorite metasomatites. Besides that, the Tekhut copper-porphyry field is located near Alaverdi.

According to the K-Ar method, the age of the Tekhut phaneritic intrusions is Neocomian (133±8 million years). The background (phanerite) igneous rocks, as well as the porphyry bodies, are essentially sodium and high-alumina and belong to the tonalite group (Кекелия и др., 1991, 1993).

According to V.Z.Yaroshevich (Ярошевич, 1985), who studied gas-liquid inclusions, the fluids from which the ore substance precipitated were chloride-sodium-potassium, highly concentrated (50-20 wt% or 30-40 g/kg in terms of NaCl); mineral formation occurred in the range of 400-220°C, the pressure could exceed 100 kbar; sulfide sulfur at the Tekhut field is characterized by a small dispersion of the $\delta^{34}S$ value and is close to the meteoric standard; sulfate sulfur (anhydrite) is heavier relative to sulfide sulfur by 13.5%. The oxygen isotope composition of the water inclusions varies from I3.0 to -4.1%, which may show some dilution of magmatic waters (fluids) by meteoric ones.

The Alaverdi ore region, which covers the extreme southwestern part of the Somkhito-Kafan tectonic zone of the fragment of the paleo-island-arc structure, is composed mainly of Bajocian-Bathonian and Late Jurassic-Early Cretaceous volcanic complexes in its central part. The Alaverdi volcanic structure was formed as a result of at least three powerful phases of volcanic activity (Бабазаде и др., 2015). It is important to emphasize that the differentiation trend of the Early Bajocian volcanites is located in the transition zone between the tholeiitic field and the calc-alkaline band on the AFM diagram (Кекелия и др., 1991, 1993), and the trends of the later Middle Jurassic volcanites are within the calc-alkaline band. According to general geological data, four groups of endogenous fields of non-ferrous metals are distinguished in the region

(Сопко, 1971). It is assumed that the earliest are baryte-polymetallic ores confined to the apical part of the Akhtal intrusion. The Alaverdi copper field was apparently formed in the late Bajocian-Bathonian, and the Shamlugh field in the late Jurassic, since the massive copper-pyrite stocks are screened by late Jurassic rhyodacites here. The recent mineralization of the subduction stage of the development of the paleo-island-arc structure is the abovementioned copper-porphyry Tekhut field, which shows a paragenetic connection with the Early Cretaceous tholeiitic complex (Кекелия и др., 1991, 1993). It follows from the available data (temperatures of homogenization of gas-liquid inclusions in quartz ores (Аревадзе, 1989; Кекелия и др., 1993) that the Alaverdi field was formed at temperatures of 205-280°C, Shamlugh at 185-210°C, and Akhtal at 170±200°C. N_2, CO_2 among the gases in the inclusions, and a small amount of water were observed. High concentrations of SO_4^{2-}, Ca, Na were observed in aqueous extracts from gas-liquid inclusions of ores of the Gafan field, which is an analogue of the Alaverdi field. In addition, significant concentrations of heavy metals were revealed in aqueous extracts, besides common cations (K, Na, Ca, Mg).

The isotopic composition of sulfur of sulfides in the fields of the Gadabay and Alaverdi ore regions is almost close to the composition of meteoric sulfur. Pyrites of the early quartz-pyrite stage of mineral formation are characterized by the value of $\delta^{34}S=4.9‰$, and 1.2-1.5‰ in the chalcopyrite-pyrite-sphalerite stage, which can be explained by the lightening of sulphide sulfur due to the accumulation of ^{34}S in baryte and anhydrite. The sulfur isotope composition of chalcopyrite 2.6‰ and sphalerite 4.2 ‰ and 7.2‰ testifies to the staged formation of the ores of the Gadabay field. The isotopic composition of oxygen in quartz from copper fields of the Gadabay ore region was equal to +8.9-+11.3‰, Mekhmana ore region (Azerbaijan) to +6.9-12.8‰, Paragachay copper-molybdenum field (Daralagoz block, Azerbaijan) to +9.7‰, Alaverdi ore region to +10.3-+0.5‰. Hydrogen of water from fluid inclusions (Alaverdi field) is characterized by 3D values equal to -75±0.5‰. New data on the isotopic ratios of sulfides sulfur and oxygen from quartz taken from fields in the Bolnisi, Gadabay and Alaverdi regions should be added to this. The analyses were carried out in the USGS laboratory (Denver, USA). The homogenization temperatures of gas-liquid inclusions in quartz from epigenetic fields of the Lesser Caucasus were determined in the same laboratory. The homogenization temperatures of liquid inclusions from copper ores were found to be 315-325°C at Madneuli, 295-305°C at the Gadabay gold-copper pyrite field, 300-320°C at the Kapaz and Tulallar gold-pyrite fields (Абдуллаева и др., 2021), 315-335°C at the Tutkhun gold-sulfide field (Azerbaijan) (Babazadeh et al., 2024); 245-250°C at the Akhtala polysulfide field (Armenia), 325-330°C at the Tekhut copper-porphyry fields (Armenia), and 340-345°C at the Garadag-Kharkhar group (Azerbaijan) (Баба-заде и др., 2015).

Oxygen isotope ratios from quartz of copper and copper-porphyry ores of the Madneuli (Georgia), Gadabay, Bitti-Bulag, Gulyatag, Janyatag, Damirli, Garadag-Kharkhar group, Paragachay (Azerbaijan) and Tekhut (Armenia) fields may show the participation of magmatic waters during the ore-forming process (Тейлор, 1982). The sulfur isotope ratios from sulfides are ambiguous at the epigenetic deposits of the Lesser Caucasus island paleoarc, but the authors of this article believe that most of the sulfur had a magmatogenic source. We state here that these data do not contradict the results of thermobarogeochemical studies previously carried out in the laboratory of the Caucasian Institute of Mineral Resources.

Geological and genetic model of gold-bearing volcanogenic fields of non-ferrous metals in paleoisland-arc structures

Volcanogenic fields are concentrated in geological complexes that were formed during the interaction of oceanic and continental plates. This is usually a zone of active continental margins, under which oceanic crust subducts. Active margins at certain stages of geological history were fragmented and are perceived as "accumulations" of microplates.

Back in the 80s of the last century, many scientists (Абрамович, Клушин, 1987; Митчел, Гарсон, 1984; Rona, 1986) emphasized blocks of the Earth's crust that corresponded (taking into account the principle of actualism) to fragments of both passive and active continental margins. It is possible to recognize geological formations Within the fragments that contain certain ore accumulations. In our case, we are dealing with the Alpine fragments of the Pontic-Lesser Caucasus island arc, which is characterized by both volcanogenic-sedimentary and epithermal fields (epigenetic), known in the literature as the Kuroko type (Франклин и др., 1984). One of them was an ore accumulation environment and acted as either physical or geochemical barriers for the ore-bearing system, while others were considered as a source of ore matter and also as a source of energy supply. These metallogenic categories are intensively used in genetic constructions. The concept of "ore-generating system" is also often used. It should be perceived as a set of interacting elements acting in a given relationship as a whole (Тюхтин, 1988).

The integrity of such systems is determined by their emergence, the so-called cognitive properties. F.A. Letnikov (Летников, 1993) emphasized that geological systems of different levels (The Earth as a whole, the components of its "levels", for example, magmatic and fluid systems) have synergetic or, in other words, self-organizing properties.

The ore process is identified with the development of a high-energy geological system, practically open to its mobile components. The following act as macroelements of dissipative fluid systems: 1) fluid formation areas (there are scientists' controversial and contradictory opinions about them (Чухров, 1976); 2) their movement paths; 3) discharge areas with structures (physical) and geochemical barriers, where the accumulation of ore matter occurs.

This paper proposes a mental-logical model of the development of ore-generating systems and, first of all, that part of it that is responsible for the precipitation and coning of ore components. The model identifies those features-factors that are necessary and sufficient for the conduct of ore-forming processes. In order to substantiate the logic of the provided constructions, besides general geological data, thermobarogeochemical data and isotopic ratios of the leading ore-forming elements are used. It is important to emphasize (Баба-заде, 2000) that the genetic model should be perceived as a kind of abstraction, which takes into account mainly not the external similarity of individuals (deposits, ore bodies), but the standard nature of the processes occurring in the system.

According to geophysical data (Рингвуд, 1981), the root parts of magmatic bodies under island arcs with developed sialic crust are usually located at depths of 60-80 km. Since these depths correspond to the lower crust, researchers (Белоусов, Кривенко, 1983; Рингвуд, 1981; Уилли, 1983) assume a connection between orogenic series magmas and partial melting of amphibolites.

Traces of intensive hydrotherm activity – hydrothermal changes in rocks and ore accumulation are usually observed under the volcanic dome (for example, Madneuli) or above the Chayeli dome. The idea of a magmatic source of fluids in volcanogenic fields has lost its appeal in recent decades due to the difficulties associated with the need to explain the involvement of significant volumes of water during the hydrothermal process. The mechanism of fluid separation is thought to be a relatively short-term phenomenon. "Traces" of the latter in magmatic bodies are expressed by autometasomatic alterations, equal distribution of submicroscopic individuals of oxides and sulfides in silicate crystals or in the intergranular space of rock-forming minerals. The results of isotope-geochemical studies of volcanogenic fields incline researchers to the conclusion on a large content of meteoric waters in hydrosystems (Синяков, 1986). Experiments also show a small content of magma water in hydrosystems, not exceeding 0.0005% of the total mass of water (Гричук и др., 1984).

It is well known that there is a relationship between ore components and their content in ore-bearing rocks (Баранов и др., 1990; Фарфель, 1988). Moreover, hydrothermally altered rocks near ore accumulations are characterized by a deficit of metals. Experimental work (Гричук и др., 1984; Hodgson, Lyndon, 1977) on the extraction of elements from rocks under PT conditions corresponding to the functioning of fluids also confirms the possibility of considering ore-bearing magmatic and sedimentary formations as a source of metals.

Hydrothermal solutions with ore elements are similar in salinity to seawater, and at the same time they are enriched in comparison with seawater by several orders of Fe, Ag, Pb, Cu and Zn (Mottl et al., 1979). The initial redistribution and separation of ore components is associated with the crystallization conditions of magmatic rocks with a specific component composition. Spherical acetates of oxide-ore segregations of liquation nature have been revealed (Прокопцев, Прокопцев, 1990) in the basalts of mid-ocean ridges, and earlier in siliceous formations. Sulfides have also been observed in the form of "drops" in the impregnations of clinopyroxene and feldspar in the ore subalkaline effusives of the rift valley of the mid-ocean ridge (Акимцев, Шарапов, 1993). These ore liquates contain nickel-pyrrhotite, sphalerite, chalcopyrite, silver, albite and potassium feldspar. As some researchers (Нортон, Кэттл, 1982) believe, the further migration path of ore elements in volcanic regions is determined by the involvement of sea and formation meteoric waters in the convective flow due to a decrease in their density under the influence of the thermal anomaly of intrusions introduced into volcanites. Aggressive heated waters acquire the properties and composition of ore-bearing fluids, interacting with intrusions and volcanites.

Large-scale ore genesis, according to materials collected from the World Ocean (Гринберг и др., 1990; Ельянова, Мирлин, 1990; Ельянова, 1999; Рона, 1986), is carried out sequentially during the process of: 1) crystallization of magmas; 2) interaction of surface waters that have acquired "aggressiveness" with volcanites; 3) stable functioning of the physicochemical barrier in the area of hydrotherm discharge (whether it is the seabed or the near-surface zone of the Earth's crust).

Volcanogenic fields of non-ferrous metals are characterized by the following peculiarities:

1. Both sedimentary-hydrothermal and veinlet-impregnated fields are confined to volcano-depressions. The former are confined to their axial zones, the latter occupy the near edge parts and are controlled by extrusive domes. The component composition of the ores depends on the petrochemical characteristics of the ore-bearing volcanites and their comagmates. Baryte-polymetallic mineralization is preferentially associated with sodium-potassium rhyodacites, and copper-zinc (Кривцов, 1989) mineralization is associated with andesite-basalts and sodium rhyolites;

2. The fluids that formed the volcanogenic fields were weak acid sodium chloride, with low salinity (Овчинников, 1988; Синяков, 1986; Франклин и др., 1984; Баба-заде, 1999, 2000). Low salinity of fluids is also characteristic of modern sulfide accumulation in the World Ocean (Бортников и др., 2004; Бортников, Викентьев, 2005). However, brines (up to 30 mol% - equiv. NaCl at a temperature of 200-400°C) have also been observed for some fields of sulfide formation (Бортников, Викентьев, 2005). Data on the Lesser Caucasus fields do not contradict this (Баба-заде и др., 1990; Баба-заде, 1999, 2000; Кекелия и др. 1991; 1993).

It is shown in the work (Yardley, Bruce, 2005), which summarizes the data on crustal fluids, that temperature is one of the main factors affecting the concentration of metals in the solution. Metals Fe, Mn, Zn, Pb in solution are most likely in chloride complexes. For example, for zinc $ZnCl^+$ and $ZnCl^{2-}_4$ (Seward, 1984). The concentration of the abovementioned metals also increases with the chloride concentration. Metals are most likely concentrated in brines – in evaporites, from which Pb-Zn fields of the Mississippi-Missouri type are formed.

According to researchers (Франклин и др., 1984), the maximum temperatures of ore deposition are comparable to the boiling temperatures of the solution. The "base" of hydrotherm evaporation with temperatures over 270°C is located at depths of 300-400 m in areas of modern volcanism (Синяков, 1986).

According to the data on the Lesser Caucasus region, the maximum homogenization temperatures at copper fields were equal to 410-390°C, and at baryte-sulfide fields ~280°C (Ярошевич, 1985). According to our data, the maximum fluid pressures at epigenetic fields of nonferrous metals in the Lesser Caucasus, as well as the diagrams (Shepherd et al., 1985) used to determine the pressure approached 150-200 bar, and mineral formation occurred at depths of 400-600 m from the paleosurfaces.

3. The known data on the isotopic composition of hydrogen and oxygen of fluid inclusions in quartz, baryte and calcite of volcanogenic baryte-polymetallic ores were previously interpreted in favor of a high content of meteoric water participation during the ore-forming process. Meteoric water could be inferior to magmatogenic water for copper ores (Кривцов и др., 1987; Франклин и др., 1984; Ярошевич, 1985).

The results we obtained for determining oxygen isotopes in the laboratory of the US Geological Survey (Denver) also do not contradict these data.

4. The data on the isotopic composition of sulfur in sulfides and sulfates, as already mentioned, are ambiguous: the isotopic composition of sulfur in sulfides approaches the composition of meteoric sulfur, and sulfates are heavier by 14±3‰.

5. Boiling of fluid at most fields with hydrothermal-sedimentary deposits did not occur at all or possibly, occurred before the thermals reached the seabed, thereby facilitating the preparation of ore-conduit systems. The most favorable conditions for the stable accumulation of hydrothermal-sedimentary ores were created at the bottom of sea basins, the depths of which varied within 2-3 km (Бортников, Викентьев, 2005; Stackelberg, 1985).

It should be stated that according to the modern data, the hydrothermal-sedimentary deposits formed due to the "black smokers" were formed following the completion of the accumulation of andesite-dacite-rhyolite complexes (deposits, as result from observations at fields of Kuroko-type, are located on rhyodacites domes). The mineral zoning that we see in hydrothermal-sedimentary deposits is explained by the redistribution of ore-forming components as a result of the destruction of "hills" and their diffusion from lower to upper levels during the process of "washing out" of ores by fluids (Hannigton et. al, 1986). An example is the modern ore structure in the Pacific Ocean, on the Explorator Ridge, where high-temperature sulfides underlie layers of lower-temperature Fe-Mn sulfides, baryte and silica. According to G.D.Grichuk (Гричук, 1999), the anhydrite-pyrite structure (they proposed a thermodynamic model) is eventually replaced by a later silica-sulfide substance. The occurrence of anhydrite in the "ore mounds" is explained by the involvement of sea waters in the discharge zones. Seawater is heated, resulting in anhydrite deposition (Черкашев и др., 1999).

The levels of mineral formation in epigenetic fields are generally comparable to the zones of "black smoker" pipes, the boundary anomalous physicochemical parameters of which caused the simultaneous crystallization of anhydrite and iron sulfides. These conditions correspond to zones of

hydrosystems with minimum activities $>PO_2$, coinciding with the lower boundary of the baryte stability field at equal activities of $H_2S - SO_4^{-2}$ (Франклин и др., 1984). The zonal distribution of metals in baryte-sulfide deposits can be explained by: 1) different stability of complex compounds (Овчинников, 1988; Франклин и др., 1984); 2) greater dependence of the solubility of copper minerals on temperature compared to the solubility of sphalerite and galena (Франклин и др., 1984); 3) dependence of metal deposition on concentration of S^{-2}. Higher concentrations of H_2S are required for precipitation of copper and zinc than for lead at equal concentrations of metals in the solution; 4) action of the hydrosulfuric barrier, the effectiveness of which is determined by low concentrations of S^{-2} (Крайнов и др., 1988).

It can also be assumed that $\sum S$ is sufficient for copper precipitation in fluid discharge zones, while lead, zinc and silver tend to pass the hydrosulfuric barrier with a alteration in ligand. Excess anion precipitator (a known phenomenon in analytical chemistry) acts as a solvent for the complexing agent.

Ch.Heinrich (Heinrich, 2005) stated that magmatic waters with low salinity are able to transport gold under high temperature conditions. His conclusion is based on physical and chemical studies. One of the main conditions is a sufficient amount of H_2S, which acts as a ligand (bisulfate complex). C. Heinrich's paper (Heinrich, 2005) deals with Au-Cu porphyry fields, but, in our opinion, the results of this author's research can also be used in the case of gold-bearing fields such as Madneuli, Dagkesaman, Tulallar, Chovdar, etc.

Conclusions

It can be concluded that ore fields of paleo-island-arc structures, in particular the Pontic-Lesser Caucasus arc, should be expected in the following geological settings: in vents and on the slopes of paleovolcanoes located in volcanodepressions: ore bodies in siliceous parts of volcanogenic-sedimentary strata or above them (in the case of hydrothermal-sedimentary deposits); as a rule, the ores are covered by basic volcanites, but there may be exceptions.

The ores of the Lesser Caucasus fields are clearly epigenetic: veinlet-impregnated and vein mineralization is superimposed on hyaloclastites and tuffites in the Gadabay and Alaverdi ore regions; veinlet-impregnated copper mineralization is occurred in silicified tuffites in Bolnisi, as well as impregnated gold and baryte-sulfide in the form of veins and flat deposits - in secondary quartzites. The ores of the Chayeli fields are similar to the "ore hills" of modern mid-ocean ridges and rifting zones of marginal seas.

Ore bodies in the Gadabay and Alaverdi ore regions are located in a cover of narrow zones of quartz-sericite-chlorite metasomatites; a vertical metasomatic column is occurred in the Bolnisi region: secondary quartzites in the upper part (near-surface solfataric alterations), and higher-temperature silicification in the lower part (quartz-chlorite-sulfide metasomatites with minor amounts of sericite). Ore metasomatites are surrounded by a cover of propylites. Veinlet-impregnated "yellow" ores are surrounded by quartz-hydromicaceous metasomatites at the fields of the Chayeli (Madenkoy) type, under hydrothermal-sedimentary deposits, in the underlying dacites against the background of regional propylites. The latter mark the paths of hydrothermal solutions moving to the marine paleo-ocean.

Stocks and thin lens-veins (group of northern lenses in Gadabay) of copper ores are found in the Gadabay and Alaverdi ore regions; large-volume copper stockworks are predominantly occurred in the Bolnisi region; besides stockworks, thick deposits of lens-shaped massive sulphide ores consisting mainly of pyrite, chalcopyrite and sphalerite in the Eastern Pontides.

It is clear that these differences are due to the different geodynamic regimes of development of individual blocks of the Earth's crust of the paleoisland-arc structure.

Thermobarogeochemical studies have shown that the main copper and gold fields as one of the main sub-ore components of the ores were formed in similar PTX conditions and belong to a single genetic volcanogenic class of fields, despite the difference in the mechanism of ore deposition.

REFERENCES

Abdullayeva Sh.F. Geological and geochemical studies and forecast of gold ore paleosystems of the Lesser Caucasus mountain-folded structure. Sputnik. Moscow, 2013, 156 p. (in Russian).

Abdullayeva Sh.F. Volcanogenic gold-bearing sulfide fields of island-arc zones, conditions of their geodynamic development, patterns of placement and forecasting criteria (the Lesser Caucasus). Abstract of diss. of Doctor of Sciences. Baku, 2018, 58 p. (in Russian).

ЛИТЕРАТУРА

Абдуллаева Ш.Ф. Вулканогенные золотосодержащие сульфидные месторождения островодужных зон, условия их геодинамичечского развития, закономерности размещения и критерии прогнозирования (Малый Кавказ). Автореф. дисс. … доктора наук. Баку, 2018, 58 с.

Абдуллаева Ш.Ф. Геолого-геохимические исследования и прогноз золоторудных палеосистем Малокавказского горно-складчатого сооружения. Спутник. Москва, 2013, 156 с.

Abdullayeva Sh.F., Babazadeh V.M., Imamverdiyev N.A. et al. Tulallar epithermal gold-sulfide fields: structural peculiarities, geological and structural characteristics and patterns of ore localization (the Lesser Caucasus). Moscow, Gorniy Zhurnal, No. 9 (2290), 2021, pp. 53-60, DOİ: 10.17580/gzh.2021.09.09 (in Russian).

Abramovich I.I., Klushin I.G. Geodynamics and metallogeny of folded regions. Nedra. Leningrad, 1987, 247 p. (in Russian).

Adamia Sh.A., Zakariadze G.S., Lordkipanidze M.B. Evolution of the ancient active continental margin on the example of the Alpine history of the Caucasus. Geotectonics, No. 4, 1977, pp. 88-103 (in Russian).

Akchay M., Arar M. Geology, mineralogy and geochemistry of the Chayeli massive sulfide ore deposit, Rize. NE Turkey. In: Mineral Deposits: Processes to processing (A.Stanley, ed.), Balkema. Rotterdam, 1999, pp. 459-462.

Akimtsev V.A., Sharapov V.N. "Ore" effusive rocks of the rift valley side of the Mid-Atlantic Ridge Papers of the Academy of Sciences of Russia, Vol. 331, No. 3, 1993, pp. 329-331 (in Russian).

Altun Y. Geology of the Chayeli-Madenkoy copper-zinc deposit and the problems related to mineralization. Ankara. Mineral Res. Expl. Bull., 89, 1977, pp. 10-24.

Arevadze V.A. Physicochemical conditions of formation of endogenous fields of Transcaucasia. Abstract of diss.... Doctor of Geological and Mineral Sciences in the form of a scientific paper. Tbilisi. Metsniereba. 1989, 65 p. (in Russian).

Babazadeh V.M. Generalized geological-genetic model of pyrite ore formation. Bulletin of Baku University. Series of Natural Sciences, No. 1, 2000, pp. 105-126 (in Russian).

Babazadeh V.M. Pyrite metallogeny and evolution of Mesozoic-Cenozoic volcanism of the Lesser Caucasus. Bulletin of Baku University. Series of natural sciences, No. 4, 1999, pp. 113-132 (in Russian).

Babazadeh V.M., Abdullayeva Sh.F. Noble metal ore-magmatic systems. Publishing house of Baku University. Baku, 2012, 276 p. (in Russian).

Babazadeh V.M., Abdullayeva Sh.F., Novruzova S.R. Structural conditions for the Tutkhun ore field the central part of the Lesser Caukasus. ANAS Transactions, Earth Sciences, No. 1, 2024, pp. 104-118, DOI:10.33677/ggianas20240100112 http://www.journalesgia.com.

Babazadeh V.M., Kekeliya S.A., Abdullayeva Sh.F. et al. Gold-bearing sulfide fields of island-arc paleosystems, their metallogenic peculiarities and conditions of geodynamic development (on the example of the Lesser Caucasus Alps). CBS Publishing House. Baku, 2015, 400 p. (in Russian).

Babazadeh V.M., Kekeliya S.A., Abdullayeva Sh.F. et al. Main peculiarities of the metallogeny of the Caucasus. Nedra. Moscow, 2000, 187 p. (in Russian).

Babazadeh V.M., Makhmudov A.I., Ramazanov V.G. Copper and molybdenum porphyry fields. Azerneshr. Baku, 1990, 377 p. (in Russian).

Babazadeh V.M., Musayev Sh.D., Nasibov T.N. et al. Gold of Azerbaijan. Azerbaijan National Encyclopedia. Baku, 2003, 424 pp. (in Russian).

Baranov A.N., Arkhangelsky A.N., L.N. Ovchinnikov (editor): Scientific foundations of the geochemical method for predicting hidden pyrite fields by alluvial halos. Theory and practice of geochemical prospecting in modern conditions. IMGRE. Moscow, 1990, pp. 108-124 (in Russian).

Belousov A.F., Krivenko A.P. Magmatogenesis of volcanic formations. Nauka. Novosibirsk, 1983, 243 p. (in Russian).

Biju-Duval B., Dercourt J., Le Richon X. From the Tethys ocean to Mediterranean seas: a plate tectonic model of the evolution of the western Alpine system. Historic Structural de Bassins Mediterraneens, 1977, pp. 143-164.

Bortnikov N.S., Simonov V.A., Bogdanov Yu.A. Fluid inclusions in minerals from modern sulfide structures: physico-

Абдуллаева Ш.Ф., Баба-заде В.М., Имамвердиев Н.А. и др. Эпитермальное золото-сульфидное месторождение Тулаллар: особенности строения, геолого-структурная характеристика и закономерности размещения оруденения (Малый Кавказ). Москва, Горный журнал, No. 9(2290), 2021, с. 53-60, DOİ: 10.17580/gzh.2021.09.09.

Абрамович И.И., Клушин И.Г. Геодинамика и металлогения складчатых областей. Недра. Ленинград, 1987, 247с.

Адамия Ш.А., Закариадзе Г.С., Лордкипанидзе М.Б. Эволюция древней активной континентальной окраины на примере альпийской истории Кавказа. Геотектоника, No. 4, 1977, с. 88-103.

Акимцев В.А., Шарапов В.Н. «Рудные» эффузивы борта рифтовой долины Срединно-Атлантического хребта. Доклады Академии Нах к России, Том. 331, 1993, No. 3, с. 329-331.

Аревадзе В.А. Физико-химические условия формирования эндогенных месторождений Закавказья. Автореф. дисс. ... докт. геол.-мин. наук в форме научного доклада. Мецниереба. Тбилиси,1989, 65с.

Баба-заде В.М. Колчеданная металлогения и эволюция мезокайнозойского вулканизма Малого Кавказа. Вестник Бакинского Университета. Серия естественных наук. No. 4, 1999, с. 113-132.

Баба-заде В.М. Обобщенная геолого-генетическая модель колчеданного рудообразования. Вестник Бакинского Университета. Серия естественных наук, No. 1, 2000, с. 105-126.

Баба-заде В.М., Абдуллаева Ш.Ф. Благороднометальные рудно-магматические системы. Изд. Бакинского Университета. Баку, 2012, 276 с.

Баба-Заде В.М., Кекелия С.А., Абдуллаева Ш.Ф. и др. Золотосодержащие сульфидные месторождения островодужных палеосистем, их металлогенические особенности и условия геодинамического развития (на примере альпид Малого Кавказа). Изд-во «CBS». Баку, 2015, 400 с.

Баба-Заде В.М., Кекелия С.А., Абдуллаева Ш.Ф., и др. Основные черты металлогении Кавказа. Недра. Москва, 2000, 187 с. IBSN 978-5-8365-0505-9

Баба-заде В.М., Мусаев Ш.Д., Насибов Т.Н. и др. Золото Азербайджана. Аз. Милли Энсиклопедиясы. Баку, 2003, 424 с.

Баба-заде В.М., Махмудов А.И., Рамазанов В.Г. Медно- и молибден-порфировые месторождения. Азернешр. Баку, 1990, 377 с.

Баранов А.Н., Архангельский А.Н. Л.Н.Овчинников (ред.). Научные основы геохимического метода прогноза скрытых колчеданных месторождений по ореолам выноса. Теория и практика геохимических поисков в современных условиях. ИМГРЭ. Москва, 1990, с. 108-124.

Белоусов А.Ф., Кривенко А.П. Магматогенез вулканических формаций. Наука. Новосибирск, 1983, 243 с.

Бортников Н.С., Викентьев И.В. Современное сульфидное полиметаллическое минералообразование в мировом океане. Геология рудных месторождений, т. 47, No. 1, 2005, с. 16-50.

Бортников Н.С., Симонов В.А., Богданов Ю.А. Флюидные включения в минералах из современных сульфидных построек: физико-химические условия минералообразования и эволюция флюида. Геология рудных месторождений, Том 46, No. I, 2004, с. 74-87.

Гринберг Г.А., Краснов С.Г., Айнемер А.И. и др. Гидротермальное сульфидное оруденение в океане. Советская геология, No. 12, 1990, с. 81-91.

Гричук Д.В. Модель образования колчеданного рудного тела в субмаринной гидротермальной системе. В.Е. Попов (ред.) Модели вулканогенно-осадочных рудообразующих систем. Тезисы докладов международной конференции. С-Петербург, 1999, с.19-21.

Гричук Д.В., Борисов М.В., Мельникова Г.Л. Термодинамическая модель гидротермальной системы в океанической

chemical conditions of mineral formation and fluid evolution. Geology of ore fields, Vol. 46, No. 1, 2004, pp. 74-87 (in Russian).

Bortnikov N.S., Vikentyev I.V. Modern sulfide polymetallic mineral formation in the world ocean. Geology of ore fields, Vol. 47, No. 1, 2005, pp. 16-50 (in Russian).

Chakir U. Geological characteristics of the Aşiköy-Toykondu (Küre-Kastamonu) massive sulfide deposits. Mineral. Res. Expl. Bull., Ankara, No. 117, 1995, pp. 29-40.

Cherkashev G.A., Zhirnov E.A., Stepanova T.V., Mozgova N.N. Zoning and model of formation of oceanic sulfide structures (based on deep-sea drilling data). Models of volcanogenic-sedimentary ore-forming systems. Abstracts of the international conference, St. Petersburg, 1999, pp. 141-142 (in Russian).

Chukhrov F.V. (editor). Sources of ore matter of endogenous fields. Nauka. Moscow, 1976, 340 p. (in Russian).

Dixon C.J., Periere J. Plate tectonics and mineralization in the Tethyan Region. Mineralium Deposita, No. 9, 1974, pp. 185-198.

Elyanova E.A. Formation of modern and ancient submarine pyrite ores: composition and structure. Models of volcanogenic-sedimentary ore-forming systems. Abstracts of the international conference, St. Petersburg, 1999, pp. 26-27 (in Russian).

Elyanova E.A., Mirlin E.G. Oceanic ore genesis. Soviet geology, No. 6, 1990, pp. 47-55 (in Russian).

Farfel L.S. Forecasting of ore fields. Nedra. Moscow, 1988, 150 p. (in Russian).

Franklin J.M., Lydon J.W., Sangster D.F. Pyrite fields of volcanic association. Genesis of ore fields, Mir. Moscow, Vol. 2, 1984, pp. 39-252 (in Russian).

Grichuk D.V. Model of formation of pyrite ore body in submarine hydrothermal system. Models of volcanogenic-sedimentary ore-forming systems. Abstracts of the international conference. St. Petersburg, 1999, pp. 19-21 (in Russian).

Grichuk D.V., Borisov M.V., Melnikova G.L. Thermodynamic model of hydrothermal system in oceanic crust: assessment of solution evolution. Geology of ore fields, No. 4, 1984, pp. 3-24 (in Russian).

Grinberg G.A., Krasnov S.G., Ainemer A.I. et al. Hydrothermal sulfide mineralization in the ocean. Soviet Geology, No. 12, 1990, pp. 81-91 (in Russian).

Gugushvili V.I., Beridze T.M., Chkhotua et al. Volcanic and metallogenic indicators of the stages of geodynamic development of the Eurasian active margin and synvolcanic and postvolcanic blocking on the example of the Bolnisi ore region. Institute of Geology. New series, Tbilisi, Issue 130, 2018, 123 p. (in Russian).

Gugushvili V.I., Kekeliya M.A., Moon Ch., Natsvlishvili M.P. Crust and mantle sources of Cretaceous volcanism and sulfide ore formation in the Bolnisi ore region. 1st Proceedings of the Institute of the Academy of Sciences of Georgia, new series, 2002, Vol. 117, pp. 412-119 (in Russian).

Güner M. Sulphide ores and geology of the Küre area, Pontides in North Turkiye. Mineral Research and Exploration Bulletin, 1980, pp. 65-109.

Hannington M.D. Peter J.M. Scott S.D. Gold in sea-floor polymetallic sulfide deposits. Econ. Geol., Vol. 81, 1986, pp. 1867-1883.

Heinrich Ch.A, The physical evolution of low-salinity magmatic fluids at the porphyry to epithermal transition: a thermodynamic study. Mineralium Deposita, No.39, 2005, pp. 864-889.

Hodgson C.L., Lyndon S.M. The geological setting of the volcanogenic massive sulfide deposits and active hydrothermal systems: some implications for explorations. Canadian Mining Metallurgical Bull., Vol.70, 1977, pp. 95-106.

Kekeliya S.A., Ambokadze A.N., Ratman I.P. Volcanogenic fields of non-ferrous metals of paleoisland-arc structures and methods of their forecasting. Metsniereba. Tbilisi, 1993, 96 p. (in Russian).

коре: оценки эволюции раствора. Геология рудных месторождений. No. 4, 1984, с. 3-24.

Гугушвили В.И., Беридзе Т.М., Чхотуа и др. Вулканические и металлогенические индикаторы этапов геодинамического развития Евразийской активной окраины и синвулканическое и поствулканическое блокирование на примере Болнисского рудного района. Тбилиси, Ин-т геологии. Нов.серия, Вып. 130, 2018, 123 с.

Гугушвили В.И., Кекелия М.А., Мун Ч. Нацвлишвили М.П. Коровые и мантийные источники мелового вулканизма и сульфидного рудообразования в Болнисском рудном районе. Труды ГИН АН Грузии, новая серия, в. 117, 2002, с.412-119.

Ельянова Е.А. Формирование современных и древних субмаринных колчеданных руд: состав и строение. В.Е. Попов (ред.). Модели вулканогенно-осадочных рудообразующих систем. Тезисы докладов международной конференции. С-Петербург, 1999, с.26-27.

Ельянова Е.А., Мирлин Е.Г. Океанический рудогенез. Советская геология. No. 6, 1990, с.47-55.

Зоненшайн А.П., Ковалёв А.А. (ред.). Новая глобальная тектоника (тектоника плит). Мир. Москва, 1974, 471 с.

Кекелия С.А., Ярошевич В.З., Ратман Н.П. Геолого-генетические модели альпийских вулканогенных месторождений цветных металлов Средиземноморского металлогенического пояса. Геология и геофизика, No. 8, 1991, с.71-79.

Кекелия С.А., Амбокадзе А.Н., Ратман И.П. Вулканогенные месторождения цветных металлов палеоостроводужных сооружений и методика их прогнозирования. Мецниереба. Тбилиси, 1993, 96 с.

Крайнов С.11., Матвеев Л.И., Соломин Г.А. Геохимические условия осаждения цинка и свинца из рассолов седиментационных бассейнов на сульфидном барьере. Геохимия, No. 2, 1988, с. 1708-1719.

Кривцов А.И. Прикладная металлогения. Недра. Москва, 1989, 288 с.

Кривцов А.И., Богданов Ю.В., Бородаевская М.Б. и др. Меднорудные месторождения типы и условия образования. Недра. Москва, 1987, 197 с.

Летников Ф.А. К проблеме синергетики геологических систем. Геология и Геофизика, No. 1, 1993, с. 34-56.

Митчел А., Гарсон М. Глобальная тектоническая позиция минеральных месторождений. Мир. Москва, 1984, 496 с.

Монин А.С., Зоненшайн Л.П. (редакторы). История океана Тетис. Институт океанологии. Москва, 155 с.

Назаров Ю.И. Особенности формирования месторождений медноколчеданной формации Южной Грузии. Недра. Москва, 1966, 227с.

Нортон Д., Кэтл А.М. Термальные аспекты рудоотложения. Геохимия гидротермальных рудных месторождений. Мир. Москва, 1982, с. 481-496.

Овчинников 31.Н. Образование рудных месторождиий. Недра. Москва, 1988, 255 с.

Прокопцев Г.И., Прокопцев Н.Г. Образование металлоносных гидрогерм на дне океана. Известия Академии Наук СССР, серия геологическая, No. 4, 1990, с. 34-44.

Рингвуд А.Е. Состав и петрология мантии Земли. Недра. Москва, 1981, 584 с.

Рона II. Гидротермальная минерализация областей спрединга в океане. Мир. Москва, 1986, 160 с.

Синяков В.И. Общие рудогенетические модели эндогенных рудных формаций. Наука. Новосибирск, 1986, 243 с.

Сопко П.Ф. Колчеданные месторождения Малого Кавказа. Недра. Москва, 1971, 256 с.

Тейлор Х.А. Изотопы кислорда и водорода в гидротермальных рудных месторождениях. Геохимия гидротермальных рудных месторождений. Мир. Москва, 1982. с. 200-237.

Kekeliya S.A., Yaroshevich V.Z., Ratman N.P. Geological and genetic models of Alpine volcanogenic fields of non-ferrous metals of the Mediterranean metallogenic belt. Geology and Geophysics, No. 8, 1991, pp. 71-79 (in Russian).

Kraynov S.I., Matveyev L.I., Solomin G.A. Geochemical conditions of zinc and lead precipitation from brines of sedimentation basins on a sulfide barrier. Geochemistry, No. 2, 1988, pp. 1708-1719 (in Russian).

Krivtsov A.I. Applied metallogeny. Nedra. Moscow, 1989, 288 p. (in Russian).

Krivtsov A.I., Bogdanov Yu.V., Borodayevskaya M.B. et al. Copper ore fields: types and conditions of formation. Nedra. Moscow, 1987, 197 p. (in Russian).

Lethch Graig H.B. Mineralogy and textures of the Lakhanos and Kizilkaya massive sulphide deposits, Northeastern Turkey and their similarity to Kuroko ores. Mineral deposita, No.16, 1981, pp. 241-257.

Letnikov F.A. On the problem of synergetics of geological systems. Geology and Geophysics, No. 1, 1993, pp. 34-56 (in Russian).

Mitchell A., Garson M. Global tectonic position of mineral fields. Mir. Moscow, 1984, 496 p. (in Russian).

Monin A.S., Zonenshain L.P. (eds). History of the Tethys Ocean. Institute of Oceanology. Moscow, 1987, 155 p. (in Russian).

Mottl M.J., Holland H.D., Corr R.F. Chemical exchange during hydrothermal alteration of basalts seawater. Experimental results for Fe, Mn and sulfur apecies. Geochim. et acta, Vol. 43, 1979, pp. 869-884.

Nazarov Yu.I. Peculiarities of the formation of fields of copper-pyrite formation of South Georgia. Nedra. Moscow, 1966, 227 p. (in Russian).

Norton D., Cattle A.M. Thermal aspects of ore deposition. In: Geochemistry of hydrothermal ore fields (H.P.Barnes, ed.). Mir. Moscow, 1982, pp. 481-496 (in Russian).

Okay Л.L, Şahintürk O. Geology of the Eastern Pontides. In: Regional and petroleum geology of the Black Sea and surrounding region (Robinson A.G. ed.), American Association Petroleum Geologists Memoir, No. 68, 1997, pp. 291-311.

Ovchinnikov N. Formation of ore fields. Nedra. Moscow, 1988, 255 p. (in Russian).

Popovic R. Auriferous mineralization in the Murgul-Artvin-Maradit area (Northeastern Turkey). Mineral Res. Expl. Bull., No. 129, 2004, pp. 17-29.

Prokoptcev G.I., Prokoptcev N.G. Formation of metal-bearing hydrotherms on the ocean floor. Bulletin of the USSR Academy of Sciences, Geological Series, No. 4, 1990, pp. 34-44 (in Russian).

Rhone II. Hydrothermal mineralization of spreading zones in the ocean. Mir. Moscow, 1986, 160 p. (in Russian).

Ringwood A.E. Composition and petrology of the Earth's mantle. Nedra. Moscow, 1981, 584 p. (in Russian).

Seward T.M. The formation of lead (II) chloride complexes to 300°C: A spectrophotometric study: Geochimica et Cosmoshimica Acta, Vol. 48, 1984, pp. 121-134.

Shepherd T.J., Rankin A.H., Aiderton D.H.M. A practical guide to fluid inclusion studies. Blaskie, Glasgow and London, 1985, 239 p.

Sherlock R.L., Barret T.I., Lewis P.D. Geological setting of the Rapu Rapu gold-rich volcanogenic massive sulfide deposits, Albay Province, Philippines. Mineralium deposita, No. 38, 2003, pp. 813-830.

Shikhalibeili E.Sh. Some problematic issues of geological structure and tectonics of Azerbaijan. Elm. Baku, 1996, 215 p. (in Russian).

Sinyakov V.I. General ore-genetic models of endogenous ore formations of Novosibirsk. Nauka. Novosibirsk, 1986, 243 p. (in Russian).

Тюхтин В.И. (ред.). Диалектика познания сложных систем. Мысль. Москва, 1988, 317 с.

Уилли Р.Дж. Петрогенез и физика Земли. Эволюция изверженных пород. Мир. Москва, 1983, с.468-503.

Фарфель Л.С. Прогнозирование рудных месторождений. Недра. Москва, 1988,150 с.

Франклин Дж.М., Лайдон Дж.У., Сангстер Д.Ф. Колчеданные месторождения вулканической ассоциации. В: Генезис рудных месторождений (Б.С.Скиннер, ред.), Т. 2. Мир. Москва, 1984, с. 39-252.

Черкашев Г.А., Жирнов Е.А., Степанова Т.В., Мозгова Н.Н. Зональность и модель формирования океанских сульфидных построек (по материалам глубоководного бурения). В: Модели вулканогенно-осадочных рудообразующих систем (В.Е.Попов ред.). Тезисы докладов международной конференции. С-Петербург, 1999, с. 141-142.

Чухров Ф.В. (ред.). Источники рудного вещества эндогенных месторождений. Наука. Москва, 1976, 340 с.

Шихалибейли Э.Ш. Некоторые проблемные вопросы геологического строения и тектоники Азербайджана. Элм. Баку, 1996, 215 с.

Ярошевич В.З. Генетические особенности месторождений основных рудных формаций Кавказа по данным изотопных исследований. Автореф. дисс. ... канд. геол.- мин. наук. Тбилиси, 1985, 23 с.

Akçay M., Arar M. Geology, mineralogy and geochemistry' of the Çayeli massive sulfide ore deposit, Rize. NE Turkey. In: A. Stanley (ed). Mineral Deposits: Processes to processing. Balkema. Rotterdam, 1999, pp. 459-462.

Altun Y. Geology of the Çayeli-Madenköy copper-zinc deposit and the problems related to mineralization. Ankara. Mineral Res. Expl. Bull., Vol. 89, 1977, pp. 10-24.

Babazadeh V.M., Abdullayeva Sh.F., Novruzova S.R. Structural conditions for the Tutkhun ore field the central part of the Lesser Caucasus. ANAS Transactions, Earth Sciences No. 1, 2024, pp. 104-118, DOI:10.33677/ggianas20240100112 http://www.journalesgia.com.

Biju-Duval B., Dercourt J., Le Richon X. From the Tethys ocean to Mediterranean seas: a plate tectonic model of the evolution of the western Alpine system. Historic Structural de Bassins Mediterraneens. 1977, pp. 143-164.

Vrielinck B. Tethys-l'histoire d'»un ocean disparu. Bureau du recherches geologiques et minieres Societe Geologique de France. Geochronique, No. 52, 1994, pp. 14-18 (in French).

Çakir Ü. Geological characteristics of the Aşiköy-Toykondu (Küre-Kastamonu) massive sulfide deposits. Mineral. Res. Expl. Bull., Ankara, No. 117, 1995, pp. 29-40.

Dixon C.J. Periere J. Plate Tectonics and Mineralization in the Tethyan Region. Mineralium Deposita, No. 9, 1974, pp. 185-198.

Güner M. Sulphide ores and geology of the Küre area, Pontides in North Turkiye. Mineral Research and Exploration Bulletin, Vol. 94, 1980, pp. 65-109.

Hannington M.D. Peter J.M. Scott S.D. Gold in sea-floor polymetallic sulfide deposits. Econ. Geol., Vol. 81, 1986, pp. 1867-1883.

Heinrich Ch.A. The physical evolution of low-salinity magmatic fluids at the porphyry to epithermal transition: a thermodynamic study. Mineralium Deposita, No. 39, 2005, pp. 864-889.

Hodgson C.L., Lyndon S.M. The geological setting of the volcanogenic massive sulfide deposits and active hydrothermal systems: some implications for explorations. Canadian Mining Metallurgical Bull., Vol. 70, 1977, pp. 95-106.

Lethch Graig H.B. Mineralogy and textures of the Lakhanos and Kizilkaya massive sulphide deposits. Northeastern Turkey and their similarity to Kuroko ores. Mineral. deposita, No. 16, 1981, pp. 241-257.

Sopko P.F. Pyrite fields of the Lesser Caucasus. Nedra. Moscow, 1971, 256 p. (in Russian).

Sosson M., Rolland Y., Muller C., Danelian T., Melkonyan R., Kekelia S., Adamia S., Babazadeh V., Kangarli T., Avagyan A., Galoyan G., Mosar J. Subduction, obduction and collision in the Lesser Caucasus (Armenia, Azerbaijan, Georgia), new insights. Geological Society, London, Special Publication No. 340, 2010, pp. 329-352.

Stackelberg L. Van and the shipboard scientific party. Hydrothermal sulfide deposits in backarc spreading centers in the Southwest Pacific. BGC Circulair, No. 27, 1985, pp. 3-14.

Taylor H.A. Oxygen and hydrogen isotopes in hydrothermal ore fields. H.L. Geochemistry of hydrothermal ore fields. Mir. Moscow, 1982, pp. 200-237 (in Russian).

Tyukhtin V.I. (ed.). Dialectics of knowledge of complex systems. Mysl. Moscow, 1988, 317 p. (in Russian).

Ustaomer T., Robertson A.H.F. Late Paleozoic-Early Mesozoic marginal basins along the active southern continental margin of Eurasia: evidence from the Central Pontides (Turkey) and adjacent regions. Geological Journal, No.120, 1993, pp.1-20.

Vrielinck B. Tethys-l'histoire d`un ocean disparu. Geochronique. Bureau du recherches geologiques et minieres Societe Geologique de France. No 52, 1994, pp. 14-18 (in French).

Willie R.J. Petrogenesis and physics of the Earth. In: Evolution of volcanic rocks (H.S.Yoder, ed.), Mir. Moscow, 1983, pp. 468-503 (in Russian).

Yardley Bruce W.D. Metal concentrations in crustal fluids and their relationship to ore formation. Economic Geology, Vol.100, No. 4, 2005, 613 p.

Yaroshevich V.Z. Genetic peculiarities of fields of the main ore formations of the Caucasus according to isotope studies. Abstract of diss. ... Cand. Geol.-Min. Sci. Tbilisi, 1985, 23 p. (in Russian)

Yigit O., Nelson E.P., Hitzman M.W. Early Tertiary epithermal gold mineralization. Bahc ecik prospect, northeastern Turkey. Mineralium Deposita, Vol. 35, 2000, pp. 689-696.

Yilmaz A., Adamia Sh,, Chabukiani A., Chkhotua T., Erdogan K., Tuzcu S., Karabiyik-oglu M. Structural correlation of the Southern Transcaucasus (Georgia) - Eastern Pontides (Turkey). In: Tectonics and Magmatism in Turkey and the Surrounding Area (Bozkurt E., Winchester L.A., Piper J.D.A., ed), Geological Society Special Publication, 173, Vol. 17, London, 2000, pp. 185-198.

Yilmaz Y., Tüysüz O., Yiğitbap E., Genç S., Şengör A.M.C. Geology and tectonic evolution of the Pontides. In: Regional and petroleum geology of the Black Sea and surrounding region (Robinson A.C., ed.), American Association Petroleum Geologists Memoir, No. 68. 1997, pp. 183-226.

Zonenshain A.P., Kovalev A.A. (eds.). New global tectonics (plate tectonics). Mir. Moscow, 1974, 471 p. (in Russian).

Mottl M.J., Holland H.D., Corr R.F. Chemical exchange during hydrothermal alteration of basalts seawater. Experimental results for Fe, Mn and sulfur apecies. Geochim. et acta, Vol. 43, 1979, pp. 869-884.

Okay Л.L., Şahintürk O. Geology of the Eastern Pontides. In: Regional and petroleum geology of the Black Sea and surrounding region (Robinson A.G., ed.), American Association Petroleum Geologists Memoir, No. 68, 1997, pp. 291-311.

Popovic R. Auriferous mineralization in the Murgul-Artvin-Maradit area (Northeastern Turkey). Mineral Res. Expl. Bull., No.129, 2004, pp. 17-29.

Seward T.M. The formation of lead (II) chloride complexes to 300°C: A spectrophotometric study: Geochimica et Cosmoshimica Acta. Vol. 48, 1984, pp. 121-134.

Sosson M., Rolland Y., Muller C., Danelian T., Melkonyan R., Kekelia S., Adamia S., Babazadeh V., Kangarli T., Avagyan A., Galoyan G., Mosar J. Subduction, obduction and collision in the Lesser Caucasus (Armenia, Azerbaijan, Georgia), new insights. Geological Society, London, Special Publication No. 340, 2010, pp. 329-352.

Sherlock R.L., Barret T.I., Lewis P.D. Geological setting of the Rapu Rapu gold-rich volcanogenic massive sulfide deposits, Albay Province, Philippines. Mineralium deposita, No. 38, 2003, pp. 813-830.

Shepherd T.J., Rankin A.H., Aiderton D.H.M. A practical guide to fluid inclusion studies. Blaskie. Glasgow and London, 1985, 239 p.

Stackelberg L. Van and the shipboard scientific party. Hydrothermal sulfide deposits in backarc spreading centers in the Southwest Pacific. BGC Circulair, No. 27, 1985, pp. 3-14.

Ustaömer T., Robertson A.H.F. Late Paleozoic-Early Mesozoic marginal basins along the active southern continental margin of Eurasia: evidence from the Central Pontides (Turkey) and adjacent regions. Geological Journal, No. 120, 1993, pp.1-20.

Yardley Bruce W.D. Metal concentrations in Crustal Fluids and Their Relationship to Ore formation. Economic Geology. V.100, No. 4, 2005, 613 p.

Yigit O., Nelson E.P., Hitzman M.W. Early Tertiary epithermal gold mineralization. Bahc ecik prospect, northeastern Turkey. Mineralium Deposita, No. 35, 2000, pp.689-696.

Yilmaz A., Adamia Sh,, Chabukiani A., Chkhotua T., Erdoöan K., Tuzcu S., Karabiyik-oğlu M. Structural correlation of the Southern Transcaucasus (Georgia) – Eastern Pontides (Turkey). In: Tectonics and Magmatism in Turkey and the Surrounding Area (Bozkurt E., Winchester L.A., Piper J.D.A, eds.). Geological Society Special Publication, Vol. 173, No. 1, London, 2000, pp. 185-198.

Yilmaz Y., Tüysüz O., Yiğitbap E., Genç S., Şengör A.M.C. Geology and tectonic evolution of the Pontides. In: Regional and petroleum geology of the Black Sea and surrounding region (Robinson A.C., ed.). American Association Petroleum Geologists Memoir, No. 68, 1997, pp. 183-226.

ЗОЛОТОСОДЕРЖАЩИЕ ВУЛКАНОГЕННЫЕ МЕСТОРОЖДЕНИЯ ЦВЕТНЫХ МЕТАЛЛОВ МАЛОГО КАВКАЗА И ВОСТОЧНЫХ ПОНТИД И ИХ ГЕНЕЗИС

Баба-заде В.М.[1], Абдуллаева Ш.Ф.[1], Новрузова С.Р.[1], Ибрагимов Дж.Р.[2]
[1]Бакинский Государственный Университет, Азербайджан
Az 1148, Баку, ул. акад. Захид Халилова, 33: vasifbabazadeh1938@bsu.edu.az;
shakhla.a@gmail.com; samiranovruzova001@gmail.com
[2]Azerbaijan International Mining Company Limited
AZ1065, Баку, ул. Измир, 2: Javid.Ibrahimov@aimc.az

Резюме. В странах Южного Кавказа и Турции наиболее представительные золотосодержащие вулканогенные месторождения известны в толщах, слагающих фрагменты Понтийско-Южнокавказской палеодуги, активно функционировавшей в течение мезозойского времени. В это время под дугу, которая являясь краевой частью Евразийского континента, субдуцировалась океаническая кора. Отдельные сегменты дуги различались своим геодинамическим развитием, в связи с чем в них возникали разнотипные вулканогенные месторождения. На западе, в пределах Понтид (Турция), помимо эпигенетических, известны и гидротермально-осадочные залежи. Примером последних может служить месторождение Чаели (Маденкой).

В статье вкратце охарактеризованы геологические обстановки нахождения месторождений Турции, Азербайджана, Армении и Грузии. Большинство из них могут быть отнесены к типу Куроко и отличаются характером накопления руд: в Турции известны медно-цинковые залежи, сформированные, по-видимому, в условиях глубоководного бассейна, а восточнее – мы имеем примеры лишь эпигенетических месторождений. Кроме того, в Болнисском районе разрабатывается Маднеульское месторождение, которое являет собой пример полиформационного месторождения и поэтому уникально.

Гядабейский и Алавердский рудные районы, интересны тем, что в них в юрских вулканодепрессиях сосредоточены медные, медно-цинковые и барит-сульфидные руды, а в приподнятых клиновидных блоках, ограничивающих вулканодепрессии, известны медно-порфировые месторождения – Карадагское и Тутхунское. Все месторождения Гядабейского и Алавердского рудных районов, включая медно-порфировые, являются промышленно значимыми.

На базе собранного литературного материала, который накапливался в течение ряда лет, а также собственных данных, была создана мысленная логическая геолого-генетическая модель вулканогенных месторождений.

Месторождения вулканогенной природы, несмотря на то что формируются в сходных РТХ-условиях, имеют свой «облик», учет которого крайне важен при прогнозировании месторождений в конкретных районах.

Ключевые слова: *месторождение, рудный район, палеодуга, включение, флюид, изотоп.*

KİÇİK QAFQAZIN VƏ ŞƏRQİ PONTİDLƏRİN ƏLVAN METALLARININ QIZILSAXLAYAN VULKANOGEN YATAQLARI VƏ ONLARIN GENEZİSİ

Babazadə V.M.[1], Abdullayeva Ş.F.[1], Novruzova S.R.[1], İbrahimov C.R.[2]
[1]Bakı Dövlət Universiteti, Azərbaycan
Az 1148, Bakı şəh., akad. Zahid Xəlilov küç., 33: vasifbabazadeh1938@bsu.edu.az;
shakhla.a@gmail.com; samiranovruzova001@gmail.com
[2]Azərbaycan İnterneyşnl Mayning Kompani Limited Şirkəti
AZ1065, Bakı şəh., İzmir küç., 2: Javid.Ibrahimov@aimc.az

Xülasə. Cənubi Qafqazda, o cümlədən Türkiyədə, mezozoy erasında aktiv olan Pontid-Cənubi Qafqaz paleoqövsünün fraqmentlərini təşkil edən təbəqələrdə qızılsaxlayan vulkanogen yataqlar müəyyən edilmişdir. Həmin dövrlərdə okean qabığı Avrasiya materikinin marjinal hissəsi olan qövsün altına gömülmüşdür. Qövsün ayrı-ayrı seqmentləri geodinamik inkişafı ilə fərqlənirdi, buna görə də onlarda müxtəlif tipli vulkanogen yataqlar yaranmışdır. Qərbdə, Pontidlər (Türkiyə) daxilində, epigenetik yataqlardan başqa hidrotermal-çökmə yataqları da mövcuddur. Sonunculara misal olaraq Çayeli yatağını (Madenköy) göstərmək olar.

Məqalədə qısaca olaraq yataqların Türkiyə, Azərbaycan, Ermənistan və Gürcüstanda yaranmasının geoloji mühitindən bəhs edilir. Onların böyük əksəriyyəti Kuroko tipinə aid edilə bilər və filizliliyin zənginliyinə görə fərqlənirlər: Türkiyədə, çox guman ki, dərin sulu hövzədə formalaşmış mis-sink kütlələri formalaşmışdır, şərqdə isə bir yalnız epigenetic yataqları görürük. Bundan başqa Bolnisi rayonunda istismar olunan Madneuli yatağının poliformasion tipə malik olmasını qəbul etməliyik və bu səbəbdən unikaldır.

Gədəbəy və Allahverdi filiz rayonları onunla maraq doğurar ki, burada yuranın vulkanodepressiyalarında mis, mis-sink və barit-sulfid filizlərin cəmləşmişlər, vulkan depresiyalarını məhdudlaşdıran yuxarı qalxmış paz şəkilli bloklarda isə mis-porfir yataqları – Qaradağ və Texut – məlumdur. Gədəbəy və Allahverdi filiz rayonlarının məlum yataqları, o cümlədən mis-porfir yataqları, sənaye əhəmiyyətlidirlər.

On illərlə toplanılan fond materialları, eləcə də aparılmış tədqiqatlarımız əsasında vulkanogen sahələrin mental məntiqi geoloji-genetik modeli yaradılmışdır.

Vulkanogen mənşəli yataqlar, oxşar geoloji şəraitdə əmələ gəlmələrinə baxmayaraq, özünə məxsus olan xüsusiyyətlərə malikdir, bu isə konkret rayonlarda yataqların proqnozlaşdırılması zamanı nəzərə alınmalıdır.

Açar sözlər: *yataq, filiz rayonu, paleoqövs, daxilolma, flüid, izotop*

THE USE OF GLOBAL GRAVITY FOR MAPPING THE RELATIONSHIP BETWEEN SEISMICITY AND GEOLOGIC STRUCTURE IN THE MIDDLE PART OF ACEH PROVINCE, INDONESIA

Yanis M.[1], Abdullah F.[1,2], Ananda R.[3], Syamsyudin F.[1,2],
Ismail N.[1,2], Zainal M.[1], Paembonan A.Y.[4]

[1]*Geophysical Engineering Department, Syiah Kuala University*
Banda Aceh 23111, Indonesia: yanis@usk.ac.id
[2]*Physics Department, Syiah Kuala University*
Banda Aceh 23111, Indonesia
[3]*Department of Geophysical Engineering, Bandung Institute of Technology*
Bandung 40132, Indonesia
[4]*Geophysical Engineering Department, Sumatra Institute of Technology*
Lampung Selatan 35365, Indonesia

Summary. Aceh is one of the Indonesian provinces prone to earthquakes because it is traversed by the Great Sumatra Fault and the subduction zones along its west coast with high seismic activity. Recently, fault mapping research has focused on the Aceh and Seulimum segments in the western part of Aceh Province. In contrast, the central part has yet to be studied significantly, even though several earthquakes in the last 10 years have occurred in the areas where fault traces still need to be mapped properly. Therefore, this study used the global gravity model Plus (GGM+) with a high resolution of 200 m/px to analyze the relationship between seismicity and fault structures in the Central part of Aceh. The residual anomaly from GGM+ indicates that the existence of geological structures such as the Aceh, Pameu, and Samalanga segments are characterized by low gravity. Several derivative methods were also applied to clarify the existence of a fault, such as the horizontal derivative anomaly for mapping the Aceh, Batee, Samalanga, and Alue Lintang – Peusangan segments. The vertical derivative shows the existence of the Tringgadeng Fault, suspected as a source of the Pidie Jaya earthquake in 2016. Therefore, the tilt derivative can also visualize the presence of the Nissam fault, which is not shown in other filter methods. We also carried out a 3D gravity modelling using the Occam algorithm and Singular Value Decomposition (SVD); the density shows the fault structure's depth and geometry, generally 8 km, thus providing reliability of GGM+ in fault studies, especially in high elevation areas, which are challenging for instrument mobilization.

1. Introduction

The province of Aceh is traversed by the Great Sumatran Fault (GSF) line, which stretches ~1.900 km from Lampung to the Andaman Islands (McCaffrey, 2009; Hill et al., 2015). Seismicity data also shows that the southern part of Sumatra has experienced a lot of seismic activities, while the northern part has not released significant earthquakes for 170 years (Sieh and Natawidjaja, 2000). So, it is estimated that the Aceh Province has a potential for a big magnitude earthquake with Mw ≥ 7 if the stored energy in that area is released over a long period (Ito et al., 2012). This is a serious future threat to the Aceh

region, considering that earthquakes on land are usually very harmful (Muksin et al., 2019). The GSF fault is divided into 19 segments, starting from the southernmost with a small strike-slip and increasing to the northern part of the island of Sumatra. Two earthquakes with a magnitude of Mw 7.7 occurred in 1936, and Mw 6.5 in 1964 caused severe damage around Banda Aceh (Fig.1), and another earthquake with a magnitude of Mw 9 in 2004 shocked Sumatra, followed by a tsunami (Lay et al., 2005). This event triggered aftershocks in the subduction zone and several segments of the GSF (Natawidjaja and Triyoso, 2007). Even though several researchers

have focused on the western part, Aceh and Seulimum Segments (Yanis et al., 2021b; Ghosal et al., 2012; Muksin et al., 2018). However, several recent earthquake events occurred at locations where the faults had not been mapped significantly, as shown in Figure 1. Significant seismic activity data from the USGS in the North Aceh region had a magnitude of Mw 2-6.5. Several destructive earthquakes also occurred in the Aceh Province, such as in Pidie Jaya in 2016 with Mw 6.5, which resulted in 101 fatalities and more than 800 people were injuries, as well as damage to various public infrastructures and the Takengon earthquake on July 2, 2013, which resulted in 30 people died.

Gravity data have been proven to be used to map subsurface fracture structures (Hiramatsu et al., 2019; Vos et al., 2006). However, for areas that are very large and difficult to access, the measurements are usually carried out by airplane, which requires a lot of funding and becomes an obstacle for developing countries. Fortunately, nowadays, there are free-access gravity satellite data with different resolutions, such as the GOCE and GRACE satellites with a resolution of 5 km/px (Rexer and Hirt, 2015), TOPEX/Poseidon satellite with a resolution of 1.3 km/px (Chatterjee et al., 2007; Yanis et al., 2021a),

and Global Gravity Model plus (GGM+) data which combines GRACE, GOCE and EGM2008 data to obtain a high gravity data of 200 m/px (Hirt et al., 2013; Yanis et al., 2022). In this study, we processed the GGM+ data using 3D transformation and inversion to find correlations between seismicity data and fault structures in the central region of Aceh.

The application of gravity method has been successfully applied in several areas, such as for mapping fault structures in the Andaman Sea (Purnachandra Rao et al., 2011; Yanis et al., 2023), the Aceh and Seulimum segments (Yanis et al., 2021b), and it is even used to visualize local faults in the Geuredong volcano in the central part of Aceh and the geological structure on the Weh Island (Abdullah et al., 2022). In addition, satellite gravity data have been confirmed to have the same anomaly responses as Shipborne Gravity data over the Indian Offshore Regions (Chatterjee et al., 2007) and in Hudson Bay (Keating and Pinet, 2013). In the regional area, the global gravity data also has the potential to map the geological structure of the eastern Mediterranean region with its complex geology, so that it can be used as an important implication for tectonic-seismological analysis in the region (Eppelbaum and Katz., 2012, 2015).
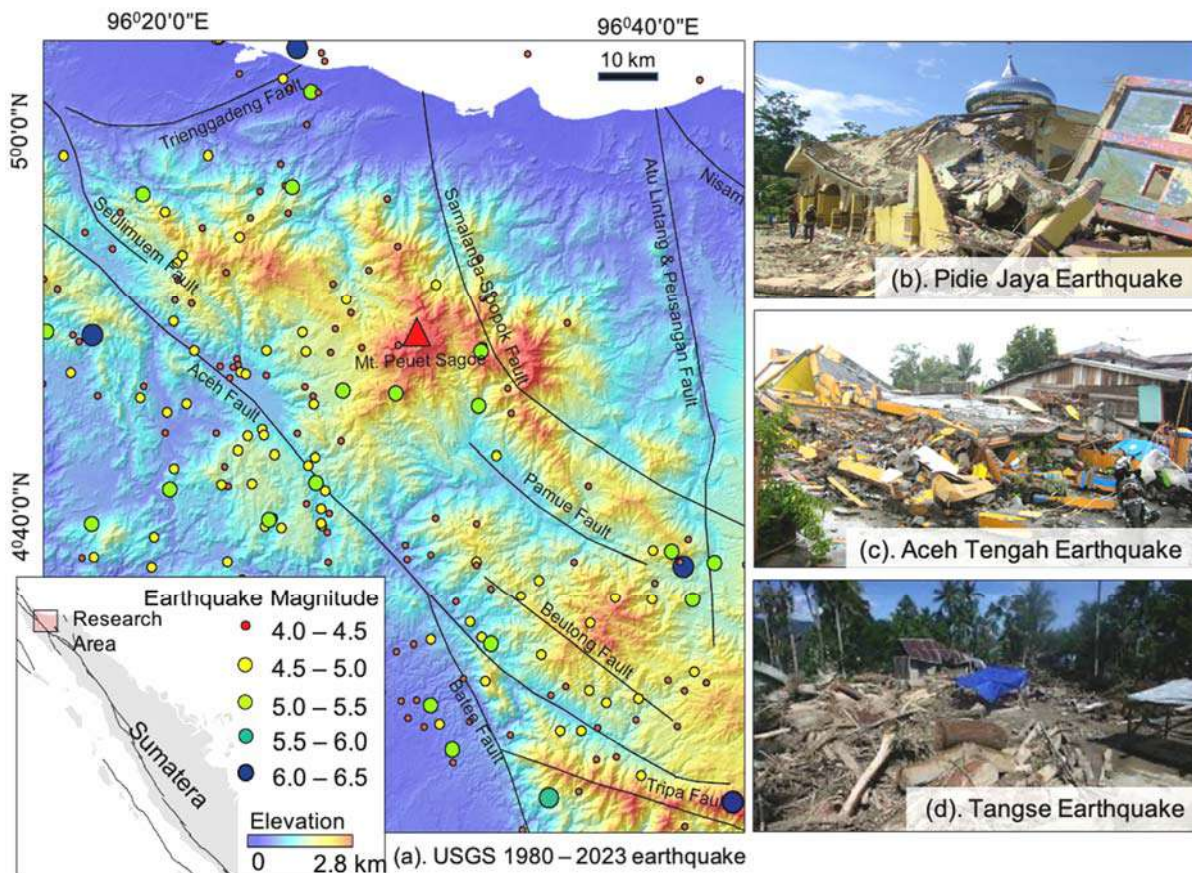
Fig. 1. (a) The distribution of earthquake magnitudes along with the Tringgadeng Segment to the Tripa Fault in the central part of Aceh from 1980-2023 obtained from the USGS, some of the damage caused by earthquakes that occurred along the Great Sumatran Fault such as (b) Pidie Jaya Earthquake on 6 December 2016, (c) Earthquake Central Aceh on Tuesday 2 July 2013, and (d) Tangse Earthquake which occurred on 22 December 2013

The data also shows a similar pattern to the ground gravity data (Yanis et al., 2021b; Yanis et al., 2023). These facts could make global gravity data, the main tool for studying geological structures on a global scale.

2. Geological and Tectonic Framework

The formation of geological structures in Aceh is generally influenced by tectonic activities from convergent forces of two plates, the Eurasian and Indo-Australian Plates, which form subduction zones along the Southwest of Sumatra Island (Bradley et al., 2017; Sieh and Natawidjaja, 2000; Yanis et al., 2023). As a result, it has produced a row of Bukit Barisan and GSF, which divides the island from the Andaman Sea to Semangko Bay. The GSF that transverses Aceh is divided into four main segments, the Aceh, Seulimuem, Tripa, and the Batee Segment, where the Aceh Segment stretches from the Central Aceh to the Aceh Island in a northwest-southeast direction for 200 km (Rizal et al., 2019; Ghosal et al., 2012; Sieh and Natawidjaja, 2000; Yanis et al., 2021b).

The Seulimuem Segment structure stretches for 120 km and continues to Weh Island in the northern part of Banda Aceh. This segment also passes the Seulawah Agam volcano in the southwest (Marwan et al., 2022; Marwan et al., 2021). The tectonic history of the Seulimuem Segment recorded earthquakes of Mw > 6.4 in 1936 and 1965 (Muksin et al., 2019; Sieh and Natawidjaja, 2000). The modified geological map (Fig, 2) shows that several rock formations, such as the Alluvium, Keutapang, Idi, Geumpang, Kluet, and Meulaboh formations dominate the study area. These rock formations are formed from various types of rocks, including intrusive and extrusive igneous rocks, clastic and non-clastic sedimentary rocks, and metamorphic rocks. Clastic sedimentary rocks dominate areas near the coast and lowlands, caused by weathering transported to those places.
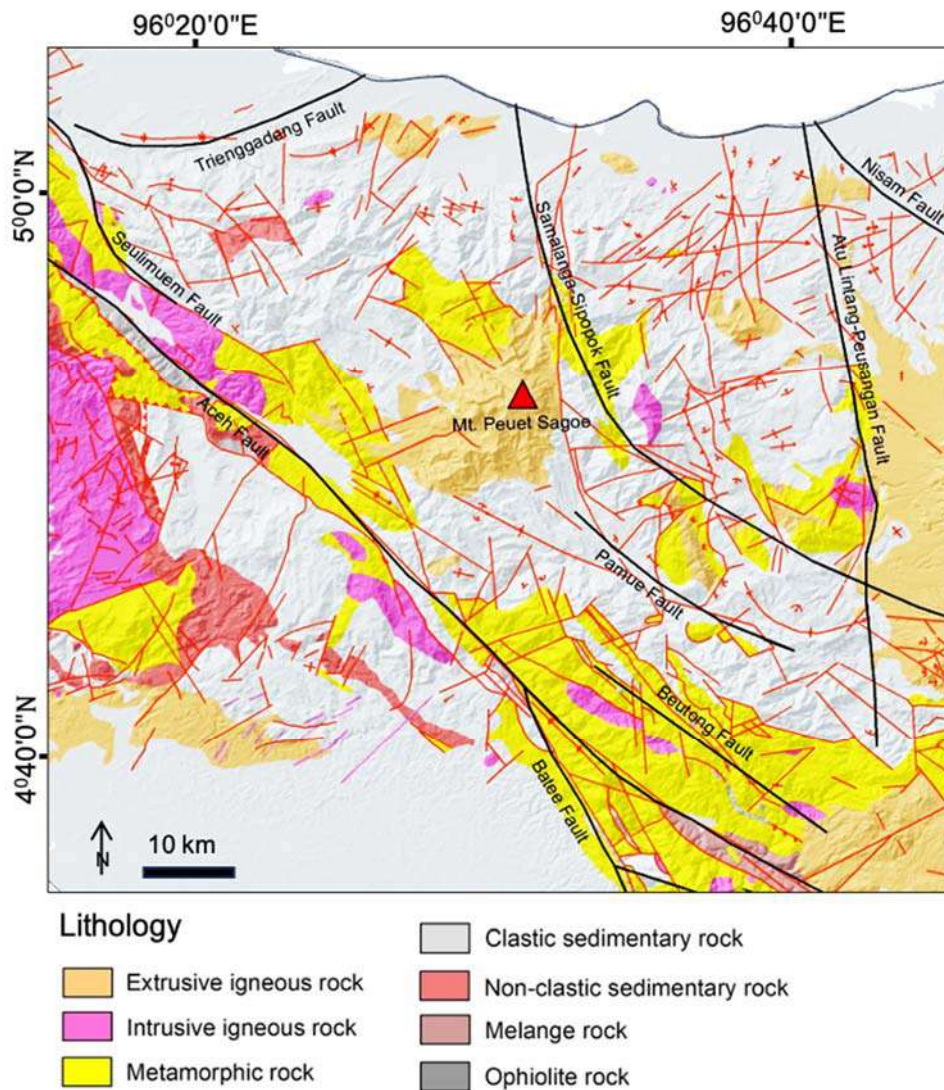
Fig. 2. A geological map shows the distribution of rocks dominated by metamorphic and igneous rock in the study area; the red line is the geological structure, while the black line is the GSF fracture from several segments

The research area also contains several fault segments of the GSF, such as the Tripa and Batee Segments. This area also has a significant role in seismic activity in Aceh, where there have been devastating earthquakes originating from the Tripa Segment with a magnitude of Mw 6.0 in 1990 and 1997. In addition, several other active faults spread across the central part of Aceh play a role in seismic activity. Tectonic activity in the subduction zone and the GSF line in Aceh has resulted in a high frequency of earthquakes. Since 2010-2023, there have been many earthquakes of various magnitudes. The strength of the earthquakes that occurred in that time interval was dominated by magnitudes Mw 4.0-5.0. In addition, several other earthquakes occurred with magnitudes Mw 5.1-7.8, and some were destructive, especially those at magnitudes Mw > 6.0 (Muzli et al., 2018; Muksin et al., 2018).

3. Theory and Data observation
3.1 Basic Theory of Gravity

The basic principle of the gravitational field is an attractive force that arises between two objects with masses as Newton's law of gravity states that the value is proportional to the multiplication of the masses and inversely proportional to the square of the distance between their centers of mass (Hinze et al., 2010). Many methods can be used to acquire gravity data, starting from marine, ground and airborne surveys, besides global observation data are freely available which is acquired using satellites (van der Meijde et al., 2015; Kern et al., 2003; Yanis et al., 2022). Satellite gravity data have been corrected for several parameters so that it is generally available in the free-air anomalies (Andersen and Knudsen, 2000; Dewanto et al., 2022). Currently, many satellites provide gravitational field data on the earth's surface, i.e. the European Space Agency, the ERS-1 satellite, and the Geodetic Satellite, which recorded gravitational field data above the earth's surface. Unfortunately, the resolution of the data is in the range of 2-25 km globally, so it is generally used for studies in large areas (Pavlis et al., 2012). In addition, there are also gravity field data, which have a high resolution of up to 200 m/px obtained from a combination of GRACE and GOCE satellite data, namely the Global Gravity Model Plus (GGM+) data, which have been widely used for various studies of geological structures in large and local areas.(Tassis et al., 2013; Yanis et al., 2022; Hirt et al., 2013; Chatterjee et al., 2007).

3.2 Global Gravity Model Plus (GGM+)

GGM+ is satellite gravitational field data obtained from the results of a combination of 3 satellites: GRACE, GOCE gravity satellites (spatial scale ~10,000 km to ~100 km), and EGM2008 (spatial scale ~100 km to ~10 km). In general, the GGM+ model data is calculated based on the following equation.

$$\left[\sum_{i=1}^{4}(A^T\Sigma(l)^{-1}A)_{GOCE,i} + (A^T\Sigma(l)^{-1}A)_{GRACE}\right]x =$$
$$= \left[\sum_{i=1}^{4}(A^T\Sigma(l)^{-1}l)_{GOCE,i} + (A^T\Sigma(l)^{-1}l)_{GRACE}\right] \quad (1)$$

where A is the Jacobian matrix, l is the observed value of gravity, and Σ is a form of realistic variances. The unknown spherical harmonic coefficient is represented as x. The GRACE calculation component consists of ITG-GRACE2010s data obtained based on GRACE's k-band spanning rates and kinematic orbit data in the 2002-2009 time interval.

3.3 Free Air Anomaly

GGM+ provides high-resolution data of 200 m/px, covering all land areas and can be accessed freely via http://ddfe.curtin.edu.au/gravitymodels/ GGM+/. Several data types are obtained from GGM+, such as gravity disturbance, acceleration, North-South deflection, East-West deflection, and quasi-geoid height. Only the gravity disturbance data is equivalent to free-air anomaly data, which is used to interpret the geological structure of Central Aceh with an area of 111 km x 111 km. Figure 3 shows a comparison of the resolution between the available gravity data from several sources in the study area, where GGM+ data has 250,000 data points, Earth Gravitational Models (EGM) 2008 has 576 points, and World Gravity Map (WGM) 2012 has 961 data stations. Hence, the resolution from GGM+ is very good for studying geological structures in the local areas, as also found by (Hirt et al., 2014) and (Dewanto et al., 2022).

3.4 Enhancement Technique

Analysis of subsurface structures such as faults can be performed through gravity data transformation. For fault studies, data transformation is carried out through several types of derivative analysis, including the first horizontal derivative, a technique for filtering the gravity value for the first derivative of the horizontal plane. HD or horizontal gradient can be used to see changes in the rate of gravity values towards x and y directions in units of mGal/m, as shown in eq.2

$$HD(x,y) = \sqrt{\left(\frac{\partial \Delta g}{\partial x}\right)^2 + \left(\frac{\partial \Delta g}{\partial y}\right)^2} \quad (2)$$

Where $\frac{\partial \Delta g}{\partial x}$ and $\frac{\partial \Delta g}{\partial y}$ are the first derivative of the gravity anomaly in the x and y horizontal directions.
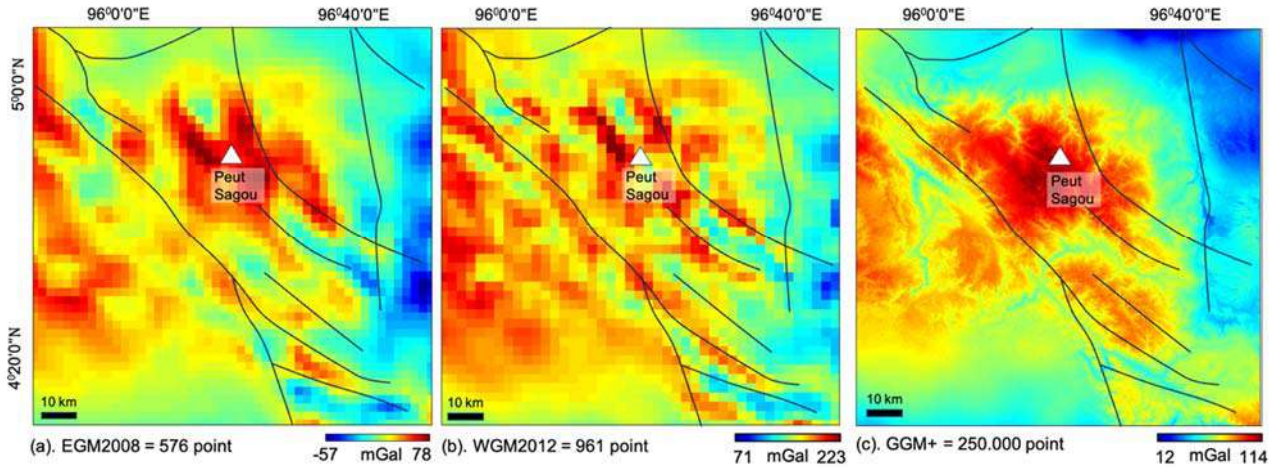
Fig. 3. Comparison of gravity anomaly from several satellite data with different resolutions in the research area, (a) Earth Gravitational Models (EGM) 2008 with a total of 576 points, (b) World Gravity Map (WGM) 2012 with 961 data points, and (c) GGM+ with a resolution of 200 m/px and 250,000 total data points

In addition, there is also a first vertical derivative method that calculates the first derivative in the vertical direction from the gravity data. The vertical derivative (VD) is mathematically calculated using the Laplace equation (Vaish and Pal, 2015).

$$VD = \frac{\partial^2 \Delta g}{\partial z^2} = - \left(\frac{\partial^2 \Delta g}{\partial x^2} + \frac{\partial^2 \Delta g}{\partial y^2} \right) \qquad (3)$$

where Δg is the value of the gravity anomaly, x and y are the components of the horizontal direction, and z is the vertical direction component. A filter was also obtained by comparing the vertical plane derivative with the absolute amplitude of the total horizontal plane derivative, namely the tilt derivative. This filter can detect the boundaries of geological structures based on the angle obtained from comparing vertical and horizontal derivatives, which can be written mathematically (Doğru et al., 2017).

$$TDR = tan^{-1} \left(\frac{\frac{\partial^2 \Delta g}{\partial z^2}}{\sqrt{\left(\frac{\partial \Delta g}{\partial x}\right)^2 + \left(\frac{\partial \Delta g}{\partial y}\right)^2}} \right) \qquad (4)$$

where $\frac{\partial \Delta g}{\partial z}$ is the vertical derivative in the z-direction.

4. Result and Interpretation
4.1 Bouguer Anomaly

To get the Bouguer anomaly, assuming the density that dominates the study area is necessary. The parameter is obtained from a geological map generally composed of alluvial clastic sedimentary rocks. The density value of this rock is in the range of 1.96-2.10 g/cm³ with an average value of 2.05 g/cm³. This average value is used in the calculation of the Bouguer correction. The results of the Bouguer anomaly were also overlaid with the fault structure obtained from several previous studies (Muksin et al., 2018; Sieh and Natawidjaja, 2000). After the Bouguer and terrain correction was made using the SRTM 30 m/px data, a complete Bouguer anomaly was obtained as shown in Fig. 4a, which varies between 12-114 mGal as a representative of the difference of rock density in the middle part of Aceh area. High Bouguer values (80-114 mGal) are found in the middle of the study area which is the response to high topography and the accumulation of densities in the form of intrusive igneous rocks from the Peut Sagoe Volcano. At the same time, the east and the south side areas are dominated by low Bouguer values (12-18 mGal), which are the response to the metamorphic rock density of the study area.

In some areas that are estimated to have regional faults, such as the Aceh and Seulimum Segments, the Bouguer data show the existence of the geological features through relatively low-value data that infiltrate high-value data. The pattern is also seen in the Pameu and Beutong Segments. However, the existence of other faults, such as the Tringgadeng Segment, which caused a 6.3 Mw earthquake in 2016, cannot be shown properly. The same things also happened in the Batee and Samalanga Segments. Therefore, we separated the residual and regional anomalies from the gravity data. The anomalies were separated using a cut-off wavelength of 50,000 m obtained from wave spectrum analysis through a Fourier transform (Pham et al., 2020). The residual anomalies were generated by applying high-pass filtering which allows high-frequency data representing near-surface anomalies as shown in Fig.4b.
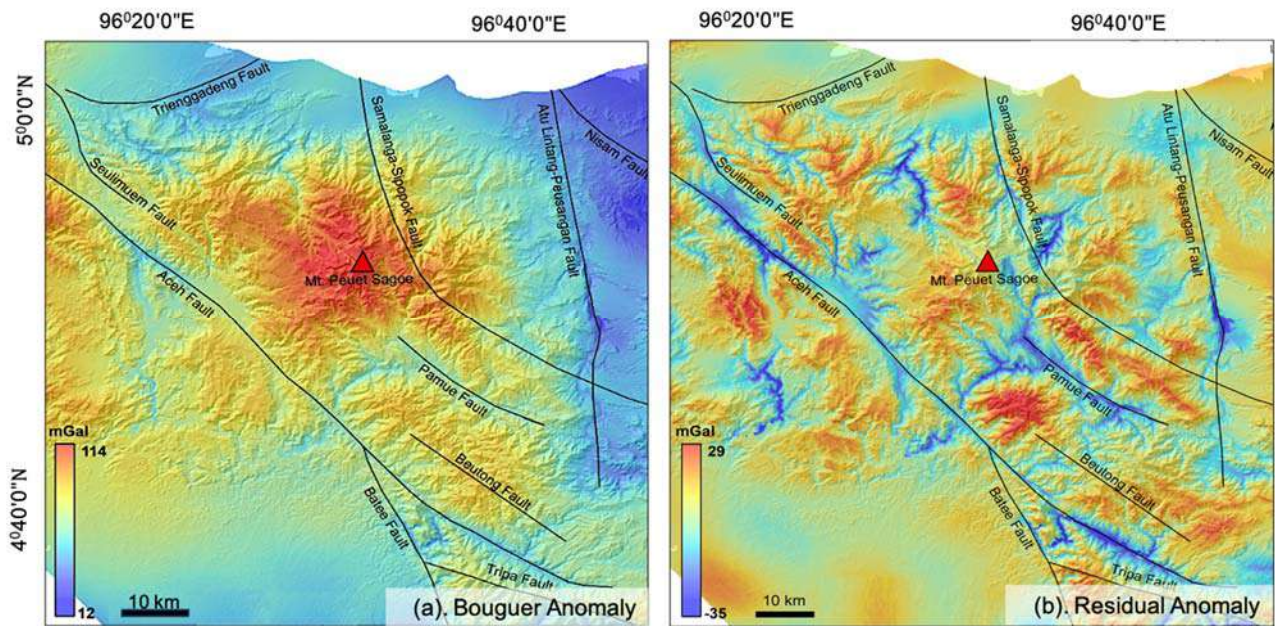
Fig. 4. (a) Complete Bouguer anomaly from GGM+ that was corrected for terrain using SRTM 30m/px data, high Bouguer values are found in the volcanic areas and several faults, while low Bouguer values dominate Tringgadeng dan Nissam Fault, while (b) is a residual anomaly from the Bouguer data indicating the presence of a fault in Central Aceh

The residual anomaly varies between -35 to 29 mGal, representing the subsurface density value from the local anomaly, where the high Bouguer value is no longer focused on the volcanic area but is evenly distributed in all places as a response to the geological features. Residual anomaly data can clearly show the existence of several faults generally characterized by low gravity values (-35 to 5 mGal), such as the Aceh Segment which runs straight from east to west of the study area. In addition, the residual anomaly data can reveal the existence of the Pameu Segment in the NW-SE direction which was previously not clear in the Bouguer anomaly. The same thing can also be seen in the Samalanga – Sipopok Segment, which is characterized by low and flanked by high anomalies. The existence of the Seulimum Segment in the NW-SE direction and the Alue Lintang-Peusangan Segment in the N-S direction, which caused significant seismic activity in Aceh Province, was also previously unclear in the Bouguer data. Still, the segments can be described clearly in the residual anomaly data. Although the residual values can show the existence of the faults, several faults still cannot be described properly, such as the Beutong Segment in the NW-SE direction and the Trienggadeng Segment in the SW-NE direction, which caused the 2016 earthquake in Pidie Jaya. Therefore, it is necessary to do some data enhancement using digital filtering to clarify the presence of subsurface geological features (Pham et al., 2020; Nasuti et al., 2012; Yanis et al., 2021a).

4.2 Derivative Anomaly

Qualitative interpretation techniques were used to clarify the existence of geological structures, such as the horizontal derivative (Fig.5a) which is the first derivative of the gravity data to its coordinates. According to Cooper (2006), fault structures and geological features from horizontal derivative results indicate areas flanked by high and low values side by side. The results of the first derivative in the horizontal direction vary between 0.045-5 mGal/m, where the low values are at the edge of the research area without geological structure (Bennett et al., 1981). Whereas in the middle area there are several faults dominated by high and low values which represent the existence of subsurface structures, such as the Aceh, Batee, Samalanga-Sipopok Segments and also the Alue Lintang-Peusangan Segment. The existence of these faults can be easily differentiated from the surrounding areas such as at the junction of three faults, The Batee, Tripa, and Aceh Segments indicated by high horizontal derivative values. However, other geological features, such as the Nisam Fault, cannot be mapped caused by slow tectonic motion. So that traces of these structures are not visible on the surface.

For that purpose, we clarify the existence of the features using another technique called tilt derivative which has a range of values from $-\pi/2$ to $\pi/2$ or -1.57 radian to 1.57 radian, as shown by Fig. 5b. where the tilt will be positive above the source of the anomaly, zero at the edge of the structure, and a negative value outside of the object. So the tech-

niques are very useful for simplicity in detecting the geological structures and the host area around the anomaly (Cooper and Cowan, 2006; Yanis et al., 2021b). Based on the tilt derivative data, it can be shown that 0 rad is the edge of the structure in an area where there are fault segments, such as the Batee Fault which is visible extending from the NW-SE direction, and the Aceh Segment which also intersects with the Batee Fault.

In addition, the Nisam Fault which previously could not be mapped by the horizontal filter, the tilt derivative can visualize the existence of the structure in the NW-SE direction which is characterized by high radian values. The same thing can be seen from the Pameu and Beutong Faults, which previously could not be mapped properly. As a complementary, the vertical derivative values were also calculated which only focused on several faults, especially for fault areas that cannot be described by the two previous filters, such as the western part (Fig. 5c) and the eastern (Fig. 5d) of the measurement location.

The vertical derivative anomaly in the vertical direction varies between -0.072 to 0.054 mGal/m. On the left side of the Trienggadeng Fault structure, the anomaly can be described well through the high derivative values which extend in the W-E direction, even though the existence of the fault that caused the Pidie Jaya Earthquake in 2016 is not visible on the surface. The same is also illustrated for the Seulimum Segment, which has significant seismic activity. The vertical anomaly can visualize a structure that extends in the NW-SE direction close to the Aceh Segment.

In the area between Trieggadeng and Seulimum Fault, several other high and low anomalies are suspected to be a response to local geological structures caused by the vertical derivative in meters. In the eastern part of the study area, the vertical derivative data can properly describe the existence of the Aceh Faults in the NW-SE direction, which is characterized by a low derivative value as a response to the edges of the subsurface anomaly structure. The same thing can be seen from the Batee Fault which is dominated by seismicity with 4.0-5.5 Mw, while at the Tripa and Beutong Segments the seismic activities are < 5 Mw which cannot be described from the previous filter. So, this vertical derivative can also show the existence of these faults with high values as a representation of the local structure from the other faults.

4.3 3D inversion model of Gravity

To obtain geological depth in the subsurface, such as faults, we carried out a 3D modelling by integrating the geological and seismicity data as the model's constraints. The 3D modelling was done using the GRABLOX 1.6 Software developed by (Pirttijarvi, 2008; Yanis et al., 2022; Yanis et al., 2023). In the calculation process, the Singular Value Decomposition (SVD) and Occam's Inversion were used to get the best density solution that correlates with the actual condition below the surface. The SVD algorithm decomposes a matrix into two matrices, while Occam's Inversion is an inversion method that utilizes the model's roughness level. Mathematically the density value from the inversion results is calculated using the following equation.

$$\Delta g\ (\boldsymbol{r}) = g_z\ (\boldsymbol{r}) = G \frac{\partial}{\partial_z} \int_v \frac{\rho(r')}{|r-r|} dV' \qquad (5)$$

G is the gravity constant $\boldsymbol{r} = (x - x_0)\boldsymbol{i} + (y - y_0)\boldsymbol{j} + (z - z_0)\boldsymbol{k}$ that provide the vector position of the data measuring, r is a vector in volume V integration, and $\rho(r')$ is the volume of material density at the location V. The initial step in this inversion is determining the number of grids as model parameters, where the x and y axes are divided into 20 blocks (nx = 20, ny = 20) while the z-axis is ten blocks (nz = 10). The initial model length in the x and y directions is 111 km (dX = 30 km, dY = 111 km) with a model depth of 30 km (dZ = 30 km). This depth information was obtained from analysis of the USGS seismicity data from 1980-2023. So, the total number of blocks (N = nX x nY x nZ) is obtained as many as 4,000 blocks, and each block represents an area of 5.5 km for the x and y directions and 3 km for the z-direction. The selected background density is 2.67 gr/cc as a response to the average density in the earth's crust. Specifically, the optimal 3D gravity inversion models and blocks in the middle of the Aceh region are shown in Fig. 6. Using a computer powered by a Core i5 processor and 8 GB RAM capacity. It took about 25 hours to complete the inversion process, with 10 times the number of iterations needed to get the best model solution. The RMS data obtained from the inversion process was 5.21%.

The interpretation of the 3D model was carried out on the slice depth that cuts through the fault structure, as shown in Fig. 7 with a density range of 2-3 gr/cc. At a depth of 0 km (Fig. 7a), there are high-density values of 2-2.3 gr/cc spread in the middle, which is suspected as an intrusive igneous rock type associated with the volcanic activities of the Peut Sagoe volcano. The high-density values of 2.4-2.65 gr/cc are also found in the western part as a representative of extrusive igneous rocks such as rhyolite and andesite. However, low-density rocks dominate the Nisam, Beutong, and Tripa Faults on the east side. The seismic traces of the earthquakes in these areas are relatively small com-

pared to the Aceh and Seulimum Segments on the west side as it is known that each fault has its characteristics, including depth and geometry which greatly affect the impact of the damage caused. For example, the identified Trienggadeng Fault is at a depth of 3 km. The density data at 0 to 10 km can show this segment's existence, characterized by high-density values. Still, this structure cannot be visualized completely due to the sedimentation process on the surface.
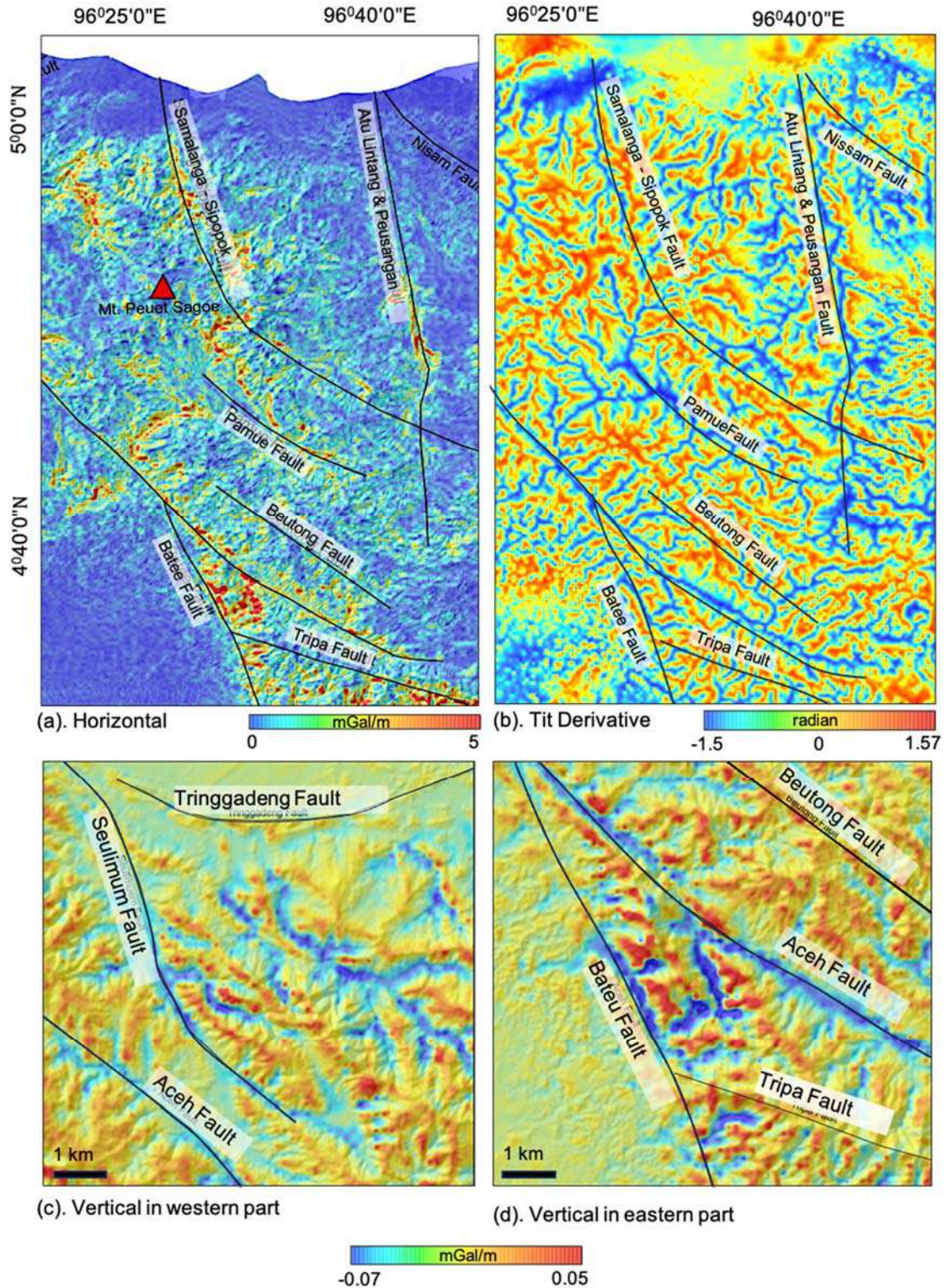
Fig. 5. The Bouguer data transformation clarifies the existence of geological structures below the surface. (a) Horizontal derivative, which is sensitive to horizontal changes, (b) Tilt derivative, while the vertical derivative is calculated for several highlight fault segments, such as in (c) the western region, which has the Trienggaden and Seulimum Segments, and (d) the eastern region which has the Bate and Aceh Segments
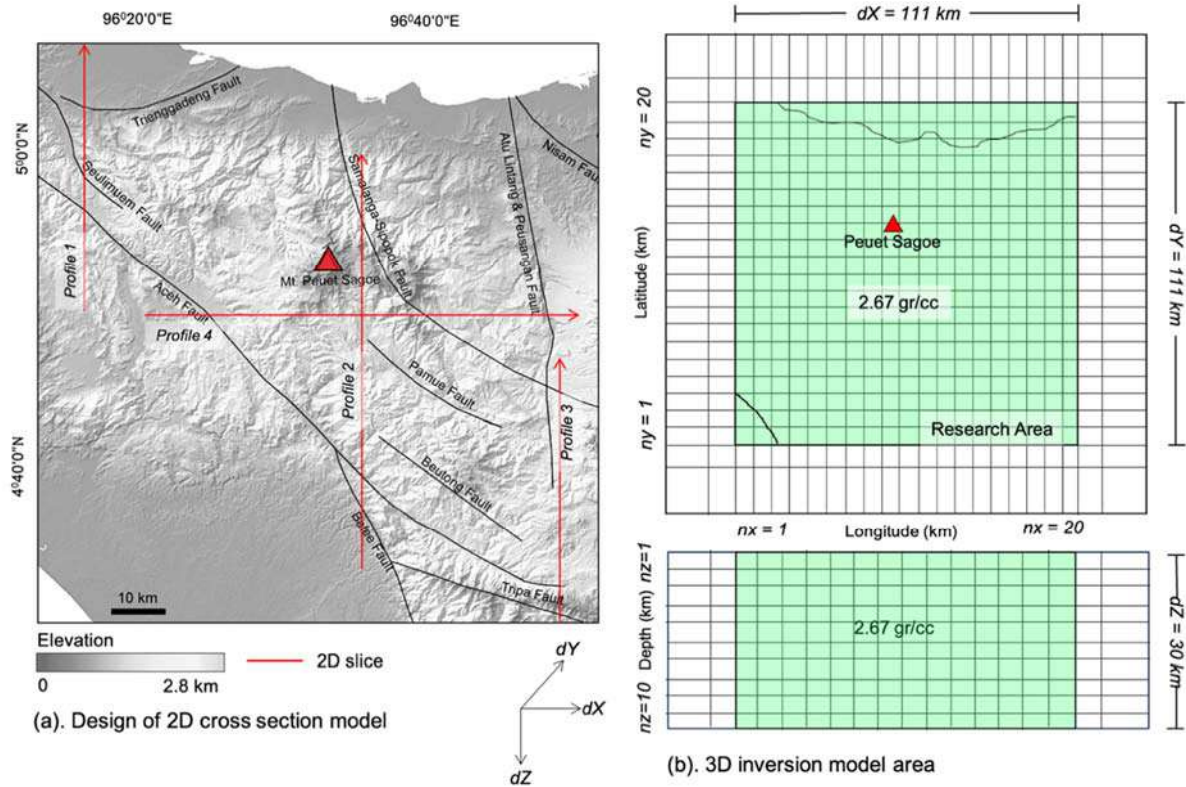
Fig. 6. Inversion of the 3D gravity data uses Occam and SVD algorithms. Where (a) designs a 2D cross-section model on several faults, while (b) is a 3D inversion model that shows a matrix of values nx and ny = 20, while nz 10 represents the subsurface depth

In addition, the Aceh and Seulimum Segments in the NW-SE direction can be described well through high-density and low-density values of the Lintang – Peusangan Fault on the east side of the measurement location. At a depth of 10 km (Fig. 7b), the whole Trienggadeng Segment can still be shown well, stretching in the W-E direction with high-density values. At this depth, the medium-density values dominate the measurement area and indicate several faults below the surface, such as the Aceh Segment on the west side and the Pameu and Beutong Segments with low-density values on the east side. At depths of 10 km (Fig. 7c) and 15 km (Fig. 7d), the anomalies generally show the same pattern; for example the high-density values are focused on the Samalanga-Sipopok Segment area in response to the subsurface metamorphic rocks, where the density models at this depth are still able to show the presence of faults with significant traces of seismic activities such as the Seulimum and Aceh Segments which extended in the NW-SE direction, the Tripa, Pameu, and Trienggadeng Segments with low seismic activities. Overall, the 3D anomaly model can show the rock density of the geological structures in the Central Aceh region. Still, this model is not very sensitive to map residual structures such as the Nisam Fault, which has relatively few seismic activities.

4.4 2D cross-section model

A 2D cross-section model was also created from the 3D gravity inversion to study the depth and geometry of the faults. There are four 2D profiles sliced intersecting several faults in the northern region of Aceh Province. For instance, Profile 1 (Fig. 8a) shows contrasting rock densities at 0-30 km depths. At a distance of 25 km from the profile, the presence of the Aceh Fault can be demonstrated at a depth of 8 km below the surface, characterized by high-density values and proofed by significant seismic activity. In addition, the Trienggadeng Fault can also be shown by a high density at the same depth as the Aceh Segment. Meanwhile, the Seulimum Segment, which is 30 km from the profile, is characterised by a low-density value extending from the surface to 25 km below the surface.

In Profile 2 (Fig. 8b), the existence of the Aceh Segment on the east side is also shown at a depth of 8 km with high density which correlates with Profile 1. The Batee Segment in the N-W direction also shows high density and is connected with the Aceh Segment on the east side. At the same time, the Samalanga-Sipopok Segment in the NW-SE direction can also be mapped at a depth of 8 km. In general, the presence of the subsurface faults is indicated by contrast differences in high-density data as shown in Profile 3 (Fig. 8c) as shown in the Samalanga-Sipopok Segment at a distance of 25-50 km and the Tripa Segment at a distance of 0-20 km.
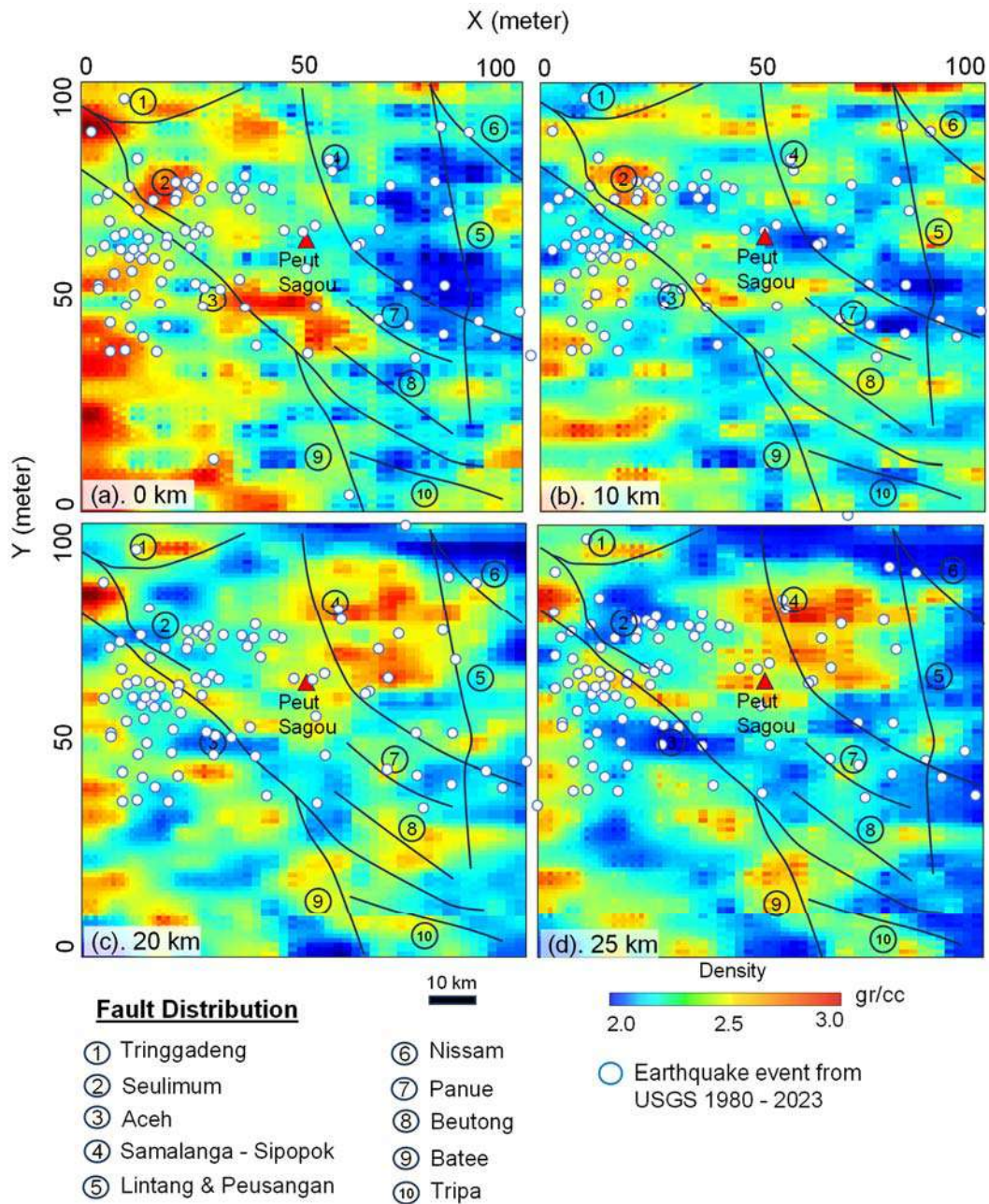
Fig. 7. The 3D slice model shows the distribution of density with depths of (a) 0 km, (b) 10 km, (c) 20 km, and (d) 25 km, which indicate the presence of a rock with a density of 2 – 3 gr/cc

This cross-sectional model can show the subsurface fault geometry. However, several faults cannot be visualized properly, such as in Profile 4 (Fig. 8d), where the rock density is unable to show the existence of the Aceh and Samalanga-Sipopok Segments instead the rock density contrast represents a weak zone that may intersect with the presence of faults.

5. Conclusion

Earthquake disaster mitigation must be done as early as possible to minimise material losses and casualties. So far, the studies on faults in Aceh Province have only focused on the Aceh and Seulimum Segments, while the North of Aceh region has yet to be studied. Even though the location also has several fault segments that can cause earthquakes. This study discusses the efficiency of the GGM+ global gravity data with a resolution of 200 m/px for mapping the geological structure in Central Aceh, which has several fault segments and many seismic activities. The approaches described here included the Bouguer anomaly, digital transformation, 2D modelling, and also 3D modelling of gravity. Based on the data analyses, the existence of a fault structure can be indicated by Bouguer anomaly of -35 to 5 mGal, such as the Seulimum Segment in the NW-SW direction and Alue Lintang – Peusangan in the N-S direction.
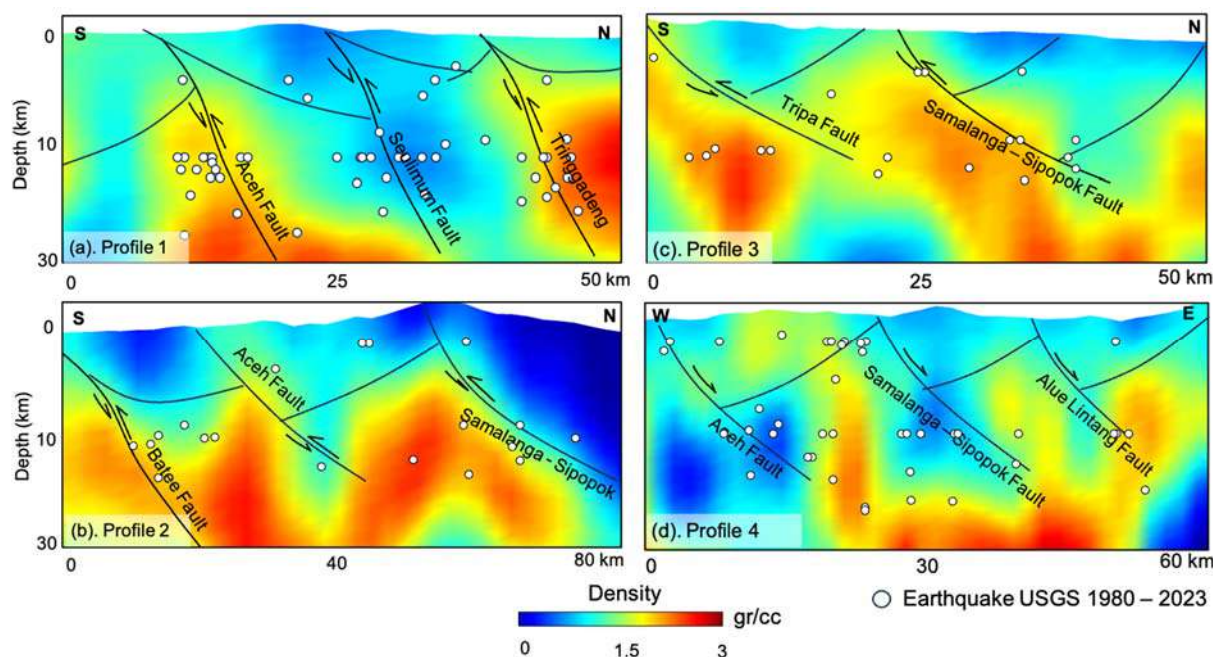
Fig. 8. The 2D cross-section model that was overlaid with the earthquake epicenter from the USGS and the interpretation of the presence of faults from the geological map, (a) Profile 1 which is traversed by several segments such as the Aceh, Seulimum, and Trienggadeng Faults, (b) Profile 2 which intersects the Samalanga-Sipopok Segment, (c) Profile 3 in Tripa Fault area, and (d) Profile 4 in the Alue Lintang Fault area. The density contrast of the inverted 3D gravity data can visualize the presence of these faults

In contrast, the existence of the Batee Fault, Tripa, and Aceh Segments can be clarified through high horizontal derivative anomaly (> 2 mGal/m). In addition, we also applied vertical derivative and tilt derivative filters to clarify structures that cannot be mapped from the previous filter, where the results obtained can clearly show the existence of the Trienggadeng Segment in the W-E direction, the Batee Segment and the Aceh Fault in NW-SE direction. The results of the 3D modelling combined with seismicity and geology data as the data constraints can show the depth of the faults in the Central Aceh region at 8 km below the surface, where the geometry of several segments such as the Aceh, Samalanga, and Trienggadeng Faults can be visualized with a density of 1.8 gr/cc as a representation of intrusive igneous rocks in the research area. GGM+ data analyses have been successfully used as a rapid and low-cost method for mapping fault structures correlated with seismic activity. It can be used as an initial stage in analysing fault presence in various other locations, especially in tropical countries with high topography where mobilising survey instruments is very difficult.

REFERENCES

Abdullah F. et al. Subsurface mapping of fault structure in the Weh island by using a 3D density of global gravity. GEO-MATE Journal, Vol. 23, No. 96, 2022, pp. 121-128.

Andersen O.B. and Knudsen P. The role of satellite altimetry in gravity field modelling in coastal areas. Physics and Chemistry of the Earth, Part A: Solid Earth and Geodesy, Vol. 25, No. 1, 2000, pp. 17-24, DOI:10.1016/S1464-1895(00)00004-1.

Bennett J.D. et al. The geology of the Banda Aceh Quadrangle, Sumatra. Geological Research and Development Center, Bandung. Explanatory Note. 1981, 19 p.

Bradley K.E. et al. Implications of the diffuse deformation of the Indian Ocean lithosphere for slip partitioning of oblique

ЛИТЕРАТУРА

Abdullah F. et al. Subsurface mapping of fault structure in the Weh island by using a 3D density of global gravity. GEO-MATE Journal, Vol. 23, No. 96, 2022, pp. 121-128.

Andersen O.B. and Knudsen P. The role of satellite altimetry in gravity field modelling in coastal areas. Physics and Chemistry of the Earth, Part A: Solid Earth and Geodesy, Vol. 25, No. 1, 2000, pp. 17-24, DOI:10.1016/S1464-1895(00)00004-1.

Bennett J.D. et al. The geology of the Banda Aceh Quadrangle, Sumatra. Geological Research and Development Center, Bandung. Explanatory Note. 1981, 19 p.

Bradley K.E. et al. Implications of the diffuse deformation of the Indian Ocean lithosphere for slip partitioning of oblique

plate convergence in Sumatra. Journal of Geophysical Research: Solid Earth, Vol. 122, No. 1, John Wiley and Sons Ltd. Jan. 2017, pp. 572-591, DOI:10.1002/2016JB013549.

Chatterjee S. et al. Validation of ERS-1 and high-resolution satellite gravity with in-Situ Shipborne gravity over the Indian Offshore Regions: Accuracies and implications to subsurface modeling. Marine Geodesy, Vol. 30, No. 3, Aug. 2007, pp. 197-216, DOI:10.1080/01490410701438323.

Cooper G.R.J. Interpreting potential field data using continuous wavelet transforms of their horizontal derivatives. Computers and Geosciences, Vol. 32, 2006, pp. 984-992, DOI:10.1016/ j.cageo.2005.10.012.

Cooper G.R.J. and Cowan D.R. Enhancing potential field data using filters based on the local phase. Computers and Geosciences, Vol. 32, No. 10, 2006, pp. 1585-1591, DOI:10.1016/ j.cageo.2006.02.016.

Dewanto B.G. et al. The 2022 Mw 6.1 Pasaman Barat, Indonesia earthquake, confirmed the existence of the Talamau segment fault based on teleseismic and satellite gravity data. Quaternary, Vol. 5, No. 4, p. 45, 2022, DOI:10.3390/quat5040045.

Doğru F. et al. Application of tilt angle method to the Bouguer gravity data of Western Anatolia. Bulletin of the mineral research and exploration, 2017, Vol. 155, No. 155, pp. 213-222.

Eppelbaum L.V. and Katz Y.I. Key features of seismo-neotectonic pattern of the Eastern Mediterranean. Proceedings of National acad. Sci. Azerb. Rep., Ser.: The Sciences of Earth, No. 3, 2012, pp. 29-40.

Eppelbaum L.V. and Katz, Yu.I. Newly developed paleomagnetic map of the Easternmost Mediterranean Joined with tectono-structural analysis Unmask geodynamic history of this region. Central European Jour. of Geosciences (Open Geosciences), Vol. 7, No. 1, 2015, pp. 95-117.

Ghosal D. et al. New insights on the offshore extension of the Great Sumatran fault, NW Sumatra, from marine geophysical studies. Geochemistry, Geophysics, Geosystems, Vol. 13, No.11, 2012, DOI:10.1029/2012GC004122.

Hill E.M. et al. The 2012 Mw 8.6 Wharton Basin sequence: A cascade of great earthquakes generated by near-orthogonal, young, oceanic mantle faults. Journal of Geophysical Research: Solid Earth, Vol. 120, No. 5, John Wiley and Sons Ltd. 2015, pp. 3723-3747, DOI:10.1002/2014JB011703.

Hinze W.J. et al. Gravity and magnetic exploration: principles, practices, and applications. cambridge university press, Jan. 2010, 512 p., DOI:10.1017/CBO9780511843129.

Hiramatsu Y. et al. Gravity gradient tensor analysis to an active fault: a case study at the Togi-Gawa Nangan fault, Noto Peninsula, Central Japan. Earth, Planets and Space, Vol. 71, No. 1, Springer. Berlin, Heidelberg, 2019, DOI:10.1186/s40623-019-1088-5.

Hirt C., Claessens S. et al. New ultrahigh-resolution picture of Earth's gravity field. Geophysical Research Letters, Vol. 40, No. 16, Aug. 2013, pp. 4279-4283, DOI:10.1002/grl.50838.

Hirt C., Kuhn M. et al. Study of the Earth's short-scale gravity field using the ERTM2160 gravity model. Computers and Geosciences, Vol. 73, Elsevier, 2014, pp. 71-80, DOI:10.1016/ j.cageo.2014.09.001.

Ito T. et al. Isolating along-strike variations in the depth extent of shallow creep and fault locking on the Northern Great Sumatran Fault. Journal of Geophysical Research, Vol. 117, No. B6, 2012, pp. 1-16, DOI:10.1029/2011JB008940.

Keating P. and Pinet N. Comparison of surface and shipborne gravity data with satellite-altimeter gravity data in Hudson Bay. The Leading Edge, Society of Exploration Geophysicists, Vol. 32, No. 4, 2013, pp. 450-458, https://doi.org/ 10.1190/tle32040450.1.

Kern M. et al. A Study on the combination of satellite, airborne and terrestrial gravity data. Journal of Geodesy, Vol. 77, pp. 217-225, 2003, DOI:10.1007/s00190-003-0313-x.

Lay T. et al. The Great Sumatra-Andaman earthquake of 26 December 2004. Science, Vol. 308, No. 5725, American Association for the Advancement of Science, May 2005, pp. 1127-33, DOI:10.1126/SCIENCE.1112250.

Marwan M. et al. A low-cost UAV based application for identify and mapping a geothermal feature in Ie Jue Manifestation, Seulawah Volcano, Indonesia. International Journal of GEOMATE, Vol. 20, No. 80, 2021, pp. 135-142, DOI:10.21660/2021.80.J2044.

Marwan M. et al. geoelectrical model of geothermal spring in Ie Jue Seulawah deriving from 2D VLF-EM and DC resistivity methods. Journal of Applied Engineering Science, Vol. 21, No. 1, 2023, pp.59-69, DOI:10.5937/JAES0-38014.

McCaffrey R. The Tectonic Framework of the Sumatran Subduction Zone. Annual Reviews, Vol. 37, Apr. 2009, pp. 345-366, DOI:10.1146/annurev.earth.031208.100212.

Muksin U. et al. Investigation of Aceh Segment and Seulimeum Fault by using seismological data; A preliminary result. Journal of Physics: Conference Series, Vol. 1011, No. 1, Apr. 2018, p. 012031, DOI:10.1088/1742-6596/1011/1/012031.

Muksin U. et al. AcehSeis Project provides insights into the detailed seismicity distribution and relation to fault structures in Central Aceh, Northern Sumatra. Journal of Asian Earth Sciences, Vol. 171, 2019, pp. 20-27, Elsevier, DOI:10.1016/J.JSEAES.2018.11.002.

Muzli M. et al. The 2016 Mw 6.5 Pidie Jaya, Aceh, North Sumatra, earthquake: Reactivation of an unidentified sinistral fault in a region of distributed deformation. Seismological Research Letter, Vol. 89, No. 5, 2018, pp. 1761-1772, DOI:10.1785/0220180068.

Nasuti A. et al. Onshore-offshore potential field analysis of the Møre-Trøndelag fault complex and adjacent structures of Mid Norway. Tectonophysics, Vol. 518-521, 20 January 2012, pp. 17-28, DOI:10.1016/J.TECTO.2011.11.003.

Natawidjaja D.H. and Triyoso W. The Sumatran fault zone – from source to hazard. Journal of arthquake and Tsunami, Vol. 1, No. 01, World Scientific, 2007, pp. 21-47.

Pavlis N.K. et al. The development and evaluation of the earth gravitational model 2008 (EGM2008). Journal of Geophysical Research: Solid Earth, Vol. 117, No. 4, 2012, pp. 1-38, DOI:10.1029/2011JB008916.

Pham L.T. et al. Enhancement of potential field source boundaries using an improved logistic filter. Pure and Applied Geophysics, Vol. 177, No. 11, 2020, pp. 5237-5249, DOI:10.1007/s00024-020-02542-9.

Pham L.T. et al. Subsurface structural mapping from high-resolution gravity data using advanced processing methods. Journal of King Saud University, Science, Vol. 33, No. 5, 2021, p. 101488, DOI:10.1016/j.jksus.2021.101488.

Pirttijarvi M. Gravity interpretation and modeling software based on 3-D block models. GRABLOX. User's Guide to Version, 2008.

Purnachandra Rao N. et al. Structure and tectonics of the Andaman Subduction Zone from modeling of seismological and gravity data. In: New Frontiers in Tectonic Research - General Problems, Sedimentary Basins and Island Arcs, Intech Publisher/ Rijeka, Croatia, 2011, DOI:10.5772/19090.

Rexer M. and Hirt Ch. Spectral analysis of the Earth's topographic potential via 2D-DFT: A new data-based degree variance model to degree 90,000. Journal of Geodesy, Vol. 89, No. 9, Sept. 2015, pp. 887-909, DOI:10.1007/s00190-015-0822-4.

Rizal M. et al. The 2D resistivity modelling on north sumatran fault structure by using magnetotelluric data. IOP Conference Series: Earth and Environmental Science, Vol. 364, Dec. 2019, p. 012036, DOI:10.1088/1755-1315/364/1/012036.

Sieh K. and Natawidjaja D. Neotectonics of the Sumatran Fault, Indonesia. Journal of Geophysical Research: Solid Earth,

Vol. 105, No. B12, 2000, pp. 28295-28326, DOI:10.1029/2000jb900120.

Tassis G.A. et al. A new Bouguer gravity anomaly field for the Adriatic Sea and its application for the study of the crustal and upper Mantle Structure. Journal of Geodynamics, Vol. 66, 2013, pp. 38-52, Elsevier, DOI:10.1016/j.jog.2012.12.006.

Vaish J. and Pal S.K. Geological mapping of Jharia Coalfield , India using GRACE EGM2008 gravity data: A vertical derivative approach. Geocarto International, Vol. 30, No. 4, 2015, pp. 388-401, DOI:10.1080/10106049.2014.905637.

van der Meijde M. et al. GOCE data, models and applications: A review. International Journal of Applied Earth Observation and Geoinformation, Vol. 35, Part A, March 2015, pp.4-15, DOI:10.1016/j.jag.2013.10.001.

Vos I.M.A. et al. Resolving the nature and geometry of major fault systems from geophysical and structural analysis: The Palmerville Fault in NE Queensland, Australia. Journal of Structural Geology,Vol. 28, No.11, November 2006, pp. 2097-2108, DOI:10.1016/j.jsg.2006.07.016.

Yanis M., Simanjuntak A.V.H., Abdullah F. et al. Application of Seismicity and Gravity Observation-Based Filtering Model for Mapping a Fault Structure in Weh Island, Indonesia. Iraqi Geology Journal, Vol. 56, July.2024, pp. 260–274. DOI:10.46717/IGJ.56.2A.20MS-2023-7-29.

Yanis M., Marwan M. et al. A pilot survey for mapping the fault structure around the Geuredong volcano by using high-resolution global gravity. Acta Geophysica, Vol.70, July 2022, pp.2057-2075, Springer, DOI:10.1007/S11600-022-00860-1.

Yanis M., Marwan M. et al. Application of GEOSAT and ERS Satellite as an Alternative method of gravity ground measurement in hydrocarbon basin in East Island. Indonesian Journal of Geography, Vol. 33, No. 2, Feb. 2020, DOI:10.22146/ mgi.50782 (in Indonesian).

Yanis M., Faisal A., Yenny A. et al. Continuity of Great Sumatran Fault in the marine area revealed by 3D inversion of gravity data. Jurnal Teknologi, Vol. 83, No. 1, Jan.2021, pp. 145-155, DOI:10.11113/jurnalteknologi.v83.14824.

Yanis M., Faisal A., Zaini N. et al. The northernmost part of the Great Sumatran Fault Map and images derived from gravity anomaly. Acta Geophysica, Vol. 69, No. 3, June 2021, pp. 795-807, DOI:10.1007/s11600-021-00567-9.

ИСПОЛЬЗОВАНИЕ ГЛОБАЛЬНОЙ ГРАВИТАЦИИ ДЛЯ КАРТИРОВАНИЯ СВЯЗИ МЕЖДУ СЕЙСМИЧНОСТЬЮ И ГЕОЛОГИЧЕСКИМ СТРОЕНИЕМ В СРЕДНЕЙ ЧАСТИ ПРОВИНЦИИ АЧЕХ, ИНДОНЕЗИЯ

Янис М.[1], Абдулла Ф.[1,2], Ананда Р.[3], Сямсюдин Ф.[1,2], Исмаил Н.[1,2], Зайнал М.[1], Паембонан А.Я.[4]
[1]Геофизический инженерный факультет, Университет Сийя Куала
Банда-Ачех 23111, Индонезия: yanis@usk.ac.id
[2]Физический факультет, Университет Syiah Kuala
Банда Ачех 23111, Индонезия
[3]Кафедра геофизической инженерии, Бандунгский технологический институт
Бандунг 40132, Индонезия
[4]Геофизический инженерный факультет, Технологический институт Суматры
Южный Лампунг 35365, Индонезия

Резюме. Ачех – одна из индонезийских провинций, подверженных землетрясениям, поскольку ее пересекают Большой Суматрский разлом и зоны субдукции вдоль западного побережья с высокой сейсмической активностью. В последнее время исследования по картированию разломов были сосредоточены на сегментах Ачех и Сеулимум в западной части провинции Ачех. В отличие от этого, центральная часть еще не изучена, несмотря на то, что за последние 10 лет произошло несколько землетрясений в районах, где трассы разломов все еще нуждаются в надлежащем картировании. Поэтому в данном исследовании использовалась глобальная гравитационная модель Plus (GGM+) с высоким разрешением 200 м/пкс для анализа взаимосвязи между сейсмичностью и структурами разломов в центральной части Ачеха. Остаточная аномалия GGM+ указывает на существование геологических структур, таких как сегменты Ачех, Памеу и Самаланга, характеризующихся низкой гравитацией. Для уточнения наличия разломов также применялись некоторые производные методы, например, горизонтальная производная аномалия для картирования сегментов Ачех, Бати, Самаланга и Алуэ Линтанг - Пеусанган. Вертикальная производная показывает существование разлома Тринггаденг, предположительно являющегося источником землетрясения Пи-

ди Джая в 2016 году. Таким образом, производная наклона может также визуализировать наличие разлома Ниссам, что не отображается в других методах фильтрации. Мы также провели 3D гравитационное моделирование с использованием алгоритма Occam и сингулярного разложения; плотность указывает на глубину и геометрию структуры разлома, в целом 8 км, что обеспечивает надежность GGM+ при изучении разломов, особенно в высокогорных районах, где использование приборов затруднено.

Ключевые слова: Гравитация, разлом, GGM +, провинция Ачех, геологическое строение, 3D инверсия

İNDONEZİYANIN AÇEH ƏYALƏTİNİN ORTA HİSSƏSİNİN SEYSMİKLİK VƏ GEOLOJİ QURULUŞU ARASINDAKI ƏLAQƏNİ XƏRİTƏLƏNDİRMƏK ÜÇÜN QLOBAL CAZİBƏ QÜVVƏSİNDƏN İSTİFADƏ

Yanis M.[1] , Abdulla F.[1,2], Ananda R.[3], Səmsyudin F.[1,2] , İsmayıl H.[1,2], Zaynal M.[1], Paembonan A.Ya.[4]

[1]Geofizika mühəndislik fakültəsi, Sia Kuala Universiteti
Banda-Açeh 23111, İndoneziya: yanis@usk.ac.id
[2]Fizika fakültəsi, Syiah Kuala Universiteti
Banda-Açeh 23111, İndoneziya
[3]Geofiziki mühəndislik kafedrası, Bandunq texnologiya institutu
Bandunq 40132, İndoneziya
[4]Geofiziki mühəndislik fakültəsi, Sumatra texnologiya institutu
Cənubi Lampunq 35365, İndoneziya

Xülasə: Açeh - Böyük Sumatra fay xəttinin və yüksək seysmik aktivliyə malik, qərb sahili boyunca subduksiya zonalarının kəsişdiyi, zəlzələlərə məruz qalan İndoneziyanın vilayətlərindən biridir. Son zamanlar fay xətlərinin xəritələnməsi ilə bağlı tədqiqatlar Açeh vilayətinin qərb hissəsindəki Açeh və Seulimum seqmentlərinə fokuslanmışdır. Bununla yanaşı, son 10 ildə fay xətlərinin düzgün xəritələnməsinə ehtiyacı olan bölgələrdə bir neçə zəlzələ baş verməsinə baxmayaraq, mərkəzi hissə hələ də öyrənilməmişdir. Buna görə də, bu tədqiqatda Açehin mərkəzi hissəsində seysmik aktivlik ilə fay strukturları arasındakı əlaqəni təhlil etmək üçün 200 m/piks yüksək həlledicilıklə Qlobal Qravitasiya Modeli Plus (GGM+) istifadə edilmişdir. GGM+ qalıq anomaliyası Açeh, Pameu və Samalanga seqmentləri kimi aşağı qravitasiya ilə səciyyələnən geoloji strukturların mövcudluğunu göstərir. Fayların varlığını dəqiqləşdirmək məqsədilə Açeh, Bati, Samalanga və Alue Lintang – Peusangan seqmentlərinin xəritələnməsi üçün üfüqi törəmə anomaliyası kimi bəzi törəmə metodları da tətbiq edilmişdir. Şaquli törəmə Tringgadeng qırılmasının mövcudluğunu göstərir, bu qırılma 2016-cı ildəki Pidie Jaya zəlzələsinin mənbəyi hesab olunur. Beləliklə, maillik törəməsi Nissam qırılmasının da mövcudluğunu vizuallaşdıra bilər, bu isə digər filtrləmə metodlarında görünmür. Biz həmçinin Occam alqoritmi və sinqulyar parçalanma metodundan istifadə edərək 3D cazibə modelləşdirilməsi apardıq; sıxlıq qırılmanın dərinliyini və strukturunu göstərir, ümumilikdə 8 km dərinliyindədir ki, bu da GGM+ metodunun etibarlılığını təmin edir, xüsusən də cihazların istifadəsinin çətin olduğu dağlıq ərazilərdə qırılmaların öyrənilməsində.

Açar sözlər: Qravitasiya, qırılma, GGM +, Açex əyaləti, geoloji quruluş, 3D inversiya

AN APPLICATION OF IMPROVISED 2D GEO-RESISTIVITY SURVEY TO ROAD FAILURE INVESTIGATION

Raji W.O.[1, 2], Sulaiman' M.O.[1]

[1]Department of Geophysics, University of Ilorin, Ilorin, Nigeria
PMB 1515, Ilorin, Kwara State, Nigeria
[2]Department of Earth Sciences, Carleton University, Ottawa, Canada
1125 Colonel By Dr, Ottawa, ON K1S 5B6: lanreraji@unilorin.edu.ng, wasiu.raji@gmail.com

Keywords: *Road failure investigation, Geophysical survey, Electrical resistivity imaging, 2D augmented array, subsurface resistivity models*

Summary. The Electrical Resistivity Imaging (ERI) method of geophysics has gained large-scale applications in civil engineering for pre-construction site assessment and post-construction investigative and remedial interventions. However, the cost of ERI equipment limits its applications in underdeveloped/developing countries and unfunded studies. This limitation is overcome in this study by applying an alternative and reliable technique of multiple imaging of subsurface for engineering applications using traditional 1D Earth Resistivity equipment and collocated electrodes array. This technique was used to investigate the principal cause of road pavement failure along University Teaching Hospital Road, Ilorin, Nigeria. Five profiles of 100 m were established at different parts of the road to acquire subsurface resistivity data. Resistivity models inverted from the data acquired by the improvised 2D surveys show low resistivity breakouts, weathered sections with high moisture content, weak zones, and elongated brittle structures in the top ten meters of the subsurface. The high resistivity layer corresponds to the stable portions of the pavement while the low resistivity breakouts in the shallow part of the resistivity models correspond to the failed pavements and potholes on the road. Elongated vertical structures were identified as weak zones that served as conduits for rainwater from the top and groundwater from subsurface accelerated weathering activities in the area. Water ingress due to lack of drainage, high moisture content in the top layers, and intense subsurface weathering were found as the cause of the road pavement failure. The study recommends some remedial interventions prior to reconstructing the road pavement**.**

Introduction

Electrical resistivity survey, ERS, is the preferred geophysical method often used for probing the subsurface in built-up areas. Because it's non-invasive and non-destructive, ERS has gained large-scale applications in construction and civil engineering works. It has been used for characterizing subsurface materials beneath the locations where engineering infrastructures are to be cited, determining foundation depth, or locating geological structures (such as fractures, and buried river channels) that may compromise the integrity of the proposed buildings or infrastructure. Recent development in field procedure, technology, instrumentation, and computer software in the field of geophysics has broadened the applications of electrical resistivity methods to other disciplines including forensic investigations, engineering, and environmental studies. In the last two decades or so, equipment for acquiring multiple resistivity data at different depth levels over large areas in real time has been developed. These data have been used to produce multi-dimensional (2D, 3D, and 4D) images of the subsurface to advise suitable locations to cite infrastructure, investigate the cause of failed buildings, roads, and dams, and determine the strength of concrete piles (Darling, 2001; Rucker, 2006; Soupios et al., 2007; Castilho, Maia, 2008; Karastathis et al., 2002; Cardarelli et al., 2018; Raji, Aluko, 2021). These images are known as subsurface resistivity models or resistivity tomograms. The process of data acquisition and processing is here known as Electrical Resistivity Imaging ERI.

Some new ERI equipment has the capacity to acquire thousands of datasets at different lateral and vertical positions in a single survey and in-built software to process data and image subsurface resistivity beneath the profile line in real time. Therefore, ERI offers on-the-spot assessments of engineering sites for timely decision making. It reduces the cost

of geotechnical studies, gives higher coverage than drilling/coring and is cheaper than soil sampling and laboratory testing. However, ERI equipment is very expensive and unaffordable to many geoscience practitioners and researchers in underdeveloped and developing countries where research funding is limited and difficult to access. The limitation caused by the unaffordability and non-availability of new ERI equipment for (non-contract projects) engineering studies is overcome in this study using an augmented 2D-resistivity survey. The augmented 2D survey uses collocated electrode arrays and traditional resistivity meters that are readily available and affordable. Details of the survey are given in the material and method section.

The augmented 2D survey was applied to investigate the cause of repeated failure of road pavement along University Teaching Hospital road, Ilorin, Kwara State, Nigeria. The failed sections of the road has been repaired three times within the three years preceding this study to ease the movement of ambulances and private vehicles conveying patients to hospital for medical attention. However, the same portions keep failing. To find a lasting solution to the perennial problem, this study was conducted to characterize the subsurface materials beneath the road pavement and to advise the best way to tackle the problem. The aim of this study is to uncover the subsurface condition responsible for the repeated failure of pavement at the designated portions of the road. The objectives of the study are: (i) to show that the augmented 2D Electrical Resistivity survey is suitable for investigating road failure in the absence of expensive and unaffordable ERI equipment, and (ii) to recommend remedial strategies to prevent future failure of pavement on the road.

Application of the electrical method of geophysics to road failure investigation and other engineering applications is based on the direct relation between the electrical conductivity of soils/rocks and concrete materials and the shear strength of the materials. Sections with high moisture content which are often associated with road failure have anomalous resistivity signatures that contrast with the competent layers beneath the stable parts of the road. Clay in-fills, subsurface erosional surfaces, fractures, weathered sections, and buried river channels known to be responsible for road failure have characteristic low resistivity properties compared to competent, dry aggregate layers commonly used as base/subbase materials for roads and other engineering constructions (Adeoti et al, 2016; Feyisa and Gebissa, 2023). Feyisa and Gebissa, (2023) investigated the cause of Gedi-Ijaji Asphalt road in Ethiopia using ERI equipment and magnetic method. 2D plots of the resistivity section showed that the failed

section of the road corresponds to the low resistivity structures in the subsurface. The low resistivity structure was interpreted as an area of highly weathered sections saturated with moisture infiltrated through surface fractures.

Similarly, Raji and Aluko (2021) applied electrical resistivity and seismic surveys to investigate the cause of excessive water leakage in Asa Dam in West Africa. Results of the study revealed the presence of a low resistivity high-permeability section in the dam foundation. The low resistivity section in the 2D tomogram coincided with a low-velocity oxbow structure in the seismic velocity tomogram. The joint interpretation of the electrical resistivity and seismic velocity tomograms suggested the presence of an extended high-permeable weak zone through which water leaks out of the dam. Other related studies (Osinowo et al., 2011; Arjwech et al., 2013; Adeoti et al., 2016; Raji et al., 2017; Ademila, 2021) found that subsurface causes of failed roads and buildings are often associated with weak zones or water-saturated sections which show up as low resistivity structures in 2D resistivity images. The current study is different from the previous similar studies because it used an augmented 2D resistivity survey technique. The technique removed the limitations placed by the unaffordability of ERI equipment.

Material and Method

Applications of electrical resistivity survey to investigate the cause of road pavement failure are based on the understanding that if subsurface conditions are responsible for the failure of a portion of the road, the subsurface conditions beneath the stable and failed portions of the road should have contrasting electrical resistivity signatures. The resistivity contrast can be best imaged by continuous and multi-level measurements of resistivity/ conductivity along the profile(s) that covered the stable and failed portions of the road pavement. Continuous and multi-level resistivity measurements are done by ERI equipment. However, this equipment was unavailable for this study due to cost. An augmented 2D ERI survey was performed using Campus Omega Terrameter and collocated electrode arrays. Other accessories used in the survey include a DC battery, 21 metallic electrodes, four reels of cable, crocodile clips, hammers, a portable Geographic Positioning System device (GPS), and measuring tapes.

The augmented 2D resistivity survey followed the Wenner array. 51 electrode positions were marked at 2 m intervals to cover a 100 m profile line. However, only 21 electrodes that were available were coupled to the ground at the beginning of the survey on a straight line (fewer or more electrodes could be used). At the start, only electrode

numbers 1, 2, 3, and 4 were connected to the resistivity meter, and they correspond to C1, P1, P2, and C2 terminals, respectively. After measurement, the connecting wires were moved to electrodes numbers 2, 3, 4, and 5 and they were connected to C1, P1, P2, and C2 terminals, respectively, and another measurement was taken, then the wires were moved to electrode numbers 3, 4, 5 and 6 for the third measurement. The sequence of connections and measurements continued until electrodes 48, 49, 50, and 51 were connected and measurements were taken.

The electrodes used at the earlier part of the profile were moved forward after measurements to cover the later part of the profile. For example, electrodes number 1 to 17, can be moved to the position marked for electrodes 22 to 38 while taking measurements with electrodes 18, 19, 20, and 21. After completing the series of measurements using electrode spacing of 2 ($a = 2, n = 1$), electrode spacing was changed to 4 m, and measurements along the 100 m profile were repeated, ($a = 4, n = 1$). Finally, the electrode spacing was changed to 6 m to complete the third level measurements, ($a = 6, n = 1$). a is greater, penetration of the injected current is deeper. The field layout for the augmented 2D survey is shown in Fig. 1. Wenner array is selected for this study because it has better depth resolution and higher signal strength than the Dipole-dipole array, and it is less susceptible to acquisition noise (Neyamadpour et al., 2010).

This measurement was repeated at other four locations along the road with each profile covering the stable and failed portions of the road pavement. The failed portions were marked out on each profile for referencing and interpretation purposes. For quality control purposes, the profiles were set out in the following pattern. The beginning and end of Profile 1 fell into the failed road pavement, between the two ends there were stable and failed portions of the pavement. The two ends of Profile 2 fell into the stable pavement, and there were stable and failed

pavement between the two ends. Profile 3 largely covered the stable pavement but has a big pothole at the beginning, Profile 4 entirely covered the failed pavement section, while Profile 5 tarted in the stable pavement and ended in the failed pavement.

Fig. 2a is the site map showing the locations of the profiles along the road. Photographs showing some failed portions of the road are shown in Fig. 2b. The bad sections of the road were marked out on each profile and recorded on the field note for reference and interpretation purposes. Data acquired on each profile line were concatenated to form 2D data. Increment in electrode separation (a= 2, 4, 6) represents greater depths penetrated by the injected current, and hence deeper probing. The data were plotted against the profile distance for different electrode separations on each profile for visual inspection. The plots were used as quality control for the 2D modelling because they represent quantitative changes in resistivity/conductivity with distance and depth. The field data were preprocessed using an in-house MATLAB program (Raji et al., 2017) to remove spurious data points that may be due to acquisition error and poor electrode contact.

The resistivity models of the subsurface beneath each profile line were obtained using least squared finite difference-based tomographic inversion (Loke, Barker, 1996). The geological model built from borehole logs and VES-based lithologic sections in the area (Abubakar et al., 2014; Aromoye et al., 2019) was fed into the inversion scheme. The starting 2D model assumed that the (i)pavement material was laid on a flat layer that comprises the subgrade/sub-grade and the topsoil and (ii) that deeper section of the subsurface is made of partially weathered crystalline rocks. The inverted resistivity models were finally processed and plotted using DiproWin Software. The resistivity models shown in Figs 3 to 5 were obtained after 5/6 iterations. The RMS error of the results ranged between 6 to 11%.
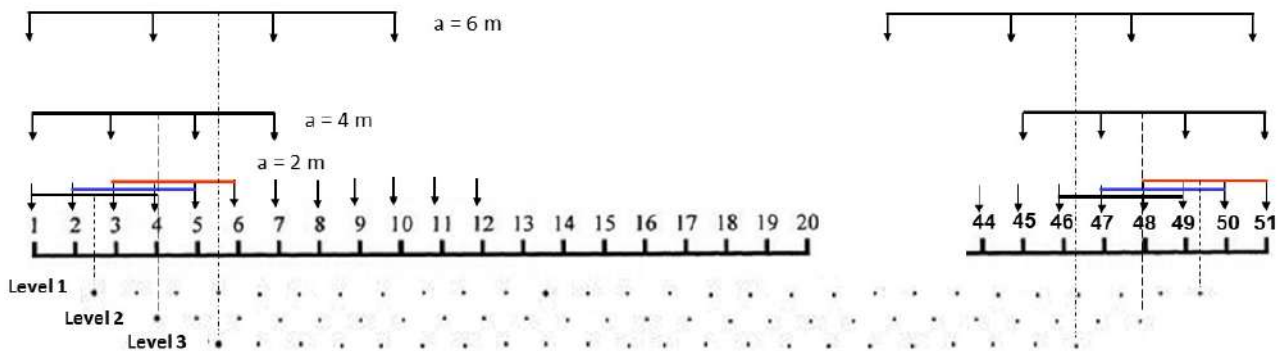
Fig. 1. Schematic image of 2D augmented survey and electrode array used for the study
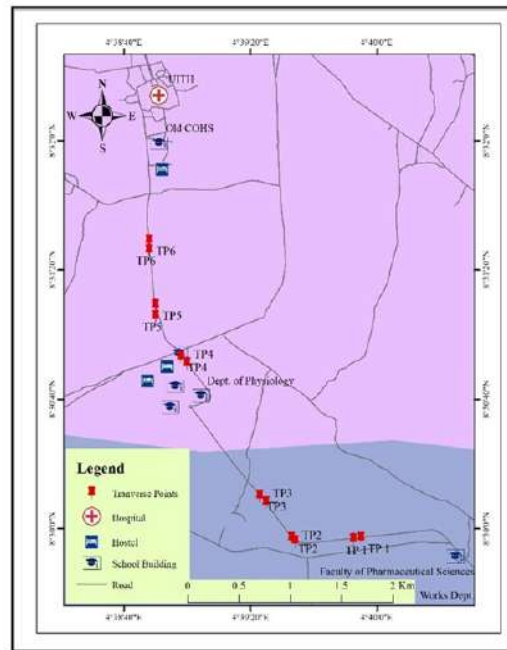
Fig. 2a. Map showing location of the 2D Survey

Fig. 2b. Photos showing parts of the road with failed pavement

Results and Discussion

Interpretations of the resistivity models for road failure in this study were based on the following background knowledge: (i) subsurface condition beneath the stable and failed portions of the road should have contrasting resistivity values and patterns; (ii) the major causes of road failure are weak zones, buried river channels, clay layers, weathered sections, and fractures that are often associated with low resistivity/high conductivity structures; and (iii) distances corresponding the failed portions of pavements marked on the profile line are compared the lateral distance on the 2D resistivity models for concurrence.

The resistivity models revealed heterogeneous resistivity distribution in the subsurface, and resistivity values range from 49 - 3008 Ωm. Based on the resistivity patterns and geo-electric features, the structures in the resistivity models are classified into four broad geo-resistivity sections. The reddish–purplish laterally continuous structure at the top 2 m from the surface represents laterally a continuous geo-resistivity layer of resistivity values ranging from 760- 2684 Ωm.

This high-resistive geo-electric layer is interpreted as the combination of the base/sub-base and the topsoil (sub-grade). The base/sub-base materials are construction aggregates of high drainage charac-

51

teristics. The subgrade/topsoil has high clay content with poor drainage characteristics. The high resistivity values in this geo-electric layer are interrupted by some low resistivity breakouts that indicate weak zones and conductive sections in some places (Soupios et al., 2007; Loke et al., 2020). The second geo-resistivity structure is represented by the greenish colour and has resistivity values ranging from 91 - 398 Ωm. This structure corresponds to the dry weathered layer. The third geo-resistivity section is represented by the blue colour and has resistivity values ranging from 48-86 Ωm.

This section is interpreted as a weathered rock with high moisture/water content. The moisture/water content of the rock is responsible for the low resistivity property of this geo-resistivity section. The fourth geo-resistivity section is represented by a reddish/purplish colour in deeper section of the resistivity models. This geo-resistivity section is interpreted as the stable (unweathered) crystalline rocks. They are generally resistant to weathering and have a characteristic massive structure which is common to rocks of igneous origin. The top 2 m of the resistivity models which correspond to the subgrade material and the topsoil layer characterized by high resistivity red/purple color contained some low resistivity breakouts. These low resistivity breakouts occur irregularly on the resistivity models but are consistent with the position of failed pavement on the road. The low resistivity is due to high moisture content in the failed parts of the pavement some of which have developed into potholes.

Figs. 3a and 3b showed the resistivity models beneath profiles 1 and 2, respectively. As described in the methodology section, the profiles were set out in a pattern that allows quality control during interpretation. Two ends of Profile 1 fell in the failed portion of the road pavement while the two ends of Profile 2 fell in the stable portions of the road pavement. Between two ends, there were failed and stable portions

of the pavement. The resistivity model in Fig. 3a showed low resistivity sections at the beginning and end of the profile, while the resistivity model in Fig. 3b shows high resistivity at two ends with low resistivity breakout between them. These two resistivity models suggest that the failed and stable portions of road pavements are characterized by low resistivity breakouts and high resistivity sections, respectively.

These results are consistent with the findings of Osinowo et al. (2011) and Feyisa, Gebbisa (2023) who used ERI surveys for road investigation studies in Nigeria and Ethiopia, respectively. The low resistivity structure lying at 70 – 80 m on Profile 2 indicates the position of a big/deep pothole filled up with compacted laterite. Generally, the low resistivity breakouts in the top 2 -3 m appear larger on the resistivity models than their actual sizes on the road. This could be due to water/moisture in the failed pavement infiltrating the layers beneath the stable pavement. Resistivity models beneath Profile 3 and 4 are shown in Figs. 4a and 4b respectively. The big pothole at the beginning of profile 3 showed up as a low resistivity breakout measuring about 15 m while the remaining part of the profile is characterized by high resistivity section which corresponds to the stable pavement.

The continuous green colour (low resistivity) at the top of the resistivity model in Figure 4b indicated the absence of pavement on the section of the road covered by the profile. The section was filled with compacted laterite to reduce the roughness of the road. The vertical structure beneath the 40 m suggests a weak zone associated with a brittle structure that extends beyond the depth of the resistivity model. The resistivity model beneath Profile 5 is shown in Fig. 5. The image showed high resistivity top layer interrupted by low-resistivity breakouts at the 15 – 20 m mark and the end of the profile. These low resistivity breakouts correspond to the position of the failed pavement on the section of the road covered by profile 5.
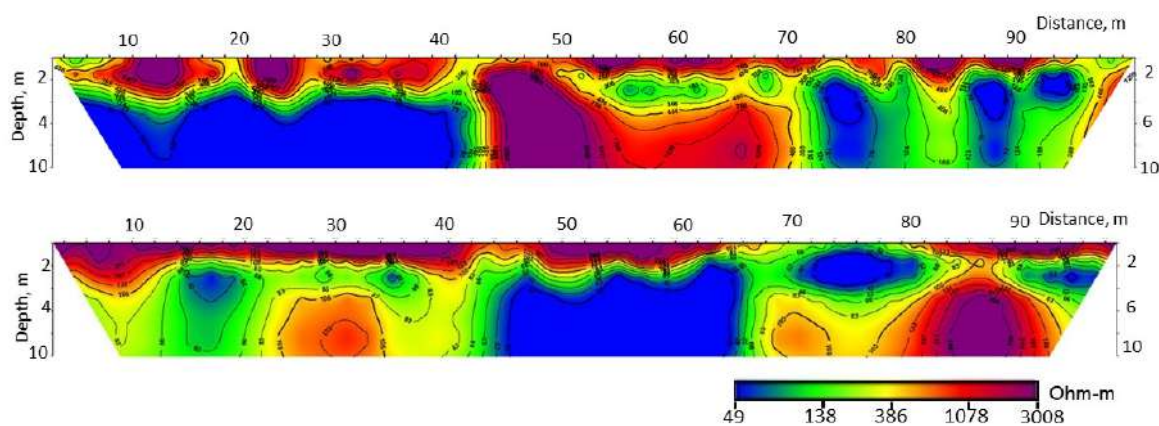
Fig. 3. 2D subsurface resistivity models beneath Profile 1(top) and Profile 2 (bottom)
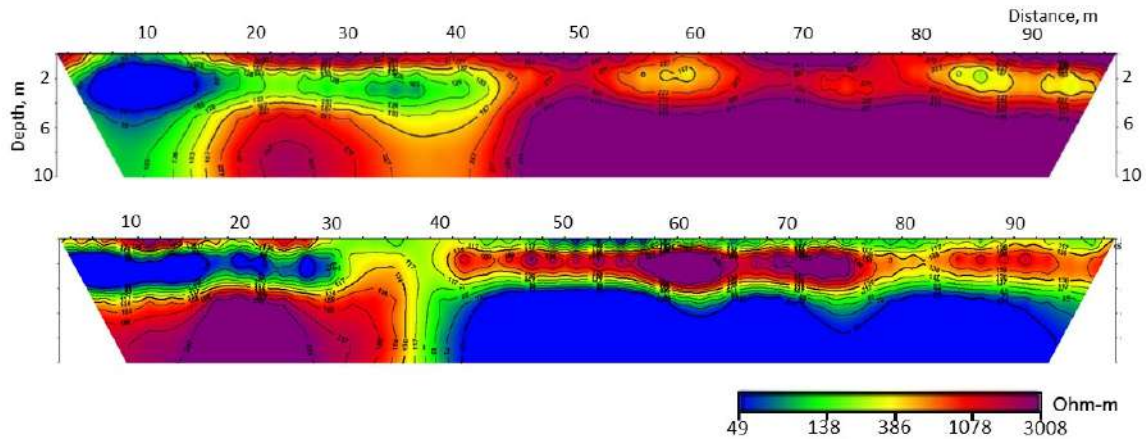
Fig. 4. 2D subsurface resistivity models beneath Profile 3 (top) and Profile 4(bottom)
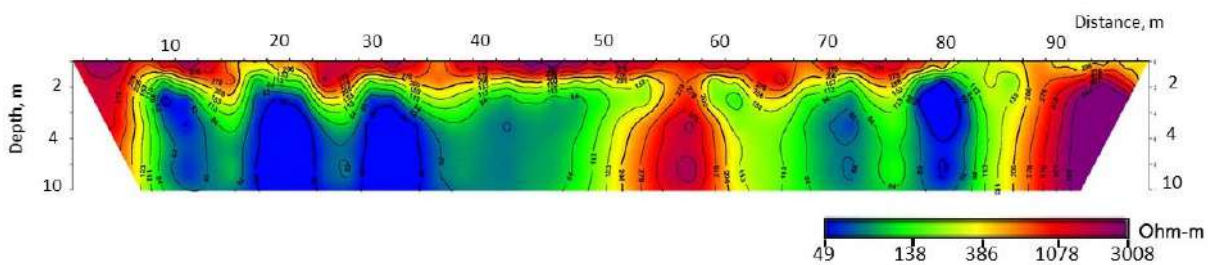
Fig. 5. 2D subsurface resistivity model beneath Profile 5

Generally, the subsurface below the topsoil is characterized by weathered rocks, water-saturated sections and vertical structures that showed shallow up as low resistivity features. These features are weak zones with high moisture content that often compromise the stability of the road. Positions 40 - 45 m on Profile 1, 65 - 68 m on Profile 2, 36 - 40 m on Profile 4, and 80 – 90 m on Profile 5 show some vertical structures that cut through the entire depth of the resistivity models. These vertical structures suggest the presence of deep-seated fractures located at depths beyond the 10 m penetrated by the survey. The structures serve as conduits for the infiltration of rainwater from the top and groundwater from the subsurface, thereby accelerating the weathering of rocks in the area. (Raji, Sulaiman, 2023).

High moisture content in the shallow part of the subsurface due to water ingress and the lack of drainage channels on the road are the main causes of pavement failure on the road. The sub-base and sub-grade contain a significant amount of clay which stores water (and swells) during the rainy season. Hydrologic data and topographic maps of the area show that the road was built on a low and flat topography and groundwater level is shallow in the area (Raji and Abdulkadir, 2020). Continuous interaction between the rocks and groundwater resulted in intense weathering of the rock in the deeper section of the subsurface. The study recommends the removal of the remaining pavement, installing thick base and sub-base materials to raise the road above the surface level, and constructing drainage channels on the two sides of the road before reconstructing new pavement.

Conclusion

The concern of road users on the cause of the repeated failure of the University of Ilorin - Teaching Hospital Road has been addressed in this study. Findings from this study have been used to propose solutions to repeat failure of the pavements along the road. The principal cause of pavement failure and pothole development on the road is the high moisture content in the near subsurface layer due to water ingress and poor drainage system. The 2D resistivity models beneath the road showed that the failed portions of the road pavement are characterized by low resistivity breakouts amidst the high resistivity layer in the top two meters. The deeper section of the road is characterized by weathered rocks of high moisture content and elongated vertical features. The vertical features suggest weak zones and brittle structures filled with low-resistivity weathered rocks that are not strong enough to support heavy loads presented by some vehicles using the road. Overall, the results showed that the augmented 2D resistivity survey is appropriate for road failure investigations. Therefore the

method removed the barrier created by the unaffordability of ERI equipment. The study recommends the removal of the remaining pavement, installing thick base and sub-base materials to raise the road above the surface level, and constructing drainage channels on the two sides of the road before reconstructing new pavement.

REFERENCES

Abubakar H.O., Raji W.O., Bayode S. Direct current resistivity and very low-frequency electromagnetic studies for groundwater development in a basement complex area of Nigeria. Science Focus, Vol. 19, No. 1, 2014, pp.1-10.

Ademila O. Combined geophysical and geotechnical investigation of pavement failure for sustainable construction of Owo-Ikare highway, Southwestern Nigeria. NRIAG Journal of Astronomy and Geophysics, Vol. 10, No. 1, 2021, pp. 183-201, DOI: 10.1080/20909977.2021.1900527.

Adeoti L., Ojo A., Adegbola R. B., Fasakin O. Geoelectric assessment as an aid to geotechnical investigation at a proposed residential development site in Ilubirin, Lagos, Southwestern Nigeria. Arabian Journal of Geoscience, Vol. 9, No. 5, 2016, DOI: 10.1007/s12517-016-2334-9.

Arjwech R., Everett M., Briaud J.L., Hurlebaus S., Medina-Cetina Z., Tucker S., Yosefpour N. Electrical resistivity imaging of unknown bridge foundations. Near Surface Geophysics. Vol. 11, No. 1, 2013, pp. 591-598, DOI: https://doi.org/10.3997/1873-0604.2013023.

Aromoye S.A, Alimi S.A., Bello O.S., Raji W.O., Olawale L.O., Bonde D.S. 2-D Electrical Resistivity Tomography for groundwater potential in basement terrain of a part of Ilorin Sheet 223 NW Nigeria. Saudi Journal of Engineering and Technology, Vol. 4, No. 9, 2019, pp. 357-362, DOI:10.36348/SJET.2019.v04i09.004.

Castilho G., Maia D. A Successful mixed land-underwater 3D resistivity survey in an extremely challenging environment in Amazônia. 21st EEGS Symposium on the Application of Geophysics to Engineering and Environmental Problems, 2008, pp. 1150-1158, DOI:10.4133/1.2963224.

Cardarelli E., Cercato M., Donno D.G. Surface and borehole geophysics for the rehabilitation of a concrete dam (Penne, Central Italy). Engineering Geology, Vol. 241, No.1, 2018, pp. 1-10, https://doi.org/10.1016/j.enggeo.2018.05.008.

Dahlin T. The development of DC resistivity imaging techniques. Computers and Geosciences, Vol. 27, No. 9, 2001, pp. 1019-1029, DOI:10.1016/S0098-3004(00)00160-6.

Feyisa H.N., Gebissa F.T. Geophysical investigation of road failure: A case study of Gedo-Ijaji Asphalt Road, Oromia Regional State, Ethiopia. Journal of Geology and Geophysics, Vol. 12, No. 3, 2023, p. 1081.

Haile T., Ayele A. Electrical resistivity tomography and magnetic surveys: Applications for building site characterization at Gubre, Wolkite University site, western Ethiopia. SINET: Ethiopian Journal of Science, Vol. 37, No. 1, 2014, pp. 13-30.

Karastathis V.K., Karmis P.N., Drakatos G., Stavrakakis G. Geophysical methods contributing to the testing of concrete dams, application at the Marathon Dam. Journal of Applied Geophysics, Vol. 50, No. 3, 2002, pp. 247-260, https://doi.org/10.1016/S0926-9851(02)00145-3.

Loke M.H., Barker R.D. Practical techniques for 3D resistivity surveys and data inversion. Geophysical Prospecting, Vol. 44, No. 3, 1996, pp. 499-523, https://doi.org/10.1111/j.1365-2478.1996.tb00162.x.

Loke M.H., Rucker D.F., Chambers J.E., Wilkinson P.B., Kuras O. Electrical resistivity surveys and data interpretation. In:

ЛИТЕРАТУРА

Abubakar H.O., Raji W.O., Bayode S. Direct current resistivity and very low-frequency electromagnetic studies for groundwater development in a basement complex area of Nigeria. Science Focus, Vol. 19, No. 1, 2014, pp.1-10.

Ademila O. Combined geophysical and geotechnical investigation of pavement failure for sustainable construction of Owo-Ikare highway, Southwestern Nigeria. NRIAG Journal of Astronomy and Geophysics, Vol. 10, No. 1, 2021, pp. 183-201, DOI: 10.1080/20909977.2021.1900527.

Adeoti L., Ojo A., Adegbola R. B., Fasakin O. Geoelectric assessment as an aid to geotechnical investigation at a proposed residential development site in Ilubirin, Lagos, Southwestern Nigeria. Arabian Journal of Geoscience, Vol. 9, No. 5, 2016, DOI: 10.1007/s12517-016-2334-9.

Arjwech R., Everett M., Briaud J.L., Hurlebaus S., Medina-Cetina Z., Tucker S., Yosefpour N. Electrical resistivity imaging of unknown bridge foundations. Near Surface Geophysics. Vol. 11, No. 1, 2013, pp. 591-598, DOI: https://doi.org/10.3997/1873-0604.2013023.

Aromoye S.A, Alimi S.A., Bello O.S., Raji W.O., Olawale L.O., Bonde D.S. 2-D Electrical Resistivity Tomography for groundwater potential in basement terrain of a part of Ilorin Sheet 223 NW Nigeria. Saudi Journal of Engineering and Technology, Vol. 4, No. 9, 2019, pp. 357-362, DOI:10.36348/SJET.2019.v04i09.004.

Castilho G., Maia D. A Successful mixed land-underwater 3D resistivity survey in an extremely challenging environment in Amazônia. 21st EEGS Symposium on the Application of Geophysics to Engineering and Environmental Problems, 2008, pp. 1150-1158, DOI:10.4133/1.2963224.

Cardarelli E., Cercato M., Donno D.G. Surface and borehole geophysics for the rehabilitation of a concrete dam (Penne, Central Italy). Engineering Geology, Vol. 241, No.1, 2018, pp. 1-10, https://doi.org/10.1016/j.enggeo.2018.05.008.

Dahlin T. The development of DC resistivity imaging techniques. Computers and Geosciences, Vol. 27, No. 9, 2001, pp. 1019-1029, DOI:10.1016/S0098-3004(00)00160-6.

Feyisa H.N., Gebissa F.T. Geophysical investigation of road failure: A case study of Gedo-Ijaji Asphalt Road, Oromia Regional State, Ethiopia. Journal of Geology and Geophysics, Vol. 12, No. 3, 2023, p. 1081.

Haile T., Ayele A. Electrical resistivity tomography and magnetic surveys: Applications for building site characterization at Gubre, Wolkite University site, western Ethiopia. SINET: Ethiopian Journal of Science, Vol. 37, No. 1, 2014, pp. 13-30.

Karastathis V.K., Karmis P.N., Drakatos G., Stavrakakis G. Geophysical methods contributing to the testing of concrete dams, application at the Marathon Dam. Journal of Applied Geophysics, Vol. 50, No. 3, 2002, pp. 247-260, https://doi.org/10.1016/S0926-9851(02)00145-3.

Loke M.H., Barker R.D. Practical techniques for 3D resistivity surveys and data inversion. Geophysical Prospecting, Vol. 44, No. 3, 1996, pp. 499-523, https://doi.org/10.1111/j.1365-2478.1996.tb00162.x.

Loke M.H., Rucker D.F., Chambers J.E., Wilkinson P.B., Kuras O. Electrical resistivity surveys and data interpretation. In:

Encyclopedia of solid earth geophysics. Cham: Springer International Publishing. 2020, pp. 1-6. Available from: https://doi.org/10.1007/978-3-030-10475-7_46-1.

Neyamadpour A., Abdullah W.A.T.W., Taib S., Neyamadpour B. Comparison of Wenner and dipole-dipole arrays in the study of an underground three-dimensional cavity. Journal of Geophysics and Engineering, Vol. 7, No. 1, 2010, pp. 30-40, DOI.org/10.1088/1742-2132/7/1/003.

Olasehinde P.I., Raji W.O. Geophysical studies on fractures of basement rocks at University of Ilorin, Southwestern Nigeria: application to groundwater exploration. Water Resources, Vol. 17, No.1, 2007, pp. 3-10.

Osinowo O.O., Akanji A.O., Akinmosin A. Integrated geophysical and geotechnical investigation of the failed portion of a road in basement complex terrain of southwestern Nigeria. RMZ-material and Geoenvironment, Vol. 58, No. 2, 2011, pp. 143-162.

Raji W.O., Aluko K.O. Investigating the cause of excessive seepage in a dam foundation using seismic and electrical surveys – a case study of Asa Dam, West Africa. Bulletin of Engineering Geology and the Environment, Vol. 80, No. 1, 2021, pp. 6445-6455, https://doi.org/10.1007/s10064-021-02329-9.

Raji W.O., Adeoye T.O., Ibrahim K.O. Geophysical investigation for Basement Rock Structures around a proposed Dam site. Adamawa State University Journal of Scientific Research, Vol. 5, No. 2, 2017, pp. 38-49.

Raji W.O., Abdulkadir K.A. Geo-resistivity data set for groundwater aquifer exploration in the basement complex terrain of Nigeria, West Africa, Data-in-brief, Vol. 31, No. 1, 2020, https://doi.org/10.1016/j.dib.2020.105975.

Raji W.O., Sulaiman M.O. Road failure investigations using improvised 2-D Geo-Resistivity Surveys. Near-surface Geophysics, 29th European Meeting of Environmental and Engineering Geophysics, Vol. 20203, 2023, pp. 1-5, DOI: https://doi.org/10.3997/2214-4609.202320062.

Rucker M. Surface geophysics as a tool for the characterization of existing bridge foundations and scour conditions. Proceedings of the Conference on Applied Geophysics, Missouri, U.S.A., December, 2006, pp. 4-7.

Soupios P.M., Georgakopoulos P., Papadopoulos N., Saltas V., Andeadakis A., Vallianatos F., Sarris A., Makris J.P. Use of engineering geophysics to investigate a site for a building foundation. Journal of Geophysics and Engineering, Vol. 4, No. 1, 2007, pp. 94-103, DOI:10.1088/1742-2132/4/1/011.

ПРИМЕНЕНИЕ ИНТЕГРИРОВАННОЙ 2D МОДЕЛИ ГЕОЭЛЕКТРИЧЕСКОГО СОПРОТИВЛЕНИЯ ДЛЯ ИССЛЕДОВАНИЯ ПРИЧИН РАЗРУШЕНИЯ ДОРОЖНОГО ПОКРЫТИЯ

Раджи У.О.[1, 2], Сулейман М.О.[1]
*[1]Факультет геофизики, Университет Илорина, Илорин, Нигерия
РМВ 1515, Илорин, Штат Квара, Нигерия
[2]Факультет наук о Земле, Карлтонский университет, Оттава, Канада
1125 Colonel By Dr,Оттава, ON K1S 5B6: lanreraji@unilorin.edu.ng, wasiu.raji@gmail.com*

Резюме. Метод визуализации удельного сопротивления (ERI) в геофизике активно используется в гражданском строительстве для предварительной оценки строительных площадок, а также для послестроительных исследований и восстановительных работ. Однако высокая стоимость оборудования ERI ограничивает его применение в слаборазвитых и развивающихся странах, а также в исследованиях без финансирования. Недавние успехи в полевых методах, технологиях, инструментах и программном обеспечении в геофизике расширили применение электрорезистивных методов в таких областях, как судебные экспертизы, инженерное дело и экологические исследования. В данном исследовании эта проблема решается путем применения альтернативной и надежной техники многократной визуализации подповерхностных слоев для инженерных целей, используя традиционное оборудование 1D измерений электрического сопротивления Земли и расположенных массивов электродов. Эта техника применялась для выяснения главной причины разрушения дорожного покрытия вдоль дороги Университетской клиники в Илорине, Нигерия. Модели сопротивления, полученные на основе экспериментальных данных 2D-съемки, показывают зоны низкого сопротивления, участки выветривания с высоким содержанием влаги, зоны слабых участков и удлиненные хрупкие структуры в верхнем десятиметровом слое недр. Слои с высоким удельным сопро-

тивлением соответствуют устойчивым участкам дорожного покрытия, в то время как зоны с низким удельным сопротивлением в верхней части моделей удельного сопротивления соответствуют поврежденным покрытиям и выбоинам на дороге. Продолговатые вертикальные структуры были определены как слабые зоны, которые служили каналами для дождевой воды сверху и грунтовых вод, что ускоряло процессы выветривания в этом районе.

Ключевые слова: Исследование разрушений дорожного покрытия, геофизическое исследование, визуализация электрического сопротивления, 2D расширенный массив, модели подповерхностной резистивности

YOL ÖRTÜYÜNÜN DAĞILMA SƏBƏBLƏRİNİN TƏDQİQATI ÜÇÜN İNTEQRASİYA OLUNMUŞ 2D GEOELEKTRİK MÜQAVİMƏT MODELİNİN TƏTBİQİ

Raji U.O.[1,2], Suleyman M.O.[1]
[1]*İlori Universitetinin Geofizika kafedrası, İlori, Nigeriya*
PMB 1515, İlori, Kvara Ştatı, Nigeriya
[2]*Karlton Universitetinin Yer Elmləri kafedrası, Ottava, Kanada*
1125 Colonel By Dr, Ottava, ON K1S 5B6: lanreraji@unilorin.edu.ng, wasiu.raji@gmail.com

Xülasə. Geofizikada xüsusi elektrik müqavimətinin (ERI) vizuallaşdırma metodu mülki inşaat işlərində ərazilərin ilkin qiymətləndirilməsi, eləcə də tikintidən sonrakı analiz və bərpa işləri üçün geniş istifadə olunur. Lakin ERI avadanlığının yüksək dəyəri onun az inkişaf etmiş və inkişaf etməkdə olan ölkələrdə, həmçinin maliyyə dəstəyi olmayan tədqiqatlarda istifadəsini məhdudlaşdırır. Geofiziki mühitdə sahə metodları, texnologiyalar, avadanlıqlar və proqram təminatında son yeniliklər elektrik müqaviməti metodlarının hüquqi ekspertiza, mühəndislik və ekoloji tədqiqatlar kimi sahələrdə tətbiqini genişləndirib. Bu tədqiqatda mühəndislik məqsədləri üçün səthaltı təbəqələrin alternativ və etibarlı çoxölçülü təsvir texnikası təklif edilir, burada ənənəvi 1D torpaq elektrik müqaviməti ölçmə avadanlığı və elektrodlar qruplarından istifadə edilir. Bu texnika, Nigeriyanın İlori şəhərindəki Universitet Klinikasının yaxınlığındakı yolun üstünün dağılma səbəbini araşdırmaq üçün tətbiq edilmişdir. 2D çəkilişlərindən əldə edilən eksperimental məlumatlara əsaslanaraq əldə olunan rezistivlik modelləri, aşağı rezistivlik zonalarını, yüksək rütubət tərkibli aşınma sahələrini, zəif hissələri və üstdəki 10 metrlik yeraltı qatında uzanan həssas strukturları göstərir. Yüksək spesifik rezistivlik qatları yol üstünün dayanıqlı hissələrinə uyğun gəlir, aşağı spesifik rezistivlik zonaları isə zədələnmiş örtüklər və yoldaki oyuqlara uyğundur. Uzunsov şaquli strukturlar zəif zonalar kimi müəyyən edilmişdir ki, bu da üst tərəfdən yağış suyunun və yeraltı suyun kanalları kimi xidmət edərək, bu ərazidə aşınma proseslərini sürətləndirir.

Açar sözlər: *Yol örtüyünün dağılmalarının tədqiqi, elektrik müqavimətinin vizuallaşdırılması, 2D formatında genişlənmiş massiv, səthaltı rezistivliyin modeli*

APPLICATION OF REMOTE SENSING AND GEOGRAPHIC INFORMATION SYSTEMS (GIS) FOR TSUNAMI POTENTIAL MAPPING IN SIKKA DISTRICT, EAST NUSA TENGGARA

Sianturi H.L., Tanesib J.L., Louk A.C., Blegur D.I., Warsito A.

Department of Physics, Faculty of Science and Engineering, Nusa Cendana University, Indonesia
Jln. Adisucipto – Penfui, Kupang 85001 NTT, Indonesia: hlsianturi@staf.undana.ac.id

Summary. This study aims to map potential tsunami areas, evacuation routes and gathering points in Sikka District, East Nusa Tenggara Indonesia. Mapping is carried out using geographic information systems through a tsunami vulnerability analysis approach. The vulnerability approach is conducted using some criteria including land elevation, slope, land use, distance from the coastline, and distance from rivers. Population factors are also used to determine the level of tsunami risk. Overall, the coastal areas of Sikka District are potentially at risk of tsunami. The level of potential is very high in the northern coastal areas of Magepanda Regency, West Alok District, Alok District, East Alok District, Kangae District, Kewapante District, Waigete District, Talibura District and some small islands in the north of Sikka District, namely Pemana Island, Big Island, and Babi Island. Areas with high vulnerability are mostly found on the north coast and a small part on the south coast. These areas with a very high and high level of risk are still relatively small, which is about 6% of the total area of Sikka District. However, these potential areas are in a dense residential area, therefore tsunami mitigation has been developed in the form of comprehensive evacuation routes and gathering points to reduce the negative impact of tsunamis. The earthquake event used as a reference is with a magnitude of 7.3 on the Richter scale at a depth of 114 km north of Sikka District.

Introduction

The Indonesian archipelago is highly prone to earthquakes and tsunamis. Being densely populated, the Indonesian archipelago has more persons exposed to such geophysical hazards than any other country in the world (Dhellemmes et al., 2021; Hall et al., 2022). Some major geophysical disasters have occurred in the region including the 2004 Indian Ocean earthquake and tsunami that killed over 165,000 people of Indonesia, making it one of the deadliest socio-natural disasters in the 21st century (Hall et al., 2022; BNPB, 2012).

To minimize the impact of tsunamis on the community, a number of studies have been conducted to investigate and develop tsunami mitigation models for some regions in Indonesia. Areas covered in the studies include Banda Aceh (Agussaini et al., 2022; Nurhayaty et al., 2015), Palu Bay (Imran et al., 2020), Pangandaran beach-West Java (Faiqoh et al., 2013), Padang city-West Sumatera (Imamura et al., 2012), Manacarra beach-West Sulawesi (Baeda, et al., 2015), and Labuan Bajo-East Nusa Tenggara (Wibowo, 2022). Such studies have provided the society including the government with more obvious tsunami mitigation concept and better mitigation strategies to minimize the negative effects of potential tsunami hazards in the future.

Sikka District, which is a part of the East Nusa Tenggara Province, is an area with a fairly high level of tsunami risk because this area is close to the subduction zone of the Australian and Eurasian tectonic plates and is influenced by active faults along the Flores Island (Fauzy, 2006; Sengaji and Nababan, 2009). Sengaji and Nababan (2009) have made tsunami level map in Sikka region but the authors have not investigated in details the tsunami disaster mitigation efforts, namely the process of seeking various preventive measures to minimize the negative impact of the tsunami disaster. Hence, the purpose of the present work is to map the level of potential Tsunami disaster and map evacuation routes and gathering points of potential Tsunami areas in Sikka District. The map will be made by applying the remote sensing systems and geographic information, which was previously used to map the tsunami potential map in Kupang Regency, East Nusa Tenggara (Rumaal et al., 2018).

METHOD
Database Building

Extensive data processing is carried out by collecting data from various sources which are then processed to obtain each parameter, namely Digital Elevation Model (DEM) data producing slope maps, elevation, distance from rivers and Landsat 8 image data (Band 4, 3, 2, & 8) for land cover maps, and coastline data producing distance maps from the coastline. Meanwhile, the preparation of evacuation route maps and gathering points uses Sikka District Road Network data and local building data. Areas at risk of tsunami impact can also be identified through population density at each monitoring location (Julkarnaen 2008; Sinaga et al., 2011).

Scoring and Weighting of Potential Levels

The rating and weighting system for each parameter corresponds to the influence exerted on the tsunami disaster, the greater the effect, the greater the weight, and vice versa, the smaller the influence, the smaller the weight (Papathoma et al., 2003; Irfani, 2002).

Spatial analysis is used for the determination of tsunami potential using the CBM method, both to classify and to overlay each parameter obtained. All parameters used will be in a grid format consisting of a set of cells. Each cell has a certain value, the magnitude of which depends on the magnitude of each parameter. In determining the level of vulnerability, calculations are also carried out by assigning scores and weights to each parameter. The score is multiplied by the weight used in each parameter. The value of each class is based on the following formula (Muzaki et al., 2009):

$$N = \sum Bi \; x \; Si \qquad (1)$$

where:

N= Total value weight
Bi = Weight on each criterion
Si = Score on each criterion
I = i^{-th} parameter

Furthermore, it is grouped based on its value into five classes (zones) namely very high potential, high, intermediate, low and very low potential. The interval of each class is obtained from the number of maximum value multiplications of each weight and score minus the number of minimum value multiplications which are then divided by the number of parameters used. Mathematically, the interval of tsunami vulnerability level classes is formulated as follows (Muzaki et al., 2009):

$$Hose \; width \; class \; (L) = \sum \frac{(Bi \; x \; Si) \max - (Bi \; x \; Si) min}{n} \qquad (2)$$

where:

L = Hose grade width
n = Number of classes

Data Interpretation

Data interpretation is carried out qualitatively and quantitatively by separating each vulnerability map, namely for vulnerability according to land cover map, slope, altitude, distance from coastline, and distance from rivers. The impact of tsunami insecurity in terms of population density is interpreted in a similar way (Eddy, 2006; Muck, 2008).

RESULTS AND DISCUSSION
Map of the Study Area

Sikka District is located between 8°22' to 8°50' south latitude and 121°55'40" to 122°41'30" east longitude. Administratively, the boundaries of Sikka District are north of the Flores Sea, south of the Sawu Sea and the west is bordered by Ende District and east of East Flores District. Sikka District consists of 21 sub-districts covering 13 villages, and has an area of 7,552.91 km^2 consisting of 1,731.90 km^2 of land area and 5,821 km^2 of sea area. The study area is presented in Fig. 1.

Slope

Slope is an important parameter in determining tsunami potential, the steeper a landmass, the higher the lower the rise (Sambah and Miura, 2014). In this study, the slope weighed 20%. The slope is derived from elevation using the Surface analyst function on the analyst's spatial menu. The slope map is visualized in Fig. 2.

The areas of the slope mapping results of Sikka District are depicted in Table 1.

Table 1

Potential Slope Area of Sikka District Elevation

No	Potential Level	Class	Area (km^2)
1	Very Low	> 40%	4.745
2	Low	15 - 40%	672.6
3	Intermediate	6 - 15%	675.87
4	Tall	2 - 6%	220.83
5	Very High	0 - 2%	79.199

The elevation classification is divided into 5 classes, namely very high class (< 10m), high class (10 - 25 m), medium (25 - 50m), low (50 - 150m), and very low (>150m). Fig. 3 shows the elevation map while the area of elevation classes in Sikka District is presented in Table 2.

Table 2

Area of elevation potential of Sikka District

No	Potential Level	Class	Area (km^2)
1	Very Low	>150 m	1389.3
2	Low	50–150 m	126.46
3	Intermediate	25 – 50 m	74.33
4	Tall	10 – 25 m	76.07
5	Very High	>10 m	20.21
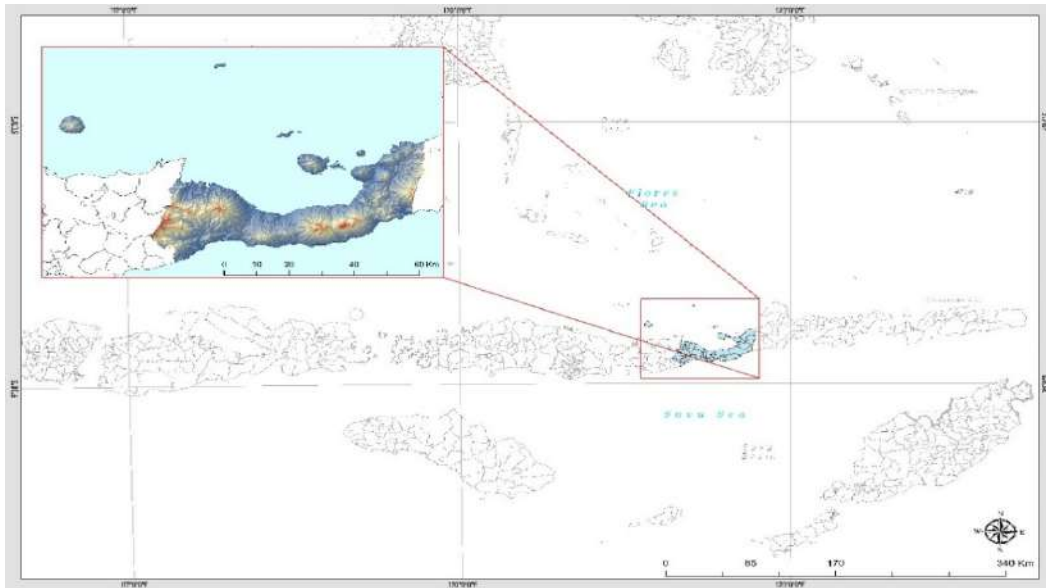
Fig. 1. Map of the study area

Fig. 2. Map of slope research area
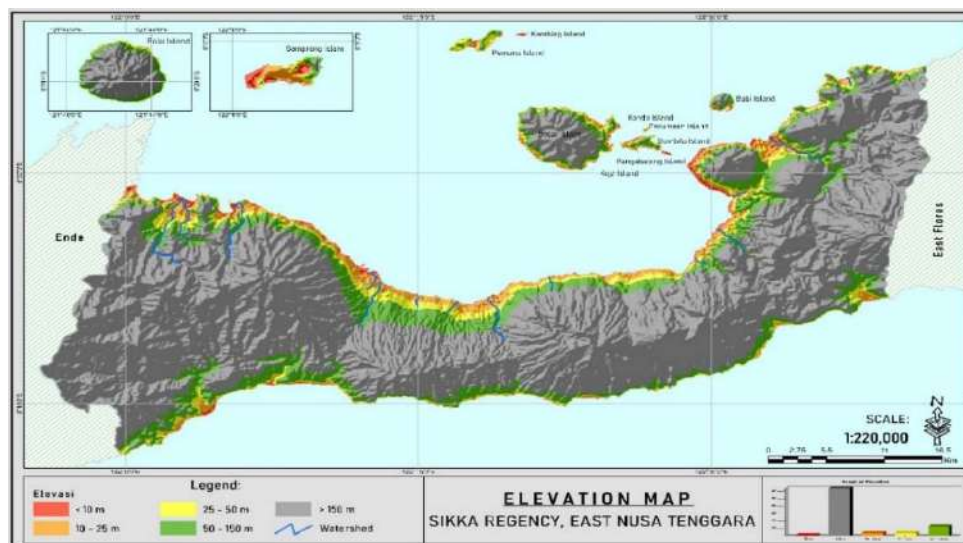
Fig. 3. The Elevation map of research area

Land use

Based on data obtained from data processing, land use including forests, community gardens, fields, dry land, settlements, and noise in the form of clouds, is visualized and can be seen in Fig. 4. From Fig. 4, the area of each land use in Sikka District is calculated and depicted in Table 3.

Table 3

Land cover area of Sikka District

No	Types of Land Use	Potential Level	Area (km²)
1	Forest	Very Low	369.5
2	Citizen Gardens (rice fields and other types of farming)	Low	425.4
3	Garden	Intermediate	436.2
4	Dry Land	Tall	330.2
5	Village	Very High	117.4
6	Cloud	Very Low	8.77

Distance from Coastline

The settlement of residents in Sikka District is directly adjacent to the sea. Therefore, in this study, the distance parameter from the coastline was one of the important factors in the analysis (Faiqoh, et al., 2013). The distance map is processed from the coastline (Fig. 5). Based on the potential class area, the distance from the coastline in Sikka District has been calculated and presented in Table 4.

Distance from the River

Tsunamis that enter the river flow will cause great damage, when the tsunami passes through a narrow area such as a river, there will be an increase in speed and an increase in water mass because the flow of the same water mass must travel a narrow distance at the same time (Pratiwi, 2017). The results of mapping the distance from the river can be seen in Fig. 6 with corresponding areas shown in Table 5.

Table 4

Distance from the coastline of Sikka District

No	Distance	Potential Level	Area (km²)
1	0 - 500 m	Very Low	102.37
2	500 - 1000 m	Low	78.65
3	1000 - 1500 m	Intermediate	70.74
4	1500 - 3000 m	Tall	184.98
5	> 3000 m	Very High	1233.34

Table 5

Area Distance from river Sikka Regency

No	Distance	Potential Level	Area (km²)
1	0 - 100 m	Very Low	102.37
2	100 - 200 m	Low	78.65
3	200 - 300 m	Intermediate	70.74
4	300 - 500 m	Tall	184.98
5	> 500 m	Very High	1233.34

Fig. 4. Land cover map

Fig. 5. Distance map from coastline

Fig. 6. Map of potential distance from Sikka Regency River

Analysis of Regional Potential for Tsunami Disaster

Analysis of tsunami potential levels is carried out using the overlay method of all parameters contained in the potential level analysis matrix. The classification of tsunami potential levels in Sikka District consists of 5 categories, namely very high, high, medium, low, very low. The map of the potential level of Sikka District is shown in Fig. 7.

Areas with very low (R5) and low (R4) tsunami disaster potential, namely most of the southern part of the area dominated by highlands with elevation conditions (topography) of 50 m to 1668 m include Nita District, south of Magepanda Regency, south of Waigete Regency, south of Waiblama District, south of Talibura, Hewakloang District, south of Kange District, south of District Nelle, Mego District, Mapitra District, Doreng District, Bola District, Lera District, Paga District. A map of the northern part of Sikka district with potential levels can be seen in Fig. 8.

Very high potential dominates the northern coastal area of Sikka district. This is supported by the state of elevation (topography) of coastal areas ranging from 0 m – 25 m with a slope of 0 – 6%. Areas that have a very large impact supported by population density are the northern coastal areas of Magepanda district, Palueisland, west Alok regency, Alok regency, east Alok regency, Kangae regency, Kewapante district, Waigete regency, Talibura regency and on the northern small island of Sikka district. Based on the calculation of tsunami potential maps, each category has an area (Table 6).

Table 6

Extent of tsunami potential in Sikka District

No	Potential Classes	Potential Level	Area (km^2)	Percentage
1	R5	Very Low	11.76	1%
2	R4	Low	85.70	5%
3	R3	Intermediate	237.27	14%
4	R2	High	1336.72	79%
5	R1	Very High	20.76	1%
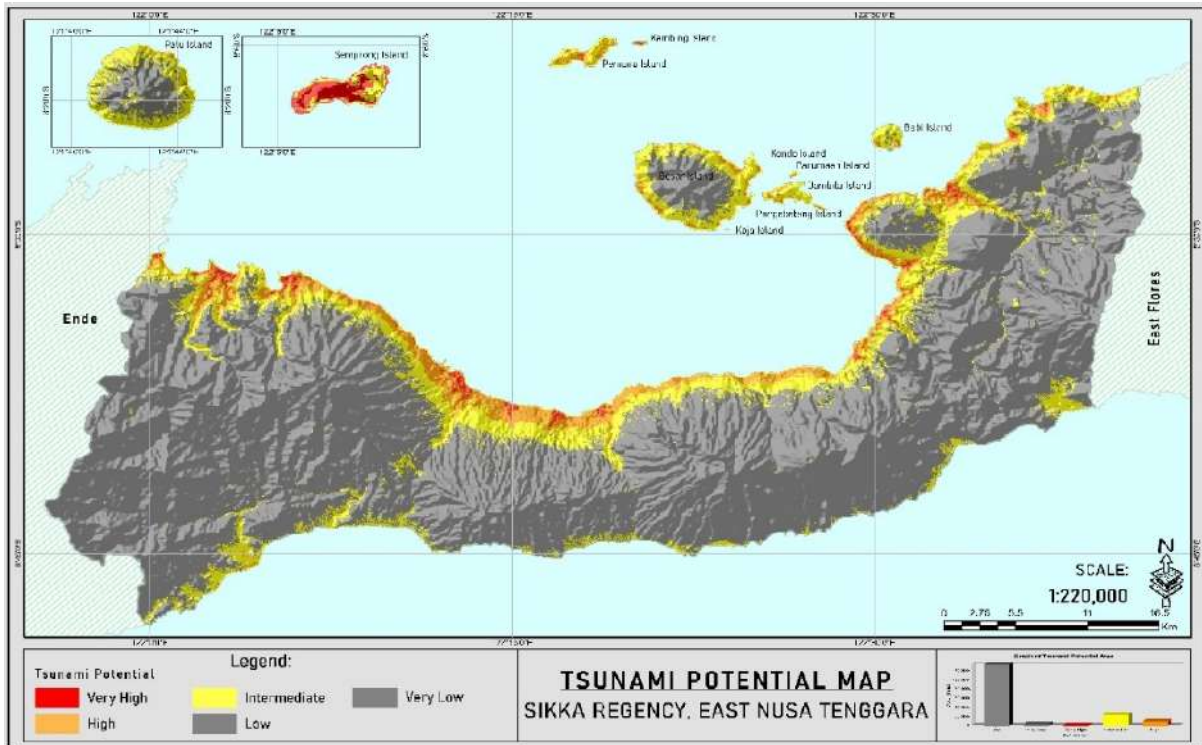
Fig. 7. Sikka District tsunami potential level map
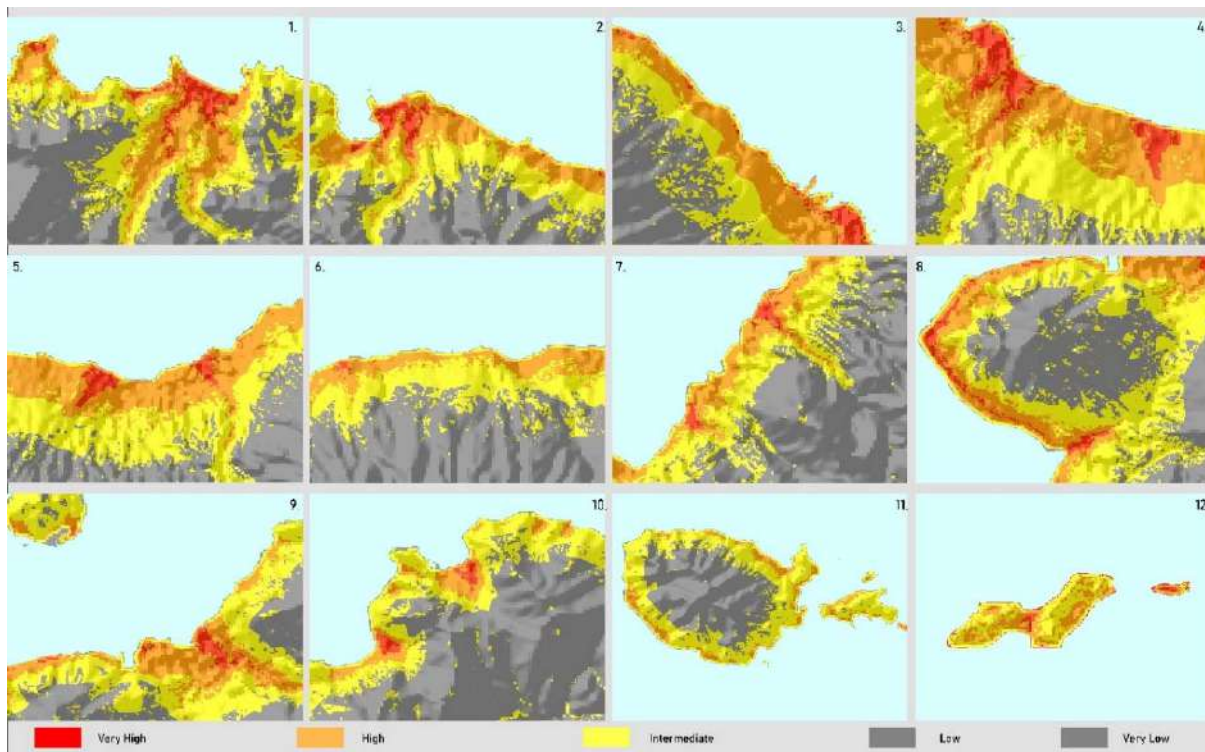
Fig. 8. Map of tsunami potential level of Northern Sikka District

Areas with high (R2) and very high (R1) vulner-ability to tsunami disasters are areas with the greatest potential for damage, both in terms of physical dam-age to the environment and casualties. Environmental damage and loss of life are included in the category of direct damage. Direct damage is defined as fiscal damage or loss that can be quantified in quantity, e.g. casualties, damage to buildings, plantation land, and agricultural land (Pramana, 2015; Primary, 2017). This area has the characteristics of low land elevation (topography), gentle slopes, land use in the form of plantations, rice fields, settlements, distance from the

coastline is relatively close, and the presence of large rivers that empty into the sea.

Areas with low (R4) and very low (R5) vulnerability categories are areas that are safe from being hit by tsunami waves. This area has the characteristics of high land elevation (topography), steep slopes, land use in the form of forests and settlements that are not too dense, and the distance from the coastline and rivers is relatively far.

Disaster Mitigation

To reduce the impact received by tsunami hazards in coastal areas, efforts to reduce the vulnerability of tsunami disasters in Sikka District are one of them through efforts by making maps of evacuation routes and gathering points so that they can help the community in dealing with tsunami disasters (Cutter, et al., 2008; Di Mauro, et al., 2013; Syamsidik, et al., 2021). In terms of reducing fatalities from the impact of the tsunami disaster, here is a map of the evacuation routes of Sikka District as shown in Fig. 9 and maps of evacuation routes and gathering points of the northern coastal area of Sikka District as presented in Fig. 10.

Table 7

Location of Tsunami Disaster Evacuation Points

Number	Name	Elevation
1	Catholic College of Philosophy	217m
2	SMPK Hewerbura Watublapi	455m
3	Hewokloang Village Office	437m
4	Umagera Village Office	185m
5	Nelle District Office	138m
6	Scalabrinian monastery	102 m
7	Convent of the sisters of Mercedaria Solm	52 m
8	Korean Sister	279m
9	Church of St. Gabriel Ladubewa	97m
10	St. John's Chapel Blidit Stasi Bath	142 m
11	Santissima Runut Catholic Church	412 m
12	Church of St. Catholic John the Baptist	401 m
13	Capela Hubin Tekaiku	340m
14	Holy Cross Parish Church Kloangrotat	551 m
15	Sacred Heart of Jesus Catholic Church	170m
16	St. Arnold Jansen Catholic Church	131 m
17	St. Catholic Church of Mary Immaculata Habi	58m
19	Napungete Dam	246m
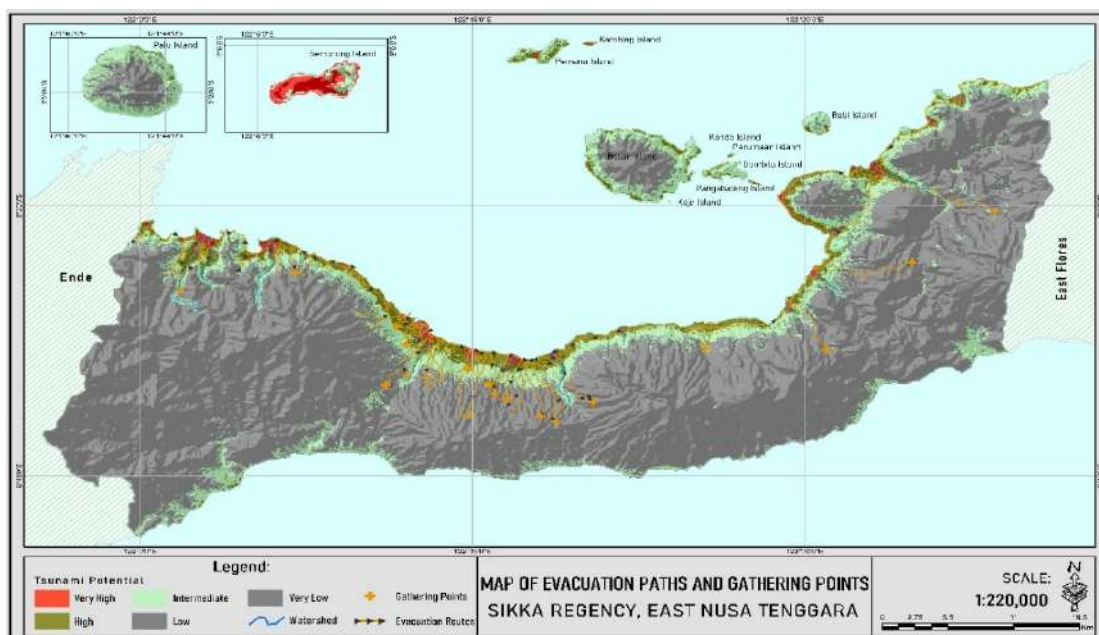
Fig. 9. Map of evacuation routes and gathering points in the northern part of Sikka District
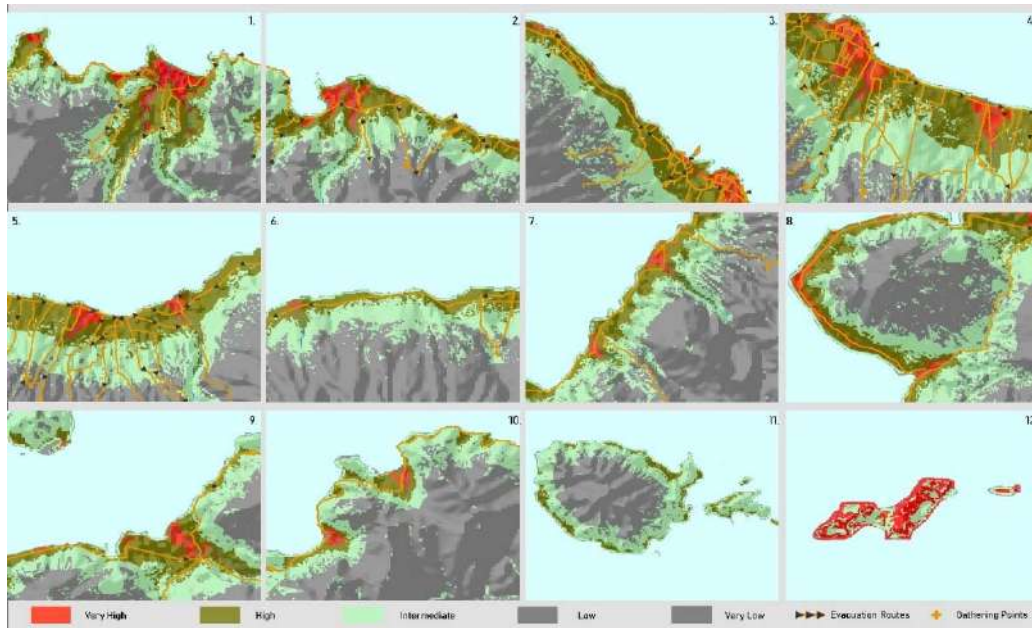
Fig.10. Map of evacuation routes and gathering points of Sikka District

Figs 9 and 10 illustrate evacuation routes and gathering points in Sikka District where the above mentioned data is obtained from spatial data, namely road networks and government facilities, religious facilities, and educational facilities. The evacuation route is a rescue route specifically designed by connecting the entire area to a safe area as a Gathering Point for residents or communities in the area. Evacuation routes serve to direct residents from the threat of danger to a safer place in the event of a disaster. The evacuation routes above include all roads that are in areas with high levels of vulnerability to safer areas or areas with very low levels of vulnerability. The gathering point between them is summarized in Table 7.

Table 7 is dominated by safe evacuation places or points and among them there are 3 temporary evacuation sites, namely the Convent of the sisters of Mercedaria Solm with an altitude of 52 m above sea level, the Catholic Church of St. Mary Immakulata Habi with an altitude of 58 m above sea level, and the Convent of the Sisters PACR Wolonmaget with an altitude of 32 m above sea level.

CONCLUSION

A map of tsunami potential, as well as evacuation routes and gathering points in Sikka District with varying degrees, have been obtained in the present work. Areas that have very high and high levels of tsunami potential include the northern coastal areas of Sikka District while areas affected by the tsunami disaster when the earthquake occurred are the north coast of Magepanda Regency, Palue Island, West Alok Regency, Alok District, East Alok District, Kangae District, Kewapante District, Waigete District, Talibura District and some small islands north of Sikka District, namely Pemana Island, Big Island, and Pig Island. Meanwhile, emergency gathering points during the tsunami were St. Gabriel Ladubewa Church, St. Mary Immaculate Habi Catholic Church, Mercedaria Solm Sisters Monastery.

REFERENCES

Agussaini H., Sirojuzilam S., Rujiman R., Purwoko A. A new approach of the tsunami mitigation strategies for the city of Banda Aceh, Indonesia. Indonesian Journal of Geography, Vol. 54, No.1, 2022, pp. 62-99.
Baeda A.Y., Suriamihardja D.A., Umar H., Rachman T. Tsunami Mitigation Plan for Manakarra Beach of West Sulawesi Province, Indonesia. Procedia Engineering, Vol. 116, No.1, 2015, pp. 134-140.
BNPB (Indonesia Disaster Management Agency). Master Plan of Tsunami Risk Reduction, Jakarta, 2015.
Cutter S.L., Barnes L., Berry M., Burton C., Evans E., Tate E., Webb J. A place-based model for understanding community resilience to natural disasters. Global environmental change, Vol. 18(4), 2008, pp. 598-606.

ЛИТЕРАТУРА

Agussaini H., Sirojuzilam S., Rujiman R., Purwoko A. A new approach of the tsunami mitigation strategies for the city of Banda Aceh, Indonesia. Indonesian Journal of Geography, Vol. 54, No.1, 2022, pp. 62-99.
Baeda A.Y., Suriamihardja D.A., Umar H., Rachman T. Tsunami Mitigation Plan for Manakarra Beach of West Sulawesi Province, Indonesia. Procedia Engineering, Vol. 116, No.1, 2015, pp. 134-140.
BNPB (Indonesia Disaster Management Agency). Master Plan of Tsunami Risk Reduction, Jakarta, 2015.
Cutter S.L., Barnes L., Berry M., Burton C., Evans E., Tate E., Webb J. A place-based model for understanding community resilience to natural disasters. Global environmental change, Vol. 18(4), 2008, pp. 598-606.

Dhellemmes A., Leonard G.S., Johnston D.M., Vinnell L.J., Becker J.S., Fraser S.A., Paton D. Tsunami awareness and preparedness in Aotearoa New Zealand: The evolution of community understanding. International Journal of Disaster Risk Reduction, Vol. 65, 2021, 102576.

Di Mauro M., Megawati K., Cedillos V., Tucker B. Tsunami risk reduction for densely populated Southeast Asian cities: analysis of vehicular and pedestrian evacuation for the city of Padang, Indonesia, and assessment of interventions. Natural hazards, Vol. 68, 2013, pp. 373-404.

Eddy. GIS in disaster management: A case study of tsunami risk mapping in Bali, Indonesia. James Cook University, 2006. Available from: http://eprints.jcu.edu.au/29297/.

Faiqoh I., Gaol J.L., Ling M.M. Vulnerability level map of tsunami disaster in Pangandaran Beach, West Java. International Journal of Remote Sensing and Earth Sciences, Vol. 10, No. 2, 2013, pp. 90-103, DOI: http://dx.doi.org/10.30536/j.ijreses.2013.v10.a1848.

Fauzi. Daerah Rawan Gempa Tektonik di Indonesia diakses pada. 2006, http://www.bmg.go.id (5 Juni 2007).

Hall S., Sloan-Aagard C., Harris R., Emmett C., Prasetyadi C., Pettersson J., Cope A., Cox M.H. Perceptions of tsunami susceptibility and self-efficacy among adolescents in Indonesia: The influence of gender, religion, location, age, hazard information source, and past experience. International Journal of Disaster Risk Reduction, Vol. 79, 2022, 103151, DOI:10.1016/j.ijdrr.2022.103151.

Imamura F., Muhari A., Mas E., Pradono M.H., Post J., Sugimoto M. Tsunami disaster mitigation by integrating comprehensive countermeasures in Padang city, Indonesia. Journal of Disaster Research, Vol. 7, No. 1, 2012, pp. 48-64, DOI:10.20965/jdr.2012.p0048.

Imran Z., Sugiarto S.W., Muhammad A.N. Coastal vulnerability index aftermath tsunami in Palu Bay, Indonesia. IOP Conference Series: Earth and Environmental Science, Vol.420, 2020, 012014, DOI 10.1088/1755-1315/420/1/012014.

Irfani M. Landscape patterns in tsunami-prone areas in the application of research results for tsunami disaster management in Indonesia (Sadikin et al. eds.). Proceedings of the Tsunami Seminar in the Framework of research on tsunami hazard and its effect on Indonesian Coastal Region, 2002, pp. 2003-2004, Available from: http://eprints. uny.ac.id/id/eprint/11520.

Julkarnaen D. Identification of spatial-based tsunami risk level in Cilegon City Industrial Estate. Doctoral dissertation, Thesis, Master of Bandung Institute of Technology, 2008, Unpublished, 106 p., Available from: http://pwk. lib.itb.ac.id/index.php/bibliografi/detail/15914.

Muck M. Tsunami evacuation modeling: development and application of spatial information systems that support tsunami evacuation planning in Southwest Bali. Institut für Geographiean der Universität Regensburg, Regensburg, 2008.

Muzaki A.A., Susilo S.B., Agus S.B. Spatial analysis of coral reef ecosystem conditions as a basis for determining marine protected areas with cell based modeling method in Karang Lebar and Karang Congkak Kepulauan Seribu, DKI Jakarta. 2009, Available from: http://repository.ipb.ac.id/handle/123456789/57577.

Nurhayaty A., Wimbarti S., Triatmadja R., Hastjarjo T.D. Model of tsunami preparedness for Indonesian Tsunami Prone Areas Communities. Journal of Disaster Research, Vol. 10, No. 5, 2015, pp. 957-965, DOI:10.20965/jdr.2015.p0957.

Papathoma M., Dominey-Howes D., Zong Y., Smith D. Assessing tsunami vulnerability: an example from Heraklion, Crete. Natural Hazards and Earth System Science, Vol. 3, No, 5, 2003, pp. 377-389, DOI: http://dx.doi.org/10.5194/nhess-3-377-2003.

Pramana B.S. Mapping of tsunami vulnerability in Pelabuhan Ratu District, Sukabumi Regency. SOCIO-DIDACTICS: Journal of Social Science Education, Vol. 2, No. 1, June 23, 2015, pp. 76-91, DOI: http://dx.doi.org/10.15408/sd.v2i1.1383 (in Indonesian).

Primary W.P. Tsunami hazard mapping and its impact on infrastructure in Benoa Bay Area, Bali Province. Brawijaya University Malang. 2017, Available from: http://repository.ub.ac.id/id/eprint/8285.

Sambah A.B., Miura F. Integration of spatial analysis for tsunami inundation and impact assessment. Journal of Geographic

Pratiwi A. Spatial analysis of the vulnerability of the west coast of Banten Province to the tsunami disaster using a Geographic Information System, 2017, Available from: http://repository.ipb.ac.id/handle/123456789/88370 (in Indonesian).

Primary W.P. Tsunami hazard mapping and its impact on infrastructure in Benoa Bay Area, Bali Province. Brawijaya University Malang. 2017, Available from: http://repository.ub.ac.id/id/eprint/8285.

Rumaal L.A., Tanesib J.L., Tarigan J. Application of remote sensing and Geographic Information System for mapping tsunami potential areas in Kupang District, East Nusa Tenggara Province. Journal of Physics: The Physics of Science and Its Applications, Vol. 3, No. 2, 2018, pp. 170-8, DOI: https://doi.org/10.35508/fisa.v3i2.623 (in Indonezian).

Sambah A.B., Miura F. Integration of spatial analysis for tsunami inundation and impact assessment. Journal of Geographic Information Systems, Vol. 6, No. 1, 2014, pp.11-22, DOI: http://dx.doi.org/10.4236/jgis.2014.61002.

Sengaji E., Nababan B. Mapping of Tsunami Risk Level in Sikka District, East Nusa Tenggara. E-Journal of Tropical Marine Science and Technology, Vol. 1, No. 1, 2009, pp. 48-61.

Sinaga T.P.T., Nugroho A., Lee Y.W., Suh Y. GIS mapping of tsunami vulnerability: A case study of Jembrana District in Bali, Indonesia, KSCE Journal of Civil Engineering, Vol. 15(3), 2011, pp. 537-43, https://doi.org/10.1007/s12205-011-0741-8.

Syamsidik, Oktari R.S., Nugroho A., Fahmi M., Suppasri A., Munadi K., Amra R. Fifteen years of the 2004 Indian Ocean Tsunami in Aceh-Indonesia: Mitigation, preparedness and challenges for a long-term disaster recovery process. International Journal of Disaster Risk Reduction, Vol. 54, 2021, 102052,doi: https://doi.org/10.1016/j.ijdrr.2021.102052

Wibowo M. Modeling the potential of tsunami hazard in Labuan Bajo towards a disaster- resilient tourism area. Indonesian Journal of Geography, Vol. 54(1), 2022, pp. 83-91.

Information Systems, Vol. 6, No. 1, 2014, pp.11-22, DOI: http://dx.doi.org/10.4236/jgis.2014.61002.

Sengaji E., Nababan B. Mapping of Tsunami Risk Level in Sikka District, East Nusa Tenggara. E-Journal of Tropical Marine Science and Technology, Vol. 1, No. 1, 2009, pp. 48-61.

Sinaga T.P.T., Nugroho A., Lee Y.W., Suh Y. GIS mapping of tsunami vulnerability: A case study of Jembrana District in Bali, Indonesia, KSCE Journal of Civil Engineering, Vol. 15(3), 2011, pp. 537-43, https://doi.org/10.1007/s12205-011-0741-8.

Syamsidik, Oktari R.S., Nugroho A., Fahmi M., Suppasri A., Munadi K., Amra R. Fifteen years of the 2004 Indian Ocean Tsunami in Aceh-Indonesia: Mitigation, preparedness and challenges for a long-term disaster recovery process. International Journal of Disaster Risk Reduction, Vol. 54, 2021, 102052,doi: https://doi.org/10.1016/j.ijdrr.2021.102052

Wibowo M. Modeling the potential of tsunami hazard in Labuan Bajo towards a disaster- resilient tourism area. Indonesian Journal of Geography, Vol. 54(1), 2022, pp. 83-91.

Wibowo M. Modeling the potential of tsunami hazard in Labuan Bajo towards a disaster- resilient tourism area. Indonesian Journal of Geography, Vol. 54(1), 2022, pp. 83-91.

Pramana B.S. Pemetaan Kerawanan Tsunami Di Kecamatan Pelabuhanratu Kabupaten Sukabum. SOCIO-DIDACTICA: Social Science Education Journal, Vol. 2, No. 1, Jun 23 2015, pp. 76-91, DOI: http://dx.doi.org/10.15408/sd.v2i1.1383

Pratiwi A., Gaol J.L., Nurjaya I.W. Analisis Spasial Kerentanan Wilayah Pesisir Barat Provinsi Banten terhadap Bencana Tsunami dengan Menggunakan Sistem Informasi Geografis, 2017, Tersedia dari: http://repository.ipb.ac.id/handle/123456789/88370.

Rumaal L.A., Tanesib J.L., Tarigan J. Aplikasi Penginderaan Jauh Dan Sistem Informasi Geografi Untuk Pemetaan Daerah Berpotensi Tsunami Di Kabupaten Kupang Provinsi Nusa Tenggara Timur. Jurnal Fisika: Fisika Sains dan Aplikasinya, Vol. 3, No. 2, 2018, DOI: https://doi.org/10.35508/fisa.v3i2. 623.

ПРИМЕНЕНИЕ ДИСТАНЦИОННОГО ЗОНДИРОВАНИЯ И ГЕОГРАФИЧЕСКИХ ИНФОРМАЦИОННЫХ СИСТЕМ (GIS) ДЛЯ КАРТИРОВАНИЯ ПОТЕНЦИАЛА ЦУНАМИ В РАЙОНЕ СИККА, ВОСТОЧНАЯ НУСА ТЕНГГАРА

Сиантури Х.Л., Танесиб Дж.Л., Лоук А.К., Блегур Д.И., Варсито А.
Кафедра физики, факультет науки и инженерии, Университет Нуса Чендана, Индонезия
Jln. Adisucipto - Penfui, Kupang 85001 NTT, Индонезия: hlsianturi@staf.undana.ac.id

Резюме. Индонезийский архипелаг очень подвержен землетрясениям и цунами. Данное исследование направлено на картирование потенциальных зон риска цунами, маршрутов эвакуации и мест сбора в районе Сикка, Восточная Нуса-Тенгара, Индонезия. Картирование выполняется с использованием географических информационных систем с применением подхода анализа уязвимости к цунами. Этот анализ проводится на основе нескольких критериев, включая высоту над уровнем моря, наклон местности, использование земель, расстояние до побережья и расстояние до рек. Также учитываются факторы населенности для определения уровня риска цунами. В целом, прибрежные зоны района Сикка потенциально подвержены риску цунами. Уровень этого риска очень высок в северных прибрежных зонах района Маджепанда, Западный Алок, Алок, Восточный Алок, Кангаэ, Кевапанте, Уайгете, Талибула, а также на некоторых мелких островах к северу от района Сикка, таких как остров Пемана, Большой остров и остров Баби. Зоны с высокой уязвимостью в основном расположены на северном побережье и частично на южном побережье. Эти зоны с очень высоким и высоким уровнем риска составляют всего около 6% от общей площади района Сикка. Однако потенциальные рисковые зоны находятся в плотнозаселенных районах, поэтому для снижения негативного воздействия цунами разработаны комплексные маршруты эвакуации и места сбора. В качестве эталонного события было выбрано землетрясение магнитудой 7.3 по шкале Рихтера на глубине 114 км к северу от района Сикка.

Ключевые слова: *Потенциал цунами, дистанционное зондирование, смягчение последствий, географическая информационная система, район Сикка*

SİKKA RAYONU, ŞƏRQİ NUSA-TENQARADA POTENSİAL SUNAMİ RİSK ZONALARININ XƏRİTƏLƏNDİRİLMƏSİ ÜÇÜN MƏSAFƏDƏN ZONDLAMA VƏ COĞRAFİ İNFORMASİYA SİSTEMLƏRİNİN (CİS) TƏTBİQİ

Sianturi H.L., Tanesib J.L., Luk A.K., Blegur D.I., Varsito A.
Fizika kafedrası, Elm və Mühəndislik fakültəsi, Nusa Cendana Universiteti, İndoneziya
Jln. Adisucipto - Penfui, Kupang 85001 NTT, İndoneziya: hlsianturi@staf.undana.ac.id

Xülasə. İndoneziya arxipelaqı zəlzələrə və sunamilərə qarşı olduqca həssasdır. Bu tədqiqat, İndoneziyanın Şərqi Nusa-Tenqaradakı Sikka rayonunda potensial sunami risk zonaları, təxliyə marşrutları və toplanma məkanlarının xəritələndirməsinə yönəlib. Xəritələndirmə sunami təhlükəsinə qarşı həssaslıq analizinə əsaslanan coğrafi informasiya sistemlərinin istifadəsi ilə həyata keçirilir. Bu analiz dəniz səviyyəsindən yüksəklik, ərazi meyli, torpaqdan istifadə, sahilə və çaylara olan məsafə kimi bir neçə kriteriyaya əsaslanır. Həmçinin əhalinin sıxlığı faktoru da nəzərə alınır ki, sunami risk səviyyəsi müəyyən edilsin. Ümumiyyətlə, Sikka rayonunun sahil zonaları potensial olaraq sunami təhlükəsinə məruz qalır. Bu risk səviyyəsi Madjepanda, Qərbi Alok, Alok, Şərqi Alok, Kangae, Kevapante, Uaygete, Talibula rayonlarının şimal sahil zonalarında, həmçinin Sikka rayonunun şimalında yerləşən Peman adası, Böyük ada və Babi adası kimi bəzi kiçik adalarda çox yüksəkdir. Yüksək həssaslığa malik zonalar əsasən şimal sahillərində və qismən cənub sahillərində yerləşir. Bu çox yüksək və yüksək risk səviyyəsinə malik zonalar Sikka rayonunun ümumi sahəsinin cəmi 6%-ni təşkil edir. Bununla belə, potensial risk zonaları əhalinin sıx yaşadığı ərazilərdə yerləşir, buna görə də sunaminin mənfi təsirini azaltmaq üçün kompleks təxliyə marşrutları və toplanma məkanları hazırlanmışdır. Etalon hadisə kimi Sikka rayonunun şimalında 114 km dərinlikdə, 7.3 bal gücündə Rixter şkalası üzrə zəlzələ seçilmişdir.

Açar sözlər: *sunami potensialı, distansion zondlama, təsirlərin azaldılması, coğrafi məlumat sistemi, Sikka rayonu*

ANALYSIS OF VULNERABILITY AND DYNAMIC CHARACTERISTICS OF A MONOLITHIC BUILDING USING MICROTREMOR MEASUREMENTS

Oripov N.[2], Alimukhamedov I.[2], Yanbukhtin I.[1], Musaev U.[1],
Zakirov A.[1], Mamarozikov T.[2]

[1]Center for Advanced Technologies within the Ministry of Higher Education,
Science and Innovation of the Republic of Uzbekistan,
3a, University str., Almazor district, Tashkent, 100174: nozim.o.k92@gmail.com,
ilhom75@mail.ru, Ilyas9348702@gmail.com, ulugbek-1975@mail.ru,
azamatzakirov@mail.ru, timur.mamarozikov@yandex.ru
[2]Institute of Seismology named after G. Mavlyanov,
Academy of Sciences of the Republic of Uzbekistan
3, Zulfiyakhanim str., Tashkent, 100128

Summary. Microtremor measurements are a widely recognized and effective method for evaluating the dynamic properties and potential seismic vulnerability of buildings. These measurements allow for the determination of critical parameters such as the dominant frequency, amplification factor, vulnerability index, and floor spectral ratio (FSR) for each floor of the building under investigation. In this study, microtremor measurements were conducted on a 26-storey monolithic reinforced concrete residential building located in the heart of Tashkent city. Recordings were made using six velocimeters simultaneously for 30 minutes. Measurements were taken on the basement floors (two floors), on the first floor, and then at two-floor intervals throughout the entire height of the building. Additionally, free-field measurements were taken on the ground outside the building to serve as a reference. The data was analyzed using GEOPSY software, which generated HVSR (Horizontal-to-Vertical Spectral Ratio) curves for the structure. The analysis showed that the building has the appropriate characteristics to effectively absorb seismic impact, indicating that it is well-constructed and capable of withstanding seismic forces. The strong structural integrity, demonstrated through low amplification and vulnerability indices, suggests that the building's design provides adequate protection against potential earthquake damage. These findings contribute to the broader understanding of how microtremor studies can be applied in the seismic evaluation of tall buildings in urban conditions.

1. Introduction

One of the parameters that cause significant damage to buildings and structures are their dynamic and seismic characteristics such as natural frequency, resonance value (Herak, 2011) and building vulnerability index (Nakamura et al., 2000). These parameters can be obtained by recording ambient noise. In this study, a 26-story apartment building was investigated using the microtremor method to obtain the building's safety performance. The main advantages of microtremor analysis are simplicity, efficiency and speed, which provide a reliable, accurate and stable assessment of building vibration modes from low-amplitude excitation.

The eigenfrequency value on soil is determined by processing microtremor data using the HVSR (Horizontal to Vertical Fourier Spectral Ratio) (Gallipoli et al., 2004, Irie et al., 2000, and Konno et al., 1998). The natural frequency value of the building is determined using the FSR (Floor Spectral Ratio) method and the analysis spectrum is obtained from each floor to get the natural frequency value of the building (Oynakov et al., 2023). The building resonance value is determined based on the spectrum for each component (NS and EW). Resonance can be used to determine the level of possibility of a building experiencing resonance during an earthquake. Resonance risk occurs if the dominant periods of the ground and buildings are close to each other. The

value of the amplification and natural frequency in soil and buildings can be the value of soil vulnerability analysis, building vulnerability analysis and building resonance (Gosar, 2007).

2. Description of the building

T1 business class residential complex with unique modern architecture will be built in 2021-2024. It is located in the center of Tashkent. Complex T1 consists of 26 floors. The 2-storey basement part of the building is intended for parking, the 1st and 2nd floors – for commercial and domestic services, the 3rd floor – for a terrace with a green area, the 4th-26th floors – for residential apartments. The foundations of the building are 218 reinforced frame piles 30 m long and 1.2 m in diameter driven into stony loess soils. The foundation, measuring 76×25×2 m and weighing 9370 tons, was poured on piles. On its top, the T1 building weighing 50,000 tons was constructed using monolithic frame technology. M600 grade concrete was used in the construction.

3. Microtremor measurements

In determining the potential risk of earthquake hazard, there is a method by analyzing the natural vibrations of the Earth, commonly known as microtremor or microseismic (Hadianfard et al., 2017). Microseismic is a vibration of the Earth. The weak vibration can originate from human activity, ocean waves, wind, traffic and others. Sources of microtremor or microseismic can be divided into natural and artificial sources. Examples of natural microseismic can come from rain, wind, running water, or ocean waves, while sources of artificial microseismic generally come from industrial and human activities, including the sound of machines, cars, people walking, and so on. The amplitude of the microseismic is so small that it is difficult for humans to detect it, but with the development of technology, instruments that can detect these waves are created, which are commonly called seismometers (Nakamura, 2009; Okada, 2003).

Microtremors have been based on ambient noise recordings to determine the dynamical characteristic parameters of buildings. Many researchers reviewed, introduced and applied ambient noise analysis for both purposes. Nakamura et al., 2000; Sato et al., 2008 identified damaged buildings using the vulnerability index of a structure estimated from transfer function parameters.

Microtremors were recorded in different parts of -2F, -1F, 1F, 3F, 6F, 9F, 12F, 15F, 18F, 21F, 24F and roof floors of a T1 business class residential complex (Fig. 1). Free-field measurements were also taken close to the building and at a sufficient distance to avoid its influence. Ambient noise measurements were made using a CMG-6TD seismometer (Guralp, UK). Each sensor provided vibration recording over a wide frequency range from 0.03 to 100 Hz.

Microtremor was recorded in three directions (EW, NS, Z) with a 1/100 second sampling rate. The recording length was 30 minutes because frequencies below 1 Hz were not of interest.
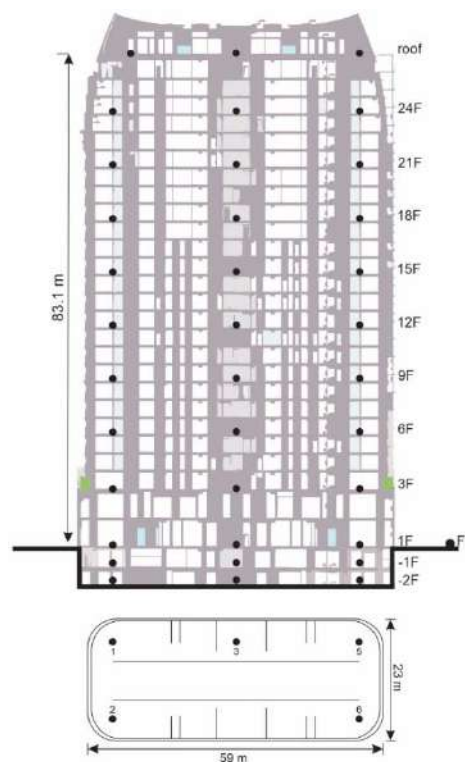
Fig. 1. The elevation and floor plan with measurement points in a newly constructed T1 building. (● - Measurement points)

4. Methodology
4.1. Horizontal to Vertical Spectral Ratio (HVSR)

Microtremor measurements can be utilized to determine the soil's predominant frequency. To prevent the resonance event, a predominant frequency of soil and structure should be calculated and compared. For this purpose, the microtremor HVRS method proposed by Nakamura (Satriyo et al., 2023) was used. To do this, using a seismometer, it is necessary to simultaneously record three components of the ground vibration velocity. Then, power spectra of ground motion should be calculated for two horizontal directions (EW and NS) and also for vertical direction (V). Finally, to determine the site frequency, the spectral ratio of the combined horizontal (H) to vertical (V) component of ground motion must be calculated. The frequency of the peak amplitude in the spectral ratio graph is the predominant (natural) frequency of the site. By comparing the fundamental frequency obtained from the microtremor H/V spec-

tral ratio with the function received from the seismic log, the researchers concluded that the H/V microtremor spectral ratio provides a reliable estimate of sediment frequency (Hadianfard et al., 2017).

The following formula is the basis for calculating the horizontal to vertical microtremor spectrum ratio (HVSR) and is expressed as follows:

$$HVSR = \frac{\sqrt{[(S_{north-south})^2 + (S_{east-west})^2]}}{S_{vertical}} \quad (1)$$

To obtain reliable HVSR curve results, quality control is required based on the SESAME 2004 standard. There are three reliable criteria for HVSR curves, including (SESAME, 2004):

1. $f_0 > 10/Iw$
2. $nc(f_0) > 200$, $nc = Iw. nw. f_0$,
3. $\sigma A(f) < 2$ to $0.5f_0 < f < 2f_0$ if $f_0 > 0.5$ Hz, or $\sigma A(f) < 3$ to $0.5f_0 < f < 2f_0$ if $f_0 < 0.5$ Hz

where *Iw* is the window length, *nw* is the number of windows selected to obtain the average H/V curve, *nc* is the number of significant cycles, σA is the standard deviation of *A* H/V (*f*), and f_0 is the peak frequency in the H/V curve.

Data processing to obtain the HVSR on the free field was performed in the following way: recorded times series were visually inspected to identify possible erroneous measurements and stronger transient noise. Each record was then split into 20-30 s-long windows tapered with a 5% cosine function. A Fast Fourier Transform (FFT) was calculated for each window in each seismometer component. The Fourier spectra were smoothed using Konno and Ohmachi (Konno et al., 1998) with 40 smoothing constants. HVSR was computed as the geometric average of both horizontal component spectra divided by the vertical spectrum for each window. This analysis was used GEOPSY software.

4.2. Floor Spectral Ratio (FSR)

The use of HVSR is not recommended when determining transfer function parameters in buildings, this is because only in a few cases it gets good results. This inaccuracy is because it cannot be assumed that the horizontal and vertical spectra have a fixed value at ground level, so there is no reason to use them in the assessment of building structures. If this is still implemented in buildings, it will likely be very dangerous in cases of very strong soil amplification, because the analysis results are not close to the actual situation. In this case, the HVSR may give an incorrect assessment or building response because it is identified as a spurious transfer function parameter. (Gallipoli et al., 2004)

The floor spectra ratio (FSR) method is a method for determining the natural and resonant frequencies of buildings that describe the characteristics of buildings against earthquakes (Gosar, 2010; Sungkono et al., 2011). In the FSR method, other building characteristics that can be obtained besides the natural frequency are the building resonance index and the building vulnerability index. The natural frequency building value is determined from the spectrum analysis of each building floor to the ground below it. The data calculation process was performed to determine the natural frequency value of the building using the equation below (Prakosa et. al., 2015).

$$f_0(FSR) = \frac{f_bNS}{f_tNS} = \frac{f_bEW}{f_tEW} \quad (2)$$

Equation (2) is the FSR analysis equation where f_b is the value of the building frequency, f_t is the value of the ground frequency, and NS-EW is the respective components of the data.

Resonance can be used to determine the level of possibility of a building experiencing resonance during an earthquake (Gosar, 2010). There are several classifications:

1. Low resonance (*R*>25%)
2. Medium resonance (15% <*R*< 25%)
3. High resonance (*R*<15%)

The building resonance index (*R*) is determined based on the spectrum of each component (NS and EW) which is calculated based on the following equation:

$$R = \left|\frac{f_b - f_t}{f_t}\right| \times 100\% \quad (3)$$

where f_b is the natural frequency of the building, and f_t is the natural frequency of the ground.

4.3. Vulnerability index

The vulnerability of buildings is one of the most important parameters for the evaluation of potential damages in urban areas caused by earthquakes. Nakamura et al. and Sato et al. showed that the vulnerability index can be used to describe the building strength in bearing the earthquake shakings. It is considered that the vulnerability of structures against earthquake disasters can be estimated by the drift angle, related to the input earthquake acceleration *a* in cm/s². Here, α is a portion that affects this structure among whole earthquake motion *a*:

$$\alpha = e \times a, \quad (4)$$

where *e* shows the efficiency of earthquake motion working for this structure.

A deformation performance and the degree of earthquake motion amplification can be estimated from the dynamic characteristics of structures. Here, the primary natural frequency of the structure that seems to influence earthquake damage is considered. Displacement δ_i of ith floor is estimated from this primary natural frequency F and amplitude A_i of ith floor as follows (Fig. 2):

$$\delta_j = A_i \times \alpha / (2\pi F_s)^2 \qquad (5)$$

Therefore, the drift angle γ_i of ith floor is shown as:

$$\gamma_i = \delta_{i+1} - \delta_i / h = \Delta A_i \times \alpha / (2\pi F)^2 / h_i$$
$$= e \times K_{bi} \times a, \qquad (6)$$

where

$$K_{bi} = \Delta A_i / (2\pi F)^2 / h_i \times 10{,}000, \qquad (7)$$
$$\Delta A_i = A_{i+1} - A_i, \qquad (8)$$

ΔA_i shows the difference in amplification of the ith floor, h_i is the height of ith floor in meters, and F is the predominant frequency of the structure.

Thus, the drift angle γ_i for each floor is estimated from the vulnerability index K_{bi} multiplied by the maximum acceleration on the surface ground in cm/s^2 and the efficiency e of earthquake motion. Here, the $_{av}K_b$ value is derived as averaged K_{bi} for each structure for the discussion as follows:

$$_{av}K_b = \frac{A}{(2\pi F)^2 \times H} \times 10{,}000, \qquad (9)$$

where A – shows the amplitude of the top floor and H – is the total height of the structure in meters.
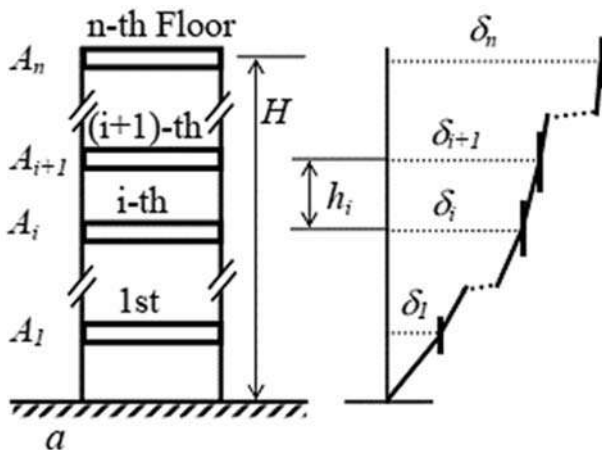
Fig. 2. Schematic model of *n*-th floor structures and its mode shape. δ_j is the horizontal displacement, h_i is the height, A_i is the amplification factor of the *i*-th story column, H is the height of the *n*-th floor structure, and a is the horizontal acceleration of the foundation ground

In addition, when $_{av}K_b$ is substituted for K_{bi} in Eq. (6), the averaged drift angle γ_{av} will be calculated. K_{bi} and $_{av}K_b$ are expressed in units of 10^{-6}, 10,000 in Eqs. (7) and (9) are multiplied for adjustment.

5. Result of analysis
5.1. Ground natural frequency

Ground natural frequency obtained from HVSR analysis is the average frequency of each vertical and horizontal spectrum. The obtained spectral ratio for the site where the T1 building is located is shown in Fig. 3. Based on this figure, the natural frequency of the site is 0.64 Hz.
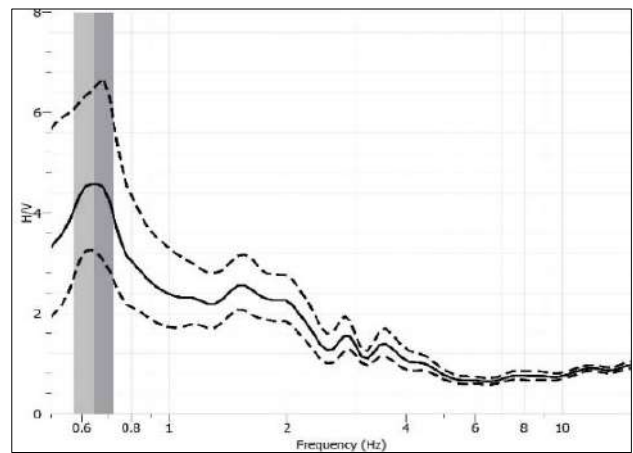
Fig. 3. Spectral ratio (H/V) for site where the T1 building is located, natural frequency 0.64 Hz

5.2. Spectrum analysis of building

Based on the analysis of microtremors recorded in the building, a spectral analysis of the horizontal components of the indicated floors was performed (Fig. 4). The values of the EW component ranged from 0.62-3.1 Hz, and the values of the NS component ranged from 0.64-3.16 Hz. The average frequency spectrum of each component was ± 1.6 Hz. In Fig. 5 it can be observed that the frequency values by floor decrease sharply after the 12th floor because the higher the building, the lower the dominant frequency of the building.

5.3. Floor Spectral Ratio Analysis

FSR (Floor Spectral Ratio) analysis was conducted to determine the natural frequency of the building (Fig. 6). The FSR analysis was calculated by dividing the dominant frequencies of the building floors determined from the spectrum analysis by the free surface frequency.

The EW component values of all floors ranged from 0.97-4.8 Hz, and the NS component values ranged from 1-4.95 Hz. The average natural frequency of each component was ±2.5 Hz.
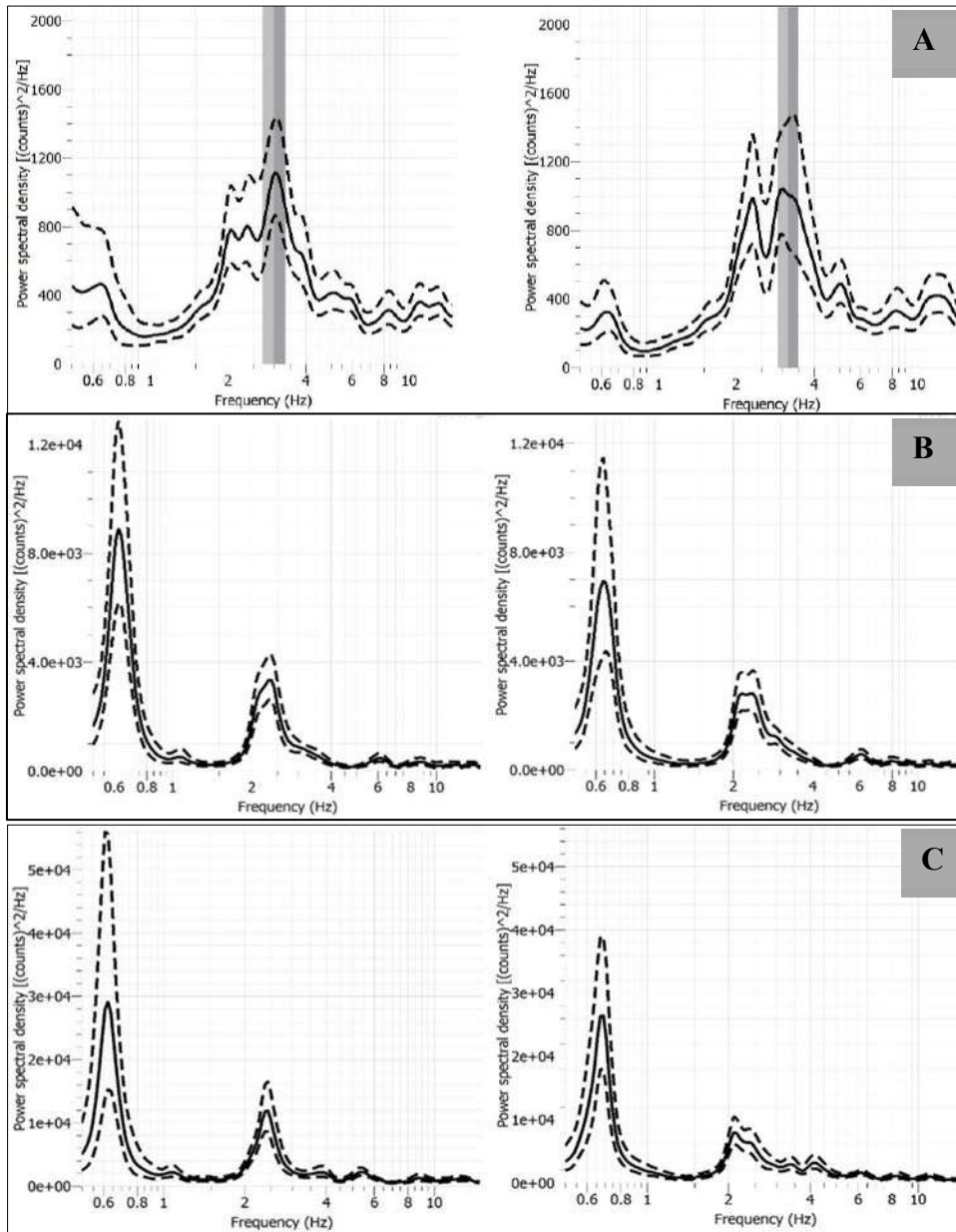
Fig. 4. Frequency and amplitude graph using spectrum analysis. A) EW and NS spectrum graph of the 3rd floor; B) EW and NS spectrum graph of the 12th floor; C) EW and NS spectrum graph of the roof.

	-2	-1	1	3	6	9	12	15	18	21	24	roof
■ EW	2.88	2.26	3.1	2.38	2.38	2.39	0.62	0.63	0.65	0.63	0.63	0.62
■ NS	2.86	3.16	2.83	2.06	2.1	2.09	0.64	0.67	0.64	0.65	0.66	0.68
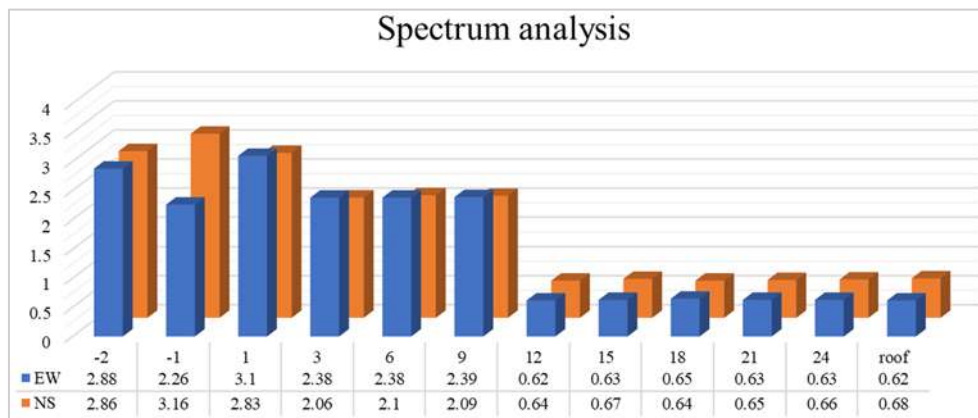
Fig. 5. Diagram of change of frequency values by floors based on spectral analysis
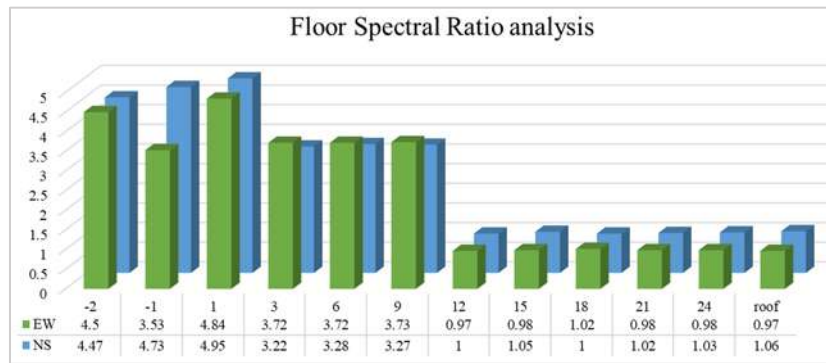
Fig. 6. Diagram of natural frequency variation by floors based on FSR analysis

5.4. Ground and Building resonance

The magnitude of building-to-site resonance ranged from 51% to 617% for the EW component and 59% to 674% for the NS component (Fig. 7). The average resonance value is ±290%. Based on the above classification (Gosar, 2010), the obtained resonance value is categorized as low resonance because the natural frequency of the building is much higher than the value of the natural frequency of the site. For the horizontal components, resonance values up to the 9th floor differed by values greater than >100%, and from the 12th floor and above, values differed by values below <100%. This significantly reduces the probability of resonance phenomenon.

5.5. Building vulnerability index

The building vulnerability index (Kb) shows the level of damage that occurs to the building in the event of an earthquake. The greater the vulnerability value of a building, the greater the potential damage that will occur (Mokhberi, 2015; Sarkowi et al., 2022).

Based on the processing results, the vulnerability index values of building T1 changed from 0.42 to 9.45 for the EW component and from 0.43 to 7.12 for the NS component. The lowest vulnerability index was observed on the 9th floor and the highest on the roof (Fig. 8). This indicates that the building is very resistant to earthquakes.
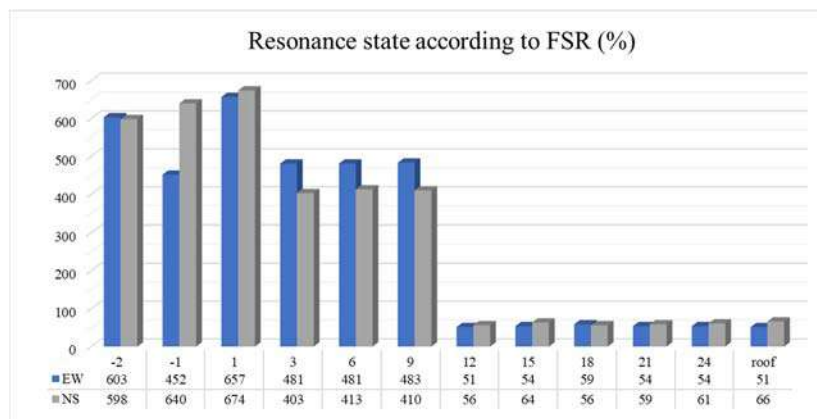
Fig. 7. Diagram of resonance variation by floor
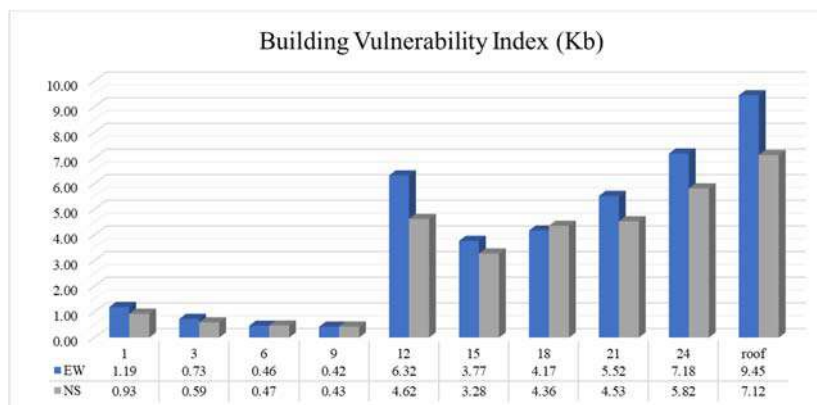
Fig. 8. Diagram of change of vulnerability index by floors

6. Conclusions

Based on the results of calculations and analysis, the soil on which building T1 is located is found to have a frequency of 0.64 Hz by the HVSR method. The FSR analysis showed that the natural frequency of the building was determined to be 0.97 Hz – 4.8 Hz in the EW component and 1 Hz – 4.95 Hz in the NS component. It should be said that above the 9th floor, there was a sharp decrease in the natural frequency of the building. This indicates that the building was divided into two parts.

The magnitude of the building and ground resonance varied between 51% – 617% in the EW component and between 59% – 674% in the NS compo-

nent. The mean value of the component resonance was ±290%. In turn, this figure is categorized as low resonance because the natural frequency of the building is much higher than the value of the natural frequency of the ground.

The vulnerability index ranged from 0.42 to 9.45 for the EW component and from 0.43 to 7.12 for the NS component. The vulnerability index values decreased from the 1st floor to the 9th floor and increased sharply from the 9th floor above. In general, the values showed a result below <10. The vulnerability index value of the building shows that the building is of low category (safe).

REFERENCES

Gallipoli M.R., Mucciarelli M., Castro R.R., Monachesi G., Contri P. Structure, soil-structure response and effects of damage based on observations of horizontal-to-vertical spectral ratios of microtremors. Soil Dynamics and Earthquake Engineering, Vol. 24(6), 2004, pp. 487-495, DOI:10.1016/j.soildyn.2003.11.009.

Gosar A. Microtremor HVSR study for assessing site effects in the Bovec basin (NW Slovenia) related to 1998 Mw5.6 and 2004 Mw5.2 earthquakes. Engineering Geology, Vol. 91, No. 2-4, 2007, pp. 178-193, DOI:10.1016/j.enggeo.2007.01.008.

Gosar A. Site effects and soil-structure resonance study in the Kobarid basin (NW Slovenia) using microtremors. Natural Hazards and Earth System Science, Vol. 10(4), 2010, pp. 761-772, DOI:10.5194/nhess-10-761-2010.

Hadianfard M.A., Rabiee R., Sarshad A. Assessment of vulnerability and dynamic characteristics of a historical building using microtremor measurements. Journal of Civil Engineering, Vol. 15, 2017, pp. 175-183, https://doi.org/10.1007/s40999-016-0086-2.

Herak M. Overview of recent ambient noise measurements in Croatia in free-field and in buildings Geofizika, Vol. 28(1), 2011, pp.21-37.

Irie Y., Nakamura K. Dynamic characteristics of a R/C building of five stories based on microtremor measurements and earthquake observations. In: Proc. of XII World. Conf. Earthq. Eng., Wellington, 2000, pp. 500-508.

Konno K. and Ohmachi T. Ground-motion characteristics estimated from spectral ratio between horizontal and vertical components of microtremor. Bulletin of the Seismological Society of America, Vol. 88, No.1, 1998, pp. 228-241, https://doi.org/10.1785/BSSA0880010228.

Mokhberi M. Vulnerability evaluation of the urban area using the H/V spectral ratio of microtremors. International Journal of Disaster Risk Reduction, Vol. 13, 2015, pp. 369-374, DOI:10.1016/j.ijdrr.2015.06.012.

Nakamura Y, Gurler E.D., Saita J., Rovelli A., Donati S. Vulnerability investigation of roman colosseum using Microtremor. In: 12th World Conference on Earthquake Engineering, Auckland, New Zealand, 2000, pp. 2660-1-8.

Nakamura Y. Basic Structure of QTS (HVSR) and Examples of Applications. In: Increasing Seismic Safety by Combining Engineering Technologies and Seismological Data, Conference proceedings, edited by Mucciarelli M. et al., Dordrecht, Netherlands, 2009, pp. 33-51, DOI:10.1007/978-1-4020-9196-4.

Okada H. The microtremor survey method. Society of Exploration Geophysicists with the cooperation of Society of Exploration Geophysicists of Japan and Australian Society of Exploration Geophysicists, SEG Books. Science. 2003, 135 p.

ЛИТЕРАТУРА

Gallipoli M.R., Mucciarelli M., Castro R.R., Monachesi G., Contri P. Structure, soil-structure response and effects of damage based on observations of horizontal-to-vertical spectral ratios of microtremors. Soil Dynamics and Earthquake Engineering, Vol. 24(6), 2004, pp. 487-495, DOI:10.1016/j.soildyn.2003.11.009.

Gosar A. Microtremor HVSR study for assessing site effects in the Bovec basin (NW Slovenia) related to 1998 Mw5.6 and 2004 Mw5.2 earthquakes. Engineering Geology, Vol. 91, No. 2-4, 2007, pp. 178-193, DOI:10.1016/j.enggeo.2007.01.008.

Gosar A. Site effects and soil-structure resonance study in the Kobarid basin (NW Slovenia) using microtremors. Natural Hazards and Earth System Science, Vol. 10(4), 2010, pp. 761-772, DOI:10.5194/nhess-10-761-2010.

Hadianfard M.A., Rabiee R., Sarshad A. Assessment of vulnerability and dynamic characteristics of a historical building using microtremor measurements. Journal of Civil Engineering, Vol. 15, 2017, pp. 175-183, https://doi.org/10.1007/s40999-016-0086-2.

Herak M. Overview of recent ambient noise measurements in Croatia in free-field and in buildings Geofizika, Vol. 28(1), 2011, pp.21-37.

Irie Y., Nakamura K. Dynamic characteristics of a R/C building of five stories based on microtremor measurements and earthquake observations. In: Proc. of XII World. Conf. Earthq. Eng., Wellington, 2000, pp. 500-508.

Konno K. and Ohmachi T. Ground-motion characteristics estimated from spectral ratio between horizontal and vertical components of microtremor. Bulletin of the Seismological Society of America, Vol. 88, No.1, 1998, pp. 228-241, https://doi.org/10.1785/BSSA0880010228.

Mokhberi M. Vulnerability evaluation of the urban area using the H/V spectral ratio of microtremors. International Journal of Disaster Risk Reduction, Vol. 13, 2015, pp. 369-374, DOI:10.1016/j.ijdrr.2015.06.012.

Nakamura Y, Gurler E.D., Saita J., Rovelli A., Donati S. Vulnerability investigation of roman colosseum using Microtremor. In: 12th World Conference on Earthquake Engineering, Auckland, New Zealand, 2000, pp. 2660-1-8.

Nakamura Y. Basic Structure of QTS (HVSR) and Examples of Applications. In: Increasing Seismic Safety by Combining Engineering Technologies and Seismological Data, Conference proceedings, edited by Mucciarelli M. et al., Dordrecht, Netherlands, 2009, pp. 33-51, DOI:10.1007/978-1-4020-9196-4.

Okada H. The microtremor survey method. Society of Exploration Geophysicists with the cooperation of Society of Exploration Geophysicists of Japan and Australian Society of Exploration Geophysicists, SEG Books. Science. 2003, 135 p.

Oynakov E., Ivanov R., Aleksandrova I., Milkov J., Popova M. Evaluation of the Nakamura vulnerability index of a cast-in-situ reinforced-concrete building from ambient noise records. In: Dobrinkova, N., Nikolov, O. (eds.) Environmental Protection and Disaster Risks. EnviroRISKs 2022. Lecture Notes in Networks and Systems, Vol. 638. Springer. Cham. 2023, pp.66-76, DOI:10.1007/978-3-031-26754-3_6.

Prakosa P.T., Ibad M.I., Kafi M.S., Burhanudin M.A., Rahmania A. (2015) Earthquake microzonation and strength building evaluation at Gelora Bung Tomo Stadium Surabaya using micro-tremor method. Proceedings of 7th International Conference on Physics and Its Applications 2014 (ICOPIA 2014), Vol. 1, 2015, pp. 14-20.

Sarkowi M., Wibowo R.C., Sunanda Yogi I.B., Yusuf M., Boka Y.S. Microtremor analysis to evaluate BMKG region III building, Bali, Indonesia. IJES – Iranian Journal of Earth Sciences, Vol. 14(2), 2022, 104-111, DOI: 10.30495/ijes.2022.1942485.1659.

Sato T., Nakamura Y., Saita J. The change of dynamic characteristics using microtremor. The 14th WCEE – The 14th World Conference on Earthquake Engineering, Beijing, China, 2008, pp 17-25.

Satriyo A., Suryanto W., Anggono T., Al Kamali M.L., Yufi H.S. Study Characteristics of a Multipurpose Reactor Building G.A. Siwabessy using Floor Spectral Ratio. E3S Web of Conferences. Vol. 468, 2023, ICST UGM –The 4th Geoscience and Environmental Management Symposium, Article Number 09003, 2023, https://doi.org/10.1051/e3sconf/202346809003.

SESAME, Guidelines for the implementation of the H/V spectral ratio technique on ambient vibrations measurements, processing and interpretation, 2004, Available: http://sesame-fp5.obs.ujfgrenoble.fr/Delivrables/Del-D23HVUser Guidelines.pdf.

Sungkono S., Warnana D.D., Triwulan, Utama W. Evaluation of Buildings Strength from Microtremor Analyses. International Journal of Civil & Environmental Engineering, Vol. 11(05), 2011, pp. 6-12.

АНАЛИЗ УЯЗВИМОСТИ И ДИНАМИЧЕСКИХ ХАРАКТЕРИСТИК МОНОЛИТНОГО ЗДАНИЯ С ИСПОЛЬЗОВАНИЕМ МИКРОТРЕМОРНЫХ ИЗМЕРЕНИЙ

Орипов Н.[2], Алимухамедов И.[2], Янбухтин И.[1], Мусаев У.[1], Закиров А.[1], Мамарозиков Т.[2]

[1]*Центр передовых технологий при Министерстве высшего образования, науки и инноваций Республики Узбекистан, 100174, г.Ташкент, Алмазарский район, ул. Университетская, дом 3а: nozim.o.k92@gmail.com, ilhom75@mail.ru, Ilyas9348702@gmail.com, ulugbek-1975@mail.ru, azamatzakirov@mail.ru, timur.mamarozikov@yandex.ru*
[2]*Институт сейсмологии им. Г.Мавлянова Академии наук Республики Узбекистан 100128, г.Ташкент, ул. Зульфияханим, дом 3*

Резюме. Микротреморные измерения являются одним из наиболее эффективных и широко применяемых методов для оценки динамических характеристик зданий и определения их сейсмической уязвимости. Данный метод позволяет выявить ключевые параметры, такие как доминирующая частота, коэффициент усиления, индекс уязвимости, а также спектральное отношение (FSR) для каждого отдельного этажа здания. В рамках данного исследования были проведены измерения на 26-этажном монолитном железобетонном жилом здании, расположенном в центре города Ташкент. Для получения данных использовались шесть велосиметров, работающих одновременно в течение 30 минут для повышения точности результатов. Измерения проводились на этажах подвала (два этажа), на первом этаже, а также на каждом втором этаже по высоте здания. Кроме того, были проведены непрерывные измерения на свободной поверхности вокруг здания для сравнительного анализа с грунтом и изучения поведения основания при сейсмическом воздействии. Данные были обработаны с использованием программного пакета GEOPSY, который позволил построить кривые HVSR (горизонтально-вертикальные спектральные отношения). Анализ показал, что здание обладает соответствующими характеристиками эффективно гасить сейсмическое воздействие, что свидетельствует о его прочной конструкции и способности противостоять сейсмическим нагрузкам. Низкий коэффициент усиления и индекс уязвимости указывают на высокую устойчивость здания к потенциальным сейсмическим воздействиям, что подтверждает его способность выдерживать землетрясения. Эти выводы являются значительным вкладом в понимание важности применения микротреморных исследований для сейсмической оценки высотных зданий, особенно в условиях плотной городской застройки и повышенной сейсмической активности.

Ключевые слова: *микротремор, собственная частота, FSR, HVSR, индекс уязвимости, резонанс*

MİKROTREMOR OLÇÜLMƏLƏRİNDƏN İSTİFADƏ ETMƏKLƏ MONOLİT BİNALARIN DAVAMLIĞININ VƏ DİNAMİK XÜSUSİYYƏTLƏRİNİN TƏHLİLİ

Oripov N.[2], Alimuxamedov I.[2], Yanbuxtin İ.[1], Musayev U.[1], Zakirov A.[1], Mamarozikov T.[2]
[1]*Özbəkistan Respublikası Ali Təhsil, Elm və İnnovasiya Nazirliyi, qabaqcıl texnologiyalar Mərkəzi,*
100174, Daşkənd şəh., Almazar rayonu, Universitetskaya küçəsi, ev 3A: nozim.o.k92@gmail.com, ilhom75@mail.ru,
Ilyas9348702@gmail.com, ulugbek-1975@mail.ru, azamatzakirov@mail.ru, timur.mamarozikov@yandex.ru
[2]*Özbəkistan Respublikasının Elmlər Akademiyasının Q.Mavlyanov adına Seysmologiya İnstitutu*
100128, Daşkənd şəh., Zülfiyahanim küç., ev 3

Xülasə. Mikrotremor ölçmələri binaların dinamik səciyyələrinin qiymətləndirilməsi və onların seysmik həssaslığının müəyyən edilməsi üçün ən təsirli və geniş istifadə olunan metodlardan biridir. Bu metod dominant tezlik, gücləndirmə əmsalı, həssaslıq indeksi və hər bir mərtəbə üçün spektral nisbət (FSR) kimi əsas parametrləri müəyyən etməyə imkan verir. Bu tədqiqat çərçivəsində ölçmələr Daşkənd şəhərinin mərkəzində yerləşən 26 mərtəbəli monolit dəmir-beton yaşayış binasında aparılmışdır. Məlumatların toplanması üçün eyni vaxtda 30 dəqiqə ərzində işləyən altı velosimetrdən istifadə edilmişdir ki, nəticələrin dəqiqliyi artsın. Ölçmələr zirzəmi mərtəbələrində (iki mərtəbə), birinci mərtəbədə və bina boyunca hər iki mərtəbədə aparılmışdır. Bundan əlavə, qeyd etmək lazımdır ki, torpaq ilə müqayisəli analiz aparmaq məqsədilə və həmçinin təməl seysmik təsir altında bazanın davranışını öyrənmək üçün binanın ətrafındakı sərbəst səthdə davamlı ölçmələr aparılmışdır. Nəticələr GEOPSY proqram təminatı vasitəsilə işlənilmişdir ki, bu da HVSR (horizontal-vertikal spektral nisbətlər) əyrilərinin qurulmasına imkan verir. Analiz göstərdi ki, bina seysmik təsirləri effektiv şəkildə zəiflədə bilir, bu da onun möhkəm quruluşa malik olduğunu və seysmik yüklərə davam gətirə biləcəyini sübut edir. Aşağı gücləndirmə əmsalı və həssaslıq indeksi binanın potensial seysmik təsirlərə qarşı dayanıqlığını göstərir və onun zəlzələlərə qarşı davamlı olduğunu təsdiq edir. Bu nəticələr mikrotremor tədqiqatlarının hündür binaların seysmik qiymətləndirilməsində tətbiqinin əhəmiyyətini anlamağa, xüsusilə sıx şəhərsalma və yüksək seysmik aktivlik şəraitində böyük töhfə verir.

Açar sözlər: *mikrotremor, xüsusi tezlik, FSR, HVSR, zəiflilik indeksi, rezonans*

CHARACTERISTICS OF GEOPHYSICAL FIELDS AND GEOPHYSICAL SIGNS OF MINERALIZATION IN THE BUKANTAU MOUNTAINS IN THE SOUTHERN TIEN-SHAN

Goipov A.B.[1], Akhmadov Sh.I.[1], Yusupov V.R.[2]

[1]*Ministry of Mining and Geology of the Republic of Uzbekistan, University of Geological Sciences, State institution. "Institute of Mineral Resources", Uzbekistan*
64, Olimlar str., Tashkent, 100041
[2]*Institute of Seismology named after G.A. Mavlyanov,*
Academy of Sciences of the Republic of Uzbekistan
3, Zulfiyakhonim str., Tashkent, 100128

Keywords: Deposits, endogenous processes, gold, structure, formation, geophysical fields, intrusive rocks

Summary. The Bukantau Mountains are located in the northwestern part of the Southern Tien Shan folded gold ore belt. In geodynamic zoning, the Bukantau Mountains are divided into the North Bukantau and the South Bukantau structural-formational zones (SFZ). They are complexly curved uplifts complicated by smaller folds. The ores of the North Bukantau SFZ form copper-zinc-pyrite with gold (Karamurun), gold-sulfide-quartz (Irlir, Dzhetymtau) and secondary copper-molybdenum-skarn (Orazaly I, II) and chromite formations. The main ore deposits of the South Bukantau SFZ are rare metal-gold ore (Altyntau deposit), gold-arsenic (Kokpatas deposit), gold-polymetallic (Turbay deposit), gold-silver (Okzhetpes deposit) mineralization, tungsten-bearing skarns and skarnoids (Sautbay deposit).

The paper contains an analysis of long-term data from complex geophysical studies of the Bukantau Mountains. The characteristics of changes in the values of the physical field of 63 objects in the Bukantau Mountains were analyzed and complexes of geophysical features and relationships with the localization of mineralization were created.

The search criteria were formulated based on a study of the features of physical fields characteristic of known ore occurrences and deposits, from the point of view of the degree of unambiguity of their reflection in electric, gravitational and magnetic fields. Comparison of remote sensing data, geophysical and geochemical data using static and metallogenic analyses made it possible to determine predictive and promising positions, confirmed by field interpretation and driving of mine workings, recommended for further geological exploration work.

1. INTRODUCTION

Currently, scientific studies are being conducted worldwide to identify the physical properties of rocks and their analysis. In particular, special attention is given to conducting extensive complex geological and geophysical studies in the USA, Russia, China, India and the states of Central Asia to meet the demand for minerals. Such a scientific approach improves the methodology to solve quantitative interpretation problems of geophysical mineralization signs in the exploration and search for mineral deposits.

Determining the main factors of gold ore localization and other manifestations of minerals is necessary to improve the efficiency of forecasting and prospecting.

To date, identifying localization factors of gold deposits is based primarily on empirical data and on the search for deposit placement patterns relative to geological structural elements of the regions. Therefore, one of the main conditions for the successful identification of localization factors of deposits is studying the geological structure and history of the geological development of territories and determining the place and time of concentration formation.

Endogenous ore deposits represent abnormal concentrations of useful elements in a relatively small volume of the Earth's crust that arose due to the confluence of favourable circumstances under the influence of various factors during the development of the Earth. Their detection is the main goal of geological research, in which there are stages of forecasting and

researching. These stages are based on identifying objective patterns of the formation and placement of specific ores in the upper horizons of the Earth's crust. To accomplish this, various geological, geophysical, geochemical, surficial, and hydrogeological methods are used, and the prerequisites for the occurrence of the desired ores in certain formations or structures and the empirical patterns of the placement of known mineralization relative to specific lithological, tectonic and magmatic factors are taken into account. A positive result is achieved only while considering the totality of all data reflecting the peculiarities of the formation of a specific mineralization type.

The purpose of this paper is a static analysis of the anomalies in the geophysical fields of the Bukantau Mountains (the western end of the southern Tien Shan (Fig. 1)) for further metallogenic prediction (Борисов и Глух, 1982; Рогачев, 1977; Сердюков, 1978; Глух и др., 2002; Goipov, et al., 2020a; 2020b; Гоипов, 2021).

The gold deposits and manifestations of the Bukantau are part of four formations: gold-sulfide veined-interspersed ores, gold-sulfide-quartz, gold-silver and gold-scarn. The deposits of the gold (sulfide)-quartz formation can be divided into two subformations: a) low-sulfide veined zones and stockwork and b) low-sulfide veins, linear vein zones and breccias.

The established main factors of the localization of ore fields are common to the entire folded system.

In addition, the roles of some of these factors may be different in each tectonic segment. For each type of gold deposit, the selected factors have slightly different meanings.

All deposits and manifestations of the Bukantau gold are located within extended intrablock crushing zones and are usually subconsistent with the host strata. Therefore, these zones play the role of ore-controlling structures and are comparable to ore-bearing faults (Гоипов, 2021). In addition to crushing, the zones are characterized by small rods and dikes of small bodies with variegated composition that often form belts and bundles, and sometimes there is an increased number of veins, including quartz veins.
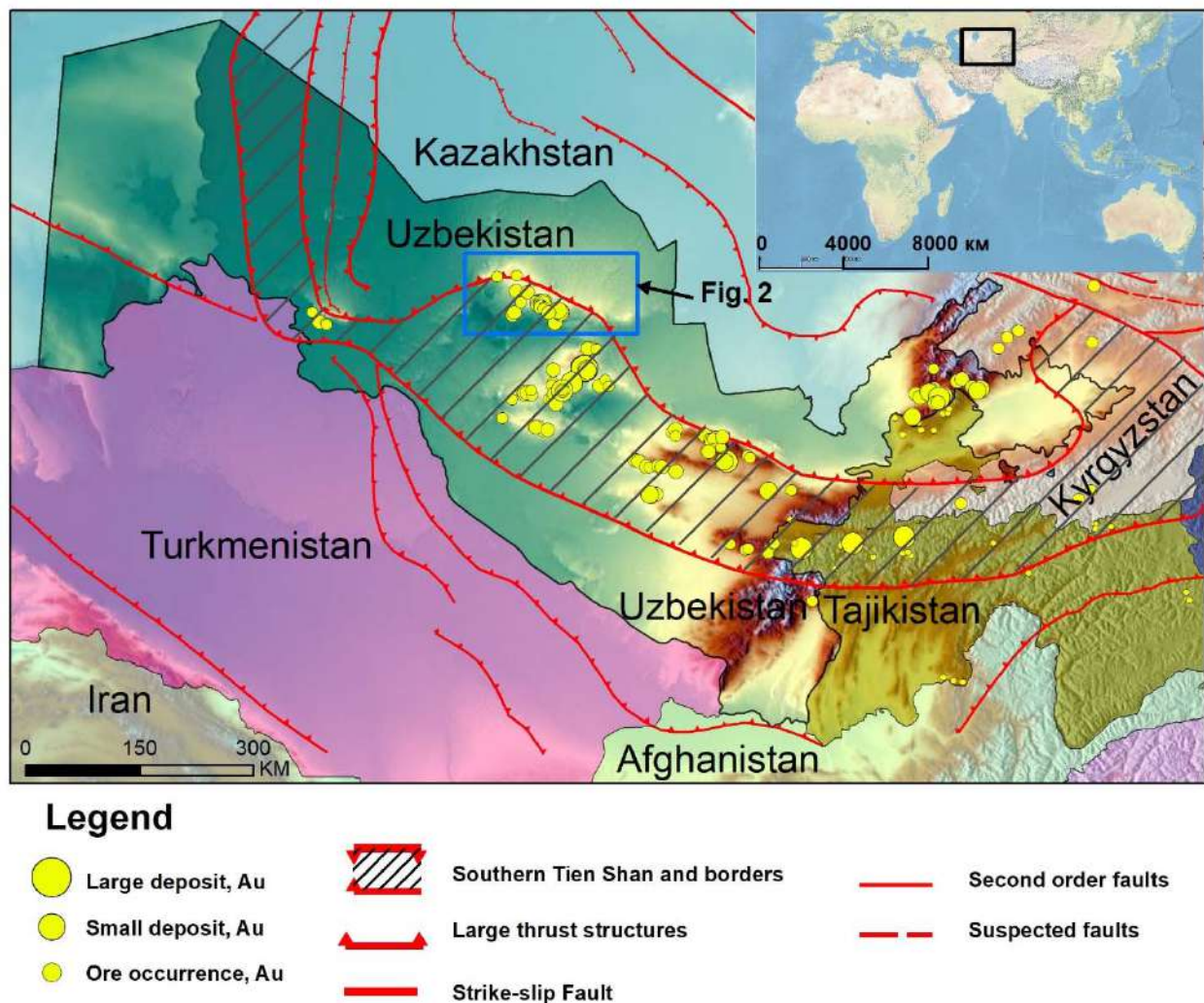
Fig. 1. Schematic zoning of the western part of the South Tien Shan orogenic system in the territory of Central Asia (Mukhin et all., 2023) with gold ore deposits and deep faults (Кремнев, 1981) based on a global digital relief model (compiled by A.B.Goipov)

The role of ore-controlling structures is played by transverse and diagonal ruptures and zones of ruptures of different orders: from small ruptures affecting the localization of ore bodies and pillars in deposits to regional transblock ruptures, near and at the intersection of which ore fields are localized with longitudinal zones.

An important role in the localization of ores, especially gold-sulfide-sulfide veined-interspersed, is played by ore-shielding surfaces, which are usually the soles and roofs of dolomite-siliceous carbonate strata, as well as thrust planes. In some cases, this is especially typical for the Bukantau, the role of ore-controlling structures in relation to ore fields is played by the folds (Исаходжаев и др., 2015).

The geophysical field characterization was carried out by qualitatively analysing the structure, intensity and geological structure of the area and determining the possible nature of the selected structural elements based on a comprehensive analysis of all available data in the Arc GIS (geospatial analysis) environment, including the results of processed remote sensing materials.

2. RESEARCH METHODS

Geophysical signs of mineralization in the territory of the Bukantau Mountains are given using the above mentioned results, especially in terms of the geological interpretation of the selected geophysical field elements. The main tasks involved in integrating the cosmogeological (remote sensing) results with geological and geophysical materials require a correlation analysis of changes in the geophysical field values.

This work was carried out according to the application of the ArcGIS program with the digitization of stock materials, and remote sensing Earth materials and maps of geochemical halos were integrated.

For gravimetric research, the morphological feature map of local gravimetric field components based on the results of zoning was digitized in the form of gravitational field intensity lines for a static analysis of the automated allocation of promising areas by known reference objects.

The geological formations composing the Bukantau Mountain structure are part of two structural and formation zones: the North Bukantau and the South Bukantau. The boundary of the structural formation zones is the North Bukantau interzonal fault, in which the formations of the North Bukantau structural formation zone (SFZ) are uplifted (thrown up) over the deposits of the South Bukantau SFZ. In the gravitational field, the North Bukantau fault is indicated by a linear zone of horizontal gradients.

The local components of the gravity field of the North Bukantau interzonal fault are accompanied by linear zones of high-frequency minima, which show the fragmented and dissociated zones accompanying the main fault plane.

The geological structural features of the structural formation zones are well displayed both by the regional component of the gravity field and on the map of anomalies in the reduced field (Кремнев, 1981).

The North-Bukantau SFZ, which is composed of dense volcanogenic and volcanogenic-sedimentary rocks and overlying upper Paleozoic molasses, is characterized mainly by positive field values ranging from 10 to 39 mGal. The intensity of the anomalies gradually decreases from West to East. This is because dense volcanogenic rocks that were developed in the West are overlapped in the eastern direction by a less dense molasse formation and then by loose Mesozoic formations.

The South-Bukantau SFZ, which is composed of terrigenous formations of the Cambro-Silurian and acidic intrusions that break through them, is characterized by low negative gravitational field values ranging from -39 to -5 mGal. The intensity of the field naturally increases from the South, where large granitoid massifs are developed to the North, and where the terrigenous section increases via carbonate formations of the Irlir Ridge.

Thus, the main geological structural elements of the Bukantau Mountains coincide with the characteristic features of the regional gravitational field component.

In the North-Bukantau SFZ, against the background of the generally higher gravity field, two gravitational maxima are distinguished: in the west, Karamurunsky, and in the east, South-Tokhtatau.

The maximum intensity of the Karamurun, which reaches 39 mGal, is caused by green shales of the Kumbulak Formation and basaltoids of the Tubabergen Formation and reaches the level of the eroded section. The boundaries of the maximum practically coincide with the geological boundaries.

The South-Tokhtatau maximum is located in the eastern part of the square. The site is covered with loose sediments up to 200 m thick. The intensity of the gravity field here reaches 11.5 mGal (Кремнев, 1992).

Wells drilled within the limits of the gravitational maximum revealed the Kumbulak and Tubabergen Formations, i.e., the geological natures of the described gravity field maxima are similar.

The maximum intensities of the gravity field of the East of the Karamurun are 6-9 mGal (Кремнев, 2005). The rocks of the Argali, Tokhtatau and Ashibulak Formations (molasse formation) are exposed here. They are underlain by basaltoids of the Tubabergen Formation and broken by numerous dikes of the main composition.

In the cores of small anticlinal folds, the Tubabergan Formation approaches the daytime surface, which is recorded by local anomalies of the linear field with an intensity reaching 11.5 mGal.

In the south-east direction, the molasse formation sinks under the loose formations of the foothill plain, the thickness of which reaches 200-250 m. Accordingly, the depths of the Tubaberg and Kumbulak Formations increase. This causes a decrease in the intensity of the field to -4 mGal.

In the northern part of the Bukantau Mountains, a section of a reduced field value is allocated inside the positive gravity field northeast of the Karamurun maximum. The intensity of the field here varies from 5 to -3 mGal. The direction of the iso-anomaly is the northeast. This area of the reduced field value corresponds to the Bokalinsky intrusive, composed of tonalites and trondhjemites, which density is 2.68 g/cm^3. Intrusions break through the rocks of the Argali Formation. Contacts with the host rocks are steep at angles of 70-75°.

An isometric negative anomaly of the gravity field with an intensity reaching -12 mGal is distinguished in the northern part of the intrusive zone. Perhaps this anomaly corresponds to an incoming magmatic channel (the "leg" of the intrusion).

Magnetometric research indicates that for the zoning of the magnetic field, a map of the anomalous magnetic field on a scale of 1:100,000 was used. The map of the regional component of the magnetic field with an average radius of 10 km and the map of the local component were auxiliary.

The magnetic field in the area of the Bukantau Mountains is quite complex and differentiated. Its intensities vary from -100 to +300 nanotesla (nT).

By the nature of the field, the area of the Bukantau Mountains is divided into two parts, namely, the northern and the southern (this is most clearly visible on the map showing the regional component of the field). The boundary of the section approximately coincides with the North-Bukantau interzonal fault.

The North-Bukantau and South-Bukantau structural formation zones are well expressed in the observed magnetic field.

In the North-Bukantau SFZ in the northern part of the area, two areal positive magnetic field anomalies with an intensity reaching 400 nT are distinguished. The western anomaly corresponds to the Bokalin intrusive tonalite-trondhjemite composition (the magnetic susceptibility of tonalites and trondhjemites reaches 1350×10^{-6} CGS (Кремнев, 2005; Крикунова и др., 2012).

The anomaly coincides with the shape and size of the intrusion mapped during the geological survey. The second anomaly is located somewhat in the northeast of the Bokalinsky intrusive. In its form, it also resembles an intrusive array. The anomaly is located above the foothill plain, i.e., the magnetically disturbing object is blocked by loose formations of considerable power. According to the shape of the anomaly and its intensity, it presumably maps an intrusion with the same composition as the Bokalin intrusion. To the southeast of this anomaly, there is another, smaller anomaly with an intensity of more than 300 nT. The depths to the upper edge of the disturbing objects according to the quantitative interpretation of these anomalies are 1000-1300 m, the effective magnetization values range from 1000 to 2400 × 10^{-6} CGS units (the eastern object has effective magnetization values that are slightly lower than 900-1000 units), and I.G. Kremnev links these anomalies with volcanogenic formations of the main composition (gabbro and gabbro porphyrites).

The East of the meridian of the Kokpatas gold deposit, the magnetic field of the North Bukantau SFZ is calm and positive with intensities of 40-50 nT. The stretch of the isodynam smoothly varies from the northwest to the northeast and back. Against the background of a calm field, anomalies of an isometric form with an intensity reaching +100 nT are observed. Their diameters are 4-5 km. Isometric anomalies are located along the North Bukantau interzonal fault (Fig. 2). Their possible geological nature is the vent facies of the Tubabergan subvolcanic complex.

In the eastern part of the area overlain by loose sediments, two rather large positive anomalies with intensities of 100-300 nT are distinguished and are obviously caused by volcanogenic formations of increased basicity.

The nature of the magnetic field over the South-Bukantau structural and formation zones is much more complicated. The magnetic field here is predominantly negative, its intensity varies from -10 nT to -100 nT, and the nature of the field is mosaic. Areal and isometric negative magnetic field anomalies map granitoid massifs and rods, and linear anomalies correspond to the terrigenous rocks containing them (Кузнецов, Муравьев, 1986; Максудов и др., 2010; 2015; 2016).

Against the background of the general negative magnetic field, linear, annular and arc-shaped positive anomalies with intensities of 50-150 nT are distinguished, giving the magnetic field a very complex differentiated character.

3. DISCUSSION OF THE RESULTS

In the southwestern part of the area, large granitoid intrusions, namely, the Altyntau and Kokpatas intrusions, are mapped by two areal negative magnetic field anomalies with an intensity of up to -100 nT. Areal negative magnetic field anomalies along the perimeter are framed by small positive intensity anomalies of up to +150 nT. Their geological nature has

been clearly established during prospecting operations at the deposits and ore occurrences of gold in Cholchoratau, Altyntau, etc. Positive magnetic field anomalies correspond to the keratinized and scarred rocks of the Kokpatas Formation in the intrusive exocontacts. Discontinuous disturbances of latitudinal, meridional, north-eastern and, less often, north-western directions are confidently distinguished in the magnetic field (Fig. 2).

In the central part of the square, in the Turbay Mountains, negative magnetic field anomalies with an intensity of up to -100-150 nT are distinguished. Their shape is isometric or elongated in the northwest direction. They are framed on the periphery by annular, linear and isometric positive magnetic field anomalies with an intensity of up to +100 nT.

The described negative magnetic field anomalies correspond to the Turbai, Sautbay and Sarytau granitoid intrusions, which in turn represent rod-shaped and ridge-shaped protrusions of the roof of a large granitoid massif – Sautbay-Sarytau – that does not reach the level of the eroded section. The Sautbay-Sarytau granitoid intrusion is uniquely installed in the gravity field. It is also possible that the Turgai and Sautbay intrusions are rods that break through the intrusion and that do not reach the level of the eroded section.

Positive magnetic field anomalies map the zones of keratinized and scarred rocks of the Kokpatass Formation, to which the gold and tungsten mineralization of the Bulutkan deposits and the Sarytau group ore occurrences are confined (Fig. 3).

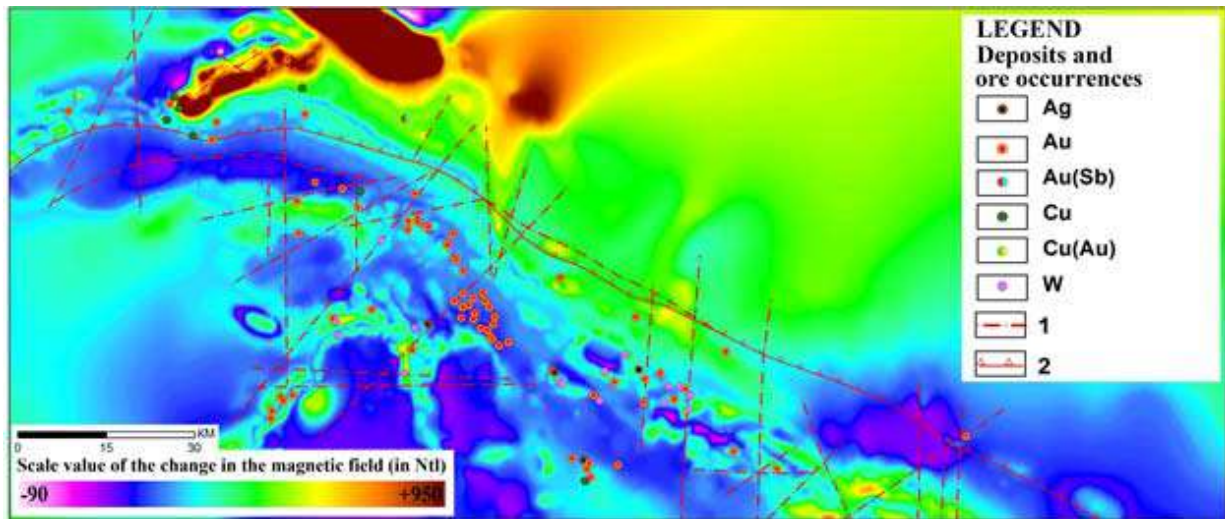**Fig. 2.** Map of morphological features of the ΔTa aeromagnetic field. 1 – boundaries between structural and formation zones; 2 – faults identified by geophysical data (using materials by Дементеенко, Киндерова, 2007)
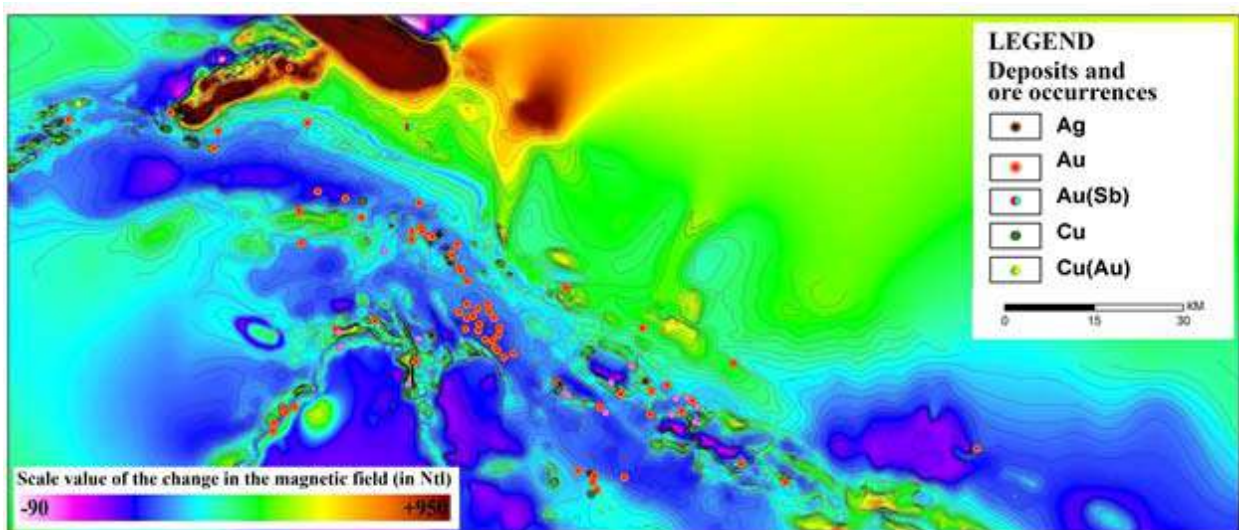

Fig. 3. Magnetic field with overlapping deposits and ore occurrences (using materials by Дементеенко, Киндерова, 2007)

In the south-eastern part of the square, a mosaic magnetic field that is sharply differentiated in intensity indicates the South-Dzhetymtau (Mullalinsky) intrusion that does not reach the level of the pre-Mesozoic foundation, as well as keratinized and scarred rocks in the exocontacts of its roof.

Small arc-shaped positive magnetic field anomalies with intensities of +20 - +30 nTl in the Boztau area are of particular interest. They are confined to the north-western periclinal immersion of the Kokpatas-Boztau anti-form and probably map serpentinites (or serpentinite melange) lying at the base of the tectonic plates. Low-lying serpentinite bodies of small capacity (10-20 m) were opened by drilling wells during prospecting operations in the Boztau area. The presence of magnetite was established while studying serpentinites.

Linear positive magnetic intensity anomalies are distinguished between the Turbay Mountains and the North Bukantau interzonal fault; the values range from +50 - +100 nT. The bedrock within these anomalies has a low magnetic susceptibility. The magnetically disturbed objects that caused a significant increase in the magnetic field are located below the level of the eroded section and are apparently caused by pyrite-pyrrhotite mineralization (Кремнев, 1981, 1992, 2005; Крикунова и др., 2012).

The exploration and informative value of the natural electric field anomalies in the Bukantau Mountains are not clear, although this method has studied almost the entire uplift area, where pre-Mesozoic deposits are exposed at the surface and are present at a depth of up to the first tens of metres. Extensive (up to 10-15 km) negative EP field potential anomalies with intensities in the first hundreds of millivolts are identified here and are usually explained by graphitized (carbonaceous) and permeable rocks.

The natural electric field in the study area is characterized by a complex structure and values of the potential intensity ΔUEP from +500 mV to -450 mV (Fig. 4). Positive EP anomalies, as a rule, correspond to intrusive formations and carbonate and monolithic rocks that have not undergone any changes (hydrothermal changes, crushing, or fracturing).

The Karamurun negative EP field is confined to the western part of the Bukantau fault. The Karamurun deposit (copper-pyrite with gold) is located in the area of weakly positive EP field values.

The Aitym negative EP field is confined to the deposits of the Koksai Formation (O_2-S_1ks), represented by an interlayer of carbonaceous siliceous-micaceous shales, with interlayers of flints of the first subformation and siltstones, sandstones, mudstone shales, and siltstone mica-quartz of the second and third subformations. The internal structure of the Aitym negative EP field is determined by negative anomalies of the second order, which fix the zones of the tectonic disturbances of the northeastern and near-latitude strike. The gold deposits of Aytym, Ayakashchi-2, as well as a number of gold ore manifestations are located in the region of negative field values or gravitate to areas of its greatest gradient.

Positive EP anomalies in the area of the Kokpatas ore field are mapped by the Karashakh volcanogenic-sedimentary complex (C_2kg) and limestones of the West Okzhetpes Formation (C_1zk).

The Okzhetpes negative EP field is confined to the deposits of the Bostau Formation (C_2bs), which is represented by siltstones, mudstones, gravelites, sandstones, conglomerates, and limestone lenses. The internal structure of the negative EP field is determined by negative anomalies of the second order, mainly of the northwestern strike, thereby fixing zones of tectonic disturbances.

In the area of the Bulutkan ore occurrence, in general, an increase in the EP potential values in the southern direction is clearly recorded, reaching a relative excess of up to 250 MV over the northern part. This pattern is explained by the spread of intrusive formations in the southern part of the site.

For the electrical exploration of the VP, in the Bukantau Mountains, various surveys using the VP method were studied, mainly individual ore fields, deposits, ore occurrences and their flanks, where pre-Mesozoic deposits are exposed on the surface or lie at a depth of up to the first metres. In this connection, a single, integral map of the anomalous VP (polarization induced) field for the entire elevation area was not compiled. The scheme of the anomalous VP field of the Bukantau Mountains has been compiled, including separate areas (sections) of work by the VP method.

4. RESULTS

In the study area, regional anomalies of the first order were identified and were associated with scattered inclusions of sulfides and an increased concentration of carbonaceous material in rocks (hc = 5-10%); regional anomalies of the second order correspond to a higher concentration of sulfides and carbonaceous material in rocks (hc =7.5-15%). The internal structure of the regional anomalies of the first and second orders of the VP is determined by local VP anomalies corresponding to local zones that are most enriched in sulfides (hc an.=20% or more).

All numerical values that were digitized and analysed are given in Table 1.
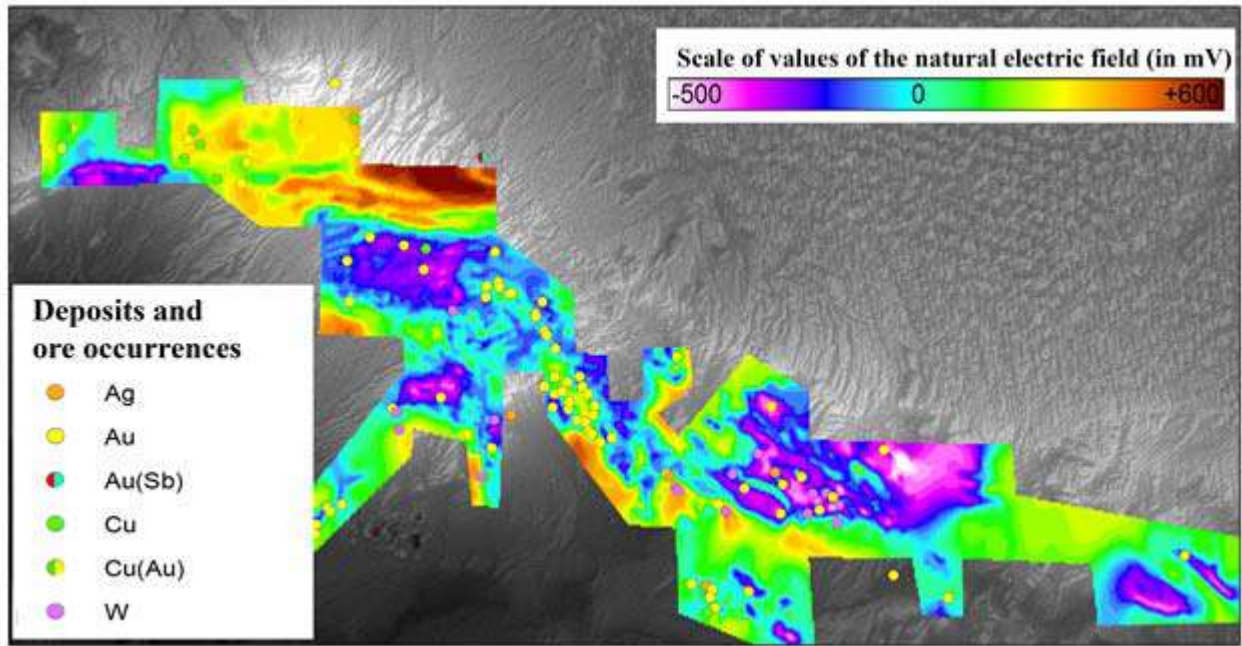
Fig. 4. Morphological map of the features of the natural field (EP) based on the results of zoning (using materials by Дементеенко, Киндерова, 2007).

<div align="right">

Table 1

</div>

The complex geophysical features and the relationship with the localization
of the mineralization of the Bukantau Mountains (compiled by A.B. Goipov)

№	Deposits and ore occurrences	Element		ₐGa in mgl	ₐTa in nTl	ΔU in mV
1	Aytym-II	🔴	Au	0-(-0,5)	-40-50	-50
2	Altyntau-VII, VIII	🔴	Au	1,5-2,0	10-20	-100
3	Argali	🟢	Cu	-1,5-2,0	260-270	300
4	Ayakashyi	🔴	Au	0 -(+0,5)	-20-30	-250
5	Barkhany	🔴	Au	0,5-1,0	-60-70	-200
6	Shoe covers	🟣	W	0,5-1,0	-110-120	0
7	Shoe covers	🟢	Cu	0, 5-1,0	-130-140	0
8	Middle-I, II	🔴	Au	0 -(+0,5)	-80-90	0
9	Budukan	🔴	Au	0 -(+0,5)	-30-40	350
10	Burgut	🟣	W	-0,5-1,0	30-40	300
11	Eastern-I, II	🔴	Au	0-(-0,5)	-50-60	50
12	Mountain	🔴	Au	0-(-0,5)	-40-50	-50
13	Farther	🔴	Au	0-(+0,5)	-30-40	-200
14	Flannelette	🔴	Au	0,5-1,0	10-20	-50
15	Dautbay	🔴	Au	0-(+0,5)	60-70	50
16	Jazzik	🔴	Au	0-(+0,5)	-70-80	-100
17	Derbez-I	🟡	Ag	0 -(+0,5)	50-60	200
18	Jelsay-II	🔴	Au	0-(+0,5)	-10-20	0
19	Jetymtav II	🟡🔴	Ag, Au	0-0,5	-60-70	-50
20	Jelandi	🟣	W	1,0-1,5	80-90	350
21	Jirakuduk	🔴	Au	0-0,5	10-20	200
22	Jirakuduk	🟢🔴	Cu, Au	0 -(+0,5)	40-50	250
23	Dolomit	🔴	Au	0-0,5	-40-50	-100
24	Irlir	🟢🔴	Cu, Au	0,5-1,0	0-10	250
25	Irintav	🟣	W	-0,5-1,0	-80-90	200

No	Name		Element			
26	Kantokken	●	Au	0,5-1,0	10-20	-10
27	Kantokken	◑	Au, W	1,0-1,5	40-50	-20
28	Karamurun	◑	Au, Cu	2,0-2,5	20-30	200
29	Karashokho-I, II	●	Au	0 -(+0,5)	-50-60	50
30	Kansay	●	Au	+0,5-1,0	-50-60	-250
31	Okzhetpes	●	Ag	0-(+0,5)	-40-50	-150
32	Orazali	●	Cu	0-(-1,5)	10-20	300
33	Pridorozhny	●	Au	0 -(+0,5)	-100-110	150
34	Prirazlomny	●	Au	0 -(+0,5)	-60-70	-70
35	Prikontaktov	●	Au	0 -(+0,5)	-90-100	0
36	Foothill	●	Au	0-(-0,5)	-60-70	0
37	Plain	●	Au	0 -(+0,5)	-60-70	0
38	Sarapan	●	W	1,0-1,5	20-30	-100
39	Sarapan	●	Au	1,0-1,5	0-10	-100
40	Sarkekazgan	●	Au	0-(-0,5)	-70-80	-250
41	Sarytau	●	W	-1,0-1,5	0-10	-100
42	Sautbau	●	W	0-(-0,5)	-20-30	300
43	North Altyntau	●	Au	1,5-2,0	70-80	50
44	North Aytym	●	Au	0,5-1,0	-40-50	-50
45	North Jilindin	●	Au	1,5-2,0	-70-80	0
46	North Karabulak	●	Au	0,5-1,0	-10-20	100
47	Northern I, II	●	Au	0-(-0,5)	-40-50	50
48	Northeast	●	Au	0-(-0,5)	-40-50	100
49	North-West I, II	●	Au	0-(+0,5)	-40-50	-200
50	Silver	◑	Ag, Au	0-(+0,5)	-60-70	0
51	Sulfide	●	Au	0-(-0,5)	-40-50	200
52	Taraubay	●	Au	0-(-0,5)	10-20	-350
53	Turbay	●	Au	0-(-0,5)	-10-20	-200
54	Turbay	●	Ag	0-(-0,5)	0-10	-100
55	Turbay (west)	◑	Au, Ag	0-(+0,5)	-20-30	300
56	Terensay	●	Au	0,5-1,0	-50-60	150
57	Ulkentau	● ● ● ●	Au, Ag, Cu, W	-0,5-1,0	-20-30 / -30-40 / -20-30 / -20-30	-100
58	Haydarkul	●	Au	0-(-0,5)	60-70	0
59	Central	●	Au	0,5-1,0	-50-60	50
60	Cholcharatau-I	●	Au	0-(+0,5)	0-10	-150
61	Latitudinal	●	Au	0,5-1,0	-60-70	200
62	Southern Bektash	●	W	1,0-1,5	10-20	-50
63	Southern-I, II, III	●	Au	0-0,5	-60-70	200

Legend for table number 1

$_\Delta$Ga in mgl	The value of the gravity of deposits and ore occurrence in the gravitational field (gravity is measured in milligals (1 mGal $= 10^{-5}m/s^2$)
$_\Delta$Ta in nTl	The value of the magnetic field of deposits and ore occurrence in nanotesla (1 nT $=$ 1 nanotesla $= 10^{-9}$Tesla $= 10^{-9}$Tl)
ΔU ЕП in mV	The value of the natural electric field of deposits and ore occurrence in millivolts (1 millivolt [mV] = 0.001 volt [V]) ΔU
🔴	Gold deposits and ore occurrences
🟡	Silver deposits and ore occurrence
◑	Gold-silver deposits and ore occurrence
◐	Silver-gold-deposits and ore occurrence
🟣	Tungsten deposits and ore occurrence
🟢	Copper occurrence

The features of the change in the values of physical fields of 63 objects (deposits and ore occurrences) were analyzed throughout the territory of the Bukantau Mountains. Then these objects for each type of mineralization (gold, silver, tungsten) were compared and the relationships were determined for the quantitative distribution of ore objects by complex geophysical features (Table 2).

Positive magnetic field anomalies map the zones of keratinized and scarred rocks of the Kokpatas Formation, to which the gold and tungsten mineralization of the Turbai, Sautbay, Bulutkan deposits and the ore occurrences of the Sarytau Group are confined.

Seven negative anomalous EP fields of the first order can be distinguished in the square (from west to east): I – Karamurun, II – Aitym, III – Cholcharatau, IV – Kokpatas, V – Okzhetpes, VI – Turbay, and VII – Jetym.

The Karamurun negative EP field is confined to the zone of the Bukantau fault (in its western part). The Karamurun deposit (copper-pyrite with gold) is located in the area of weakly positive EP field values.

Positive EP field anomalies correspond to the limestones of the Okzhetpes Formation (D$_{2-3}$ok). At the Okzhetpes site (Ващенко и др., 1980), all manifestations of gold are located either in the gradient region of the EP field or (less often) in the negative EP field but in areas with relatively elevated potential values. Considering the position of the Bulutkan and

Barkhan ore occurrences, one can ensure that they are also located in the marginal parts of large negative natural electric field anomalies.

In the area of the Bulutkan ore occurrence, in general, an increase in the EP potential values in the southern direction is clearly recorded, reaching a relative excess of up to 250 MV over the northern part. This pattern is explained by the spread of intrusive formations in the southern part of the site.

The increased polarizability of ores was established and used in studies via the method of induced polarization at a number of sites in Dzhetymtau (Ващенко и др., 1980) in the Turbay Mountains and Okzhetpes site (Усманов и др., 1984). Gold sulfide ores, as a rule, are distinguished by an increase in apparent polarizability (hc); however, the allocation of anomalies in many cases is difficult due to the influence of graphitization and uneven sulfidization of the host rocks. Their separation is a simultaneously important and very difficult task, the solution of which probably lies in the way of studying the transient characteristics of the decline in the VP and nonlinear processes.

The South Bukantau regional EP anomaly is confined to the southern branch of the Bukantau fault, which is represented by crushed, fractured rocks with scattered inclusions of sulfides and is located within the limits of the Karamurun negative EP anomaly.
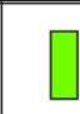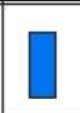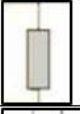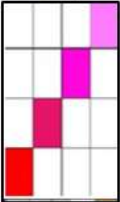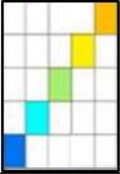
Quantitative distribution and interrelations of ore objects of Bukantau
mountains according to complex geophysical features
(compiled by A.B. Goipov)

№	Deposits and ore occurrences	ΔU mV ΔGₐ mgl	ΔTa in nTl
1	Karamurun		
2	Altyntau VII, VIII		
3	North Altyntau		
4	North Jilindinskoe		
5	Jelands		
6	Cantroken		
7	Sarapan (Au)		
8	Sarapan (W)		
9	Yu. Bektash		
10	Barkhany		
11	Shoe covers (W)		
12	Shoe covers (Au)		
13	Flannelette		
14	Irlir		
15	Cantroken		
16	Kansai		
17	Sev. Aitym		
18	Sev. Karabulak		
19	Terensai		
20	Central		
21	Latitudinal		
22	Ayakashi II		
23	Middle I, II		
24	Budukan		
25	Far		
26	Dautby		
27	Jazz		
28	Derbez I		
29	Jelsai II		

ΔU mV: -200 -100 0 100 200
ΔGₐ mgl: -2,5 -1,5 0 1,5 2,5
ΔTa in nTl: -200 -100 0 100

№	Deposits and ore occurrences	ΔU mV ΔGa mgl	ΔTa in nTl
30	Jirakuduk		
31	Karashoho I, II		
32	Okzhetpes I		
33	Pridorozhny		
34	Prirazlomny		
35	Prikontaktovy		
36	Ravninny		
37	Severo-zapadnoye I, II		
38	Serebryany		
39	Turbay (Zapad.)		
40	Cholcharatau I		
41	Aitym II		
42	Vostochny I, II		
43	Gorny		
44	Jetymtau II		
45	Jirakuduk		
46	Dolomite		
47	Predgorny		
48	Sarcecasgan		
49	Southbay		
50	Severnoye I, II		
51	Severo-vostochnoye		
52	Sulfide		
53	Tarabay		
54	Turbay (Au)		
55	Turbay (Ag)		
56	Haidarkul		
57	Yuzhny I, II III		
58	Burgut		
59	Irintau		
60	Ulkentau		
61	Orazaliyev		
62	Sarytau		
63	Arhar		

Legend for table number 2

Sign	Values	Materials used
	Negative values of the natural electric field	The value of the natural electric field is given in millivolts (mV) according to the map of the natural field at a scale of 1:200,000 [Дементеенко и Киндерова, 2007].
	Positive values of the natural electric field	
	Zero values of the natural electric field	
	Positive values of the gravitational field	ΔGa is given mGl according to the local component of the gravitational field on a scale of 1:200,000 [Дементеенко и Киндерова, 2007].
	Zero values of the gravitational field	
	Negative values of the abnormal magnetic field	ΔTa is given in nTl according to the map of the anomalous magnetic field on a scale of 1:200,000 [Дементеенко и Киндерова, 2007].
	Positive values of the abnormal magnetic field	

5. CONCLUSION

Within the Central and Northern Altyntau areas, the zone of local gravimetric anomalies is associated with geochemical halos of gold and tungsten and characteristic minerals of quartz, gold, scheelite, pyrite, and arsenopyrite. According to structural tectonic factors, mineralization is controlled by faults in the northeastern and northwestern directions, which consist of a zone of fractured and crushed rocks and feathered structures. The magmatic factor of mineralization is represented by granite-granodiorite intrusions and an exocontact zone of magmatic formations complicated by large faults. The ore formation according to the reference sites is rare gold and quartz.

Local negative gravimetric anomalies and positive anomalies of induced polarizations associated with the sulfide mineralization zone were detected within the Karashakh, near-contact, dike, and latitudinal sections. According to geochemical data, halos of gold and arsenic are present. The types of mineralization are gold, pyrite, and arsenopyrite. Structurally, it is represented by the arched zone of the anticline fold, faults, and thrusts. The ore formation is gold-sulfide.

In some areas of the Dzhelsai, Barkhannoy and Okzhetpes ore fields, VP anomalies and zones of negative magnetic anomalies are associated with geochemical halos of gold. The type of mineralization is gold quartz and sulfide. The structural factors of mineralization are the northeastern, northwestern and submeridional faults, the brachianticline, and the feathering structures of the Kokpatas deep fault. The type of ore formation according to the reference sites is gold-quartz.

In the Sautbay, Sarytau, and Cholcharatau areas, negative magnetic field anomalies correlate with geochemical halos of tungsten, molybdenum, and copper. Characteristic minerals are scheelite, fluorite, molybdenum, pyrrhotite, chalcopyrite and antimony. Magmatic mineralization includes rod-shaped granodiorite intrusions and scarn zones at the contacts of intrusions. The type of ore formation is gold-rare-metal quartz. On a detailed scale, the magnetic field value for each object changes, but the nature of the negative or positive anomaly remains.

Changes in the values of the physical field are associated with the geological and tectonic structure of the region and the occurrence of the foundation, as well as the composition of rocks.

All available values are used for static analysis and are converted to a raster format for the automated allocation of promising areas by known reference objects.

Thus, the prospecting signs and ore-controlling factors of mineralization and their interrelations with the values of the anomalous geophysical and geochemical fields were analysed in the territory of the Bukantau Mountains.

As a result of the integration of remote sensing, geophysical, and geochemical data using static and metallogenic analyses, predictive and promising positions have been identified and certified by field decryption (Goipov et al., 2020) and the sinking of mine workings, which are recommended for subsequent geological prospecting.

6. GRATITUDE

REFERENCES

Borisov O.M., Glukh A.K. Ring structures and lineaments of Central Asia. Fan. Tashkent, 1982, 122 p. (in Russian).

Dementenko L.I., Kinderova L.P. Allocation of priority forecast areas for gold and other minerals within the Bukantau Mountains based on the creation and processing of a database of geological, geophysical, geochemical and remote sensing information using field zoning methods and computer forecasting technologies for 2004-2007. Project report. State Geological Fund. Tashkent, 2007, 164 p. (in Russian).

Glukh A.K. et al. Remote maps are the basis of metallogenic and predictive studies. Geology and Mineral Resources, No. 3, 2002, pp. 28-32 (in Russian).

Goipov A.B. Automated lineament analysis in the Lessa program in order to identify structural factors of mineralization in the Bukantau mountains. Bulletin of NUUz, No. 3/1, 2021, pp. 161-167 (in Russian).

Goipov A.B., Akhmadov Sh.I., Movlanov Zh.Zh. The study of mineralized zones of the Bukantau mountains from satellite images in the short-wave infrared range. Mining Journal of Kazakhstan, No. 8, 2020, pp. 10-14 (in Russian).

Goipov A.B., Khasanov N.R., Akhmadov Sh.I. Study of the mineralized zones of the Bukantau mountains on space images in the short-wave infrared range. Journal of Critical Reviews, Vol. 7, No. 06, 2020a, pp. 2070-2074.

Goipov A.B., Rakhmatovich K.N., Axmadov S.I., Musaxonov Z.M. Application of ratio bands of space images for mapping minerals on the example of Kokpatas-Okzhetpes trend in Mountain Bukantau (South Tien Shan). The American Journal of Applied Sciences, Vol. 2, No. 07, 2020b, pp. 94-103, DOI:10.37547/tajas/Volume02Issue07-16.

Isakhodzhaev B.A., Tangirov A.I., Urunov B.N. Boztau-Kokpatas-Okzhetpessky trend. Scientific and practical journal "Geology and mineral resources", Tashkent, No. 6, 2013, pp. 23-30 (in Russian).

Kremnev I.G. Complex interpretation in the "Target Forecast" system of the Russian Academy of Sciences, Irkutsk, 1992 (in Russian).

Kremnev I.G. Mapping of the anomalous magnetic field and gravimetric map scale 1: 500000 - 1:1000000 of the territory of the Republic of Uzbekistan for 2004-2005, Geolfond RUz, 2005 (in Russian).

Kremnev I.G. Principles of allocation structures of physical fields according airborne geophysical surveys, Tashkent, "FAN" of the Uzbek SSR, No. 6, 1981, p. 49-52 (in Russian).

Krikunova L.M., Zahidov A.R., Gafurbekov A.A. Geological and industrial types of iron ores of Uzbekistan. SE "NIIMR". Tashkent, 2012, 100 p. (in Russian).

ЛИТЕРАТУРА

Борисов О.М., Глух А.К. Кольцевые структуры и линеаменты Средней Азии. Фан Ташкент, 1982, 122 с.

Ващенко В.П., Ларин Н.М. и др. Отчет по геологической съемке м-ба 1:50000. Фонды Мингео. Уз.ССР, 1980.

Глух А.К. и др. Дистанционные карты – основа металлогенических и прогнозных исследований. Геология и минеральные ресурсы, No. 3, 2002, с. 28-32.

Гоипов А.Б. Автоматизированный линеаментный анализ в программе «Lessa» с целью выявления структурных факторов оруденения в горах Букантау. Вестник НУУз., No. 3/1, 2021, с. 161-167.

Гоипов А.Б., Ахмадов Ш.И., Мовланов Ж.Ж. Изучение минерализованных зон гор Букантау по космическим снимкам в коротковолновом инфракрасном диапазоне. Горный журнал Казахстана, No. 8, 2020, с. 10-14.

Дементеенко Л.И., Киндерова Л.П.Выделение первоочередных прогнозных площадей на золото и другие полезные ископаемые в пределах гор Букантау на основе создания и обработки базы данных геолого-геофизической, геохимической и дистанционной информации методами районирования полей и технологий компьютерного прогноза за 2004-2007 г.г. Гос. Геол.фонд. Ташкент, 2007, 164 с.

Исаходжаев Б.А., Тангиров А.И., Урунов Б.Н. Бозтау-Кокпатас-Окжетпесский тренд. Научно-практический журнал "Геология и минеральные ресурсы", Ташкент, No. 6, 2013, с. 23-30.

Кремнёв И.Г. Комплексная интерпретация в системе «Целевой прогноз» РАН СО ИЗК, Иркутск, 1992 г.

Кремнёв И.Г. Принципы выделения структур физических полей по данным аэрогеофизических съемок, «ФАН». Ташкент, УзССР, No. 6, 1981, с. 49-52

Кремнёв И.Г. Составление карт аномального магнитного поля и гравиметрической карты масштаба 1: 500000 – 1: 1000000 территории Республики Узбекистан за 2004-2005 гг., Геолфонд РУз, 2005.

Крикунова Л.М., Захидов А.Р., Гафурбеков А.А. Геолого-промышленные типы железных руд Узбекистана. ГП «НИИМР». Ташкент, 2012, 100 с.

Кузнецов О.Л., Муравьев В.В. Физико-геологическая природа концентрически-зональных объектов дистанционного зондирования. Обзор, Общая и рег.геол. ВИЭМС. Москва, 1986, 40 с.

Максудов С.Х., Кремнев И.Г., Рустамов А.И., Смирнов А.Н., Туйчиев А.И., Юсупов В.Р. Предварительные результаты высокоточных магниторазведочных работ на территории Восточного Букантау. В: Актуальные проблемы геологии, геофизики и металлогении, Ташкент, 2015, с.43-46.

Kuznetsov O.L., Muravyev V.V. Physical and geological nature of concentric-zonal remote sensing objects. Overview, General and reg.geol. All-Union Research Institute of Economics of Mineral Raw Materials and Geological Exploration. 1986, 40 p. (in Russian).

Maksudov S. Kh., Kremnev I.G., Rustamov A.I., Smirnov A.N., Tuichiev A.I., Yusupov V.R. Preliminary results of high-precision magnetic exploration in the territory of Eastern Bukantau. In: "Actual problems of geology, geophysics and metallogeny", Tashkent, 2015, pp.43-46 (in Russian).

Maksudov S. Kh., Pak V.A., Karimova G.G., Umarova M.E., Juraev I. Some results of the use of high-precision magnetic prospecting to identify ore objects on the Yertashsai square in the Angren district. Geol. and Mineral Resources, No. 3, 2010, pp. 17-20 (in Russian).

Maksudov S.Kh., Tuichiev A.I., Yusupov V.R., Kremnev I.G., Rustamov A.I., Smirnov A.N. Results of high-precision magnetic survey on the territory of Eastern Bukantau. International Scientific and Technical Conference "Integration of science and practice as a mechanism for effective development of the geological industry of the Republic of Uzbekistan", Part I. SE "NIIMR" Tashkent. 2016, pp.292-293 (in Russian).

Mukhin P., Mirkamalov R., Seltmann R. Structure of the Muruntau gold ore region in the Kyzyl-Kum desert (Central Asia). Int. J. Earth Sci. (Geol.Rundsch.), Vol. 112, 2023, pp. 659-683, https://doi.org/10.1007/s00531-022-02262-6.

Rogachev B.V. Geophysical methods in the search for gold ore deposits. In the collection "Geophysics of gold deposits" Moscow, 1977, pp. 13-21 (in Russian).

Serdyukov M.K. Acquisition of geophysical, geochemical and geological studies. In the collection "Geophysical research in the search and exploration of ore deposits in Kazakhstan", Alma-Ata, 1978, pp. 6-8 (in Russian).

Usmanov R.R. et al. Report on the compilation of an aerial geological map of the Northern Nuratau mountains and adjacent territories, scale 1:50000 on an area of 12700 km^2. Mingeo funds. Uz.SSR, 1984 (in Russian).

Vashchenko V.P., Larin N.M. et al. Geological survey scale 1:50000 report. Mingeo funds, Uz.SSR, 1980 (in Russian).

Максудов С.Х., Пак В.А, Каримова Г.Г., Умарова М.Э., Джураев И. Некоторые результаты применения высокоточной магниторазведки для выявления рудных объектов на площади Ерташсай в Ангренском районе. Геол. и минеральные ресурсы, No. 3, 2010, с. 17-20.

Максудов С.Х., Туйчиев А.И., Юсупов В.Р., Кремнев И.Г., Рустамов А.И., Смирнов А.Н. Результаты высокоточной магнитной съемки на территории Восточного Букантау. Интеграция науки и практики как механизм эффективного развития геологической отрасли Республики Узбекистан. Материалы Международной научно-технической конференции. Часть-I. ГП «НИИМР». Ташкент, 2016, с. 292-293.

Рогачев Б.В. Геофизические методы при поисках золоторудных месторождений. В сб.: Геофизика золоторудных месторождений Москва, 1977, с. 13-21.

Сердюков М.К. Комплектование геофизических, геохимических и геологических исследований. В сб.: Геофизические исследования при поисках и разведке рудных месторождений в Казахстане, Алма-Ата, 1978, с. 6-8.

Усманов Р.Р. и др. Отчет по составлению аэрофотогеологической карты гор Северный Нуратау и прилегающих территорий м-ба 1:50000 на площади 12700км^2. Фонды Мингео, Уз.ССР. 1984.

Goipov A.B., Khasanov N.R., Akhmadov Sh.I. Study of the mineralized zones of the Bukantau mountains on space images in the short-wave infrared range. Journal of Critical Reviews, Vol. 7, No. 06, 2020a, pp. 2070-2074.

Goipov A.B., Rakhmatovich K.N., Axmadov S.I., Musaxonov Z.M. Application of ratio bands of space images for mapping minerals on the example of Kokpatas-Okzhetpes trend in Mountain Bukantau (South Tien Shan). The American Journal of Applied Sciences, Vol.2, No. 07, 2020b, pp. 94-103, DOI:10.37547/tajas/Volume02Issue07-16.

Mukhin P., Mirkamalov, R., Seltmann R. Structure of the Muruntau gold ore region in the Kyzyl-Kum desert (Central Asia). Int. J. Earth. Sci. (Geol. Rundsch.), Vol. 112, 2023, pp. 659–683, https://doi.org/10.1007/s00531-022-02262-6.

ХАРАКТЕРИСТИКА ГЕОФИЗИЧЕСКИХ ПОЛЕЙ И ГЕОФИЗИЧЕСКИХ ПРИЗНАКОВ ОРУДЕНЕНИЯ ГОР БУКАНТАУ ЮЖНОГО ТЯНЬ-ШАНЯ

Гоипов А.Б.[1], Ахмадов Ш.И.[1], Юсупов В.Р.[2]

[1]Министерство горной промышленности и геологии Республики Узбекистан, Университет геологических наук, ГУ «Институт минеральных ресурсов», Узбекистан, 100041, г. Ташкент, ул. Олимлар, 64
[2]Институт сейсмологии имени Г.А. Мавлянова Академии наук Республики Узбекистан
100128, г. Ташкент, ул. Зульфияхоним-3

Резюме. В северо-западной части Южного Тянь-Шаньского складчатого золоторудного пояса расположены горы Букантау. В геодинамическом районировании горы Букантау разделены на Северобукантаускую и Южнобукантаускую структурно-формационные зоны (СФЗ). Они представляют собой сложно изогнутые поднятия, осложнённые более мелкими складками.

Руды Северобукантауской СФЗ образуют медно-цинково-колчеданную с золотом (Карамурун), золото-сульфидно-кварцевую (Ирлир, Джетымтау) и второстепенные медно-молибденово-скарновую (Оразалы I, II) и хромитовую формации. Проявления золота относятся к золото-сульфидно-кварцевому геолого-промышленному типу. Основные рудные объекты Южнобукантауской СФЗ образуют редкометально-золоторудную (месторождение Алтынтау), золотомышьяковую (месторождение Кокпатас), золотополиметаллическую (месторождение Турбай), золотосеребряную (месторождение Окжетпес) минерализации, вольфрамоносные скарны и скарноиды (месторождение Саутбай).

Геофизическими признаками могут служить различные элементы геофизических полей – интенсивность поля, оси положительных и отрицательных аномалий, градиенты поля и др. Районирование физических полей горы Букантау на структурно-формационной основе позволило типизировать и разделить гравитационные и магнитные аномалии на однородные группы.

Статья содержит анализ многолетних данных комплексных геофизических исследований гор Букантау. Были проанализированы характеристики изменения значений физического поля 63 объектов на территории гор Букантау и созданы комплексы геофизических признаков и взаимосвязей с локализацией оруденения.

Поисковые критерии формулировались на основе изучения особенностей физических полей, характерных для известных рудопроявлений и месторождений, с точки зрения степени однозначности их отражения в электрическом, гравитационном и магнитном полях. Сопоставление данных Дистанционного зондирования Земли, геофизических и геохимических данных с

использованием статического и металлогенического анализов позволило определить прогнозно-перспективные позиции, под-тверждённые полевым дешифрированием и проходкой горных выработок, рекомендованные для дальнейших геолого-поис-ковых работ.

Ключевые слова: Месторождения, эндогенные процессы, золото, структура, формирование, геофизические поля, интру-зивные породы.

CƏNUBİ TYAN-ŞANIN BUKANTAU DAĞLARININ GEOFİZİKİ SAHƏLƏRİNİN VƏ ƏLAMƏTLƏRİNİN SƏCİYYƏSİ

Goipov A.B.[1], Əhmədov Ş.İ.[1], Yusupov V.R.[2]
Özbəkistan Respublikasının dağ sənaye və geologiya nazirliyi, Geoloji elmlər universiteti, ÖR
«Mineral xammal resursları institutu», Özbəkistan, 100041, Daşkənd şəh., Olimlar küç. 64
[2]Özbəkistan Respublikasının Elmlər Akademiyasının Q.Mavlyanov adına Seysmologiya İnstitutu
100128, Daşkənd şəh., Zülfiyahanim küç., ev 3

Xülasə. Cənubi Tyan-Şanın şimal-qərb hissəsində yerləşən Bukantau dağları qızıl filizli qurşağında yerləşir. Geodinamik ra-yonlaşdırmada Bukantau dağları Şimal Bukantau və Cənub Bukantau struktur-formasiya zonalarına (SFZ) bölünür. Onlar mürəkkəb əyilmiş qalxımlar olub, daha kiçik qırışıqlarla mürəkkəbləşmişdir. Şimal Bukantau SFZ filizləri mis-çink-pirit (Karamurun), qızıl-sulfid-kvars (İrlir, Cetimtau) və az miqdarda mis-molibden-skarnoid (Orazalı I, II) və xromit formasiyalarına bölünürlər. Qızıl təzahürləri qızıl-sulfid-kvars geoloji-sənaye tipinə aid edilir. Cənub Bukantau SFZ-də əsas filiz obyektləri nadir metal-qızıl filiz (Altyntau yatağı), qızıl-arsen (Kokpatas yatağı), qızıl-polimetal (Turbay yatağı), qızıl-gümüş (Okjetpes yatağı) mineralizasiyası, volfram skarn və skarnoidləri (Sautbay yatağı) olaraq göstərilir. Geofiziki təsirlər - geofiziki sahələrin özünəməxsus elementləri - əsas sahələr, müsbət və mənfi anomaliyalar, sahələrin qradientləri və s. kimi qəbul edilə bilər. Bukantau dağlarının struktur-formasiya əsasında fiziki sahələrinin rayonlaşdırılması, qravitasiya və maqnit anomaliyalarını homogen qruplara və tiplərə ayırmağa imkan verir.

Məqalədə Bukantau dağlarının çoxillik kompleks geofiziki tədqiqatları məlumatlarının təhlili aparılmışdır. Bukantau dağları ərazisində 63 obyektin fiziki sahə göstəricilərinin dəyişmə xüsusiyyətləri təhlil edilmiş və filizləşmənin lokallaşması ilə əlaqəli geofiziki əlamətlərin və qarşılıqlı əlaqələrin kompleksləri yaradılmışdır.

Axtarış meyarları, mövcud filiz təzahürləri və yataqlarına xas olan fiziki sahələrin xüsusiyyətlərinin, onların elektrik, qravitasiya və maqnit sahələrində nə dərəcədə dəqiq əks olunduğu baxımından öyrənilməsi əsasında formalaşdırılmışdır. Yerin məsafədən zondlanması məlumatları, geofiziki və geokimyəvi məlumatların statistik və metallogenik təhlillərlə müqayisəsi nəticəsində, sahə dekodlaşdırılması və dağ qazma işlərilə təsdiqlənmiş, gələcək geoloji-axtarış işləri üçün tövsiyə olunan perspektivli mövqelər müəyyən edilmişdir.

Açar sözlər: Yataqlar, endogen proseslər, qızıl, struktur, formalaşma, geofiziki sahələr, intruziv süxurlar

POTENTIAL OPPORTUNITIES FOR ORGANIZATION OF GEOPARK IN NAKHCHIVAN AUTONOMOUS REPUBLIC

Kangarli T.N., Ibrahimov V.B., Rashidov T.M., Kangarli I.T.

Ministry of Science and Education of the Republic of Azerbaijan,

Institute of Geology and Geophysics, Azerbaijan

119, H.Javid ave., Baku, AZ1143: tkangarli@gmail.com

Summary. Azerbaijan is distinguished by a great variety of geoheritage sites, including those of a regional and global importance. In 1982, 37 geosites were included in the country's first of protected nature monuments. In 2009-2012, special National Action Plan was implemented, resulting in the development of an extended inventory of 484 geosites of global, regional, national and local importance. As some groups of the identified geosites are located within relatively small geographic areas with outstanding natural, cultural and historical heritage, the most promising way of organizing their conservation is the establishment of geological parks. As of now, there are 6 areas in Azerbaijan, characterized by high potential for the organization of a geopark. One of such areas is the Nakhchivan Autonomous Republic – a landlocked exclave of Azerbaijan, characterized by exceptionally rich geological and biological diversity, as well as representative cultural-historical heritage. In 2020-2022, Azerbaijani specialists have studied the feasibility of integrating most important geosites of the province within the framework of a single Ilandagh geopark which resulted in the development of a detailed inventory of 171 rare and unique geosites. The territory of the planned geopark is also known as one of the key biodiversity areas of Azerbaijan and the Caucasus ecoregion. As to cultural and historical heritage, there are 66 historical and 108 archaeological monuments, including 2 historical and 28 archaeological monuments of global importance. All these factors make Ilandagh one of the best places in Azerbaijan to create a global geopark.

Potential of the country

Thanks to the complexity of geological structure and the specifics of geological evolution background, territory of Azerbaijan is distinguished by a great variety of geoheritage sites, including those of a regional and, in several cases, global importance. There are many unique geosites in Azerbaijan, all having certain value from the perspectives of scientific research, visual perception and tourism potential. Apparently, the most prominent component of the national geoheritage is the world's largest mud volcano concentration represented by more than 400 active volcanoes detected within the relatively small geography of the Eastern Azerbaijan. Besides that, the list of Azerbaijan's unique geosites includes, but is not limited to, the world's richest Quaternary fauna deposits, Naftalan oil with strong healing properties, thermal and mineral water sources, multi-origin magmatic and tectonic landforms, rare lithological-stratigraphic sections, relic mountain lakes, etc.

In 1982, 37 of the most prominent geosites of the country were included in the "List of state nature monuments – geological (paleontological) objects taken under state protection", approved by the Cabinet of Ministers of Azerbaijan. In 2009-2012, "National Action Plan for the Protection and Sustainable Use of Rare Geological Objects in Azerbaijan Republic" was implemented, resulting in the development of an extended inventory of geosites located on the territory of Azerbaijan. The new inventory included 484 geosites of global, regional, national and local importance. According to the Plan, the identified geosites have been grouped in a number of categories, including stratigraphic and paleontological (75 geosites), mineralogical and ore-petrographic (132 geosites), geotectonic (132 geosites), geomorphological (94 geosites), hydrological-hydrogeological (94 geosites) and historical-geological objects (Kangarli, Babayev, 2012).

Following development of the above detailed inventory, the government and the scientific society of Azerbaijan started working on how to organize individual protection of the identified geosites by mandating them status of individual nature monuments, conserving them as part of existing or newly

conserving them as part of larger special protection areas. As some groups of the identified unique geosites are located within relatively small geographic areas with outstanding natural, cultural and historical heritage, the most promising way of organizing their conservation is the establishment of geological parks. As of now, there are the following 5 areas on the map of Azerbaijan, characterized by high potential for organization of a geopark.

Mud volcanoes

Azerbaijan has gained a fame of the country with the highest mud volcano concentration. There are over 350 mud volcanoes in the eastern part of the country, including 156 offshore volcanos active on the bottom of the Caspian Sea (Alizadeh et al., 2016b; Rashidov, 2014; Rashidov et al., 2019). Total area occupied by the volcanoes amounts to 60 thousand km^2. Back in 1982, 4 most famous mud volcanos became the first geosites in Azerbaijan to be mandated the status of specially protected area. In 2007, the State Nature Reserve "Mud Volcanoes Group of Baku and Absheron Peninsula" was established on a total area of 123 km^2, which covered 43 mud volcanoes and their surroundings. Besides its' geoheritage, development area of the mud volcanism is known for rich cultural and historical heritage (Aliyev et al., 2024).

Girmaki

Occupying small area in the east of the Absheron peninsula, Girmaki site contains several valuable geosites, including an original erosive relief, daylighting bitumen deposits and an exposed stratotype of the oil-bearing productive series. Besides its' geological landmarks, the area is known as a habitat of rare semi-arid flora species, and due to a natural gas fire blazing continuously at the foot of the Yanardagh hill. Girmaki site is also known for its' mining-historical heritage represented by a number of preserved ancient oil pits used back in 17th to 19th centuries.

Khaltan depression

Located in the river valley of Gilgilchay in the north-western Azerbaijan, the area is characterized by rich landscape diversity and presence of several unique geosites. One of such landmarks is a stratotype section of the Jurassic and Cretaceous sediments of the continental slope and foot facies of the southern margin of the Scythian Epi-Hercynian platform. Another important geosite is a well-exposed complete lithological-stratigraphic section of the Cretaceous deposits of the Greater Caucasus marginal sea facies, building up the geological structure of the Khaltan mould – the largest structural basin in the Southeastern Caucasus region. Geomorphologi-

cal diversity of the area is also very pronounced, represented by multiple exotic landforms emerged as a result of nappe tectonics of the Austrian phase of tectogenesis. Finally, the area is famous for the thermal mineral water outcrops, as well as a number of historical and archaeological monuments.

Basgal

Located on Mikhtokan range in the Ismayilli district of Azerbaijan, Basgal area is renowned for a number of unique geosites formed as a result of nappe tectonics of the Aptian-Rhuddanian tectogenesis, including the stratotype section and structural forms of the island-arc margin of the South Caucasus continental massif, unique outcrops of the Quaternary tectonics, Mudresa structural basin, and the Caucasus' only Earle Paleocene intrusion (Buynuz gabbro-sienites). Other-than-geological sites of the area are represented by famous medieval villages of Lahij and Basgal.

Nakhchivan

Territory of Nakhchivan Autonomous Republic is known for especially rich geodiversity. Nakhchivan geoheritage amounts to over 150 geosites located all over the territory of the province. The region also stands out for rich landscape and biological variety, as well as historical, cultural, and archaeological monuments.

Geopark potential of the Nakhchivan Autonomous Republic

One of the most geodiversity-rich provinces of Azerbaijan is Nakhchivan Autonomous Republic – a landlocked exclave of Azerbaijan, bordered by Armenia in the north and east, Iran in the south and west and Turkey in the northwest. Occupying a relatively small area of 5500 km^2, the province is characterized by high density and rich diversity of geosites. Rich geoheritage of the province include lithological-stratigraphic sections reflecting 400 myr geological history of the region, magnificent magmatic landforms, easy to access and study faulting zones and rupture dislocations, numerous sources of mineral waters with a wide range of balneological properties, rich ore and non-ore deposits, mining-historical monuments, etc. The province is also characterized by diverse geo-morphology represented by spectacular river valleys, terraces and alluvial cones, glacial cirques, trough valleys and moraines, exotic rocks and rock compositions, mountain peaks, ancient volcanic structures, karst and pseudo-karst formations, and different-age peneplains.

In 2009-2012, an inventory and passportization of the geoheritage of the Nakhchivan province was implemented within the framework of the "National Action Plan for the Protection and Sustainable Use of

Rare Geological Objects in Azerbaijan Republic". As a result of the implemented studies, over 150 rare and unique geosites were identified in the province, including 22 lithology-stratigraphic, 25 hydrological and hydrogeological, 18 magmatic, 14 ore-petrographic, 68 geomorphological and 5 mining-historical sites.

In 2020-2022, specialists from the Institute of Geology and Geophysics have studied the feasibility of integrating most important geosites of the province within the framework of a single geopark. The study resulted in the outlining of the geopark's border, and the development of a detailed inventory of 171 rare and unique geosites. Covering a total area of 1700 km^2 between the drainage divide of the Zangezur range in the northeast and the riverbed of Araz in the south, the geopark will cover the territories belonging to Ordubad (872 km^2), Julfa (582 km^2) and Babek (246 km^2) districts of Nakhchivan AR (Kangarli et al., 2018; Kangarli et al., 2019) (Fig. 1).

On the territory of the planned geopark there are 1 city, 3 urban-type settlements and 65 villages with a total population of 75,570 thsd people. As local community livelihoods depend mainly on beekeeping, animal husbandry, gardening and olericulture, almost an entire territory of the geopark is characterized by low levels of manmade environmental impacts. Thus, there are no large cities or industrial enterprises, whereas 70% of electricity needs are provided by renewable sources. In addition to the geological heritage, the area is renowned for rich biodiversity and historical heritage.

Based on the study results, a special task force was created to develop a detailed inventory of the planned geopark and undertake the other steps required for its' organization. In the beginning of 2023, a proposal was sent to the respective national autho-rities of Azerbaijan in connection to the establishment of the "Ilandagh" geopark, named after the most prominent geological and geomorphological landmark of the Nakhchivan AR.

Insight into the geological heritage of Ilandagh geopark

The inventory of 171 geosites studied and described by the task force, include 73 geomorphological, 54 geological, 34 hydrogeological and 10 hydrological objects of global, national and regional importance located in the different parts of the Ilandagh geopark. The below paragraphs provide for the characteristics of each of the above categories supplied with Illustrated description of the most valuable monuments.

Geomorphological sites

On the territory of Ilandagh geopark, there are a large number of rare geomorphological objects, reflecting historical and modern relief-forming processes. The most remarkable morphosculptures are volcanic domes, intrusive massifs, caves, exotic rocks, picturesque mountain peaks, canyons, etc. (Alizadeh et al., 2016a). The inventory includes 72 rare geomorphological sites, including majestic mountain peaks, 32 exotic rocks, 11 caves, 8 canyons and river valleys.

Fig. 1. Map of Ilandagh Geopark

Majestic mountains

In Nakhchivan, mountains do not only form ranges, but also act as individual peaks, standing out against a predominantly flat surface of the Nakhchivan sloping plain. 22 majestic mountain peaks been identified as rare geosites (Fig. 2). These mountains are cone-, plateau-, table- and dome-shaped structures with true altitudes varying from 876 amsl (Mt. Plovtapa) to 3829 amsl (Mt. Gemigaya). According to their genesis, many of these mountains are also classified as tectonic geosites. On several mountains, there are also the archaeological and historical monuments dating back to prehistorical, antique and medieval periods.

Exotic rocks

Widely developed in the eastern part of the province, exotic rock landforms had emerged due to erosion of Cenozoic volcanosedimentary complexes. Unique outlines of such rocks and rock compositions are very attractive for tourists, while geological structure of the outcrops is very informative for researchers (Fig. 3). The total of 32 exotic rocks were included in the inventory, including 13 standalone cliffs, 12 rock compositions, 1 earthen pyramid and 2 rocky areas (Kangarli, Babayev, 2012).

Caves

Geosites inventory of Ilandagh geopark includes 11 enclosed limestone and limestone-dolomite karst, as well as pseudo-karst caves with outstanding value of national and regional importance. Some caves are also popular for their archaeological and cultural value (Fig. 4). For example, there are early men's sites discovered in the caves of Havush piri, Gazma, Dashgala and Bibgatal. The other caves are known as sacred places of worship. The most famous one is the Ashab-i Kehf cave – one of the most important sacred places of Azerbaijan, popular for the Islamic communities of the Caucasus and Middle East regions (Kangarli, Babayev, 2012).

Canyons

In different parts of the Zangezur and Daralayaz ranges, there are several undisturbed valleys and canyons with unique geological and geomorphological characteristics and magnificent landscapes. The most picturesque 8 canyons, each extending for the distance of 3-7 km in the river valleys of Ganzachay, Goydara, Kilit, Saggarsu, Nakhchivanchay and Araz, were included in the geopark's inventory (Fig. 5).

Geological sites

In Nakhchivan, there are a lot of rare geosites associated with different-age and multi-genesis geological and tectonic processes. 54 of such geosites have been studied and inventoried by the task force of Ilandagh Geopark. Identified geosites were grouped in the categories of stratigraphic, tectonomagmatic, ore-historical and petrographic monuments.

Fig. 2. Majestic mountain peaks: a) Alinja (1811.9 m), b) Bardik (2053.6 m), c) Ilandagh (2415.8 m), d) Nahajir (1807.3 m**)**
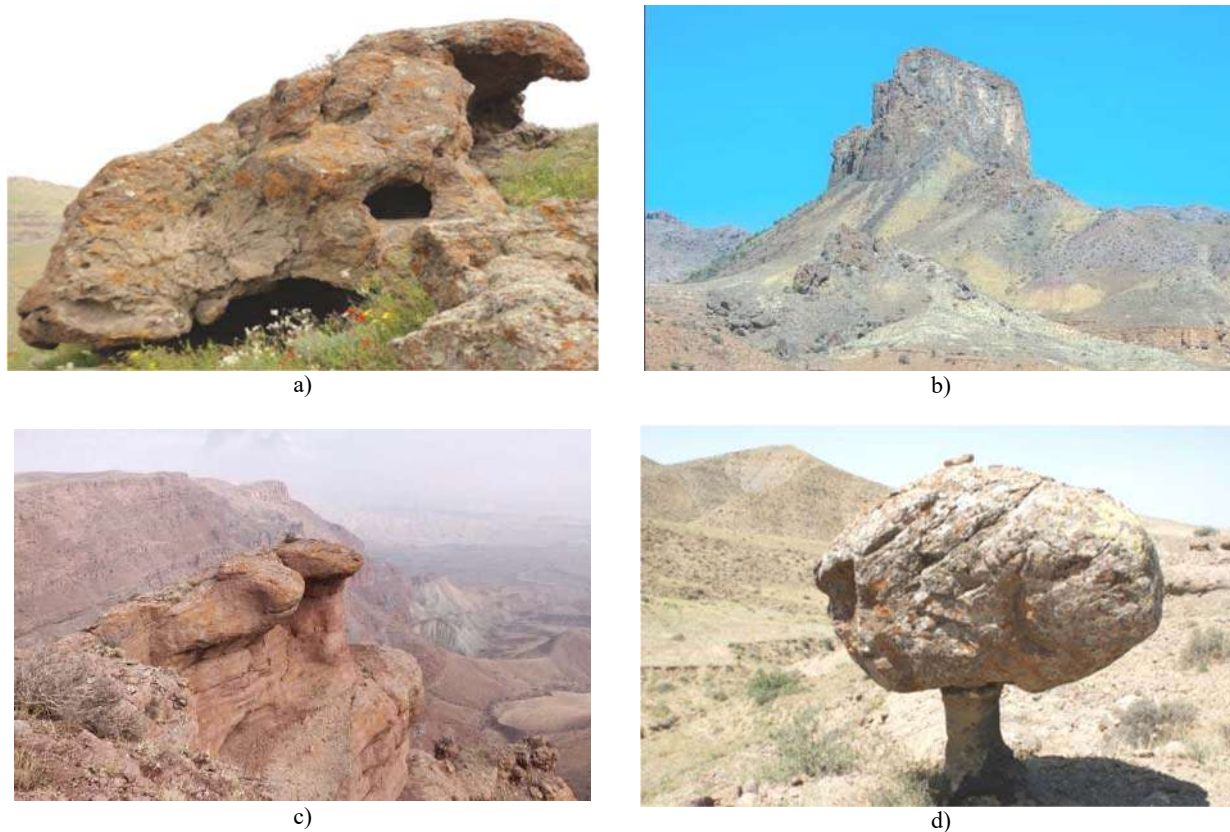
Fig. 3. Exotic rocks: a) Ayigaya, b) Babek Galasi, c) Jutbash Kertenkele, d) Papagdash
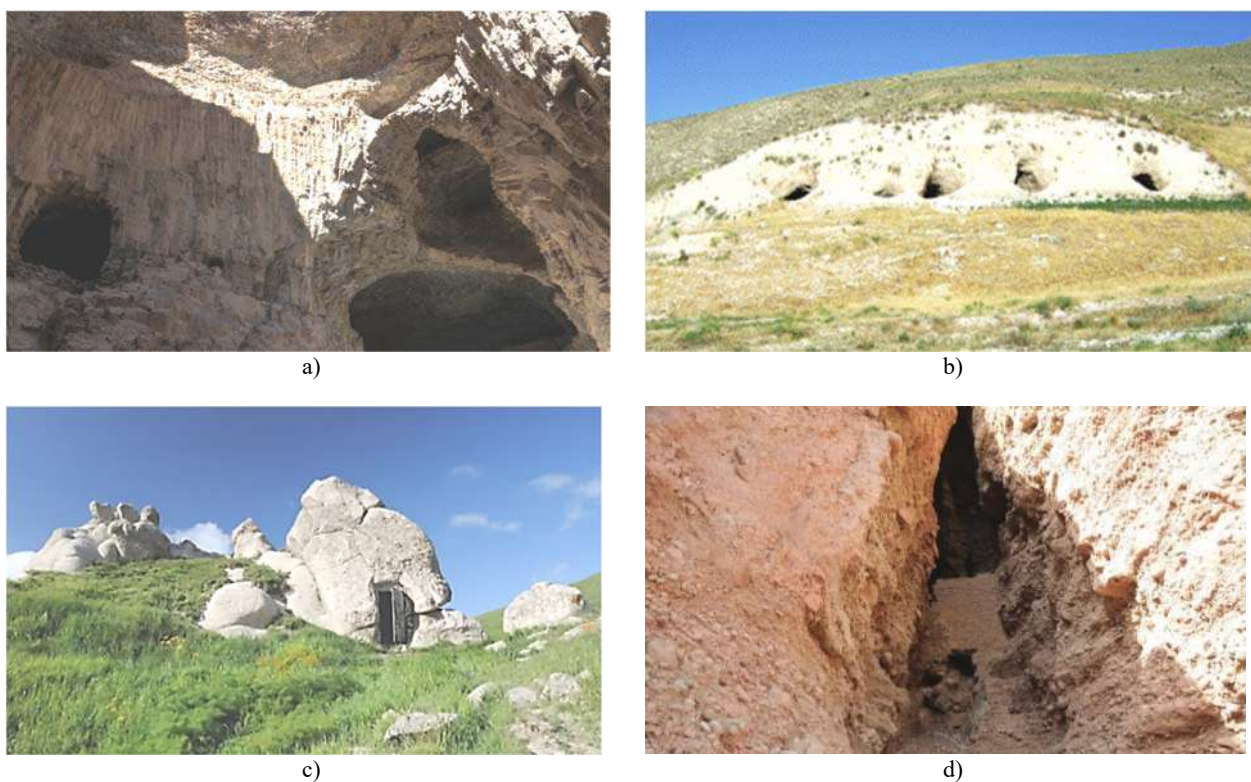
Fig. 4. Caves: a) Ashab-i Kehf, b) Lizbirt, c) Farhad evi, d) Darasham

Fig. 5. Canyons: a) Koydara, b) Saggarsu, c) Nakhchivanchay

Stratigraphic geosites

Unique stratigraphic sections are of a high priority in the list of rare geosites of the Nakhchivan province, as they reflect some of the key milestones in the geological evolution of the Caucasus, Middle East and Anatolia regions. Lithological and stratigraphic sections exposed in the province belong to the Paleozoic, Mesozoic and Cenozoic complexes of the Araz megazone. On the territory of Ilandagh geopark, there are 17 unique lithology-stratigraphic sections, including the most remarkable stratotype sections of Aza (Paleocene-Eocene terrigenous complex), Paradash (Bartonian-Priabonian formation), Chashirdagh (Lower-Middle Miocene series), Kukukchay (Lower Lutetian formation), Darasham (Upper Permian terrigenous-carbonate complex) and Kotam (Upper Cretaceous volcanosedimentary complex) (Fig. 6) (Kangarli, Babayev, 2012).

Tectonomagmatic geosites

Rare tectonomagmatic geosites of the Nakhchivan province are represented by intrusive and subvolcanic massifs, as well as ancient blocks of the rocks with unique petrographic and tectonic parameters (Alizadeh et al., 2016c). 13 such geosites are located on the territory of Ilandagh geopark, including famous Nakhchivan laccoliths – the group of spectacular intrusives – abovementioned magnificent mountains of Ilandagh, Nahajir, Khanegah and Bardik (Fig. 7).

Ore-petrographic geosites

Ore-petrographic geosites are one of the most representative parts of the Nakhchivan's geoheritage. There are 14 ore deposits on the relatively small territory of the province, and 12 of them are located on the territory of Ilandagh geopark. These are the only in the entire Caucasus and Middle East regions deposits of silty agates in Daralik and andalusite in Paraghachay, Buzgov travertine deposit known for rich reserves of the high-quality minerals, the world's largest dolomite deposit in Nokhutdagh, the Caucasus' largest rock salt deposit in Duzdagh (developed for 5 thsd years) and melanterite deposit in Nehram valley, as well as Ganzin granodiorite, Kilit

hornfels and monzonite, Ordubadchay granodiorite-granosyenite Gapijig rutile and Sirab aragonite de- posits known as the only deposits of these minerals in Azerbaijan (Fig. 8).

Fig. 6. Lithology-stratigraphic sections: a) Chashirdagh, b) Kukukchay, c) Aza, d) Kotam

Fig. 7. Tectonomagmatic geosites: a) Aghridagh intrusive, b) Bardik intrusive, c) Gal intrusive, d) Nahajir intrusive

Fig. 8. Ore-petrographic deposits: a) Nokhutdagh dolomite deposit, b) Sirab aragonite deposit

Mining-historical geosites

Some of the numerous mineral deposits of the Nakhchivan province have been developed since ages. For example, mining of salt from the Duzdagh deposit has been carried out since the 3rd millennium BC. The copper-arsenic deposits of Daridagh were exploited back in the 3rd century BC. According to the 12th century historian Hamdullah Ghazvini, there were several copper mines in the vicinity of Nakhchivan town, production of which was exported to the other countries in the region. The total of 7 ore-historical geosites were identified and inventoried as part of the Ilandagh geopark. In addition to the de-posits mentioned above, the list includes Gomur sulphur (18th century), Paraghachay molybdenum (18th century), "Safar evleri" construction stone (15th century), as well as Sirab and Vaykhir copper (3rd-1st millenniums B.C.) deposits (Fig. 9).

Hydrogeological sites

One of the most famous and valuable elements of the geological heritage of Nakhchivan province are the numerous sources of mineral and thermal waters. So far, only 54 of the 220 mineral water sources discovered in the region have been studied in detail.
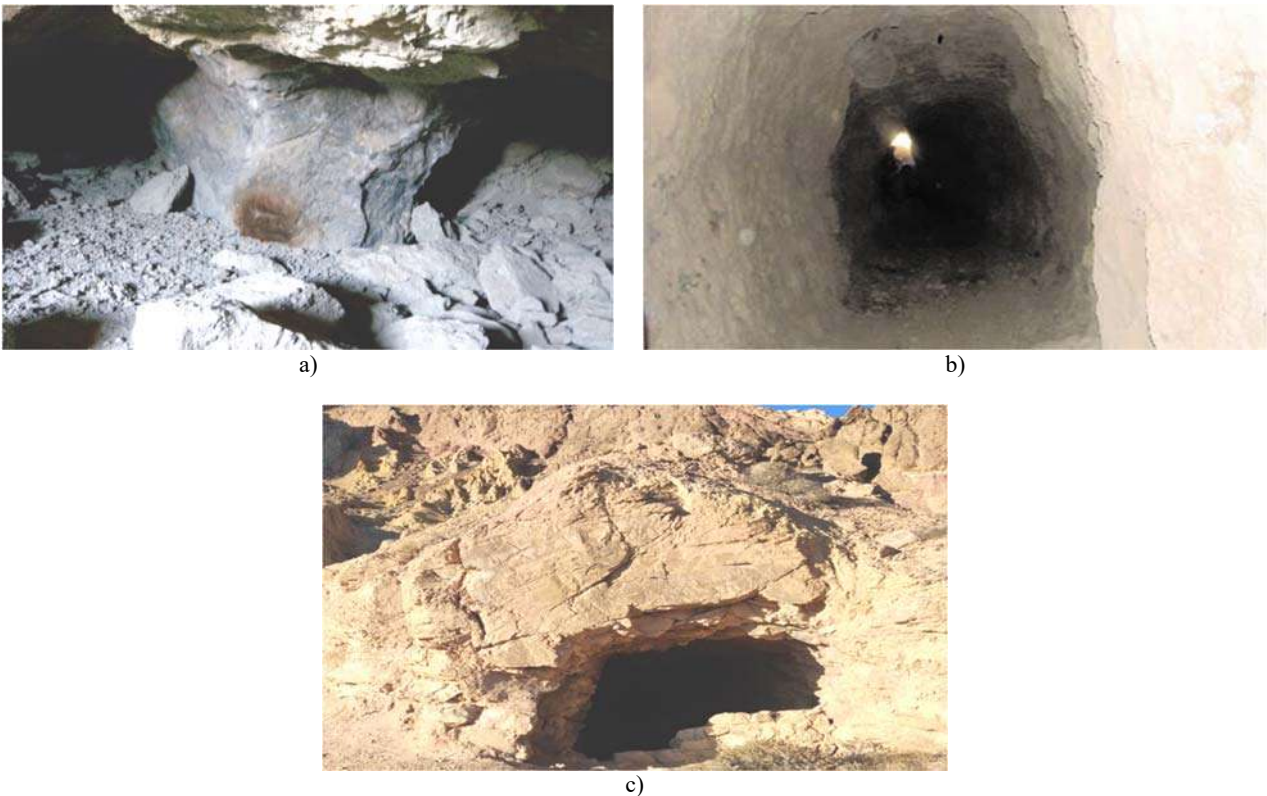
Fig. 9. Ore-historical geosites: a) Duzdagh salt deposit, b) Vaykhir copper deposit, c) Daridagh copper-arsenic deposit

In general, mineral waters are divided into 6 types, 8 classes and 33 types and, according to their balneological properties, are represented by chloride-sulphate, sulphide, magnesium-iron and radon groups. The total flow rate of the studied sources reaches 15 million litres per day. In the relatively small geography of the province, analogues of many world-famous mineral waters are produced, including the Russian "Sinegorskaya", "Narzan", "Yessentuki", "Kislovodsk" and "Pyatigorsk", the Georgian "Borjomi", "Tsaghveri" and "Java", Czech "Frantiskovy", Hungarian "Kevert", Polish "Kudova",

French "La Bourboule", German "Dürkheim", Ukrainian "Shoima", etc. Of particular interest are the fissure-vein waters emerging from subsoil of the Badamli, Vaykhir, Gahab, Sirab, Nahajir, Gizilvang and Daridagh mineral water deposits. The temperature of the water taken from the operating wells of the Sirab and Daridagh sources reaches 41-52ºC. There is a balneological hospital operating on the basis of the Daridagh carbonate-Margumush reservoir. 35 natural and drilled mineral water sources were included in the inventory of the Ilandagh geopark (Fig. 10).

a)

b)

c)

d)

Fig. 10. Hydrogeological sites: a) Sirab, b) Vaykhir, c) Daridagh, d) Ganza

Hydrological sites

The list of rare hydrological monuments of Nakhchivan includes mountain lakes and waterfalls with different hydrological parameters, hydrodynamic regime and chemical properties of water. Standalone part of this heritage is a rock salt waterfall - a unique natural monument at the Duzdagh deposit. The picturesque mountain lakes Goygol, Salvarty, Ganlygel and Batabat, located between absolute heights of 2100-3100 m on the slopes of the Zangezur and Daralayaz ranges, are the highest mountain lakes in the Azerbaijani part of the Lesser Caucasus. Also, there are 11 beautiful 10-20 m tall waterfalls located in different reaches of the major rivers of the province. Hydrological sites of Ilandagh geopark include Batabat, Goygol, Ganligol and Salvarti high-mountain lakes, as well as Balliduz, Jamalchay, Arafsa, Gavakh, Pazmara and Zidara waterfalls.

Biodiversity

An important condition for achieving sustainability of a global geopark is the richness of a candidate territory in the other types of natural, as well as tangible and intangible cultural and historical heritage. The territory of Nakhchivan province is distinguished not only for its' rich landscape diversity and large accumulation of rare geosites, but also for its biodiversity.

Most of the flora and fauna species spread on the territory of Azerbaijan (60 and 56%, respectively) are present in the Nakhchivan ecosystems. The biodiversity of the province is represented by about 3,000 species of plants, 373 species of animals and 226 species of birds. Among them, 58 animal, 39 plant and 3 bird species are listed in the Red Book of Azerbaijan. On the territory of the autonomous re-

public there are Zangezur National Park, as well as Shahbuz, Arpachay, Ordubad and Araz state reserves.

The territory of the planned geopark is known as one of the key biodiversity areas of not only Nakhchivan, but also Azerbaijan and the Caucasus ecoregion. The geopark's fauna is represented by 403 species of vertebrates and 2030 species of invertebrates. 142 species, including 9 fish, 6 amphibian, 14 reptile, 71 bird and 42 mammal species, are included in the second edition of the Red Book of Azerbaijan. The flora diversity of the province is also very rich, amounting to 3021 species of alpine, petrophytic and desert vegetation.

Cultural and historical heritage

Another element of the wealth of the Nakhchivan province is its historical and cultural heritage. In total, there are more than 280 archaeological and 400 historical monuments registered on the territory of the Nakhchivan Autonomous Republic. On the territory of the planned geopark, there are 66 historical and 108 archaeological monuments. 2 historical monuments are of global, 60 of national, and 4 of

local importance. 28 archaeological sites are of global, 61 of national, and 19 of local importance.

Conclusions

Geological and natural diversity, as well as rich cultural and historical heritage of the Nakhchivan Autonomous Republic make it one of the most promising regions of Azerbaijan in terms of the creation and successful functioning of a global geopark. Concentration of a large number of easily accessible geosites in a relatively small area with developed transport and energy infrastructure facilitates the solution of problems associated with the organization of the Ilandagh geopark. Ilandagh geopark will integrate geological, geomorphological, and culture-historical heritage of the province, as well as its' key biodiversity areas (Zangezur National Park) into a single legal nature protection system. In addition, the proposed geopark will allow creating an original protection mechanism of natural sites and human heritage, with the involvement of local societies. Moreover, it will promote organizing education and awareness raising activities, and developing geotourism in the province.

REFERENCES

Aliyev A.A., Huseynov D.A, Abbasov O., Rashidov T., Kangarli I. Mud volcanoes of Azerbaijan: The unique natural objects of the geoheritage. Geoheritage, Vol. 16(1), article id. 20, 2024, DOI: 10.1007/s12371-024-00931-3.

Alizadeh A.A., Guliyev I.S., Kadirov, F.A., Eppelbaum L.V. Geomorphology. In: Geosciences of Azerbaijan. Regional Geology Reviews. Springer. Cham., 2016a, pp. 11-29, DOI:10.1007/978-3-319-27395-2_2.

Alizadeh A.A., Guliyev I.S., Kadirov F.A., Eppelbaum L.V. Mud Volcanism. In: Geosciences of Azerbaijan. Regional Geology Reviews. Springer. Cham., 2016b, pp. 215-233, DOI: 10.1007/978-3-319-27395-2_7.

Alizadeh A.A., Guliyev I.S., Kadirov F.A., Eppelbaum L.V. Tectonics. In: Geosciences of Azerbaijan. Regional Geology Reviews. Springer. Cham., 2016c, pp. 129-201, DOI:10.1007/978-3-319-27395-2_5.

Kangarli T., Babayev S. Geological heritage of Azerbaijan Republic. Nafta-Press. Baku, 2012, 78 p.

Kangarli T., Ibrahimov V., Rashidov T. et al. Feasibility study of the "Ilandagh" Geopark creation in Nakhchivan Autonomous Republic (Azerbaijan). Geoheritage, Vol. 11, pp. 1973-1980, 2019, DOI: 10.1007/s12371-019-00409-7.

Kangarli T., Kangarli I., Rashidov T., Ibrahimov V. Creation of "Ilandag" Geopark in the Nakhchivan Autonomous Republic (Azerbaijan). Priroda, No. 11, 2018, pp. 44-51, DOI: 10.31857/S0032874X0002323-4 (in Russian).

Rashidov T. The diversity of mud volcanoes in the landscape of Azerbaijan. EGU General Assembly Conference Abstracts. Vienna, 2014, 1610019R, DOI: 10.13140/RG.2.2.23100.74883.

Rashidov T., Kangarli I., Ibragimov V. The quaternary mud volcanism in Azerbaijan as the geological phenomenon of the Ponto-Caspian region of the Alpine-Himalayan folded belt. The Third Plenary Meeting and Field Trip of INQUA IFG 1709F POCAS. Tehran and Guilan Province, I.R. Iran, 2019, pp. 121-123.

ЛИТЕРАТУРА

Aliyev A.A., Huseynov D.A, Abbasov O., Rashidov T., Kangarli I. Mud volcanoes of Azerbaijan: The unique natural objects of the geoheritage. Geoheritage, Vol. 16(1), article id. 20, 2024, DOI: 10.1007/s12371-024-00931-3.

Alizadeh A.A., Guliyev I.S., Kadirov, F.A., Eppelbaum L.V. Geomorphology. In: Geosciences of Azerbaijan. Regional Geology Reviews. Springer. Cham., 2016a, pp. 11-29, DOI:10.1007/978-3-319-27395-2_2.

Alizadeh A.A., Guliyev I.S., Kadirov F.A., Eppelbaum L.V. Mud Volcanism. In: Geosciences of Azerbaijan. Regional Geology Reviews. Springer. Cham., 2016b, pp. 215-233, DOI:10.1007/978-3-319-27395-2_7.

Alizadeh A.A., Guliyev I.S., Kadirov F.A., Eppelbaum L.V. Tectonics. In: Geosciences of Azerbaijan. Regional Geology Reviews. Springer. Cham., 2016c, pp. 129-201, DOI:10.1007/978-3-319-27395-2_5.

Kangarli T., Babayev S. Geological heritage of Azerbaijan Republic. Nafta-Press. Baku, 2012, 78 p.

Kangarli T., Ibrahimov V., Rashidov T. et al. Feasibility study of the "Ilandagh" Geopark creation in Nakhchivan Autonomous Republic (Azerbaijan). Geoheritage, Vol. 11, pp. 1973-1980, 2019, DOI: 10.1007/s12371-019-00409-7.

Rashidov T. The diversity of mud volcanoes in the landscape of Azerbaijan. EGU General Assembly Conference Abstracts. Vienna, 2014, 1610019R, DOI: 10.13140/RG.2.2.23100.74883.

Rashidov T., Kangarli I., Ibragimov V. The quaternary mud volcanism in Azerbaijan as the geological phenomenon of the Ponto-Caspian region of the Alpine-Himalayan folded belt. The Third Plenary Meeting and Field Trip of INQUA IFG 1709F POCAS. Tehran and Guilan Province, I.R. Iran, 2019, pp. 121-123.

Кенгерли Т.Н., Кенгерли И.Т., Рашидов Т.М., Ибрагимов В.Б. Создание геопарка «Иландаг» в Нахчыванской Автономной Республике (Азербайджан). Природа, No. 11, 2018, с. 44-51, DOI: 10.31857/S0032874X0002323-4

ПОТЕНЦИАЛЬНЫЕ ВОЗМОЖНОСТИ ОРГАНИЗАЦИИ ГЕОПАРКА В НАХЧЫВАНСКОЙ АВТОНОМНОЙ РЕСПУБЛИКЕ

Кенгерли Т.Н., Ибрагимов В.Б., Рашидов Т.М., Кенгерли И.Т.
*Министерство науки и образования Азербайджанской Республики,
Институт геологии и геофизики, Азербайджан
AZ1143, Баку, просп. Г.Джавида, 119: tkangarli@gmail.com*

Резюме. Территория Азербайджанской Республики отличается исключительным богатством геологического наследия, включающего в себя в том числе редкие геологические объекты (РГО) регионального и мирового значения. В 1982 году 37 РГО были включены во впервые разработанный список охраняемых природных памятников Азербайджана. В 2009-2012 гг., в целях расширения этого списка был реализован «План действий по охране и устойчивому использованию редких геологических объектов в Азербайджанской Республике», в ходе которого были изучены и инвентаризированы 484 РГО мирового, регионального, национального и местного значения. Учитывая, что некоторые из выявленных групп РГО расположены на сравнительно небольших территориях, характеризующихся богатством природного и историко-культурного наследия, наиболее перспективным способом организации охраны этих объектов можно считать создание геологических парков. В настоящее время в Азербайджане имеется 5 территорий, отличающихся высоким потенциалом для организации геопарков. Одной из таких территорий является Нахчыванская Автономная Республика, отличающаяся исключительным геологическим и историко-культурным наследием, а также богатым биологическим разнообразием. В 2020-2022 гг. группа азербайджанских ученых исследовала потенциал интеграции важнейших РГО региона в рамках правового режима геопарка «Иландаг». В результате проделанных работ были составлены паспорта для 171 объектов геологического наследия Нахчыванской АР. Территория планируемого геопарка также признана одной из основных зон биоразнообразия Азербайджана и Кавказского экорегиона. Что касается культурно-исторического наследия, то здесь насчитывается 66 исторических и 108 археологических памятников, в том числе 2 исторических и 28 археологических памятников мирового значения. Все эти факторы делают геопарк «Иландаг» одним из самых благоприятных мест для создания глобального геопарка в Азербайджанской Республике.

Ключевые слова: *геоконсервация, редкие геологические объекты, геопарк, геология, геоморфология, Нахчыван, Азербайджан*

NAXÇIVAN MUXTAR RESPUBLİKASINDA GEOPARKIN TƏŞKİLİ ÜÇÜN POTENSİAL İMKANLAR

Kəngərli T.N., İbrahimov V.B., Rəşidov T.M., Kəngərli İ.T.
*Azərbaycan Respublikası Elm və Təhsil Nazirliyi, Geologiya və Geofizika İnstitutu, Azərbaycan
AZ1143, Bakı, H.Cavid prosp., 119: tkangarli@gmail.com*

Xülasə. Azərbaycanda regional və dünya əhəmiyyətinə malik təbiət abidələri daxil olmaqla, bir çox geoloji irs obyektləri mövcuddur. 1982-ci ildə 37 nadir geoloji obyekt (NGO) Azərbaycanda ilk dəfə tərtib olunmuş qorunan təbiət abidələrinin siyahısına daxil edilmişdir. Həmin siyahının genişləndirilməsi məqsədilə 2009-2012-ci illərdə həyata keçirilmiş "Azərbaycan Respublikasında nadir geoloji obyektlərin qorunması və davamlı istifadəsinə dair Tədbirlər Planı"nın icrası nəticəsində ölkə ərazisində yerləşən qlobal, regional, milli və yerli əhəmiyyətli 484 NGO tədqiq edilmiş və inventarlaşdırılmışdır. Müəyyən edilmiş bəzi qrup NGO-ların təbii və tarixi-mədəni irsin zənginliyi ilə səciyyələnən nisbətən kiçik coğrafi ərazilərdə yerləşdiyini nəzərə alaraq, həmin obyektlərin mühafizəsinin təşkili üçün ən perspektivli yol geoloji parkların yaradılması hesab edilə bilər. Hazırda Azərbaycanda geoparkların təşkili üçün yüksək potensialı ilə seçilən 5 ərazi mövcuddur ki, bunlardan biri də müstəsna geoloji və tarixi-mədəni irsi, habelə zəngin bioloji müxtəlifliyi ilə seçilən Naxçıvan Muxtar Respublikasıdır. 2020-2022-ci illərdə Azərbaycanlı alimlər vilayətin ən mühüm NGO-larının "İlandağ" Geoparkının hüquqi rejimi çərçivəsində inteqrasiyasının potensialını təhqiq etmiş və nəticədə 171 obyektin pasportlarını işləyib hazırlamışdır. Planlaşdırılan geoparkın ərazisi həm də Azərbaycanın və Qafqaz ekoregionunun əsas biomüxtəliflik ərazilərindən biri kimi tanınır. Mədəni-tarixi irsə gəlincə, burada 66 tarixi və 108 arxeoloji abidə, o cümlədən dünya əhəmiyyətli 2 tarixi və 28 arxeoloji abidə mövcuddur. Bütün bu amillər "İlandağ" Geoparkını Azərbaycan Respublikasında qlobal geopark yaratmaq üçün ən əlverişli yerlərdən birinə çevirir.

Açar sözlər: *geokonservasiya, nadir geoloji obyektlər, geopark, geologiya, geomorfologiya, Naxçıvan, Azərbaycan*

LANDSLIDE MODELING USING GIS AND A STATISTICAL METHOD UPSTREAM OF PORT TANGIER MED (TANGIER, MOROCCO)

Maktite A., Faleh A.

Faculty of Letters and Human Sciences, Saïs-Fès, Department of Geography, Sidi Mohammed ben Abdellah University, Fès, Morocco: maktiteabderrahim@gmail.com, ali.faleh@usmba.ac.ma

Keywords: port, Mediterranean Tangier, informative value, success curves, forecast curves

Summary. The context of this study is crucial for understanding the challenges faced by the Tanger Med Port, a strategic hub for international trade. Located in a mountainous region, this port is particularly vulnerable to natural hazards, especially landslides. A study conducted on a 193 km² test site recorded 277 slope movements, representing about 11% of the total area. This evaluation of terrain susceptibility used the information value method to map the movements over recent decades as well as six predisposing factors.

The results show that nearly 31% of the total area is highly susceptible to mass movements, 22% is very sensitive, and 23.3% presents a low threat. These findings were rigorously compared and validated using success rate and prediction rate curves. Five major risk classes for landslides were identified in areas that are undeveloped or sparsely developed with low to negligible values and developed areas on mountain slopes with very high-risk values.

Accurate mapping and risk analysis are essential for developing management and prevention strategies to minimize potential impacts on port infrastructure and associated economic activities. This study thus contributes to a better understanding of geological risks in the region and more importantly, to the implementation of appropriate measures to ensure the safety and resilience of the port.

Introduction

The mountains of the Moroccan Rif are subject to instabilities, often in the form of mass movements, which can have a direct impact on urban constructions (Flageollet, 1989; Maate, 1996). These instabilities are caused by various factors, such as an aggressive climate, rugged terrain, the presence of soft ground (such as marl and flysch), as well as aggravating anthropogenic factors. In the Ksar-Sghir area, for example, several landslides have caused varying degrees of damage to the urban area, including the destruction of some houses and the temporary closure of important roads, leading to major disruptions in road traffic. However, the loss of human life associated with these phenomena has always been rare in this region. To deal with these problems, the Directorate of Equipment and Transport allocates about 50% of its annual budget to either strengthen or repair the roads and hydraulic infrastructures damaged by landslides, according to a source from MATEE. In 2005, however, these unforeseen events caused significant economic losses on a national scale and compromised the development of the region.

It is therefore essential to study and map the risks of mass movements in order to implement preventive actions against these complex phenomena. This is why the establishment of landslide risk maps is of crucial importance. Indeed, the United Nations Office for Natural Disaster Reduction (UNDRO, 1979) was the first international institution to emphasize the importance of this type of cartographic documents for estimating the risks associated with a natural phenomenon in particular. Later, during the "International Decade for the Prevention of Natural Disasters" (DIPCN) in Paris in 1999, the usefulness of hazard maps for the prevention of natural disasters and the management of the territory was reaffirmed (El Kharim, 2002). In Morocco, the only documents drawn up so far relating to the hazard linked to landslides have been:

a. the hazard map of the movements of the slopes of the Rif at the scale of 1/1000000 drawn up by Milliés-Lacroix in 1968

b. the mapping work landslide risks in the Taounate region carried out by Avenard in 1965 and Fares in 1994

c. the landslide risk mapping trial in the Al Hoceima region carried out by Margaa in 1994, landslide risk mapping in the Tetouan region drawn up by El Kharim in 2002 and the mapping

of the hazard linked to landslides in the Tangier peninsula carried out by Sossey Alaoui in 2005 and Faleh et al. in 2002.

Initially, researchers faced the difficulty of superimposing and analyzing geographical information that varies in time and space. However, the emergence of Geographic Information Systems (GIS) and the development of computer science have made it possible to carry out complex spatial analyses. This made it possible to analyze geographic information, apply particular algorithms, perform statistical analyses and model the results. Several researchers have underlined the importance of this approach for mapping the hazard associated with landslides (Brabb, 1984, 1987; Wadge, 1988; van Westen et al., 1993; Brabb, 1995; Carrara et al., 1995; Irigaray, 1995; Soeters and Van Westen, 1996; El Kharim, 2002; Maquaire and Ambrose, 2002). Furthermore, some researchers have highlighted the interest of combining satellite imagery with GIS to establish maps of the hazard linked to landslides (Rouzeau and Scanvic, 1992; Leroi et al., 1992; van Westen, 1993).

As part of our study, we mapped the risk associated with landslides in order to benefit from precise knowledge of this phenomenon in the region studied. This detailed cartographic representation is all the more justified as human activity in these areas is becoming increasingly intense. Our work is therefore divided into several stages:

– Listing the slope movements described in the bibliography.

– Understanding their distribution by identifying predisposing and triggering factors.

– Mapping each factor contributing to the genesis of mass movements (predictive factors).

– Determining the areas impacted by these phenomena, as well as the infrastructure, equipment and vulnerable populations.

– Developing a representation of the risk of landslides in order to prevent hazards by integrating the data into a GIS.

I.   Presentation of the Study Area

The study area extends over an area of 193 km² and is located upstream of the Mediterranean port complex of Tangier, in the Tangier peninsula in northwestern Morocco. It encompasses the three basins of Oued R'mel, Oued Ksar Sghir and Oued Ghlala (Fig.1).

The geomorphological characteristics of this area include slopes which are rather steepy as well as a very rugged mountainous relief composed of mountains and valleys extending from East to West.

From a geological point of view, the study region is composed of several distinct formations: the Internal Domain, including the Ghomaride and the Limestone Dorsal, the External Domain, including the Internal Tangier Unit and the External Tangier Unit, as well as the flysch nappes, which include the Predorsalian Unit, the Tisirène Beni Ider Unit and the Numidian facies sandstone Unit (Fofana, 2009). The climate in this area is of the subhumid type, with annual rainfall varying between 800 and 1000 mm and average annual temperatures ranging from 17 to 20°C. The main studied rivers in the region are Oued Ksar Sghir, Oued Rhlâlâ and Oued Rmel.
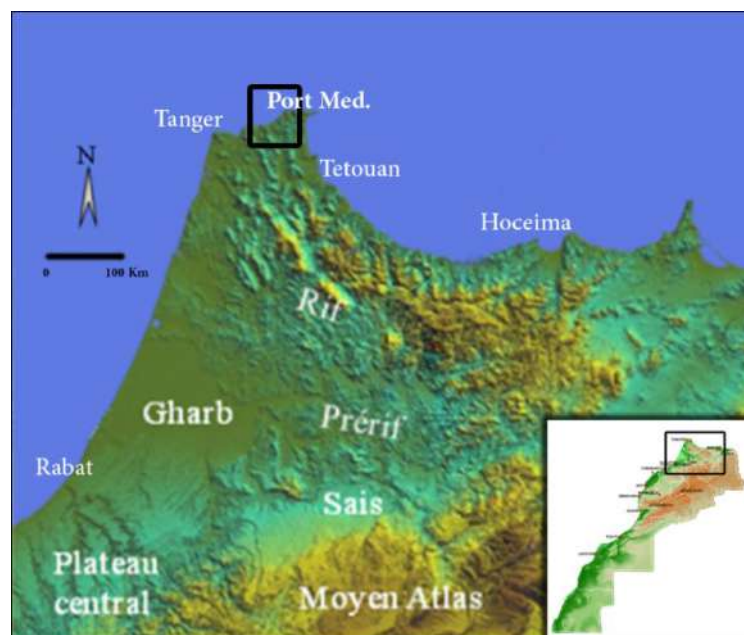
Source: Google Earth Image
Directed by: Maktite Abderrahim

Fig. 1. Location of the studied area

II. Methodology

The method adopted to carry out this study is the method of informative values (VI). It is a statistical method used to assess the forecasting quality of a forecasting model. It measures the ability of a model to correctly predict the actual value of a target variable. The VI is defined as the sum of the absolute differences between the predicted values and the actual values weighed by the relative importance of each target variable. However, the lower the value of the VI, the more accurate the model is considered.

The method is then based on the creation of a risk index map using variable maps, maps of the probability of occurrence of landslides, and maps of the vulnerability of the area studied according to the following steps (Fig. 2):

A. The landslide Hazard

The criteria taken into account to assess landslides generally include their area, speed, depth and the volume of soil displaced. The propensity of lands to undergo landslides is determined by their physical characteristics such as slopes, aspect, concavity, and other factors related to their stability. In addition, the probability of occurrence is used to estimate the risk of landslide in each specific area over a given period.

The process of creating the hazard map involves two steps: on the one hand, the determination of the predisposition of the land to instability (susceptibility), taking into account their physical characteristics (slope, exposure, concavity, etc.) and, on the other hand, the determination of the temporal probability that a given area will experience a landslide in a given period of time.

1. Landslide Inventory

In order to measure the propensity of land to landslides, it is important to identify the areas that have been affected in the past and to observe the characteristics of the affected land. The susceptibility maps that are typically created by the adopted method are based on the idea that future landslides will occur under conditions similar to those that caused previous landslides (Hansen, 1984).

To create a landslide inventory, aerial photo interpretation is usually used for confirmation by fieldwork. This method is considered the best tool for identifying landslides. In this study, we have established the inventory of landslides based on aerial images from Google Earth pro and work already carried out in the region.

2. Predisposing Factors

The method adopted to assess the susceptibility of land in this study area is based on a statistical approach called "Informative Values Method" (VI). This method was chosen because of its objectivity and easy reproducibility. Its fundamental principle is to collect data on the characteristics of the land where landslides have already occurred in order to assess their susceptibility to landslides.

To construct the susceptibility map, six variables were identified using all the data available on the land in the study area, as well as information extracted from the digital terrain model (DTM). These variables are presented in Fig. 4. This data collection allowed us to establish a complete list of the characteristics of the lands; characteristics which were then used to evaluate those lands' susceptibility to landslides.

3. Evaluation and Production of the Susceptibility Map

The informative value of a class in a variable is determined according to the number of landslides that have occurred on lands with the same characteristics as the considered class. More specifically, it is obtained by comparing the number of landslides occurring on the lands of the class to the proportion of lands of this class over the total area studied according to the following formula:

$$VI(i) = Ln\left(\frac{S_i/N_i}{S/N}\right) \qquad (1)$$

Si: the area of class i slipped
Ni: the area of class i
S: the total area that slipped
N: the total area of the studied area

Once the informative value of each class of each variable has been determined, they are combined to produce an estimate of the overall susceptibility of the terrain in the area. The combination of the informative values is generally carried out using a mathematical model which takes into account the relative importance of each variable in the generation of landslides.

In the Raster representation, each pixel of each variable has a VI value. To create the susceptibility map, these VI values of each variable present in each pixel are summed up and then grouped into different classes.

4. Construction of Success and Forecast Curves

The accuracy of this model is assessed using hit and prediction rates, as defined by Yin and Yan in 1988; Chung and Fabbri in 2003 and cited by Zêzere et al., 2004. The hit rate measures the reliability of the model using the slips that were used to build it. It makes it possible to determine the extent to which the model is capable of correctly reproducing the slips already observed.

The prediction rate, on the other hand, is calculated by introducing part of the slippage into the

model and comparing the results obtained with the success and prediction curves. This step verifies the ability of the model to accurately predict landslides based on the characteristics of the terrain.

The analysis of the success and prediction curves, as well as the measurement of the areas under these curves, make it possible to determine the accuracy of the model developed. The more the curves overlap and the larger the areas under the curves, the more accurate the model is considered to be in its ability to assess the susceptibility of the land to landslides.

The analysis of the accuracy of the model is an important aspect to assess the reliability of the susceptibility map obtained. The success and prediction rates provide a measure of the correspondence between the actual slip zones and the slip zones pre-

dicted by the model. If the success and prediction rates are high, it means that the model is well adjusted to the real data and can therefore be used with good confidence to predict landslide risk areas in the future. However, if the rates are low, it means the model needs to be improved by using additional variables or changing the methodology used to build the model.

B. The definition of Temporal Probability

The frequency at which the phenomenon occurs is measured by the temporal occurrence probability component of the hazard. To calculate this component, we generally use the recurrence period of the cause that triggered the landslide. In the case of the landslides that have occurred in northern Morocco over the past fifty years, the main cause is heavy rainfall.
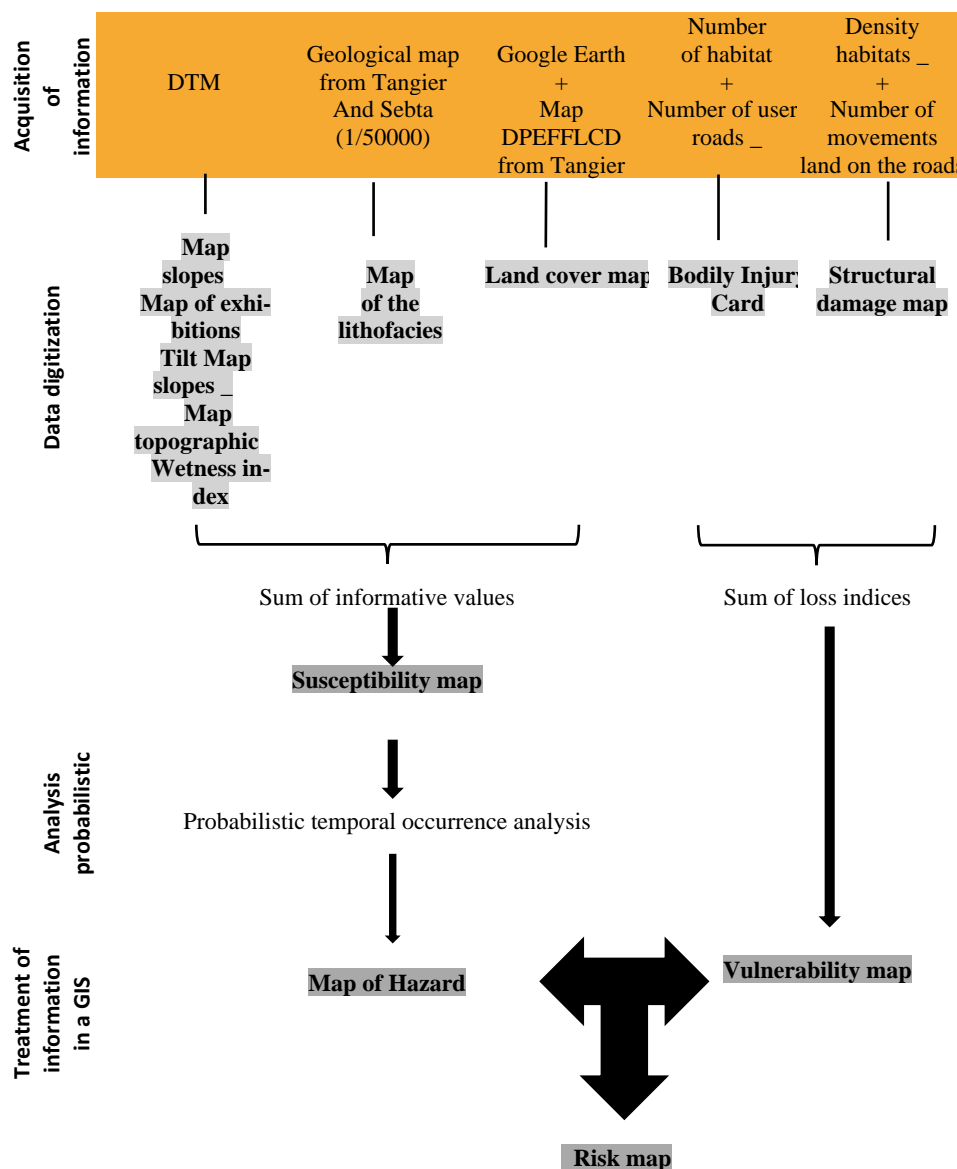
Source: Description of the method
Directed by: Maktite Abderrahim

Fig. 2. Methodological scheme

To estimate the probability of temporal occurrence of landslides, the most common rainfall scenarios that have caused landslides since the 1980s have been identified. It is assumed that the same rains will produce the same types of landslides and will affect the same surfaces. Using formula (2), the probability of temporal occurrence is determined for each landslide susceptibility class.

$$\mathbf{Pi = 1 - (1 - \frac{T\ affect\acute{e}e}{Ti} * Pr)} \qquad (2)$$

Pi: the probability of the susceptibility class
T affected: the total area of the area that will slip
Ti: the area of the susceptibility class i
Pr: the predictive value of the susceptibility class i

The temporal probability values are determined by the calculations performed to measure the susceptibility, which will be described in detail in the results part. The predictive value, on the other hand, measures the model's ability to predict the location of future landslides based on past landslides.

C. Vulnerability Assessment

To quantify vulnerability, an index is used that takes into account two major criteria: bodily injury and structural damage (Leone, 1996).

➢ The personal injury assessment includes two factors: the number of inhabitants in the different regions of the study area and the number of vehicles using the different roads in the study area (Fig. 10).

➢ Structural damage is assessed by taking into account two factors: the population density of each Douar and the number of landslides affecting each road (Fig. 11).

Each pixel in each theme is assigned a value between 0 and 1 based on the loss index. The maximum loss index value is set at 1. Generally, the value 1 is attributed to the most vulnerable class, then the other values are attributed according to this one.

D. Realization of the Risk Map:

Finally, we produced the risk map by superimposing the hazard map with the vulnerability map and based on a matrix that determines the risk classes (Table 1).

The levels of hazard and vulnerability were divided into four classes using quantiles. By crossing these classes, the level of risk was determined.

III. Results and Discussions:
A. Landslide Hazard Map
1. Inventory of Landslides

Before proceeding with the elaboration of the susceptibility map, a preliminary step was carried out. It consisted of an inventory of ground instabilities based on several sources. First, the work of El Gharbaoui B., produced in 1981 were consulted, in particular its geomorphological map of the Tangier peninsula at scale 1/100,000. In addition, the geological maps of the Ministry of Energy and Mines (MEM) at scale 1 /50,000 of Ksar Sghir and Sebta were examined.

In addition to these sources, information from the landslide map produced by Fonseca André Filipe in 2014 was used. This work, which constituted a doctoral thesis entitled "Large deep-seated landslides in the northern Rif Mountains (Northern Morocco): inventory and analysis", provided a valuable contribution to our study. Digital images from Google Earth Pro were also used to complete our information.

Then, field observations were carried out in order to complete and validate the data collected. This step made it possible to obtain additional information and to check the consistency of the data obtained from the various sources mentioned above.

In this way, 277 landslides were identified, of which 38.6% were debris screes, 16% were solifluctions, 23% were mudslides and 22.4% were complex movements (Table 2).

Table 1

Matrix determining the risk classes

		Hazard			
	×	Very weak (Class 1)	Weak (Class 2)	Strong (Class 3)	Very strong (Class 4)
Vulnerability	Very weak (Class 1)	2	3	4	5
	Weak (Class 2)	3	4	5	6
	Strong (Class 3)	4	5	6	7
	Very strong (Class 4)	5	6	7	8

	acceptable risk		Medium high risk		High risk

Distribution of landslides in the study area

Type of slips	Number of elaborate slips of:			The sum	The surface in (m²)
	Map by André Filipe, 2014	Geomorphological and geological map	Image from Google Earth		
Complex movements	3	7	52	62	2623700
Mudslides	1	0	63	64	748700
Solifluction	11	16	17	44	8519100
Landslide	4	82	21	107	10082300
Sum	19	105	153	277	21973800

Directed by: Maktite Abderrahim

The landslides identified are aligned in a North-South direction and are distributed around the water-courses of the study area. The number of landslides recorded decreases slightly from northeast to south-west, as shown in Fig. 3.
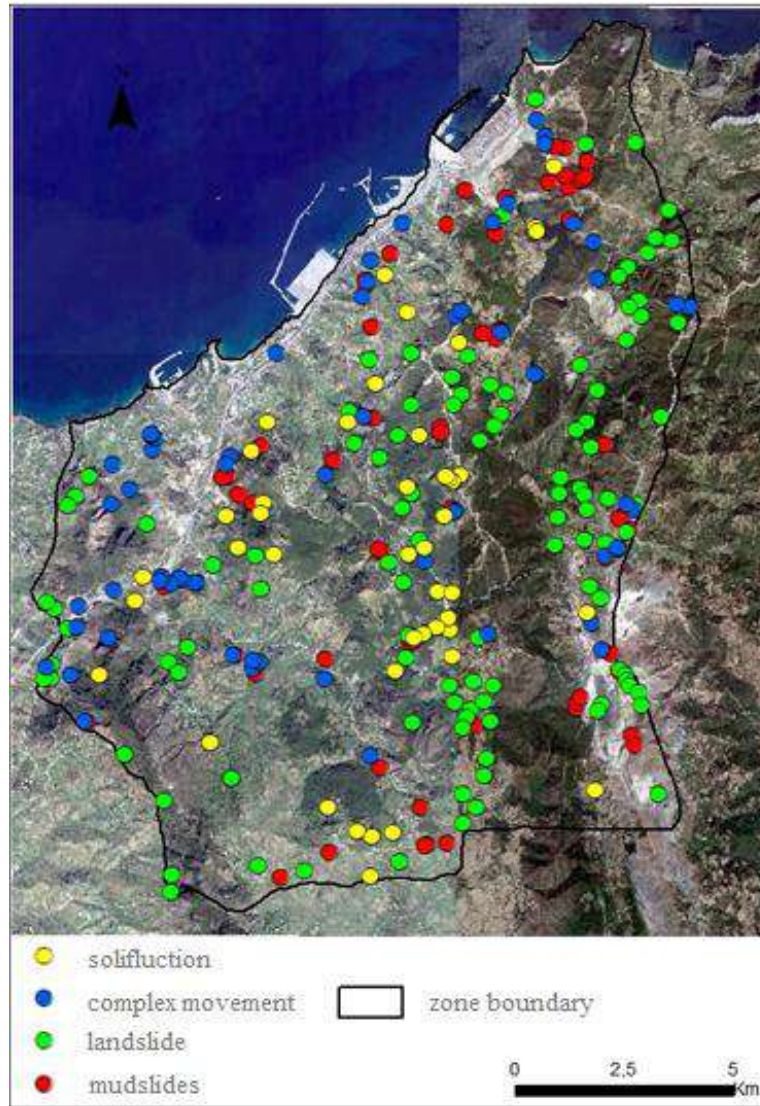
Source: Satellite Image 2016
Directed by: Maktite Abderrahim

Fig. 3. Inventory and location of landslides in the study area

2. Predisposing Factors

Then, it is necessary to list the variables or predisposition factors of the lands that have undergone landslides. Some of these factors come from a digital terrain model (DTM) of the studied area, obtained by digitizing contour lines from 1/25000 topographic maps.

The DTM (Digital Terrain Model) of the study area was created using a pixel size of ten meters on a side. This resolution was determined based on the contour spacing available for building the DEM. Moreover, this pixel size was considered as an ap-

propriate compromise between data precision and the amount of data generated, considering the size of the studied area which is 193 km². Thus, the DEM consists of 1,930,000 pixels, with each pixel representing an area of 100 m².

In the context of this study, the pixel size chosen for each theme is also ten meters per side, with the exception of the concavity/convexity of the slopes. For this variable, the precision of the DEM has been reduced and the pixel size has been increased to 50 meters per side to better represent this specific topographic feature.
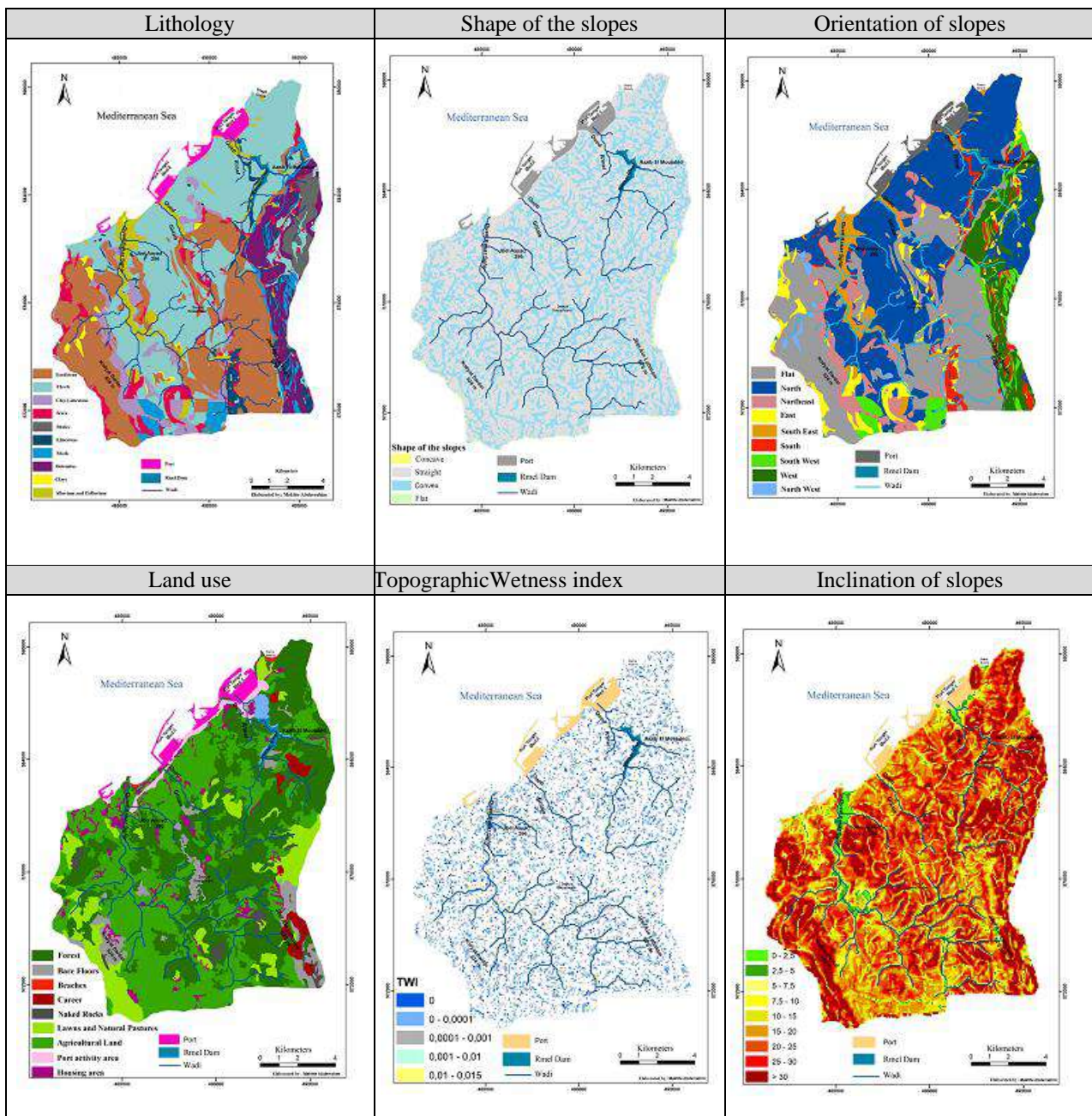
Source: - DTM (1/25000)
-IFN (2014)

Fig. 4. Predisposing factors for susceptibility assessment

With regard to topography Wetness Index (TWI), this is an index used to assess the presence of water in soils and areas of external saturation. For each pixel, this index is calculated according to the following formula:

$$\text{TWI} = In(A/\tan B)$$

A: Flow Accumulation
B: slope

Using GIS, we were able to determine the number of suspected landslides as well as the total area of each landslide for each of the six themes. We also calculated the informative values for each class using a specific formula (equation 1). For each class of each theme, we measured the area affected by the slip by counting the number of pixels of this class containing a slip point. It should be noted that the slips were represented by dots in this study, with only one slip dot typically present per pixel. Although it is a simplification of reality, this model produced excellent results even if it does not allow an accurate estimation of the volume of earth displaced by a landslide, which would require an evaluation in the field.

The susceptibility is represented by the average value of the VI of each class present in each theme, calculated for each pixel (Dai et al., 2002). However, it is necessary to prove the robustness of this model by evaluating it using the methods of success rate and prediction rate.

3. Evaluation and Production of the Susceptibility Map

Fig. 8 presents the future slip probability for each pixel. The informative values, which reflect the probabilities of the different classes, are divided into "quantiles", in such a way that each class contains the same number of pixels. Classes are defined as follows:

➢ Class 1 includes the lowest values, located between -5.3348 and 1.1242.
➢ Class 2 includes values ranging from 1.1243 to 2.4187.
➢ Class 3 includes values between 2.4188 and 3.8052.
➢ Finally, class 4 corresponds to the maximum values, which extend from 3.8053 to 6.6827.

According to the hypothesis that the conditions predisposing to landslides are likely to be repeated and based on the values used to construct the success curve, it is possible to affirm that, in an indeterminate period of time, 79.2 % of landslides will occur in class 4, 15.7% – in class 3, 5.0% – in class 2 and 0.1% – in class 1. It can therefore be concluded that

class 4 represents areas with very high probability of slippage.

However, it should be emphasized that these values only reflect the susceptibility of risk areas spatially, which differs from the hazard map which also takes into account the temporal probability of occurrence.

4. Assessment of the Robustness and Accuracy of the Model used to Map Susceptibility

4.1. Development of the Success Curve

To assess the reliability of the model used to map the susceptibility of terrains, you can actually create a logarithmic curve by following the process described below:

➢ Export the informative values (VI) used to construct the susceptibility map from the GIS and place them in a column of a table, sorted in descending order.
➢ The second column of the table represents the number of pixels assigned to each VI value, while the third column indicates the land area where landslides occurred in those pixels.
➢ Create a fourth column using the following formula: each cell in this column is the sum of the pixels of the first n cells in the second column, divided by the total pixels. Given that each pixel corresponds to an elementary surface of the study area (10 meters by 10), this column represents the accumulation of surfaces classified in decreasing order of VI, divided by the total surface. The values in this column are therefore all between 0 and 1.
➢ Create a fifth column in the same way as the fourth but using the values of the land areas where landslides have occurred.
➢ Construct the success curve using the values in the fourth column on the abscissa and those in the fifth column on the ordinate, using a logarithmic scale.

In summary, this process allows you to create a logarithmic curve that represents the success rate of the model used for terrain susceptibility mapping. This curve is constructed by using the informative values exported from the GIS and by calculating the accumulations of the land surfaces classified in descending order of VI.

The Fig.6 presents the value "AUC", which is the abbreviation of "Area Under the Curve". This value is a measure of the reliability of the model and has no unit. The higher the AUC value, the more robust the model is considered. In general, a value greater than 0.85 indicates a good model for representing susceptibility. In this case, the value of the AUC is 0.86, which constitutes a first element of validation of the model created.
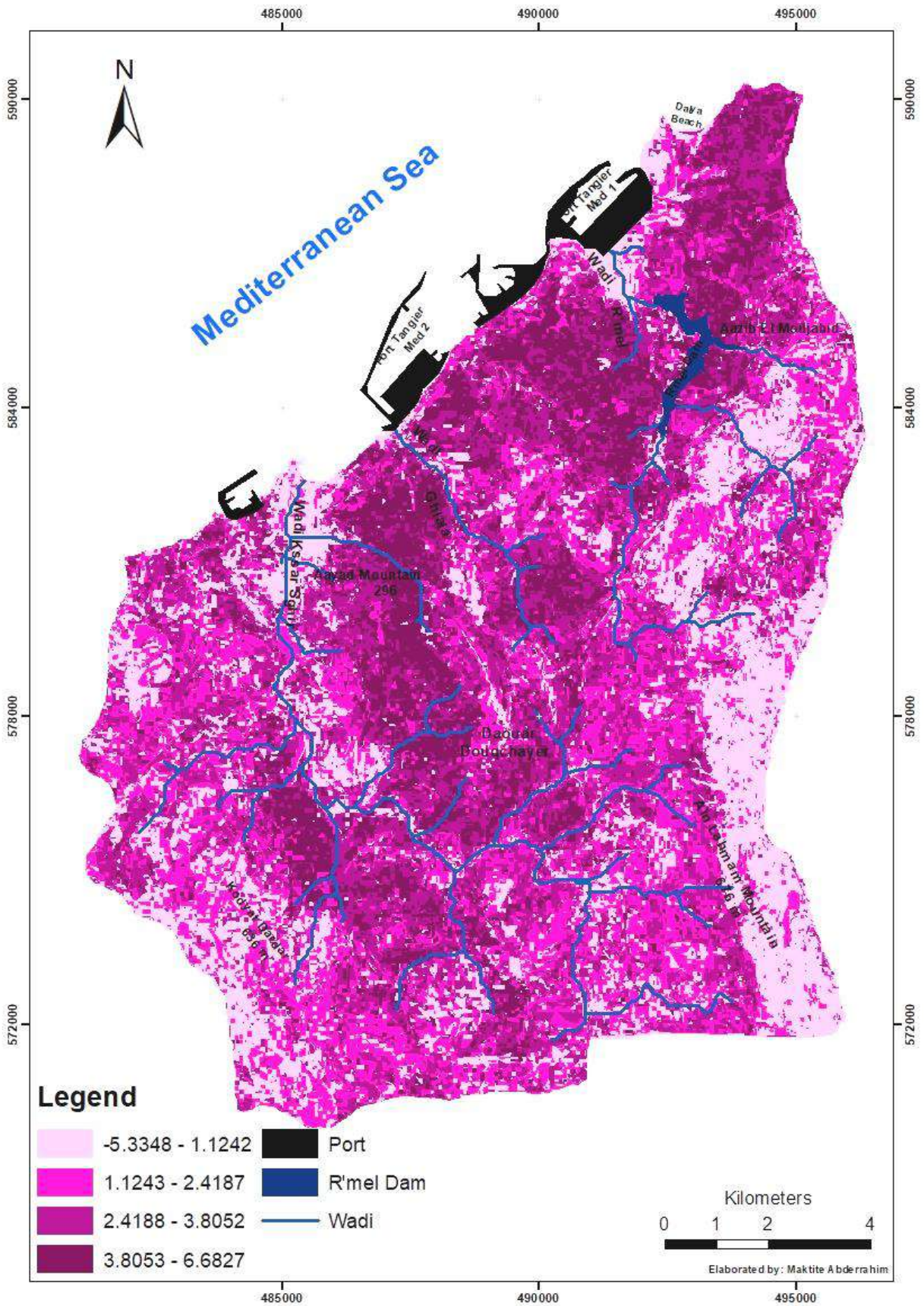
Fig. 5. Susceptibility map of the study area

111
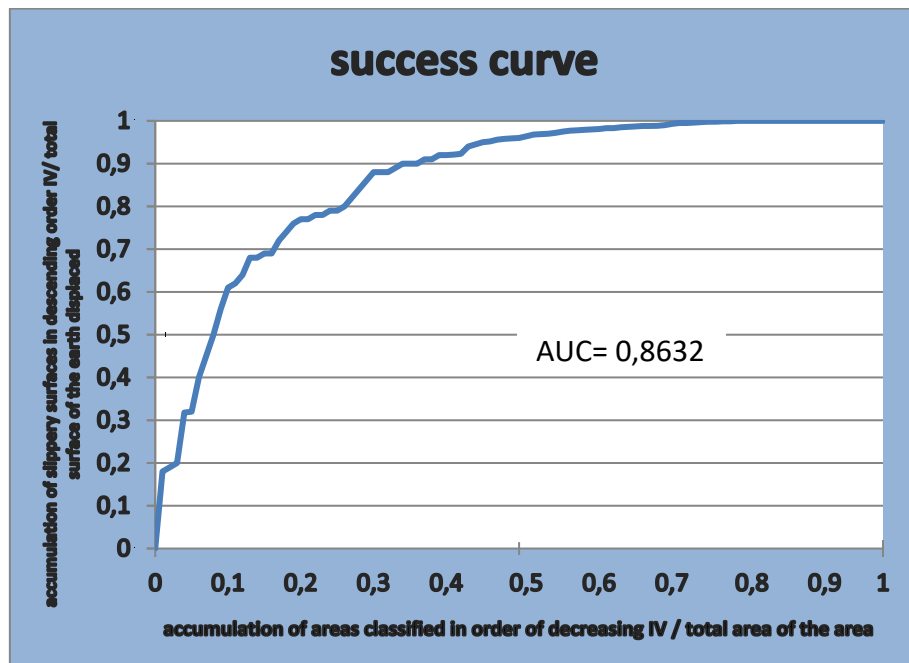
Source: Susceptibility map database

Fig. 6. Success curve

It can be observed on the curve that the value 0.1 on the abscissa axis corresponds to a value of 0.61 on the ordinate axis. This means that the 10% of the surface of the study area that was identified by the model as having the greatest susceptibility contains 61% of the suspected landslides. Additionally, 79% of suspected landslides are in the 25% most likely terrain. These results testify to the reliability of the model, which succeeded in identifying the surfaces most susceptible to slippage. Assuming that, the next slides will take place under conditions similar to the previous ones.

The validity of the constructed model was confirmed using the landslide data that was used to construct it. However, to more accurately assess its accuracy, it would be necessary to introduce another method and to verify whether the model produces comparable results. This principle was used to create the forecast curves.

A common practice is to randomly divide a dataset into two groups in order to construct a forecast curve from a single dataset. The process involves using the first group to develop a susceptibility model, which is then assessed using the second group. This method was used in the case of 277 presumed landslides, where the first group of 124 landslides (land movement cited by: André A. and El Gharbaoui B., 1973) was used to create a susceptibility model. The latter was then validated based on the 153 points of the second group (quoted from Google Earth images). Using this approach, a prediction curve was established (shown in red in Fig. 6) and can be compared to the success curve (in blue in Fig. 5) to assess model performance.

4.2. Development of Forecast Curves

To assess the performance of the susceptibility representation model, two prediction curves were developed in this study.

The first curve was constructed by randomly separating the 277 presumed landslides into two groups. The first group, comprising 124 landslides from the geomorphology map (El Gharbaoui, 1981) and the André Filipe map (table 2), was used to generate the susceptibility map, which should not be confused with the map constructed from all 277 slips. Then, the remaining 153 swipes from the second group were used to validate the same map. A prediction curve was then created using the same methods as for the success curve.

The prediction curves are visually compared to the success curve and their accuracy is assessed by calculating the area under each curve. This analysis makes it possible to assess the accuracy of the susceptibility model and to determine its reliability for predicting new landslides.

4.2.1. Forecast Curve 1

The model used for this validation was developed from the 277 points. The prediction curve 1 obtained (in red in Fig. 6) was compared to the success curve (in blue in Fig. 5).

The prediction and success curves have notable similarities, while their area under the curve (AUC) values is close.

The analysis of the success curve shows that the model is highly effective. Specifically, 10% of the area identified as most likely to experience slips contains 59% of the actual slips, while 25% of the most likely area includes 78.5% of the slips. This indicates that the model is very reliable in predicting where slips will occur.
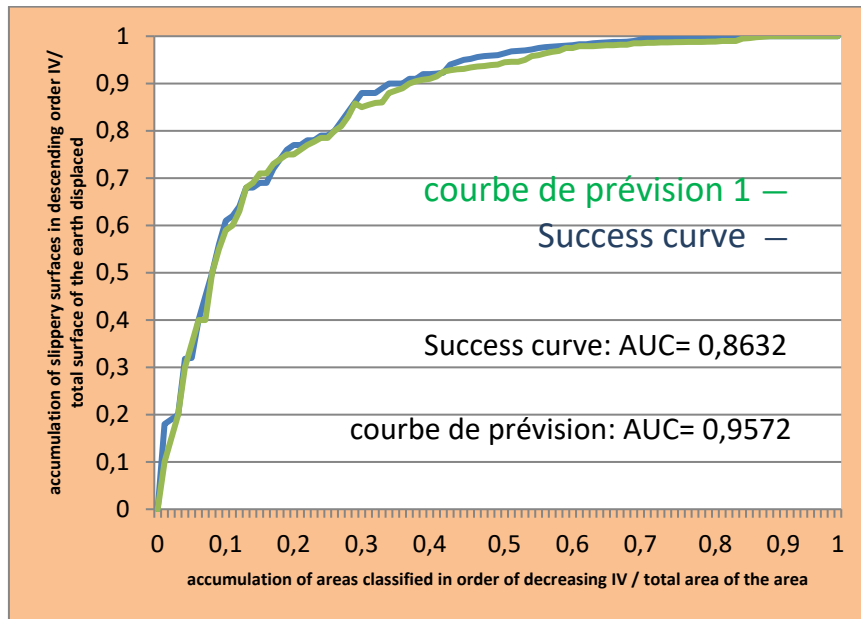
Source: Susceptibility map database

Fig. 7. Forecast curve 1

The prediction curve 1 obtained using the model created from the 124 points is very close to the success curve (Fig. 5). The shape of their plot is similar, and their AUC is higher than that of the success prediction curve, which was 0.8632.

4.2.2. Forecast Curve 2

Nevertheless, the evaluation focused on the resistance of the model developed from the points of group 1. Thus, a second forecast curve was established to evaluate the one created from the 277 po-

tential slips, which were used to establish the susceptibility map of the study area.

The results of forecast curve 2 confirm the accuracy of the model developed, where the most likely 10% of the surface contains 57% of the confirmed landslides and the most likely 25% contains 78% of these landslides. These results demonstrate the effectiveness of the inventory carried out to create a model of land susceptibility. Consequently, the information collected on this area is sufficient to create a fairly accurate terrain susceptibility model.
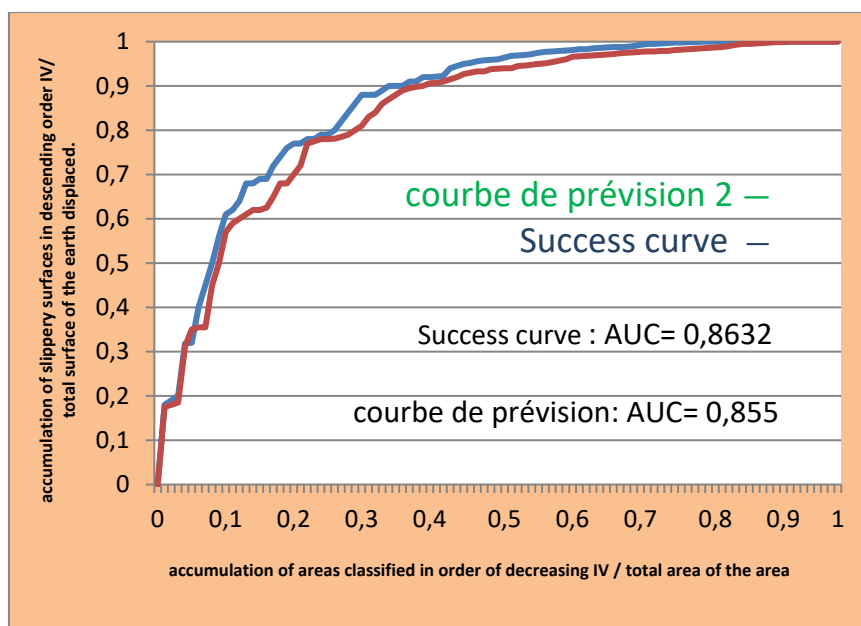
Source: Susceptibility map database

Fig. 8. Forecast curve 2

113

B. Hazard Map of the Area

The hazard map is generated from the susceptibility map based on the 277 presumed landslides and validated by the success and prediction curves. Each class in the susceptibility map is associated with a probability of temporal occurrence (Zêzere et al., 2004), assuming that the amount of land that will slip in the study area over the next forty years will be similar to that which has slipped in the past forty years. The choice of this forty-year period was motivated by the availability of data from a previous study carried out by El Gharbaoui in 1981, a period marked by heavy rainfall that triggered numerous landslides, thus offering a learning opportunity.

Using this assumption, the estimate of the total area of the area that will experience landslides over the next forty years is obtained by adding the areas of landslides that have occurred in this area over the past forty years. This sum gives a value of 21,973,800 m².

Quantiles were used to distribute the hazard values, creating four classes with approximately equal areas containing an equivalent number of values. However, it is important to note that the number of pixels in each class may vary slightly due to the grouping of pixels with similar values in the same class. The probability P for each class was calculated using the x and y coordinates of the success curve, which helps to determine the probability of a slip occurring in a pixel belonging to a given class over the next 40 years. For example, class 3 has a probability of 0.017, which means that there is a 1 in 59 chance of experiencing landslide within the next forty years (as shown in Table 3).

Thus, the hazard map presented indicates the probability of occurrence of a landslide for each pixel of the study area over the next forty years.

The hazard map is based on the susceptibility map of the studied area (Zêzere et al., 2008), which was presented previously. However, the hazard map differs from the susceptibility map because it incorporates not only the spatial susceptibility, but also the temporal probability of landslide for each pixel over the next forty years. The values obtained make it possible to assess the severity of the hazard according to the probability of a landslide. The results are presented in Table 4 and will be used to generate the risk map.

C. Vulnerability Map

Research on landslide vulnerability on a global scale is limited, which makes the assessment method proposed in this study rather forward-looking and potentially in need of further study. However, this method allows an overall assessment of the vulnerability of an area, as well as its impact on the representation of risk.

The study of the vulnerability of the study area was based on two main criteria: the first is the criterion of bodily harm, which includes a population index and a road use index (Tables 5 and 6), while the second is the structural damage criterion, which includes a population density index and a road damage index (Tables 7 and 8).

Table 3

Values of the probability of temporal occurrence obtained by equation (2)

Hazard classes	Surface m²	Contact details		$P_r = y_i - y_{i-1}$	Probability P	Chance of slipping in 40 years
		x	y			
1	48437165	0.25	0.79	0.79	0.358	1⁄3
2	48375733	0.50	0.96	0.17	0.077	1⁄13
3	48585329	0.75	0.997	0.037	0.017	1⁄59
4	48288816	1	1	0.003	0.0014	1⁄714

Table 4

Qualification of hazard classes

Class	Probability	Chance of experiencing slippage in 40 years	Hazard
1	0.358	One in 3	Very weak
2	0.077	One in 13	Weak
3	0.017	One in 59	Strong
4	0.0014	One in 714	Very strong

The global vulnerability map was developed based on two separate maps assessing structural damage and bodily harm. To build these maps, loss index values were assigned to different elements at risk. For each pixel, the sum of the loss indices of these different elements was calculated, then the results were normalized on a scale of 0 to 1 to represent the vulnerability. A value of 1 corresponds to areas most likely to sustain significant damage.
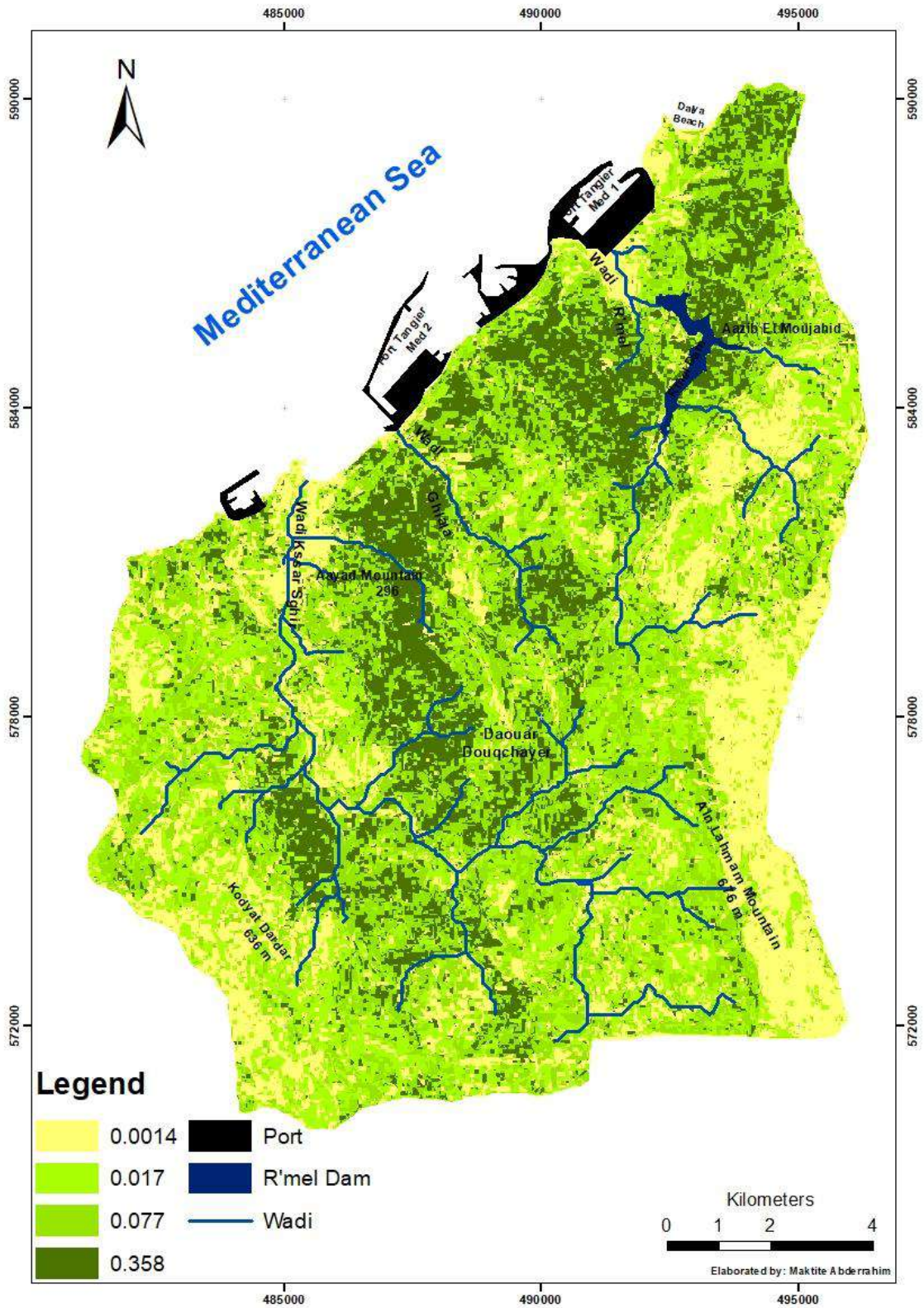
Source: Susceptibility map database
Directed by: Maktite Abderrahim

Fig. 9. Hazard map of the study area

Table 5

Risk index related to road use

Type of roads	Number of users	IV value
National Road N16	5230	1
A4 motorway	5003	0.957
Regional Road P4701	2554	0.488
Regional Road P4613	1962	0.375
Regional Road P4703	1700	0.325
Road Walking	Between 5 and 30	0.001 – 0.006
Railway	4	0.001

Source: fieldwork + DRETL

Table 6

Risk index linked to the number of populations

Regions	Number of habitats	IV value	Regions	Number of habitats	IV value
AIN CHOUKA	510	0.27	ANASSAR	512	0.28
AIN LAAKAYZ	177	0.09	MANSOURA	466	0.25
OUED GHLALA	545	0.29	ELHAMA	209	0.11
AIN RMEL	989	0.53	ZHARA	404	0.22
BOUAAYAD	1355	0.73	ELGHOUJIN	991	0.53
DALYA	267	0.14	HTATECH	242	0.13
DCHER BIN LWIDAN	1075	0.58	KSSER LMAJAZ CENTER	927	0.50
DHER LGHAROUB	1856	1	KSSER SGHIR	490	0.26
LACHBA	753	0.41	MLICH	1075	0.58
DKCHER	614	0.33	OUED RMEL	260	0.14
DCHICHA	488	0.26	TAGHREMT	475	0.26

Source: 2014 census

Table 7

Risk index linked to the density of habitats

Municipality or city	Habitat density index	Municipality or city	Habitat density index
Ksser Sghir	1	Melloussa	0.624
Anjra	0.904	Alain	0.314
Ksser lmajaz	0.669	Taghremt	0.309

Source: 2014 census

Table 8

Risk index linked to the number of ground movements

Type of roads	Landslide inventory	IV value
Regional Road P4701	23	1
Regional Road P4703	15	0.652
Regional Road P4613	14	0.609
National Road N16	9	0.391
Road Walking	Between 1 and 3	0.130 – 0.043
A4 motorway	0	0
Railway	0	0

Source: fieldwork

Source: field work + census 2014
Directed by: Maktite Abderrahim
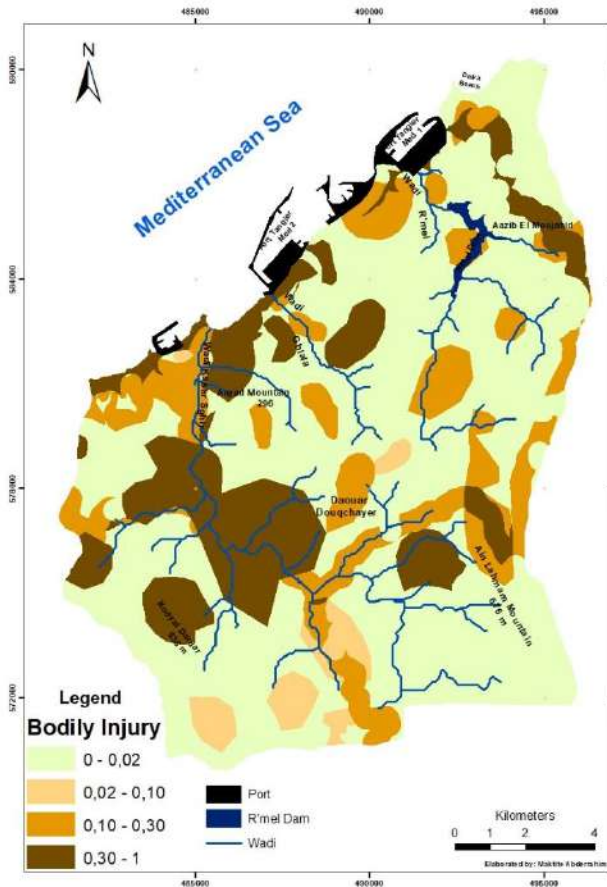
Fig. 10. Bodily injury map
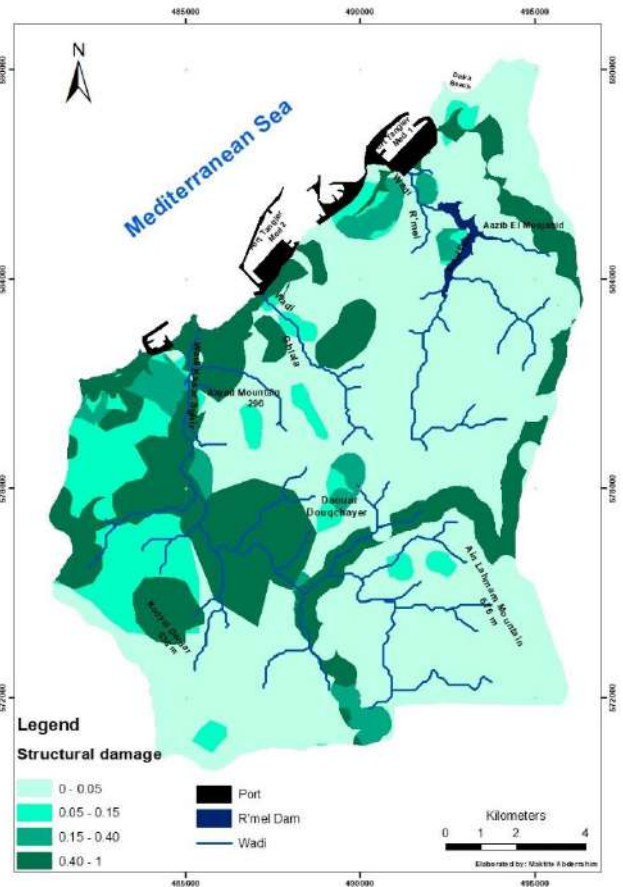
Fig. 11. Structural damage map

Body and structural vulnerability maps have significant similarities due to the risk elements taken into account when developing them. Areas where there is a significant concentration of at-risk elements such as inhabitants, Douars and roads display a higher vulnerability compared to areas where these elements are less present. In addition, there is a correlation between certain forms of vulnerability for certain elements at risk, especially for roads, where bodily and structural vulnerabilities are high.

The vulnerability values have been divided into four classes separated into quantiles, in the same way as for the susceptibility of the terrain or for the hazard. The results, shown in Table 9, were used to create the risk map.

By examining Figs 9 and 12, it can be seen that the areas with very high vulnerability are mainly

found in the northern part of the study area, while the land exposed to a strong hazard is located in the northern half near the port and forest projects. This suggests that the inhabitants have not developed a certain awareness of the risks, choosing to settle in areas where the hazard is higher.

D. Risk Map

Quantiles of hazard and vulnerability classes have been established (see Tables 4 and 9). The risk is then assessed by crossing these hazard and vulnerability classes (see Table 1).

The risk map results from the combination of the hazard and vulnerability maps. The areas most at risk are mainly located in the northern half of the study area, which corresponds to the most vulnerable area.

Table 9

Qualification of vulnerability classes

Classes	Loss index value	Vulnerability
1	From 0 to 0.24	**very low**
2	From 0.25 to 0.30	**Weak**
3	From 0.31 to 0.36	**Strong**
4	From 0.37 to 1	**Very strong**

117
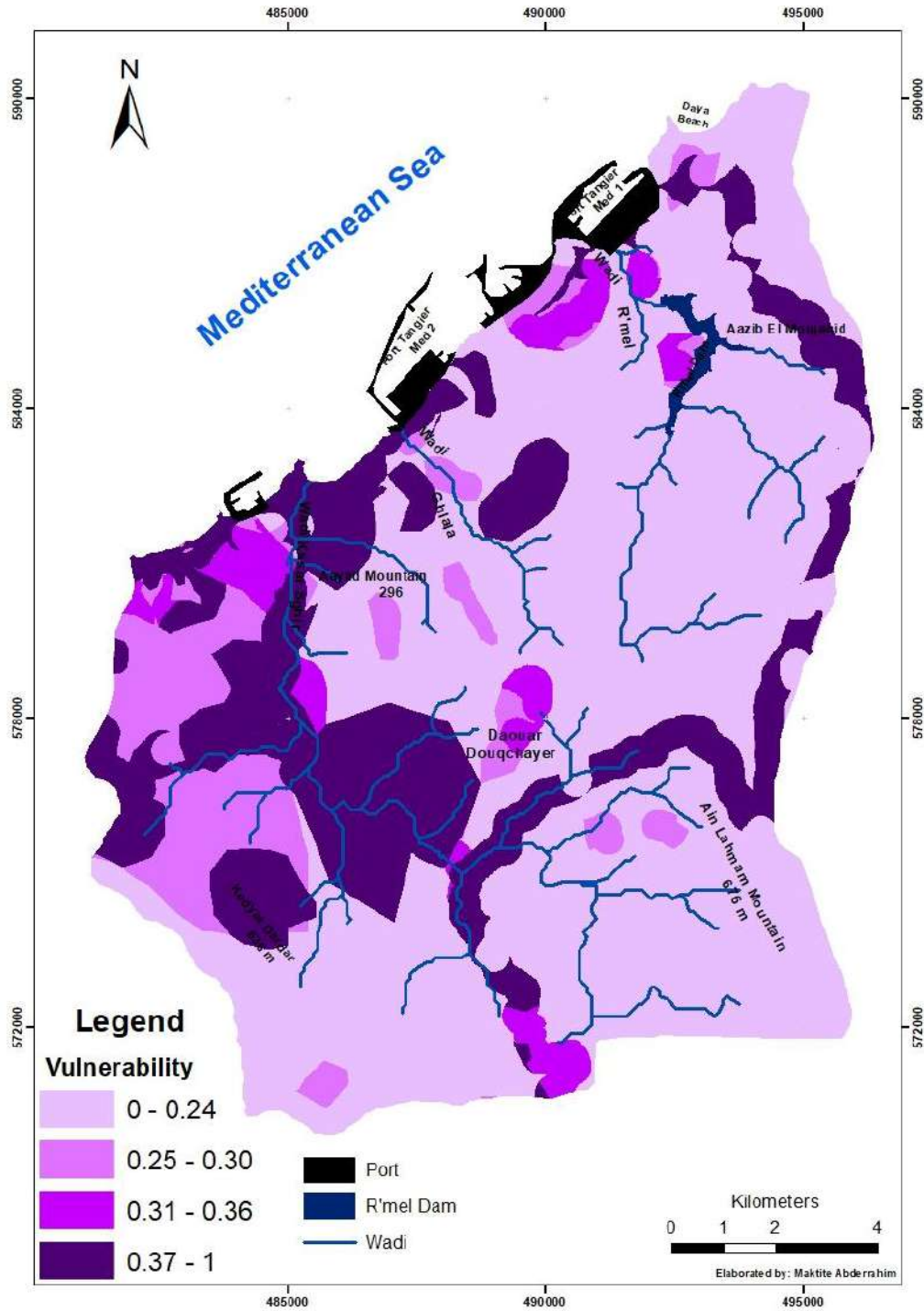
Source: Overlay of maps Figs 10 and 11
Directed by: Maktite Abderrahim

Fig. 12. Vulnerability map of the study area

Table 10

Qualification of risk classes

Classes	Risk index value	Type of risk
1	From 0 to 0.24	Very weak
2	From 0.25 to 0.30	Weak
3	From 0.31 to 0.36	Strong
4	From 0.37 to 1	Very strong

Source: Description of the method
Directed by: Maktite Abderrahim

Legend

Risk Index

- (2) Acceptable Risk
- (3) Acceptable Risk
- (4) Moderately High Risk
- (5) Moderately High Risk
- (6) Moderately High Risk
- (7) High Risk
- (8) High Risk
- Port
- R'mel Dam
- Wadi
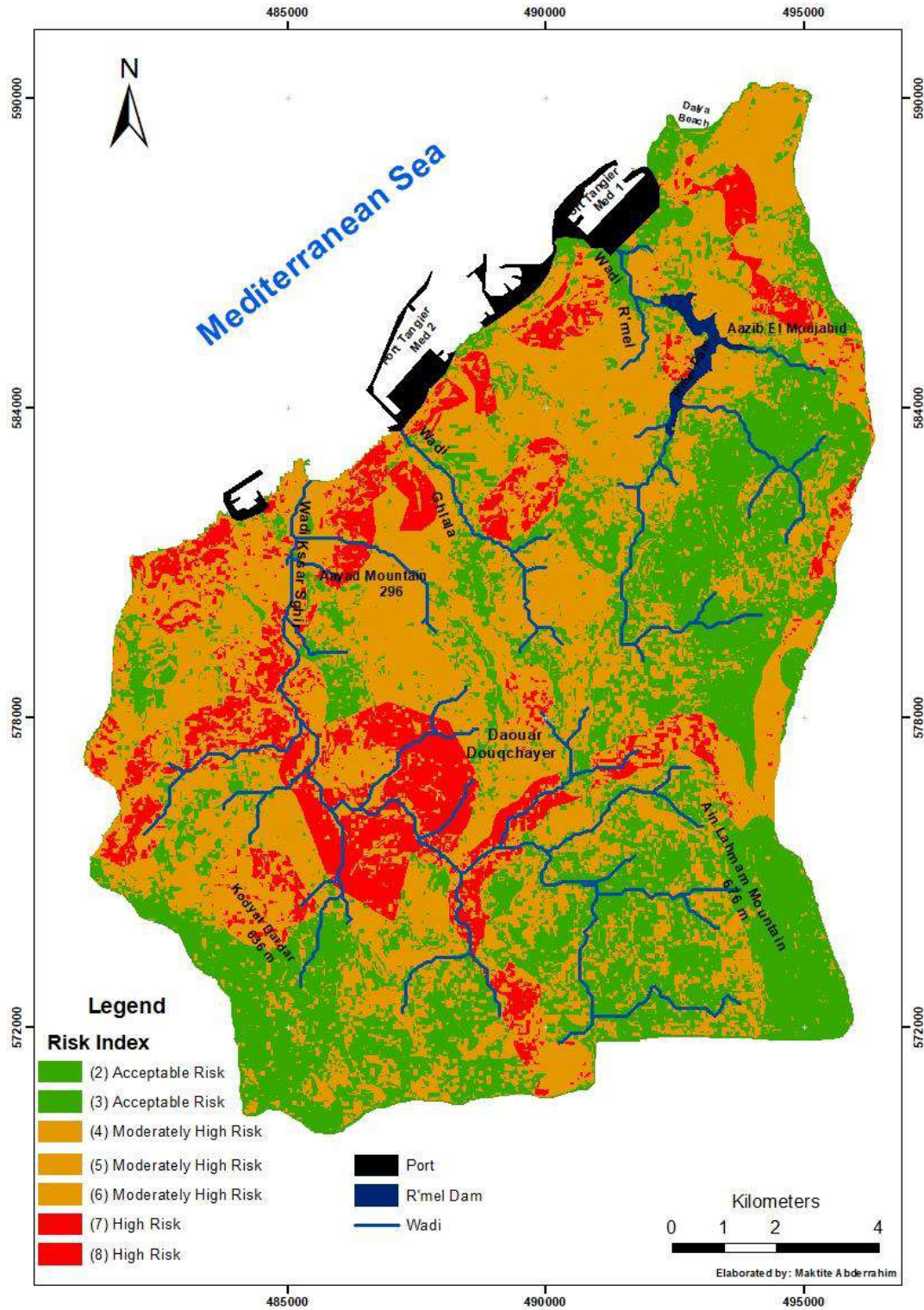
Source: overlay of maps Figs 9 and 12
Directed by: Maktite Abderrahim

Fig. 13. Landslide risk map

Although the accuracy of the susceptibility map was confirmed by the success and prediction rates, the validity of the risk map can be questioned as it was developed from the vulnerability map which requires study with a more in-depth methodology. Additionally, the vulnerability map only considers risk items for which data are available, which may affect the accuracy of the risk map.

In order to ensure effective land use planning, regions presenting a high risk will require the implementation of prevention and protection measures. One of the most important preventive measures is to

prohibit construction in high-hazard areas. Drainage can be used to prevent slope erosion, while reforestation can reduce the impact of water on soils. Excavating the top of rotational landslides can help stabilize these areas, while building retaining walls along roads can retain soils.

For areas with moderately high risk, it is essential to design them in such a way that they do not increase the existing risk. Prevention and protection measures can also be put in place to reduce the level of risk and bring it down to an acceptable level, thus ensuring a more secure development.

IV. Conclusion

The objective of this study is to develop methods for assessing the hazard and risk associated with landslides using a common conceptual model. This method made it possible to generate a susceptibility map for the study area, as well as hazard, vulnerability and risk maps associated with this same area. The resolution of the Digital Terrain Model (DTM) used for this study was 10 meters, which provided detailed results for in-depth regional analysis. The evaluation of the quality of the susceptibility model was carried out using success and prediction curves, thus demonstrating the reliability and accuracy of the method employed.

The hazard map was developed based on the assumption that the amount of land that will slip in the study area over the next forty years will be similar to that which has slipped in the same area over the past forty years. This hypothesis is interesting because it only requires information on the area of the landslides and their approximate date to calculate the temporal probability of occurrence of the landslides, thus making it possible to obtain the hazard map.

By crossing the hazard and vulnerability maps, a risk map was generated. The method developed in this study is promising because it allows obtaining significant results with a relatively small volume of data. This represents a considerable advantage for its application in the Regional Development Plans.

REFERENCES

Avenard J.M. The current erosion in the Sebou basin. Report of the National Institute of Agricultural Research (INRA). Rabat, 1965, 114 p. (in French).

André A. and El Gharbaoui A. Aspects of the coastal morphology of the Tangier peninsula. Journal of the Geography of Morocco, No. 23-24, 1973, pp. 125-149 (in French).

Brabb E.E. Innovative approaches to landslide hazard mapping. Proceed. IV lnt. Symp. Landslides, Toronto, Vol. 1, 1984, pp. 307-324.

Brabb E.E. Analyzing and portraying geologic and cartographic information for land-use planning, emergency response, and decision making in San Mateo County, California. Proc. GIS'78, San Fransisco, ll-nd Annual Int. Conf. on GIS, 1987, pp. 362-374.

Brabb E.E. The San Mateo County GIS project for predicting the consequences of hazardous geologic processes. In: Geographical information system in assessing natural hazards (Carrara A. and Guzzetti F., eds.). Kluwer Academic Publishers. Dordrecht, 1995, pp. 299-334.

Carrara A., Cardinali M., Guzzetti F., Reichenbach P. GIS-based techniques for mapping landslide hazard. In: Geographical information system in assessing natural hazard (Carrara A. and Guzzetti F., eds.), Kluwer Acad. Publ. Dordrecht, 1995, pp. 135-176.

Chung C.F. and Fabbri A. Validation of spatial prediction models for landslide hazard mapping. Natural Hazards, Vol. 30, 2003, pp. 451-472, https://doi.org/10.1023/B:NHAZ.0000007172.62651.2b.

Dai F.C., Lee C.F., Ngai Y.Y. Landslide risk assessment and management: an overview. Engineering Geology, Vol. 64, No. 1, 2002, pp. 65-87, https://doi.org/10.1016/S0013-7952 (01)00093-X.

El Gharbaoui A. Earth and man in the Tingitan Peninsula. Essay on man and the natural environment in the Western Rif. Work of the Scientific Institute, Geology and Physical Geography Series, No. 15, 1981, Rabat (in French).

El Kharim Y. Study of slope movements in the Tetouan region (Western Rif): Inventory, analysis and mapping. PhD thesis Es-Sciences, Abdelmalek Essaadi University, Tetouan, Morocco, 2002, 250 pp. (in French).

REFERENCE

Avenard J.M. L'érosion actuelle dans le bassin de Sebou. Rapport de l'institut national de recherche Agronomique (INRA). Rabat, 1965, 114 p.

Andre A. et El Gharbaoui A. Aspects de la morphologie littorale de la péninsule de Tanger. Revue de la Géographie du Maroc, No. 23-24**,** 1973, pp. 125-149.

Brabb E.E. Innovative approaches to landslide hazard mapping. Proceed. IV lnt. Symp. Landslides, Toronto, Vol. 1, 1984, pp. 307-324.

Brabb E.E. Analyzing and portraying geologic and cartographic information for land-use planning, emergency response, and decision making in San Mateo County, California. Proc. GIS'78, San Fransisco, ll-nd Annual Int. Conf on GIS, 1987**,** pp. 362-374.

Brabb E.E. The San Mateo County GIS project for predicting the consequences of hazardous geologic processes. In: Geographical information system in assessing natural hazards (Carrara A. and Guzzetti F., eds.). Kluwer Academic Publishers. Dordrecht, 1995**,** pp. 299-334.

Carrara A., Cardinali M., Guzzetti F., Reichenbach P. GIS-based techniques for mapping landslide hazard. In: Geographical information system in assessing natural hazard (Carrara A. and Guzzetti F., eds.), Kluwer Acad. Publ. Dordrecht, 1995, pp. 135-176.

Chung C.F. and Fabbri A. Validation of spatial prediction models for landslide hazard mapping. Natural Hazards, Vol. 30, 2003, pp. 451-472, https://doi.org/10.1023/B:NHAZ.0000007172.62651.2b.

Dai F.C., Lee C.F., Ngai Y.Y. Landslide risk assessment and management: an overview. Engineering Geology, Vol. 64, No. 1, 2002, pp. 65-87, https://doi.org/10.1016/S0013-7952 (01)00093-X.

El Gharbaoui A. La Terre et l'Homme dans la Péninsule Tingitane. Essai sur l'Homme et le milieu naturel dans le Rif occidental. Travaux de l'Institut Scientifique, Série géologie et géographie physique, No. 15, 1981, Rabat.

El Kharim Y. Etude des mouvements de versants dans la région de Tétouan (Rif occidental): Inventaire, analyse et cartographie. Thèse de Doctorat Es-Sciences, Université Abdelmalek Essaadi, Tétouan. Maroc, 2002, 250 p.

Faleh A., Sadiki A., Haloui B., Akdim B. Application of mineralogical and geotechnical analyses of clays in the study of landslides: examples from the Central Prerif (northern Morocco). Geography Papers, No. 35, January-June, 2002, pp. 115-128, Spain (in Spanish).

Fares A., Rollet M., Broquet P. Methodology for mapping natural hazards related to ground movements. French Journal of Geotechnics, No. 69, 1994, pp. 63-72 (in French).

Flageollet J-C. Field movements and their prevention. Geographical Collection. Paris, Masson, 1989, 224 p. (in French).

Fofana O. Preparation of a landslide risk map of the Kser SGHIR area (northern Rif, Morocco). Final thesis for the Diploma of State Engineer in Agronomy. Institute of Agronomy and Veterinary Medicine Hassan II, 2009 (in French).

Fonseca André Filipe. Large deep-seated landslides in the northern Rif Mountains (Northern Morocco): inventory and analysis. Doctoral thesis, 2014.

Hansen A. Landsat hasard analysis. In: Slope instability (Brunsden D. et Prior D.B., eds.). John Wiley ans Sons. Chichester, 1984, pp. 523-602.

Irigaray C. Hillside movements: Inventory, analysis and susceptibility mapping using a Geographic Information System. Application to the areas of Colmenar (Malaga), Rute (Córdoba) and Montefrio (Granada). PhD thesis, Granada University, 1995, 384 p. (in Spanish).

Leone F. Concept of vulnerability applied to the assessment of the risks generated by field movements. Orleans. BRGM, Doctoral thesis, 1996 (in French).

Leroi E., Rouzeau O., Scanvic J.Y., Weber C.C, Vergas-Curvo G. Remote sensing landslide hazard mapping using GIS technology in Colombia Andes. Episode, Vol. 15, No. 1, 1992, pp. 32-35, DOI:10.18814/epiiugs/1992/v15i1/006.

Maate A. Alpine paleogeographic stratigraphy and evolution of the Gomaride domain (internal Rif, Morocco). Doctoral thesis, University of Granada, Department of Stratigraphy and Paleontology, Spain, 1996, 397 p., http://hdl.handle.net/10481/53657 (in Spanish).

Margaa Kh. Natural hazards mapping test: application to the development of the Al Hoceima region (Rif, northern Morocco). PhD thesis, University of Franche-Comté, 1994, 196 p., Corpus ID: 127852669 (in French).

Maquaire O., Ambrose B. Geomorphological hazards (ground movements) – process, operation, maps. Strasbourg: s.n, 2002.

Milliès-Lacroix A. Landslides. Presentation of a forecast map of mass movements in the Rif (northern Morocco). Mining and Geology, Vol. 27, 1968, pp. 43-53 (in French).

Rouzeau O. and Scanvic J.Y. Use of satellite data for the study of ground movements and the production of susceptibility maps. Géo Observateur, No. special, Marisy 92, Rabat, 1992, pp. 265-270 (in French).

Soeters R. and van Westen C.J. Slope instability recognition, analysis and zonation. In: Landslides: Investigation and Mitigation (Turner A.K., Schuster R.L., éds.), Transportation Research Board, National research Council, Special report 247, National Academy Press. Washington D.C., USA, 1996, pp. 129-177.

Sossey A. Processing and integration of optical and radar satellite data in a GIS with a view to obtaining a map of the hazard linked to the instability of the terrain in the Tangier peninsula (northern Rif, Morocco). PhD, Mohamed V University, Faculty of Sciences, Rabat, 2005, 175 p. (in French).

UNDRO (Office of the United Nations Disaster Relief Coordinator). Natural disasters and vulnerability analysis. Report of Expert Group Meeting, 1979, 19 p.

van Westen C.J. Remote sensing and geographic information systems for geologic hazard mitigation. ITC Journal, No. 4, 1993, pp. 393-399.

Faleh A., Sadiki A., Haloui B., Akdim B. Application des analyses minéralogique et géotechniques des argiles dans l'étude des glissements de terrains: exemples du Prérif central (Maroc septentrional). Papeles de Geografía, No. 35, enero-junio, 2002, pp. 115-128, España.

Fares A., Rollet M., Broquet P. Méthodologie de la cartographie des risques naturels liés aux mouvements de terrain. Revue Française de Géotechnique, No. 69, 1994, pp. 63-72.

Flageollet J-C. Les mouvements de Terrain et leur prévention. Collection Géographique. Paris, Masson, 1989, 224 p.

Fofana O. Elaboration d'une carte de Risque de Glissement de terrain de la zone de Kser SGHIR (Rif septentrional, Maroc). Mémoire de fin d'étude pour l'obtention du Diplôme d'ingénieur d'Etat en Agronomie. Institut Agronomique Et Vétérinaire Hassan II, 2009.

Fonseca André Filipe. Large deep-seated landslides in the northern Rif Mountains (Northern Morocco): inventory and analysis. Doctoral thesis, 2014.

Hansen A. Landsat hasard analysis. In: Slope instability (Brunsden D. et Prior D.B., eds.). Chichester. John Wiley ans Sons. 1984, pp. 523-602.

Irigaray C. Movimientos de ladera: Inventario, analisis y cartografia de susceptibilidad mediante un Systema de Informaciòn Geografica. Aplicacion a las zonas de Colmenar (Malaga), Rute (Cordoba) y Montefrio (Granada). Thèse de Doctorat, Université de Granada, 1995, 384 p.

Leone F. Concept de vulnérabilité appliquée à l'évaluation des risques générés par les phénomènes de mouvements de terrain. Orléans. BRGM, Thèse de doctorat, 1996.

Leroi E., Rouzeau O., Scanvic J.Y., Weber C.C, Vergas-Curvo G. Remote sensing landslide hazard mapping using GIS technology in Colombia Andes. Episode, Vol. 15, No. 1, 1992, pp. 32-35, DOI:10.18814/epiiugs/1992/v15i1/006.

Maate A. Estratigrafía y evolución paleogeográfica alpina del dominio gomáride (Rif interno, Marruecos). Tesis doctoral, Universidad de Granada, Departamento de Estratigrafía y Paleontología, España, 1996, p 397, http://hdl.handle.net/10481/53657.

Margaa Kh. Essai de cartographie des risques naturels: application à l'aménagement de la région d'Al Hoceima (Rif, Nord-Maroc). Thèse Doctorat, Université de Franche-Comté, 1994, 196 p., Corpus ID: 127852669.

Maquaire O., Ambroise B. Aléas géomorphologiques (mouvements de terrains) –processus, fonctionnement, cartographies. Strasbourg: s.n, 2002.

Milliès-Lacroix, A. Les glissements de terrain. Présentation d'une carte prévisionnelle des mouvements de masse dans le Rif (Maroc septentrional). Mines et Géologie, 27, 1968, pp. 43-53.

Rouzeau O. et Scanvic J.Y. Utilisation des données satellitaires pour l'étude des mouvements de terrain et la réalisation de cartes de susceptibilité. Géo Observateur, No. spécial, Marisy 92, Rabat, 1992, pp. 265-270.

Soeters R. and van Westen C.J. Slope instability recognition, analysis and zonation. In: Landslides: Investigation and Mitigation (Turner A.K., Schuster R.L., éds.), Transportation Research Board, National research Council, Special report 247, National Academy Press. Washington D.C., USA, 1996, pp. 129-177.

Sossey A. Traitement et intégration des données satellitaires optiques et Radar dans un SIG en vue de l'obtention de carte de l'aléa lié aux instabilités de terrain dans la péninsule de Tanger (Rif septentrional, Maroc). Doctorat, Université Mohamed V, Faculté des Sciences, Rabat. 2005, 175 p.

UNDRO (Office of the United Nations Disaster Relief Coordinator). Natural disasters and vulnerability analysis. Report of Expert Group Meeting, 1979, 19 p.

van Westen C.J. Remote sensing and geographic information systems for geologic hazard mitigation. ITC Journal, No. 4, 1993, pp. 393-399.

van Westen C.J., van Duren I., Kruse H.M.G., Terlien M.T.J. GISSIZ: training package for Geographic Information Systems in slope instability zonation. ITC-Publication Number 15, ITC, Enschede, The Netherlands. Volume 1 – Theory, 245 pp., Volume 2 – Exercises, 1993, 359 pp.

Wadge G. The potential for volcanic disaster in the Lesser Antilles arc. Bulletin of Volcanology, Vol. 50(2), 1988, pp. 198-215.

Yin K.L. and Yan T.Z. Statistical prediction model for slope instability of metamorphosed rocks. Proceeding 5th International Symposium on Landslides, Lausanne, Switzerland, Vol. 2, 1988, pp.1269-1272.

Zêzere J.L., Garcia RAC., Oliveira SC, Reis E. Probabilistic Landslide risk analysis considering direct costs in the area north of Lisbon (Portugal). Geomorphology, Elsevies. Vol. 94, 2008, pp. 467-495.

Zêzere J.L., Reis E., Garcia R., Oliveira S., Rodrigues M.L., Vieira G., Ferreira A.B. Integration of spatial and temporal data for the definition of different landslide hazard scenarios in the area north of Lisbon (Portugal). Natural hazards and Earth system Sciences, European Geosciences Union, Vol. 4, 2004, pp.133-146, https://doi.org/10.5194/nhess-4-133-2004.

МОДЕЛИРОВАНИЕ ОПОЛЗНЕЙ, ОБРАЗУЮЩИХСЯ В ВЕРХНЕЙ ЧАСТИ ПОРТА ТАНЖЕР-МЕД (ТАНЖЕР, МАРОККО), С ИСПОЛЬЗОВАНИЕМ ГИС И СТАТИСТИЧЕСКОГО МЕТОДА

Мактит А., Фалех А.

*Факультет литературы и гуманитарных наук, Саис-Фес, кафедра географии,
Университет Сиди Мохаммед бен Абделла, Фес, Марокко*

Резюме. Данное исследование имеет решающее значение для понимания проблем, с которыми сталкивается порт Танжер-Мед – стратегический узел международной торговли. Расположенный в горном регионе, этот порт очень уязвим для стихийных бедствий, особенно оползней. Нужно подчеркнуть, что с учетом полученных данных, исследование, проведенное на испытательном полигоне площадью 193 км², зафиксировало 277 движений по склону, что составляет около 11% от общей площади. При оценке восприимчивости местности использовался метод информационной ценности для картирования перемещений за последние десятилетия, а также шесть предрасполагающих к ним факторов.

Результаты показывают, что почти 31% общей площади очень восприимчивы к массовым движениям, 22% очень чувствительны, а 23,3% представляют малую угрозу. Эти результаты были сопоставлены и подтверждены с использованием успешных показателей и кривых прогнозирования. Кроме того, надо отметить, что было выделено пять основных классов риска оползней на неосвоенных или малоосвоенных территориях с низким или незначительным значением риска и на освоенных территориях горных склонов с очень высоким его значением.

Таким образом, точное картирование и анализ рисков необходимы для разработки стратегий управления и предотвращения оползней с целью минимизации потенциального воздействия на портовую инфраструктуру и связанную с ней экономическую деятельность. В заключение можно сказать, что данное исследование способствует лучшему пониманию геологических рисков в регионе и, что более важно, реализации соответствующих мер по обеспечению безопасности и устойчивости порта.

Ключевые слова: *порт, Средиземноморский Танжер, информативность, кривые успешности, кривые прогноза*

QGT VƏ STATİSTİK METODDAN İSTİFADƏ EDİLMƏKLƏ, TANJER-MED LİMANININ (TANJER, MƏRAKEŞ) YUXARI HİSSƏSİNDƏ ƏMƏLƏ GƏLMİŞ SÜRÜŞMƏLƏRİN MODELLƏŞDİRİLMƏSİ

Maktit A., Faleh A.

*Ədəbiyyat və humanitar elmlər fakültəsi, Sais-Fes, coğrafiya kafedrası,
Sidi Moxammed ben Abdella Universiteti, Fes, Marakeş*

Xülasə. Bu tədqiqat, beynəlxalq ticarətin strateji mərkəzi olan Tanca-Med portunun qarşılaşdığı problemlərin başa düşülməsi üçün həlledici əhəmiyyət daşıyır. Dağlıq bir bölgədə yerləşən bu port, təbii fəlakətlərə, xüsusilə sürüşmələrə qarşı çox həssasdır. 193 km² sahəsi olan sınaq poliqonunda aparılan tədqiqat, ümumi sahənin təxminən 11%-ni təşkil edən 277 yamac hərəkətini qeydə almışdır. Əlavə olaraq, qeyd etmək lazımdır ki, ərazinin həssaslığının qiymətləndirilməsində son onilliklərdə baş vermiş yerdəyişmələri xəritələşdirmək üçün məlumatın qiyməti metodu və onlara səbəb olan altı amildən istifadə edilmişdir. Bundan əlavə əldə edilən nəticələr göstərir ki, ümumi sahənin təxminən 31%-i kütləvi hərəkətlərə çox həssasdır, 22%-i isə yüksək dərəcədə həssasdır və 23,3%-i az risk daşıyır. Həmçinin bu nəticələr uğurlu göstəricilər və proqnozlaşdırma əyrilərindən istifadə edilərək təsdiq edilmişdir. Aşağı və ya əhəmiyyətsiz risk dərəcəsi olan inkişaf etməmiş və ya az inkişaf etmiş ərazilər və yüksək risk dərəcəsi olan dağ yamaclarında yerləşən inkişaf etmiş ərazilər üzrə beş əsas sürüşmə riski sinfi müəyyən edilmişdir. Port infrastrukturuna və ona bağlı iqtisadi fəaliyyətə potensial təsiri azaltmaq məqsədi ilə sürüşmələrin idarə olunması və qarşısının alınması üçün dəqiq xəritələşdirmə və risklərin təhlili vacibdir. Nəticə etibarilə, bu tədqiqat regiondakı geoloji risklərin daha yaxşı başa düşülməsinə və daha da əhəmiyyətlisi, port təhlükəsizliyi və davamlılığını təmin etmək üçün müvafiq tədbirlərin həyata keçirilməsinə töhfə verir.

Açar sözlər: *port, Tanca Aralıq dənizi, məlumatlılıq,uğurluq əyriləri, proqnoz əyriləri*

СЛАНЦЕВЫЕ НЕФТЕГАЗОВЫЕ СИСТЕМЫ ЮЖНО-КАСПИЙСКОЙ ВПАДИНЫ

Керимов В.Ю.[1,3], Гулиев И.С.[2], Джавадова А.С.[1],
Мустаев Р.Н.[3], Гурбанов В.Ш.[1], Гусейнова Ш.М.[1]

[1]Министерство науки и образования Азербайджанской Республики,
Институт нефти и газа, Азербайджан
AZ1000, Баку, ул. Ф.Амирова, 9: huseynova_shalala@yahoo.com
[2]Президиум Национальной академии наук Азербайджана, Азербайджан
AZ1001, Баку, ул. Истиглалият, 30: i.s.guliyev@gmail.com
[3]Российский государственный геологоразведочный университет
имени Серго Орджоникидзе, Российская Федерация
117997, Москва, ул. Миклухо-Маклая, 23: mustaevrn@mgri.ru

SHALE OIL AND GAS SYSTEMS OF THE SOUTH CASPIAN DEPRESSION

Kerimov V.Yu.[1,3], Guliyev I.S.[2], Javadova A.S.[1], Mustaev R.N.[3], Gurbanov V.Sh.[1], Huseynova Sh.M.[1]
[1]Ministry of Science and Education of the Republic of Azerbaijan, Institute of Oil and Gas, Azerbaijan
 9, F.Amirov str., Baku, AZ1000
[2]Presidium of Azerbaijan National Academy of Sciences, Azerbaijan
 30, Istiglaliyyat Str., Baku, AZ1001: i.s.guliyev@gmail.com
[3]Sergo Ordzhonikidze Russian State University for Geological Prospecting, Russian Federation
 23, Miklouho-Maclay Str., Moscow,117997: mustaevrn@mgri.ru

Keywords: *South Caspian depression, shale strata, hydrocarbon system, kerogen, catagenesis, organic porosity, adsorption*

Summary. The paper describes the shale oil and gas bearing systems of the South Caspian basin based on the results of basin modeling. Identification and assessment of the prospects for shale accumulations at the regional level is based largely on the results of numerical modeling with subsequent calibration of the resulting model.

The largest masses of oil are concentrated in shale strata, and OM is present there initially, and oil (light components of OM) emigrates from shale to neighboring reservoir rocks. Changes in the structure of kerogen during catagenetic maturation occur in contact areas. In dense immature kerogen, organic pores ("kerogen porosity") begin to form, which, by the end of the main phase of oil formation, form a connected system that provides space for newly formed petroleum hydrocarbons. Organic porosity or porosity in the texture of kerogen, formed during the thermal maturation of rock OM, can affect the adsorption of the resulting oil by the porous surface of the kerogen. The results of organic porosity studies suggest that organic pores in the kerogen texture make a significant contribution to the space of newly formed reservoirs in the thickness of oil source rocks.

It is concluded that the following shale oil and gas systems were formed in the South Caspian basin: diatomaceous shale oil and gas system, Oligocene-Miocene shale oil and gas system and Eocene shale oil and gas system, which are combined unconventional oil and gas systems with hydrocarbons, partially emigrated from the oil and gas source rock and partially preserved (unrepressed).

Введение

Проблема изучения и освоения нефтегазовых ресурсов сланцевых формаций относится к числу сложных, наукоемких и мультидисциплинарных. В петрологической терминологии под нефтегазоносными сланцами понимается целый ряд твердых, многослойных пелитовых пород: глина, мергель, глинистый известняк, аргиллит, алевролит и собственно сланец, которые вмещают всевозможные формы органического вещества (ОВ), отражающие стадии его зрелости. Отличаясь текстурными характеристиками от других пелитовых пород, сланцы способны расщепляться на пластинки. Нефть и газ в таких породах располагаются преимущественно в диффузно рассеянном состоянии и в микротрещинах. Сланцевые толщи,

с низкопроницаемыми коллекторами, вмещающие скопления углеводородов (УВ), являются в последние годы предметом пристального внимания в связи с существенным ростом промышленной значимости.

Опыт изучения и освоения скоплений УВ, приуроченных к сланцевым комплексам в США, обеспечил серьезный стимул к изучению подобных объектов по всему миру, включая европейские страны, Китай и многие другие государства. В Северной Америке благодаря использованию новейших технологий произошла «сланцевая революция». Начав 30 лет назад с бурения на сланцевых полях мелких скважин, США добыли из сланцевых формаций около 180 млрд. м³ газа и более 40 млн. т нефти. В США интерес к разработке газа из сланцевых формаций был настолько высоким, что в 19 бассейнах (Marccllus, Antrim, New Albany, Barnett, Lewis и др.) было пробурено более 35000 скважин.

Мировые геологические запасы нефти из сланцев оценены на уровне более чем 3 трлн. барр. (рис. 1). Последняя оценка ресурсов нефти из сланцев для других стран (в млрд. барр. н.э.): Китай – 333; Россия – 248; Демократическая Республика Конго – 100; Иордания – 90; Бразилия – 82; Италия – 73; Марокко – 53; Австралия – 32; Эстония – 16; Израиль – 250 (Beckwith, 2012).

Перспективы изучения и освоения нефти из сланцевых формаций почти во всех нефтегазоносных провинциях (НГП) России, весьма впечат-

ляющи, в первую очередь это относится к баженовской свите и ее аналогам в Западной Сибири. По данным Международного энергетического агентства (IEA, 2013), она оценена как наиболее богатая сланцевая толща в мире – 144 млрд. барр. нефти и более 36.9 трлн. м³ газа. Повышенный интерес представляют отложения доманикового типа в промышленно развитых районах Тимано-Печорской и Волго-Уральской НГП, майкопская и кумская свиты Предкавказья, рифей-кембрийские отложения в Восточной Сибири (Якуцени, 2009; Прищепа, Аверьянова, 2013).

Понятийная база и терминология при исследовании сланцевых формаций и сланцевых скоплений УВ

Среди специалистов существуют некоторые разночтения при исследовании сланцевых формаций и сланцевых скоплений УВ, связанные с несовпадением понятий (и неточностями перевода) в англоязычной, российской, а вслед за ними и в азербайджанской специализированной литературе и критериев, применяемых в зарубежных и российских классификациях запасов и ресурсов, коллекторов и литологических свойств пород. По этой причине некоторые исследователи, обсуждая проблемы изучения сланцевых нефти и газа, включают сюда тематику горючих сланцев, которые, безусловно, являются самостоятельными группами нетрадиционных источников УВ, но не имеют никакого отношения к сланцевым скоплениям УВ.
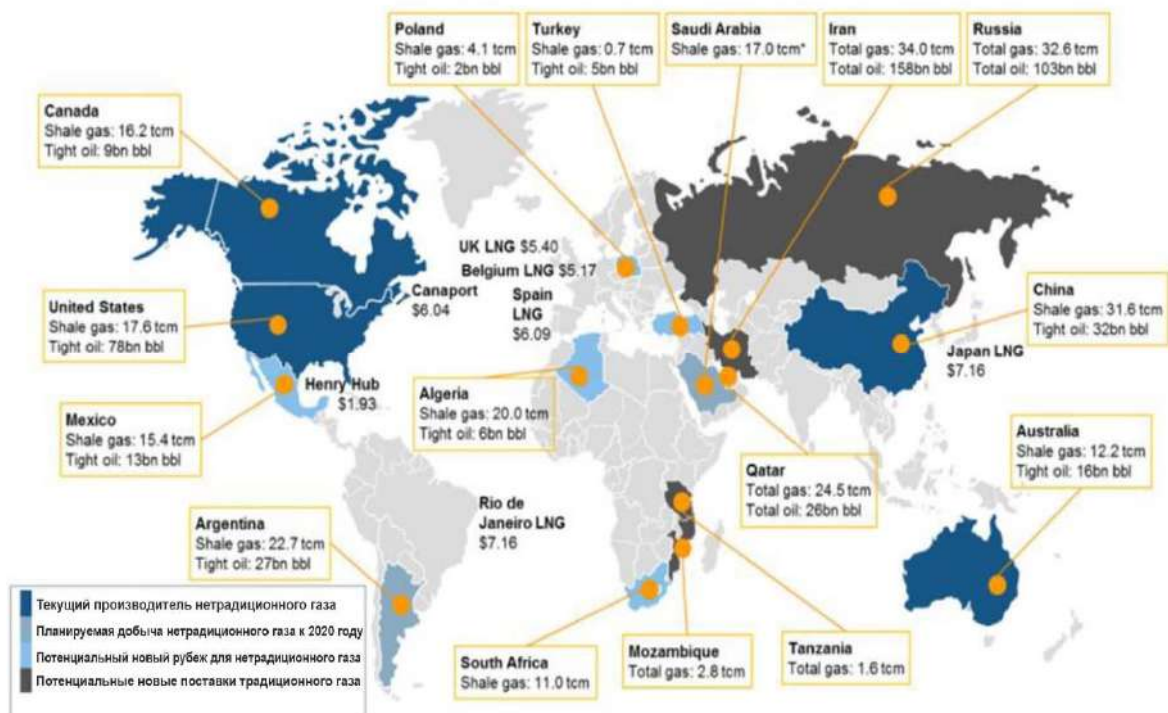

Рис. 1. Мировой потенциал запасов сланцевых УВ

Некоторые исследователи, в том числе и в Азербайджане, сланцевые толщи называют фациями, что противоречит учениям о геологических формациях и фациях, описанных в известных трудах Н.С.Шатского, Н.М.Страхова, Д.В.Наливкина, В.И.Попова, Л.Б.Рухина, В.В.Белоусова, Н.Н. Хераскова, Ю.А. Жемчужникова, Г.Ф. Крашенинникова, М.В. Коровина, Л.В.Пустовалова, М.А.Усова, Ю.А.Кузнецова, В.Е.Хаина, А.Л.Яншина и др. Понятия «фация» и «формация» различаются прежде всего масштабом: формация состоит из нескольких, а в некоторых случаях из одной фаций. Если для фаций главным определяющим фактором формирования является *физико-географическая обстановка осадконакопления,* то для формаций – *тектонический фактор.* Фация – это определенный тип породы, образовавшейся в определенных физико-географических условиях, то есть тип фации определяется «обстановкой осадконакопления», в общем случае включает физико-географическую и топографическую характеристики, условия существования флоры и фауны, динамику и физико-химическую обстановку среды осадконакопления или образования пород. Поэтому называть сланцевые толщи сланцевой фацией некорректно, так как в природе не существует физико-географической обстановки осадконакопления, в которой образовались сланцы. Фации характеризуются петрографическими и геохимическими характеристиками осадочных пород, которые представляют палеогеографическую и геохимическую среды осадочных отложений. В природе существует следующая генетическая цепочка глинистых пород*: глинистые илы – глина – аргиллитоподобные глины – аргиллиты – глинистые сланцы.* Таким образом, сланцы, являясь последним звеном этой цепочки, относятся к метаморфическим породам, образовавшимся в результате длительного воздействия внешних факторов (температуры, давления и т. д.). А горючие сланцы – это метаморфические породы, относящиеся к группе твердых каустобиолитов, поэтому их нельзя называть фациями.

Таким образом, целесообразно сланцевые толщи называть формациями. Такие формации широко известны на территории зарубежных стран, с которыми связаны «сланцевая нефть» и «сланцевый газ» – формации Barnett, Bakken и Green River (США); формации бассейнов Sichuan, Tarim, Junggar и Songliao (Китай); позднеюрско-нижнемеловая формация Vaca Muerta и среднеюрская формация Los Molles (Аргентина); силурийские и доггерские формации (Румыния), сланцевые формации бассейнов Paris и South-East (Франция), бассейнов Basque-Cantabrian и Ebro (Испания), Lover Saxony (Германия), бассейна West Nethcrland (Нидерланды), сланцевого бассейна Alum (Швеция), а также сланцевых бассейнов Дании, Норвегии и др.

Под формацией (по В.Е. Хаину) понимают естественное и закономерное сочетание горных пород (осадочных, вулканогенных, интрузивных), связанных общностью условий образования и возникающих на определенных стадиях развития основных структурных зон земной коры. В связи с изложенным, выделяемые сланцевые толщи на территории Азербайджана целесообразно называть диатомовой сланцевой формацией, олигоцен-миоценовой сланцевой формацией и палеоцен-эоценовой сланцевой формацией.

Нефть и газ, добыча которых ведется из низкопроницаемых коллекторов, приуроченных или сопряженных непосредственно с толщей, генерирующей их (in situ), в англоязычной литературе называются «нефть и газ сланцев» **(shale oil & gas)**. Принципиальными отличиями скоплений, образованных в таких нефтегазовых системах, от широко распространенных и традиционных, является низкое качество коллекторов. Основной набор процессов, характеризующих такую систему, является сокращенным по сравнению с традиционным (генерация, миграция, аккумуляция, консервация) в части процессов миграции и аккумуляции. Для нетрадиционных углеводородных скоплений предлагается использовать следующие термины, соответствующие англоязычным: **oil shale** – сланец, содержащий кероген; **shale oil** – нефть глинистых сланцев; **shale gas** – газ глинистых сланцев; **tight oil** – нефть низкопроницаемых (плотных) пород; **tight gas** – газ низкопроницаемых (плотных) пород.

Традиционная нефтегазовая система характеризуется набором процессов, определяемых подвижностью УВ в системе: генерацией УВ, вытеснением, миграцией и аккумуляцией. Многообразие типов нефтегазовых систем вызвано различиями во взаимоотношениях между толщами генерации и транзитными толщами, доминирующими путями миграции УВ и ее способами, характеристиками зон аккумуляции УВ и качеством флюидоупоров.

Для нетрадиционных нефтегазовых систем характерен неполный (сокращенный) набор процессов. В первую очередь это касается резкого ограничения миграции и аккумуляции. Наиболее общим является случай, когда нетрадиционная нефтегазовая система образуется за счет сохранения (удерживания) генерированных УВ непосредственно в нефтегазоматеринской толще (НГМТ). В случае частичного вытеснения генерированных УВ из НГМТ образуется комбинированная нетрадиционная нефтегазовая система с УВ, частично

эмигрировавшими из НГМТ и частично сохраненными (не вытесненными).

Таким образом, вмещающие породы сланцевой нефти и газа представляют собой гибридное явление, которое одновременно генерирует и накапливает УВ. Такие системы называются системой сланцевой нефти ("**shale-source oil system**") и системой сланцевого газа **("shale-source gas system**"). Поиск и разведку запасов нефти и газа в сланцевых пластах следует направить в ту часть системы, где наиболее сконцентрированы (в свободной и сорбированной формах) УВ.

В Южно-Каспийском бассейне можно выделить *диатомовую сланцевую нефтегазовую систему, олигоцен-миоценовую сланцевую нефтегазовую систему и эоценовую сланцевую нефтегазовую систему*. Они являются комбинированными нетрадиционными нефтегазовыми системами с УВ, частично эмигрировавшими из НГМТ и частично сохраненными (не вытесненными).

Результаты исследований

Информация о распространении сланцевых парод на территории Азербайджана дана в трудах А.А.Али-Заде, В.В.Вебера, А.Ж.Султанова, Р.Х.Султанова, С.Г.Салаева, В.Ю.Керимова и др. Особо стоит отметить в этом направлении труды Ад.А.Алиева (2015) и О.Р.Аббасова (2022), исследовавших сланцы на территории Азербайджана

как на наземных обнажениях, так и на образцах из выбросов грязевых вулканов. Сланцевые формации, выявленные в Прикаспийско-Губинском, Шамахы-Гобустанском, Абшеронском и Приталышском (Джалилабадском) нефтегазоносных районах, связаны с меловым, среднеэоценовым, майкопским и диатомовым периодами (рис. 2) (Abbasov, 2022; Алиева и др., 2019).

Сланцы эоценового возраста выявлены в обнажениях, охватывающих полосу юго-востока – северо-запада, начиная от площади Гейтепе (Багир-Заде и др., 1988) Абшеронского полуострова до села Дияллы в районе Исмаиллы. Нижнемайкопские сланцы сложены с небольшим количеством песчанистых и глинисто-конгломератовых пород, обнаруженных в Прикаспийско-Губинском (на окраине рек Бабачай и Агчай), Шамахы-Гобустанском (в районах ручьев реки Гирдиманчай, Лагич) районах, в Центральном Гобустане (вокруг горы Гаиблар) и в Ярдымлы (в районе ручья реки Вилашчай). А полоса, протянувшаяся от Агчалы до сел Исмаиллы, расположенных в верховьях Гирдыманчая, характерна для распространения сланцев, принадлежащих верхнему майкопу. На юге и юго-востоке этой полосы установлены сланцевые структуры (Шихзарли, Гаибляр, Шаибляр и др.). Пространственное распространение горючих сланцев диатома выявлены в Прикаспийско-Губинском регионе (Гаджиев, 1989).
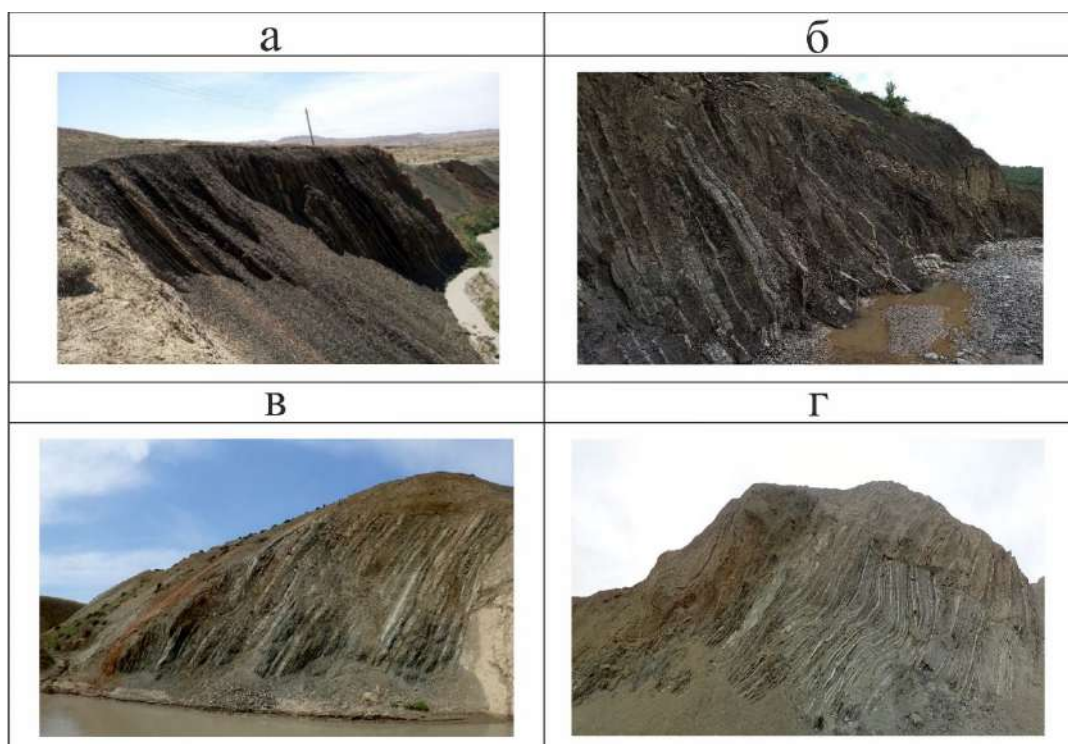
Рис. 2. Обнажения сланцевых толщ эоценового возраста на участке Чайлы (а, б), нижнемайкопского возраста в Лагидже (б) (по материалам Аббасова, 2022), палеоценового (в) и среднеэоценового возраста (г) на участке Перекюшкиль (по материалам Aghayeva и др., 2021). В обнажениях сланцевые слои и пластины чередуются глинистыми, аргиллитовыми, алевролитовыми и другими слоями

На территории Азербайджана сланцевые породы встречаются не только в поверхностных обнажениях, но и в выбросах грязевых вулканов (Галимов, 1973; Глумов и др. 2004; Гулиев и др., 1992, Гулиев, Фейзуллаев, 1996). Этот факт свидетельствует о присутствии сланцевых формаций на больших глубинах кайнозойского комплекса Южно-Каспийского бассейна – аналогов формаций сланцев, наблюдаемых на земной поверхности. Проведенные исследования свидетельствуют о сланцевой природе диатомовой свиты, майкопской серии. Эоценовые отложения Южно-Каспийской впадины также являются объектами формирования в них нетрадиционных (сланцевых) скоплений УВ. Эти толщи представляют собой гибридные феномены, включающие как традиционные, так и нетрадиционные скопления УВ.

Результаты исследований диатомовой сланцевой, олигоцен-миоценовой сланцевой и палеоцен-эоценовой сланцевой формаций показали, что они являются естественным и закономерным сочетанием горных пород, формирование которых произошло на альпийском этапе развития Южно-Каспийского бассейна. На основании проведенного палеотектонического и геодинамического анализа в составе осадочного чехла Южно-Каспийского бассейна выделены основные структурно-формационные (тектоно-формационные) комплексы (СФК), которые являются отражением эволюционного развития этого бассейна. При формировании этих СФК определяющими являлись этапы геотектонического цикла, с которыми связаны вышеуказанные сланцевые формации – диатомовый СФК сформировался на *роданской фазе*, олигоцен-миоценовый СФК – на *пиренейской фазе* и палеоцен-эоценовой СФК – на *новоларамийской* и *пиренейской* фазах альпийского тектогенеза.

Это подтверждается также исследованиями П.З.Мамедова (2010): палеоцен-эоценовый СФК сформировался на *этапе островодужного вулканизма и расширения*; олигоцен-миоценовый СФК – на этапе сжатия и постепенного сокращения, а диатомовый СФК – на этапе экстремального сокращения и быстрого погружения.

Керогенсодержащие сланцевые толщи представлены целым рядом твердых, многослойных пелитовых пород (глина, мергель, глинистый известняк, аргиллит, алевролит и собственно сланец), вмещающих всевозможные формы ОВ, находящегося на различной стадии преобразованности (рис. 3). Отличаясь текстурными характеристиками от других пелитовых пород, сланцы способны расщепляться на пластинки. Эти отложения отличаются фациальной изменчивостью, сопровождающейся широким развитием разнофациальных, не сходных по составу комплексов.

Сланцы выражены трещиноватыми, тонкоплитчатыми, листоватыми аргиллитоподобными глинами и мергелями, перемежающимися с плотными разновидностями глин и мергелей. Так, диатомовая сланцевая толща расщепляется на сланцевые пластины и пласт толщиной около 60 м бумажных сланцев (Калмыков и др., 2019). Олигоцен-миоценовая сланцевая толща с нефтематеринской толщей майкопской серии (включая пшехскую и нижнесоленовскую толщи) состоит из многослойных пелитовых пород, чередующихся сланцевыми пластами. Эоценовая сланцевая толща сложена чередованием дискретных интервалов сланцевых пластин с богатыми органическими веществами многослойных пелитовых пород. Обобщение результатов показывает, что матрицы в исследованных образцах этих пород сложены глинистыми агрегатами на 45% с добавками ОВ и обломочными компонентами алеврито-пелитовой размерности. В матрицах изучаемых объектов поровое пространство представлено межагрегатными или межкристаллическими порами, морфология которых была определена процессами литогенеза (условиями осадконакопления и последующими диа- и катагенезом) (Керимов и др., 1990; Лебедев и др., 1987; Гулиев и др., 2003; Леонов и др., 2010).

В общем комплексе исследований, направленных на прогноз нефтегазоносности сланцевых отложений, существенную роль играют геохимические методы (Левин, Сенин, 2003; Дахнова и др., 2015). На любых уровнях геохимических исследований первостепенная задача при выявлении нефтегазообразования в НГМТ – определение фациально-генетического состава ОВ. Для прогнозирования границ зон нефтегазообразования и фазового состояния УВ в недрах необходимо учитывать фациальные и генетические разновидности ОВ, его тип и содержание в породе, характер и особенности катагенеза ОВ. Важное значение имеют термобарические условия нахождения НГМТ. Для исследования сланцевых толщ Южно-Каспийской впадины – диатомовой толщи, майкопской серии и палеоцен-эоценового комплекса – были обобщены результаты пиролитических исследований (Левин, Федоров, 2001).

Диатомовая свита. Часть образцов попадает в раннюю стадию углеводородообразования – градации катагенеза ПК$_3$–МК$_1$. Для некоторых образцов T_{max} достигает 440-458°C и более (рис. 4).

Олигоцен – нижний миоцен (майкопская серия) характеризуется широким диапазоном значений по углеводородно-генерационному потенциалу – от удовлетворительного до превосходного (рис. 6).

Отложения майкопской серии отличаются высоким содержанием $C_{орг}$, достигающим 15.1% при среднем содержании 1.86%. Качество и содержание ОВ майкопских отложений улучшаются в восточном направлении в сторону Каспийского моря. В образцах выделяется равнозначное значение керогена III и II типов. Часть полученных значений T_{max} лежит в пределах от 420-445°C и более, а рассчитанные значения температуры составляют 171-200°C и соответствуют градации катагенеза $МК_3$–$МК_4$. В этой зоне интенсивно протекают термические и термокаталитические процессы преобразования, а также происходит перестройка молекулярной структуры в процессе катагенеза, которая приводит к преобразованию пелитовых пород (глина, мергель, глинистый известняк, аргиллит) в сланцы. Отложения майкопского возраста в очагах генерации находятся в интервалах глубин, находящихся в зоне нефтяного окна (**oil window**), в которой происходит генерация УВ с максимальной активностью, в том числе и легких (до 4 %). С переходом в зону $МК_4$ в майкопские отложения в главной зоне газообразования начинают генерировать газообразные УВ (рис. 7). Майкопская серия считается наиболее важной нефтематеринской породой в Южно-Каспийском бассейне.
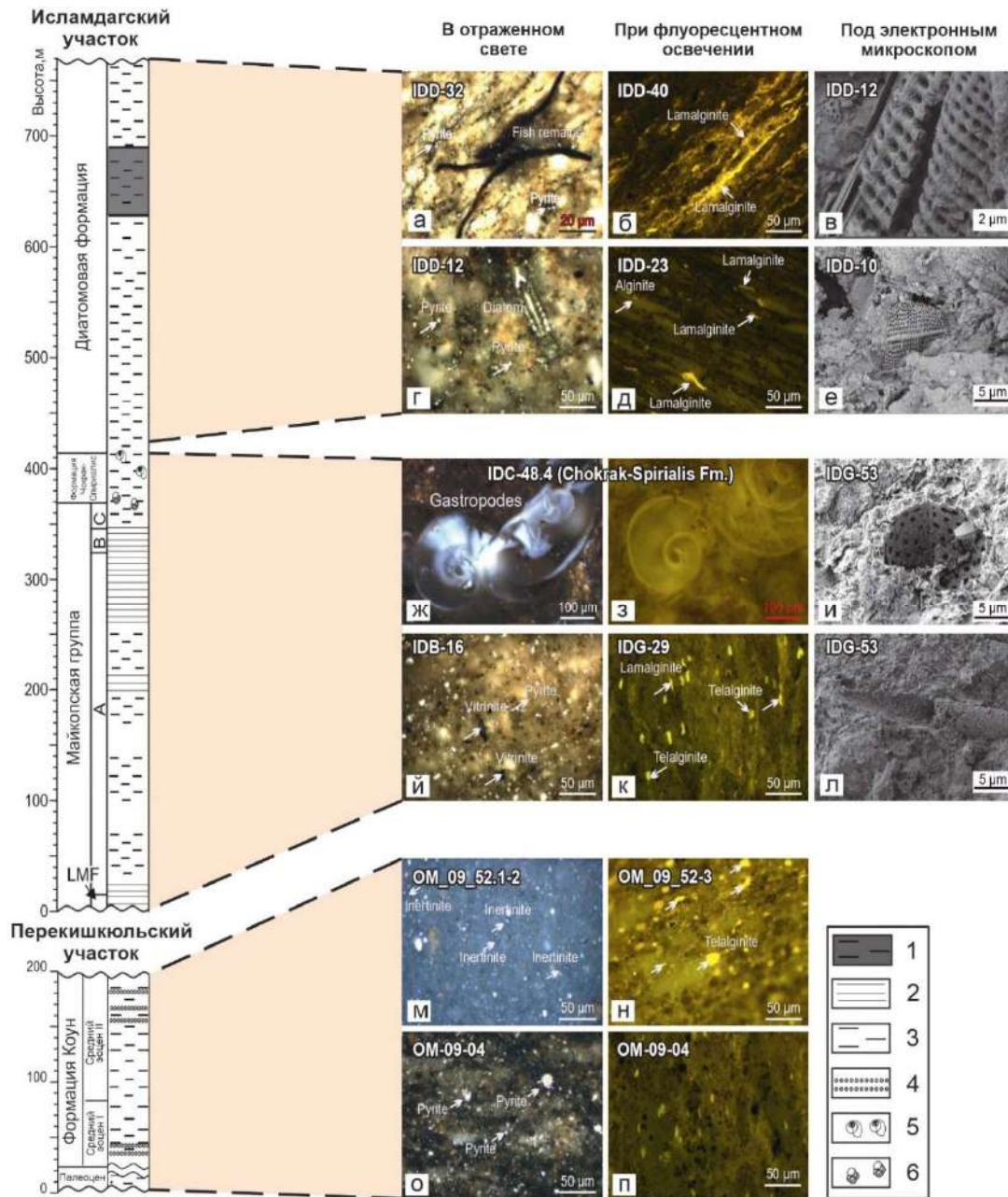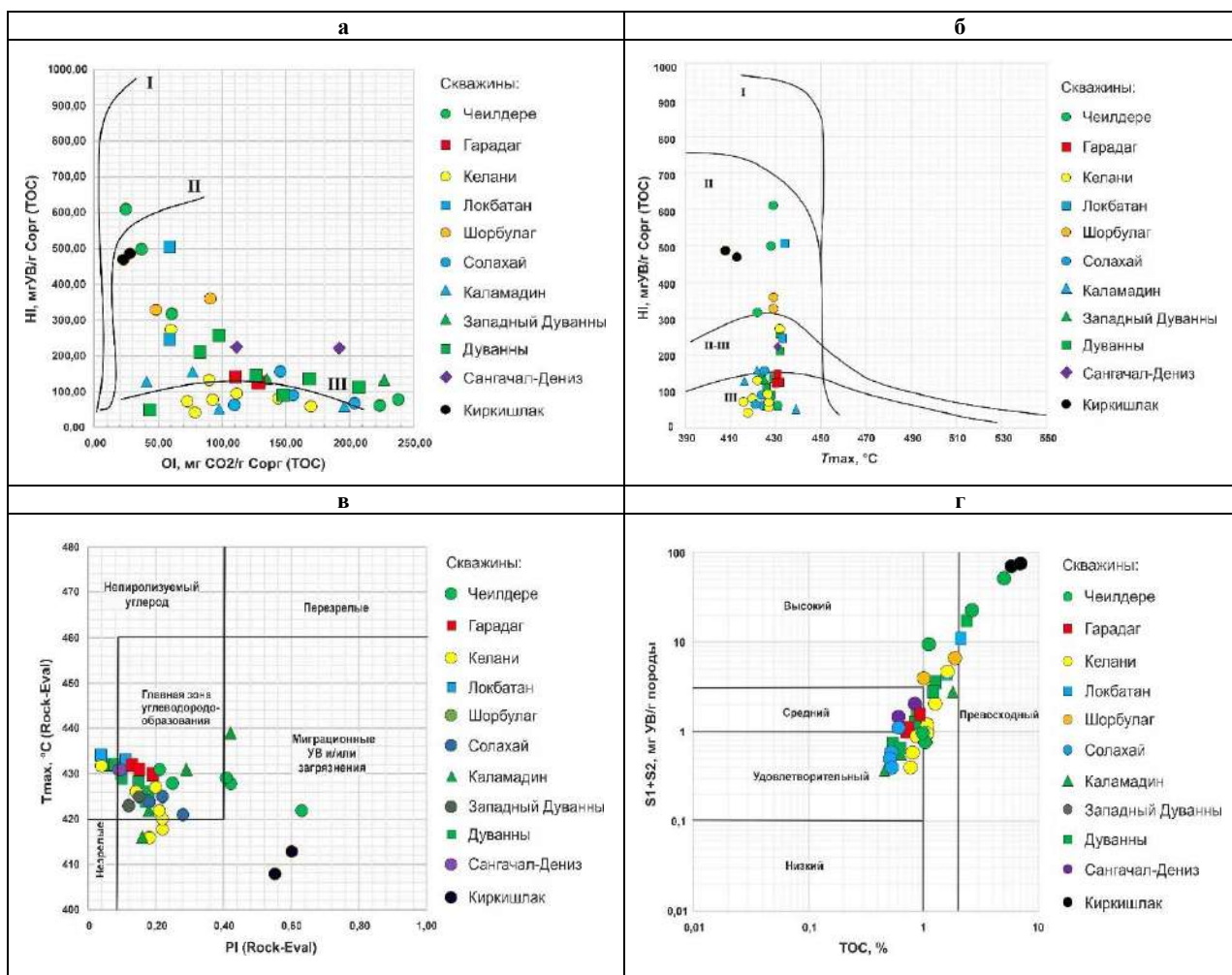

Рис. 3. Шлифы образцов из обнажений:
а–е – диатомовая формация; ж, з – чокракская-спириалисская формация; и–л – майкопская серия; м, н – средний эоцен II; о, п – палеоцен (по материалам Aghayeva и др., 2021); 1 – бумажные сланцы, 2 – глины и глинистые сланцы, 3 –аргиллит, 4 – песчаник, 5 – птероподы, 6 – планктонные фораминиферы

Рис. 4. Интерпретация результатов пиролитических исследований образцов миоценового комплекса:
а – модифицированная диаграмма Ван Кревелена – зависимость водородного индекса HI от кислородного индекса OI; б – зависимость водородного индекса HI от максимальной температуры пиролиза T_{max}; в – диаграмма соотношения максимальной температуры пиролиза T_{max} и индекса продуктивности PI; г – диаграмма соотношения генерационного потенциала материнской породы и общего содержания органического углерода C_{opr}

***Палеоцен-эоценовый комплекс отложений.*** Эоценовые отложения характеризуются широким диапазоном значений по углеводородно-генерационному потенциалу – от низкого до превосходного (рис. 8). В образцах преобладает кероген III типа. Результаты исследований показывают, что рассчитанные значения температуры составляют $210°С$ и более, а образцы эоценовых отложений соответствуют градации катагенеза $МК_4$–$МК_5$, в результате чего интенсивно протекают термические и термокаталитические процессы преобразования, а также происходит перестройка молекулярной структуры, которая приводит к интенсивному сланцеобразованию и преобразованию пелитовых пород в сланцы. Эоценовые отложения входят в главную зону газообразования. Содержание углерода в керогене достигает 85-86%, что свидетельствует об уплотнении углеродной структуры, связанной с потерей водорода, содержание которого менее 2%. Удаление водорода

происходит за счет интенсивной генерации газообразных УВ. На этом этапе возникает резкое снижение объемов генерации УВ, даже метана, что подтверждается также результатами моделирования процесса генерации УВ в эоценовых отложениях (рис. 9).

Принципиально важно не путать *кероген в сланцевых отложениях* и уже генерированные *нефть и газ* в НГМТ, содержащиеся в рассеянном состоянии в микропорах и микротрещинах, в послойной трещиноватости в пределах НГМТ (shale oil & gas), одновременно выступающих резервуарами для произведенных ими УВ.

Последнее крайне важно для оценки потенциала первоочередных для разработки сланцевых объектов на территории Азербайджана нефтегазоматеринских свит, таких как диатомовая свита и майкопская серия, обладающих огромным генерационным потенциалом.
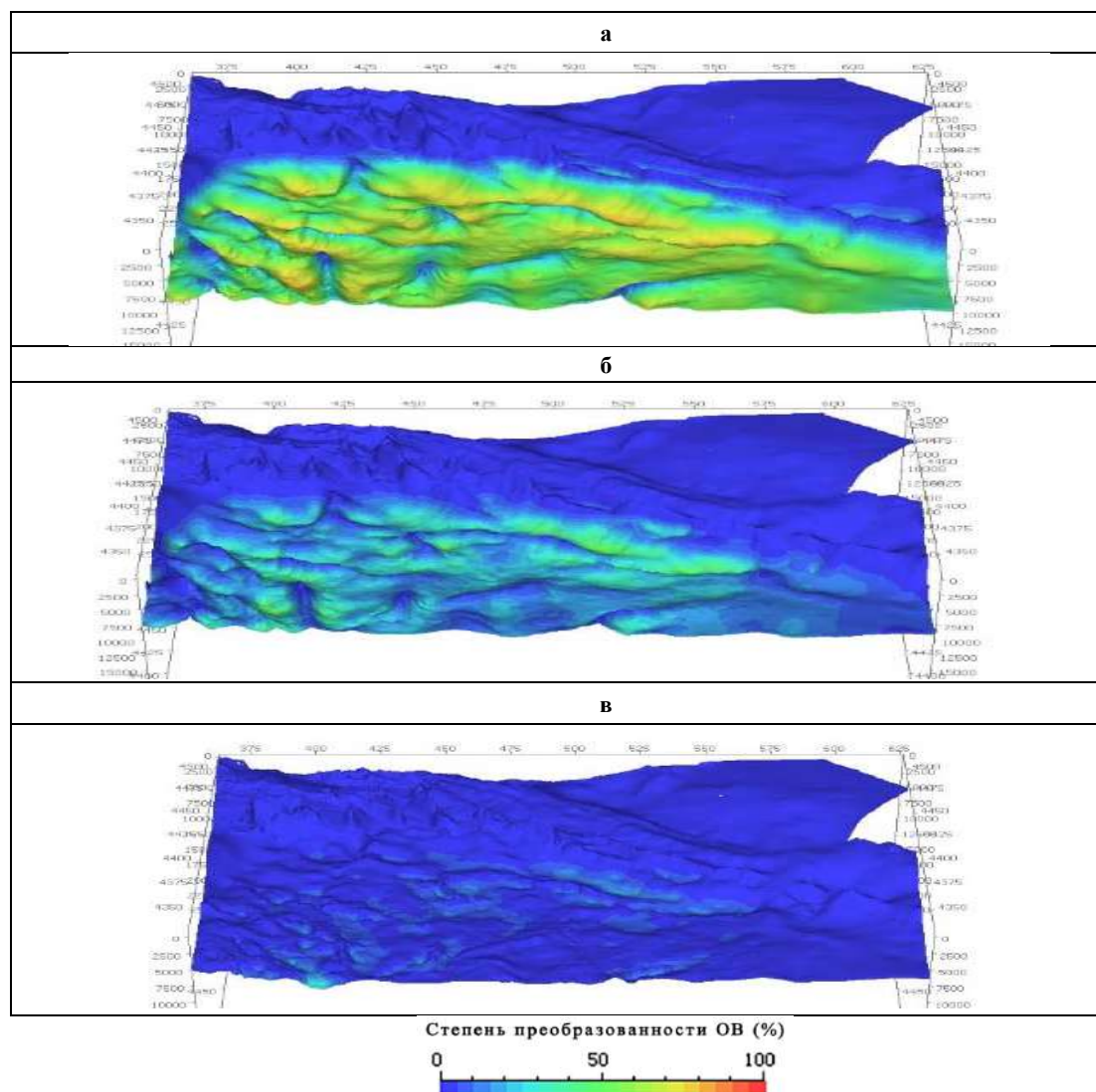
Рис. 5. 3D-реконструкция процесса катагенетической эволюции диатомовых отложений Южно-Каспийского бассейна: а – к настоящему времени; б – к концу абшеронского времени (1.1 млн. лет); в – концу акчагыльского времени (2 млн. лет)

Исследования свидетельствуют, что скопления УВ в низкопроницаемых сланцевых толщах формируются в процессе аккумуляции УВ в НГМТ за счет процессов сорбции, сгенерированных УВ как керогеном, так и незрелыми продуктами его преобразования – асфальтенами, тяжелыми (спиртобензольными) смолами (Мехтиев, 1956; Обсуждение книги Ш.Ф.Мехтиева…, 1957). Важной особенностью скоплений УВ в таких толщах является то, что УВ (газ и нефть) находятся преимущественно в связанном, сорбированном, диффузно-рассеянном состоянии в керогене и продуктах преобразования керогена – начальных, наиболее незрелых продуктах сингенетичной нефти (асфальтенах, смолах, твердых парафинах), изначально рождающейся в объеме керогена в процессе его химического (каталитического, термического, радиационного и т. д.) преобразования (Мехтиев, 1985). Согласно концепциям В.И.Вернадского и И.М.Губкина, «в диффузно-рассеянном

состоянии нефть занимает огромные пространства на земном шаре». В настоящее время нахождение рассеянной нефти реально установлено в осадочной толще земной коры, во много раз превышающей ее во всех известных залежах. Диффузно-рассеянные нефтяные компоненты присутствуют в скрытом виде в нефтематеринском органическом веществе (ОВ) в отличие от «макронефти», выделившейся и эмигрирующей из материнской породы в коллектор. В сланцевых толщах сконцентрированы наибольшие массы нефти, а ОВ присутствует там изначально, и нефть (легкие компоненты ОВ) эмигрирует из сланцев в соседние породы-коллекторы. Когда смежные коллекторы отсутствуют, нефть консервируется в глинах. На адсорбцию сгенерированных УВ активно влияет органическая пористость на поверхности керогена. Процесс адсорбции приводит к увеличению концентрации вещества на границе раздела фаз (Гаджиев, 1989).
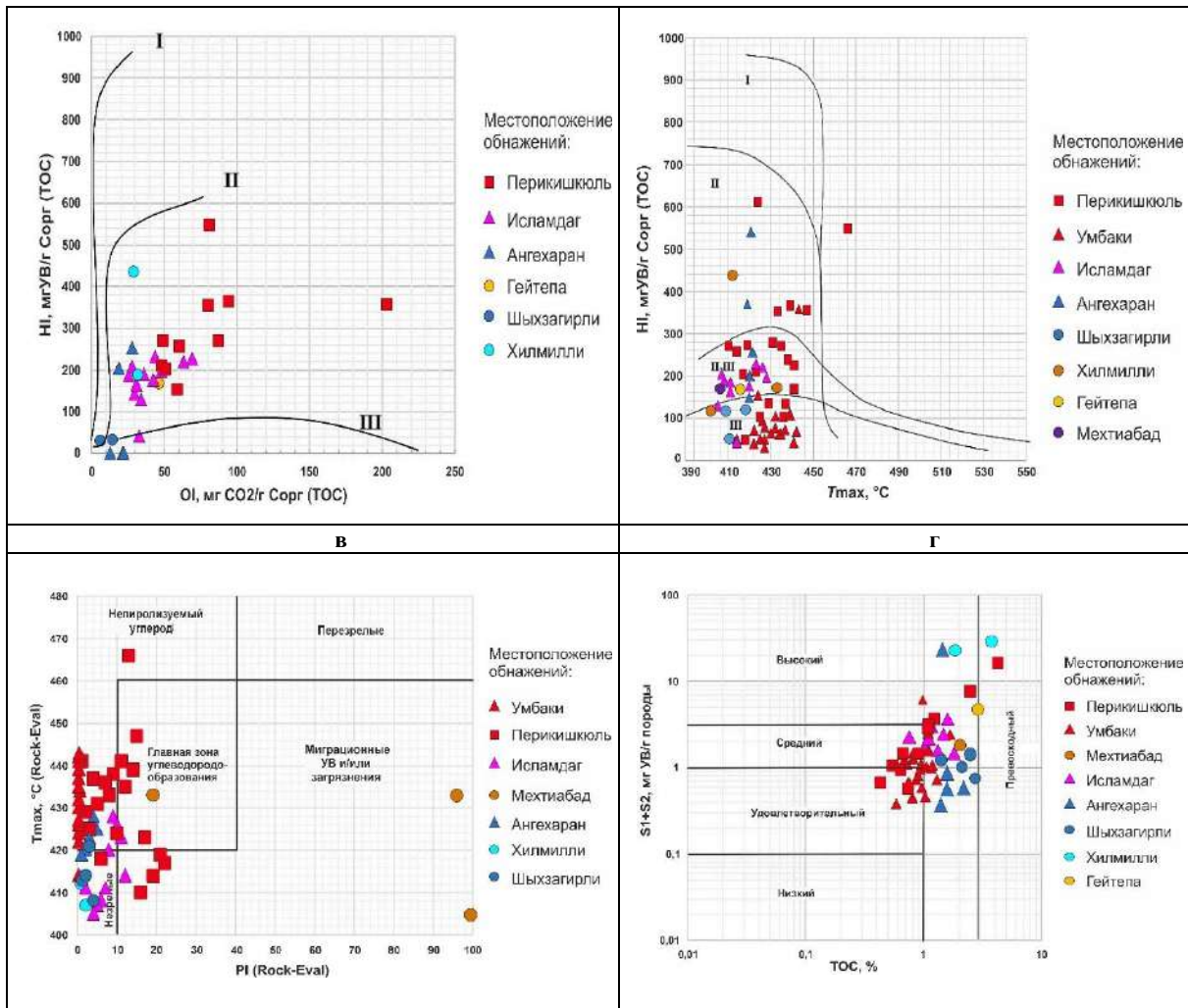
Рис. 6. Интерпретация результатов пиролитических исследований образцов майкопской серии:
а – модифицированная диаграмма Ван Кревелена – зависимость водородного индекса HI от кислородного индекса OI; б – зависимость водородного индекса HI от максимальной температуры пиролиза T_{max}; в – диаграмма соотношения максимальной температуры   пиролиза T_{max} и индекса продуктивности PI; г – диаграмма соотношения генерационного потенциала материнской породы и общего содержания органического углерода $C_{орг}$

Полученные результаты подтверждают сделанное ранее предположение (Керимов и др., 1990) о различиях в преобразованности ОВ, которые влияют на формирование пористой структуры в породах, появление и распространение керогеновой пористости. Изменение структуры керогена в процессе катагенетического созревания происходит в контактовых участках (Керимов и др., 2023). В связи с катагенетическим расходом ОВ на образование УВ и неуглеводородных продуктов происходит снижение массы органического вещества в процессе катагенеза, и на каждом этапе преобразования имеют место остаточные концентрации. В плотном незрелом керогене начинают образовываться **органические поры («керогеновая пористость»)** (рис. 10, 11), которые к концу главной фазы нефтеобразования формируют связанную систему, обеспечивающую пространство для вновь образуемых нефтяных УВ.

Примером «органической пористости» являются нанометрические поры в низкопроницаемых глинистых сланцевых толщах. Диаметр этих пор обычно составляет менее 1 мкм. Размеры нанометровых пор в керогене в основном варьируются от 80 до 100 нм (Прищепа, Аверьянова, 2013; Сенин и др., 2022; Лебедев и др., 2016).

«Органическая пористость», или пористость в текстуре керогена, формирующаяся в процессе термического созревания ОВ породы, способна влиять на адсорбцию образующейся нефти пористой поверхностью керогена. Результаты проведенных исследований «органической пористости» позволяют считать, что органические поры в текстуре керогена существенно сказываются на пространстве новообразованных резервуаров в толще нефтематеринских пород.
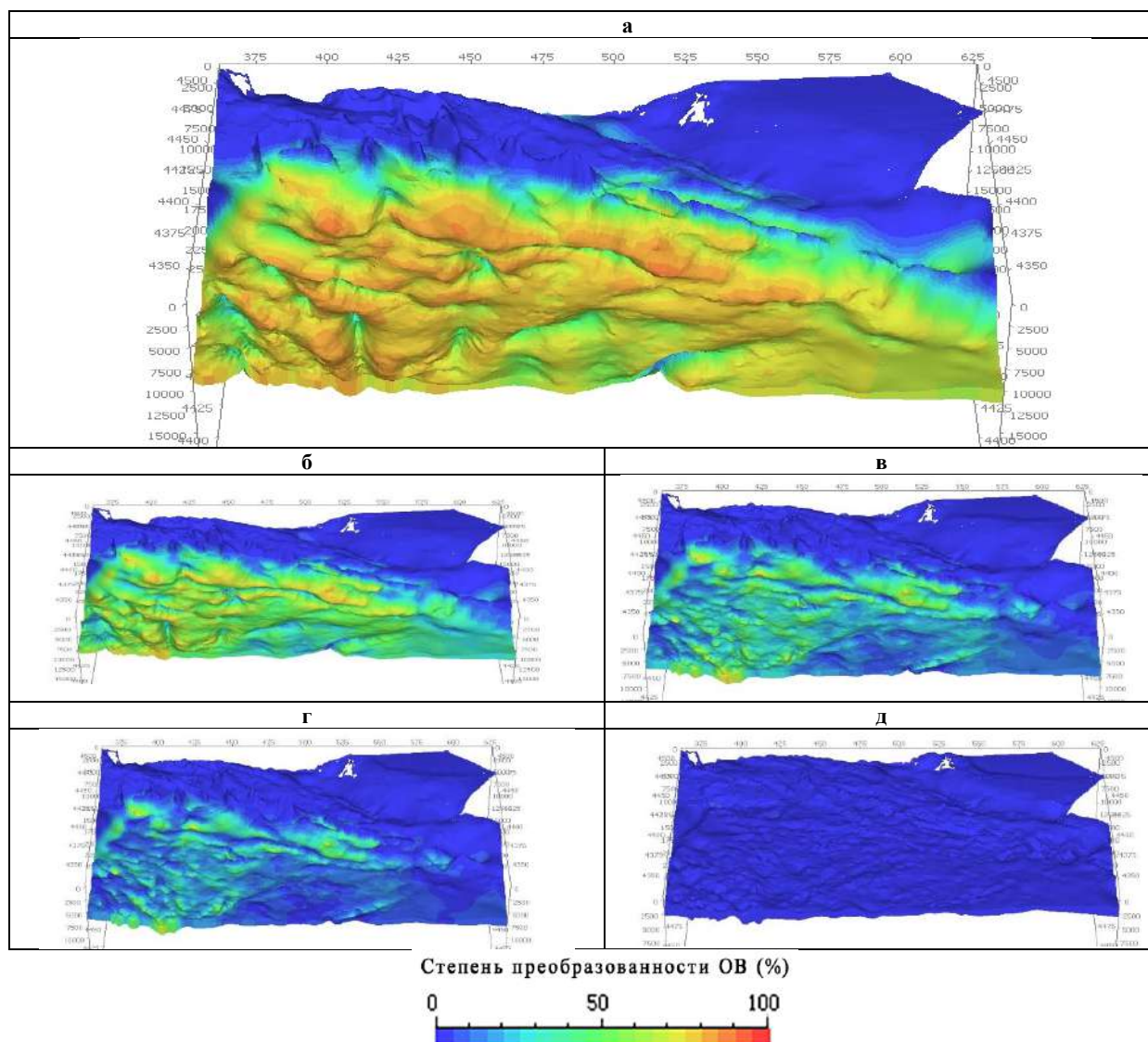
Рис. 7. 3D-реконструкция процесса катагенетической эволюции майкопских отложений Южно-Каспийского бассейна:
а – к настоящему времени; б – к концу абшеронского времени (1.1 млн. лет); в – к концу акчагыльского времени (2 млн. лет);
г – к концу плиоценового (ПТ) времени (2.8 млн. лет); д – к концу диатомового времени (5.8 млн. лет)

Таким образом, можно считать, что органические поры в текстуре керогена вносят значительный вклад в пространство новообразованных резервуаров в толще продуктивных пород (Dolson, 2016; Inan et al., 1997; Katz et al., 2005; Malovitsky, 2000; Керимов и др., 2023; Керимов, 2023). Процесс адсорбции сгенерированных УВ приводит к увеличению концентрации вещества на границе раздела фаз. Модель адсорбции молекул УВ в органических порах показана на рис. 12.

Адсорбция УВ основывается на следующих принципах:

● *является локализованной (происходит на адсорбционных центрах), в данном случае адсорбция нефти и газа может происходить на поверхности органических пор в керогене;*

● *происходит не на всей поверхности адсорбента, а на активных центрах, которыми являются выступы либо впадины на поверхности адсорбента;*

● *каждый активный центр способен взаимодействовать только с одной молекулой адсорбента;*

● *процесс адсорбции находится в динамическом равновесии с процессом десорбции.*

Скопления УВ в низкопроницаемых глинистых и сланцевых нефтегазоматеринских толщах формируются в процессе аккумуляции УВ за счет процессов сорбции отгенерированных УВ как керогеном, так и незрелыми продуктами его преобразования – асфальтенами, тяжелыми (спиртобензольными) смолами (Прищепа, Аверьянова, 2013).
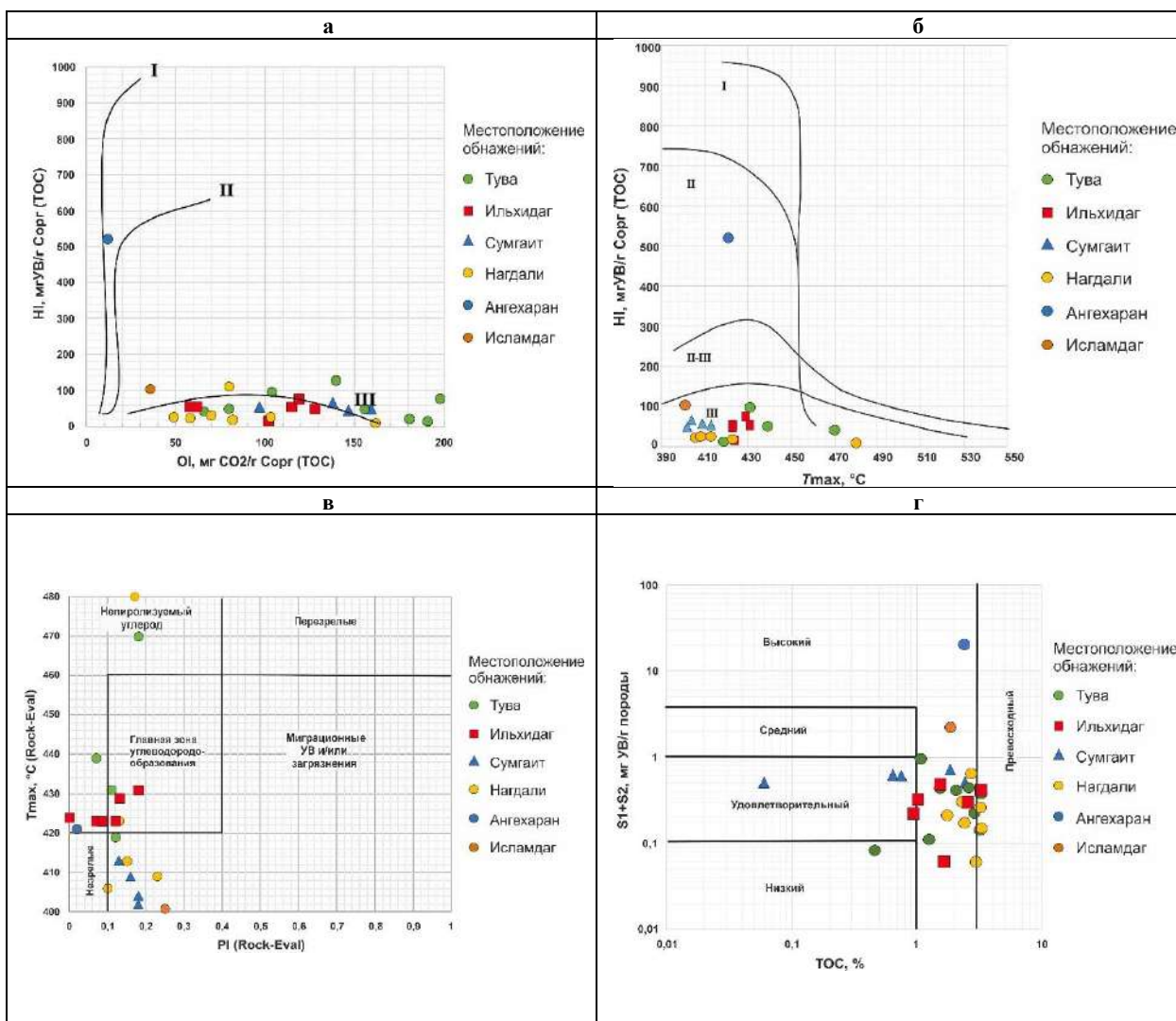
Рис. 8. Интерпретация результатов пиролитических исследований образцов палеоцен-эоценового комплекса из обнажений: а – модифицированная диаграмма Ван Кревелена – зависимость водородного индекса HI от кислородного индекса OI; б – зависимость водородного индекса HI от максимальной температуры пиролиза T$_{max}$; в – диаграмма соотношения максимальной температуры пиролиза T$_{max}$ и индекса продуктивности PI; г – диаграмма соотношения генерационного потенциала материнской породы и общего содержания органического углерода C$_{орг}$

Важной отличительной чертой скоплений УВ в таких толщах является то, что газ и нефть находятся в преимущественно связанном, сорбированном, растворенном, диффузно-рассеянном состоянии в керогене и продуктах преобразования керогена – начальных, наиболее незрелых продуктах сингенетичной нефти (асфальтенах, смолах, твердых парафинах), изначально рождающейся в объеме керогена в процессе его химического (каталитического, термического, радиационного и т. д.) преобразования. На адсорбцию сгенерированных УВ активно влияет «органическая пористость» пористой поверхности керогена. Процесс адсорбции приводит к увеличению концентрации вещества на границе раздела фаз. Адсорбция происходит из жидкой или газовой фазы на границе раздела газ – твердое, жидкость – твердое, газ – жидкость, жидкость – жидкость (Сенин и др., 2022).

Скопления в сланцевых толщах имеют некоторые общие черты. С одной стороны, это высококачественные достаточно зрелые материнские породы, содержащие УВ, которые можно добыть, с другой – это достаточно хрупкие отложения, позволяющие провести гидроразрыв пласта и получить хорошие притоки в скважинах.

Однако у каждого сланцевого скопления есть свои особенности, которые необходимо учитывать в процессе разработки, чтобы обеспечить эффективную добычу. К основным критериям скрининга сланцевых скоплений относятся: содержание органического углерода, зрелость НГМТ (отражательная способность витринита), мощность толщи, количество свободных УВ, количество адсорбированных УВ (Inan et al., 1997; Katz et al., 2005; Malovitsky, 2000).
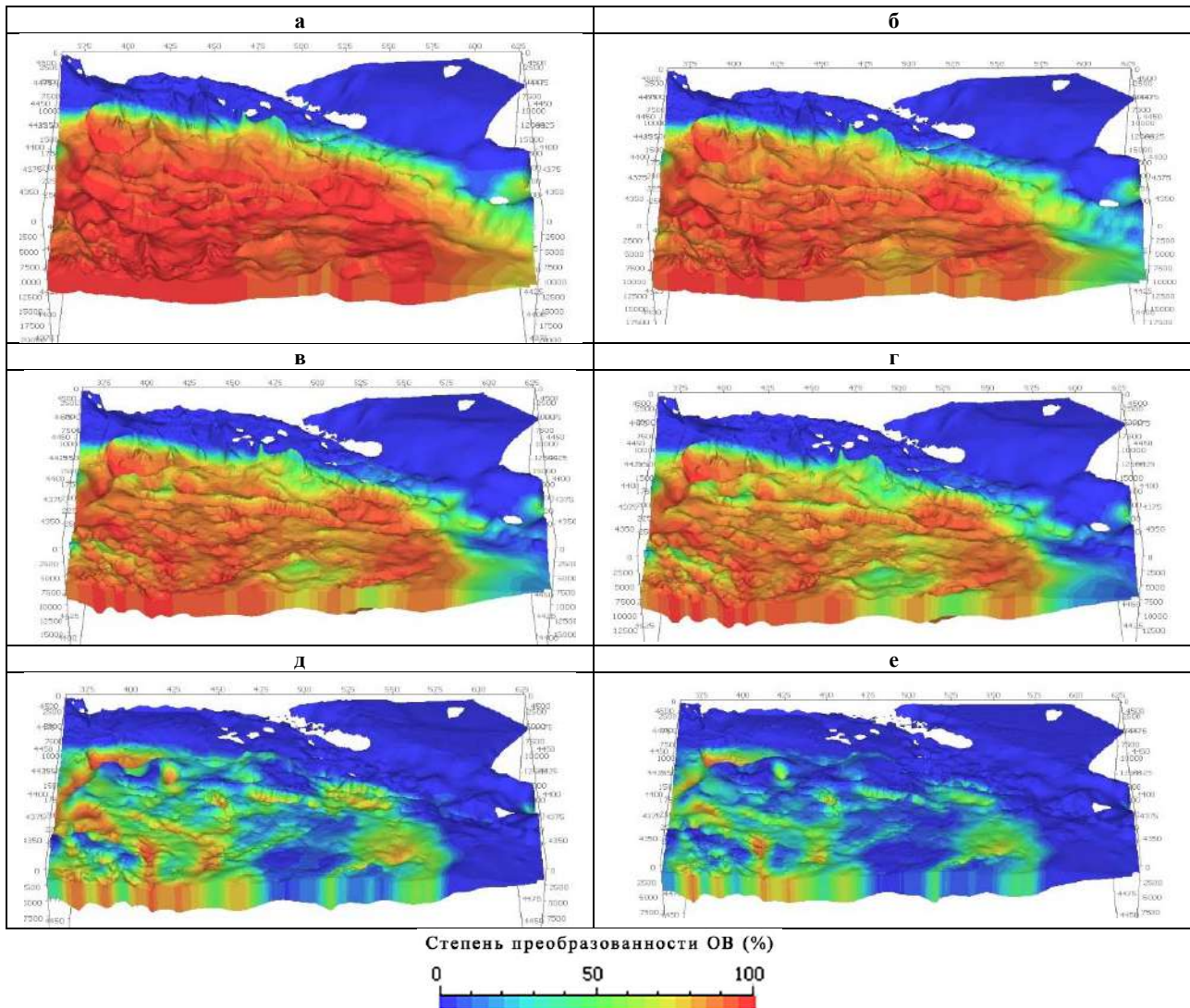
Рис. 9. 3D-реконструкция процесса катагенетической эволюции эоценовых отложений:
а – к настоящему времени; б – к концу абшеронского времени (1.1 млн. лет); в – к концу акчагыльского
времени (2 млн. лет); г – к концу плиоцена (ПТ) (2.8 млн. лет); д – к концу диатомового времени (5.8 млн.
лет); е – к концу майкопского времени (17 млн. лет)

Более расширенный список параметров включает: проницаемость, поровое давление (предпочтительно повышенное), хрупкость (предпочтительно высокая), минералогический состав (предпочтительно присутствие значительного количества кварца или карбонатов), непроницаемые породы выше и ниже НГМТ (для удержания гидравлической трещиноватости), естественную трещиноватость, пластовую температуру (предпочтительно выше 110°C), простое наклонное залегание толщи (таблица 1). Для выявления наиболее продуктивных областей формируются карты по каждому критерию, а области перекрытия по максимальному их количеству указывают на Sweet Spots – это области в пределах сланцевой толщи, геологические условия которых могут обеспечить

наиболее продуктивную и стабильную (длительную) работу скважин.

Карты строят на основании скважинных и других геолого-геофизических и геохимических данных с привлечением результатов численного моделирования. Выделение и оценка перспектив сланцевых скоплений на региональном уровне базируются в значительной степени на результатах численного моделирования с последующей калибровкой полученной модели (Керимов и др., 2016; Керимов и др., 2014; Lapidus et al., 2018; Керимов и др., 2017; Mustaev et al., 2023; Ottman, Bohacs, 2014; Гулиев, 2018; Гулиев и др. 1991; Abrams,1997; Aghayeva et al., 2021; Sondergeld et al., 2010; Фейзуллаев и др., 2022; Лисицын, 1988; 2009; Ализаде и др., 2018).
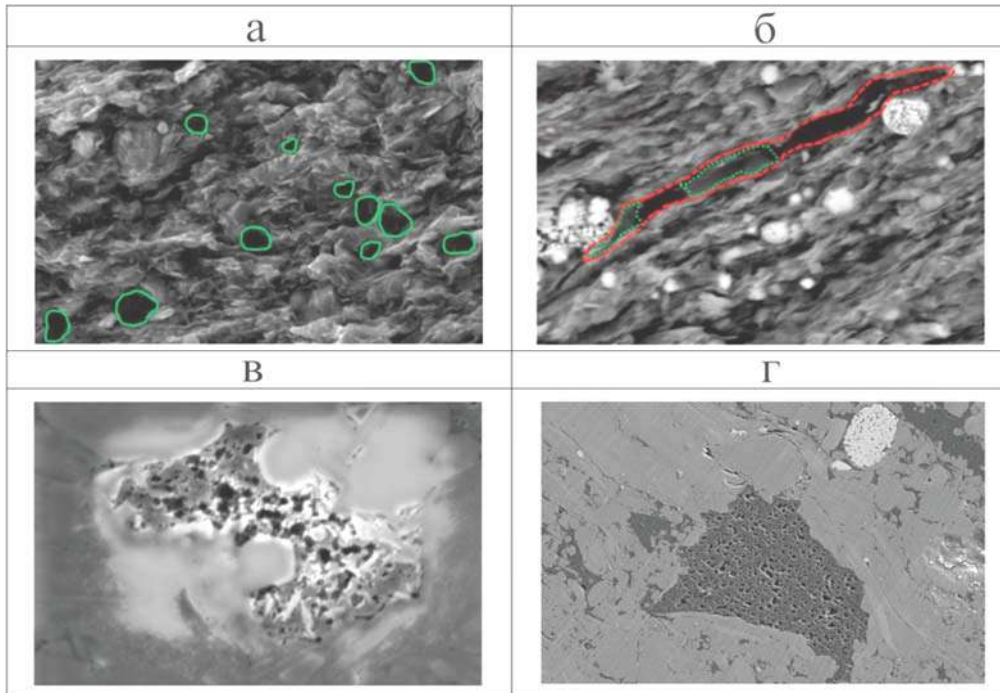
Рис. 10. Органические поры:
а – изометрические в глинистой массе породы, заполненные УВ; б – щелевидные, частично заполненные УВ; в, г – органическая поверхностная пористость в толще Longmaxi Shale на юго-востоке Чунцина (Китай) с порами разного диаметра в двух SEM-изображениях в среднем составляет 30.19% (Алиева и др., 2019)
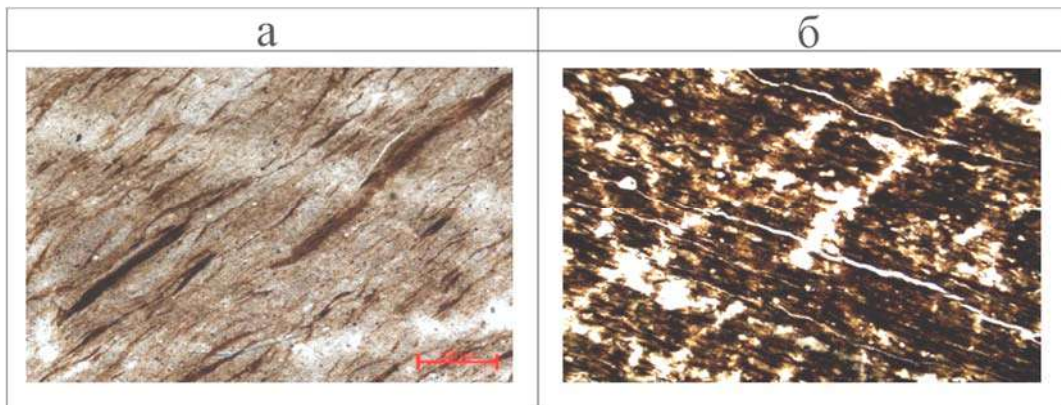
Рис. 11. Следы ОВ в порах и соединениях сланцевых толщ в нижнем миоцене из обнажения Джангидаг (а) и в среднем эоцене из выбросов грязевого вулкана Шыхзегирли (б) (по материалам Аббасова, 2022)
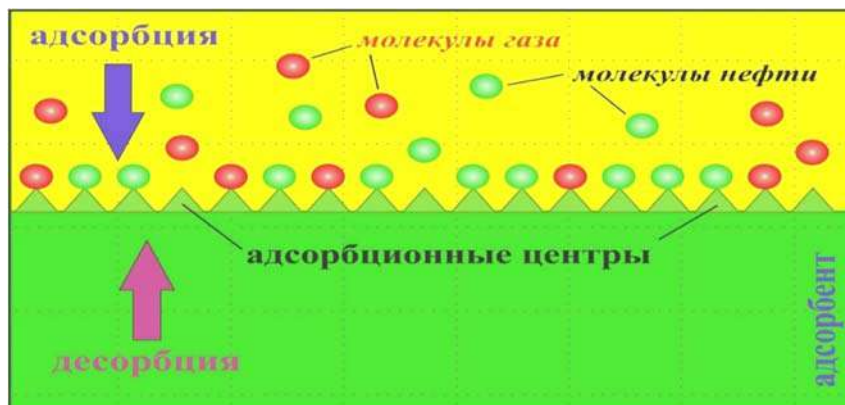
Рис. 12. Модель адсорбции молекул УВ в органических порах

Таблица 1

Критерии оценки перспектив нефтегазоносности сланцевых скоплений УВ
(по данным Dolson, 2016 со ссылкой на Sondergeld et al., 2010)

Критерий оценки	Предпочтительное значение	Источник данных
Зрелость ОВ	> 1.4 – для сланцевого газа, > 1.0 – для сланцевой нефти	Любые палеотермометры
Содержание углерода, %	> 2	Rock Eval
Тип керогена	Нефтепроизводящий	Геохимические данные
Мощность толщи	> 30 м, но может варьировать в зависимости от экономики	ГИС, сейсмические данные
Глубина залегания	Наименьшая глубина, поздней газогенерации для поиска сланцевого газа или поздней генерации нефти для поиска сланцевой нефти	Моделирование ГАУС
Давление, МПа	> 3.5	ГИС
Пластовая температура, °C	> 110	ГИС, моделирование
Флюидоупоры	Наличие непроницаемых пластичных барьеров ниже и выше сланцевой толщи	Керн, каротаж
Количество сорбированных и свободных УВ в породе	Зависит от экономических критериев	Моделирование
Трещиноватость	Вертикальная и горизонтальная, открытые трещины	Региональное картирование, ГИС, геомеханическое моделирование
Структурное строение	Простое наклонное залегание толщи, отсутствие разломов	Сейсмические данные, структурное картирование
Фациальная изменчивость породы	Чем меньше, тем лучше	Межскважинная корреляция
Минералогия (для оценки хрупкости)	> 40 % кварца или карбонатов	Исследование керна, ГИС
Модуль Юнга, коэффициент Пуассона	> 3.0 и < 0.25, соответственно	Исследование керна
Проницаемость, нД	> 100	Капиллярное давление, ГИС
Водонасыщение, %	< 40	ГИС (сопротивление)
Состав газа	Низкое содержание CO_2 и H_2S, наличие газа в порах более 2 %, высокое API для сланцевой нефти	ГИС, моделирование, расход бурового раствора

Заключение

Проведенные исследования свидетельствуют о сланцевой природе диатомовой свиты, майкопской серии, эоценовых отложений Южно-Каспийской впадины. Сланцевые НГМТ являются гибридными феноменами, которые не только генерируют, но и аккумулируют УВ и образуют углеводородные системы. Такие системы называют **«сланцевые нефтегазовые системы»** ("shale-source oil system" и "shale-source gas system".) Границы такой системы совпадают с границами зрелой НГМТ, которая одновременно является и резервуаром. В Южно-Каспийском бассейне сформировались сланцевые нефтегазовые системы: *диатомовая сланцевая нефтегазовая система, олигоцен-миоценовая сланцевая нефтегазовая система и эоценовая сланцевая нефтегазовая система,* которые являются комбинированными нетрадиционными нефтегазовыми системами с УВ, частично эмигрировавшими из НГМТ и частично сохраненными (невытесненными).

ЛИТЕРАТУРА

Аббасов О.Р., Алиев А.А., Агаев А.М., Худузаде А., Хасанов Е. Минералогия, геохимия и особенности палеовыветривания горючих сланцев палеоген миоценовых отложений Азербайджана. SOCAR Proceedings, No. 1, 2022, с. 24-36. DOI:10.5510/OGP20220100625.
Алиев Ад.А., Гулиев И.С., Дадашев Ф.Г., Рахманов Р.Р. Атлас грязевых вулканов мира. Nafta-Press. Баку, 2015, 323 с.

REFERENCES

Abbasov O.R., Aliyev A.A., Agayev A.M., Khuduzade A.İ., Hasanov E. Mineralogy, geochemistry and features of paleoweathering of oil shale of Paleogene-Miocene deposits of Azerbaijanş. SOCAR Proceedings. 2022, pp. 24-36, DOI:10.5510/OGP20220100625 (in Russian).
Abrams M.A., Narimanov A.A. Geochemical evaluation of hydrocarbons and their potential sources in the western South

Алиева С.А., Авербух Б.М., Серикова У.С., Мустаев Р.Н. Геология и нефтегазоносность Каспийской впадины. ИНФРА-М. Москва, 2019, 486 с.

Ализаде А.А., Гулиев И.С., Мамедов П.З. Продуктивная толща Азербайджана: монография в 2-х т. Недра. Москва, Т. I, 2018, 305 с.

Ализаде А.А., Гулиев И.С., Мамедов П.З. Продуктивная толща Азербайджана: монография в 2-х т. Т.II. Недра. Москва, 2018, 236 с.

Обсуждение книги Ш.Ф. Мехтиева "Вопросы происхождения нефти и формирования нефтяных залежей Азербайджана". Изв. АН Аз. ССР, No. 6, 1957, с. 215-228.

Багирзаде Ф.М., Нариманов А.А., Бабаев Ф.Р. Геолого-геохимические особенности месторождений Каспийского моря. Недра. Москва, 1988, 206 с.

Гаджиев А.Н. Палеогеографическая обстановка доплиоценового времени и роль Палео-Волги в формировании осадочных бассейнов Восточного Паратетиса. В кн.: Структура и нефтегазоносность впадин внутренних морей. Москва, ИГиРГИ, 1989, с. 65-69.

Галимов Э.М. Изотопы углерода в нефтегазовой геологии. Недра. Москва, 1973, 384 с.

Глумов И.Ф., Маловицкий Я.П., Новиков А.А., Сенин Б.В. Региональная геология и нефтегазоносность Каспийского моря. ООО «Недра-Бизнесцентр». Москва, 2004, 342 с.

Гулиев И.С., Кляцко Н.В., Мамедова С.А., Сулейманова С.Ф. Нефтегазопродуцирующие и коллекторские свойства отложений Южно-Каспийской впадины. Литология и полезные ископаемые, No. 2, 1992, с. 110.

Гулиев И.С., Сулейманова С.Ф., Кляцко Н.В. Прогноз коллекторских свойств пород осадочного чехла Южно-Каспийской впадины. Советская геология, No.7, 1991, с.7-15.

Гулиев И.С., Левин Л.Э., Федоров Д.Л. Углеводородный потенциал Каспийского региона (системный анализ). Nafta-Press. Москва-Баку, 2003, 127 с.

Гулиев И.С., Фейзуллаев А.А. Зональность углеводообразования и ресурсы нефти и газа в Южно-Каспийской впадине. АНХ, No.4, 1996, с. 6-8.

Гулиев И.С., Мустаев Р.Н., Керимов В.Ю., Юдин М.Н. Дегазация Земли: масштабы и последствия. Горный журнал, No. 11, 2018, pp. 38-42, DOI:10.17580/gzh.2018.11.06.

Дахнова М.В., Можегова С.В., Назарова Е.С., Пайзанская И.Л. Оценка запасов «сланцевой нефти» с использованием геохимических параметров. Геология нефти и газа, No. 4, 2015, с. 55-61.

Калмыков А.Г., Карпов Ю.А., Топчий М.С. Влияние катагенетической зрелости на формирование коллекторов с органической пористостью в баженовской свите и особенности их распространения. Георесурсы, Т. 21, No. 2, 2019, с. 159-171.

Керимов В.Ю., Авербух Б.М., Мильничук В.С. Тектоника северного Каспия и перспективы нефтегазоносности. Советская геология, No. 7, 1990, с. 23-30.

Керимов В.Ю., Бондарев А.В., Мустаев Р.Н., Хоштария В.Н. Оценка геологических рисков при поисках и разведке месторождений углеводородов. Нефтяное хозяйство, No.8, 2017, с. 36-41, DOI:10.24887/0028-2448-2017-8-36-41.

Керимов В.Ю., Сенин Б.В., Серикова У.С., Мустаев Р.Н., Романов П.А. Оценка условий формирования и распределения ловушек и залежей углеводородов в черноморско-каспийском регионе. ANAS Transactions, Earth Sciences. No. 1, 2023, с. 81-99, DOI:10.33677/ggianas20230100096.

Керимов В.Ю., Серикова У.С. Основатель современного Азербайджанского государства Гейдар Алиев – автор концепции о нефтяной стратегии Азербайджана. ANAS Transactions, Earth Sciences, Special Issue, 2023, p. 18-21, DOI: 10.33677/ggianasconf20230300004.

Caspian depression, Republic of Azerbaijan. Marine and Petroleum Geology, Vol. 14 (4), 1997, pp. 451-468, DOI:10.1016/s0264-8172(97)00011-1.

Aghayeva V., Sachsenhofer R.F., Van Baak C.G.C. et al. New geochemical insights into cenozoic source rocks in Azerbaijan: implications for petroleum systems in the South Caspian region. Journal of Petroleum Geology, July 2021, Vol. 44 (3), pp. 349-384, DOI:org/10.1111/ipg.12797.

Aliev Ad.A., Guliev I.S., Dadashev F.G., Rakhmanov R.R. Atlas of mud volcanoes of the world. Nafta-Press. Baku, 2015, 323 p. (in Russian).

Alieva S.A., Averbukh B.M., Serikova U.S., Mustaev R.N. Geology and oil and gas potential of the Caspian Basin. INFRA-M. Moscow, 2019, 486 p. (in Russian).

Alizadeh A.A., Guliev I.S., Mamedov P.Z. Productive strata of Azerbaijan. Monograph in 2 volumes. Nedra. Moscow, Vol. I., 2018, 305 p. (in Russian).

Alizadeh A.A., Guliev I.S., Mamedov P.Z. Productive strata of Azerbaijan: Monograph in 2 volumes. Nedra. Moscow, Vol. II, 2018, 236 p. (in Russian).

Discussion of Sh.F.Mehdiyev's book "Issues of oil origin and formation of oil deposits of Azerbaijan." Izv. AN Az. SSR, No. 6, 1957, pp. 215-228 (in Russian).

Bagirzadeh F.M., Narimanov A.A., Babaev F.R. Geological and geochemical features of the fields of the Caspian Sea. Nedra. Moscow, 1988, 206 p. (in Russian).

Beckwith R. The Tantalizing Promise Of Oil Shale. JPT/JPT Online, January 2012.

Dakhnova M.V., Mozhegova S.V., Nazarova E.S., Paizanskaya I.L. Estimation of "shale oil" reserves using geochemical parameters. Geologia nefti i gaza, No. 4, 2015, pp. 55-61 (in Russian).

Dolson J. Understanding oil and gas shows and seals in the search for hydrocarbons. Springer International Publishing, Switzerland, 2016, 486 p.

Feyzullayev A.A., Huseynov D.A., Rashidov T.M. Isotopic composition of the products of the mud volcanoes activity in the South-Caspian basin in connection with petroleum potential of the deeply buried sediments. ANAS Transactions. Earth Sciences, No. 1, 2022, pp. 68-80, DOI: 10.33677/ggianas20220100073 (in Russian).

Gadzhiev A.N. Paleogeographical environment of the pre-Pliocene time and the role of the Paleo-Volga in the formation of sedimentary basins of the Eastern Paratethys. In the book: Structure and oil and gas content of the depressions of inland seas. IGiRGI, Moscow, 1989, pp. 65-69 (in Russian).

Galimov E.M. Carbon isotopes in oil and gas geology Nedra. Moscow, 1973, 384 p. (in Russian).

Glumov I.F., Malovitsky Ya.P., Novikov A.A., Senin B.V. Regional geology and oil and gas potential of the Caspian Sea. «Nedra-Business Center» LLC, Moscow, 2004, 342 p. (in Russian).

Guliev I.S., Feizullaev A.A. Zoning of oil and gas formation and oil and gas resources in the South Caspian depression. Azerbaijan Oil Economy, No. 4, 1996, pp. 6-8 (in Russian).

Guliev I.S., Klyatsko N.V., Mamedova S.A., Suleymanova S.F. Oil and gas producing and reservoir properties of sediments of the South Caspian basin. Litologia i poleznye iskopajemye, No. 2, 1992, pp. 110 (in Russian).

Guliev I.S., Levin L.E., Fedorov D.L. Hydrocarbon potential of the Caspian region (system analysis). Nafta-Press. Baku, 2003, 127 p. (in Russian).

Guliev I.S., Mustaev R.N., Kerimov V.Y., Yudin M.N. Degassing of the earth: Scale and implications. Gornyi Zhurnal, No. 11, 2018, pp. 38-42, DOI:10.17580/gzh.2018.11.06 (in Russian).

Guliev I.S., Suleymanova S.F., Klyatsko N.A. Rocks reservoir properties prediction for sedimentary cover of the South Caspian depression Sovetskaya Geologia, No. 7, 1991, pp. 7-15 (in Russian).

Керимов В.Ю., Шилов Г.Я., Мустаев Р.Н., Дмитриевский С.С. Термобарические условия формирования скоплений углеводородов в сланцевых низкопроницаемых коллекторах хадумской свиты Предкавказья, Нефтяное хозяйство, No. 2, 2016, с. 8-11.

Лебедев Л.И., Алексина И.А., Кулакова Л.С. Каспийское море: геология и нефтегазоносность. Наука. Москва, 1987, 296 с.

Лебедев С.А., Костяной А.Г. и др. Система Каспийского моря. Российская академия наук, Институт океанологии им. П.П. Ширшова. Научный мир. Москва, Т. 1, 2016, 479 с.

Левин Л.Э., Сенин Б.В. Глубинное строение и динамика осадочных бассейнов в Каспийском регионе. ДАН, Т. 338, No. 2, 2003, с. 216-219.

Левин Л.Э., Федоров Д.Л. Среднекаспийский и Южно-Каспийский бассейны: геолого-геофизические параметры нефтегазоносных систем и распределение потенциальных ресурсов углеводородов. В кн.: Современные проблемы геологии нефти и газа, Научный мир. Москва, 2001, с. 278-286.

Леонов Ю.Г., Волож Ю.А., Антипов М.П. Консолидированная кора Каспийского региона: опыт районирования. ГЕОС. Москва, 2010, 64 с.

Лисицын А.П. Закономерности осадкообразования в областях быстрого и сверхбыстрого осадконакопления (лавинной седиментации) в связи с образованием нефти и газа в Мировом океане. Геология и геофизика, Т. 50, No. 4, 2009, с. 373-400.

Лисицын А.П. Лавинная седиментация и перерывы в осадкообразовании в морях и океанах. Наука. Москва, 1988, 310 с.

Мамедов П.З. Современная архитектура Южно-Каспийского мегабассейна – результат многоэтапной эволюции литосферы в центральном сегменте Альпийско-Гималайского подвижного пояса. Известия НАНА, Науки о Земле, No. 4, 2010, с. 46-72.

Мехтиев Ш.Ф. Вопросы происхождения нефти и формирования нефтяных залежей Азербайджана. Изд-во АН Аз. ССР, Баку, 1956, 319 с.

Мехтиев Ш.Ф. Процессы формирования и преобразования состава нефти и газа в природе. Элм. Баку, 1985, 144 с.

Керимов В.Ю. Осипов А.В., Мустаев Р.Н., Монакова А.С. Моделирование углеводородных систем в регионах со сложным геологическим строением. Геомодель – 2014. Россия, г. Геленджик, 08-11 сентября 2014, DOI:10.3997/2214-4609.20142245.

Прищепа О.М., Аверьянова О.Ю. К обсуждению понятийной базы нетрадиционных источников нефти и газа – сланцевых толщ. Нефтегазовая геология. Теория и практика. Т. 8, No. 3, 2013, с.11.

Сенин Б.В., Керимов В.Ю., Мустаев Р.Н., Леончик М.И. Структурно-геодинамические системы фундамента Черноморско-Каспийского региона и их эволюция в позднем палеозое-кайнозое. Геотектоника, No. 1, 2022, с. 27-50.

Фейзуллаев А.А., Гусейнов Д.А., Рашидов Т.М. Изотопный состав продуктов деятельности грязевых вулканов Южно-Каспийского бассейна в связи с нефтегазоносностью глубокопогруженных отложений. ANAS Transactions, Earth Sciences. No.1, 2022, с. 68-80, DOI: 10.33677/ggianas20220100073.

Якуцени С.П. Влияние геоструктурных и литофациальных особенностей нефтегазоносного бассейна на масштабы накопления потенциально токсичных элементов в углеводородах. Вестник Санкт-Петербургского университета. Серия 7. Геология. География. No. 4, 2009, с. 58-63.

Abrams M.A., Narimanov A. A. Geochemical evaluation of hydrocarbons and their potential sources in the western South Caspian depression, Republic of Azerbaijan. Marine and Petroleum

Inan U.S., Barrington-Leigh C., Hansen S. et al. Rapid lateral expansion of optical luminosity in lightning-induced ionospheric flashes referred to as 'elves'. Geophys. Res. Lett., No. 24 (5), 1997, pp. 583-586.

Kalmykov A.G., Karpov Yu.A., Topchiy M.S. The influence of catagenetic maturity on the formation of reservoirs with organic porosity in the Bazhenov formation and the features of their distribution. Georesursy, Vol. 21, No. 2, 2019, pp. 159-171, https://doi.org/10.18599/grs.2019.2.159-171 (in Russian).

Katz M.E., Wright J.D., Miller K.G. et al. Biological overprint of the geological carbon cycle. Marine Geology, No. 217, 2005, pp. 323-338.

Kerimov V.Y., Bondarev A.V., Mustaev R.N. Estimation of geological risks in searching and exploration of hydrocarbon deposits. Neftyanoe Khozyaystvo, No. 8, 2017, pp. 36-41, DOI:10.24887/0028-2448-2017-8-36-41 (in Russian).
Kerimov V.Y., Osipov A.V., Mustaev R.N., Monakova A.S. Modeling of petroleum systems in regions with complex geological structure. 16th Science and Applied Research Conference on Oil and Gas Geological Exploration and Development, GEOMODEL, 2014, DOI:10.24887/0028-2448-2017-8-36-41, (in Russian).

Kerimov V.Yu., Averbukh B.M., Milnichuk V.S. Tectonics of the northern Caspian Sea and oil and gas potential. Otechestvennaya geologiya, No. 7, 1990, p. 23-30 (in Russian).

Kerimov V.Yu., Senin B.V., Serikova U.S., Mustaev R.N., Romanov P.A. Assessment of the conditions of formation and distribution of structural, lithological, stratigraphic and combined traps in the Black Sea – Caspian region. ANAS Transactions. Earth Sciences, No. 1, 2023, pp. 81-99, (in Russian), DOI:10.33677/ggianas20230100096.

Kerimov V.Yu., Serikova U.S. ANAS Transactions, Earth Sciences, Special Issue, 2023, pp. 18-21, DOI: 10.33677/ggianas-conf 20230300004 (in Russian).

Kerimov V.Yu., Shilov G.Ya., Mustayev R.N., Dmitrievskiy S.S. Thermobaric conditions of hydrocarbons accumulations formation in the low-permeability oil reservoirs of khadum suite of the Pre-Caucasus. Neftyanoe Khozyaystvo, No. 2, 2016, pp. 8-11, (in Russian).

Lapidus A.L., Kerimov V.Y., Mustaev R.N. et al. Natural Bitumens: Physicochemical properties and production technologies. Solid Fuel Chemistry, No. 52 (6), 2018, pp. 344-355, DOI:10.3103/S0361521918060071.

Lebedev L.I., Aleksina I.A., Kulakova L.S. Caspian Sea: geology and oil and gas potential. Nauka. Moscow, 1987, 296 p. (in Russian).

Lebedev S.A., Kostyanoy A.G. et al. Caspian Sea system. Russian Academy of Sciences, Institute of Oceanology named after P.P.Shirshova. Scientific world. Moscow, Т. 1, 2016, 479 p. (in Russian).

Leonov Yu.G., Volozh Yu.A., Antipov M.P. Consolidated crust of the Caspian region: experience of zoning. GEOS. Moscow, 2010, 64 p. (in Russian).

Levin L.E., Fedorov D.L. Middle Caspian and South Caspian basins: geological and geophysical parameters of oil and gas bearing systems and distribution of potential hydrocarbon resources. Modern problems of oil and gas geology. Nauchny mir. Moscow, 2001, pp. 278-286 (in Russian).

Levin L.E., Senin B.V. Deep structure and dynamics of sedimentary basins in the Caspian region. DAN, Vol. 338, No. 2, 2003, pp. 216-219 (in Russian).

Lisitsyn A.P. Avalanche sedimentation and breaks in sedimentation in the seas and oceans. Nauka. Moscow, 1988, 310 p.

Lisitsyn A.P. Patterns of sedimentation in areas of rapid and ultrafast sedimentation (avalanche sedimentation) in connection with the formation of oil and gas in the World Ocean.

Geology, Vol. 14 (4), 1997, 451-468, DOI:10.1016/s0264-8172(97)00011-1.

Aghayeva V., Sachsenhofer R.F., Van Baak C.G.C. et al. New geochemical insights into cenozoicsource rocks in Azerbaijan: implications for petroleum systems in the South Caspian region. Journal of Petroleum GeologyVol. 44 (3), July 2021, pp. 349-384.

Beckwith R. The Tantalizing Promise of Oil Shale, JPT/JPT Online, January 2012.

Dolson J. Understanding Oil and Gas Shows and Seals in the Search for Hydrocarbons. Springer International Publishing. Switzerland, 2016, 486 p.

Inan U.S., Barrington-Leigh C., Hansen S. et al. Rapid lateral expansion of optical luminosity in lightning-induced ionospheric flashes referred to as 'elves' Geophys. Res. Lett. Vol. 24(5), 1997, pp. 583-586.

Katz M.E., Wright J.D., Miller K.G. et al. Biological overprint of the geological carbon cycle. Marine Geology, Vol. 217, 2005, pp. 323-338.

Lapidus A.L., Kerimov V.Y., Mustaev R.N. et al. Natural Bitumens: Physicochemical Properties and Production Technologies. Solid Fuel Chemistry. Vol. 52(6), 2018, pp. 344-355, DOI:10.3103/S0361521918060071.

Mamedov P.Z. The modern architecture of the South Caspian megabasin as result of a multi-stage evolution of the lithosphere in the central segment of the Alpine-Himalayan mobile belt. Proceeding of Azerbaijan National Academy of Sciences. The Sciences of Earth, Vol. 4, 2010, pp. 46-72.

Malovitsky Ya.P., Senin B.V. Black Sea-Caspian Region Comparative Petroleum Geology of Deep-Water Basins of different Age. In: 62nd EAGE Conf. and Techn. Exhib. SECC, Glasgow. 29.05-02.06.2000. Extended Abst. Vol. 2, pp. 1-4.

Mustaev R.N., Kerimov V.Yu., Senin B.V., Lavrenova E.A. Structural-geodynamic and hydrocarbon systems in the Black Sea-Caspian region. ANAS Transactions, Earth Sciences, Special Issue, 2023, pp. 41-45.

Ottman J., Bohacs K. Conventional reservoirs hold keys to the 'Un's. AAPG Explorer. Feb., 2014.

Rachinsky M.Z., Kerimov V.Y. Fluid Dynamics of Oil and Gas Reservoirs. New Jersey: Wiley, 2015, 617 p., DOI: 10.1002/9781118999004. EDN XNGONX.

Sondergeld C.H., Newsham K.E., Comisky J.T. et al. Petrophysical Considerations in Evaluating and Producing Shale Gas Resources. Soc. Petrol. Engineers. SPE Unconventional Gas Conference, 23-25 February, Pittsburgh, Pennsylvania, USA, 2010, pp. 1-34, DOI:10.2118/131768-MS.

Gelogiya i Geofizika, Vol. 50, No. 4, 2009, pp. 373-400 (in Russian).

Malovitsky Ya.P., Senin B.V. Black Sea-Caspian Region Comparative Petroleum Geology of Deep-Water Basins of different Age. In: 62nd EAGE Conf. and Techn. Exhib. SECC., Glasgow. 29.05-02.06.2000. Extended Abst. Vol. 2, pp. 1-4.

Mamedov P.Z. The modern architecture of the South Caspian megabasin as result of a multi-stage evolution of the lithosphere in the central segment of the Alpine-Himalayan mobile belt. Proceeding of Azerbaijan National Academy of Sciences. The Sciences of Earth. Vol. 4, 2010, pp. 46-72.

Mehdiev Sh.F. Issues of the origin of oil and the formation of oil deposits in Azerbaijan. – Baku: Publishing House of the Academy of Sciences of Az. SSR, 1956, 319 p. (Rec.) (in Russian).

Mehdiev Sh.F. Processes of formation and transformation of the composition of oil and gas in nature. Elm. 1985, 144 p. (in Russian).

Mustaev R.N., Kerimov V.Yu., Senin B.V., Lavrenova E.A. Structural-geodynamic and hydrocarbon systems in the Black Sea-Caspian region. ANAS Transactions. Earth Sciences. – Special Issue. 2023, pp. 41-45.

Ottman J., Bohacs K. Conventional reservoirs hold keys to the 'Un's. AAPG Explorer. Feb., 2014.

Prishchepa O.M., Averyanova O.Yu. To discuss the conceptual basis of unconventional sources of oil and gas - shale strata. Neftegazovaya geologiya. Teoriya i praktika. Vol. 8, No. 3, 2013, p.11 (in Russian).

Rachinsky M.Z., Kerimov V.Y., Fluid Dynamics of Oil and Gas Reservoirs. New Jersey: Wiley, 2015, 617 p., DOI: 10.1002/9781118999004. EDN XNGONX.

Senin B.V., Kerimov V.Yu., Mustaev R.N., Leonchik M.I. Structural-geodynamic systems of the basement of the Black Sea-Caspian region and their evolution in the late Paleozoic-Cenozoic. Geotektonika, No. 1, 2022, pp. 27-50. (in Russian).

Sondergeld C.H., Newsham K.E., Comisky J.T. et al. Petrophysical Considerations in Evaluating and Producing Shale Gas Resources. Soc. Petrol. Engineers. SPE Unconventional Gas Conference, 23-25 February, Pittsburgh, Pennsylvania, USA. 2010, pp. 1-34.

Yakutseni S.P. The influence of geostructural and lithofacies features of an oil and gas basin on the scale of accumulation of potentially toxic elements in hydrocarbons. Bulletin of St. Petersburg University. Series 7. Geology. Geography, No. 4, 2009, pp. 58-63 (in Russian).

СЛАНЦЕВЫЕ НЕФТЕГАЗОВЫЕ СИСТЕМЫ ЮЖНО-КАСПИЙСКОЙ ВПАДИНЫ

Керимов В.Ю.[1,3], Гулиев И.С.[2], Джавадова А.С.[1], Мустаев Р.Н.[3], Гурбанов В.Ш.[1]

[1]*Министерство науки и образования Азербайджанской Республики,Институт нефти и газа, Азербайджан*
AZ1000, Баку, ул. Ф.Амирова, 9
[2]*Президиум Национальной академии наук Азербайджана, Азербайджан*
AZ1001, Баку, ул. Истиглалият, 30: i.s.guliyev@gmail.com
[3]*Российский государственный геологоразведочный университет имени Серго Орджоникидзе, Российская Федерация*
117997, Москва, ул. Миклухо-Маклая, 23: mustaevrn@mgri.ru

Резюме. В статье по результатам бассейнового моделирования описаны сланцевые нефтегазоносные системы Южно-Каспийской впадины. Выделение и оценка перспектив сланцевых скоплений на региональном уровне базируются в значительной степени на результатах численного моделирования с последующей калибровкой полученной модели.

В сланцевых толщах сконцентрированы наибольшие массы нефти, а органическое вещество (ОВ) присутствует там изначально, и нефть (легкие компоненты ОВ) эмигрирует из сланцев в соседние породы-коллекторы. Изменение структуры керогена в процессе катагенетического созревания происходит в контактовых участках. В плотном незрелом керогене начинают образовываться органические поры («керогеновая пористость»), которые к концу главной фазы нефтеобразования формируют связанную систему, обеспечивающую пространство для вновь образуемых нефтяных углеводородов. Органическая пористость, или пористость в текстуре керогена, формирующаяся в процессе термического созревания органического вещества

породы, способна влиять на адсорбцию образующейся нефти пористой поверхностью керогена. Результаты проведенных исследований органической пористости позволяют считать, что органические поры в текстуре керогена вносят значительный вклад в пространство новообразованных резервуаров в толще нефтематеринских пород. Сделаны выводы, что в Южно-Каспийском бассейне сформировались следующие сланцевые нефтегазовые системы: диатомовая сланцевая нефтегазовая система, олигоцен-миоценовая сланцевая нефтегазовая система и эоценовая сланцевая нефтегазовая система, которые являются комбинированными нетрадиционными нефтегазовыми системами с УВ, частично эмигрировавшими из нефтегазоматеринской толщи и частично сохраненными (невытесненными).

Ключевые слова: Южно-Каспийская впадина, сланцевые толщи, углеводородная система, кероген, катагенез, органическая пористость, адсорбция

CƏNUBİ XƏZƏR ÇÖKƏKLİYİNİN ŞİSTLİ NEFT-QAZ SİSTEMLƏRİ

Kərimov V.Y.[1,3], Quliyev İ.S.[2], Cavadova A.S.[1], Mustayev R.N.[3], Qurbanov V.Ş.[1], Hüseynova Ş.M.[1]

[1]Azərbaycan Respublikasının Elm və Təhsil Nazirliyi, Neft və Qaz İnstitutu, Azərbaycan
AZ1000, Bakı, F.Əmirov küç., 9
[2]Azərbaycan Milli Elmlər Akademiyasının Rəyasət Heyəti, Azərbaycan
AZ1001, Bakı ş., İstiqlaliyyət küç., 30: i.s.guliyev@gmail.com
[3]Serqo Orconikidze adına Rusiya Dövlət Geoloji Kəşfiyyat Universiteti, Rusiya Federasiyası
117997, Moskva, Mikluxo-Maklay küç., 23: r.mustaev@mail.ru

Xülasə. Məqalədə hövzə modelləşdirilməsi nəticələrinə əsasən Cənubi Xəzər çökəkliyinin şistli neft-qaz sistemləri təsvir edilir. Regional səviyyədə şistli karbohidrogen yığımlarının müəyyən edilməsi və perspektivlərinin qiymətləndirilməsinə, rəqəmsal modelləşdirmə və alınmış modelin kalibrlənməsi nəticələrinə əsaslanır.

Üzvi maddənin (ÜM) əvvəlcədən mövcud olduğu və neft (ÜM-nin yüngül komponentləri) şistlərdən qonşu kollektor süxurlarına emiqrasiya etdiyi məkanda ən böyük karbohidrogen yığımları şistli təbəqələrində cəmləşir. Kerogenin katagenetik yetişməsi prosesi zamanı onun strukturunun dəyişməsi təmas zonalarında baş verir. Sıx yetişməmiş kerogenin daxilində üzvi məsamələr ("kerogen məsaməliliyi") əmələ gəlməyə başlayır ki, bunlar neft əmələgəlmə prosesinin əsas mərhələsinin sonuna yeni yaranan neft karbohidrogenləri üçün məkan təmin edən əlaqəli sistem təşkil edir. Süxurlardakı üzvi maddənin termik yetişməsi zamanı əmələ gələn üzvi məsaməlilik və ya kerogenin teksturasındakı məsaməlilik, kerogenin səthi ilə əmələ gələn neftin adsorbsiyasına təsir edə bilir. Üzvi məsaməliliyin tədqiqatları nəticələri göstərir ki, kerogenin teksturasındakı üzvi məsamələr neft ana süxurlarında yeni əmələ gələn rezervuarların həcminə əhəmiyyətli töhfə verir.

Belə nəticəyə gəlmək olar ki, Cənubi Xəzər hövzəsində aşağıdakı şist neft-qaz sistemləri: diatomlu şist neft-qaz sistemi, oliqosen-miosen şist neft-qaz sistemi və qeyri-ənənəvi neft-qaz sistemlərini birləşdirən Eosen şist neft-qaz sistemi formalaşmışdır. Bu sistemlər neft-qaz ana süxur qatından qismən emiqrasiya etmiş və saxlanılmış (repressiya edilməmiş) üzvi maddələrlə mükəmməl birləşmiş qeyri-ənənəvi neft-qaz sistemləridir.

Açar sözlər: *Cənubi Xəzər çökəkliyi, şist təbəqələri, karbohidrogen sistemi, kerogen, katagenez, üzvi məsaməlilik, adsorbsiya*

IDENTIFICATION OF OIL FAMILIES IN HORIZONS XIII-XV OF UZEN AND KARAMANDYBAS FIELDS BY OIL FINGERPRINTING ANALYSIS

Seitkhaziyev Y.Sh.[1,2], DaumsharovA.A[1].

[1]*Atyrau Branch of LLP «KMG Engineering», Atyrau, Kazakhstan
Building 10, pr. Elorda, md. Nursaya, Atyrau, Atyrau region,
Republic of Kazakhstan, 060097: esimhan89-89@mail.ru*
[2]*«Oilgasscientificresearchproject» Institute, SOCAR, Baku, Azerbaijan
88A, Zardabi avenue, Baku, AZ1012*

Keywords: oil fingerprinting, Ward's dendrogram, sterane ternary

Summary. Geological exploration data indicates that effective application of available databases in combination with other methods enables to avoid drilling dry exploration wells. For instance, the integration of geochemical and geophysical data has been shown to enhance exploration outcomes by a factor of more than two when compared to the use of geophysical data in isolation. For this present study 201 oil samples were collected from wellheads of producing wells in Uzen and Kara-mandybas fields in 2023. The objectives of the study were (i) to assess reservoir continuity and com-partmentalization studies by oil fingerprinting analysis of oils from horizons XIII-XV, (ii) to characterize source rocks of representative oil samples in terms of environmental condition and thermal maturity by biomarker analysis and (iii) to integrate the obtained outcomes to draw viable conclusion from geological point of view. Oil fingerprinting analysis showed three distinct groups in horizon XIII and four different groups in horizon XV. It should be noted that the oils from the first group (red) predominate in both horizons XIII and XV indicating good reservoir continuity between them. Biomarker analysis of representative oils showed that oils from upper horizons (XIII-XV) were generated from shaly lacustrine organic matters (OM), while those of lower horizons were from shaly marine OM(XXII-XXIV) and with depth increase the thermal maturity of oil samples rise.

Introduction

A review of global practice reveals that the effective application of available databases in conjunction with techniques can prevent from drilling dry holes. The combination of geochemical and geophysical data has been demonstrated to yield exploration results that are more than double those obtained from geophysical data alone (Ganz et al., 1999; Ganz, Hempton, 2005; Peters, Fowler, 2002; McCaffrey et al., 2012; Pim et al., 2018; Dekker et al., 2017; Stout et al., 2001; Chemodanov et al., 2023; Suleimanov, Abbasov, 2022; Suleimanov et al., 2023; Suleimanov et al., 2017; Suleimanov et al., 2022; Suleimanov et al., 2022a; Vishnyakov et al., 2019).

For instance, according to experts from Shell, oil fingerprinting from drilled well #21116-A10 (green) did not correspond to oils from neighbouring fields such as Eider (red), Tern (yellow), and Cormoran (blue) (Fig. 1). However, using the North Sea Oil fingerpinning Atlas, this oil appeared to be similar with that from Otter field, indicating the secondary hydro-carbon migration pathway from the northeast direction. According to this data, a well was drilled in the vaulted part along the fault direction and high amount of oil was found highlighting the significance of the geochemical atlas application. Shell experts claimed that successful well would not have been drilled without this information.

As can be observed, geochemistry yields favorable outcomes at the outset of geological exploration although the role of geophysics becomes increasingly significant with the increasing depth of drilled wells. Geochemical studies of oil are conducted on a variety of gas chromatography and chromato-mass spectrometer, enabling the detailed genetic characterization of oils (Sarsenbekov et al. 2018; Seitkhaziyev 2019, 2020, 2021, 2022).

Oil fingerprinting

For this present study, 201 oil samples were collected from wellheads of producing wells in Uzen and Karamandybas fields in 2023. The objectives of the
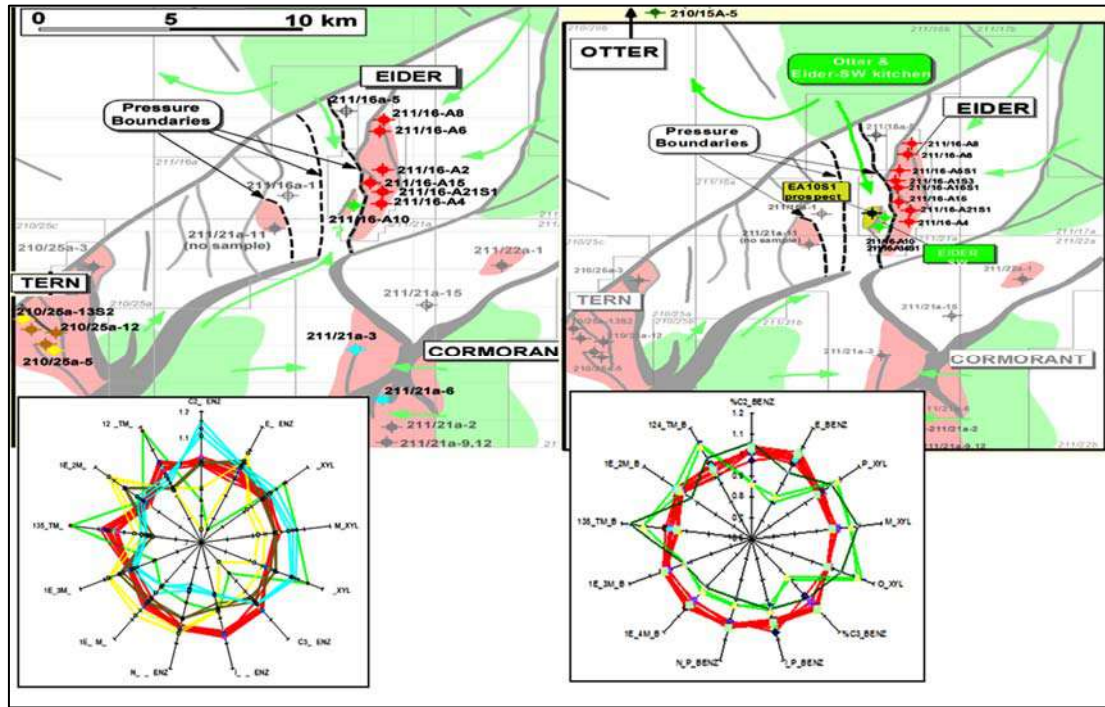
Fig. 1. The reproduction of oil migration direction and reservoir filling is based on the results of oil fingerprinting (Ganz et al., 1999).

study were: (i) to assess reservoir continuity and compartmentalization studies by oil fingerprinting analysis of oils from horizons XIII-XV, (ii) to characterize source rocks of representative oil samples in terms of environmental condition and thermal maturity by biomarker analysis and (iii) to integrate the obtained outcomes to draw viable conclusion from geological point of view.

As oil fingerprinting method, 12 aromatic peaks in oils from Low-thermal mass-multidimensional gas-chromatography (LTM-MD-GC) were employed to plot star-diagrams which exhibit similarities and differences between different oils derived from various pay zones: Identical star diagrams of oils attest to good reservoir continuity, whereas the opposite trend is true for reservoir compartmentalization.

Oil fingerprinting studies demonstrated the presence of 16 oil families within Uzen and Karamandybas fields. For convenience of comparison of oil compositions, samples were grouped according to their pay zones.

Oil fingerprinting of Horizon XIII

47 oil samples were used from this pay zone for this analysis, and the results demonstrated the identification of three distinct groups. This is clearly illustrated in the form of a Ward's dendrogram (Fig. 2) and on a structural map (Fig. 3) in the form of 'star' diagrams. The samples shown in red comprise the first group, while only two oil samples show the second group(orange). The samples in the north-west part of the field comprises the third group (blue).

Oil fingerprinting of Horizon XV

The results of the fingerprinting of 16 oil samples that penetrate this horizon indicate the presence of four distinct groups: (Fig. 4). In the structural map the oils of the first group are shown in red, while the only one sample(orange) comprises the second group. The samples in green and purple comprise the third and fourth groups correspondingly.

It should be noted that the oils from the first group predominate in both horizons XIII and XV indicating reservoir continuity between them.
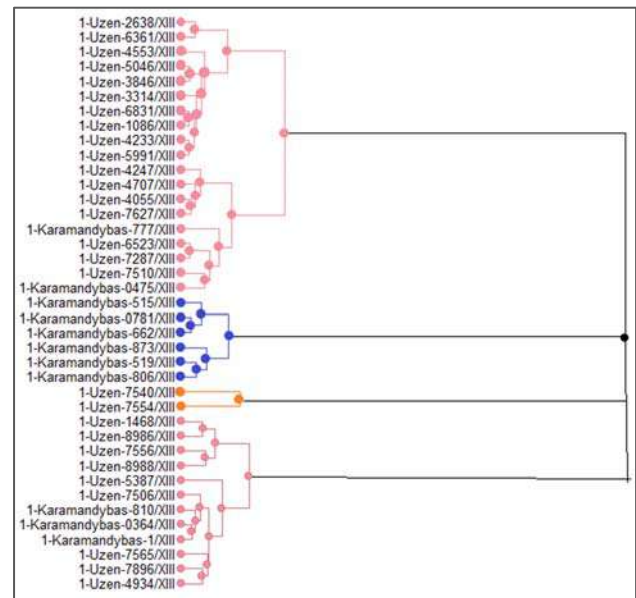

Fig. 2. Ward's dendrogramme on XIII horizon

Fig. 3. Results of fingerprinting of oil from Uzen and Karamandybas fields (XIII horizon)

Fig. 4. Results of fingerprinting of oil from Uzen and Karamandybas fields (XV horizon)

Biomarker analysis of oil:
Environmental condition of OM

A plot of pristane to phytane ratios on the C_{29} sterane/C_{30} hopane ratio (Fig. 5) was used to differentiate organic matters deposited in marine, lacustrine, or deltaic environments. The plot demonstrates that the oils of Uzen field exhibit a higher contribution of marine OM with the depth increase. For instance, the oils from the 21st horizon (red triangles) exhibit a greater contribution of marine sapropelic OM in comparision with those of the upper horizons XIII (red circles) and XVI (red rhombuses), as evidenced by their elevated C_{29} sterane/C_{30} terpane ratios.

To differentiate OM deposited in marine and lacustrine environments, sterane ternary of oils was also employed (Fig. 6). Based on this analysis, analogous conclusions are drawn. This plot clearly demonstrates a regular transition in the composition of oil from lacustrine to marine source towards the lower horizons. It is noteworthy that the oil from well No. 7554 (orange circle) and well No. 9782 (orange square) differs from the other oils from horizons XIII and XV (red figures), indicating genetic difference.

Thermal maturity

As illustrated in Fig. 7, the graph of the dependence of sterane isomers C29αααα (S/S+R) on C29 αβββ(S+R)/αβββ(S+R)+ αααα(S+R), the oils of the upper horizons XIII and XV (red figures) exhibit the lowest thermal maturity, while the oils of the lower horizon XXII display the highest thermal maturity. It

can be observed that there is a notable increase in thermal maturity with depth increase It is noteworthy that the oils from wells No. 7554 (orange circle) and No. 9782 (orange square) exhibit distinct characteristics that differentiate them from the other oils, thereby attesting to their genetic difference.

Fig. 8 also shows that the oils from the upper horizon (XIII) (red circles) exhibit relatively lower thermal maturity, whereas the oils from the lower horizon (XXII) (red triangles) display the highest thermal maturity. Similarly, the thermal maturity of the oils from the XIII, XIV, XVI and XXI horizons demonstrates a consistent increase with depth of occurrence. Furthermore, the oils from wells #7554 (orange circle) and #9782 (orange square) exhibit distinct characteristics that differentiate them from the other oils, thereby confirming their genetic divergence.

The results of the fingerprinting of oil samples from the Uzen field demonstrated the separation of distinct oil groups.

Conclusion

In this study oil fingerprinting and biomarker analysis were performed (i) to assess reservoir continuity and compartmentalization studies by oil fingerprinting analysis of oils from horizons XIII-XV, (ii) to characterize source rocks of representative oil samples in terms of environmental condition and thermal maturity by biomarker analysis and (iii) to integrate the obtained outcomes to draw viable conclusion from geological point of view.
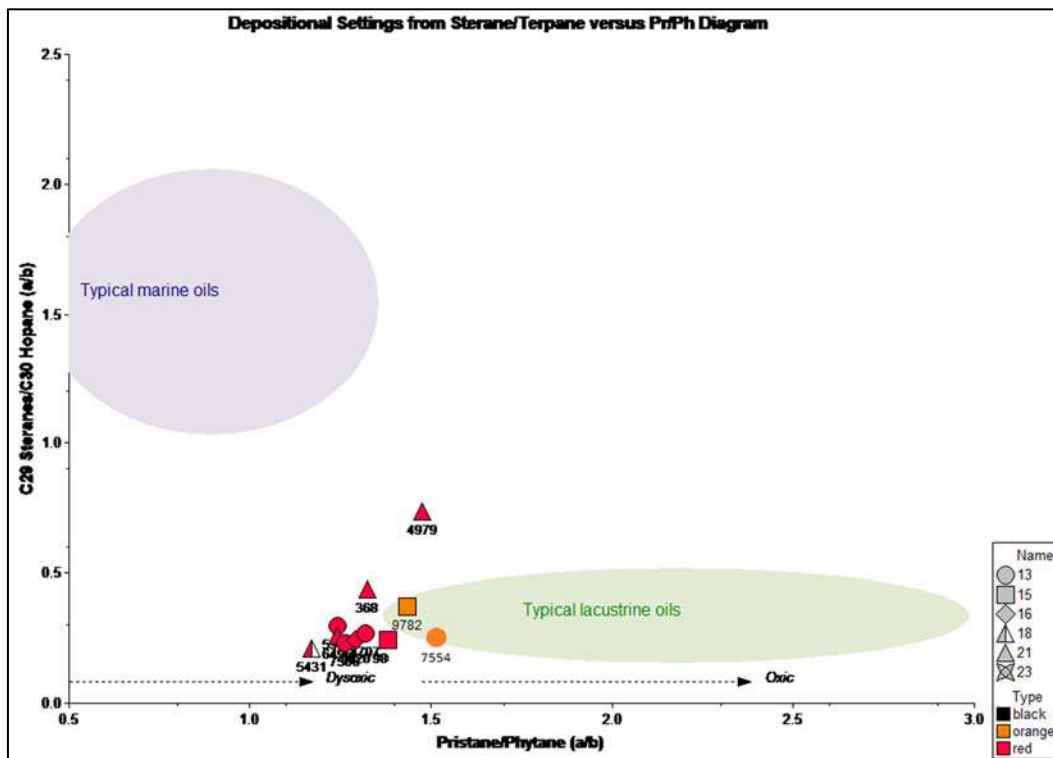

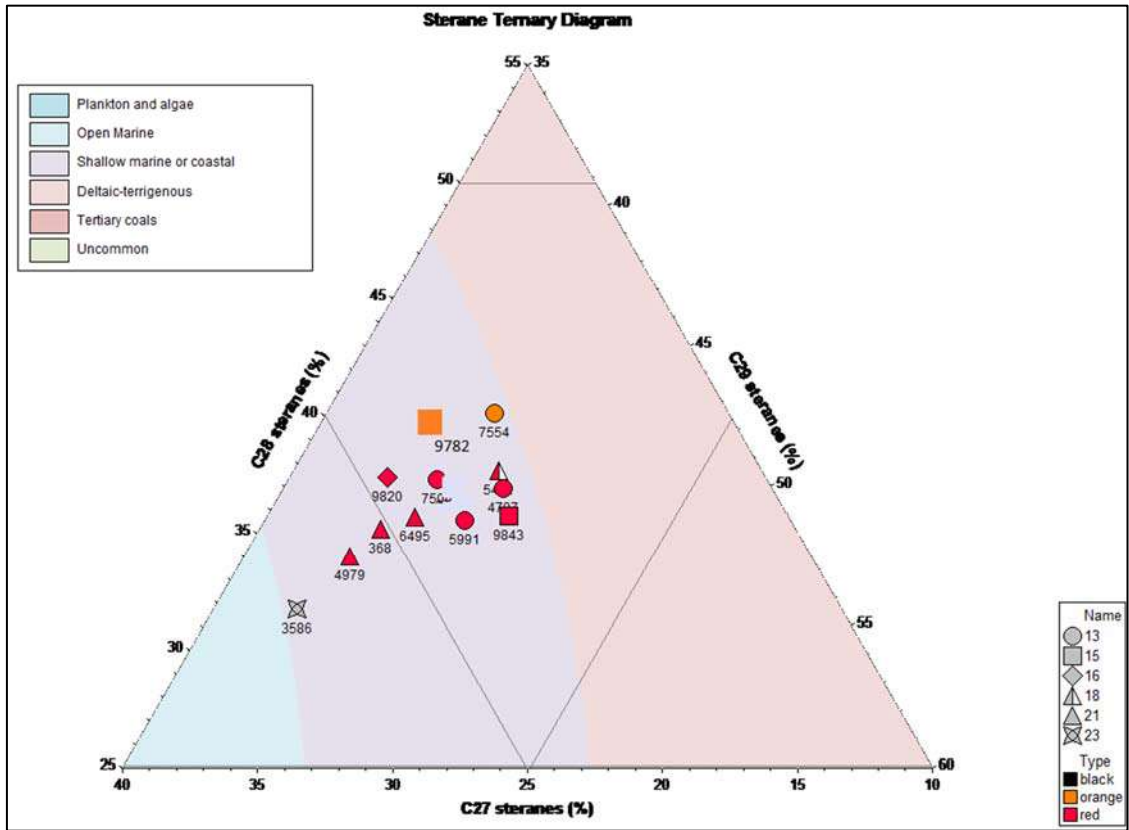**Fig. 5.** Plot of C29 sterane/C30 terpane against Pr/Ph

Fig. 6. Graph of pristan/phytane (Pr/Ph) to steraneC$_{29}$/gopaneC$_{30}$ dependence in oil samples
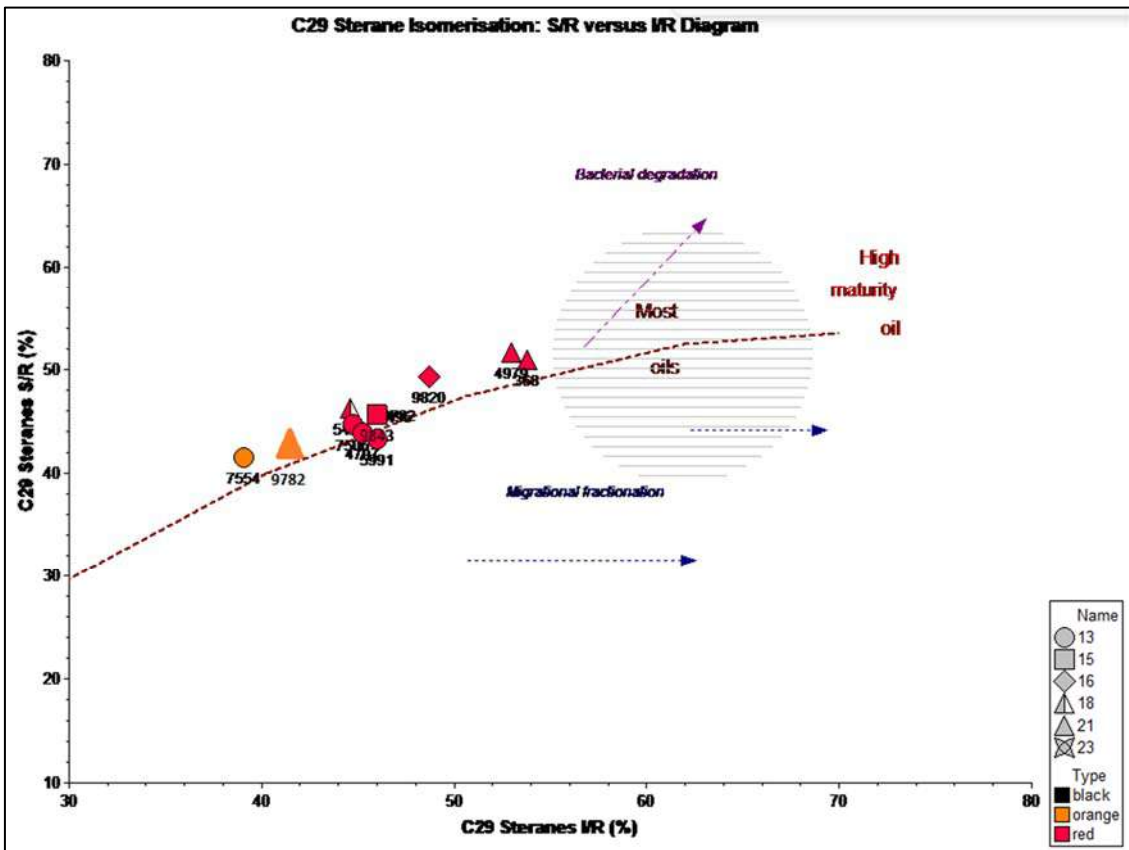

Fig. 7. Graph of dependence of sterane isomers C29αααα (S/S+R) on C29 αββ(S+R)/αββ(S+R)+ αααα(S+R) in Uzen oils
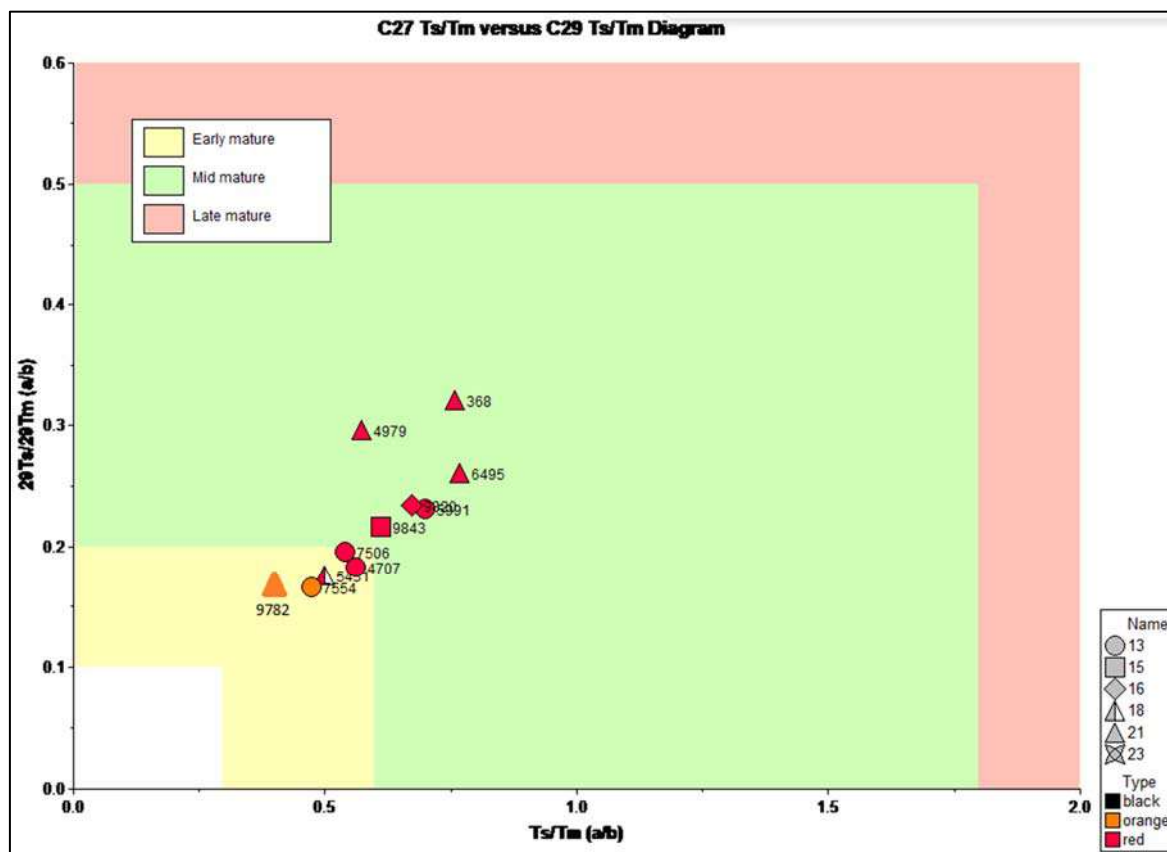
Fig. 8. Graph of dependence of terpanes C27Ts/Tm on C29Ts/Tm in oils from the Uzen field

Oil fingerprinting analysis demonstrated three distinct groups in horizon XIII and four different groups in horizon XV. It is worthy to note that the oils from the first group (red) predominate in both horizons XIII and XV indicating good reservoir continuity between them. According to biomarker analysis of representative oils, oils from upper horizons (XIII-XV) were generated from shaly lacustrine OM, while those of lower horizons (XXII-XXVI) were from shaly marine OM and with depth increase the thermal maturity of oil samples rise.

REFERENCES

Chemodanov A.E., Shipaeva M.S., Nurgaliev D.K., Sudakov V.A., Shakirov A.A., Ganiev B.G. Geochemical properties of the Upper Devonian deposits (Semiluk, Mendym and Kynovian horizons) of the Volga-Ural province for improving the Romashkinskoye oil field development efficiency. SOCAR Proceedings, No. 3, 2023, pp. 8-14, DOI: 10.5510/OGP20230300881.

Dekker R., Tegelaar E., Perrotta S., Miller S.D., Varlet X. L., Hasler Narhari C.-A., Rao J.D., Neog N., Dwindt A.A., Al-Haidar S., Dashti Q. Determination of fluid connectivity in the Middle Marrat of the Jurassic Fields of North Kuwait using oil fingerprinting. SPE-188375-MS. Proc. Abu Dhabi International Petroleum Exhibition and Conference, Abu Dhabi, UAE, November 2017.

Ganz H., Hempton M. Integrated reservoir geochemistry in Nigeria. Aberdeen, Scotland, Society of Petroleum Engineers, 2005.

Ganz H., Hempton M., van der Veen F., Kreulen R. Integrated reservoir geochemistry: finding oil by reconstructing migration pathways and paleo oil-water condition. Aberdeen, Scotland, Society of Petroleum Engineers, 1999.

Mccaffrey M.A., Baskin D.K., Patterson B.A. et al. Oil fingerprinting dramatically reduces production allocation costs. World Oil, Vol. 233, No. 3, 2012, pp. 55-60.

ЛИТЕРАТУРА

Chemodanov A.E., Shipaeva M.S., Nurgaliev D.K., Sudakov V.A., Shakirov A.A., Ganiev B.G. Geochemical properties of the Upper Devonian deposits (Semiluk, Mendym and Kynovian horizons) of the Volga-Ural province for improving the Romashkinskoye oil field development efficiency. SOCAR Proceedings, No. 3, 2023, pp. 8-14, DOI: 10.5510/OGP20230300881.

Dekker R., Tegelaar E., Perrotta S., Miller S.D., Varlet X. L., Hasler Narhari C.-A., Rao J.D., Neog N., Dwindt A.A., Al-Haidar S., Dashti Q. Determination of fluid connectivity in the Middle Marrat of the Jurassic Fields of North Kuwait using oil fingerprinting. SPE-188375-MS. Proc. Abu Dhabi International Petroleum Exhibition and Conference, Abu Dhabi, UAE, November 2017.

Ganz H., Hempton M. Integrated reservoir geochemistry in Nigeria. Aberdeen, Scotland, Society of Petroleum Engineers, 2005.

Ganz H., Hempton M., van der Veen F., Kreulen R. Integrated reservoir geochemistry: finding oil by reconstructing migration pathways and paleo oil-water condition. Aberdeen, Scotland, Society of Petroleum Engineers, 1999.

Mccaffrey M.A., Baskin D.K., Patterson B.A. et al. Oil fingerprinting dramatically reduces production allocation costs. World Oil, Vol. 233, No. 3, 2012, pp. 55-60.

Peters K., Fowler M. Applications of petroleum geochemistry to exploration and reservoir management. Organic Geochemistry, Vol. 33, No. 1, 2002, pp. 5-36.

Pim F., Bergen V., Gordon M. Production geochemistry: fluids don't lie and the devil is in the detail. Geological Society, London, Special Publications, Vol. 484, 2018, pp. 9-28, DOI:10.1144/SP484.1.

Sarsenbekov N.D., Yakupova E.N., Kairbekov S.B., Seyithaziyev Ye.Sh. The role of petroleum geochemistry in enhancing multizone oil and gas reservoirs development. SOCAR Proceedings, No. 3, 2018, pp. 65-74, http://dx.doi.org/ 10.5510/OGP20180300363.

Seitkhaziyev Y.Sh. Comprehensive geochemical study of core and cutting samples from postsalt deposits of southern parts of precaspian basin and «oil-source rocks» correlation studies. SOCAR Proceedings, No. 2, 2020, pp. 30-49.

Seitkhaziyev Y.Sh. Genetic classification of oil samples of carbonate origin from fields of the southern part of the Caspian Basin. SOCAR Proceedings, No. 3, 2019, pp. 40-60.

Seitkhaziyev Y.Sh. Geochemical analysis of oil and core samples derived from oil and gas fields in the South-Mangyshlak basin. SOCAR Proceedings, No. 4, 2022, pp. 76-86, DOI: 10.5510/OGP20220400786.

Seitkhaziyev Y.Sh. Geochemical studies of gases from oil and gas fields in the southern part of the caspian basin and their correlation with the results of oil geochemistry. SOCAR Proceedings, No. 4, 2021, pp. 43-51.

Stout S.A., Uhler A.D., Boehm P.D. Recognition of and allocation among multiple sources of PAH in Urban sediments. Environmental Claims Journal, Vol. 13(4), 2001, pp.141-158.

Suleimanov B.A, Abbasov H.F. Enhanced oil recovery mechanism with nanofluid injection. SOCAR Proceedings, No. 3, 2022, pp. 28-37.

Suleimanov B.A, Abbasov H.F., Ismayilov R.H. Thermophysical properties of suspensions with [NI$_3$(μ_3-PPZA)$_4$CL$_2$] metal string complex microparticles. SOCAR Proceedings, No. SI2, 2023, pp.194-204.

Suleimanov B.A., Abbasov H.F., Ismayilov R.H. Enhanced oil recovery with nanofluid injection. Petroleum Science and Technology, Vol. 41(18), 2022a, pp. 1734-1751, DOI:10.1080/10916466.2022.2094959.

Suleimanov B.A., Gurbanov A.Q., Tapdiqov Sh.Z. Isolation of water inflow into the well with a thermosetting gel-forming. SOCAR Proceedings, No.4, 2022, pp. 21-26, DOI:10.5510/OGP20220400779.

Suleimanov B.A., Ismayilov R.H., Abbasov H.F., Wen-Zhen Wang, Shie-Ming Peng. Thermophysical properties of nano- and microfluids with [Ni$_5$(μ_5-pppmda)$_4$Cl$_2$] metal string complex particles. Colloids and Surfaces A: Physicochemical and Engineering Aspects, Vol. 513, 2017, pp.41-50.

Vishnyakov V.V., Suleimanov B.A., Salmanov A.V., Zeynalov E.B. Primer on enhanced oil recovery. Gulf Professional Publishing. Elsevier. 2019, 222 p.

ТИПЫ НЕФТЕЙ, ВЫДЕЛЕННЫЕ В РЕЗУЛЬТАТЕ ГЕОХИМИЧЕСКИХ АНАЛИЗОВ НА МЕСТОРОЖДЕНИЯХ УЗЕНЬ И КАРАМАНДЫБАС

Сейтхазиев Е.Ш.[1,2], Даумшаров А.А.[1]

[1]Атырауский филиал ТОО «КМГ Инжиниринг», Атырау, Казахстан
060097 Атырауская область, Атырау, мкр. Нурсая, пр. Элорда, Здание 10: esimhan89-89@mail.ru
[2]НИПИ "Нефтегаз", SOCAR, Азербайджан
Просп. Зардаби, 88А, Баку, AZ1012

Резюме. Мировая практика показывает, что при геологоразведочных работах эффективное применение имеющейся базы данных в сочетании с другими методами позволяет избежать бурения сухих поисково-разведочных скважин. Например, сопоставление геохимических и геофизических данных увеличивает результаты разведки более чем в два раза, по сравнению с использованием только геофизических данных. В данной работе рассматривались образцы нефтей в количестве 201 единиц,

которые были отобраны с устьев скважин месторождений Узень и Караманбыбас в 2023 г. Целью исследования являлось определение генетического происхождения нефтей и их сопоставление с анализированными пробами нефти (2016 г.) в имеющейся базе данных. Представлены результаты геохимических исследований указанных образцов нефти основных продуктивных горизонтов (XIII, XV) месторождений Узень и Караманбыбас. Для корреляции нефтей продуктивных пластов использовались соотношения 12 ароматических пиков на хроматограммах LTM, по которым строились так называемые звездные диаграммы, наглядно иллюстрирующие сходство и различие флюидов. Многомерная газовая хроматография компонентов с низкой термальной массой (Low Thermal Mass Gas Chromatography-далее LTM) позволяет произвести качественную оценку «отпечатков» каждого индивидуального пласта, горизонта или объекта разработки. Все исследованные пробы были пригодны для фингерпринтинга. Как эмпирически, так и практически установлено, что в едином хорошо сообщающемся резервуаре звездные диаграммы нефтей идентичны, в то время как для нефтей из разобщенных резервуаров они существенно различаются. В целом все исследуемые нефти месторождений Узень и Карманбыбас по результатам «фингерпринтинга» были разделены на 16 групп. Также для удобства интерпретации все образцы нефти были сгруппированы по принадлежности к горизонтам (XIII-XXIV).

Ключевые слова: фингерпринтинг нефти, дендрограмма Варда, тригонограмма стеранов

UZEN VƏ KARAMANDIBAS SAHƏLƏRİNDƏ APARILMIŞ GEOKİMYƏVİ TƏHLİLLƏR NƏTİCƏSİNDƏ MÜƏYYƏNLƏŞDİRİLMİŞ NEFT TİPLƏRİ

Seytxaziev E.Ş.[1,2], Daumşarov A.A.[1]
[1]Atırau filialı, «KMG Engineering» MMC, Atırau, Qazaxıstan
[2]NQETLİ "Neft və Qaz", SOCAR, Azərbaycan

Xülasə. Dünyada təcrübəsi göstərir ki, geoloji-axtarış işlərində mövcud məlumat bazasından effektiv istifadə və digər metodlarla birləşdirilmə quru axtarış-kəşfiyyat buruq qazılmasından imtina etməyə imkan verir. Məsələn, geokimyəvi və geofiziki məlumatların müqayisəsi, yalnız geofiziki məlumatlardan istifadə etməklə müqayisədə kəşfiyyat nəticələrini iki dəfə artırır. Bu işdə 2023-cü ildə Uzen və Karamandıbas sahələrindəki quyulardan götürülmüş 201 nümunə neftin tədqiqi aparılmışdır. Araşdırmanın məqsədi neftlərin genetik mənşəyini müəyyənləşdirmək və onları 2016-cı il tarixli mövcud məlumat bazasında olan neft nümunələri ilə müqayisə etmək idi. Uzen və Karamandıbas sahələrinin əsas istehsal qatları (XIII, XV) üzrə göstərilən neft nümunələrinin geokimyəvi tədqiqatlarının nəticələri təqdim olunmuşdur. İstehsal qatları neftlərini korrelyasiya etmək üçün LTM xromatoqramlarında 12 aromatik maksimumun nisbətləri əsasında, neftlərin oxşarlığını və fərqlərini vizual şəkildə göstərən "ulduz diaqramları" qurulmuşdur. Aşağı İstilik Kütləsi Qaz Xromatoqrafiyası (Low Thermal Mass Gas Chromatography - LTM) hər bir fərdi qatın, horizontun və ya inkişaf obyektinin "izi"nin keyfiyyətli qiymətləndirilməsinə imkan verir. Araşdırılmış bütün nümunələr "fingerprinting" üçün uyğun olmuşdur. Empirik və praktik olaraq müəyyən edilmişdir ki, bir-biri ilə yaxşı əlaqələndirilmiş bir yataqda ulduz diaqramları eynidir, halbuki ayrılmış yataqlardan alınan neftlər əhəmiyyətli dərəcədə fərqlənir. Ümumilikdə, Uzen və Karamandıbas sahələrinin araşdırılmış bütün neftləri iz (fingerprinting) nəticələrinə görə 16 qrupa ayrılmışdır. Həmçinin, interpretasiyanı asanlaşdırmaq üçün bütün neft nümunələri XIII-XXIV qatlarına aid olanlara görə qruplaşdırılmışdır.

Açar sözlər: fingerprinting, Varda dendroqramı, steranların triqonometriyası

ВОЗМОЖНОСТИ МОНИТОРИНГА РАБОТЫ ГАЗОВЫХ СКВАЖИН МЕТОДОМ ШУМОМЕТРИИ С ПРИМЕНЕНИЕМ СИСТЕМЫ РАСПРЕДЕЛЕННЫХ АКУСТИЧЕСКИХ ДАТЧИКОВ

Колычев И.Ю.[1], Белов С.В.[1], Чистяков Н.Ю.[1], Гурбанов В.Ш.[1,2], Галкин С.В.[1]

*[1]Пермский Национальный Исследовательский Политехнический Университет, Россия
614990, Пермь, Комсомольский проспект, 29: igorek999@yandex.ru, sv.belov63@mail.ru,
Nikita.Chistyakov@fxc-png.ru, shum5011@gmail.com, vaqifqurbanov@mail.ru
[2]Министерство науки и образования Азербайджанской Республики,
Институт нефти и газа, Азербайджан
AZ1000, Баку, ул. Ф.Амирова, 9: vaqifqurbanov@mail.ru*

THE POSSIBILITIES OF MONITORING THE OPERATION OF GAS WELLS BY NOISE MEASUREMENT USING A SYSTEM OF DISTRIBUTED ACOUSTIC SENSORS

Kolychev I.J.[1], Belov S.V.[1], Chistyakov N.Yu.[1], Gurbanov V.Sh.[1,2], Galkin S.V.[1]
*[1]Perm National Research Polytechnic University, Russia
29, Komsomolsky prospect, Perm, 614990: igorek999@yandex.ru, sv.belov63@mail.ru,
Nikita.Chistyakov@fxc-png.ru, shum5011@gmail.com, vaqifqurbanov@mail.ru
[2]Institute of Oil and Gas, MSERA, Azerbaijan
9 Baku, F. Amirov str., Baku, AZ1000: vaqifqurbanov@mail.ru*

Keywords: spectral noise logging, fiber optic distributed acoustic sensing, gas-saturated formations, frequency range

Summary. The experience of using fiber-optic distributed acoustic sensing (DAS) for spectral noise logging based on a geophysical cable when monitoring the development of a gas condensate field is considered. Studies have been carried out to assess the spectral sensitivity of the DAS method. A technique has been developed for filtering the original signal with calculation of the signal energy in various frequency ranges, which carries information about the movement of fluid inside the well. Using these methods, the moment of stopping the well is clearly identified. By combining sound logging of wells with studies based on a fiber-optic system of distributed temperature sensing (DTS), intervals of gas-saturated formations operating in the well were identified.

It has been established that the information content of the DAS and DTS systems depends on the location of the cable. For monitoring development using the DTS technology, it is optimal to place the cable inside or outside the production casing. When the cable is located inside the tubing, the temperature field is distorted by counter-current fluid flows. The sensitivity of the DAS system to noise from the rock and the production casing can also be increased by optimizing the cable location, which can be justified with a wider implementation of this technology in production.

To be able to record noise from fluid movement behind the column and in the rock, it is necessary to expand the frequency range of the recorded vibrations by using special cables with increased sensitivity and an expanded directional diagram.

Введение

Главным преимуществом применения волоконно-оптических систем распределенных акустических датчиков (DAS) является возможность осуществлять непрерывный мониторинг, регистрируя акустические события в реальном времени по всей длине скважины. Точечные акустические датчики, имея большую по сравнению с DAS-системами разрешающую способность, позволяют осуществлять измерение сигнала на конкретной глубине только в ограниченный момент времени, не позволяя вести полноценный мониторинг за работой скважины. Технологии DAS более десяти лет применяются в наземной сейсморазведке и вертикальном сейсмопрофилировании (ВСП) (Parker et.al., 2014; Wu et al., 2017). Применение DAS-систем для шумометрии скважин в значительно меньшей степени освещено в науч-

ной литературе, анализ показывает их ограниченное применение преимущественно на месторождениях Северной Америки и Китая. При этом одной из значимых задач, решаемых методом шумометрии, является выделение работающих интервалов скважин с определением характера насыщения притока (Daley et al.,, 2013; Gabai, Eyal, 2016).

DAS-системы обладают рядом важных преимуществ перед традиционными измерительными системами, прежде всего это высокая плотность виртуальных датчиков и неограниченная в пределах скважины длина расстановки, нечувствительность к электромагнитным полям (Mateeva и др., 2012; Кислов, Гравиров, 2022). К недостаткам DAS можно отнести более низкую чувствительность оптического волокна в отношении акустического воздействия по сравнению с точечным микрофоном, используемым при геофизических исследованиях скважин (ГИС). В том числе, снижение разрешающей способности DAS происходит ввиду возрастания искажений спектра акустического сигнала на частотах более 150-300 Гц (Dean et al., 2017; Stork et al., 2020; Näsholm et al., 2022). Сигналы с меньшими частотами подходят для решения задач нефтяной сейсморазведки и ВСП. При регистрации шумовых сигналов искажения спектра менее значимы, поэтому необходимо определить возможность применения DAS на основе геофизического грузонесущего кабеля для шумометрии в скважинах. Ранее проведенные исследования по оценке спектральной чувствительности такой DAS-системы (Колычев и др., 2022) показали, что максимальная частота регистрируемых сигналов ограничена 2.5 кГц. Верхняя частота шумов от движения флюида в пласте может доходить до 15-30 кГц (Nikolaev, Ovchinnikov,1992; Асланян и др., 2016), однако спектр шумов при движении флюида в скважине не превышает 3 кГц (Асланян и др., 2016). В данной работе рассмотрены результаты применения шумометрии DAS на основе геофизического грузонесущего кабеля при контроле за разработкой газоконденсатного месторождения.

Исследования методом спектральной шумометрии DAS целесообразно комплексировать с методом распределенных волоконно-оптических датчиков температуры (DTS). К настоящему времени метод DTS для задач мониторинга работы нефтяных и газовых скважин разработан в значительно большей степени чем DAS. Системы DTS широко применимы для получения профиля притока или поглощения, задач мониторинга прорыва газа или воды (Lee et al., 2018; Ипатов и др., 2021), мониторинга гидроразрыва пласта (Näsholm et al., 2020). Однако только по величине температурной аномалии в скважине невозможно

достоверно судить об ее истинной природе. Данная задача может быть решена на основе анализа и классификации спектра шумометрии DAS.

Материалы и методы

Исследования методами спектральной шумометрии DAS и DTS в рамках опытно-промышленных работ проводились на четырех эксплуатационных скважинах Губкинского газоконденсатного месторождения. Исследуемый продуктивный пласт сеноманского возраста представлен переслаиванием песчано-алевролитовых и глинистых пород с подчиненной ролью последних. Сверху он перекрыт толщей турон-датских глин морского генезиса мощностью 500-800 м, что определяет высокие экранирующие свойства покрышки, позволившие сформироваться гигантским газовым залежам.

В скважину спускался бронированный грузонесущий геофизический кабель с оптоволоконным модулем (КГ 4ОВ-20-120). При исследованиях использовался программно-аппаратный комплекс «Горизонт», в состав которого входят модули DAS и DTS, работу которых можно считать синхронизированной благодаря применению единого регистрирующего сервера. Разрешающая способность методов DAS и DTS дополнительно контролировались комплексом ГИС и исследованиями точечных датчиков шумометрии и термометрии. При этом использовался высокочувствительный акустический датчик отрытого типа, который эффективно работает в газовой среде. В качестве контроля метода DTS также были проведены широко используемые на производстве исследования станцией термоконтроля «SILIXA».

Исследования проводились на двух режимах: работающей и остановленной скважины. Во время операции спуска осуществлялась запись локальными устройствами, смонтированными на конце кабеля. По окончании операции спуска осуществлялась запись работающей скважины, температура (DTS) и спектральный шум (DAS) по оптоволокну, находящемуся в кабеле сразу по всей длине скважины. Остановка скважины происходила при продолжающейся записи температуры и шума. Далее по разработанному регламенту продолжалась запись процессов, происходящих внутри скважины после остановки. Время записи в каждом из режимов варьировалось в скважинах в диапазоне от 1 до 2 часов.

Перед исследованиями были проведены опытные работы по оценке спектральной чувствительности DAS на основе геофизического грузонесущего кабеля при различном шаге квантования по времени. Эксперименты показали, что отношение сигнал/шум (SNR) на частотах более 1 кГц становится недостаточным для выделения событий в

скважине, поэтому был выбран шаг квантования по времени 0.5 мс, что обеспечило регистрацию сигналов с частотой до 1 кГц.

Обработка данных DAS включала несколько шагов (Рис. 1):

1) транспонирование данных для получения временных рядов на каждой глубине $s(t, h) \to s(h, t)$;

2) подавление специфических помех регистратора «Горизонт»;

3) расчет энергии сигнала $E(h, t)$ во временных окнах с шагом по времени 1 с;

4) расчет средних энергетических спектров сигнала $S_t(h, f)$ во временных окнах с шагом по времени 5 мин;

5) расчет энергии сигнала $E_{\Delta f}(h, t)$ в нескольких диапазонах частот Δf (0-125 Гц, 125-250 Гц, 250-500 Гц, 500-1000 Гц) во временных окнах с шагом по времени 1 с.
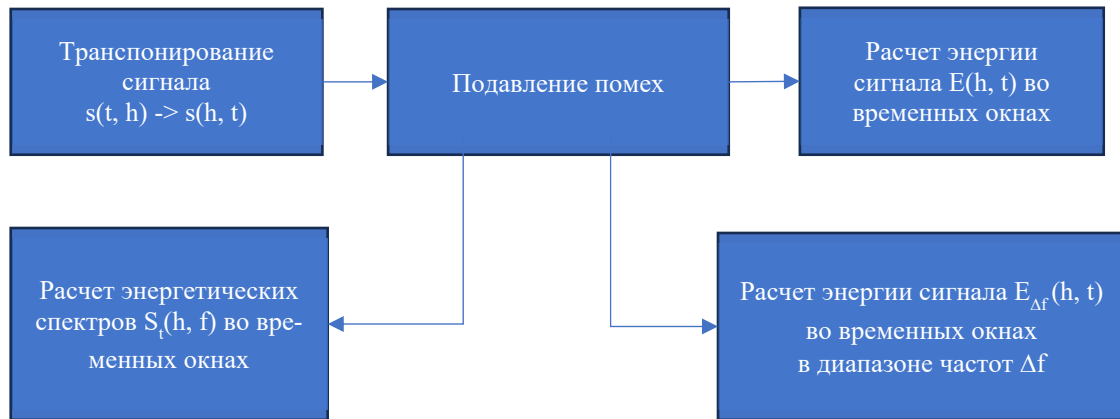

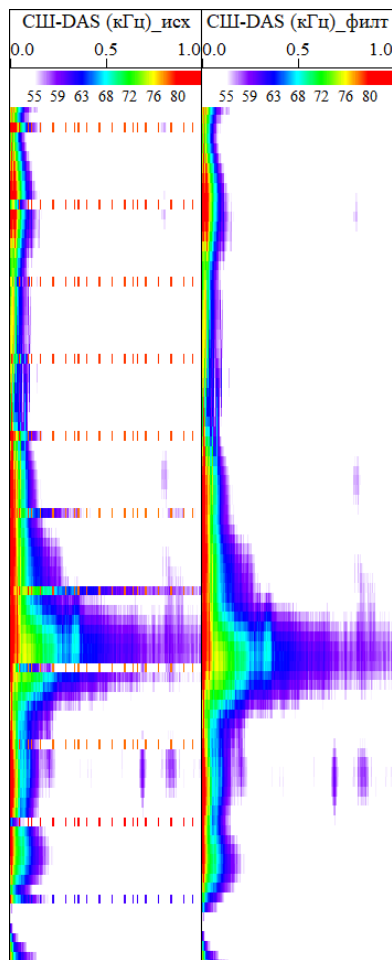**Рис. 1.** Блок-схема обработки данных метода шумометрии DAS

Рис. 2. Сравнение исходного акустического сигнала DAS (СШ-DAS$_{\text{исх}}$) и после применения процедуры фильтрации (СШ-DAS$_{\text{филт}}$)

Предварительная обработка сигнала DAS в регистрирующем сервере может содержать нелинейные преобразования, которые влияют на форму и спектр сигнала. Чтобы исключить неопределенности данного типа применена специальная программа записи исходного сигнала шумометрии DAS, поступающего с регистратора. Записанный с регистратора сигнал содержал помехи (Рис. 2), которые удалялись с помощью специально разработанной процедуры.

Обработка данных с визуализацией результатов проводилась в программном комплексе обработки и интерпретации данных геофизических исследований скважин «Соната-2019». Из рис. 2 видно, что применение процедуры фильтрации сигнала существенно подавляет помехи, которые в исходном сигнале проявляются по всему стволу скважины.

Результаты

Сравнение результатов измерений акустического шума точечными и распределенными датчиками в режимах остановленной и работающей скважины приведены на рис. 3. По аномалиям шумометрии на глубине 773 м обоими методами выявлена негерметичность насосно-компрессорной трубы (НКТ), которая возможно вызвана выносом песка из работающего пропластка. Как видно из рисунка положение аномалий шума, зарегистрированного системой DAS, соответствует положению аномалий от дискретного датчика.
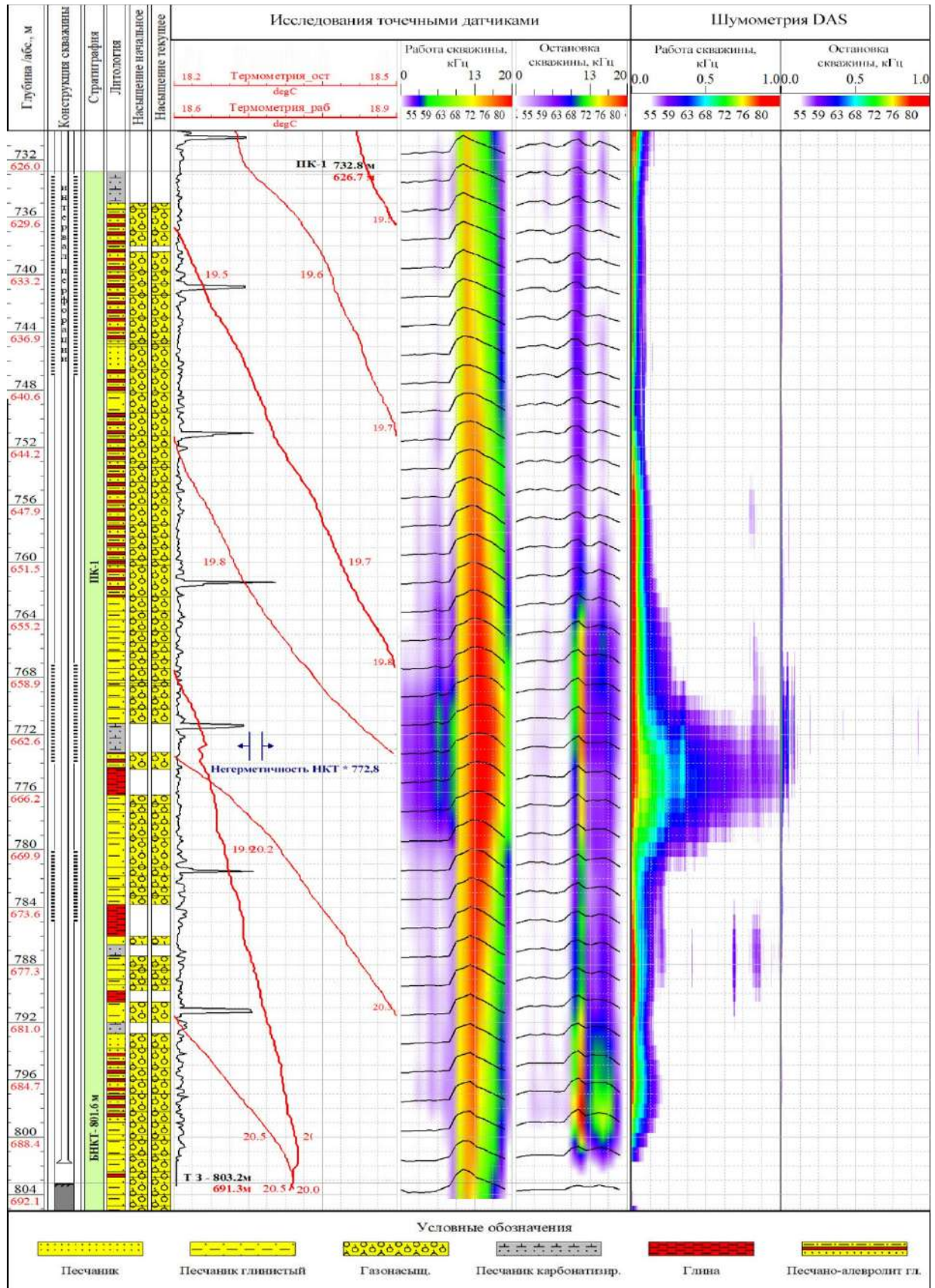
Рис. 3. Сопоставление измерений спектра акустического шума точечными и распределенными датчиками DAS

Интенсивность установленной аномалии при шумометрии DAS меньше чем при регистрации точечным датчиком. Энергия зарегистрированного системой DAS шума сосредоточена в диапазоне 0-700 Гц, в то время как энергия шума, зарегистрированного точечным датчиком, преобладает в диапазоне

10-18 кГц. Это является следствием нескольких факторов. Диаграмма направленности распределенных датчиков имеет максимум в вертикальном направлении и минимум в горизонтальном (Kuvshinov, 2016), плотная оболочка из стальной проволоки дополнительно препятствует передаче деформаций внутрь кабеля, что приводит к ограничению регистрируемого спектра частотой 2.5 кГц. В исследуемой скважине кабель находился в газовой среде, поэтому частота регистрируемых колебаний не превышала 1 кГц. Исследования диаграммы направленности DAS-систем (Чулков и др., 2023; Чугаев, Тарантин, 2023) показали, что для повышения чувствительности распределенных датчиков необходимо применять оптоволоконный кабель со спиральной навивкой оптоволокна. Такая конструкция обеспечивает равномерную диаграмму направленности при угле намотки около 57°. Применение специальных кабелей со спиральным уложением волокна позволит расширить возможности оптоволоконных систем для решения сейсмоакустических задач, в частности задач шумометрии.

Дополнительные искажения в регистрируемый сигнал и, соответственно, спектр сигнала вносят помехи самого регистратора DAS. Помехи связаны с дрейфом частоты лазера (LSFD), который приводит к дрейфу фазового сигнала, полученного системой DAS, вверх и вниз вместе с дрейфом частоты лазера. Кроме того, из-за неоднородности внешней среды и накопления фазового шума, генерируемого при передаче света в системе DAS, как прямо, так и косвенно влияют на отношение сигнал/шум (SNR) регистрируемого сигнала (Жирнов и др., 2019). Для подавления таких помех предложено несколько способов (Wu et al., 2013; Chen et al., 2021; Mao et al., 2022). Наиболее эффективный способ SEE-SGMD-PCC изложен в работе (Bai et al., 2023). Указанные способы повышения SNR сигнала рассчитаны на детерминированный сигнал, который наблюдается при ВСП и сейсморазведке. Эффективность подавления шумов LSFD для применения в акустической шумометрии требует дополнительной апробации на скважинах.

Данные мониторинга по технологии DAS по всему стволу скважины отображены на рисунке 4. На диаграммах энергии во всех диапазонах частот хорошо виден момент остановки скважины. В диапазоне частот 0-125 Гц преобладают шумы от движения газа в скважине. Шум фильтрации газа через обнаруженный дефект НКТ уверенно выделяется в диапазонах 125-250 Гц и 250-500 Гц. После остановки скважины этот шум прекращается. При этом наблюдаемый после остановки скважины небольшой шум в верхней ее части на низких частотах вероятно связан с работами на поверхности.

Форма спектра позволяет делать выводы об источнике шума (Nikolaev, Овчинников, 1992; Асланян и др., 2016). Как видно на рис. 4, шум от движения газа по стволу скважины сосредоточен в диапазоне 0-250 Гц. На глубине негерметичности НКТ спектр расширяется и охватывает весь регистрируемый диапазон частот.

Мониторинг распределения температуры в скважине выполнен двумя видами аппаратуры DTS. Аппаратурой «SILIXA» и «Горизонт» получены близкие по форме изменения распределения температуры по скважине, при этом для «SILIXA» отмечен несколько меньший диапазон выделенной аномалии. В обоих случаях на диаграммах DTS отчетливо фиксируется момент остановки скважины, с выделением положительной аномалии в интервале работающих пропластков вблизи негерметичности НКТ. При этом абсолютные значения температуры отличаются значительно, разница достигает 6°C.

При сравнении результатов DTS с измерением точечным термометром установлено, что чувствительность распределенных датчиков заметно ниже. Аномалия температуры от негерметичности колонны составляет 0.02-0.05 C° и на данных DTS выделяется только по градиенту. Данный факт объясним меньшей разрешающей способностью распределённого датчика DTS по сравнению с точечным датчиком. Также влияет инерционность датчика DTS, обусловленная конструкцией кабеля (оболочка, броня и т.д.) и тем, что оптоволоконный модуль находится в центре конструкции кабеля. В целом перед проведением измерений для повышения качества сигнала необходима дополнительная калибровка аппаратуры DTS с конкретным кабелем.

Сопоставление результатов шумометрии DAS с DTS (Рис. 5) показывает, что разрешающая способность метода DAS ниже чем DTS, так как шум от источника колебаний может распространяться на значительные расстояния по элементам конструкции вдоль скважины. При этом между показаниями DAS и DTS наблюдается высокая сходимость выделенных аномалий по глубине скважины с выделением притока газа в диапазоне глубин 772 – 775 м.

Выводы

Применение системы распределенных акустических датчиков DAS позволяет выполнять мониторинг акустического шума по стволу скважины с выделением интервалов притока газа. Регистрируемый диапазон спектра частот несет информацию о движении флюида и событиях внутри скважины.
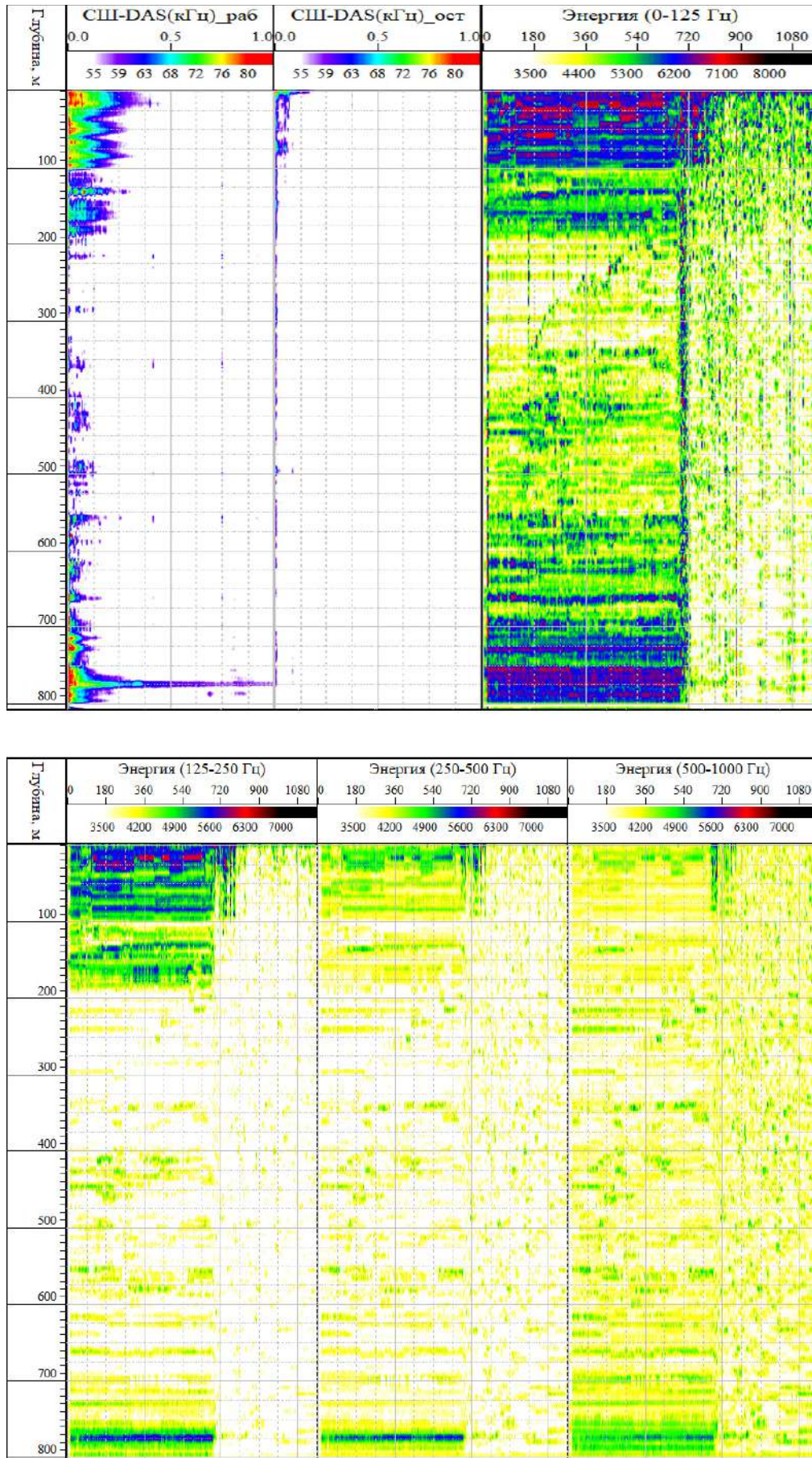
Рис. 4. Мониторинг акустического шума по стволу скважины методом DAS с выделением частотного диапазона шумометрии
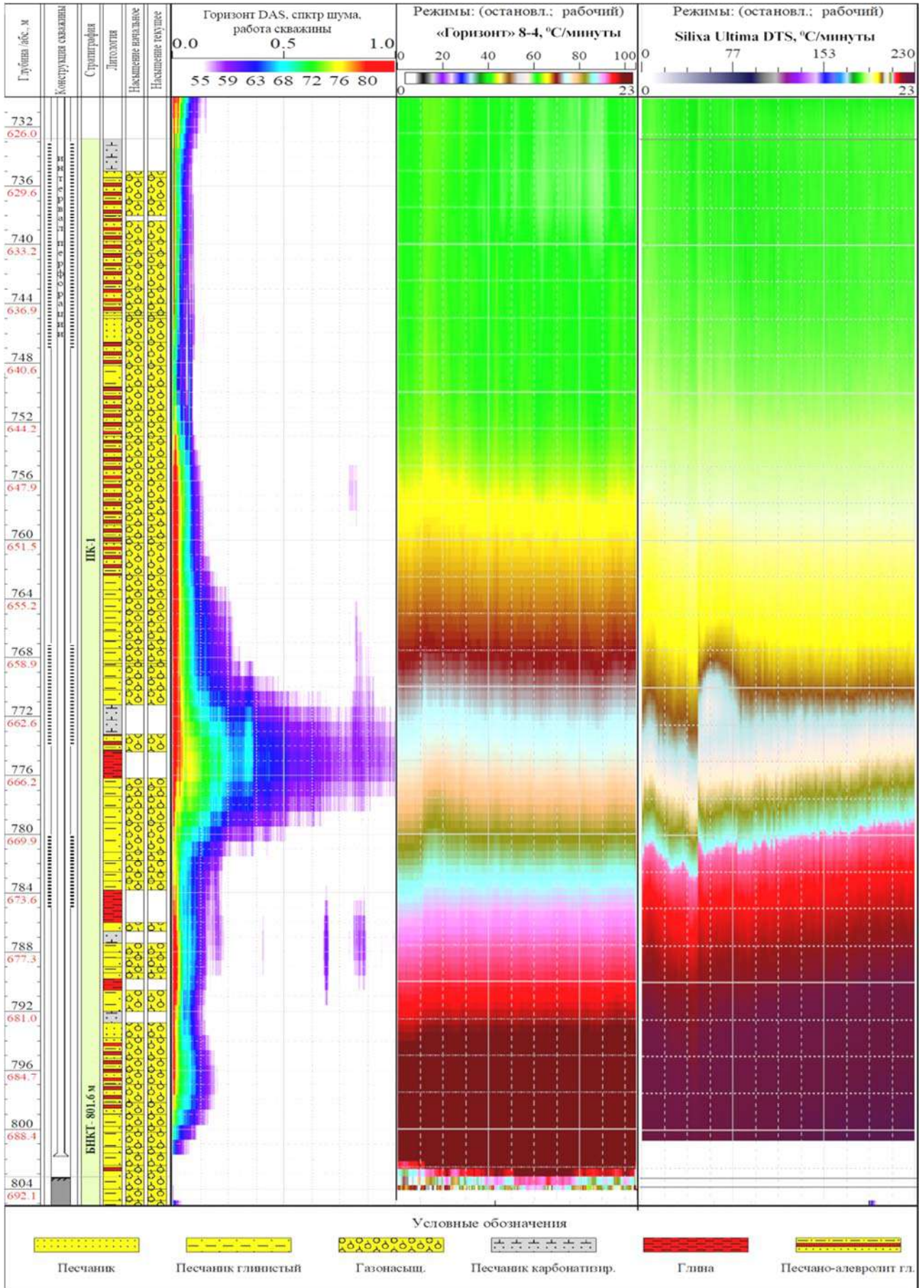
Рис. 5. Сопоставление результатов измерений методов шумометрии DAS и DTS по стволу скважины

Для повышения достоверности выделения в скважине работающих интервалов целесообразно комплексировать данные методов DAS и DTS. Информативность систем DAS и DTS зависит от места расположения кабеля. Для контроля за разработкой по технологии DTS оптимально размещать кабель внутри или снаружи эксплуатационной колонны. При расположении кабеля внутри НКТ поле температуры искажается встречными потоками флюида. Чувствительность системы DAS к шуму от породы и эксплуатационной колонны также может быть повышена оптимизацией расположения кабеля, что может быть обосновано при более широком внедрении данной технологии на производстве.

Для возможности регистрации шума от движения флюида за колонной и в породе необходимо расширить частотный диапазон регистрируемых колебаний за счет применения специальных кабелей с повышенной чувствительностью и расширенной диаграммой направленности. Достоверность исследований методом шумометрии DAS может быть существенно повышена путем тестирования программных алгоритмов для улучшения соотношения сигнал/шум.

В перспективе предложенные подходы могут позволить не только судить по шумометрии DAS об интервалах фильтрации флюидов, но и на основе анализа спектров регистрируемых шумов определять характер их насыщения (нефть, вода, газ). С учетом этого, опытно-промышленные работы методом шумометрии DAS представляются весьма перспективными в плане тиражирования технологии для обеспечения мониторинга работы скважин.

Благодарности

ЛИТЕРАТУРА

Aslanian A.M., Aslanian I.Yu., Maslennikova Y.S. et al. Diagnostics of gas overflows by a complex of high-precision thermometry, spectral noise measurement and pulsed neutron-neutron logging. Territory of Oil and Gas, No. 6, 2016, pp. 74-81 (in Russian).

Bai X., Zhang F., Lin L. et al. Phase drift and noise suppression method based on SEE-SGMD-PCC in a distributed acoustic sensor. Optics Express, Vol. 31, No. 19, 2023, pp. 31463-31485, https://doi.org/10.1364/OE.495356.

Chen W., Ma X., Ma Q. et al. Denoising method of the φ-OTDR system based on EMD-PCC. IEEE Sensors Journal, Vol. 21, No. 10, 2021, pp. 12113-12118, DOI: 10.1109/JSEN.2020. 3033674.

Chugaev A.V., Tarantin M.V. Amplitude-frequency response of distributed acoustic sensor DAS with spiral winding of fiber. Mining Science and Technology, Vol. 8, No. 1, 2023, pp. 13-21, DOI: 10.17073/2500-0632-2022-06-10 (in Russian).

Chulkov E., Tikhotsky S.A., Dubinya N.V. Design of seismic sensors based on the DAS principle: analysis and numerical modeling. Proceedings of the International Geological and Geophysical Conference, March 27-29, 2023. Vol. 3, PolyPRESS. Tver, 2023, 234 p. (in Russian).

Daley T.M. et al. Field testing of fiber-optic distributed acoustic sensing (DAS) for subsurface seismic monitoring. The Leading Edge, Vol. 32, No. 6, 2013, pp. 699-706, DOI:10.1190/ tle32060699.1.

Dean T., Cuny T., Hartog A.H. The effect of gauge length on axially incident P-waves measured using fibre optic distributed vibration sensing: Gauge length effect on incident P-waves. Geophysical Prospecting, Vol. 65, No. 1, 2017, pp. 184-193, DOI: 10.1111/1365-2478.12419.

Gabai H., Eyal A. On the sensitivity of distributed acoustic sensing. Optics Letters, Vol. 41, No. 24, 2016, pp. 5648-5651, https://doi.org/10.1364/OL.41.005648.

REFERENCES

Bai X., Zhang F., Lin L. et al. Phase drift and noise suppression method based on SEE-SGMD-PCC in a distributed acoustic sensor. Optics Express, Vol. 31, No. 19, 2023, pp. 31463-31485, https://doi.org/10.1364/OE.495356.

Chen W., Ma X., Ma Q. et al. Denoising method of the φ-OTDR system based on EMD-PCC. IEEE Sensors Journal, Vol. 21, No. 10, 2021, pp. 12113-12118, DOI: 10.1109/JSEN.2020. 3033674.

Daley T.M. et al. Field testing of fiber-optic distributed acoustic sensing (DAS) for subsurface seismic monitoring. The Leading Edge, Vol. 32, No. 6, 2013, pp. 699-706, DOI:10.1190/ tle32060699.1.

Dean T., Cuny T., Hartog A.H. The effect of gauge length on axially incident P-waves measured using fibre optic distributed vibration sensing: Gauge length effect on incident P-waves. Geophysical Prospecting, Vol. 65, No. 1, 2017, pp. 184-193, DOI: 10.1111/1365-2478.12419.

Gabai H., Eyal A. On the sensitivity of distributed acoustic sensing. Optics Letters, Vol. 41, No. 24, 2016, pp. 5648-5651, https://doi.org/10.1364/OL.41.005648.

Kislov K.V., Gravirov V.V. Distributed acoustic sounding: a new tool or a new paradigm. Seismic Instruments, Vol. 58, No. 2, 2022, p. 5-38, DOI: 10.21455/si2022.2-1.

Kuvshinov B.N. Interaction of helically wound fibre-optic cables with plane seismic waves. Geophysical Prospecting, Vol. 64, No. 3, 2016, pp. 671-688, DOI: 10.1111/1365-2478.12303.

Lee D., Park K.G., Lee C.-N., Choi S.-J. Distributed temperature sensing monitoring of well completion processes in a CO2 Geological Storage Demonstration Site. Sensors, Basel, Vol. 18, No. 12, 2018, 4239 p., https://doi.org/10.3390/s18124239.

Mao B., Bu Z. Xu B. et al. Denoising method based on VMD-PCC in φ-otdr system. Optical Fiber Technology, Vol. 74, No. 3, 2022, 103081, DOI: 10.1016/j.yofte.2022.103081.

Mateeva A., Mestayer J., Cox B. et al. Advances in distributed acoustic sensing (DAS) for VSP. SEG Technical Program Expanded Abstracts, 2012, 4609 p., DOI: 10.1190/segam2012-0739.1.

Ipatov A.I. et al. Monitoring of reservoir production in horizontal wellbores based on the results of unsteady thermometry by distributed fiber-optic sensors. PRONEFT - Professionally About Oil, 2021, No. 4 (22), pp. 81-91 (in Russian).

Kislov K.V., Gravirov V.V. Distributed acoustic sounding: a new tool or a new paradigm. Seismic Instruments, Vol. 58, No. 2, 2022, p. 5-38, DOI: 10.21455/si2022.2-1.

Kolychev I.Yu., Denisov A.M., Belov S.V. et al. Assessment of possibilities of application of vibroacoustic impact technology (DAS) in monitoring of oil and gas wells operation. Problems of Development of Hydrocarbon and Ore Mineral Deposits, Vol. 1, 2022, pp. 250-255 (in Russian).

Kuvshinov B.N. Interaction of helically wound fibre-optic cables with plane seismic waves. Geophysical Prospecting, Vol. 64, No. 3, 2016, pp. 671-688, DOI: 10.1111/1365-2478.12303.

Lee D., Park K.G., Lee C.-N., Choi S.-J. Distributed temperature sensing monitoring of well completion processes in a CO_2 Geological Storage Demonstration Site. Sensors, Basel, Vol. 18, No. 12, 2018, 4239 p., https://doi.org/10.3390/s18124239.

Mao B., Bu Z. Xu B. et al. Denoising method based on VMD-PCC in φ-otdr system. Optical Fiber Technology, Vol. 74, No. 3, 2022, 103081, DOI: 10.1016/j.yofte.2022.103081.

Mateeva A., Mestayer J., Cox B. et al. Advances in distributed acoustic sensing (DAS) for VSP. SEG Technical Program Expanded Abstracts, 2012, 4609 p., DOI: 10.1190/segam2012-0739.1.

Moradi P., Dande S., Angus D. Fibre-optic sensing and microseismic monitoring evaluate and enhance hydraulic fracturing via real-time and post-treatment analysis. First Break, Vol. 38, No. 9, 2020, pp. 65-72.

Näsholm S.P., Iranpour K., Wuestefeld A. et al. Array signal processing on distributed acoustic sensing data: directivity effects in slowness space. Journal of Geophysical Research: Solid Earth, Vol. 127, No. 2, 2022, pp. 1-24, DOI: 10.1029/2021JB023587.

Nikolaev S.A., Ovchinnikov M.N. Sound generation by a filtrational flow in porous. Akusticeskij zurnal, Vol. 38, No. 1, 1992, pp. 114-118 (in Russian).

Parker T., Shatalin S., Farhadiroushan M. Distributed acoustic sensing – a new tool for seismic applications. First Break, Vol. 32, No. 2, 2014, pp. 61-69, DOI: 10.3997/1365-2397.2013034.

Stork A.L., Baird A.F., Horne S.A. et al. Application of machine learning to microseismic event detection in distributed acoustic sensing data. Geophysics, Vol. 85, No. 5, 2020, pp. 149-160, DOI: 10.1190/geo2019-0774.1.

Wu H., Li X., Li H. et al. An effective signal separation and extraction method using multi-scale wavelet decomposition for phase-sensitive OTDR system. The International Society for Optical Engineering, Vol. 8916, 2013, 89160Z, DOI: 10.1117/12.2035836.

Wu X., Willis M.E., Palacios W. et al. Compressional and shear-wave studies of distributed acoustic sensing acquired vertical seismic profile data. The Leading Edge, Vol. 36, No. 12, 2017, pp. 962-1044, DOI: 10.1190/tle36120987.1.

Moradi P., Dande S., Angus D. Fibre-optic sensing and microseismic monitoring evaluate and enhance hydraulic fracturing via real-time and post-treatment analysis. First Break, Vol. 38, No. 9, 2020, pp. 65-72.

Näsholm S.P., Iranpour K., Wuestefeld A. et al. Array signal processing on distributed acoustic sensing data: directivity effects in slowness space. Journal of Geophysical Research: Solid Earth, Vol. 127, No. 2, 2022, pp. 1-24, DOI: 10.1029/2021JB023587.

Nikolaev S.A., Ovchinnikov M.N. Sound generation by a filtrational flow in porous. Akusticeskij zurnal, Vol. 38, No. 1, 1992, pp. 114-118 (in Russian).

Parker T., Shatalin S., Farhadiroushan M. Distributed acoustic sensing – a new tool for seismic applications. First Break, Vol. 32, No. 2, 2014, pp. 61-69, DOI: 10.3997/1365-2397.2013034.

Stork A.L., Baird A.F., Horne S.A. et al. Application of machine learning to microseismic event detection in distributed acoustic sensing data. Geophysics, Vol. 85, No. 5, 2020, pp. 149-160, DOI: 10.1190/geo2019-0774.1.

Wu H., Li X., Li H. et al. An effective signal separation and extraction method using multi-scale wavelet decomposition for phase-sensitive OTDR system. The International Society for Optical Engineering, Vol. 8916, 2013, 89160Z, DOI: 10.1117/12.2035836.

Wu X., Willis M.E., Palacios W. et al. Compressional and shear-wave studies of distributed acoustic sensing acquired vertical seismic profile data. The Leading Edge, Vol. 36, No. 12, 2017, pp. 962-1044, DOI: 10.1190/tle36120987.1.

Zhirnov A.A., Stepanov K.V., Chernutsky A.O. et al. Influence of laser frequency drift in phase-sensitive optical time domain reflectometry. Optics and Spectroscopy. Vol. 127, No. 10, 2019, pp. 656-663, DOI: 10.21883/OS.2019.10.48364.177-19 (in Russian).

Асланян А.М., Асланян И.Ю., Масленникова Ю.С. и др. Диагностика заколонных перетоков газа комплексом высокоточной термометрии, спектральной шумометрии и импульсного нейтрон-нейтронного каротажа. Территория нефти и газа, No. 6, 2016, с. 74-81.

Жирнов А.А., Степанов К.В., Чернуцкий А.О. и др. Влияние дрейфа частоты лазера в фазочувствительной рефлектометрии. Оптика и спектроскопия, Том 127, No. 10, 2019, с. 603-610, DOI: 10.21883/OS.2019.10.48364.177-19.

Ипатов А.И. и др. Мониторинг выработки коллектора в горизонтальных стволах по результатам нестационарной термометрии распределенными оптоволоконными датчиками. PRONEFTЬ – Профессионально о нефти, 2021, No. 4 (22), с. 81-91.

Кислов К.В., Гравиров В.В. Распределенное акустическое зондирование: новый инструмент или новая парадигма. Сейсмические приборы, Том 58, No. 2, 2022, с. 5-38, DOI: 10.21455/si2022.2-1.

Колычев И.Ю., Денисов А.М., Белов С.В. и др. Оценка возможностей применения технологии виброакустического воздействия (DAS) при мониторинге работы нефтяных и газовых скважин. Проблемы разработки месторождений углеводородных и рудных полезных ископаемых. Т. 1, 2022, с. 250-255.

Чугаев А.В., Тарантин М.В. Амплитудно-частотный отклик распределенного акустического сенсора DAS со спиральной намоткой волокна. Горные науки и технологии, Т. 8, No.1, 2023, с. 13-21, DOI: 10.17073/2500-0632-2022-06-10.

Чулков Е., Тихоцкий С.А., Дубиня Н.В. Дизайн сейсмических датчиков на основе принципа DAS: анализ и численное моделирование. Материалы Международной геолого-геофизической конференции, 27–29 марта 2023 года. Том 3, ПолиПРЕСС. Тверь, 2023, 234 с.

ВОЗМОЖНОСТИ МОНИТОРИНГА РАБОТЫ ГАЗОВЫХ СКВАЖИН МЕТОДОМ ШУМОМЕТРИИ С ПРИМЕНЕНИЕМ СИСТЕМЫ РАСПРЕДЕЛЕННЫХ АКУСТИЧЕСКИХ ДАТЧИКОВ

Колычев И.Ю.[1], Белов С.В.[1], Чистяков Н.Ю.[1], Гурбанов В.Ш.[1,2], Галкин С.В.[1]

[1]Пермский Национальный Исследовательский Политехнический Университет, Россия
614990, Пермь, Комсомольский проспект, 29
[2]Министерство науки и образования Азербайджанской Республики, Институт нефти и газа, Азербайджан
AZ1000, Баку, ул. Ф.Амирова, 9: vaqifqurbanov@mail.ru

Резюме. Рассмотрен опыт применения оптоволоконных распределенных акустических систем (DAS) при шумометрии скважин на основе геофизического кабеля при контроле за разработкой газоконденсатного месторождения. Проведены исследования по оценке спектральной чувствительности метода DAS. Разработана методика фильтрации исходного сигнала с расчетом энергии сигнала в различных диапазонах частот, что несет информацию о движении флюида внутри скважины. Путем комплексирования шумометрии скважин с исследованиями на основе волоконно-оптической системы распределенных датчиков температуры (DTS) выделены интервалы работающих в скважине газонасыщенных пластов. По методам DAS и DTS отчетливо выделяется момент остановки скважины.

Установлено, что информативность систем DAS и DTS зависит от места расположения кабеля. Для контроля за разработкой по технологии DTS оптимально размещать кабель внутри или снаружи эксплуатационной колонны. При расположении кабеля внутри НКТ поле температуры искажается встречными потоками флюида. Чувствительность системы DAS к шуму от породы и эксплуатационной колонны также может быть повышена оптимизацией расположения кабеля, что может быть обосновано при более широком внедрении данной технологии на производстве.

Для возможности регистрации шума от движения флюида за колонной и в породе необходимо расширить частотный диапазон регистрируемых колебаний за счет применения специальных кабелей с повышенной чувствительностью и расширенной диаграммой направленности. Достоверность исследований методом шумометрии DAS может быть существенно повышена путем тестирования программных алгоритмов для улучшения соотношения сигнал/шум. В перспективе предложенные подходы могут позволить не только судить по шумометрии DAS об интервалах фильтрации флюидов, но и на основе анализа спектров регистрируемых шумов определять характер их насыщения (нефть, вода, газ).

Ключевые слова: *шумометрия скважин, оптоволоконных распределенные акустические системы, газонасыщенные пласты, частотный диапазон*

QAZ QUYULARININ FƏALİYYƏTİNİ İZLƏMƏK ÜÇÜN AKUSTİK SENSORLARDAN İSTİFADƏ EDİLƏN SƏSÖLÇMƏ METODUNUN İMKANLARI

Kolıçev İ.Yu.[1], Belov S.V.[1], Çistyakov N.Yu[1]., Qurbanov V.Ş.[1,2], Qalkin S.V.[1]

[1]Perm Milli Araşdırma Politexnik Universiteti, Rusiya
614990, Perm, Komsomol prospekti, 29
[2]Azərbaycan Respublikası Elm və Təhsil Nazirliyi, Neft və Qaz İnstitutu, Azərbaycan
AZ1000, Bakı, F. Əmirov küçəsi, 9: vaqifqurbanov@mail.ru

Xülasə. Geofiziki kabeldən istifadə edərək qaz-kondensat yatağının işlənməsinə nəzarət zamanı quyularda optik lifli paylanmış akustik sistemlərin (DAS) tətbiq təcrübəsi təhlil edilmişdir. DAS metodunun spektral həssaslığını qiymətləndirmək məqsədilə araşdırmalar aparılmışdır. Fərqli tezlik diapazonlarında siqnalın enerjisini hesablamaqla ilkin siqnalın filtrasiya metodu işlənmişdir ki, bu da quyunun daxilində flüidin hərəkəti barədə məlumat verir. Quyularda səs-küy ölçmə prosesini optik lifli paylanmış temperatur sensorları (DTS) əsasında aparılan tədqiqatlarla birləşdirərək, quyuda qazla doymuş lay intervalları müəyyən edilmişdir. DAS və DTS metodları vasitəsilə quyunun dayanma anı dəqiq şəkildə izlənilə bilir.

Məlum olmuşdur ki, DAS və DTS sistemlərinin məlumat effektivliyi kabelin yerləşmə mövqeyindən asılıdır. DTS texnologiyası ilə nəzarət üçün kabelin istismar kolonunun içində və ya xaricində yerləşdirilməsi optimal hesab edilir. Kabel nasos-kompressor boruları (NKT) daxilində olduqda flüidlərin əks axınları temperatur sahəsində xətalar yaradır. DAS sisteminin süxur və istismar kolonu tərəfindən yaranan səs-küyə həssaslığı kabelin yerləşmə mövqeyinin optimallaşdırılması ilə artırıla bilər ki, bu da texnologiyanın daha geniş tətbiqi ilə əsaslandırıla bilər.

Kolon arxasında və süxurda flüidin hərəkətindən yaranan səs-küyün qeydiyyatı üçün daha geniş tezlik diapazonunu əhatə edən xüsusi yüksək həssas kabellərin istifadəsi tələb olunur. DAS metodunda səs-küy analizinin dəqiqliyi, siqnal-küy nisbətini yaxşılaşdırmaq məqsədilə proqram alqoritmlərinin sınaqdan keçirilməsi ilə xeyli artırıla bilər. Gələcəkdə təklif olunan yanaşmalar yalnız DAS vasitəsilə flüid filtrasiyası intervallarını müəyyənləşdirməyə deyil, həm də səs-küy spektrlərini analiz edərək onların tərkibini (neft, su, qaz) müəyyən etməyə imkan verə bilər.

Açar sözlər: *quyuların səs-küymetriyası, akustik sistemlərinin optiki lif paylanması, qazdoyumlu qatlar, tezlik diapazonu*

ТЕРМОГРАВИМЕТРИЧЕСКОЕ ИССЛЕДОВАНИЕ ГОРЮЧИХ СЛАНЦЕВ НЕКОТОРЫХ МЕСТОРОЖДЕНИЙ ВОСТОЧНОГО АЗЕРБАЙДЖАНА МЕТОДОМ МИКРОВОЛНОВОГО ВОЗДЕЙСТВИЯ

Мурадова П.А.[1], Литвишков Ю.Н.[1], Аббасов О.Р.[2]
[1]Министерство науки и образования Республики Азербайджан,
Институт катализа и неорганической химии им. М.Ф.Нагиева
AZ1143, Баку, просп. Г.Джавида, 113: muradovaperi@rambler.ru
[2]Министерство науки и образования Республики Азербайджан,
Институт геологии и геофизики AZ1143, Баку, просп. Г. Джавида, 119

THERMOGRAVIMETRIC STUDY OF OIL SHALES OF SOME DEPOSITS IN EASTERN AZERBAIJAN BY THE METHOD OF MICROWAVE IMPACT

Muradova P.A.[1], Litvishkov Yu.N.[1], Abbasov O.R.[2]
[1]Institute of Catalysis and Inorganic Chemistry named after M.F. Nagiev, Ministry of Science and Education of Azerbaijan
AZ1143, Baku, H. Javid Ave., 113: muradovaperi@rambler.ru
[2]Institute of Geology and Geophysics, Ministry of Science and Education of Azerbaijan
AZ1073, Baku, H. Javid Ave., 119

Keywords: Oil shale, thermolysis, microwave radiation, microwave penetration depth, chromatographic analysis

Summary. East Azerbaijan contains huge oil shale reserves, which according to available data amount to several billion tons. Among the deposits with large predicted resources, Guba, Jangichay and Diyally are of particular importance. Despite its widespread use worldwide, especially for producing oil and gas hydrocarbons and thermal power, oil shale, found in more than 100 areas in East Azerbaijan, is still not used. The prospect of obtaining the listed products from oil shale requires the study of their thermal properties, including the patterns associated with the decomposition of kerogen in various temperature ranges. An attempt to thermolysis shale samples from some deposits of East Azerbaijan using microwave irradiation was made in this study. A high absorption rate and penetration depth of ultra-high-frequency electromagnetic radiation into the mass of the studied samples were established, which made it possible to predict a high degree of extraction of organic high-molecular and gaseous components in a shorter exposure time compared to traditional heating. The group composition of high-molecular organic products and gaseous compounds was studied using liquid-adsorption column chromatography in combination with gas chromatographic analysis of thermally desorbed components. The characteristics of the group composition of the organic part of the samples of oil shale from the studied deposits are presented, distributed by fractions as saturates, aromatics, resins and asphaltenes (SARA).

Введение

Из-за значительной истощенности сырьевых запасов нефти и природного газа в настоящее время внимание уделяется разработке альтернативных источников углеводородов, в частности, горючих сланцев, которые как по значительному объему и распространению месторождений, так и по относительно высокому содержанию органической составляющей следует рассматривать в качестве перспективных источников для получения углеводородного сырья (Зеленин, Озеров, 1983; Стрижакова, 2008; Стрижакова, Усова,

2006; Стрижакова и др., 2006; Лапидус и др., 2017; Рудин, Серебрянников, 1988). Кроме того, уникальный состав органического вещества горючих сланцев позволяет использовать их не только в качестве энергоносителей, но и как источник ценных химических продуктов (Aliyev et al., 2018; Aliyev et al., 2022).

Как видно из данных, приведенных в таблице 1, запасов горючих сланцев в мире существенно больше, чем запасов нефти и природного газа (Череповский,1988).

Таблица 1

Мировые ресурсы природных энергоносителей

Доказанные мировые ресурсы	
Углеводороды	Мировые ресурсы, млрд. т
Каменный уголь	1035
Горючие сланцы	825
Нефть	240
Природный газ	194

В Азербайджане сосредоточены огромные запасы горючего сланца, которые по имеющимся данным составляют около нескольких миллиардов тонн (Aliyev and Abbasov, 2020). Среди более 100 определенных на данный момент проявлений (выходов) горючих сланцев по прогнозным ресурсам наблюдаются также таковые, как Губинское, Джангичайское и Дияллинское, которые высоко оцениваются и классифицируются как месторождения (Aliyev and Abbasov, 2019; Алиев и др., 2000; Abbasov et al., 2025).

Исследование природы горючих сланцев, извлекаемых из 16 месторождений Азербайджана, и сопоставление их с характеристиками сланцев 15 месторождений стран ближнего и дальнего зарубежья позволяет отнести первые к категории наилучших среди низкокалорийных горючих сланцев (Алиев и др., 2002).

Так, сланцы месторождений Азербайджана выгодно отличаются по ряду качественных и количественных параметров, в частности, содержанием органического вещества (5-32%), серы (0,3-1,2%), зольностью (65-84%) и теплотой сгорания (3-14 МДж/кг), что намного превосходит аналогичные свойства низкокалорийных горючих сланцев месторождений Германии, КНР, Румынии и др. (Алиев, Белов, 2003; Aho et al., 2013; Aliyev and Abbasov, 2020).

В настоящее время основным способом извлечения органических продуктов из нефтегазоносных сланцев является их термическая обработка с использованием традиционных источников нагрева, в том числе различных теплоносителей, электронагрева и т.д. (Стрижакова, Усова, 2008; Стрижакова и др., 2010; Лапидус и др., 2018; Лапидус и др., 2020). Существенным недостатком данных способов является большая протяженность во времени (низкая скорость) термической обработки сланцев до полного извлечения органической массы, занимающая несколько часов, вследствие чего происходят нежелательные процессы коксования, влияющие на выход извлекаемой жидкой части углеводородов и образование оксидов углерода на завершающей стадии нагрева.

В последние годы в лабораторной и производственной практике все более широкое применение находят нетрадиционные способы энергетического воздействия физических полей на технологические среды, основанные, например, на использовании микроволнового электромагнитного излучения (Литвишков и др., 2015; 2019; Muradova et al., 2018). В связи с тем, что скорость и способ нагрева сланцев являются важнейшими факторами, влияющими на выход и свойства извлекаемых органических продуктов, в данной работе предпринята попытка термолиза горючих сланцев из некоторых месторождений Азербайджана, в частности, Губинского в Губинском, Джангичайского в Гобустанском и Дияллинского в Исмаиллинском районах при воздействии высокоскоростного источника сверхвысокочастотного (СВЧ) микроволнового излучения.

Экспериментальная часть

Исследования воздействия микроволнового излучения на образцы сланцев проводились на установке, сконструированной на базе лабораторной микроволновой печи марки «Sanyo EM-G5593V (Panasonic)» с объемом резонатора 23 л. Выходная мощность магнетрона варьировалась в диапазоне 200-800 Вт при рабочей частоте 2450 МГц. Контроль температуры образцов в резонаторе печи осуществлялся дистанционным инфракрасным пирометром марки «CEM DT-8858» со шкалой измерения температуры (50-1300°C).

Экспозиция измельченных до фракции 1-5 мм образцов осуществлялась в размещенном в резонаторе печи прозрачном для микроволнового излучения кварцевом реакционном сосуде емкостью 100 мл, снабженном входной и газоотводной линией.

Для предотвращения окислительного превращения термически десорбированных органических продуктов в воздушной атмосфере микроволновый нагрев образцов проводился в редуцированном потоке азота, подаваемого со скоростью 100-150 мл/мин.

Установка оснащена системой конденсации и улавливания жидких продуктов термолиза. Газообразные продукты улавливались в змеевиковой ловушке, охлаждаемой в сосуде Дьюара, заполненном твердым диоксидом углерода.

Во избежание неожиданного перегрева образцов в резонаторе печи устанавливалась шунтирующая емкость с циркулирующей дистиллированной водой.

Разделение жидкой части десорбированных углеводородов на компоненты осуществлялось методом жидкостно-адсорбционной хроматографии (saturates, aromatics, resins and asphaltenes) с использованием колонки с силикагелем марки

«КСК». Сложная углеводородная смесь разделялась при этом на четыре аналитические группы соединений: насыщенные углеводороды, ароматические соединения, смолы и асфальтены (ASTM).

Качественно-количественный анализ газообразной составляющей десорбированных соединений проводился на хроматографе марки «ЛХМ-8 МД» (колонка l=3,6 м, $d_{вн}$=3мм, заполненная фазой «Porapak QS»), при программированном нагреве термостата в диапазоне температур 30÷65^{0}C со скоростью подъема температуры 3-5^{0}C/мин.

Обсуждение результатов

Как известно, эффективность воздействия СВЧ излучения на неоднородные по своему составу технологические среды, к которым, в частности, относятся горючие сланцы, в значительной степени определяется их термотрансформационными свойствами, т.е. уровнем поглощения энергии генерируемого электромагнитного поля (ΔPx) и трансформации ее в теплоту (Валитов и др., 1984; Бердоносов и др., 2000; Бурлуцкий, Калеева, 2011). При этом независимо от параметров электромагнитного излучения, результатом измерения будет среднее значение потери его мощности:

$$\Delta P_x = \frac{c \cdot m \cdot \Delta T}{0.24\tau} \ (Дж/с) \qquad (1)$$

где: 0.24 – тепловой эквивалент работы, m – масса исследуемого образца, (г); c – удельная теплоемкость образца (кДж/кг·K); ΔT – измеряемое приращение температуры образца (K); τ – время экспозиции в микроволновой печи (с).

При оценке эффективности воздействия микроволнового излучения немаловажное значение имеет глубина его проникновения в объем образцов. Эмпирическое определение глубины проникновения электромагнитной волны в состав образцов заключается в выявлении такой толщины слоя среды $\boldsymbol{\delta}_E$, при которой обеспечивается практически полное поглощение воздействующей энергии СВЧ излучения (Еремин, Сюняев, 2016; Pavlenok et al., 2010; Даминев и др., 2002; Abramovitch et al., 1991; Бикбулатов и др., 2002):

$$\delta_E \approx \frac{\lambda}{\pi\sqrt{2\varepsilon'(\sqrt{1+tg^2}\delta - 1)}} \qquad (2)$$

Здесь: δ_E – расстояние, на котором амплитуда вектора напряженности электрического поля E_0 уменьшается в e раз ($e \approx 2,7$ – основание натурального логарифма), ε' – действительная часть относительной диэлектрической проницаемости материала катализатора, $tg\delta$ – тангенс угла диэлектрических потерь, λ – длина СВЧ волны.

На рис. 1 представлена гистограмма, иллюстрирующая зависимость потери мощности микроволнового излучения образцами горючего сланца, взятыми из залежей Губинского, Джангичайского, и Дияллинского месторождений. Видно, что диэлектрические потери излучения для образцов всех месторождений имеют достаточно высокий уровень, что способствует достижению температурного режима их микроволнового термолиза.
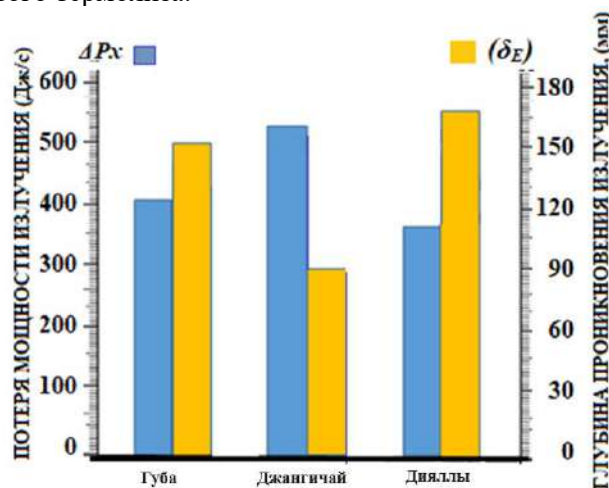
Рис. 1. Потери мощности СВЧ-излучения при микроволновом воздействии на образцы горючих сланцев, отобранных из месторождений Губа, Джангичай и Дияллы, и глубина проникновения излучения в их шихту. Условия экспозиции образцов: количество загрузки – 50 г.; мощность магнетрона – 600 Вт; рабочая частота – 2450 МГц; время экспозиции – 10 мин.; скорость потока N₂ – 120мл/мин.

Установлено, также, что величина глубины проникновения излучения в объем образцов превышает линейные размеры шихты, размещенной в резонаторе микроволновой печи, что обеспечивает отсутствие радиального градиента температуры при трансформации СВЧ излучения в теплоту.

Исследование динамики возрастания температуры образцов (рис. 2), при варьировании мощности излучения и времени экспозиции в резонаторе печи, позволило выявить различие скорости их нагрева, что, вероятно, связано с различием диэлектрических потерь в минеральной, неорганической составляющей сланцев, состав которой определяется собственно месторождением и доминирует над органическим веществом – керогеном. Так, для достижения температуры сланцевой шихты, необходимой для полной десорбции органической составляющей (400-600^{0}C), в случае Дияллинского месторождения необходимо воздействие излучения мощностью 800 Вт и время экспозиции ~20 минут, в то время как для микроволнового термолиза сланцев Джангичайского и Губинского место-

рождений необходим подъем мощности излучения до ~600 Вт.
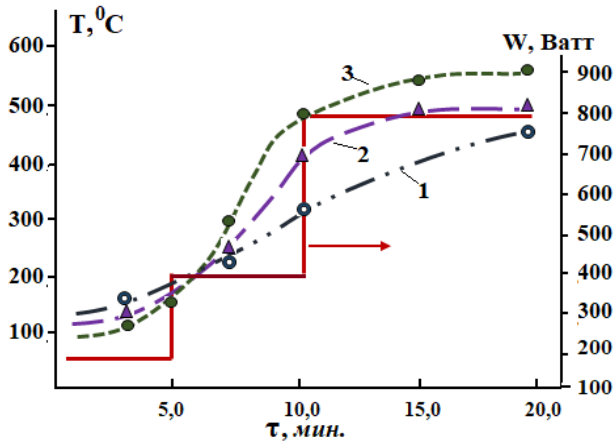
Рис. 2. Динамика возрастания температуры образцов горючих сланцев Дияллинского (1), Губинского (2) и Джангичайского (3) месторождений при варьировании мощности микроволнового излучения и времени экспозиции в резонаторе печи. Условия экспозиции образцов: количество загрузки – 50 г; рабочая частота – 2450 МГц; скорость потока N₂ – 120мл/мин.

После завершения экспозиции в резонаторе печи наблюдается относительно большое различие в потере веса исследуемых образцов. Максимальная потеря веса за счет десорбции углеродных компонентов происходит после микроволновой обработки образцов, взятых из месторождения Джангичай. Следует также отметить, что образцы сланцев этого месторождения характеризуются наибольшим соотношением десорбированной жидкой фазы к газообразной.

Учитывая данное обстоятельство, с практической точки зрения представляло целесообразным проведение дальнейших экспериментов по микроволновому термолизу с образцами Джангичайского месторождения. Так, было установлено, что потеря веса при десорбции связанных с органической частью сланца углеводородных компонентов происходит стадийно (рис. 3). При этом наблюдаются три основные температурные области потери веса образцов.

В первой области воздействия излучения в течение 5 минут экспозиции (при температуре ~200⁰С) с образованием воды происходит десорбция первичных газообразных компонентов, таких как C_1-C_4, CO и CO_2 (небольшое количество H_2S не исключается).

Продолжение экспозиции образцов в течение последующих 5 минут приводит к повышению температуры до ~ 400°С, и при этом наблюдается конденсация тяжелой составляющей углеводородных компонентов в ловушке. Для исследованного образца термическое битумообразо-

вание происходит при температуре около 400°С. Это очень хорошо коррелируется с критической температурой образования битума в мировых сланцах (340-360°С, Abbasov, 2023), включая эстонские (380°С, Shi et al., 2017). На завершающей стадии микроволнового воздействия на образцы происходит повышение их температуры до 600⁰С и выше. Эту стадию можно рассматривать как образование сланцевой нефти и газа вместе с коксом за счет распада более прочных связей С–С. Более подробно, после разложения органической части, содержащей относительно слабые связи С–N, С–S и С–О при температурах до 400°С, разложение органических компонентов с прочными связями С–С происходит при более высоких температурах в соответствии с требованием высокой энергии активации. По нашему мнению, сланцы Джангичая обладают более высоким потенциалом нефтегенерации, чем углеводородные газы. Что касается коксообразования, то этот процесс происходит за счет обильного выделения ароматического углерода при 500-600°С. Это объясняется тем, что алифатические соединения в органической части сланцев могут сохраняться при температуре около 500°С (Abbasov, 2023). В диапазонах выше этой температуры различные процессы, такие как поликонденсация ароматических углеводородов, ароматизация циклоалканов и реакция монооксида углерода с водой, могут отрицательно влиять на концентрацию водорода.
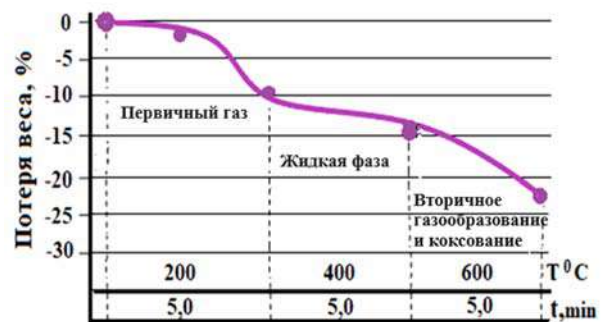
Рис. 3. Динамика потери веса образца горючего сланца месторождения Джангичай в результате десорбции газообразных и жидких органических компонентов. Условия: мощность магнетрона – 600 Вт, масса образца фракции 3-5 мм – 50 г

В таблице 2 приводятся результаты SARA-анализа группового состава десорбированных органических продуктов из образцов сланцев, в процентах от их массы.

Видно, что образцы сланцев всех трех месторождений характеризуются достаточно высоким отношением органической составляющей (20-23%) к общей массе образцов.

163

При этом максимальное количество извлеченных при микроволновом термолизе насыщенных углеводородов содержится в образцах горючих сланцев Губинского месторождения, в то время как образцы Джангичайского месторождения характеризуются относительно высоким общим содержанием органических соединений, а также содержанием ароматических и смолообразных продуктов.

В таблице 3 приведены результаты газохроматографического анализа газообразной части, десорбируемой в начальной стадии микроволнового воздействия на образцы горючих сланцев.

Видно, что в сравнении с образцами горючих сланцев Дияллинского и Губинского месторождений, образцы месторождения Джангичай характеризуются минимальным содержанием сероводорода и относительно высоким содержанием водорода.

Заключение

Таким образом, на основе совокупности представленных данных можно сделать вывод, что богатые органической частью сланцы некоторых изученных месторождений Восточного Азербайджана указывают на высокие перспективы получения углеводородов нефти и газа, а метод микроволновой термообработки, применяемый в этом исследовании, является эффективным, альтернативным методом исследования помимо горючих сланцев и других органических пород.

Таблица 2

Содержание в образцах сланцев органических продуктов, десорбированных
при воздействии микроволнового излучения мощностью 600-800 Вт,
при частоте магнетрона 2.45 ГГц. Количество использованных образцов – 50 г.

Образец сланца месторождения	Содержание органических продуктов, % (масс)			
	Насыщенные углеводороды	Ароматика	Смолы	Асфальтены
Губа	3.2	5.2	8.7	3.5
Джангичай	2.7	8.5	8.8	3.1
Дияллы	2.2	6.5	8.6	3.2

Таблица 3

Содержание в образцах сланцев газообразных продуктов, десорбированных
при воздействии микроволнового излучения мощностью 600-800 Вт,
при частоте магнетрона 2.45 ГГц. Количество использованных образцов – 50 г.

Образец сланца месторождения	Содержание газообразных продуктов, % (масс)				
	Монооксид углерода (CO)	Диоксид углерода (CO_2)	Сероводород (H_2S)	Метан (CH_4)	Водород (H_2)
Губа	0.6	0.8	1.3	2.5	1.5
Джангичай	0.5	0.4	0.7	3.1	2.3
Дияллы	0.8	1.6	1.8	2.2	1.7

ЛИТЕРАТУРА

Алиев Ад.А., Белов И.С., Алиев Г.М.А. Горючие сланцы миоцена Азербайджана. Азерб.Нефт.Хозяйство, No. 5, 2000, с. 7-11.

Алиев Ад.А., Белов И.С., Ибадзаде А.Д. Горючие сланцы Азербайджана (геология, геохимия и использование). Труды ИГ НАНА, No. 30, 2002, с.5-24.

Алиев Ад.А., Белов И.С. Горючие сланцы. В кн.: Геология Азербайджана, Том VI – Полезные ископаемые, Nafta-Press. Баку, 2003, с. 518-531.

Бердоносов С.С., Бердоносова Д.Г., Знаменская И.В. Микроволновое излучение в химической практике. Химическая технология, No. 3, 2000, с. 2-8.

Бикбулатов И.Х., Даминев Р.Р., Кузеев И.Р. и др. Реактор для проведения эндотермических процессов под действием СВЧ-излучения. Башкирский химический журнал, Том 9, No. 1, 2002, с.57-62.

REFERENCES

Abbasov O.R., Baloglanov E.E., Yolchuyeva U.J., Khuduzade A.I., Akhundov R.V. Factors controlling the formation and oil generating potential of the middle Eocene organic-rich shales of eastern Azerbaijan. Boletín de la Sociedad Geológica Mexicana, Vol. 77, No. 1, 2025, A020724, http://dx.doi.org/ 10.18268/BSGM2025v77n1a020724.

Abbasov O.R. Oil shale of Azerbaijan: Formation condition, distribution patterns, geochemical characteristics and assessment of prognostic resources. Doctor of Science Dissertation (Earth Sciences), Baku, Azerbaijan, 2023, 351 p. (in Azerbaijani).

Abramovitch R., Abramovitch D., Iyanar K., Tamareselvy K. Application of microwave energy to organic synthesis: improved technology. Tetrahedron Letters, Vol. 32, No. 39, 1991, pp. 5251-5254, https://doi.org/10.1016/S0040-4039 (00)92356-6.

Aho G.D. All oil shales are not the same. International Oil Shale Symposium. Tallinn, 2013, 20 p.

Бурлуцкий Д.С., Калеева Ж.Г. Изменение физических свойств материалов в результате экспериментального воздействия шарового электрического разряда, полученного с помощью сверхвысокочастотного излучения. Современные наукоемкие технологии, No. 5, 2011, с. 22-32.

Валитов Р.А., Дюбко С.Ф., Макаренко Б.И., Кузьмичев В.М., Мериакри В.В. Измерения на миллиметровых и субмиллиметровых волнах. Радио и связь. Москва, 1984, 296 с.

Еремин М.В., Сюняев Д.А. Температурная зависимость глубины проникновения магнитного поля при наличии дисперсии у параметров порядка сверхпроводимости и волн зарядовых плотностей. Письма в ЖЭТФ, Том 103, Вып. 3, 2016, с. 209-213.

Зеленин Н.И., Озеров И.М. Справочник по горючим сланцам. Недра. Ленинград, 1983, 248 с.

Лапидус А.Л., Шпирт М.Я., Малиновская Ю.А., Мовсумзаде Э.М., Худяков Д.С. Горючие сланцы – перспективное сырье для переработки твердых горючих ископаемых. Химия твердого топлива, No. 6, 2017, с. 15-21.

Лапидус А.Л., Бейлина Н.Ю., Худяков Д.С. Переработка горючих сланцев Волжского бассейна. Химия твердого топлива, No. 2, 2018, с. 6-13.

Лапидус А.Л., Бейлина Н.Ю., Худяков Д.С., Жагфаров Ф.Г. Исследование пека и кокса, полученных из смолы полукоксования высокосернистых горючих сланцев Волжского бассейна. Химия твердого топлива, No. 1, 2020, с. 26-29.

Литвишков Ю.Н., Гасанкулиева Н.М., Зульфугарова С.М., Мурадова П.А., Шакунова Н.В., Кашкай А.М., Марданова Н.М. Исследование характеристических параметров СВЧ-поглощающих носителей активной массы катализаторов для реакций, стимулируемых микроволновым излучением. Нефтепереработка и нефтехимия, Научно-технические достижения и передовой опыт, No. 4, 2015, с. 33-37.

Литвишков Ю.Н., Мурадова П.А., Третьяков В.Ф. Микроволновый синтез Ni-Co-Cr/Al$_2$O$_3$/Al-катализаторов с наноструктурированным активным компонентом и их активность в реакции деалкилирования толуола с водяным паром. Наногетерогенный катализ, Том 4, No. 1, 2019, с. 64-69.

Рудин М.Г., Серебрянников Н.Д. Справочник сланцепереработчика. Химия. Ленинград, 1988, 256 с.

Стрижакова Ю.А. Горючие сланцы. Генезис, составы, ресурсы. Недра. Москва, 2008, 192 с.

Стрижакова Ю.А., Усова Т.В, Третьяков В.Ф. Горючие сланцы – потенциальный источник сырья для топливно-энергетической и химической промышленности. Вестник МИТХТ, No. 4, 2006, с. 76-85.

Стрижакова Ю.А., Усова Т.В. Процессы переработки горючих сланцев. История развития. Технологии. Недра. Москва, 2008, 120 с.

Усова Т.В., Козлов А.М., Лапидус А.Л., Мовсумзаде Э.М. Стрижакова Ю.А. Каталитическая конверсия Кашпирских горючих сланцев. Нефтепереработка и нефтехимия, No. 8, 2010, с. 3-8.

Череповский В. Ф. Месторождения горючих сланцев мира. Наука. Москва, 1988, 263 с.

Abbasov O.R. Azərbaycanın yanar şistləri: əmələgəlmə şəraiti, yayılma qanunauyğunluqları, geokimyəvi xüsusiyyətləri və proqnoz resurslarının qiymətləndirilməsi. Elmlər doktorluğu dissertasiyası (Yer elmləri), Bakı, Azərbaycan, 2023, 351 s.

Abbasov O.R., Baloglanov E.E., Yolchuyeva U.J., Khuduzade A.I., Akhundov R.V. Factors controlling the formation and oil generating potential of the middle Eocene organic-rich shales of eastern Azerbaijan. Boletín de la Sociedad Geológica Mexicana, Vol. 77, No. 1, 2025, A020724, http://dx.doi.org/ 10.18268/BSGM2025v77n1a020724.

Aliyev A.A. and Abbasov O.R. Distribution patterns, organic geochemistry and mineralogy of oil shales in Azerbaijan. Gornyi Zhurnal, No 8, 2020, pp. 13-18, https://doi.org/ 10.17580/gzh.2020.08.02.

Aliyev A.A. and Abbasov O.R. Mineralogical and geochemical proxies for the Middle Eocene oil shales from the foothills of the Greater Caucasus, Azerbaijan: Implications for depositional environments and paleoclimate. Mineralia Slovaca, Vol. 51, No. 2, 2019, pp. 157-174.

Aliyev A.A., Abbasov O.R., Aghayev A.M., Khuduzade A.I., Hasanov E.H. Mineralogy, geochemistry and paleoweathering characteristics of Paleogene-Miocene oil shales in Azerbaijan. SOCAR Proceedings, No. 1, 2022, pp. 24-36, https://doi.org/10.5510/ogp20220100625.

Aliyev A.A., Abbasov O.R., Ibadzade A.J., Mammadova A.N. Genesis and organic geochemical characteristics of oil shale in Eastern Azerbaijan. SOCAR Proceedings, No. 3, 2018, pp. 4-15, https://doi.org/10.5510/OGP20180300356.

Aliyev Ad.A., Belov I.S., Aliyev H.M.A. Miocene oil shales of Azerbaijan. Azerbaijan Oil Industry Journal, No. 5, 2000, pp. 7-11 (in Russian).

Aliyev Ad.A., Belov I.S., Ibadzade A.J. Oil shale of Azerbaijan (geology, geochemistry and use). Proceedings of Geology Institute Nat., Acad.of Sciences of Azerbaijan, No. 30, 2002, pp. 5-24 (in Russian).

Aliyev Ad.A., Belov I.S. Oil shale. In.: Geology of Azerbaijan. Vol. VI. Mineral resources. Nafta-Press. Baku, 2003, pp. 518-531 (in Russian).

ASTM D 4124 – 09. Standard test method for separation of asphalt into four fractions. ASTM International. West Conshohocken. Pennsylvania, 2009, 8 p.

Berdonosov S.S., Berdonosova D.G., Znamenskaya I.V. Microwave radiation in chemical practice. Chemical technology, No. 3, 2000, pp. 2-8 (in Russian).

Bikbulatov I.Kh., Daminev R.R., Kuzeev I.R. et al. Reactor for endothermic processes under the action of microwave radiation. Bashkir Chemical Journal, Vol. 9, No. 1, 2002, p. 57-62.

Burlutskiy D.S., Kaleeva Zh.G. Changes in the physical properties of materials as a result of experimental exposure to a ball electric discharge obtained using microwave radiation. Modern science-intensive technologies, No. 5, 2011, pp. 22-32 (in Russian).

Cherepovsky V. F. Oil shale deposits of the world. Nauka. Moscow, 1988, 263 pp. (in Russian).

Daminev R.R., Bakhonin A.V., Kuzeev I.R., Bikbulatov I.Kh., Rakhmankulov D.L., Shulaev N.S., Bakhonina E.I. Reactor for carrying out endothermic processes under the influence of microwave radiation. Bashkir chemical journal, Vol. 9, No.1, 2002, p. 57-62 (in Russian).

Eremin M.V., Sunyaev D.A. Temperature dependence of the magnetic field penetration depth in the presence of dispersion in the order parameters of superconductivity and charge density waves. Letters to JETP (Journal of Experimental and Theoretical Physics), Vol. 103, No. 3, 2016, pp. 209-213 (in Russian).

Shi J., Ma Y. et al. Characteristics of Estonian oil shale kerogen and its pyrolysates with thermal bitumen as a pyrolytic intermediate. Energy and Fuels, Vol. 31, No. 5, 2017, pp. 4808-4816, https://doi.org/10.1021/acs.energyfuels.7b00054.

Lapidus A.L., Shpirt M.Ya., Malinovskaya Yu.A., Movsumzade E.M., Khudyakov D.S. Oil shale – a promising raw material for processing solid fossil fuels. Chemistry of solid fuel, No. 6, 2017, pp. 15-21 (in Russian).

Lapidus A.L., Beilina N.Yu., Khudyakov D.S. Processing of oil shale of the Volga basin. Chemistry of solid fuel, No. 2, 2018, pp. 6-13 (in Russian).

Lapidus A.L., Beilina N.Yu., Khudyakov D.S., Zhagfarov F.G. Study of pitch and coke obtained from the resin of semi-coking of high-sulfur oil shales of the Volga basin. Chemistry of Solid Fuel, No. 1, 2020, pp. 26-29 (in Russian).

Abramovitch R., Abramovitch D., Iyanar K., Tamareselvy K. Application of microwave energy to organic synthesis: improved technology. Tetrahedron Letters, Vol. 32, No. 39, 1991, pp. 5251-5254, https://doi.org/10.1016/S0040-4039(00)92356-6.

Aho G.D. All oil shales are not the same. International Oil Shale Symposium. Tallinn, 2013, 20 p.

Aliyev A.A. and Abbasov O.R. Distribution patterns, organic geochemistry and mineralogy of oil shales in Azerbaijan. Gornyi Zhurnal, No. 8, 2020, pp. 13-18, https://doi.org/10.17580/gzh.2020.08.02.

Aliyev A.A. and Abbasov O.R. Mineralogical and geochemical proxies for the Middle Eocene oil shales from the foothills of the Greater Caucasus, Azerbaijan: Implications for depositional environments and paleoclimate. Mineralia Slovac, Vol. 51, No. 2, 2019, pp. 157-174.

Aliyev A.A., Abbasov O.R., Aghayev A.M., Khuduzade A.I., Hasanov E.H. Mineralogy, geochemistry and paleoweathering characteristics of Paleogene-Miocene oil shales in Azerbaijan. SOCAR Proceedings, No. 1, 2022, pp. 24-36, DOI: 10.5510/OGP20220100625

Aliyev A.A., Abbasov O.R., Ibadzade A.J., Mammadova A.N. Genesis and organic geochemical characteristics of oil shale in Eastern Azerbaijan. SOCAR Proceedings, No. 3, 2018, pp. 4-15, https://doi.org/10.5510/OGP20180300356.

ASTM D 4124 – 09. Standard test method for separation of asphalt into four fractions. ASTM International. West Conshohocken. Pennsylvania, 2009, 8 p.

Muradova P.A, Zulfugarova S.M, Graser E, Strekov A.S, Litvishkov Y.N. Microwaves induced thermolysis of petroleum under contact with heterogenous catalysts. Chemie Ingenieur Technik, Vol. 90, No. 3, 2018, pp. 393-397, https://doi.org/10.1002/cite.201700010.

Shi J., Ma Y. et al. Characteristics of Estonian oil shale kerogen and its pyrolysates with thermal bitumen as a pyrolytic intermediate. Energy and Fuels, Vol. 31, No. 5, 2017, pp. 4808-4816, https://doi.org/10.1021/acs.energyfuels.7b00054.

Pavlenok A.V., Boiko A.A., Poddenezhny E.N. Synthesis of nano-structuredpowders ZnO using microwave energy. In: Abstracts book of International Symposium devoted to the 80th anniversary of Academician O.O.Chuiko: Modern problems of surface chemistry and physics, Kyiv, 18-21 May 2010, pp. 222-223.

Litvishkov Yu.N., Gasangulieva N.M., Zulfugarov S.M., Muradova P.A., Shakunova N.V., Kashkai A.M., Mardanova N.M. Study of characteristic parameters of microwave-absorbing carriers of active mass of catalysts for reactions stimulated by microwave radiation. Oil refining and petrochemistry. Scientific and technical achievements and advanced experience, No. 4, 2015, pp. 33-37 (in Russian).

Litvishkov Yu.N., Muradova P.A., Tretyakov V.F. Microwave synthesis of Ni-Co-Cr/Al/Al₂O₃ catalysts with nanostructured active component and their activity in the reaction of toluene dealkylation with water vapor. Nanoheterogeneous catalysis, Vol. 4, No. 1, 2019, pp. 1-6 (in Russian).

Muradova P.A, Zulfugarova S.M, Graser E, Strekov A.S, Litvishkov Y.N. Microwaves induced thermolysis of petroleum under contact with heterogenous catalysts. Chemie Ingenieur Technik, Vol. 90, No. 3, 2018, pp. 393-397, https://doi.org/ 10.1002/cite.201700010.

Pavlenok A.V., Boiko A.A., Poddenezhny E.N. Synthesis of nanostructuredpowders ZnO using microwave energy. Abstracts book of International Symposium devoted to the 80th anniversary of Academician O.O. Chuiko: Modern problems of surface chemistry and physics, Kyiv, 18-21 May 2010, pp. 222-223.

Rudin M.G., Serebryannikov N.D. Handbook of the shale processor. Chemistry. Leningrad, 1988, 256 p. (in Russian).

Strizhakova Yu.A. Oil shale. Genesis, compositions, resources. Nedra. Moscow, 2008, 192 p. (in Russian).

Strizhakova Yu.A., Usova T.V., Tretyakov V.F. Oil shale is a potential source of raw materials for the fuel, energy and chemical industries. Bulletin of Moscow State Academy of Fine Chemical Technology named after M.V. Lomonosov, No. 4, 2006, pp. 76-85 (in Russian).

Strizhakova Yu.A., Usova T.V., Processes of oil shale processing. History of development. Technologies. Nedra. Moscow, 2008, 120 p. (in Russian).

Strizhakova Yu.A., Usova T.V., Kozlov A.M., Lapidus A.L., Movsumzade E.M. Catalytic conversion of Kashpir oil shale. Oil refining and petrochemicals, No. 8, 2010, pp. 3-8 (in Russian).

Valitov R.A., Dyubko S.F., Makarenko B.I., Kuzmichev V.M., Meriakri V.V. Measurements on millimeter and submillimeter waves. Radio and communication. Moscow, 1984, 296 p. (in Russian).

Zelenin N.I., Ozerov I.M. Handbook of oil shale. Nedra. Leningrad, 1983, 248 p. (in Russian).

ТЕРМОГРАВИМЕТРИЧЕСКОЕ ИССЛЕДОВАНИЕ ГОРЮЧИХ СЛАНЦЕВ НЕКОТОРЫХ МЕСТОРОЖДЕНИЙ ВОСТОЧНОГО АЗЕРБАЙДЖАНА МЕТОДОМ МИКРОВОЛНОВОГО ВОЗДЕЙСТВИЯ

Мурадова П.А.[1], Литвишков Ю.Н.[1], Аббасов О.Р.[2]

[1]Министерство науки и образования Республики Азербайджан,
Институт катализа и неорганической химии им. М.Ф.Нагиева
AZ1143, Баку, просп. Г.Джавида, 113: muradovaperi@rambler.ru
[2]Министерство науки и образования Республики Азербайджан,
Институт геологии и геофизики AZ1143, Баку, просп. Г. Джавида, 119

Резюме. В Восточном Азербайджане сосредоточены огромные запасы горючего сланца, которые по имеющимся данным составляют несколько миллиардов тонн. Богатые органической частью сланцы некоторых изученных месторождений Восточного Азербайджана указывают на высокие перспективы получения углеводородов нефти и газа. Среди месторождений с большими прогнозными ресурсами особое значение имеют Губинское, Джангичайское и Дияллинское. Несмотря на широкое применение во всем мире, особенно для получения нефтегазовых углеводородов и теплоэлектроэнергии, горючий сланец, обнаруженный более чем в 100 объектах Восточного Азербайджана, до сих пор не используется. Перспектива получения перечисленных продуктов из горючих сланцев требует изучения их термических свойств, в том числе закономерностей, связанных с разложением керогена в различных температурных диапазонах. Известны некоторые методы, применяемые для проведения подобных исследований. В данном исследовании была предпринята попытка термолиза образцов сланцев некоторых месторождений Восточного Азербайджана на основе микроволнового воздействия. Установлены высокая скорость поглощения и глубина проникновения сверхвысокочастотного электромагнитного излучения в массу исследуемых образцов, что позволило прогнозировать высокую степень извлечения органических высокомолекулярных и газообразных компонентов за меньшее время экспозиции по сравнению с традиционным нагревом. Методом жидкостно-адсорбционной

колончатой хроматографии в сочетании с газохроматографическим анализом термически десорбированных компонентов исследован групповой состав высокомолекулярных органических продуктов и газообразных соединений. Приведена характеристика группового состава органической части образцов горючих сланцев исследуемых месторождений, распределенной по таким фракциям, как насыщенные, ароматические углеводороды, асфальтены и смолы.

Ключевые слова: Горючие сланцы, термолиз, СВЧ-излучение, глубина проникновения микроволнового излучения, хроматографический анализ

MİKRODALĞALI TƏSİR ÜSULU İLƏ ŞƏRQİ AZƏRBAYCANIN BƏZİ YATAQLARININ YANAR ŞİSTLƏRİNİN TERMOQRAVİMETRİK TƏDQİQİ

Muradova P.A.[1], Litvişkov Yu.N.[1], Abbasov O.R.[2]
*[1]Azərbaycan Elm və Təhsil Nazirliyinin M.F.Nağıyev adına Kataliz və Qeyri-üzvi Kimya İnstitutu
AZ1143, Bakı, H.Cavid pr., 113: muradovaperi@rambler.ru
[2]Azərbaycan Elm və Təhsil Nazirliyinin Geologiya və Geofizika İnstitutu
AZ1073, Bakı, H. Cavid pr., 119*

Xülasə. Şərqi Azərbaycanda nəhəng şist ehtiyatları var ki, bu, məlum olduğu kimi, mövcud məlumatlara görə bir neçə milyard ton təşkil edir. Böyük proqnozlaşdırılan ehtiyatlara malik yataqlar arasında Quba, Cangiçay və Diyallı xüsusi əhəmiyyət kəsb edir. Bütün dünyada, xüsusilə neft və qaz karbohidrogenləri və istilik enerjisi istehsalı üçün geniş istifadə olunmasına baxmayaraq, 100-dən çox sahədə aşkar edilməsinə baxmayaraq Şərqi Azərbaycanda neft şistindən hələ də istifadə olunmur. Belə ki, sadalanan məhsulların neft şistindən əldə edilməsi perspektivi onların istilik xassələrinin, o cümlədən, müxtəlif temperatur diapazonlarında kerogenin parçalanması ilə bağlı qanunauyğunluqların öyrənilməsi zərurəti yaranır. Belə tədqiqatların aparılması üçün istifadə edilən bəzi məlum üsullar mövcuddur. Bu tədqiqatda Şərqi Azərbaycanın bəzi yataqlarından mikrodalğalı sobanın təsiri ilə şist nümunələrinin termolizinə cəhd edilmişdir. Mikrodalğalı elektromaqnit şüalanmanın tədqiq olunan nümunələrin kütləsinə yüksək udma dərəcəsi və nüfuz dərinliyi müəyyən edilmişdir ki, bu da ənənəvi istiliklə müqayisədə daha qısa ekspozisiya müddətində üzvi yüksək molekulyar və qazlı komponentlərin yüksək dərəcədə çıxarılmasını proqnozlaşdırmağa imkan verir. Bundan başqa, yüksək molekulyar ağırlıqlı üzvi məhsulların və qazlı birləşmələrin qrup tərkibi maye adsorbsiya sütununun xromatoqrafiyasından istifadə etməklə, termik desorbsiya olunmuş komponentlərin qaz xromatoqrafik analizi ilə birlikdə tədqiq edilmişdir. Tədqiq olunan yataqlardan doymuş, aromatik, asfalten və qatranlar kimi fraksiyalar arasında paylanmış neftli şist nümunələrinin üzvi hissəsinin qrup tərkibinin xüsusiyyətləri verilmişdir.

Açar sözlər: Neft şisti, termoliz, mikrodalğalı radiasiya, mikrodalğalı şüalanmanın nüfuz dərinliyi, xromatoqrafik analiz

EFFECTIVE MANAGEMENT OF ENVIRONMENTAL RISKS IN THE OIL AND GAS INDUSTRY

Alizada E.K.[1], Bagirov A.A.[2], Bogopolsky V.O.[3], Shirinov M.M.[4]

[1]CJSC "Ekol Engineering Services", Azerbaijan
64, 8 November Ave., Baku, AZ1026: elnur.alizade@ekol.az;
[2-4]Azerbaijan State Oil and Industry University, Azerbaijan
16/21, Azadlig Ave., Baku, AZ1010: azad-baqirov@mail.ru,
vadim46.46@mail.ru[3], shirinov46@mail.ru

Keywords: *risk management, environmental risks, environmental safety, oil enterprises, environmental insurance, environmental protection*

Summary. The application of the corporate governance system of transnational oil and gas companies and the formation of a positive rating are based on comprehensive risk management against the backdrop of rapid technological development in the modern world. Risk factors that form the investment attractiveness rating of territories, especially environmental risks are not always taken into account while assessing their impact. From an economic point of view, managing environmental risks of projects is more effective if they are implemented at earlier stages of project implementation and organization. Unfortunately, due attention is not paid to calculating lost environmental benefits. Active risk management should be systemic but currently more attention is paid to financial risks. At the same time, recent discussions of safety declarations for hazardous industrial facilities practically allow creating a system of detailed analysis of exposure to environmental risks during the entire production period at the pre-investment, investment and operational stages of oil field development and industry enterprises. As a rule, environmental risks are not taken into account in feasibility study documentations, and managerial documents substantiating investment projects indicate the conduct of such studies at environmental impact prices. In many cases, environmental risks at oil enterprises are classified as operational risks. Quantitative and qualitative assessment of economic risks at the stages of the project life cycle has a serious methodological and practical nature. The importance of such studies is due, firstly, to possible violations of natural laws and, secondly, to natural climatic factors, risks that have a negative impact on all stages of the project.

Introduction. Oil and gas fields, pipelines, processing plants, and fuel tanks have a high potential for accidents of various types and man-made disasters that can pose a danger to people and the environment.

The variety of risks emerging at oil and gas industry enterprises, the importance of defining an integrated approach to minimizing accidents and disasters, as well as the importance of solving environmental risks, which occupy not the least place in the risk management system are considered important.

Safe operation of fuel areas will only be effective if they meet the highest requirements of international standards.

These are mainly standards ISO 9000 (quality management system), ISO 14000 (environmental management system) and ISO 45000 (occupational health and safety management system), other international documents related to environmental management and audit.

In the context of the integration of the Azerbaijani economy into the world economic system, as well as environmental problems, the tasks of assessing the activities of oil sector enterprises are very relevant.

From an economic point of view, if they are carried out at earlier stages of project implementation and organization, the costs of environmental discussion of projects including environmental risk assessment will be more effective. These costs are mainly reduced by creating an effective management system and avoiding environmental costs by oil industry enterprises reducing risks at production sites. However, unfortunately, at the pre-project stage, due attention is not paid to the discussion of calculations of lost environmental benefits (Бараненко, 2004).

Methodological principles of environmental risk management at oil and gas industry enterprises. Active risk management should be systematic, but currently more attention is being paid to fi-

nancial risks. At the same time, recent discussions of safety declarations for hazardous industrial facilities practically make it possible to create a system of detailed analysis of exposure to environmental risks throughout the entire production period at the pre-investment, investment and operational stages of oil field development and industry enterprises.

However, as a rule, environmental risks are not taken into account in feasibility study documents, and management documents justifying investment projects indicate the conduct of such studies at environmental impact prices.

In many cases, environmental risks in oil companies are classified as operational risks.

Quantitative and qualitative assessment of economic risks at the stages of the project implementation life cycle and product life cycle has a serious methodological and practical nature.

The importance of such studies is due, firstly, to possible violations of natural laws and, secondly, to natural climatic factors and risks that have a negative impact on all stages of the project.

The latter factors play a decisive role in pre-investment discussions. At the same time, regulatory requirements, especially environmental ones may change dramatically.

Environmental risks differ from the risks of force majeure in that most of them can be prevented.

However, insurance companies prefer to deal with the latter, although the profit from such a strategy is not so noticeable, even if an insured event occurs, the loss is huge.

Considering the current technological state of pipeline systems, berths and many technical structures in the oil industry, it is not so difficult to calculate the environmental risks and possible economic damage, for example, from the destruction of pipes in many places (Ализаде и др., 2010).

Even according to the roughest estimates, the annual costs of eliminating the consequences of accidents (excluding compensation for environmental damage) can amount to millions.

Therefore, registration of environmental risks of oil enterprises creates great opportunities for insurance activities (Aliyev, Alizade, 2012).

In addition, now it is necessary for oil companies to begin work on risk classification and the creation of a risk reporting system, as a result of which it will be possible to manage risks. Namely, risk management will be a somewhat integrative function that should be applied to all divisions and activities of oil enterprises. Environmental risks will not be given the last role in such an integration function.

This is confirmed by the fact that, unlike other production and project risks, a real basis for creating an environmental risk management system has al-

ready been created - this is the transition to ISO 14000 and ISO 31000 standards.

Stages of risk analysis. In general, the following main problems can be identified (Məhərrəmov və b., 2014) while considering individual stages of risk analysis of oil and gas industry enterprises:
– risk exposure and hazard identification;
– assessment of dependence;
– risk characteristics.

Assessing and managing environmental risks requires more than just an analysis of the likelihood of negative events occurring. Another main factor in risk analysis is the economic assessment of the consequences of negative events.

For environmental risks, this assessment describes the determination of the amount of environmental and economic damage. Some of the existing problems have been discussed for a long time, others are specific to the field of economic risk assessment and environmental insurance (Буянов, 2004).

The risk is calculated using the following formula (Попов и др., 2008):

$$R = P * X$$

R – volume of environmental and economic risk; P – possibility or probability of the occurrence of a negative moment or conditions (requiring financial costs); X – damage (volume of value).

First of all, the problem is linking the environmental consequences of this damage, its monetary measurement and moral damage for any violation of the state of the natural environment.

It should be noted that any assessment here is always controversial.

In addition to the difficulties of assessing moral damage, there are many controversial issues in such a precise definition, but these are the long-term consequences of negative environmental events (for example, assessing the significance of obvious changes in the ecosystem as a result of the influence of negative events). The hidden and far-reaching effects that occur and will occur in the ecosystem affect human health.

Another challenge is the outdated existing methods for calculating environmental and economic damage. When assessing environmental and economic damage, more objective and comprehensive methods are needed than those based on price indicators of the 90s of the XX century.

Significant difficulties in determining the economic assessment of environmental damage are associated with the incompleteness or lack of accuracy of existing methods.

Many of them rely on indirect methods for determining harm, which themselves require the use of more successful "cookie cutter" assessments.

In many cases, the lack of "ecological accuracy" is due to the fact that the resulting assessments are primarily human-centered.

Thus, the thresholds for the probability of effects are taken into account when assessing damage are determined primarily for humans, and not for other components of the environment (possibly more sensitive) or economic objects.

This problem is also associated with the lack of measures for assessing many representatives of the animal and plant world, taking into account their territorial "value," as well as the lack of unified territorial inventories of natural resources and calculations of the ecological potential of various species (Aliyev, Alizade, 2012).

Problems of environmental and economic assessment (including insurance cases) must be solved by developing new methods for calculating damage.

Such methods should be based on a modern method of assessing natural resources, modern methods for determining changes in the environment, damage caused by negative impacts on its components, and should be focused not only on humans, but also on other realities of the environment.

The feasibility of such work is also due to the importance of an accurate economic assessment of negative environmental consequences. It is clear that effective risk management should ultimately lead to risk reduction. However, for this it is necessary to compare the results of economic activity with the income received and costs aimed at eliminating the negative results, the so-called "environmental costs".

In this case, the effectiveness of environmental risk management will be fully assessed by comparing the funds invested in preventive measures and the costs incurred for liquidation and compensation of damage. Environmental payments must fully cover environmental costs, and tariffs must fully cover the costs of accidents at enterprises.

In such conditions, taking into account environmental payments, enterprises are faced with a choice: either to hide the fact of the accident and evade payments (due to force majeure), or to solve the problems of environmental insurance strictly by assessing the relevant environmental risks (Sylvia Adipah, 2018).

The latter is considered preferable, since "every hidden secret is revealed sooner or later," and the possible financial payout can be very difficult even for large companies.

Thus, the environmental organization of each individual type of risk is transferred to a strategic category, which is considered relevant in corporate risk management (Буянов, 2004).

Currently, the functions of environmental insurance in developed countries are receiving more and more attention. It is known that this primarily expresses the interests of the population, the state and legal entities regarding various risks in the natural scientific environment. Expanding the essence of environmental insurance as a mechanism for environmental management involves giving it preventive, monitoring, compensation and investment functions (Israfilov et al., 2016).

It is necessary to provide for the development of the following promising types of environmental insurance for oil and gas industry enterprises:

– environmental insurance;
– agreement of liability for failure to comply with the terms of the contract for the use of natural resources;
– insurance against extreme natural disasters;
– insurance of financial, investment and business risks in the environmental environment.

Risk management should focus primarily on minimizing financial risks. The main goal of this approach is to ensure predictable financial results, including those aimed at eliminating accidents and compensating for environmental damage (Хисметов и др., 2009).

In other words, the formation of environmental insurance funds should not be blind and should be reflected as a separate line item in environmental protection expenditures.

Accounting for economic risks. A rather serious problem is that state statistics authority only register major accidents associated with fires, floods and other situations. It is known that there are other accidents that do not have huge consequences and they are covered at the expense of own funds of the company and do not require wide discussion.

This summary applies not only to fixed assets, and calculating the loss is not difficult since the book values of fixed assets are known.

It is more difficult to calculate the damage caused to the environment and people by the collapse of one or another engineering equipment as a result of emergency situations (Ализаде и др., 2023).

Oil sector facilities in a market economy, first of all, do not accurately take into account economic risks; they usually ignore man-made and environmental (natural) risks (Israfilov et al., 2016).

However, presenting such categorical risks in monetary terms can radically change the attitude towards environmental issues at oil sector enterprises. Therefore, the basis for regulating safety in the technogenic environment should be based on an economic assessment, since in market conditions the main role is played by the interaction of the "cost-effectiveness" criteria.

To summarize the above, I would like to propose that the development of an economic mechanism for ensuring the environmental safety of enterprises in the oil sector should be carried out considering the following areas:

– the emergence of economic regulation of environmental safety (for example, strategies for reducing environmental risks and integrated environmental risk management);

– preparation of an economic mechanism for regulating environmental safety and its approval (for example, an action plan to reduce environmental risks);

– experimental modeling of the mechanism for environmental safety control;

– legal and regulatory support;

– development of a monitoring mechanism for environmental safety regulation;

– formation of environmental insurance funds for environmental protection costs;

– development of a mechanism for stimulating the head of the enterprise and risk managers and vesting high powers to resolve a specific issue in order to prevent an environmental disaster.

The goal of integrated environmental risk management in the oil and gas industry is to regulate rules, ensure the safety of enterprise workers and the environment, identify and implement preventive measures before an accident or risk occurs, and eliminate consequences, conscious risk and conducting appropriate training (Aliyev, Alizade, 2012).

To achieve the environmental safety goals and the upcoming strategic goal, it is necessary to start by defining responsibilities in environmental risk management (Aliyev, Alizade, 2013).

Namely, the strategic management and employees of an oil company or enterprise are responsible for risk management within the limits of their authority.

To achieve this, the powers and responsibilities must be clear to each responsible person.

• **The powers of a strategic manager of an enterprise include:**

– determine the criteria for the significance of risks, approve methodological documents, determine priorities, approve measures, make decisions on rapid response measures by reviewing reports, evaluate the effectiveness of measures aimed at managing and eliminating risks and monitoring the implementation of the program of measures.

• **The powers of the head of a structural unit (risk owner) include:**

– be responsible for risk management within the scope of activities of divisions, bring into action general control over the risk management process, identify and assess risks within the division, develop measures aimed at risk management and organize

the monitoring process, as well as provide information (reports) to management on changes.

• Risk management units (risk managers) are responsible for: developing standards and methodologies for risk assessment, providing guidelines in the field of identifying, assessing and managing risks within their competence, monitoring the risk management process by structural units and risk management to monitor the implementation of the plan actions.

• Environmental departments are responsible for: identifying environmental problems and risks for the structural divisions of the enterprise, determining appropriate measures and monitoring the implementation of environmental programs. He instructs employees in this area, constantly monitors the implementation of environmental programs and monitors the implementation of the environmental action plan.

On the system for monitoring the implementation of environmental protection measures.

In order to ensure the effective functioning of the environmental risk management system, it is necessary to carry out regular monitoring in the relevant areas of activity of structural units.

Responsibility for monitoring lies with the management of this structural unit, the environmental department and the risk management department.

In order to monitor the implementation of pre-planned activities, the results of the implemented monitoring and identified deficiencies should be recorded, analyzed and given the necessary recommendations to the risk owner, and the final report compiled on the monitoring results should be submitted to the company management.

Conclusion. Based on the above, as well as practical experience, it is possible to classify environmental risks identified in the oil and gas industry into the following seven areas according to their characteristics:

1. Field of geology and geophysics;
2. Oil and gas well drilling site;
3. Oil and gas production area;
4. Oil and gas transportation area;
5. Oil and gas processing area;
6. Petrochemical industry;
7. Construction site.

In general, environmental risks identified in areas of activity can be divided into two groups according to the degree of impact:

✓ Environmental risks that directly affect the environment;

✓ Environmental risks that led to disasters.

Based on practical experience, the authors proposed to apply the following innovative measures in order to improve the system and mechanism for managing environmental risks in oil and gas companies:

1. Preparation of an environmental impact assessment (EIA) document, conducting an environmental assessment and other necessary environmental regulatory and technical documents before carrying out work in accordance with the requirements of environmental legislation;

2. Environmental monitoring, accounting and reporting on the environmental impact of economic activities that may cause environmental hazards;

3. Carrying out constant laboratory monitoring of the compliance of discharges into the environment on the territory of the enterprise with permissible maximum standards;

4. Monitoring compliance with environmental standards and safety rules when disposing of all oils and other waste oils containing polychlorinated biphenyl (PCB) used in electrical equipment (in electrical equipment with a chlorine content of more than 50 ppm);

5. Approval and implementation of the documents "Strategy for reducing the impact on climate change" and "Plan for reducing greenhouse gas emissions";

6. Approval and implementation of the document "Waste Management Plan";

7. Approval and implementation of the document "Oil Spill Response Plan";

8. In order to prevent the spread of environmental damage, the forming of teams that will take immediate action in case of accidents and provide technical means;

9. Regular propaganda of environmental risks and their consequences, installation of warning and propaganda posters and billboards at workplaces;

10. Development of an appropriate training program on environmental risk management.

Research methods. Significant difficulties in determining the economic assessment of environmental damage are associated with the incompleteness or lack of accuracy of existing methods. Many of them rely on indirect methods for determining harm, which themselves require the use of more successful "cookie cutter" assessments.

Problems of environmental and economic assessment (including insurance cases) must be solved by developing new methods for calculating damage.

Such methods should be based on a modern method of assessing natural resources, modern methods for determining changes in the environment, damage caused by negative impacts on its components, and should be focused not only on humans, but also on other realities of the environment.

Scientific novelty. In order to improve the system and mechanism for managing environmental risks in oil and gas companies, it is considered advisable to apply the following innovative measures: preparation of EIA and other necessary environmental regulatory and technical documents; accounting and reporting on the environmental impact of economic activities that may cause environmental hazards; carrying out constant laboratory monitoring of the compliance of discharges into the environment on the territory of the enterprise with permissible maximum standards; regular propaganda of environmental risks and their consequences at workplaces.

Results. Environmental risks identified in the oil and gas industry were classified based on their characteristics in seven areas (geology and geophysics; oil and gas well drilling area; oil and gas production area; oil and gas transportation area; oil and gas processing area; petrochemical industry; construction area). In general, environmental risks identified in areas of activity were considered according to the degree of their impact and divided into those that directly affect the environment and those that led to disasters.

Practical value. Based on practical experience, the authors proposed to apply the following innovative measures in order to improve the system and mechanism for managing environmental risks in oil and gas companies:

1. Preparation of an environmental impact assessment (EIA) document, conducting an environmental assessment and other necessary environmental regulatory and technical documents before carrying out work in accordance with the requirements of environmental legislation;

2. Environmental monitoring, accounting and reporting on the environmental impact of economic activities that may cause environmental hazards;

3. Carrying out constant laboratory monitoring of the compliance of discharges into the environment on the territory of the enterprise with permissible maximum standards;

4. Monitoring compliance with environmental standards and safety rules while disposing of all oils and other waste oils containing polychlorinated biphenyl (PCB) used in electrical equipment (in electrical equipment with a chlorine content of more than 50 ppm);

5. Approval and implementation of the documents "Strategy for reducing the impact on climate change" and "Plan for reducing greenhouse gas emissions";

6. Approval and implementation of the document "Waste Management Plan";

7. Approval and implementation of the document "Oil Spill Response Plan";

8. In order to prevent the spread of environmental damage, the forming of teams that will take immediate action in case of accidents and provide technical means;

9. Regular propaganda of environmental risks and their consequences, installation of warning and propaganda posters and billboards at workplaces;

10. Development of an appropriate training program on environmental risk management.

REFERENCES	ЛИТЕРАТУРА

REFERENCES

Aliyev A.G., Alizade E.K. Environmental protection and oil spill management in the State Oil Company of the Azerbaijan Republic. Ecology and Industry of Kazakhstan, Alma-Ata, No. 1(37), 2013, pp. 56-58 (in Russian).

Aliyev A.H., Alizade E.K. Main risks in oil and gas industry companies and their efficient management. Azerbaijan Oil Industry, No. 2, 2012, pp. 60-65.

Alizade E., Bogopolskiy V., Samedov V., Shirinov M., Bagirov A. Effective risk management measures in oil industry companies in crisis conditions. Equipment, technologies, materials, No. 17 (05), 2023, pp. 4-11 (in Azerbaijani).

Alizade E.K., Ragimov R.A., Salimov S.M. Ways to create a competitive economy based on the effective use of oil and gas revenues. Problems of economics and management of the oil and gas complex, Moscow, No. 2, 2010. pp. 34-37 (in Russian).

Baranenko S.P. Risks and their management in the enterprise management system. In: Risk management (Baranenko S.P., Shemetov V.V.), Baku, No. 2, 2004, pp. 32-35 (in Russian).

Buyanov V.P. Analysis of risks in the activities of an enterprise. Issues of Economics, No. 8. 2004, pp. 128-134 (in Russian).

Israfilov Y.H., Israfilov R.H., Guliyev H.H., Efendiyev G.M. Risk assessment of the water resources losses of the Azerbaijan republic due to climate changes. Proceedings of ANAS, the sciences of Earth, No. 3-4, 2016

Khismetov T.V., Efendiev G.M., Jafarov K.A. Analysis and assessment of the risk level of accidents during well drilling. Oil Industry, No.10, 2009, pp.46-48 (in Russian).

Maharramov A., Salimov S., Alizade E. Improvement of the risk management system in oil companies in the conditions of sustainable development of the economy. Journal of international law and integration problems, Baku, No. 3(39), 2014, pp. 371-380 (in Azerbaijani).

Popov V.M., Lyapunov S.I., Kasatkin A.A. Business planning: analysis of errors, risks and conflicts. KnoRus. Moscow, 2008, 448 p. (in Russian).

Sylvia Adipah. The Ecological effects of oil mitigation associated with environmental risk. Journal of Environmental Science and Public Health, No. 2, 2018, pp. 160-167.

ЛИТЕРАТУРА

Aliyev A.H., Alizade E.K. Main risks in oil and gas industry companies and their efficient management. Azerbaijan Oil Industry, No. 2, 2012, pp. 60-65.

Israfilov Y.H., Israfilov R.H., Guliyev H.H., Efendiyev G.M. Risk assessment of the water resources losses of the Azerbaijan republic due to climate changes. – Proceedings of ANAS, the sciences of Earth, No. 3-4, 2016

Sylvia Adipah. The Ecological effects of oil mitigation associated with environmental risk. Journal of Environmental Science and Public Health, No. 2, 2018, pp. 160-167.

Ализаде Е.К., Рагимов Р.А., Салимов С.М. Пути создания конкурентоспособной экономики на основе эффективного использования нефтегазовых доходов. Проблемы экономики и управления нефтегазовым комплексом, Москва. No. 2, 2010, с. 34-37.

Алиев А.Г., Ализаде Э.К. Охрана окружающей среды и управление разливами нефти в Государственной нефтяной компании Азербайджанской Республики. Экология и промышленность Казахстана, Алма-Ата, No. 1 (37), 2013, с. 56-58.

Бараненко С.П. Риски и управление ими в системе управления предприятием. В: Управление рисками (С.П. Бараненко, В.В. Шеметов), Баку, No. 2, 2004, с. 32-35.

Буянов В.П. Анализ рисков в деятельности предприятия. Вопросы экономики, No. 8. 2004, с. 128-134.

Попов В.М., Ляпунов С.И., Касаткин А.А. Бизнес-планирование: анализ ошибок, рисков и конфликтов. КноРус. Москва, 2008, 448 с.

Хисметов Т.В., Ефендиев Г.М., Джафаров К.А., Абдиров А.А. Анализ и оценка уровня риска аварий при бурении скважин. Нефтяное хозяйство, No. 10, 2009, с. 46-48.

Əlizadə E., Boqopolski V., Səmədov V., Şirinov M., Baqirov A. Böhran şəraitində neft sahəsi şirkətlərində risklərin səmərəli idarə olunması tədbirləri. Avadanlıq, texnologiyalar, materiallar, No. 17(05), 2023, с. 4-11.

Məhərrəmov A., Səlimov S., Əlizadə E. İqtisadiyyatın davamlı inkişafı şəraitində neft şirkətlərində risklərin idarə edilməsi sisteminin təkmilləşdirilməsi. Beynəlxalq hüquq və inteqrasiya problemləri jurnalı, Bakı, No. 3 (39), 2014, s. 371-380.

ЭФФЕКТИВНОЕ УПРАВЛЕНИЕ ЭКОЛОГИЧЕСКИМИ РИСКАМИ НА ПРЕДПРИЯТИЯХ НЕФТЕГАЗОВОЙ ОТРАСЛИ

Ализаде Э.К.[1], Багиров А.А.[2], Богопольский В.О.[3], Ширинов М.М.[4]

[1]ЗАО «Ekol Engineering Services», Азербайджан
AZ1026, Баку, просп. 8 Ноября, 64: elnur.alizade@ekol.az;
[2-4]Азербайджанский государственный университет нефти и промышленности, Азербайджан
AZ1010, Баку, просп. Азадлыг,16/21: azad-baqirov@mail.ru, vadim46.46 @ mail.ru, shirinov46@mail.ru

Резюме. На фоне бурного развития технологий в современном мире применение системы корпоративного управления транснациональных нефтегазовых компаний и формирование положительного рейтинга основаны на комплексном управлении рисками. Факторы риска, формирующие рейтинг инвестиционной привлекательности территорий, особенно экологические риски, не всегда учитываются при оценке их воздействия.

В условиях интеграции национальной экономики в мировую экономическую систему задача оценки деятельности предприятий нефтяного сектора является весьма актуальной. С экономической точки зрения управление экологическими рисками проектов более эффективно, если они реализуются на более ранних стадиях реализации и организации проекта. К сожалению, подсчету утраченных экологических выгод не уделяется должного внимания.

Активное управление рисками должно носить системный характер, однако в настоящее время больше внимания уделяется финансовым рискам. В то же время недавние обсуждения деклараций безопасности опасных промышленных объектов практически позволяют создать систему детального анализа подверженности экологическим рискам в течение всего периода добычи на прединвестиционном, инвестиционном и эксплуатационном этапах разработки нефтяных месторождений, предприятиях отрасли. Однако, как правило, в документах технико-экономического обоснования экологические риски не учитываются, а в управленческих документах, обосновывающих инвестиционные проекты, указывается проведение таких исследований по ценам воздействия на окружающую среду.

Во многих случаях экологические риски на нефтяных предприятиях относят к операционным рискам. Количественная и качественная оценка экономических рисков на этапах жизненного цикла проекта имеет серьезный методический и практи-

ческий характер. Важность подобных исследований обусловлена, во-первых, возможными нарушениями естественных законов и, во-вторых, природными климатическими факторами, рисками, оказывающими негативное влияние на все этапы реализации проекта.

Ключевые слова: *управление рисками, экологические риски, экологическая безопасность, нефтегазовые предприятия, экологическое страхование, охрана окружающей среды.*

NEFT VƏ QAZ SƏNAYESİ MÜƏSSİSƏLƏRİNDƏ
EKOLOJİ RİSKLƏRİN EFFEKTİV İDARƏ EDİLMƏSİ

Əlizadə E.K.[1], Bağırov A.Ə.[2], Boqopolskiy V.O.[3], Şirinov M.M.[4]
[1]«Ekol Engineering Services» QSC, Azərbaycan
8 Noyabr prosp., 64, Bakı, AZ1026: elnur.alizade@ekol.az;
[2-4]Azərbaycan Dövlət Neft və Sənaye Universiteti, Azərbaycan
16/21, Azadlıq prospekti, Bakı, AZ1010: azad-baqirov@mail.ru, vadim46.46@mail.ru, shirinov46@mail.ru

Xülasə. Müasir dünyada texnologiyanın sürətli inkişafı fonunda transmilli neft-qaz şirkətlərinin korporativ idarəetmə sisteminin tətbiqi və müsbət reytinqin formalaşması risklərin hərtərəfli idarə olunmasına əsaslanır. Sahələr üzrə investisiya cəlbediciliyi reytinqini formalaşdıran risk faktorları, xüsusilə ekoloji risklər təsirini qiymətləndirərkən heç də həmişə nəzərə alınmır.

Milli iqtisadiyyatın dünya təsərrüfat sisteminə inteqrasiyası şəraitində neft sektoru müəssisələrinin fəaliyyətinin qiymətləndirilməsi vəzifələri olduqca aktualdır. İqtisadi nöqteyi-nəzərdən, əgər onlar layihənin icrasının və təşkilinin daha erkən mərhələlərində həyata keçirilərsə, layihələrin ekoloji risklərinin idarə olunması daha səmərəli olar. Lakin təəssüf ki, itirilmiş ekoloji faydaların hesablamalarına lazımi diqqət yetirilmir.

Risklərin aktiv idarə edilməsi sistemli olmalıdır, lakin hazırda maliyyə risklərinə daha çox diqqət yetirilir. Eyni zamanda, təhlükəli sənaye obyektləri üçün təhlükəsizlik bəyannamələrinin son müzakirələri praktiki olaraq neft yataqlarının işlənməsinin investisiyadan əvvəlki, investisiya və istismar mərhələlərində bütün istehsal dövrü ərzində ekoloji risklərə məruz qalmanın ətraflı təhlili sistemini yaratmağa imkan verir.

Bununla belə, bir qayda olaraq, texniki-iqtisadi əsaslandırma sənədlərində ekoloji risklər kifayət qədər nəzərə alınmır və investisiya layihələrini əsaslandıran idarəetmə sənədləri belə tədqiqatların ətraf mühitə təsir qiymətləri ilə aparılmasını göstərir.

Bir çox hallarda neft şirkətlərində ekoloji risklər əməliyyat riskləri kimi təsnif edilir. Layihənin həyata keçirilməsinin dövrü mərhələlərində iqtisadi risklərin kəmiyyət və keyfiyyətcə qiymətləndirilməsi ciddi metodoloji və praktik xarakter daşıyır. Belə tədqiqatların əhəmiyyəti, birincisi, təbii qanunların mümkün pozuntuları, ikincisi, təbii iqlim amilləri və layihənin bütün mərhələlərinə mənfi təsir göstərən risklərlə bağlıdır.

Açar sözlər: *risklərin idarə edilməsi, ekoloji risklər, ekoloji təhlükəsizlik, neft müəssisələri, ekoloji sığorta, ətraf mühitin mühafizəsi*

PETROGRAPHY AND GEOCHEMISTRY OF THE LOWER CRETACEOUS DEPOSITS OF THE VANDAM ZONE (SOUTHERN SLOPE OF THE GREATER CAUCASUS): INSIGHTS INTO PALEOWEATHERING, PROVENANCE AND TECTONIC SETTING

Guliyev E.Kh.

Ministry of Science and Education of the Republic of Azerbaijan,
Institute of Geology and Geophysics, Azerbaijan
H.Javid Ave., 119, Baku, AZ1143: guliyevemin@outlook.com

Keywords: *provenance, tectonic setting, paleoweathering, Vandam zone, Kepuch and Gyrkhbulag Formations*

Summary. This study examines the paleoweathering conditions, provenance, and tectonic setting of Neocomian deposits, focusing on the Kepuch and Gyrkhbulag Formations within the Vandam tectonic zone on the northern flank of the South-Caucasian microplate, characterized by complex Cretaceous flysch and volcanogenic formations. By integrating petrographic and geochemical data, this research aims to identify distinctive geochemical features reflecting provenance, weathering processes, and depositional environments, deepening the understanding of the regional geodynamic evolution. Petrographic analysis of the sandstones reveals a composition primarily consisting of rock fragments, quartz, and feldspar, with a significant clay matrix exceeding 15%, classifying them as lithic wackes and highlighting the dominance of volcanic and metamorphic rock fragments along with authigenic calcite cement. All geochemical proxies for paleoweathering, such as the Chemical Index of Alteration (CIA), Chemical Index of Weathering (CIW), and Plagioclase Index of Alteration (PIA), suggest that the source regions underwent a low to moderate degree of weathering. Provenance analysis suggests that the sediments are derived from a mixed source, primarily consisting of felsic and intermediate igneous rocks, consistent with a continental island arc tectonic environment. Discrimination diagrams – including SiO_2 versus K_2O/Na_2O, Al_2O_3/SiO_2 versus Fe_2O_3+MgO, La–Th–Sc, Ti/Zr versus La/Sc, and $Eu/Eu*–Gd_N/Yb_N$ – place the samples within active continental margin and continental island arc fields, supporting a subduction-related sediment source. This analysis highlights the significant role of tectonic processes in shaping the geochemical characteristics of these siliciclastic rocks.

Introduction

The geochemistry of sedimentary rocks plays a crucial role in deciphering their provenance, tectonic setting, and the processes involved in their formation. The chemical composition of these rocks is greatly influenced by the nature of their source areas, extent of weathering, and the tectonic environment from which they originate. These multiple factors create distinct geochemical signatures that provide insights into the provenance, depositional conditions, and the tectonic settings. Thus, the application of geochemical techniques, including the analysis of major, trace, and rare earth elements (REE), has become crucial for understanding the tectonic settings of sedimentary rocks, as it sheds light on their provenance, weathering processes, and associated depositional environments (Bhatia, 1983, Bhatia, Crook, 1986; Roser and Korsch, 1986; McLennan, 1993; Floyd & Leveridge 1987; Roeser

and Korsch, 1988; Floyd et al. 1990; Schieber, 1992; Rodrigo et. al., 2020; Masidul et.al., 2020; Haunhar et.al., 2021). Moreover, the integration of petrographic and geochemical data has been proved to be a powerful tool to evaluate tectonic setting of deposit.

The Cretaceous deposits on the southern slope of the Greater Caucasus have a well-established history of their study; however, there is a limited amount of research specifically focusing on the petrography and geochemistry of these deposits. This research is dedicated to a comprehensive mineralogical-geochemical analysis of sedimentary facies, aimed at identifying indicative associations within the sedimentary rocks to elucidate the geodynamic setting of the Vandam zone during the Early Cretaceous period. To achieve this, petrographic and geochemical studies have focused on the siliciclastic rocks of the Kepuch and Gyrkhbulag Formations, which are well-exposed in the Vandam zone.

Geological setting and lithostratigraphy

The Kakheti-Vandam-Gobustan megazone corresponds to the northern flank of the South-Caucasian microplate with an Alpine cover composed of sedimentary and magmatogenic formations. From west to east, the Girdimanchay-Velvelychay flexure divides the megazone into two tectonically distinct zones. In the west, it is represented by the Vandam geoanticlinal uplift, where predominantly Cretaceous flysch deposits and volcanogenic formations are well exposed. Structurally this zone is composed of series of anticlines-synclines associated with several south directed thrusts. To the south, the Vandam zone is separated from Ganih-Ayricay zone by the fault of the same name. Most part of arch and southern slope of uplift is concealed under Pleistocene-Holocene continental formations of Ganih-Ayricay depression. In the east (interfluve of the Girdimanchay and Agsuchay rivers) the Mesozoic core of the Vandam uplift is flexurally downwarped along the Girdimanchay-Velvelyachay flexure and its southeastern continuation opens up into the wide Shamakhi-Gobustan depression, which is primarily composed of Paleocene-Pliocene terrigenous-clayey deposits. These deposits are folded into small, often overturned to the south sharp and isoclinal folds (Fig.1) (Alizadeh et al., 2005a).

Lithostragraphically the Neocomian deposits in the Vandam zone is divided into lithostratigraphic units based mostly on lithologic characteristics. These units include the Kepuch Formation followed by the Gyrkhbulag Formation in a sequence. The Lower Cretaceous deposits of the Vandam zone are characterized by slope facies sediments primarily composed of carbonate and siliciclastic turbidites. The lower part of the Kepuch Formation, represented by Berriasian deposits in the Vandam zone, is characterized by massive conglomerate layers interspaced with sections of limestones, marls, and tuffaceous sandstones.
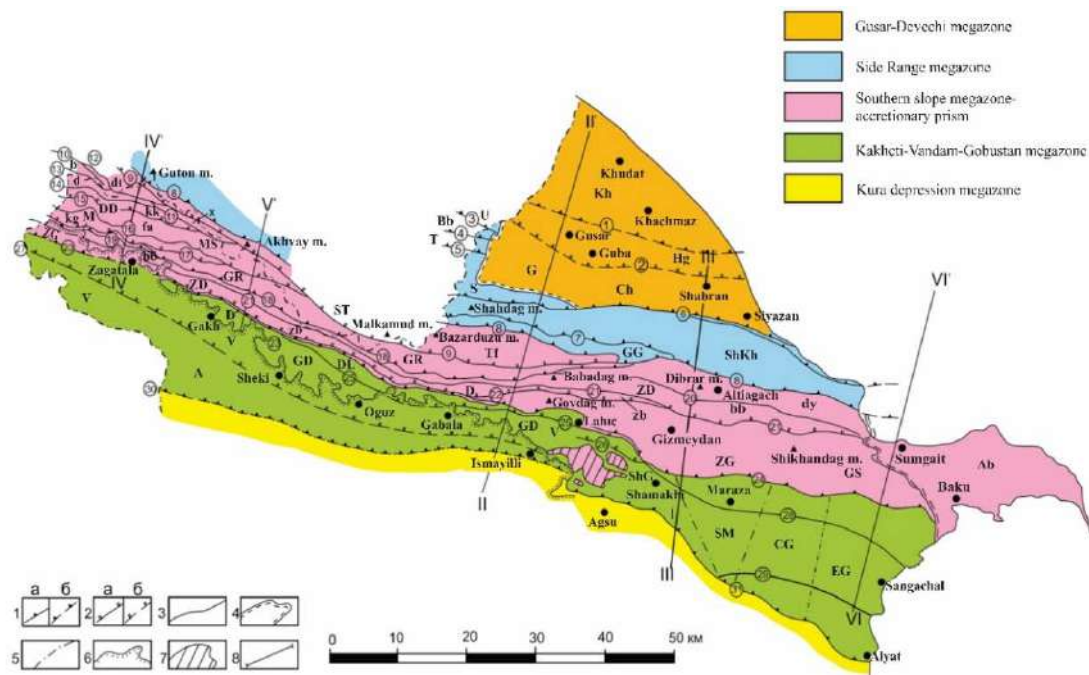
Fig. 1. Tectonic scheme of the Azerbaijani part of Greater Caucasus (Kangarli, 2012)

Boundary of strucrure: 1 – interzone tectonic boundaries (a – traced on surface; b – buried); 2 – tectonic boundaries between subzones (a – traced on surface; b – buried); 3 – boundaries of tectonic schuppens; 4 – stratigraphic boundaries; 5 – conventional boundaries; 6 – distribution boundary of modern sediements on Ganikh-Ayrichay superposed depression; 7 – Basgal nappe; 8 – lines of synthesized geological-geophisical sections

Structures: Gusar-Devechi megazone: zones: Kh – Xachmaz; G – Quba; subzones: Hg – Hasangala; Ch – Chilagir. Side Range megazone: zones: U – Ulluchay; Bb – Beybulag; T – Tairdjal; S – Sudur; ShKh – Shakhdag-Khizi; GG – Guton-Gonagkend. Southern Slope megazone: zones: ST – Speroz-Tufan; ZG – Zagatala-Govdag; Ab – Absheron; subzones: Tf – Tufan; DD – Djikhikh-Dindidag; MS – Mazim-Saribash; M – Megikan; GR – Galal-Rustambaz; ZD – Zagatala-Dibrar; D – Durudja; GS – Govdag-Sumqait; schuppens (nappe plates): dt – Djurmut-Tunsaribor; kh – Khalakhel; p – Rokhnor; b – Boskal; d – Djikhikh; кк – Kasdag-Kasmala; fa – Filizchay-Attagay; kg – Katekh-Gumbulchay; dy – Dibrar-Yashma; bb – Balakan-Babadag; zb – Zagatala-Burovdal. Kakheti-Vandam-Gobustan megazone: zones: V – Vandam; ShamG – Shamakhi-Gobustan; subzonesr: DL – Dashagil-Lahidj; GD – Gulluk-Dadagunash; A – Ayrichay; segments: Sh – Shamakhi; SM – Sundi-Maraza; CG – Central-Gobustan; EG – East-Gobustan

Fractures: 1 – İmamgulukend-Khachmaz; 2 – Khazra-Guba-Kuchay; 3 – Ashagimaki; 4 – Tendi-Keyda; 5 – Tairdjal; 6 – Siyazan; 7 – Shakhdag-Gonagkend; 8 – Major Caucasus; 9 – Khuray-Malkamud; 10 – Djoakhor-Gudurdag; 11 – Khalakhel; 12 – Kasmaldag; 13 – Machkhalor; 14 – Djikhikh-Chugak; 15 – Kokhnamadan; 16 – Hamzagor-Saribash; 17 – Suvagil; 18 – Gamarvan; 19 – Megikan; 20 – Altiagach; 21 – İlisu-Aladash; 22 – Gaynar-Gozluchay; 23 – Mamrux-Galadjig; 24 – Zangi-Garadjuzlu; 25 – Dashagil-Madrasa; 26 – Mudji; 27 – Shambul-İsmailli; 28 – Ganikh-Ayrichay; 29 – Adjichay-Alat
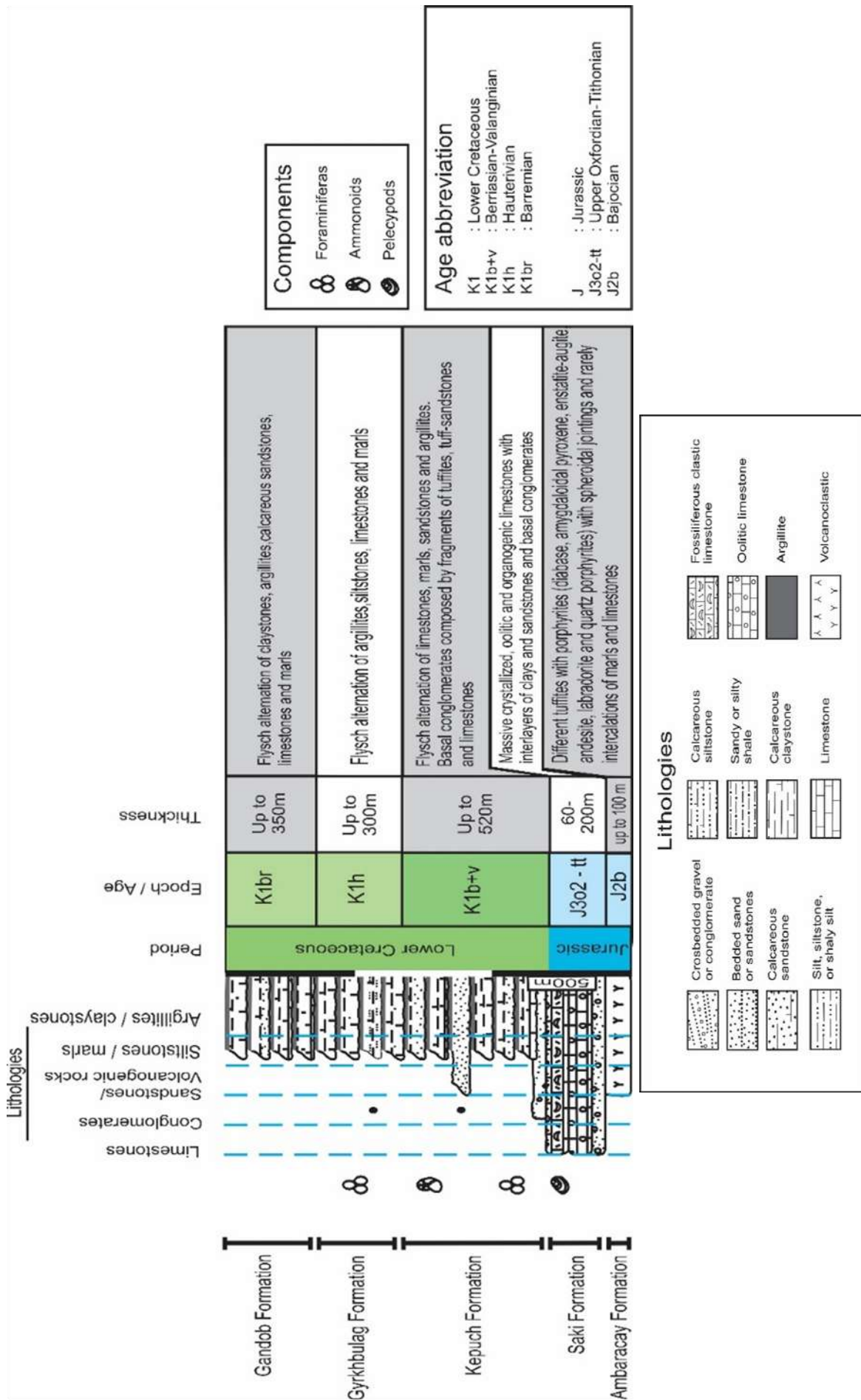
Fig. 2. Lithostratigraphic column of the Lower Cretaceous deposits of the Vandam zone (Alizadeh et al., 2005b)

The Valanginian deposits constitute the upper part of Kepuch Formation in the Vandam zone and are represented by a rhythmic alternation of grey, fine- to medium-grained calcareous sandstones and sandy limestones. In some places, pelitomorphic limestones alternate with marly clays and grey non-carbonate clays. The Hauterivian succession is comprised of terrigenous-carbonate flysch series and correspond to the Gyrkhbulag Formation. The thickness of these deposits reaches 300 m. These sediments are sharply different from the marly Kepuch Formation in their almost exclusively terrigenous character. The Hauterivian stage is dominated by argillites with interlayers of siltstones and sandstones. There are also individual interbeds of pelitomorphic limestone with a schistose structure (Alizadeh et al., 2005b) (Fig. 2).

Samples and methodology

In this study, ten samples were obtained from the Kepuch and Gyrkhbulag Formations, which are exposed in the Vandam zone on the southern slope of the Greater Caucasus. Sampling was conducted at five key outcrops: four riverbank locations along the Behmezchay (BC), Kishchay (KC), Damiraparanchay (DC), and Galachay (FL) rivers, and one roadside location (SQ) along the Sheki-Gakh route (Fig. 3). Initially, the samples were crushed for 20 minutes using a planetary ball mill to produce a homogeneous powder. This material was then further ground in a pulverizer. The fine powder (<100 μm) was placed in a porcelain crucible and subjected to drying at 1000°C overnight to eliminate moisture. Subsequently, the dried powder was combined with a binder (citric acid in a 1:10 ratio with the powder) and pulverized for an additional two minutes. This mixture was transferred into a 30 mm aluminum cap and compressed between two tungsten carbide pellets. A manual hydraulic press was used to apply a pressure of 10-15 tons per square inch for two minutes, followed by a gradual release of the pressure. The resulting compressed powder pellet was prepared for analysis. Major and trace elements were quantified via inductively coupled plasma mass spectrometry (ICP-MS) at the Laboratory of Geochemistry, Geochronology, and Isotope Geology, Department of Earth Sciences "Ardito Desio," at the Università degli Studi di Milano Statale, Italy.

For petrographic analysis, thin sections of ten representative samples were prepared at the geological laboratories of the University of Milano-Bicocca to assess mineralogical composition and microstructure. The unconsolidated samples were impregnated with epoxy resin, then cut and mounted on glass slides with Canada balsam. Slide preparation involved a three-stage grinding process, with inspections between each stage to ensure consistency in interference color reduction. The completed slides were labeled and examined under a petrographic microscope with a transmitted light and flat stage. Photomicrographs were captured to document mineral grain characteristics, which were analyzed based on their optical properties.
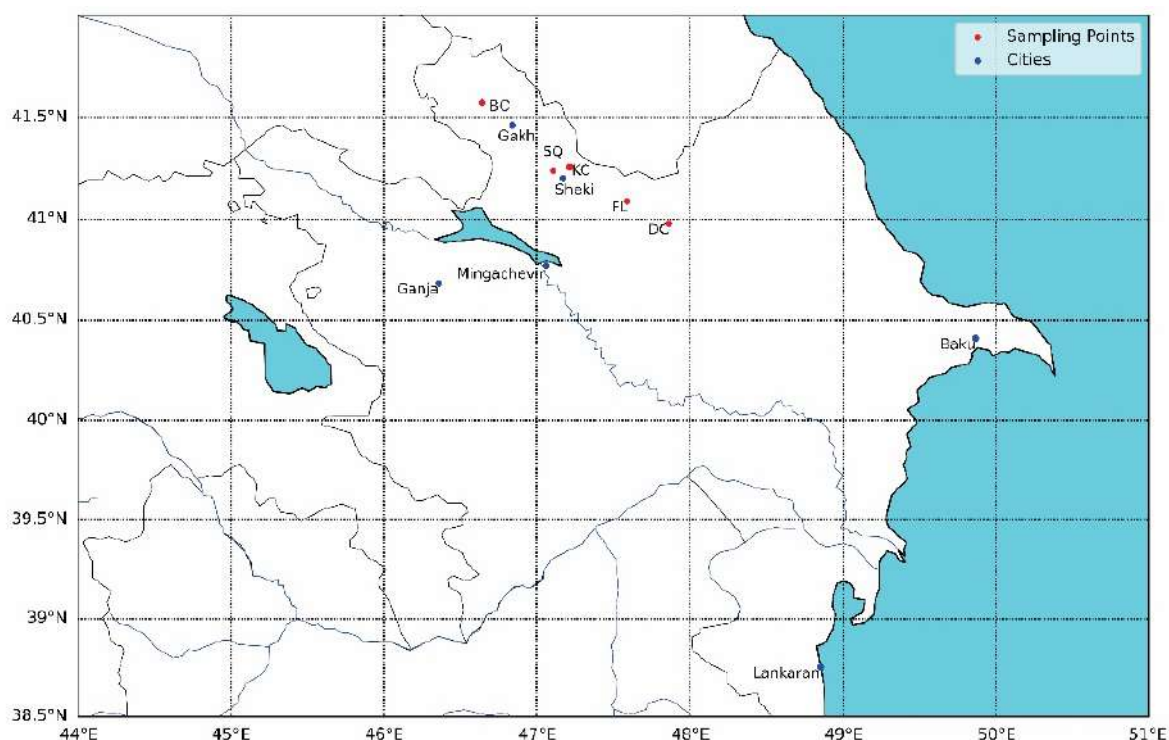
Fig. 3. Location map showing sampling points for the datasets used in the present work

Sandstone petrography

The sandstones analyzed are generally fine- to medium-grained. Microscopic examination of thin sections reveals that these sandstones comprise variable proportions of rock fragments, quartz, feldspars, matrix, and accessory minerals. The framework grains are predominantly composed of lithic clasts, with substantial contributions from quartz and feldspar (including both plagioclase and K-feldspar). Lithic fragments are primarily of volcanic (Lv) and metamorphic (Lm- quartz-mica lithic grain with schistosity) origin, with a minor component of sedimentary lithic fragments (Ls) (Fig. 4A, 4B, 4E). Volcanic lithic fragments (Lv) constitute the majority of the total lithic content. Quartz occurs mainly as monocrystalline grains, though polycrystalline quartz is also present in certain samples. Petrograph-

ic analysis reveals a lower proportion of K-feldspar relative to plagioclase (Fig. 4C). Majority of the samples contain varying proportions of mica, and muscovite (Fig. 4D) is more abundant than biotite since it is more resistant to weathering.

In accordance with the sandstone classification framework by (Pettijohn et.al.,1973), arenites are defined by a clay matrix content below 15%, whereas wackes are distinguished by a matrix exceeding 15%. As the matrix in the analyzed samples surpasses this 15% threshold and predominantly comprises clay minerals with minor detrital silts, these sandstones are classified as wackes. Furthermore, due to the dominance of lithic fragments within the framework grains, these sandstones are more precisely identified as lithic wackes. The cementing material is mainly authigenic calcite (Fig. 4F).
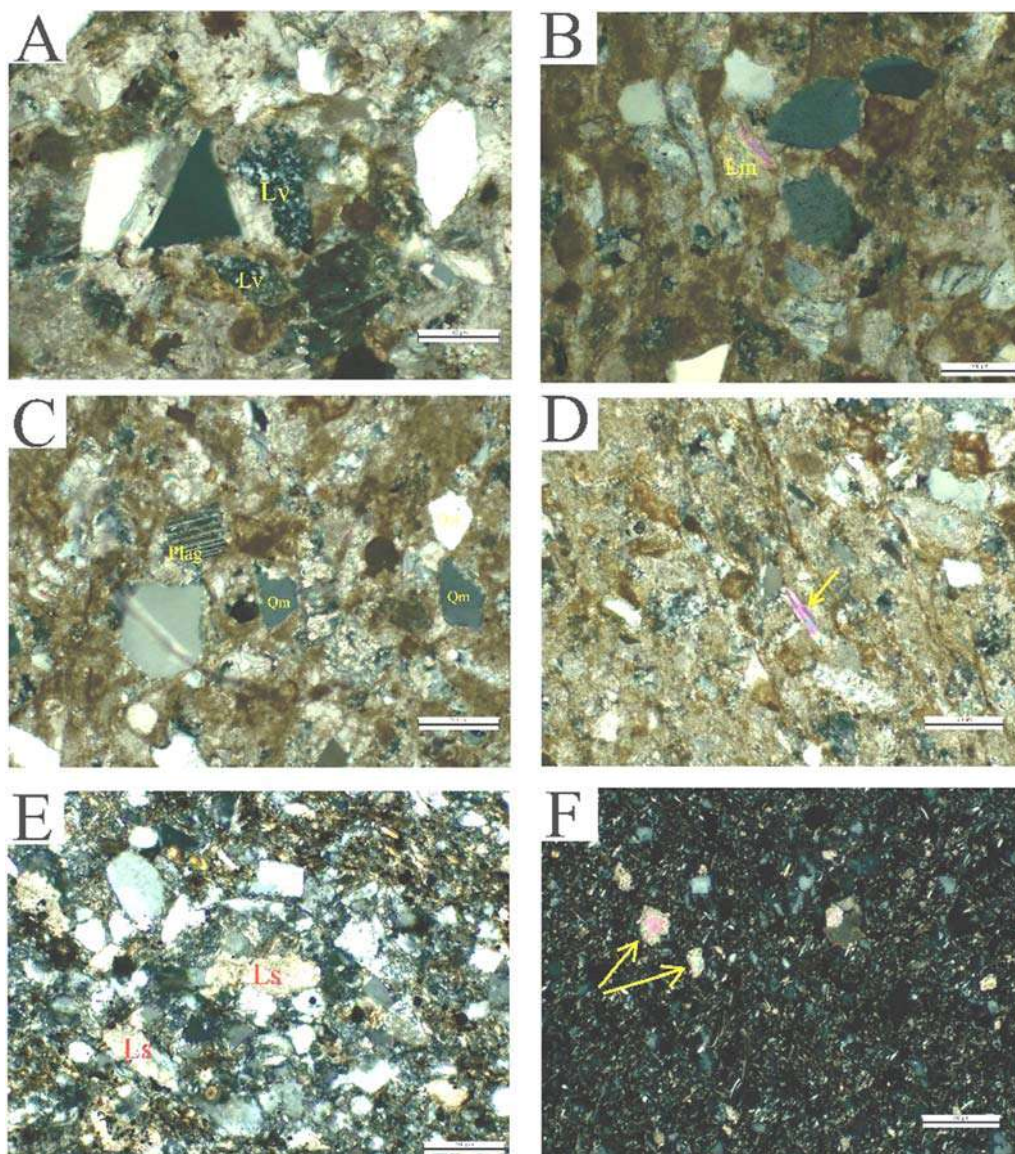
Fig. 4. Photomicrographs (in XPL) of thin-sectioned sandstones of the Kepuch and Gyrkhbulag formations showing: (A) felsic volcanic lithic fragment (Lv); (B) metamorphic lithic fragment (Lm); (C) angular to subangular monocrystalline quartz grains (Qm) and plagioclase (Plag); (D) detrital muscovite (yellow arrow) (E) sedimentary lithic fragment (Ls) (F) calcite cement (yellow arrows)

Geochemistry

Major elements

The major and trace element data are shown in Table 1 alongside average values of the Upper Continental Crust (UCC) for comparison (Taylor, McLennan, 1985). As shown in Table 1, the concentration of SiO_2 is high, varying between 55.61wt % and 79.27 wt % in the Kepuch Formation (KF), while it is between 60.33 wt% and 70.14 wt% in the Gyrkhbulag Formation (GF). The proportion of Al_2O_3 varies between 6.41wt% and 10.36 wt% in the KF, and 10.71-17.55 wt% in the GF. Compared to the upper continental crust (UCC), the SiO_2 and Al_2O_3 contents in the GF are the most similar to those of the UCC. Except for MnO and CaO, major element concentrations of samples from the KF are lower than the average values of the UCC (Fig.5). The samples from both formations are depleted in Na_2O, K_2O and P_2O_5. The GF that is distinguished by pronounced depletion in CaO (as is well seen in samples FL-1 and BC-1) have relatively high TiO_2 and FeO_2.

The K_2O/Al_2O_3 ratio in sandstone provides insight into the relative abundances of alkali feldspar and clay minerals prior to final burial. K-feldspar typically exhibits a K_2O/Al_2O_3 ratio as high as 0.9, while illite and kaolinite have lower ratios of approximately 0.3 and 0.04, respectively. (Cox et al., 1995). The low K_2O/Al_2O_3 ratios displayed by the KF and GF (0.18 and 0.16) are compatible with the predominantly illitic nature of these formations.

Trace elements and rare earth elements

Trace and rare earth element concentrations of the Kepuch and Gyrkhbulag formations are presented in Tables 1 and 2, respectively. Compared with average upper continental crust (UCC), the sandstones of the KF are characterized by relatively low concentrations of high field-strength elements (HFSE), whereas the concentrations of HFSE of rocks from the GF are close to UCC values (Fig.6). The distribution of Zr and Hf seems to be controlled by heavy mineral, such as zircon as indicated by the high correlation coefficient between Zr and Hf (r=0.97). This is supported by Zr/Hf ratios between 33 and 42, aligning well with those reported by Murali et al. (1983) for zircons.

The large ion lithophile elements (LILEs) are compared to UCC, among which Rb, Th and U are depleted in the KF samples. They are characterized by variable amounts of Ba and Sr. The samples of the GF exhibit a slight to strong depletion in Ba and Sr and minor enrichment in Cs and U (Fig.6). The siliciclastic rocks of both formations show a strong positive correlation between Rb and K_2O (r=0.99) indicating that Rb is mainly hosted by K-bearing clay mineral such as illite. In general, concentrations of transition trace elements (TTE) in the KF are lower than the average UCC concentrations. However, in a case study on the GF the average values of some TTE, such as Cr and Ni are comparable with those of UCC (Fig.6).
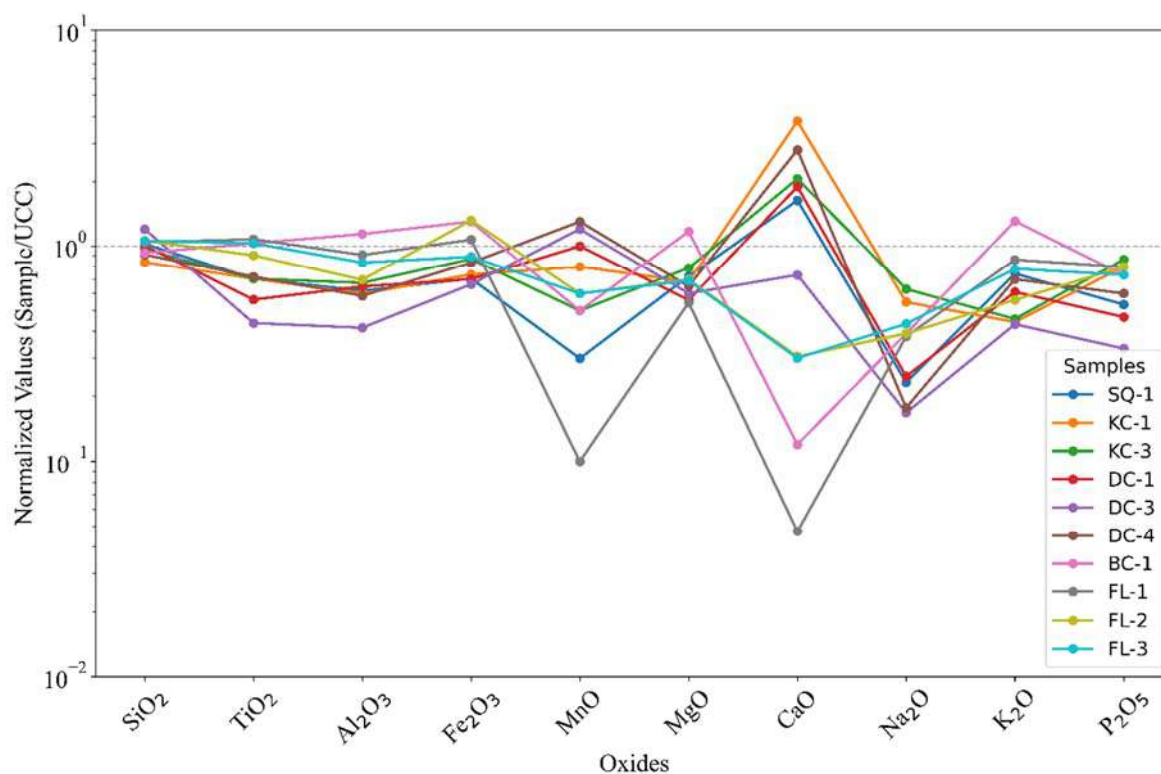
Fig. 5. Spider plot of major elements in Lower Cretaceous (Neocomian) deposits normalized against UCC (upper continental crust)
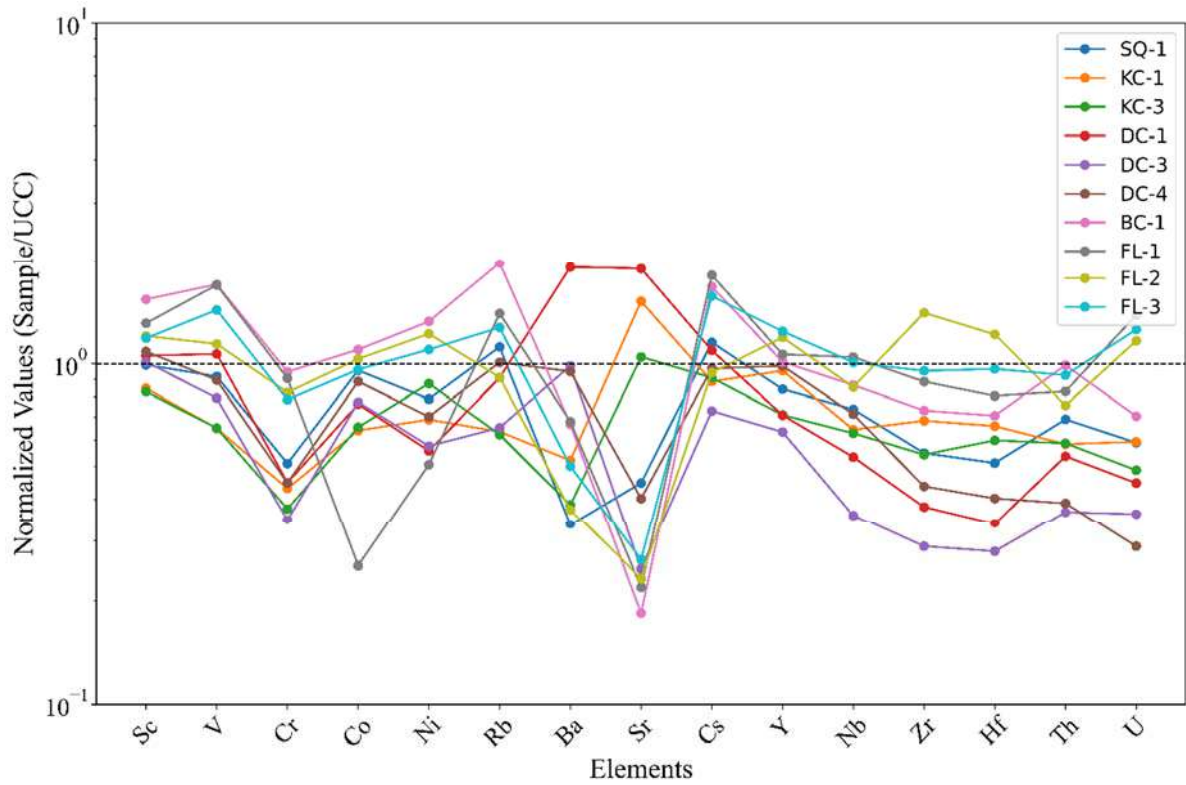
Fig. 6. Spider plot of trace element concentrations in Lower Cretaceous (Neocomian) deposits normalized against UCC (upper continental crust)

Table 1

Major (wt%) and trace element (ppm) concentrations of the samples from the Kepuch and Gyrkhbulag Formations

Formation	Kepuch Formation						Gyrkhbulag Formation					
Sample no.	SQ-1	KC-1	KC-3	DC-1	DC-3	DC-4	BC-1	FL-1	FL-2	FL-3	UCC	PAAS
SiO_2	67.70	55.61	63.82	66.33	79.27	60.33	61.41	68.69	70.14	69.98	65.89	62.9
TiO_2	0.45	0.45	0.45	0.36	0.28	0.46	0.66	0.69	0.58	0.66	0.50	0.99
Al_2O_3	9.52	9.24	10.36	9.97	6.41	9.02	17.55	14.02	10.71	12.91	15.17	18.9
Fe_2O_3	3.55	3.71	4.39	3.53	3.34	4.22	6.56	5.40	6.65	4.50	4.49	7.22
MnO	0.03	0.08	0.05	0.10	0.12	0.13	0.05	0.01	0.06	0.06	0.07	0.11
MgO	1.79	1.69	1.96	1.39	1.49	1.61	2.90	1.35	1.73	1.71	2.20	2.20
CaO	5.86	13.64	7.38	6.78	2.63	10.04	0.43	0.17	1.10	1.08	4.19	1.29
Na_2O	0.76	1.79	2.06	0.81	0.55	0.58	1.28	1.24	1.28	1.42	3.89	1.18
K_2O	2.08	1.24	1.28	1.71	1.21	1.96	3.66	2.42	1.57	2.19	3.39	3.70
P_2O_5	0.08	0.12	0.13	0.07	0.05	0.09	0.11	0.12	0.12	0.11	0.20	0.16
LOI	8.17	12.42	8.12	8.95	4.66	11.58	5.38	5.88	6.06	5.37	-	-
Sc	13.90	11.87	11.60	14.79	14.19	15.20	21.63	18.40	16.89	16.63	13.6	16
V	89.09	62.90	63.03	103.56	77.02	86.99	165.83	165.13	110.82	139.50	107	130
Cr	47.05	39.74	34.60	41.36	32.05	41.25	87.16	83.44	75.89	72.27	85	110
Co	16.56	11.06	11.30	13.20	13.38	15.36	19.03	4.39	17.87	16.65	17	23
Ni	37.08	32.32	41.16	26.19	27.06	32.95	62.53	23.87	57.53	51.74	44	55
Cu	14.54	15.02	17.01	61.98	34.78	64.19	47.25	48.51	44.84	45.35	25	50
Zn	55.56	60.61	75.53	65.52	53.22	57.47	134.38	63.80	138.38	90.05	71	85
Rb	94.07	53.26	52.23	76.49	54.70	84.83	166.17	117.91	76.75	107.27	112	160
Sr	143.40	488.02	335.03	609.42	79.39	129.09	59.02	70.28	74.54	84.57	350	200
Zr	106.00	131.73	104.84	73.50	55.78	84.60	141.06	171.22	272.17	184.02	190	210
Cs	5.66	4.35	4.46	5.36	3.57	4.75	8.25	8.92	4.62	7.74	4.6	9.3
Ba	211.74	328.01	242.46	1208.43	619.72	596.55	418.54	426.20	234.42	315.47	550	650
Pb	15.14	12.13	14.36	13.69	8.33	25.46	28.66	19.26	15.63	20.34	17	20
Th	7.23	6.12	6.16	5.64	3.86	4.10	10.40	8.72	7.94	9.73	10.7	14.6
U	1.59	1.60	1.32	1.21	0.98	0.78	1.90	3.75	3.15	3.40	2.8	3.1

The TTE show a slight enrichment of Sc and V for the GF. For the GF samples, Al_2O_3 exhibits a significant positive correlation with Sc and V (r=0.93 and r=0.86, n=4 respectively), indicating phyllosilicates as a major controlling factor for V and Sc concentrations.

The total Rare Earth Elements ($\sum$REE) in KF ranges from 65.86 to 105.43 ppm (mean = 85.80 ppm) while in GF it varies from 115.05 ppm to 132.94 ppm (mean = 123.73 ppm). If normalized to chondrite values (Fig.7), both Kepuch and Gyrkhbu-

lag samples exhibit enrichment in LREE (La_{cn}/Sm_{cn}; 2.38-3.37 and 2.79-3.89) and have an almost flat HREE (Gd_{cn}/Yb_{cn}; 1.18-1.86 and 1.05-1.55, respectively) patterns with a negative Eu anomaly (Eu/Eu* = 0.69–0.75 for KF, and 0.63-0.73 for GF). Eu anomalies were calculated as $Eu/Eu^*=(Eu)_{cn}/[(Sm)_{cn} \times (Gd)_{cn}]^{0.5}$ (McLennan 1989), where cn expresses chondrite-normalized values of the element (Taylor and McLennan 1985). The values of $\sum$LREE/$\sum$HREE are variable and range from 6.05 to 7.93, where the average value is 6.97.
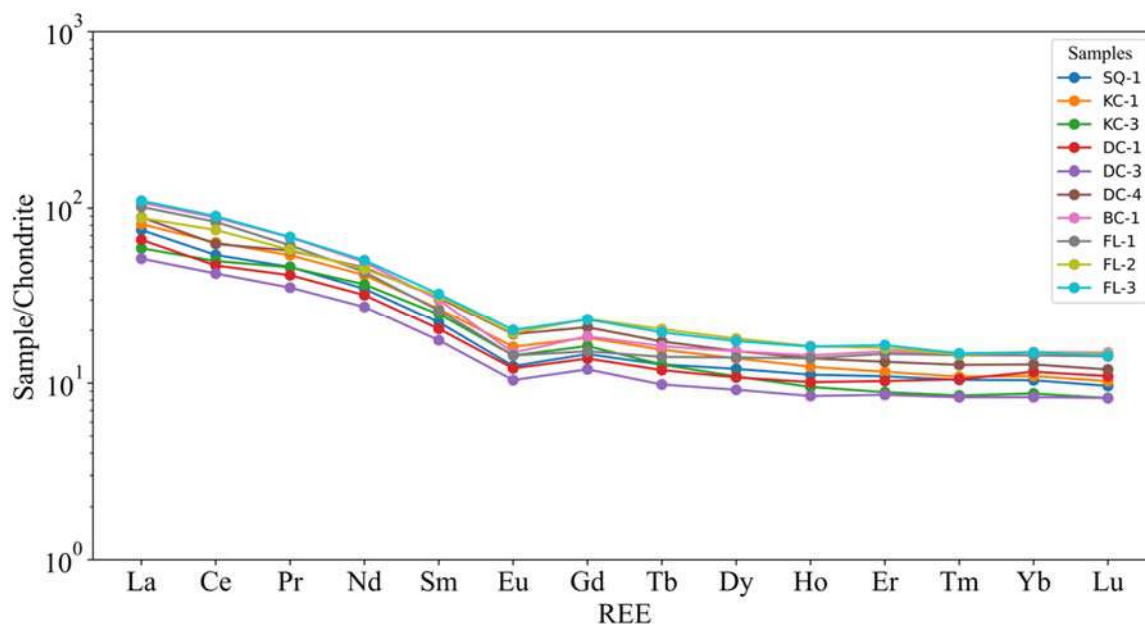
Fig.7 Chondrite-normalized rare earth elements plot for Lower Cretaceous (Neocomian) deposits of Vandam zone

Table 2

Rare earth element concentrations (ppm) of the samples from Kepuch and Gyrkhbulag Formations

Formation	Kepuch Formation						Gyrkhbulag Formation				
Sample №	SQ-1	KC-1	KC-3	DC-1	DC-3	DC-4	BC-1	FL-1	FL-2	FL-3	Chondrite Values
La	17.82	19.24	14.03	15.68	12.24	21.05	25.46	24.12	20.86	26.11	0.237
Ce	33.24	39.12	30.69	28.95	26.06	38.42	54.24	51.27	46.12	55.22	0.613
Pr	4.30	5.02	4.28	3.86	3.28	5.33	6.34	5.71	5.39	6.36	0.0928
Nd	15.88	19.04	16.82	14.63	12.51	20.96	22.53	19.83	20.62	23.11	0.457
Sm	3.30	3.96	3.68	3.02	2.60	4.57	4.45	3.86	4.67	4.80	0.148
Eu	0.70	0.91	0.81	0.68	0.59	1.07	0.84	0.81	1.08	1.13	0.0563
Gd	2.91	3.61	3.24	2.75	2.38	4.14	3.68	3.02	4.63	4.59	0.199
Tb	0.46	0.56	0.46	0.43	0.35	0.62	0.59	0.51	0.73	0.70	0.0361
Dy	2.96	3.41	2.69	2.65	2.26	3.74	3.74	3.44	4.41	4.27	0.246
Ho	0.61	0.68	0.52	0.55	0.46	0.76	0.79	0.76	0.89	0.88	0.0546
Er	1.75	1.86	1.42	1.64	1.37	2.12	2.43	2.35	2.53	2.63	0.16
Tm	0.26	0.27	0.21	0.26	0.21	0.31	0.36	0.36	0.36	0.36	0.0247
Yb	1.67	1.77	1.41	1.87	1.34	2.06	2.42	2.32	2.41	2.41	0.161
Lu	0.24	0.25	0.20	0.27	0.20	0.29	0.37	0.35	0.36	0.35	0.0246

Results and discussion

Geochemical Classification

Pettijohn et al. (1972) and Herron (1988) established classification frameworks that utilize geochemical characteristics to categorize sedimentary rocks. Utilizing the classification diagram from Herron (1988) (Fig. 8A), it was determined that most of the analyzed samples are situated within the wacke classification field, indicating a degree of immaturity. In accordance with the classification scheme proposed by Pettijohn et al. (1972), as illustrated in Figure 8B, the studied samples are predominantly classified as litharenites, with a minority being classified as arkoses.

Inferences on Paleoweathering

Chemical weathering is a key process influencing interelemental fractionation, leading to elemental ratios that differ from those in the source rocks. The intensity and extent of chemical weathering in clastic rocks can be assessed through various indices, including the Chemical Index of Alteration (CIA), Plagioclase Index of Alteration (PIA), and Chemical Index of Weathering (CIW) (Nesbitt and Young, 1982, 1984; Fedo et al., 1995; Harnois, 1988).

The Chemical Index of Alteration (CIA), introduced by Nesbitt and Young (1982), is one of the most widely used indicators of chemical weathering. Higher CIA values correlate with increased chemical weathering and a higher presence of residual clay minerals, such as illite, chlorite, kaolinite, and gibbsite. High CIA values signify intense weathering or sediment recycling, often under warm, humid paleoclimatic conditions, which results in the depletion of soluble cations (Ca^{2+}, Na^+, K^+) favor of less soluble cations like Al^{3+} and Ti^{4+}. In contrast, low CIA values reflect limited or negligible chemical weathering, generally associated with cool or arid climates. The CIA is expressed as CIA= $[Al_2O_3/(Al_2O_3+CaO+ Na_2O+K_2O)]x100$, where Al_2O_3, CaO, Na_2O, and K_2O are in molar proportions, and CaO* incorporated in silicate fraction of sediments. The CIA excludes the influence of carbonate minerals, thus reflecting the weathering intensity of silicate minerals and providing insights into the chemical weathering conditions in the source area. For the samples in this study, CIA values ranging from 55.9 to 73.7 suggest a weak to moderate degree of chemical weathering in the source rocks.

CIA values can be plotted on a Al_2O_3-(CaO+ Na_2O)-K_2O (A-CN-K) ternary diagram to refine assessments of weathering processes and evaluate potential K-metasomatism effects more precisely. This diagram also facilitates the delineation of the primary geochemical composition of the source rocks (Nesbitt and Young, 1982, 1984; Fedo et al., 1995). In this study, the samples plot along the weathering trend for granodioritic compositions, progressing towards illite without any detectable influence of K-metasomatism (Fig. 9).
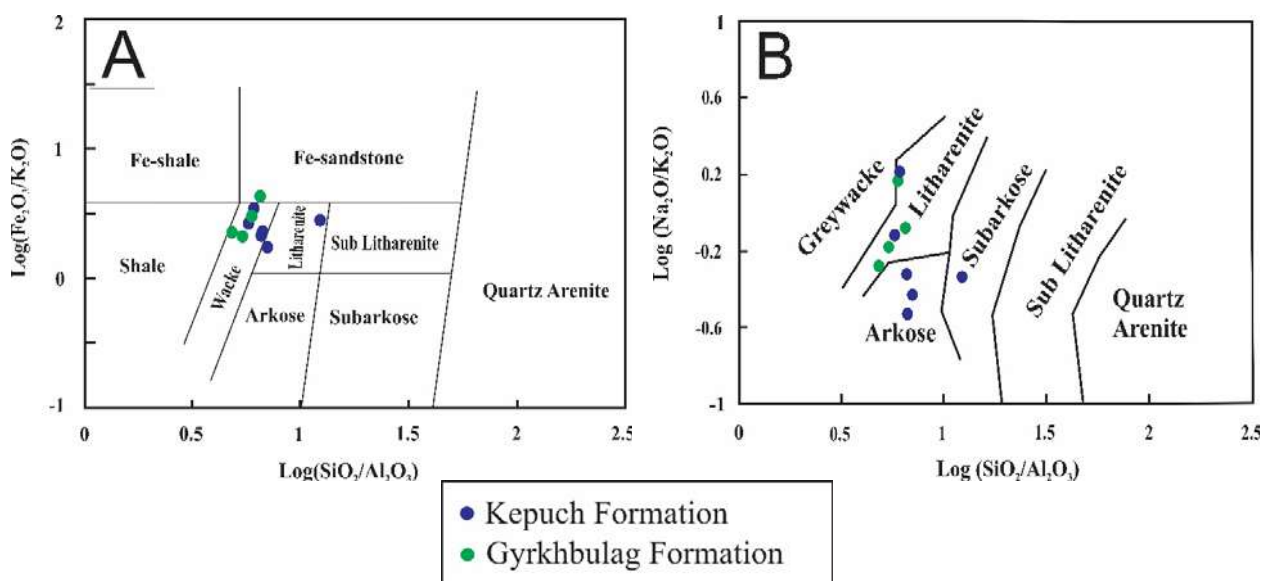
Fig. 8. Geochemical classification of samples (A) log ratios of SiO_2/Al_2O_3 – Fe_2O_3/K_2O (Herron, 1988); (B) log ratios of SiO_2/Al_2O_3 – Na_2O/K_2O (Pettijohn et al., 1972)
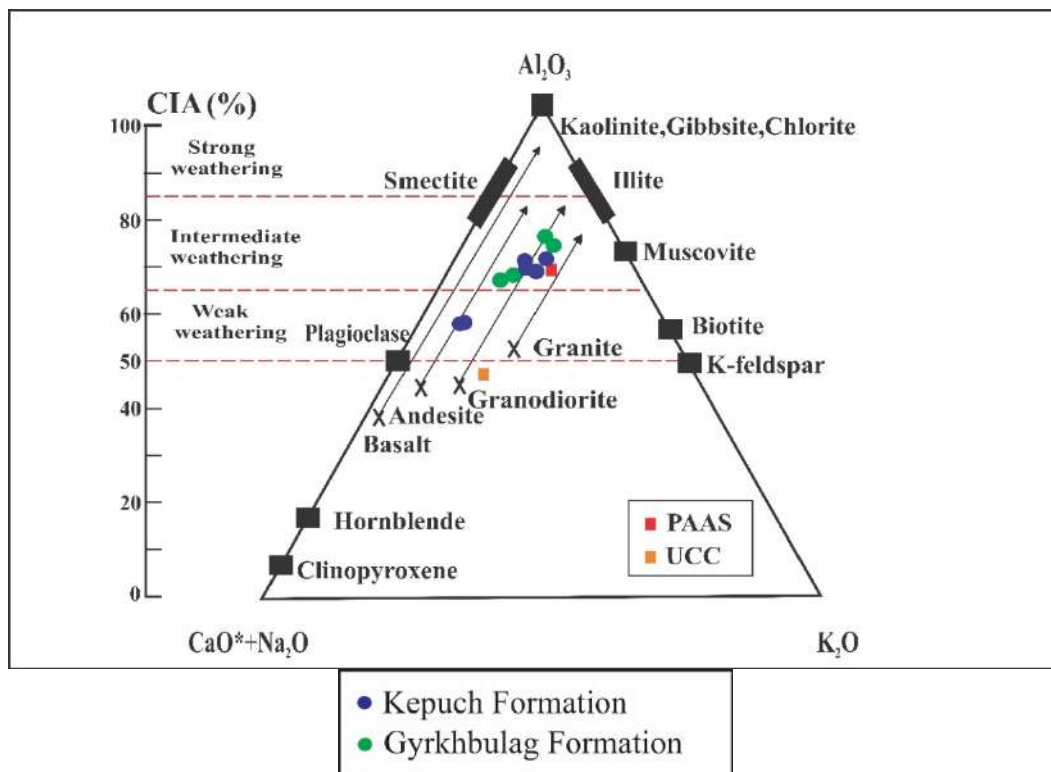
Fig. 9. The A-CN-K ternary plot of the samples; Al, Al_2O_3; CN, CaO^* + Na_2O; K, K_2O (oxides are plotted as molar); (PAAS-Post-Archean Australian Shale; UCC-Upper Continental Crust)

The extent of weathering can also be assessed by analyzing the molecular percentages of oxide components using the Chemical Index of Weathering (CIW), as proposed by Harnois (1988). Like the CIA, the CIW gauges the degree of chemical weathering and the alteration of feldspar to clay minerals (Nesbitt and Young, 1984, 1989; Fedo et al., 1995; Maynard et al., 1995). It is defined as: $CIW=[Al_2O_3/(Al_2O_3+CaO^*+Na_2O)]\times100$, where Al_2O_3, CaO, and Na_2O are in molar proportions and CaO^* is restricted to the amount of CaO in the silicate fraction only. The CIW calculation resembles that of CIA but omits K_2O, accounting for the possible leaching or retention of potassium in weathering products during sedimentation. Due to its higher cation exchange capacity, potassium is more easily incorporated into clay minerals compared to Na^+ and Ca^+ (Kroonenberg, 1994). This exclusion of K_2O minimizes complications associated with K mobilization during diagenesis or metamorphism. CIA and CIW values are interpreted similarly, with values around 50 indicating unweathered upper continental crust and values near 100 reflecting highly weathered materials (e.g., kaolinite and gibbsite). The CIW values for the samples, ranging from 60 to 85 with an average of 75, indicate low to moderate levels of weathering in the source materials, aligning with the CIA.

The Plagioclase Index of Alteration (PIA), developed by Fedo et al. (1995), serves as an alternative to the Chemical Index of Weathering (CIW), targeting specifically the alteration of plagioclase feldspar, a prevalent mineral in silicate rocks. This index is particularly useful when the focus is on assessing plagioclase weathering independently. An unweathered plagioclase has a PIA value of 50, while a fully weathered material reaches a maximum value of 100. The PIA is calculated using the formula:

$$PIA=[(Al_2O_3-K_2O)/(Al_2O_3+CaO^*+Na_2O-K_2O)]\times100,$$

where CaO^* represents only the CaO bound within the silicate fraction, and all oxide quantities are expressed in moles. For the samples examined, PIA values ranged from 56.9 to 82.8, with an average of 72.1, indicating a low to moderate degree of chemical weathering.

Implications for provenance

Various discrimination diagrams on the basis of the major-element compositions of clastic rocks have been established in order to infer their provenance characteristics. The major-element-based provenance discrimination functions diagram, introduced by Roser and Korch (1988), was applied to discriminate the source area into four major prove-

nance fields. They are the mafic igneous (P1), intermediate igneous (P2), felsic igneous (P3) and quartzose sedimentary or recycled (P4). As can be noted from discrimination plot all data lie in the fields of intermediate igneous provenance and quartzose sedimentary provenance, implying mixed source area (Fig.10A).

Additionally, since Al, Ti, and Zr oxides and hydroxides exhibit low solubility, they are often considered immobile elements; as a result, the Al_2O_3/TiO_2 ratio in the samples closely matches that of their source rocks. The Al_2O_3/TiO_2 ratio values range from 3 to 8 for mafic rocks, 8 to 21 for intermediate rocks, and 21 to 70 for felsic igneous rocks, providing insights into the source area composition (Schieber, 1992). The Al_2O_3/TiO_2 ratio of the analyzed samples varies from 18.46 to 27.69, with an average of 22.03, which is in agreement with felsic to intermediate source rock (Fig.10B). In addition, the bivariate Al_2O_3 versus TiO_2 diagram shows a concentration of data in the felsic rock field, and

only few samples plot within the field for intermediate igneous rocks. This analysis is supported by the bivariate plot of K_2O versus Rb (Fig.10C), which shows that source rocks of samples are felsic to intermediate igneous source rocks (Floyd et.al., 1989).

Apart from the major elements, trace element compositions and REEs can be used to judge the sediment provenance and the source-area rock composition due to their relatively immobile behaviour in the sedimentary environment. La/Th ratios in clastic sedimentary rocks are regarded as a powerful tool for reconstructing the source composition of sediments, while Hf concentration of a sediment typically reveals the degree of recycling that has occurred (Floyd et.al., 1987). In a cross-plot of La/Th versus Hf, apart from two metapsammite samples plotted within the andesitic arc source field, most analysed samples are characterized by low Hf content (1.48-6.46 ppm) and La/Th ratios (typically less than 3.5 ppm) plotting within the mixed felsic/basic source field (Fig.10D).
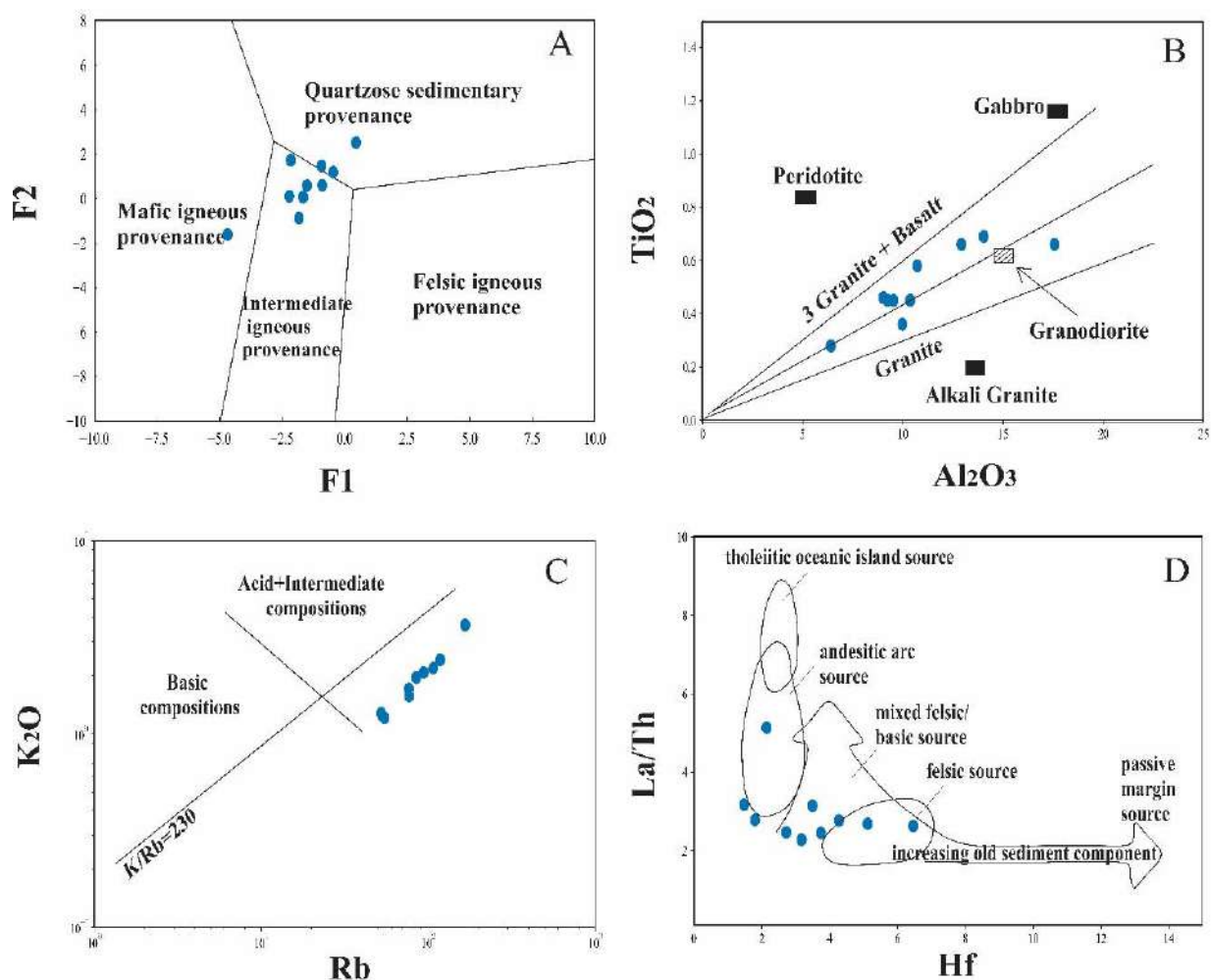
Fig.10. A) Sediment provenance diagram using major element discriminant function analysis after (Roser and Korsch, 1986) **B)** Provenance diagram of Al_2O_3 versus TiO_2 after (Schieber,1992) **C)** The K_2O vs Rb diagram (Floyd & Leveridge 1987; Floyd et al., 1990) **D)** Binary plot of Hf vs. La/Th showing the provenance of the studied sediments (fields after Floyd and Leveridge, 1987)

Tectonic Setting

The distribution of major, trace, and rare earth elements in sedimentary rocks serves as a robust tool for elucidating the nature of their tectonic environment, as distinct geochemical characteristics are often associated with specific plate tectonic environments. Roser and Korsch (1986) have proposed a tectonic discrimination diagram based on bivariate plot of SiO_2 versus K_2O/Na_2O in order to define tectonic setting of terrigenous sedimentary rocks. Figure 11A shows that majority of samples plotted in the field of active continental margin. Active continental margin setting described by Roser and Korsch suggests that sediments were derived from subduction-related basins formed in continental arcs or strike-slip basins along convergent margins.

The major element-based discriminant function diagrams of Bhatia (1983) are divided into four different fields such as oceanic island arc (OIA), continental island arc (CIA), active continental margin (ACM), and passive margin (PM). On multiparametric major-element based discriminant function diagram (Fig.11B) developed by Bhatia (1983), samples falls on active tectonic setting field. Tests on known samples showed that there is a marked increase in Fe_2O_3*+MgO and Al_2O_3/SiO_2 as the tectonic setting changes in the following sequence: PM-ACM-CIA-OIA (Bhatia, 1983). On the Al_2O_3/SiO_2 versus Fe_2O_3+MgO discrimination diagram (Bhatia 1983), most of analysed samples fall within continental island arc field (CIA) (Fig. 11C).

Moreover, elements La, Th, Zr, Nb, Y, Sc, Hf, Co and Ti are also very useful in tectonic setting discrimination because of their strong stability and high discriminating strength. La–Th–Sc discrimination diagram after Bhatia (1983) reveals that most of samples have the characteristics of a continental island arc as expected, which is in good agreement with major element tectonic discrimination (Fig. 12). In the bivariate Ti/Zr versus La/Sc plot after Bhatia and Crook (1986), once again most of the samples are found to concentrate on the continental island arc environment (Fig. 11D).
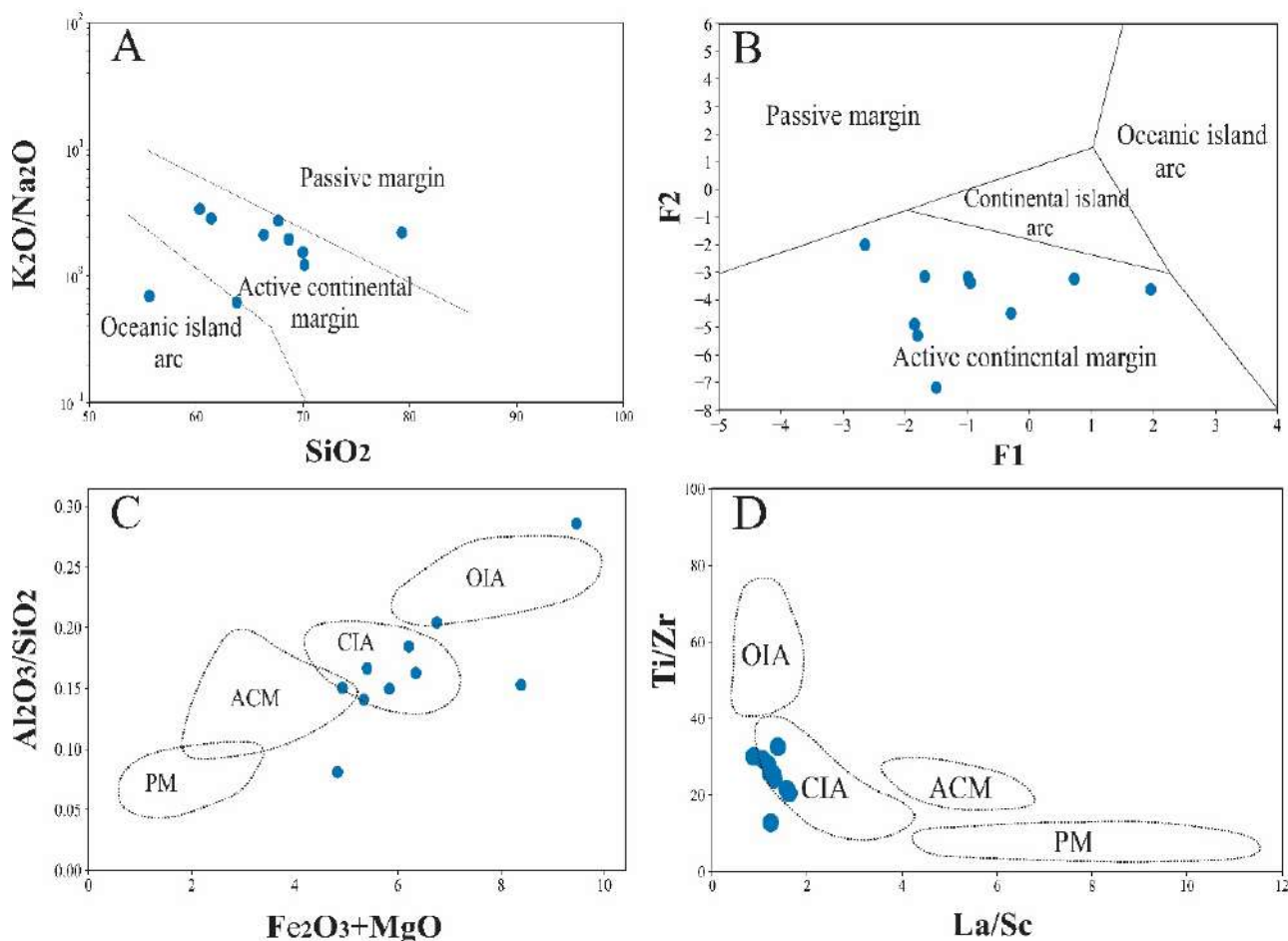
Fig.11 A) The K_2O/Na_2O vs. SiO_2 discrimination diagram (Roser and Korsch, 1986) showing tectonic setting fields for Neocomian deposits of Vandam zone **B)** discriminant function diagram of Bhatia (1983) **C)** Tectonic setting diagram a $Fe_2O_3 + MgO$ vs. Al_2O_3/SiO_2 after Bhatia (1983) **D)** Discrimination plot La/Sc vs. Ti/Zr for tectonic settings (Bhatia and Crook, 1986)

Similarly, more detailed results can be obtained using Eu/Eu*–La$_N$/Yb$_N$ diagram after McLennan (1993). In this diagram depicted in Figure 13, the La$_N$/Yb$_N$ ratio varies within the range of 5.88 to 9.26, and the Eu/Eu* value of most samples is less than 0.85, indicating that most sample parameters in this area are within the continental island arc tectonic setting.

According to Bhatia (1985), the chondrite normalized patterns of continental island arc-derived sediments are characterized by moderate enrichment of LREE relative to HREE accompanied by slight negative anomaly of Eu (mean Eu/Eu*=0.79). Applying these parameters to the analysed samples (Fig. 7), their REE characteristics indicate a strong match with a continental island arc environment.
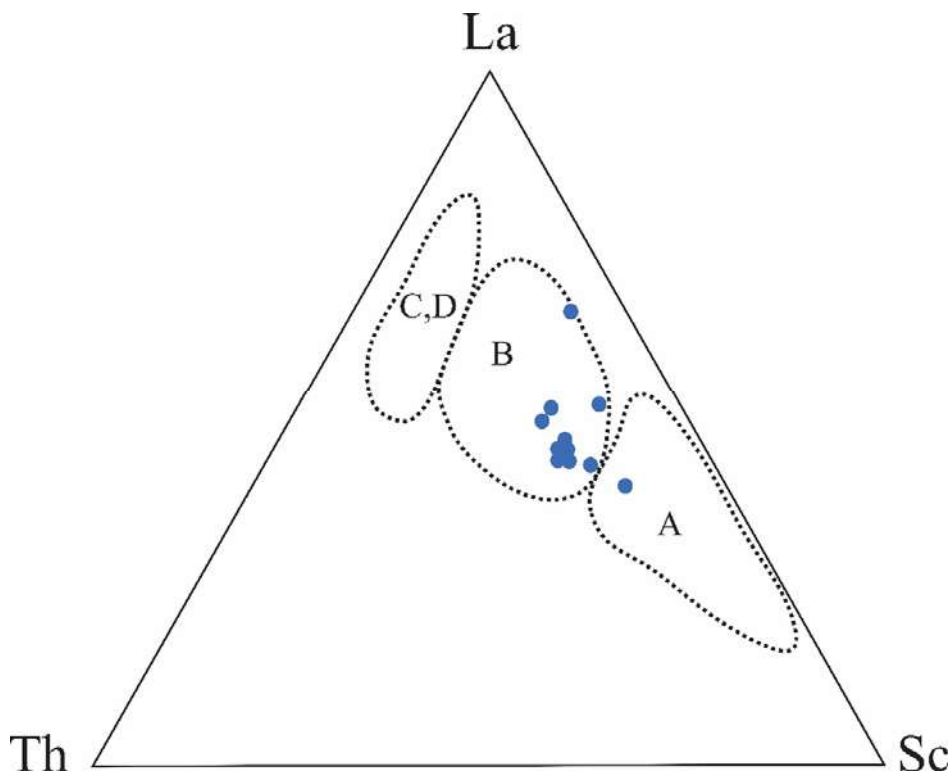
Fig. 12. Discrimination plots La-Th-Sc and Th-Sc-Zr/10 for tectonic settings (Bhatia and Crook, 1986). The tectonic regimes active (C) and passive (D) continental margins and continental (B) and oceanic (A) island arcs are distinct
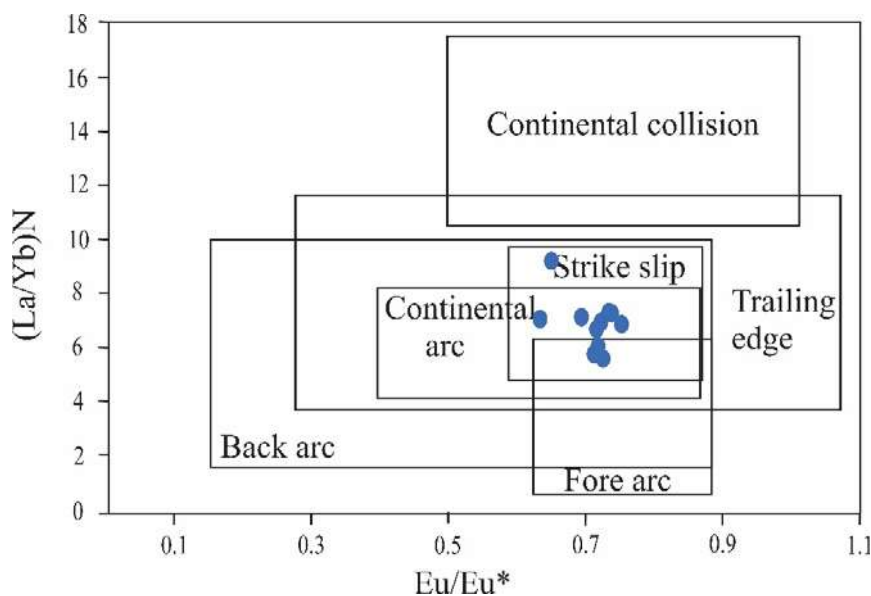
Fig. 13. Eu/Eu* versus LaN/YbN diagram after McLennan et al. (1993) showing samples clustering within the continental island arc region. The Eu/Eu* is computed using the equation Eu/Eu*=(Eu)$_{cn}$/[(Sm)$_{cn}$ x (Gd)$_{cn}$]$^{0.5}$, where "cn" represents the values of each element normalized to chondrite

Conclusion

The analyzed samples are categorized as wackes and litharenites according to geochemical classification diagrams. However, since the matrix content exceeds 15%, they are more precisely classified as greywackes.

The Chemical Index of Alteration (CIA) values for the analyzed sandstones vary from 55.9 to 73.7, suggesting a low to moderate extent of chemical weathering in their source regions. Additionally, the ratios of the Chemical Index of Weathering (CIW) and the Plagioclase Index of Alteration (PIA) further indicate that the sediments in the source areas underwent low to moderate weathering before being deposited in the basin. The A-CN-K diagram further defines the primary composition of the source rocks, revealing that the analyzed samples align with the ideal weathering trend for granodiorite toward an illite composition, without indicating any evidence of K-metasomatism.

The analysis of provenance suggests that the sandstones originate from a mixed source area, primarily composed of intermediate igneous rocks, as indicated by major-element discrimination diagrams. Additionally, trace element ratios like La/Th and Hf concentrations reinforce the notion that the source rocks are predominantly felsic to intermediate, with minimal signs of recycling.

The geochemical analysis of major, trace, and rare earth elements in the studied siliciclastic rocks strongly suggests a provenance linked to a continental island arc tectonic setting. Discriminant diagrams, including the SiO_2–K_2O/Na_2O plot by Roser and Korsch and the Al_2O_3/SiO_2 versus Fe_2O_3+ MgO diagram by Bhatia, robustly position the samples within fields characteristic of active continental margins and continental island arcs, indicating a subduction-influenced sediment source. Additionally, the La–Th–Sc ternary diagram and Ti/Zr versus La/Sc bivariate plot provide further evidence, with most samples aligning closely with continental island arc signatures. The Eu/Eu^*–La_N/Yb_N plot reveals rare earth element patterns that are emblematic of sediments derived from a continental island arc setting. Altogether, these geochemical indicators emphasize the significant influence of tectonic processes on the composition of the studied siliciclastic rocks, underscoring their tectonic heritage.

These results exhibit a strong correlation with the geodynamic interpretation of the region, as demonstrated by the works of R.N. Abdullayev and M.I. Rustamov, thereby enhancing our understanding of the tectonic dynamics involved. According to M.I. Rustamov, at the onset of the Jurassic, rifting and uncompensated subsidence initiated along the boundary between the Scytho-Turanian and South Caucasian plates, characterized by spreading in the Goitkh-Tfan trough. This area, extending from Crimea to the Absheron threshold, exhibited a distinct pattern of rift-related magmatism, including intrusive bodies and basalt flows. During the pre-Bajocian phase, diffuse spreading ceased, marking a shift to an Andean-style margin of the Scythian Plate. At this critical stage of compression, aspido-slate complex with magmatic bodies in the axial trough of the Greater Caucasus transforms into an accretionary prism, augmenting the active Scythian margin and zones of differentiated magmatism. The increasing compression phase led to southward subduction, resulting in the formation of the Kakheti-Vandam and Gagra-Dzhava zones as sites for continental island-arc volcano-plutonic associations. The Late Jurassic-Neocomian period marked the culmination of late Kimmerian tectogenesis, characterized by granitoid intrusions and the stabilization of the compressional geodynamic setting.

REFERENCES

Abdullaev R.N., Mustafaev M.A., Samedova R.A., Shafiev Kh.I., Mamedov M.N. Petrology of Magmatic Complexes of the Southern Slope of the Greater Caucasus (Vandamskaya Zone). Elm. Baku. 1990 (in Russian).
Alizadeh Ak.A. (ed.). Geology of Azerbaijan. Volume 4: Tectonics. Nafta Press. Baku, 2005a, 580 p. (in Russian).
Alizadeh Ak.A. (ed.). Geology of Azerbaijan. Volume 1: Stratigraphy. Nafta Press. Baku, 2005b, 580 p. (in Russian).
Bhatia M.R. Plate tectonics and geochemical composition of sandstone. The Journal of Geology, Vol. 91,1983, pp. 611-627, http://dx.doi.org/10.1086/628815
Bhatia M.R., Crook K.A.W. Trace element characteristics of graywackes and tectonic setting discrimination of sedimentary basins. Contributions to Mineralogy and Petrology, Vol. 92(2), 1986, pp. 181-193, https://doi. org/10.1007/BF00375292.
Cox R., Lowe D.R., Cullers R.L. The influence of sediment recycling and basement composition on evolution of mudrock chemistry in the Southwestern United States. Geo-

ЛИТЕРАТУРА

Абдуллаев Р.Н., Мустафаев М.А., Самедова Р.А., Шафиев Х.И., Мамедов М.Н. Петрология магматических комплексов южного склона Большого Кавказа (Вандамская зона). Элм. Баку, 1990, 204 с.
Ализаде Ак.А (под ред.). Геология Азербайджана. Том 4: Тектоника. Нафта Пресс. Баку, 2005a, 580 с.
Ализаде Ак.А (под ред.). Геология Азербайджана. Том 1: Стратиграфия. Часть 2: Мезозойская и кайнозойская эры. Нафта Пресс. Баку, 2005a, 580 с.
Рустамов М.И. Геодинамика и магматизм Загрос-Кавказского сегмента в фанерозое. Palmarium Academic Publishing. 2016, 543 с.
Bhatia M.R. Plate tectonics and geochemical composition of sandstone. The Journal of Geology, Vol. 91,1983, pp. 611-627, http://dx.doi.org/10.1086/628815
Bhatia M.R., Crook K.A.W. Trace element characteristics of graywackes and tectonic setting discrimination of sedimentary basins. Contributions to Mineralogy and Petrology, Vol. 92(2), 1986, pp. 181-193, https://doi. org/10.1007/BF00375292.

chimica et Cosmochimica Acta, Vol. 59, No. 14, 1995, pp. 2919-2940, https://doi.org/10.1016/0016-7037(95)00185-9.

Fedo C.M., Nesbitt H.W., Young G.M. Unravelling the effects of potassium metasomatism in sedimentary rocks and paleosols, with implications for palaeo-weathering conditions and provenance. Geology, Vol. 23, No. 10, 1995, pp. 921-924, https://doi.org/10.1130/0091-7613(1995)023<0921: UTEOPM>2.3.CO;2.

Floyd P.A. and Leveridge B.E. Tectonic environment of the Devonian Gramscatho Basin South Cornwall: Framework mode and geochemical evidence from turbiditic sandstones. Journal of the Geological Society (London), Vol. 144, 1987, pp. 531-542, http://dx.doi.org/10.1144/gsjgs.144.4.0531.

Floyd P.A. and Leveridge B.E. Tectonic environment of the Devonian Gramscatho Basin South Cornwall: Framework Mode and Geochemical Evidence from Turbiditic Sandstones. Journal of the Geological Society (London), Vol. 144, 1987, pp. 531-542, http://dx.doi.org/10.1144/gsjgs.144. 4.0531.

Floyd P.A., Shail R., Leveridge B.E., Franke W. Geochemistry and provenance of Rhenoher-cynian synorogenic sandstone: Implications fortectonic environment discrimination. In: Developments in Sedimentary Provenance (Morton A., Todd S.P., Haughton P.D.W. eds), Geological Society Special Publication 57, 1990, pp. 173-88, Geological Society of London, London.

Floyd P.A., Winchester J.A. and Park R.G. Geochemistry and tectonic setting of Lewisian clastic metasediments from the Early Proterozoic Loch Maree Group of Gairloch, N.W. Scotland. Precambrian Research, Vol.45, 1989, pp. 203-214, http://dx.doi.org/10.1016/0301-9268(89)90040-5.

Harnois L. The CIW index: A new chemical index of weathering. Sedimentary Geology, Vol. 55, No. 3-4, 1988, pp. 319-322, https://doi.org/10.1016/0037-0738(88)90137-6.

Hauhnar M., Lalnunmawia J., Dawngliana O.M.S. Geochemistry of Barail sandstone in Champhai, Mizoram: Implications on provenance and weathering history. J. Earth Syst. Sci., Vol. 130, No. 27, 2021, pp. 2-19, https://doi.org/10.1007/s12040-020-01515-9.

Herron M.M. Geochemical classification of terrigenous sands and shales from core or log data. Journal of Sedimentary Petrology, Vol. 58, No. 5, 1988, pp. 820-829.

Kangarli T.N. Mass overthrust within the structure of Greater Caucasus (Azerbaijan). In: The modern problems of geology and geophysics of Eastern Caucasus and the South Caspian Depression. 34th International Geological Congress. Special Issue Papers. Nafta-Press. Baku, 2012, pp. 163-201.

Kroonenberg S.B. Effects of provenance, sorting and weathering on the geochemistry of fluvial sands from different tectonic and climatic environments. In: Proc. 29th Int. Geol. Congr. Part A. (Kumon F., Yu K.M. eds.), Kyoto, Japan 1992, VSP Publ., Utrecht, 1994, pp. 69-81.

McLennan S.M. Rare earth elements in sedimentary rocks: influence of provenance and sedimentary processes. In: Geochemistry and Mineralogy of Rare Earth Elements (Lipin B.R. and McKay G.A., eds.), De Gruyter. Berlin, Vol. 21, No. 1, 1989, pp. 169-200, https://doi.org/10.1515/97815015 09032-010.

McLennan S.M. Weathering and global denudation. The Journal of Geology, Vol. 101(2), 1993, pp. 295-303. https://doi.org/ 10.1086/648222.

Md. Masidul Haque, Mrinal Kanti Roy. Sandstone-Shale Geochemistry of Miocene Surma Group in Bandarban Anticline, SE Bangladesh: Implications for Provenance, Weathering, and Tectonic Setting. Earth Sciences, Vol. 9(1), 2020, 38-51, https://doi.org/10.11648/j.earth.20200901.15.

Murali A.V., Parthasarathy R., Mahadevan T.M., Das M.S. Trace element characteristics, REE patterns and partition coefficients of zircons from different geological environments

Cox R., Lowe D.R., Cullers R.L. The influence of sediment recycling and basement composition on evolution of mudrock chemistry in the Southwestern United States. Geochimica et Cosmochimica Acta, Vol. 59, No. 14, 1995, pp. 2919-2940, https://doi.org/10.1016/0016-7037(95)00185-9.

Fedo C.M., Nesbitt H.W., Young G.M. Unravelling the effects of potassium metasomatism in sedimentary rocks and paleosols, with implications for palaeo-weathering conditions and provenance. Geology, Vol. 23, No. 10, 1995, pp. 921-924, https://doi.org/10.1130/0091-7613 (1995)023<0921: UTEOPM>2.3.CO;2.

Floyd P.A. and Leveridge B.E. Tectonic environment of the Devonian Gramscatho Basin South Cornwall: Framework mode and geochemical evidence from turbiditic sandstones. Journal of the Geological Society (London), Vol. 144, 1987, pp. 531-542, http://dx.doi.org/10.1144/gsjgs.144.4.0531.

Floyd P.A. and Leveridge B.E. Tectonic environment of the Devonian Gramscatho Basin South Cornwall: Framework Mode and Geochemical Evidence from Turbiditic Sandstones. Journal of the Geological Society (London), Vol. 144, 1987, pp. 531-542, http://dx.doi.org/10.1144/gsjgs.144.4.0531.

Floyd P.A., Shail R., Leveridge B.E., Franke W. Geochemistry and provenance of Rhenoher-cynian synorogenic sandstone: Implications fortectonic environment discrimination. In: Developments in Sedimentary Provenance (Morton A., Todd S.P., Haughton P.D.W. eds), Geological Society Special Publication 57, 1990, pp. 173-88, Geological Society of London, London.

Floyd P.A., Winchester J.A. and Park R.G. Geochemistry and tectonic setting of Lewisian clastic metasediments from the Early Proterozoic Loch Maree Group of Gairloch, N.W. Scotland. Precambrian Research, Vol.45, 1989, pp. 203-214, http://dx.doi.org/10.1016/0301-9268(89)90040-5.

Harnois L. The CIW index: A new chemical index of weathering. Sedimentary Geology, Vol. 55, No. 3-4, 1988, pp. 319-322, https://doi.org/10.1016/0037-0738(88)90137-6.

Hauhnar M., Lalnunmawia J., Dawngliana O.M.S. Geochemistry of Barail sandstone in Champhai, Mizoram: Implications on provenance and weathering history. J. Earth Syst. Sci., Vol. 130, No. 27, 2021, pp. 2-19, https://doi.org/10.1007/s12040-020-01515-9.

Herron M.M. Geochemical classification of terrigenous sands and shales from core or log data. Journal of Sedimentary Petrology, Vol. 58, No. 5, 1988, pp. 820-829.

Kangarli T.N. Mass overthrust within the structure of Greater Caucasus (Azerbaijan). In: The modern problems of geology and geophysics of Eastern Caucasus and the South Caspian Depression. 34th International Geological Congress. Special Issue Papers. Nafta-Press. Baku, 2012, pp. 163-201.

Kroonenberg S.B. Effects of provenance, sorting and weathering on the geochemistry of fluvial sands from different tectonic and climatic environments. In: Proc. 29th Int. Geol. Congr. Part A. (Kumon F., Yu K.M. eds.), Kyoto, Japan 1992, VSP Publ., Utrecht, 1994, pp. 69-81.

McLennan S.M. Rare earth elements in sedimentary rocks: influence of provenance and sedimentary processes. In: Geochemistry and Mineralogy of Rare Earth Elements (Lipin B.R. and McKay G.A., eds.), De Gruyter. Berlin, Vol. 21, No. 1, 1989, pp. 169-200, https://doi.org/10.1515/9781501509032-010.

McLennan S.M. Weathering and global denudation. The Journal of Geology, Vol. 101(2), 1993, pp. 295-303. https://doi.org/ 10.1086/648222.

Md. Masidul Haque, Mrinal Kanti Roy. Sandstone-Shale Geochemistry of Miocene Surma Group in Bandarban Anticline, SE Bangladesh: Implications for Provenance, Weathering, and Tectonic Setting. Earth Sciences, Vol. 9(1), 2020, 38-51, https://doi.org/10.11648/j.earth.20200901.15.

– A case study on Indian zircons. Geochimica et Cosmochimica Acta, Vol. 47, 1983, pp. 2047-2052.

Nesbitt H.W. and Young G.M. Early Proterozoic climates and plate motions inferred from major element chemistry of lutites. Nature, Vol. 299, 1982, pp. 715-717, https://doi.org/10.1038/299715a0.

Nesbitt H.W. and Young G.M. Prediction of some weathering trends of plutonic and volcanic rocks based on thermodynamic and kinetic considerations. Geochimica et Cosmochimica Acta, Vol. 48, No. 7, 1984, pp. 1523-1534, DOI:10.1016/0016-7037(84)90408-3.

Pettijohn F.J., Potter P.E., Siever R. Sand and sandstone. Springer-Verlag. New York, 1973, 618 p.

Rodrigo J.D., Gabo-Ratio J.A.S., Queaño K.L., Fernando A.G.S., Silva L.P., Yonezu K., Zhang Y. Geochemistry of the Late Cretaceous Pandan Formation in Cebu Island, Central Philippines: Sediment contributions from the Australian plate margin during the Mesozoic. The Depositional Record, Vol. 6(2), 2020, pp. 309-330, DOI:10.1002/dep2.103.

Roser B.P. and Korsch R.J. Determination of Tectonic Setting of Sandstone-Mudstone Suites Using SiO2 Content and K2O/Na2O Ratio. Journal of Geology, Vol. 94, 1986, pp. 635-650, https://doi.org/10.1086/629071.

Rustamov M.I. Geodynamics and magmatism of the Zagros-Caucasus Segment in the Phanerozoic. Palmarium Academic Publishing. 2016, 543 p. (in Russian).

Schieber J. A combined petrographical-geochemical provenance study of the Newland formation, Mid-Proterozoic of Montana. Geological Magazine, Vol. 129, 1992, pp. 223-237.

Taylor S.R. and McLennan S.M. The continental crust: Its composition and evolution. Blackwell Scientific Publications. Oxford, 1985, pp. 1-312.

Taylor S.R., McLennan S.M. The continental crust: Its composition and evolution. Oxford, London, Edinburgh, Boston, Palo Alto, Melbourne: Blackwell Scientific. Geological Magazine, Vol. 122(6), 1985, pp. 673-674, DOI:10.1017/S0016756800032167.

Murali A.V., Parthasarathy R., Mahadevan T.M., Das M.S. Trace element characteristics, REE patterns and partition coefficients of zircons from different geological environments – A case study on Indian zircons. Geochimica et Cosmochimica Acta, Vol. 47, 1983, pp. 2047-2052.

Nesbitt H.W. and Young G.M. Early Proterozoic climates and plate motions inferred from major element chemistry of lutites. Nature, Vol. 299, 1982, pp. 715-717, https://doi.org/10.1038/299715a0.

Nesbitt H.W. and Young G.M. Prediction of some weathering trends of plutonic and volcanic rocks based on thermodynamic and kinetic considerations. Geochimica et Cosmochimica Acta, Vol. 48, No. 7, 1984, pp. 1523-1534, DOI:10.1016/0016-7037(84)90408-3.

Pettijohn F.J., Potter P.E., Siever R. Sand and sandstone. Springer-Verlag. New York, 1973, 618 p.

Rodrigo J.D., Gabo-Ratio J.A.S., Queaño K.L., Fernando A.G.S., Silva L.P., Yonezu K., Zhang Y. Geochemistry of the Late Cretaceous Pandan Formation in Cebu Island, Central Philippines: Sediment contributions from the Australian plate margin during the Mesozoic. The Depositional Record, Vol. 6(2), 2020, pp. 309-330, DOI:10.1002/dep2.103.

Roser B.P. and Korsch R.J. Determination of Tectonic Setting of Sandstone-Mudstone Suites Using SiO2 Content and K2O/Na2O Ratio. Journal of Geology, Vol. 94, 1986, pp. 635-650, https://doi.org/10.1086/629071.

Schieber J. A combined petrographical-geochemical provenance study of the Newland formation, Mid-Proterozoic of Montana. Geological Magazine, Vol. 129, 1992, pp. 223-237.

Taylor S.R. and McLennan S.M. The continental crust: Its composition and evolution. Blackwell Scientific Publications. Oxford, 1985, pp. 1-312.

Taylor S.R., McLennan S.M. The continental crust: Its composition and evolution. Oxford, London, Edinburgh, Boston, Palo Alto, Melbourne: Blackwell Scientific. Geological Magazine, Vol. 122(6), 1985, pp. 673-674, DOI:10.1017/S0016756800032167.

ПЕТРОГРАФИЯ И ГЕОХИМИЯ НИЖНЕМЕЛОВЫХ ОТЛОЖЕНИЙ ВАНДАМСКОЙ ЗОНЫ (ЮЖНЫЙ СКЛОН БОЛЬШОГО КАВКАЗА): ПАЛЕОВЫВЕТРИВАНИЕ, ИСТОЧНИКИ СНОСА И ТЕКТОНИЧЕСКАЯ ОБСТАНОВКА

Гулиев Э.Х.

Министерство науки и образования Республики Азербайджан, Институт геологии и геофизики
AZ1143, Баку, просп. Г.Джавида, 119: guliyevemin@outlook.com

Резюме. Исследование посвящено палеогеографическим условиям выветривания, источникам сноса и геодинамическим условиям формирования неокомских отложений. Основное внимание уделено кепучской и гырхбулагской свитам Вандамской тектонической зоны, расположенной на северном борту Южно-Кавказской микроплиты, которая характеризуется комплексом меловых флишевых и вулканогенных формаций. Посредством интеграции петрографических и геохимических данных исследование направлено на выявление характерных геохимических признаков, отражающих источники осадков, процессы выветривания и среды осадконакопления, что способствует углублению понимания геодинамической эволюции региона. Петрографический анализ песчаников показывает, что они состоят преимущественно из обломков пород, кварца и полевого шпата, акцессорных минералов и глинистого матрикса, превышающего 15%, что позволяет классифицировать их как литарениты, и подчёркивает преобладание обломков вулканических и метаморфических пород, а также аутигенного кальцитового цемента. Геохимические индикаторы палеовыветривания, такие как индекс химического выветривания (CIA), индекс выветривания (CIW) и индекс выветривания плагиоклаза (PIA), указывают на низкую и умеренную степень выветривания областей источника сноса. Геохимический анализ терригенных пород указывает на их смешанное происхождение, преимущественно из кислых и средних магматических пород, что соотносится с тектоническими условиями континентальной островной дуги. Дискриминационные диаграммы (SiO_2–K_2O/Na_2O, Al_2O_3/SiO_2 – Fe_2O_3+MgO, La–Th–Sc, Ti/Zr–La/Sc, Eu/Eu*–Gd_N/Yb_N) указывают на размещение образцов в полях активной континентальной окраины и континентальной островной дуги, указывая на субдукционное происхождение. Эти результаты подчёркивают влияние тектонических процессов на геохимические характеристики терригенных пород.

Ключевые слова*: источники сноса, геодинамический режим, палеовыветривание, Вандамская зона, кепучская и гырхбулагская свиты*

VƏNDAM TEKTONİK ZONASININ (BÖYÜK QAFQAZIN CƏNUB YAMACI) ALT TƏBAŞİR ÇÖKÜNTÜLƏRİNİN PETROQRAFİYASI VƏ GEOKİMYASI: PALEOAŞINMA, AŞINMA MƏNBƏLƏRİ VƏ TEKTONİK ŞƏRAİT

Quliyev E.X.
*Azərbaycan Respublikası Elm və Təhsil Nazirliyi, Geologiya və Geofizika İnstitutu, Azərbaycan
AZ1073, Bakı, H. Cavid prospekti, 119: guliyevemin@outlook.com*

Xülasə. Bu tədqiqat Alt Təbaşir yaşlı çöküntü laylarının paleocoğrafi aşınma şəraitini, gətirilmə mənbələrini və geodinamik şəraitini araşdırmağa həsr olunmuşdur. Tədqiqatda əsas diqqət Cənubi Qafqaz mikroplitəsinin şimal cinahında yerləşən və mürəkkəb Təbaşir yaşlı fliş və vulkanogen formasiyaları ilə xarakterizə olunan Vəndam tektonik zonasındakı Kepuç və Qırxbulaq lay dəstələrinə yönəldilmişdir. Petroqrafik və geokimyəvi məlumatların inteqrasiyası vasitəsilə bu tədqiqat çöküntü mənbələrini, aşınma proseslərini və çökmə mühitlərini əks etdirən xarakterik geokimyəvi göstəriciləri aşkar etməklə, regionun geodinamik inkişafını daha dərindən anlamağı hədəfləyir. Qumdaşlarının petroqrafik təhlili zamanı onların əsasən süxur fraqmentlərindən, kvarsdan və çöl şpatından ibarət olduğunu, 15%-dən artıq gil matriksinə malik olduğunu göstərir ki, bu da onları litarenitlər kimi təsnif etməyə imkan verir. Petroqrafik metodun tətbiqi nəticəsində süxurlarda vulkanik qırıntıların miqdarı metamorfik və çökmə mənşəli qırıntılardan daha çox olduğu, həmçinin sementin əsasən karbonat tərkibli və kalsitdən ibarət olduğu aydınlaşmışdır. Paleoaşınma üçün geokimyəvi göstəricilər, o cümlədən Kimyəvi Aşınma İndeksi (CIA), Aşınma İndeksi (CIW) və Plagioklazın Aşınma İndeksi (PIA), aşınma mənbələrinin zəif və orta dərəcədə aşındığını göstərir. Mənşə analizi göstərir ki, çöküntü materialları əsasən turş və orta maqmatik süxur növlərindən ibarət qarışıq mənşədən gəlir və bu kontinental ada qövsü tektonik mühiti ilə uyğundur. Diskriminasiya diaqramları (SiO_2-K_2O/Na_2O, Al_2O_3/SiO_2 – Fe_2O_3+MgO, La–Th–Sc, Ti/Zr–La/Sc, Eu/Eu*-Gd_N/Yb_N) nümunələrin aktiv kontinental kənar və kontinental ada qövsü sahələrində yerləşdiyini və subduksiya ilə əlaqəli çöküntü mənbəyinə işarə etdiyini göstərir. Bu analiz tektonik proseslərin terrigen süxurların geokimyəvi xüsusiyyətlərinin formalaşmasında mühüm rol oynadığını vurğulayır.

Açar sözlər: aşınma mənbələri, geodinamik rejim, paleoaşınma, Vəndam zonası, Kepuç və Qırxbulaq lay dəstələri

ANAS Transactions   Earth Sciences   2 / 2024

http://www.journalesgia.com

MÜNDƏRİCAT

CONTENTS

ОГЛАВЛЕНИЕ